

Zinc Isotope Systematics in Terrestrial Food Webs: Implications for the Trophic Ecology of Tropical Hunter-Gatherer of Late Pleistocene Southeast Asia

Nicolas Bourgon

A dissertation submitted in fulfilment
of the requirements for the degree of
Doctor rerum naturalium (Dr. rer. nat.)
of the
Johannes Gutenberg University



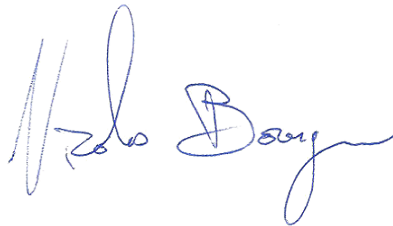
Faculty of Chemistry, Pharmaceutical Sciences, Geography and Geosciences
Institute of Geosciences
Applied and Analytical Paleontology Group

2022

Declaration

I hereby declare that I wrote the dissertation submitted without any unauthorized external assistance and used only sources acknowledged in the work. All textual passages, which are appropriated verbatim or paraphrased from published and unpublished texts, and all information obtained from oral sources, are duly indicated and listed in accordance with bibliographical rules. In carrying out this research, I complied with the rules of standard scientific practice formulated in Johannes Gutenberg-University Mainz's statutes to ensure standard scientific practices.

Signed:

A handwritten signature in blue ink, appearing to read "Helmut Berger". The signature is written in a cursive style with a large initial "H" and a long, sweeping underline.

Date: 25.01.2022

Abstract

Nicolas Bourgon

Zinc Isotope Systematics in Terrestrial Food Webs: Implications for the Trophic Ecology of Tropical Hunter-Gatherer of Late Pleistocene Southeast Asia

This thesis explores the use of “non-traditional” stable isotopes in archeology and paleontology, specifically isotopes of the trace element zinc (Zn) from tooth enamel to obtain dietary information from fossil specimens. Throughout this thesis, the use of zinc stable isotopes is explored through methodological and application perspectives, addressing some analytical challenges and developing study designs that are optimized for extracting robust dietary data from fossil materials. In particular, this method allows assessing the trophic level of a consumer, i.e., its relative dietary reliance on plant or animal resources. While nitrogen stable isotope ($\delta^{15}\text{N}$) analysis of bone or dentin collagen is an established method for trophic level assessment, such method is limited by protein preservation. Trophic level assessment of fossils beyond the Late Pleistocene, or coming from adverse taphonomic settings such as tropical and subtropical environments, are mostly unfeasible with this conventional method. However, the $^{66}\text{Zn}/^{64}\text{Zn}$ ratio (expressed as $\delta^{66}\text{Zn}$ value) in bioapatite shows promise as a proxy to infer trophic and dietary information from fossil vertebrates, even under adverse taphonomic conditions. Indeed, zinc is incorporated as a trace element in the enamel bioapatite and thus has a better long-term preservation potential of diet-related isotope compositions than collagen-bound nitrogen.

The first part of this thesis aims at giving an overview of zinc isotope analysis in paleodietary reconstructions, outlining principles of zinc isotope systematics and highlighting the potential and challenges of this analysis for archeology and paleontology. The lack of a strongly defined interpretative framework and comparative data are key obstacles to using zinc stable isotopes for paleodietary reconstructions.

The second part of this thesis examines the preservation potential of pristine diet-related zinc isotope ratios under tropical conditions with poor collagen preservation, such as the studied depositional context in Southeast Asia. Analyses were conducted on the enamel of fossil teeth from the Late Pleistocene (38.4–13.5 ka) mammalian assemblage of Tam Hay Marklot (THM) cave in northeastern Laos, representing the first use of zinc isotopes on fossils for paleodietary studies. Distinct trophic discriminations according to expected feeding habits were obtained from enamel $\delta^{66}\text{Zn}$ values of the fossil taxa. Moreover, trace element and zinc concentration profiles suggest an excellent long-term preservation potential of original zinc isotope compositions and validate the use of this method for paleodietary studies.

The third part of this thesis comprises an assessment of zinc contamination from gloves used during sample preparation, using teeth of a population of early Holocene hunter-gatherers from Lapa do Santo, Brazil. No sign of significant zinc contamination was identified, and the primary source of zinc isotope variability in the Lapa do Santo population appeared associated with dietary transitions. For the first time, the potential of zinc stable isotope values as a proxy to trace age at weaning was demonstrated.

The fourth part of this thesis involves the application of zinc isotope ratios to assess the reliance on plant or animal resources of a Late Pleistocene (63–46 ka) fossil *Homo sapiens* individual from Tam Pà Ling, one of the earliest-known anatomically modern humans in tropical Southeast Asia. The results highlighted a diet comprised of substantial amounts of plant and animal matter, which contrasts with most trophic level assessments of contemporaneous hunter-gatherer humans from other regions that comprise higher proportions of animal matter in their diet. It also reinforces a growing body of evidence for early human foragers' occupation and adaptation to tropical rainforest environments. These results further illustrate the potential of the isotopic ratios of zinc in bioapatite to bypass the taphonomical limitations of collagen-bound nitrogen isotopes, allowing insights otherwise unobtainable.

Zusammenfassung

Nicolas Bourgon

Zink-Isotopen-Systematik in terrestrischen Nahrungsnetzen: Implikationen für die trophische Ökologie der tropischen Jäger und Sammler im späten Pleistozän Südostasiens

Diese Dissertation untersucht die Anwendung "nicht-traditioneller" stabiler Isotope in der Archäologie und Paläontologie, insbesondere die Anwendung von Isotopen des Spurenelements Zink (Zn) aus Zahnschmelz, um Informationen über die Ernährung aus fossilen Proben zu erhalten. Mit dieser Methode lässt sich insbesondere die trophische Ebene eines Konsumenten beurteilen, d. h. seine relative Abhängigkeit von pflanzlichen oder tierischen Ressourcen in der Ernährung. Die Analyse der stabilen Stickstoffisotope ($\delta^{15}\text{N}$) von Knochen- oder Dentinkollagen ist zwar eine etablierte Methode zur Bewertung der trophischen Ebene, doch wird die Anwendung dieser Methode durch die Proteinkonservierung limitiert. Bei Fossilien, die älter als ~ 100.000 sind oder aus ungünstigen taphonomischen Verhältnissen stammen, ist eine Bestimmung der Trophiestufe mit dieser herkömmlichen Methode meist nicht möglich. Das $^{66}\text{Zn}/^{64}\text{Zn}$ -Verhältnis (ausgedrückt als $\delta^{66}\text{Zn}$ -Wert) in Bioapatit ist jedoch ein vielversprechender Indikator, um trophische und ernährungsbezogene Informationen aus fossilen Wirbeltieren abzuleiten, selbst unter ungünstigen taphonomischen Bedingungen. Zink ist nämlich als Spurenelement in den Bioapatit des Zahnschmelzes eingebaut und hat daher ein besseres Potenzial für die langfristige Erhaltung nahrungsspezifischer Isotopenzusammensetzungen als kollagengebundener Stickstoff.

Der erste Teil dieser Arbeit soll einen Überblick über die Zink-Isotopenanalyse bei als Werkzeug zur paläodiätischen Ernährungsrekonstruktion Rekonstruktionen geben, die isotopischen Prinzipien der Isotopensystematik von Zink umreißen und das Potenzial und die Herausforderungen dieser Analyse für die Archäologie und Paläontologie aufzeigen. Für paläodiätische Ernährungsrekonstruktionen werden das Fehlen eines

klar definierten Interpretationsrahmens und von Vergleichsdaten als zentrale Herausforderungen bei der Verwendung von Isotopen des Spurenelements Zink genannt.

Im zweiten Teil dieser Arbeit wird das Erhaltungspotenzial ursprünglicher ernährungsbezogener Zinkisotopenverhältnisse unter tropischen Bedingungen mit schlechter Kollagenerhaltung untersucht. Die Analysen wurden am Schmelz fossiler Zähne aus der spätpleistozänen (38,4–13,5 ka) Assemblage Fossilassoziaton von Tam Hay Marklot (THM) durchgeführt. Anhand der $\delta^{66}\text{Zn}$ -Werte im Zahnschmelz der fossilen Taxa konnten eindeutige trophische Unterscheidungen entsprechend den erwarteten Ernährungsgewohnheiten getroffen werden. Darüber hinaus deuten die Profile der Spurenelement- und Zinkkonzentration auf ein ausgezeichnetes Langzeit-Erhaltungspotenzial der nahrungsbezogenen Zn-Isotopenzusammensetzung hin und bestätigen die Verwendung dieser Methode für paläodiätetische Studien die Ernährungsrekonstruktion.

Der dritte Teil dieser Arbeit befasst sich mit der Bewertung der Zinkkontamination von Handschuhen, die bei der Probenvorbereitung verwendet wurden, bei für Zähne einer Population von Jägern und Sammlern aus dem frühen Holozän in Lapa do Santo, Brasilien. Es wurden keine Anzeichen für eine signifikante Zinkkontamination festgestellt, und die primäre Quelle der Zinkisotopenvariabilität in der Bevölkerung von Lapa do Santo scheint mit Ernährungsumstellungen Ernährungsänderungen zusammenzuhängen. Zum ersten Mal wurde das Potenzial des Zink-Isotopenverhältnisses als Näherungswert möglicher Indikator für das EntwöhnungsAlter beim Absetzen von der Muttermilch nachgewiesen.

Der vierte Teil dieser Arbeit befasst sich mit der Anwendung von Zink-Isotopenverhältnissen, um die Abhängigkeit von pflanzlichen oder tierischen Ressourcen eines spätpleistozänen (63–46 ka) fossilen *Homo sapiens*-Individuums aus Tam Pà Ling, einem der frühesten anatomisch bekannten modernen Menschen in Südostasien, zu bewerten. Die Ergebnisse weisen auf eine Ernährung hin, die erhebliche Mengen sowohl an pflanzlichen pflanzlicher und als auch an tierischen tierischer Stoffen Kost enthält, was im Gegensatz zu den meisten Bewertungen der tropischen Ebene zeitgenössischer Jäger und Sammler Menschen aus anderen Regionen steht, die einen höheren tierischen Proteinanteil in ihrer Ernährung aufweisen.

Contents

Declaration	3
Abstract	5
Zusammenfassung	7
Acknowledgments	Error! Bookmark not defined.
Contents	9
List of tables and figures	13
List of tables and captions	13
Tables	13
Supplementary information tables	13
List of figures and captions	19
Figures	19
Supplementary information figures	24
Dietary reconstruction in archeology	35
1.1 Introduction	35
1.2 Stable isotope analysis in paleodietary studies	36
1.3 Zinc stable isotope analysis in (paleo)dietary studies	41
1.4 Hominin biogeography and tropical forest reliance in Southeast Asia during the Pleistocene	46
1.5 This study	48
1.5.1 Aims and objectives	49
Preservation of diet-related zinc isotope ratios in fossil tooth enamel	53
Acknowledgements	55
Abstract	56
Significance	56
2.1 Introduction	57
2.2 Results	61
2.3 Discussion	64
2.3.1 Preservation of diet-related zinc isotope compositions in fossils teeth	64

2.3.2 Variation in zinc isotopic compositions in tooth enamel	65
2.4 Conclusion	67
2.5 Methods	68
Assessment of contamination and dietary transitions on zinc isotope variations	71
Acknowledgements	73
Abstract	74
3.1 Introduction	75
3.2 Material and methods	77
3.2.1 Background information on cultural and dietary behavior of humans from Lapa do Santo	77
3.2.3 TEST 2: Experiment sample contamination using different types of gloves	81
3.2.4 TEST 3: Post hoc assessment of contamination during sample preparation using linear mixed model	82
3.3 Results	82
3.3.1 TEST 1: Experiments on gloves	83
3.3.2 TEST 2: Experiment sample contamination using different types of gloves	85
3.3.3 TEST 3: Post hoc assessment of contamination during sample preparation using linear mixed model	88
3.4 Discussion	89
3.4.1 Zinc contamination during sample preparation in the clean lab	89
3.4.2 Zinc contamination during the enamel sampling procedure	90
3.4.3 Life history and dietary effects on human enamel $\delta^{66}\text{Zn}$ values	91
3.5 Conclusion	97
Trophic ecology of a Late Pleistocene early modern human from tropical Southeast Asia	99
Acknowledgements	101
Abstract	102
4.1 Introduction	103
4.2 Material and methods	106
4.3 Results	107
4.4 Discussion	111
4.4.1 Variability in tooth enamel $\delta^{66}\text{Zn}$ and trophic level	111
4.4.2 Stable zinc isotope measurements of the TPL1 <i>H. sapiens</i> individual	113

4.5 Conclusions	117
Synthesis and outlook	119
Conclusion	133
Supplementary information appendix	135
Supplementary information 1	135
Supplementary information 1.1: Context	135
Supplementary information 1.2: Stable isotope analyses	147
Supplementary information 1.3: Methods	153
Supplementary information 1.4: Results	158
Supplementary information 2	165
Supplementary information 2.1: Archeological context	165
Supplementary information 2.2: Methods	165
Supplementary information 2.3: Results and discussion	166
Supplementary information 3	168
Supplementary information 3.1: Stable isotope analyses	168
Supplementary information 3.2: Material and methods	172
Supplementary information 3.3: Variation of zinc stable isotope values in fossil tooth enamel from Tam Pà Ling and Nam Lot	177
Supplementary information tables	180
Supplementary information figures	230
References	283

List of tables and figures

List of tables and captions

Tables

Table 1. List of the gloves tested in this study and associated characteristics. One glove per box was used.	78
--	----

Supplementary information tables

Table S1. Preliminary $\delta^{66}\text{Zn}$ results (in ‰) of rats from a controlled-feeding experiment. Animals were fed a custom-made diets, either pelleted (plant-, insect-, meat-based or meat-based & bone) or natural (day-old-chicks and vegetable mix). The diet "Bone" consist in an animal-based pelleted diet with an addition of 14% of bone-like supplement. Various material (tissues, organs, body fluids and feeds) were analyzed for their zinc stable isotope compositions to investigate biological fractionation and specific diet-tissue spacings. Abbreviation: SEVA = Stable isotope-Evolutionary Anthropology (the numbering system used in the Human Evolution department of the Max Planck Institute for Evolution Anthropology, Leipzig, for every sample analyzed for isotope analysis), RBC = Red blood cell, WB = Whole blood.....	182
---	-----

Table S2. Full list of fossil tooth specimens from Tam Hay Marklot cave (Laos) analyzed in this study, with corresponding SEVA number, original number, broad dietary category and anatomical element. The dietary category assigned to each taxon was taken from Nowak (1999) ⁽¹⁾ , Macdonals (2009) ⁽²⁾ and Johnsingh and Manjrekar (2013, 2015) ⁽³⁻⁴⁾ . Abbreviation: SEVA = Stable isotope-Evolutionary Anthropology (the numbering system used in the Human Evolution department of the Max Planck Institute for Evolution Anthropology, Leipzig, for every sample analyzed for isotope analysis).	184
--	-----

Table S3. Sediment and dentin $\delta^{66}\text{Zn}$ isotope values (‰) from Tam Hay Marklot cave (Laos) used to assess the impact of diagenesis on $\delta^{66}\text{Zn}$ values. Abbreviation: SEVA = Stable isotope-Evolutionary Anthropology (the numbering system used in the Human Evolution department of the Max Planck Institute for Evolution Anthropology, Leipzig, for every sample analyzed for isotope analysis).....	185
Table S4. Enamel stable isotope results of $\delta^{13}\text{C}_{\text{apatite}}$, $\delta^{18}\text{O}_{\text{apatite}}$, $^{87}\text{Sr}/^{86}\text{Sr}$ and $\delta^{66}\text{Zn}$ from the 72 fossil tooth specimens from Tam Hay Marklot cave (Laos). Abbreviation: SEVA = Stable isotope-Evolutionary Anthropology (the numbering system used in the Human Evolution department of the Max Planck Institute for Evolution Anthropology, Leipzig, for every sample analyzed for isotope analysis).....	188
Table S5. Dentin $\delta^{13}\text{C}$ and $\delta^{15}\text{N}$ values (‰) from collagen extraction for the four of the 23 of the sub sample of 23 dentin samples, for which collagen extraction was attempted. Abbreviation: SEVA = Stable isotope-Evolutionary Anthropology (the numbering system used in the Human Evolution department of the Max Planck Institute for Evolution Anthropology, Leipzig, for every sample analyzed for isotope analysis).....	188
Table S6. List of reference materials with their respective measured and expected values for different isotopes.	189
Table S7. Results of the linear mixed model modelling $\delta^{66}\text{Zn}$ values as a function of several predictors (estimates and standard errors, confidence limits of the model, results of likelihood ratio tests, and the range of estimates obtained for the model when dropping levels of random effects one at a time).	190
Table S8. Inventory of specimens (isolated teeth) of mammals recovered at the Tam Hay Marklot site. <i>N</i> : Total number of specimens.	191
Table S9. Sample description from fossil teeth of the Tam Hay Marklot assemblage prepared for U-series dating.	192
Table S10. U-series results for the Tam Hay Marklot rhinoceros tooth specimen SCUMKR1 (<i>Dicerorhinus sumatrensis</i>).	192
Table S11. U-series results for the Tam Hay Marklot bovid tooth specimen SCUMK01 (large bovid).	193

Table S12. U-series results for the Tam Hay Marklot ourangutan tooth specimen SCUMK02 (<i>Pongo</i> sp.).....	193
Table S13. U-series results for the Tam Hay Marklot bovid tooth specimen SCUMK03 (<i>Bos</i> sp. (<i>Bos</i> cf. <i>frontalis</i>)).	194
Table S14. DAD model results for each fossil tooth sample from the Tam Hay Marklot assemblage prepared for U-series dating.	194
Table S15. Sediment and dentin $\delta^{66}\text{Zn}$ isotope values (‰) from Tam Hay Marklot cave (Laos) used to assess the impact of diagenesis on $\delta^{66}\text{Zn}$ values. Abbreviation: SEVA = Stable isotope-Evolutionary Anthropology (numbering system used in the Human Evolution department of the Max Planck Institute for Evolution Anthropology, Leipzig, for every sample analyzed for isotope analysis).....	195
Table S16. Measured and expected $\delta^{66}\text{Zn}$ values for NIST SRM 1400 and in-house AZE reference materials used in this study, and information about the type of gloves used during sample preparation and instrument (ICPMS) used for measurements.....	196
Table S17. The $\delta^{66}\text{Zn}$ values (‰) and zinc content (ng) for each of the glove tests and different type of gloves used in this study.	197
Table S18. Tooth enamel $\delta^{66}\text{Zn}$ values (‰) and zinc concentration ($\mu\text{g/g}$) from the Lapa do Santo (Minas Gerais, Brazil) hunter-gatherers, with anthropological data. Abbreviation: SEVA = Stable isotope-Evolutionary Anthropology (the numbering system used in the Human Evolution department of the Max Planck Institute for Evolution Anthropology, Leipzig, for every sample analyzed for isotope analysis).....	200
Table S19. Isotope data for the Couvent des Jacobins teeth (individual 63049 and 20106). The $\delta^{66}\text{Zn}$ values are obtained from the enamel, whereas the $\delta^{13}\text{C}$ and $\delta^{15}\text{N}$ from collagen extracted from the teeth's root. Delta values are expressed in ‰. The type of teeth sampled, the part sampled as well as the corresponding forming ages (init. and compl.: respectively the age of initiation and completion of the sampled enamel (ena.) and root) are also listed. Abbreviation: SEVA = Stable isotope-Evolutionary Anthropology (the numbering system used in the Human Evolution department of the Max Planck	

Institute for Evolution Anthropology, Leipzig, for every sample analyzed for isotope analysis). 202

Table S20. Full list of Late Pleistocene fossil tooth specimens from Nam Lot and Tam Pà Ling cave (Laos) analyzed for $\delta^{66}\text{Zn}$ and $^{87}\text{Sr}/^{86}\text{Sr}$ in this study, with corresponding laboratory internal SEVA number, original sample number, broad dietary category and tooth type. Taxonomic units range from species to family levels. The dietary category assigned to each taxon was taken from Nowak (1999), Macdonald (2009) and Johnsingh and Manjrekar (2013, 2015). Abbreviations: SEVA = Stable isotope-Evolutionary Anthropology (the numbering system used in the Human Evolution department of the Max Planck Institute for Evolution Anthropology, Leipzig, for every sample analyzed for isotope analysis), r = right, l = left. 207

Table S21. Full list of the Late Pleistocene fossil tooth specimens sub sample from Nam Lot cave (Laos) for which dentin collagen extraction was attempted. Abbreviation: SEVA = Stable isotope-Evolutionary Anthropology (the numbering system used in the Human Evolution department of the Max Planck Institute for Evolution Anthropology, Leipzig, for every sample analyzed for isotope analysis). 208

Table S22. Enamel zinc and strontium stable isotope results ($^{87}\text{Sr}/^{86}\text{Sr}$ and $\delta^{66}\text{Zn}$) and concentration (Zn [$\mu\text{g/g}$] and Sr [$\mu\text{g/g}$]) from the Late Pleistocene fossil tooth specimens from Nam Lot and Tam Pà Ling caves (Laos). Abbreviation: SEVA = Stable isotope-Evolutionary Anthropology (the numbering system used in the Human Evolution department of the Max Planck Institute for Evolution Anthropology, Leipzig, for every sample analyzed for isotope analysis). 212

Table S23. Enamel $\delta^{13}\text{C}_{\text{apatite}}$ and $\delta^{18}\text{O}_{\text{apatite}}$ stable isotope results, as well as body mass (kg), $\delta^{13}\text{C}$ (‰) enrichment factor and $\delta^{13}\text{C}_{\text{diet}}$ (‰) from the Late Pleistocene fossil tooth specimens from Tam Pà Ling, Nam Lot and Tam Hay Marklot caves (Laos). Average body mass for each species was estimated from modern day analogous species (Nowak, 1999; Macdonald, 2009; Johnsingh and Manjrekar, 2013, 2015). Most of Nam Lot $\delta^{13}\text{C}_{\text{apatite}}$ and $\delta^{18}\text{O}_{\text{apatite}}$ values used in this study had already been measured and published (Bacon et al., 2018a), as were the $\delta^{13}\text{C}_{\text{apatite}}$ and $\delta^{18}\text{O}_{\text{apatite}}$ values from Tam Hay Marklot (Bourgon et al., 2020). The M² from TPL-1 individual was not measured for $\delta^{13}\text{C}_{\text{apatite}}$ and $\delta^{18}\text{O}_{\text{apatite}}$ analysis due to lack of material. Abbreviation: SEVA = Stable

isotope-Evolutionary Anthropology (the numbering system used in the Human Evolution department of the Max Planck Institute for Evolution Anthropology, Leipzig, for every sample analyzed for isotope analysis).....	219
Table S24. Results of the linear mixed model modeling $\delta^{66}\text{Zn}$ values as a function of several predictors (diet: carnivore, bone-eating carnivore, omnivore and herbivore; $^{87}\text{Sr}/^{86}\text{Sr}$, $\delta^{13}\text{C}_{\text{apatite}}$, $\delta^{18}\text{O}_{\text{apatite}}$, locality, zinc concentration and body mass). The table shows the estimates and standard errors (SE), lower and upper confidence limits of the model (CI), results of likelihood ratio tests, and the range of estimates obtained for the model when dropping levels of random effects one at a time (Min, Max). A total of 145 specimens was used from all three Late Pleistocene Southeast Asian cave sites (Laos) of Nam Lot, Tam Pà Ling and published data from Tam Hay Marklot (Bourgon et al., 2020). Abbreviation: CI = confidence interval.	220
Table S25. List of reference materials with their respective measured and expected values for different isotopes.....	221
Table S26. Results of Tukey post-hoc pair-wise comparisons for $\delta^{66}\text{Zn}$ values between dietary categories (bone-eating carnivore, omnivore, herbivore, and carnivore). A total of 145 specimens was used from all three Late Pleistocene Southeast Asian cave sites (Laos) of Nam Lot, Tam Pà Ling and published data from Tam Hay Marklot (Bourgon et al., 2020). Abbreviation: CI = confidence interval.	222
Table S27. List of samples from Tam Pà Ling with their associated depth at which they were recovered and their associated dating according to the latest chronology of the site (Shackelford et al., 2018). Abbreviation: SEVA = Stable isotope-Evolutionary Anthropology (numbering system used in the Human Evolution department of the Max Planck Institute for Evolution Anthropology, Leipzig, for every sample analyzed for isotope analysis), C14 = Radiocarbon dating (also referred to as carbon dating or carbon-14 dating), OSL = Optically-stimulated luminescence dating, IRSL = Infrared stimulated luminescence dating.....	223
Table S28. Preliminary $\delta^{66}\text{Zn}$ results from the Late Pleistocene sites of Duoi U’Oi and Coc Muoi, Vietnam, respectively 70-60 ka and 148–117 ka. Abbreviation: SEVA = Stable isotope-Evolutionary Anthropology (the numbering system used in the Human Evolution department of the Max Planck Institute for	

Evolution Anthropology, Leipzig, for every sample analyzed for isotope analysis).....229

List of figures and captions

Figures

- Figure 1.** Box and whisker plots presenting the range of $\delta^{66}\text{Zn}$ values (‰, relative to the JMC-Lyon zinc isotope standard) in some plants (Viers et al., 2007; Moynier et al., 2009; Aucour et al., 2011; Tang et al., 2016; van der Ent et al., 2021), highlighting the general enrichment in heavy isotopes in the roots (brown square) relative to the source (orange diamond) and the general trend of lower $\delta^{66}\text{Zn}$ values in shoots (light green circle; here including stem and/or shoots data) and leaves (turquoise triangle) relative to the roots. The isotopic composition of the known or likely source (e.i., litter, soil, or nutrient solution in experimental settings) of zinc uptake from the plant does not contribute to the boxes and whiskers, which represent the 25th–75th percentiles, with the median represented by a bold horizontal line, for each plant. 44
- Figure 2.** The zinc isotope compositions (‰, relative to the JMC-Lyon zinc isotope standard) of red blood cells, bones, feces, muscle, kidney, liver, and respective feeds of animals, as reported from controlled-feeding experiments, highlights the generally low $\delta^{66}\text{Zn}$ values in soft tissues and higher values in bones compared to the diet. The beige squares correspond to data from sheep of Balter et al. (2010), the green circles from mice of Moynier et al. (2013), blue triangles from mice of Balter et al. (2013), and red diamonds from rats of a preliminary dataset (*SI Appendix, Table S1*). The dashed lines correspond to the mean $\delta^{66}\text{Zn}$ values of the diet provided to the animals in each study..... 45
- Figure 3.** (A) Range of $\delta^{66}\text{Zn}$ values (relative to the JMC-Lyon zinc isotope standard; Maréchal et al., 1999) in tooth enamel for carnivores (red), omnivores (turquoise), and herbivores (blue) of the THM cave assemblage. The boxes from the box and whisker plots represent the 25th–75th percentiles, with the median as a bold horizontal line. (B) Distribution of enamel $\delta^{66}\text{Zn}$ versus $\delta^{13}\text{C}_{\text{apatite}}$ values of the THM cave assemblage (*SI Appendix, Table S4*), where “C₃ environment” and “C₄ environment” are defined by $\delta^{13}\text{C}_{\text{apatite}} < -8$ ‰ and > -2 ‰, respectively. Dashed lines represent the full range of variation, and full lines represent 40% predictive ellipses (using R statistical software and package “SIBER”; Jackson et al., 2011; R Core Team, 2018). 61
- Figure 4.** Natural log.transformed spatial element concentration profiles (ln.Concentration, as $\mu\text{g/g}$) of Zn, Fe, Mn, Al, Mg, and REE in caprine teeth

- for a fossil (*Capricornis* sp., left) and a modern (*H. jemlahicus*, right) specimen. The Fe, Mn, Al, and REE (calculated as the sum of all measured REE concentrations) were selected as tracers for diagenetic alteration because of their relative abundance in soil-matter, as well as their tendency to be enriched postmortem in fossil bioapatite. Thus, they most likely trace postmortem taphonomic alterations and element uptake from soil pore water. Note that in both photomicrographs the tracks of laser ablation line scans are visible. 63
- Figure 5.** Schematic setup of the different leaching tests of gloves in acidic and aqueous solution. See text for more details. 80
- Figure 6.** Schematic setup of the different dry contact tests with gloves and tubes cleaned in acidic and aqueous solutions. See text for more details. 80
- Figure 7.** Amount of zinc obtained for each test and each type of gloves following the protocol described in **Figure 5** and the corresponding text. “Latex C” corresponds to the coated latex gloves and “Latex T” to the textured latex gloves. 83
- Figure 8.** Zinc isotope composition of the gloves from (1) Garçon et al. (2017) (open circles) and (2) this study (filled circles). For this study, the symbols represent the average value for the four tests and the whiskers correspond to the standard deviation. T stands for textured, C for coated. 84
- Figure 9.** Zinc isotope ratios measured for the four types of gloves tested in this study. C stands for coated, T for textured. The description of the tests is provided in the text and **Figure 5**. 85
- Figure 10.** Zinc isotope ratios for each Lapa do Santo tooth sampled either with nitrile gloves (TEST 2A), latex gloves (TEST 2B), or without gloves (TEST 2C). The numbers on the x-axis correspond to the tooth specimen ID (see *SI Appendix, Table S18*), to note that several teeth may belong to the same individual. Typical analytical error for zinc isotope ratios is 0.05 ‰ to 0.08 ‰ (2σ), and the standard deviation of the different standards (AZE and SRM 1400) run on the columns ranges from 0.08 to 0.1 ‰ (2σ). 86
- Figure 11.** Relationship between zinc concentrations ($\mu\text{g/g}$) and isotope values for the six teeth on which all three TESTS 2 A, B, and C have been performed. The

- numbers 2 to 30 corresponds to the identification number of the teeth, which are also given in **SI Appendix, Table S18**. 87
- Figure 12.** Relationship between zinc concentrations ($\mu\text{g/g}$) and $\delta^{66}\text{Zn}$ values for the Lapa do Santo teeth (black circles). All samples are plotted together, independently from the sampling method used. The blue square represents the nitrile gloves, and the empty triangles are the latex gloves. 87
- Figure 13.** Correlation between the difference of concentration and the difference of $\delta^{66}\text{Zn}$ values of tooth samples from Lapa do Santo prepared with nitrile or latex gloves. P3 = first premolar. The typical analytical error for zinc isotope ratios ranges from 0.05 to 0.08 ‰ (2σ), and the standard deviation of the different standards (AZE and SRM 1400) run on the columns are 0.08 to 0.1 ‰ (2σ). 88
- Figure 14.** Zinc isotope values in teeth of the Lapa do Santo population. Tooth types are ordered from the earliest to the latest crown initiation and formation times: from in utero (deciduous molars) to puberty (permanent third molar). A) All single measurements pooled together (sample preparation with gloves nitrile or latex- or without), B) average $\delta^{66}\text{Zn}$ value per dental specimen. The error bars represent the variation within a tooth (1σ). 90
- Figure 15.** Zinc isotope values from the enamel of different tooth types at (A) Lapa do Santo (Brazil) and (B) Jacobins convent (Rennes, France). Note the trend of decreasing $\delta^{66}\text{Zn}$ values in enamel with increasing crown formation age for humans from both archeological sites. 93
- Figure 16.** Zinc isotope compositions of all the tooth types sampled for two individuals of the Jacobins convent. The teeth are ranked from the earliest forming enamel to the latest forming crowns. 94
- Figure 17.** Zinc isotope ratios in the different teeth of Child 63949, recovered from the Jacobin convent (Rennes, France), with the corresponding formation ages of the areas of enamel sampled (**SI Appendix, Table S19**) (AlQahtani et al., 2010). Different parts of the tooth crowns were sampled: top (T); middle (M); bottom (B); whole height (W). The age at introduction of solid food and weaning is here fully hypothetical (i.e., there is no archeological record for this specimen) but is based on nitrogen isotope data measured in the tooth roots as well as historical data on the population (**SI Appendix, Supplementary**

- Information 2.1 and 2.3).** Because the actual weaning age could be slightly younger or older, it is provided only for illustrative purposes. 94
- Figure 18.** Possible scenarios for the evolution of enamel $\delta^{66}\text{Zn}$ values in teeth during childhood. 95
- Figure 19.** Box and whisker plots of the range of $\delta^{66}\text{Zn}$ values (relative to the JMC-Lyon zinc isotope standard) in tooth enamel for each taxon and the TPL1 *H. sapiens* individual (63–46 ka; black star). Each of the other colors and symbols represents specimens from different sites: Tam Pà Ling (70–1.1 ka; orange triangles), Nam Lot (86–72 ka; blue squares), and previously published data from Tam Hay Marklot (Bourgon et al., 2020; 38.4–13.5 ka; yellow circles). Note the inclusion of the bone-eating carnivore *C. crocuta* with other carnivores. The boxes represent the 25th–75th percentiles, with the median represented by a bold horizontal line. The average analytical repeatability of samples was 0.01 %. 108
- Figure 20.** Violin plots presenting the range of $\delta^{66}\text{Zn}$ values (relative to the JMC-Lyon zinc isotope standard) of tooth enamel from each site for carnivores (excluding the bone-eating carnivore *C. crocuta*), omnivores, and herbivores. Each of the colors and symbols represents specimens coming from different sites: Tam Pà Ling (70–1.1 ka; orange triangles), Nam Lot (86–72 ka; blue squares), previously published data from Tam Hay Marklot (Bourgon et al., 2020; 38.4–13.5 ka; yellow circles), and all sites combined (brown diamonds). The outline of the plots illustrates kernel probability density, where the width represents the proportion of the data found therein. The boxes from the box and whisker plots inside the violin plots represent the 25th–75th percentiles, with the median represented by a bold horizontal line. 109
- Figure 21.** Distribution of enamel $\delta^{66}\text{Zn}$ versus $\delta^{13}\text{C}_{\text{diet}}$ values for TPL1 individual (black star), carnivores (red square), bone-eating carnivore *C. crocuta* (yellow diamond), omnivores (turquoise circle), herbivores (blue triangle) for A) all three Late Pleistocene sites of Tam Pà Ling (70–1.1 ka), Nam Lot (86–72 ka) and previously published data from Tam Hay Marklot (Bourgon et al., 2020; 38.4–13.5 ka) and B) only Tam Pà Ling and Nam Lot (this study and Bacon et al., 2018a). 'C₃ environment' and 'C₄ environment' are respectively defined by $\delta^{13}\text{C}_{\text{diet}} < -21.7\text{‰}$ and $> -15.7\text{‰}$. Dashed lines for convex hulls represent the

full range of variation and full lines for ellipses represent 40% predictive ellipses. VPDB = Vienna Pee Dee Belemnite..... 110

Figure 22. Violin plots presenting the range of $\delta^{66}\text{Zn}$ values (‰, relative to the JMC-Lyon zinc isotope standard) of tooth enamel in mammals, highlighting the low $\delta^{66}\text{Zn}$ values in carnivores (red), intermediate in bone-eating carnivores (yellow; here comprised only of *C. crocuta*) and omnivores (turquoise), and high in herbivores (blue). The data aggregates specimens of three Late Pleistocene sites of Laos (n = 148, of which 13 are carnivores, 6 are bone-eating carnivores, 43 are omnivores, and 86 are herbivores): Tam Pà Ling (70–1.1 ka), Nam Lot (86–72 ka), and Tam Hay Marklot (38.4–13.5 ka). The outline of the plots illustrates kernel probability density, where the width represents the proportion of the data found therein. The boxes from the box and whisker plots represent the 25th–75th percentiles, with the median represented by a bold horizontal line..... 125

Figure 23. Violin plots presenting the range of $\delta^{66}\text{Zn}$ values (‰ and relative to the JMC-Lyon zinc isotope standard) of tooth enamel between broad localities for carnivores (red), bone-eating carnivores (yellow; here comprised only of *C. crocuta*), omnivores (turquoise), and herbivores (blue). The data aggregates specimens of different sites into three broad groups: Laos, Vietnam, and Koobi Fora. The Laos group (n = 148, of which 13 are carnivores from 5 different taxa, 6 are *C. crocuta* bone-eating carnivores, 43 are omnivores from 5 different taxa, and 86 are herbivores from 10 different taxa) includes data from Late Pleistocene sites of Tam Pà Ling (70–1.1 ka), Nam Lot (86–72 ka), and Tam Hay Marklot (38.4–13.5 ka). The Vietnam group (n = 141, of which 12 are carnivores from 4 different taxa, 52 are omnivores from 5 different taxa, and 77 are herbivores from 10 different taxa) includes preliminary data from Late Pleistocene sites of Coc Muoi (148–117 ka) and Duoi U'Oi (70–60 ka) (see *SI Appendix, Table S28*). The Koobi Fora group (n = 26, of which 9 are carnivores from 3 different taxa, 3 *C. crocuta* bone-eating carnivores, and 14 are herbivores from 6 different taxa) includes data of modern-day fauna from Koobi Fora (Jaouen et al., 2016a). The outline of the plots illustrates kernel probability density, where the width represents the proportion of the data found therein. The boxes from the box and whisker plots represent the 25th–75th percentiles, with the median represented by a bold horizontal line. 127

Figure 24. Box and whisker plots of the range of $\delta^{66}\text{Zn}$ values (relative to the JMC-Lyon zinc isotope standard) in tooth enamel for each taxon from Late Pleistocene sites from Laos and the preliminary data from Vietnam (see *SI Appendix, Table S28*). Each color corresponds to the two broad regional groups: Laos (orange) and Vietnam (light blue). Each of the symbols represents specimens from different sites: Tam Pà Ling (70–1.1 ka; circle), Nam Lot (86–72 ka; upside-down triangle), Tam Hay Marklot (38.4–13.5 ka; diamond), Duoi'U'oi (70–60 ka; triangle) and Coc Muoi (148–117 ka; square). Note the inclusion of the bone-eating carnivore *C. crocuta* with other carnivores. The boxes represent the 25th–75th percentiles, with the median represented by a bold horizontal line..... 128

Supplementary information figures

- Figure S1.** Map of the Indochinese Peninsula with the location of the studied area in northeast Laos. 230
- Figure S2.** Map of Laos showing the studied area in the Hua Pan Province, 130 km NNE from Luang Prabang..... 231
- Figure S3.** Satellite view of the studied area with the location of the cave 6 km SE from the city of Xoneuna (Muang Xon)..... 231
- Figure S4.** (A) Tam Hay Marklot cave at the foot of a tower karst covered by the forest, and (B, C) the first chamber at the entrance. (D, E) First passageway that leads to the gallery..... 232
- Figure S5.** Map of the entire Tam Hay Marklot cave from the first chamber at the entrance to the dead-end after a 235 m extent, with three views of the gallery. 233
- Figure S6.** Map of the Tam Hay Marklot cave showing the three sections of the cave and their sedimentary fillings (see **Figure S7** for the legend of sedimentary sections)..... 234
- Figure S7.** Detail of the section/trench 2 showing the main sedimentary facies of the cave. In A and B, the arrows give the direction of the paleocurrents from inside to outside of the cave..... 235

- Figure S8.** Distribution of carbon ($\delta^{13}\text{C}_{\text{apatite}}$) and oxygen ($\delta^{18}\text{O}_{\text{apatite}}$) stable isotope values in fossil tooth enamel from Tam Hay Marklot cave. 236
- Figure S9.** Distribution of carbon ($\delta^{13}\text{C}_{\text{collagen}}$) and nitrogen ($\delta^{15}\text{N}_{\text{collagen}}$) stable isotope values in root dentin of the few fossil teeth from Tam Hay Marklot cave with collagen preservation. 237
- Figure S10.** Relationship between radiogenic strontium isotope ratios ($^{87}\text{Sr}/^{86}\text{Sr}$) and zinc ($\delta^{66}\text{Zn}$) stable isotope values in enamel of fossil teeth from Tam Hay Marklot cave..... 238
- Figure S11.** Relationship between the strontium concentration (1/Conc, as $\mu\text{g/g}$) and the radiogenic strontium isotope ratios ($^{87}\text{Sr}/^{86}\text{Sr}$) in enamel of fossil teeth from Tam Hay Marklot cave. The boxes from the box and whisker plot represent the 25th–75th percentiles, with the median as a bold horizontal line, of Sr concentration from modern enamel of mammal teeth found elsewhere (Copeland et al., 2008; Britton et al., 2009; Kohn et al., 2013). 239
- Figure S12.** Spatial element concentration profiles for the element Zn, Fe, Mn, Al, Mg, Sr, Pb, U and rare earth elements (REE, calculated as the sum of all measured REE concentrations) of all LA-ICP-MS linescan analysis (1 to 3) of the Tam Hay Marklot cave fossil tooth (m3 right) specimen 34493 (*Capricornis* sp.). All concentration data ($\mu\text{g/g}$) were natural log.transformed ($\ln.\text{Concentration}$). The different shaded areas, delimited by dotted lines, represent the different histological parts: white for enamel, light gray for dentin and medium gray for pulp cavity. The profiles follow a left-to-right direction as seen from the picture on the left. 240
- Figure S13.** Spatial element concentration profiles for the element Zn, Fe, Mn, Al, Mg, Sr, Pb, U and rare earth elements (REE, calculated as the sum of all measured REE concentrations) of all LA-ICP-MS linescan analysis (1 and 2) of the Tam Hay Marklot cave fossil tooth (M2 left) specimen 34501 (*Ursus thibetanus*). All concentration data ($\mu\text{g/g}$) were natural log.transformed ($\ln.\text{Concentration}$). The different shaded areas, delimited by dotted lines, represent the different histological parts: white for enamel, and light gray for dentin. The profiles follow a left-to-right direction as seen from the picture on the left..... 241
- Figure S14.** Spatialement concentration profiles for the element Zn, Fe, Mn, Al, Mg, Sr, Pb, U and rare earth elements (REE, calculated as the sum of all measured

REE concentrations) of all LA-ICP-MS linescan analysis (1 to 3) of the Tam Hay Marklot cave fossil tooth (P4 left) specimen 34505 (*Panthera pardus*). All concentration data ($\mu\text{g/g}$) were natural log.transformed ($\ln.\text{Concentration}$). The different shaded areas, delimited by dotted lines, represent the different histological parts: white for enamel, and light gray for dentin. The profiles follow a left-to-right direction as seen from the picture on the left242

Figure S15. Spatial element concentration profiles for the element Zn, Fe, Mn, Al, Mg, Sr, Pb, U and rare earth elements (REE, calculated as the sum of all measured REE concentrations) of all LA-ICP-MS linescan analysis (1 to 3) of the Tam Hay Marklot cave fossil tooth (p2/p3 left) specimen 34524 (*Bubalus bubalis*). All concentration data ($\mu\text{g/g}$) were natural log.transformed ($\ln.\text{Concentration}$). The different shaded areas, delimited by dotted lines, represent the different histological parts: white for enamel, and light gray for dentin. The profiles follow a left-to-right direction as seen from the picture on the left.....243

Figure S16. Spatial element concentration profiles for the element Zn, Fe, Mn, Al, Mg, Sr, Pb, U and rare earth elements (REE, calculated as the sum of all measured REE concentrations) of all LA-ICP-MS linescan analysis (1 to 3) of the Tam Hay Marklot cave fossil tooth (p4 left) specimen 34538 (*Sus sp.*). All concentration data ($\mu\text{g/g}$) were natural log.transformed ($\ln.\text{Concentration}$). The different shaded areas, delimited by dotted lines, represent the different histological parts: white for enamel, and light gray for dentin. The profiles follow a left-to-right direction as seen from the picture on the left.244

Figure S17. Spatial element concentration profiles for the element Zn, Fe, Mn, Al, Mg, Sr, Pb, U and rare earth elements (REE, calculated as the sum of all measured REE concentrations) of the single LA-ICP-MS linescan analysis of the Tam Hay Marklot cave fossil tooth (m1/m2 left) specimen 34548 (*Macaca sp.*). All concentration data ($\mu\text{g/g}$) were natural log.transformed ($\ln.\text{Concentration}$). The different shaded areas, delimited by dotted lines, represent the different histological parts: white for enamel, and light gray for dentin. The profiles follow a left-to-right direction as seen from the picture on the left.....245

Figure S18. Spatial element concentration profiles for the element Zn, Fe, Mn, Al, Mg, Sr, Pb, U and rare earth elements (REE, calculated as the sum of all

measured REE concentrations) of all LA-ICP-MS linescan analysis (1 and 2) of the Center of Natural History of Hamburg modern tooth (m3 right) specimen SEVA 34707 / ZMH-S-10461 (*Bison bison*). All concentration data ($\mu\text{g/g}$) were natural log.transformed ($\ln.\text{Concentration}$). The different shaded areas, delimited by dotted lines, represent the different histological parts: white for enamel, light gray for dentin, medium gray for pulp cavity, and dark gray for calculus. The profiles follow a left-to-right direction as seen from the picture on the left..... 246

Figure S19. Spatial element concentration profiles for the element Zn, Fe, Mn, Al, Mg, Sr, Pb, U and rare earth elements (REE, calculated as the sum of all measured REE concentrations) of all LA-ICP-MS linescan analysis (1 to 3) of the Center of Natural History of Hamburg modern tooth (m3 left) specimen SEVA 34708 / ZMH-S-10963 (*Hemitragus jemlahicus*). All concentration data ($\mu\text{g/g}$) were natural log.transformed ($\ln.\text{Concentration}$). The different shaded areas, delimited by dotted lines, represent the different histological parts: white for enamel, light gray for dentin, medium gray for pulp cavity, and dark gray for calculus. The profiles follow a left-to-right direction as seen from the picture on the left. 247

Figure S20. Spatial element concentration profiles for the element Zn, Fe, Mn, Al, Mg, Sr, Pb, U and rare earth elements (REE, calculated as the sum of all measured REE concentrations) of the single LA-ICP-MS linescan analysis of the Center of Natural History of Hamburg modern tooth (p3/p4) specimen SEVA 34709/ZMH-S-10612 (*Pteronura brasiliensis*). All concentration data ($\mu\text{g/g}$) were natural log.transformed ($\ln.\text{Concentration}$). The different shaded areas, delimited by dotted lines, represent the different histological parts: white for enamel, light gray for dentin, and medium gray for pulp cavity. The profiles follow a left-to-right direction as seen from the picture on the left. 248

Figure S21. Typical concentrations ($\mu\text{g/g}$) observed through spatial element concentration profiles for the element Zn, Fe, Mn, Al, Mg, Sr, Pb, U and rare earth elements (REE, calculated as the sum of all measured REE concentrations) of the Tam Hay Marklot cave fossil tooth (m3 right) specimen 34493 (*Capricornis* sp.). The different shaded areas, delimited by dotted lines, represent the different histological parts: white for enamel, light gray for dentin, and medium gray for pulp cavity. The profiles follow a left-to-right direction as seen from the picture on the left. 249

Figure S22. Typical concentrations ($\mu\text{g/g}$) observed through spatial element concentration profiles for the element Zn, Fe, Mn, Al, Mg, Sr, Pb, U and rare earth elements (REE, calculated as the sum of all measured REE concentrations) of the Tam Hay Marklot cave fossil tooth (M2 left) specimen 34501 (*Ursus thibetanus*). The different shaded areas, delimited by dotted lines, represent the different histological parts: white for enamel, and light gray for dentin. The profiles follow a left-to-right direction as seen from the picture on the left..... 250

Figure S23. Typical concentrations ($\mu\text{g/g}$) observed through spatial element concentration profiles for the element Zn, Fe, Mn, Al, Mg, Sr, Pb, U and rare earth elements (REE, calculated as the sum of all measured REE concentrations) of the Tam Hay Marklot cave fossil tooth (P4 left) specimen 34505 (*Panthera pardus*). The different shaded areas, delimited by dotted lines, represent the different histological parts: white for enamel, and light gray for dentin. The profiles follow a left-to-right direction as seen from the picture on the left..... 251

Figure S24. Typical concentrations ($\mu\text{g/g}$) observed through spatial element concentration profiles for the element Zn, Fe, Mn, Al, Mg, Sr, Pb, U and rare earth elements (REE, calculated as the sum of all measured REE concentrations) of the Tam Hay Marklot cave fossil tooth (p2/p3 left) specimen 34524 (*Bubalus bubalis*). The different shaded areas, delimited by dotted lines, represent the different histological parts: white for enamel, and light gray for dentin. The profiles follow a left-to-right direction as seen from the picture on the left..... 252

Figure S25. Typical concentrations ($\mu\text{g/g}$) observed through spatial element concentration profiles for the element Zn, Fe, Mn, Al, Mg, Sr, Pb, U and rare earth elements (REE, calculated as the sum of all measured REE concentrations) of the Tam Hay Marklot cave fossil tooth (p4 left) specimen 34538 (*Sus* sp.). The different shaded areas, delimited by dotted lines, represent the different histological parts: white for enamel, and light gray for dentin. The profiles follow a left-to-right direction as seen from the picture on the left. 253

Figure S26. Typical concentrations ($\mu\text{g/g}$) observed through spatial element concentration profiles for the element Zn, Fe, Mn, Al, Mg, Sr, Pb, U and rare earth elements (REE, calculated as the sum of all measured REE

concentrations) of the Tam Hay Marklot cave fossil tooth (m1/m2 left) specimen 34548 (*Macaca* sp.). The different shaded areas, delimited by dotted lines, represent the different histological parts: white for enamel, and light gray for dentin. The profiles follow a left-to-right direction as seen from the picture on the left..... 254

Figure S27. Typical concentrations ($\mu\text{g/g}$) observed through spatial element concentration profiles for the element Zn, Fe, Mn, Al, Mg, Sr, Pb, U and rare earth elements (REE, calculated as the sum of all measured REE concentrations) of the Center of Natural History of Hamburg modern tooth (m3 right) specimen SEVA 34707 / ZMH-S-10461 (*Bison bison*). The different shaded areas, delimited by dotted lines, represent the different histological parts: white for enamel, light gray for dentin, and medium gray for pulp cavity. The profiles follow a left-to-right direction as seen from the picture on the left. 255

Figure S28. Typical concentrations ($\mu\text{g/g}$) observed through spatial element concentration profiles for the element Zn, Fe, Mn, Al, Mg, Sr, Pb, U and rare earth elements (REE, calculated as the sum of all measured REE concentrations) of the Center of Natural History of Hamburg modern tooth (m3 left) specimen SEVA 34708 / ZMH-S-10963 (*Hemitragus jemtahicus*). The different shaded areas, delimited by dotted lines, represent the different histological parts: white for enamel, light gray for dentin, medium gray for pulp cavity, and dark gray for calculus. The profiles follow a left-to-right direction as seen from the picture on the left. 256

Figure S29. Typical concentrations ($\mu\text{g/g}$) observed through spatial element concentration profiles for the element Zn, Fe, Mn, Al, Mg, Sr, Pb, U and rare earth elements (REE, calculated as the sum of all measured REE concentrations) of the Center of Natural History of Hamburg modern tooth (p3/p4) specimen SEVA 34709/ZMH-S-10612 (*Pteronura brasiliensis*). The different shaded areas, delimited by dotted lines, represent the different histological parts: white for enamel, light gray for dentin, and medium gray for pulp cavity. The profiles follow a left-to-right direction as seen from the picture on the left..... 257

Figure S30. Zinc concentration ($\mu\text{g/g}$) distribution of every analyzed fossil enamel cross section segment, normalized to the relative enamel thickness (0% = outermost enamel layer, 100% = full thickness prior to analysis of enamel-

dentin mixture). The gray area represents the concentration range observed in modern enamel cross section segments, colored lines those of the fossil enamel.	258
Figure S31. Relationship between $\delta^{15}\text{N}_{\text{collagen}}$ and $\delta^{66}\text{Zn}_{\text{enamel}}$ stable isotope values in fossil teeth from Tam Hay Marklot cave that yielded collagen from the dentin.	259
Figure S32. Relationship between the zinc concentration (1/Conc [$\mu\text{g/g}$]) and $\delta^{66}\text{Zn}$ stable isotope values in enamel of fossil teeth from Tam Hay Marklot cave.	260
Figure S33. Relationship between $\delta^{67}\text{Zn}$ and $\delta^{66}\text{Zn}$ stable isotope values in enamel of fossil teeth from Tam Hay Marklot cave.	261
Figure S34. Relationship between $\delta^{68}\text{Zn}$ and $\delta^{66}\text{Zn}$ stable isotope values in enamel of fossil teeth from Tam Hay Marklot cave.	262
Figure S35. Distribution between ln.Concentration Fe ($\mu\text{g/g}$) and $\delta^{66}\text{Zn}$ stable isotope values in enamel of fossil (Marklot: Tam Hay Marklot) and modern (Hamburg: Center of Natural History of Hamburg, originally zoo animals from Hagenbeck Tierpark in Hamburg) teeth.....	263
Figure S36. Distribution between ln.Concentration Al ($\mu\text{g/g}$) and $\delta^{66}\text{Zn}$ stable isotope values in enamel of fossil (Marklot: Tam Hay Marklot) and modern (Hamburg: Center of Natural History of Hamburg, originally zoo animals from Hagenbeck Tierpark in Hamburg) teeth.....	264
Figure S37. Distribution between ln.Concentration Mn ($\mu\text{g/g}$) and $\delta^{66}\text{Zn}$ stable isotope values in enamel of fossil (Marklot: Tam Hay Marklot) and modern (Hamburg: Center of Natural History of Hamburg, originally zoo animals from Hagenbeck Tierpark in Hamburg) teeth.....	265
Figure S38. Distribution between ln.Concentration REE ($\mu\text{g/g}$; calculated as the sum of all measured REE concentrations) and $\delta^{66}\text{Zn}$ stable isotope values in enamel of fossil (Marklot: Tam Hay Marklot) and modern (Hamburg: Center of Natural History of Hamburg, originally zoo animals from Hagenbeck Tierpark in Hamburg) teeth.....	266
Figure S39. Distribution between the zinc concentration (1/Zn Concentration, $\mu\text{g/g}$) and $\delta^{66}\text{Zn}$ stable isotope values in enamel of fossil (Marklot: Tam Hay	

Marklot) and modern (Hamburg: Center of Natural History of Hamburg, originally zoo animals from Hagenbeck Tierpark in Hamburg) teeth. 267

Figure S40. Distribution of $\delta^{66}\text{Zn}$ stable isotope values in dentin and enamel of fossil teeth from Tam Hay Marklot cave. Fossil teeth from various taxa: *Capricornis* sp. (34489, 34490 and 34492), *Helarctos malayanus* (34498), *Panthera pardus* (34505), *Bubalus bubalis* (34524) and *Rhinoceros sondaicus* (34556) were analyzed. Note that enamel has systematically lower $\delta^{66}\text{Zn}$ values compared to dentin of the same tooth. 268

Figure S41. Distribution of zinc concentration (1/Zn Concentration, $\mu\text{g/g}$) and $\delta^{66}\text{Zn}$ stable isotope values in dentin and enamel of fossil teeth, and sediment from Tam Hay Marklot cave. The line between samples indicate they are from the same specimen. Samples of fossil teeth include specimens from various taxa: *Capricornis* sp. (34489, 34490 and 34492), *Helarctos malayanus* (34498), *Panthera pardus* (34505), *Bubalus bubalis* (34524) and *Rhinoceros sondaicus* (34556). Sediment samples include fossiliferous layer (sandy to gravelly silty clay, with calcitic cementation), conglomerate/breccias from adjacent layer, and clay from the conglomerate). The boxes from the box and whisker plots represent the 25th–75th percentiles, with the median as a bold horizontal line, of zinc concentration from modern dentin (D) and enamel (E) found elsewhere (Lappalainen et al., 1981; Falla-Sotelo et al., 2005; Kohn et al., 2013; Teruel et al., 2015; Jaouen et al., 2016a). 269

Figure S42. Distribution between the zinc concentration (1/Zn Concentration, $\mu\text{g/g}$) and $\delta^{66}\text{Zn}$ stable isotope values in enamel and dentin of fossil teeth and sediment from Tam Hay Marklot cave. 270

Figure S43. DAD model for the Tam Hay Marklot tooth specimen SCUMK-R1 (*Dicerorhinus sumatrensis*) that was prepared and analyzed for U/Th series dating. Relative distance is calculated from the EDJ to the extremity of the dental tissues between [-1;1], being respectively the enamel tip in contact with the sediment and the pulp cavity. 271

Figure S44. DAD model for the Tam Hay Marklot tooth specimen SCUMK-01 (large Bovid) that was prepared and analyzed for U/Th series dating. Relative distance is calculated from the EDJ to the extremity of the dental tissues between [-1;1], being respectively the enamel tip in contact with the sediment and the pulp cavity. 271

- Figure S45.** DAD model for the Tam Hay Marklot tooth specimen SCUMK-02 (*Pongo* sp.) that was prepared and analyzed for U/Th series dating. Relative distance is calculated from the EDJ to the extremity of the dental tissues between [-1;1], being respectively the enamel tip in contact with the sediment and the pulp cavity.272
- Figure S46.** DAD model for the Tam Hay Marklot tooth specimen SCUMK-03A (*Bos* sp. (*Bos* cf. *frontalis*)) that was prepared and analyzed for U/Th series dating. Relative distance is calculated from the EDJ to the extremity of the dental tissues between [-1;1], being respectively the enamel tip in contact with the sediment and the pulp cavity.272
- Figure S47.** Zinc isotope composition in different teeth coming from the same Lapado Santo individuals. Single enamel $\delta^{66}\text{Zn}$ measurements per tooth and of each individual are connected by a line. Burial 23 contains 4 individuals (yellow), while burials 11, 15 and 16 involve only one individual (blue, green and red respectively).273
- Figure S48.** Three-dimensional model of the left permanent maxillary first molar (Specimen ID: SEVA 3598_3) of the Jacobins convent child showing the sampling strategy used for the zinc isotope analysis. A chunk of enamel and dentin is first detached from the crown using a pre-existing fracture (darker grey in the sectioned enamel). This piece of tooth is then cut in three subsamples, from which the dentin will be removed to leave only the enamel to be used for the zinc analyses. The middle portion of the sample (natural colors) is preserved and was not used for analyses. The red subsample concerns the cuspal part of the crown and thus represents the earliest stages of enamel growth (until ~1.5 years), while the green subsample represents crown completion (~until 3 years of age).274
- Figure S49.** Nitrogen isotopes obtained on the tooth roots of the child 63949 (Jacobins convent, Rennes).274
- Figure S50.** Matching of the stress events observed in the dentin on the 3D model of the lower left M1 of the child of the Jacobins convent and a 200 μm -thick virtual 2D section (taken where the red line is on the 3D model). The turquoise arrows show the perfect alignment of the virtual 2D section and the 3D model. A strong stress precedes crown completion (pink arrows in enamel and dentin) and produce a marked enamel hypoplasia on the enamel outer surface. From

crown completion (~3 years) to death (~6 years), the child has undergone strong and chronic stress events (green and orange)..... 275

Figure S51. Relationship between zinc concentrations (ppm, as $\mu\text{g/g}$) and isotope ratios in the teeth of the child and the adult from the Jacobins convent. 275

Figure S52. A) Map of Laos showing the geographical locations of the three fossiliferous Late Pleistocene karst cave sites of Tam Pà Ling, Nam Lot and Tam Hay Marklot (~50 km north of TPL and NL). B) Photograph of Pà Hang mountain (1170 m a.s.l), showing the close proximity (~150 m) of Tam Pà Ling and Nam Lot caves. Note that the *H. sapiens* TPL1 was found in the Tam Pà Ling cave. 276

Figure S53. Non-significant relationship between the zinc concentration ($1/\text{Zn}$ concentration, $\mu\text{g/g}$) and $\delta^{66}\text{Zn}$ values in enamel of fossil teeth of carnivores (red squares), omnivores (turquoise circles), herbivores (blue triangles), bone-eating carnivore *C. crocuta* (yellow diamonds) and TPL1 individual (white six-pointed stars), from Nam Lot (top) and Tam Pà Ling (bottom) caves. 276

Figure S54. Relative frequency (%) of each herbivorous taxon from Tam Pà Ling (70–1.1 ka), Nam Lot (86–72 ka) and published data from Tam Hay Marklot (38.4–13.5 ka) (Bourgon et al., 2020), ordered by their overall across-sites average $\delta^{66}\text{Zn}$ values. 277

Figure S55. Distribution of radiogenic strontium isotope ratios ($^{87}\text{Sr}/^{86}\text{Sr}$) and zinc ($\delta^{66}\text{Zn}$) stable isotope values in enamel of fossil teeth of each taxon from the three Late Pleistocene cave sites (Laos) of Tam Pà Ling (orange), Nam Lot (blue) and published data from Tam Hay Marklot (Bourgon et al., 2020; yellow). Small-sized Felidae, large-sized Felidae, *Elephas* sp. and TPL1 were excluded here as they only have one $^{87}\text{Sr}/^{86}\text{Sr}$ observation each. 278

Figure S56. Violin plots of theoretical $\delta^{66}\text{Zn}$ values distribution for each dietary group and observed taxon and $\delta^{66}\text{Zn}$ values from TPL. Carnivore (red), omnivore (turquoise) and herbivore (blue). The plots illustrate the simulated theoretical $\delta^{66}\text{Zn}$ distribution for each dietary group. The observed $\delta^{66}\text{Zn}$ values for each taxon (point and shapes) from TPL are plotted on the violin plots to show where the TPL samples are located on the theoretical $\delta^{66}\text{Zn}$ distribution. 279

Figure S57. Box and whisker plots of distributions of simulated $\delta^{66}\text{Zn}$ datasets (simulation runs 1 to 10) with introduced missingness, compared to the

distribution from the fossiliferous assemblage of Tam Pà Ling (TPL). The total number of specimen and the number of specimens per taxon mirror that of TPL, so that each simulation has 24 specimens and each taxon 1 to 15. The number of taxa per dietary category were randomly selected from the full dataset from Nam Lot, Tam Pà Ling and published data from Tam Hay Marklot (Bourgon et al., 2020). Carnivore (red), omnivore (turquoise) and herbivore (blue). The boxes represent the 25th–75th percentiles, with the median represented by a bold horizontal line..... 280

Figure S58. Proportion of overlap (as overlap percentage: ov. perc.) between overlapping area (represented by black wavy lines) of kernel density estimations for $\delta^{66}\text{Zn}$ values from each dietary category (carnivore = red, bone-eating carnivore *C. crocuta* = yellow, omnivores = turquoise, and herbivores = blue). ‘Overlapping’ can be defined as the area intersected by two (or more) probability density functions..... 281

Chapter 1

Dietary reconstruction in archeology

1.1 Introduction

Determining the dietary habits of fossil humans provides us with crucial insights into their behavior and ecology, and represents a key concern in the study of human evolution. The relationships between diet, hominin evolution, and behaviors are much discussed and highly debated (e.g., Lee-Thorp et al., 1994; Aiello and Wheeler, 1995; Sponheimer and Lee-Thorp, 1999a; Teaford and Ungar, 2000; Richards et al., 2001; Braun et al., 2010; Sponheimer et al., 2013), not least due to a lack of unequivocal tracers and the persistent challenge of relating existing records to past human activities. Pre-Holocene archeological sites are seldom found, and most of the artifacts present during their occupation disappeared through time. Even when archeological material such as organic remains (i.e., animal bones or plant remains) and stone tools are found, they mostly prove inadequate in providing reliable insight into overall dietary reliance, as they merely offer an indirect measure of past diets. Indeed, they could very well relate to single isolated events such as hunting, butchering, and food processing, or constitute a time-averaged assemblage covering an unknown lapse of time (e.g., Kidwell and Behrensmeyer, 1993; Dibble et al., 1997; Garvey, 2018), and their representation of everyday diets can hardly be assessed. The archeological record as a whole is thus most likely biased and unrepresentative of the daily subsistence practices of hominids.

Moreover, archeological material that survives the best (i.e., animal bones and stone tools) also strongly bias inferences towards a strongly meat-based subsistence since plant remains are missing from a large part of the archeological record (e.g., Miksicek, 1987; Wright, 2010). Fortunately, it is possible to directly assess the overall dietary

reliance of past hominids through stable isotopes analyses of surviving tissue, primarily bone collagen (e.g., Ambrose, 1986; Bocherens et al., 1991; Richards and Hedges, 1999; Richards et al., 2001; Müldner and Richards, 2005; Fischer et al., 2007; Richards and Trinkaus, 2009) and tooth enamel (e.g., Lee-Thorp et al., 1994; Sponheimer and Lee-Thorp, 1999a; Sponheimer et al., 2006b, 2013; Roberts et al., 2015, 2017a). However, these methods are confronted with limitations of their own, most notably arising from protein preservation in the case of stable isotopes analyses of collagen. This thesis explores the potential of another chemical dietary tracer, specifically of the zinc isotope method in tooth enamel, for providing dietary and trophic information in fossil communities. More specifically, the work presented here seeks to assess diagenetic post-mortem alterations and the preservation potential of a diet-related zinc isotope composition in tooth enamel, explore sampling strategies and contamination-related issues, expand on the interpretative framework of this isotope system, and provide exemplary application studies that highlight the usefulness of zinc isotopic composition for exploring paleodietary habits.

The following sections outline traditional isotopic approaches linking dietary habits and archeological evidence (*Section 1.2*) and compare this with the zinc isotope composition approach (*Section 1.3*). *Section 1.4* offers background information relative to Southeast Asia's archeological context and implications relative to human evolution. Finally, *Section 1.5* details the specific aims and objectives of this thesis, followed by the results of the application studies (*Chapters 2-4*) conducted as part of this thesis project. A synthesis of these results, an outlook and a concluding summary can be found in *Chapter 5 and 6*.

1.2 Stable isotope analysis in paleodietary studies

One of the biggest revolutions in paleodietary reconstruction studies was the introduction of stable isotope analysis, which allowed the direct exploration of past human populations' diets. Historically, most dietary studies have relied on the study of isotopes from two light elements of bone collagen: carbon ($^{13}\text{C}/^{12}\text{C}$, expressed as $\delta^{13}\text{C}$ values) and nitrogen ($^{15}\text{N}/^{14}\text{N}$, expressed as $\delta^{15}\text{N}$ values). These elements are also found in calcified tissues like bones and teeth, the most common vertebrate tissues surviving into the archeological record, making them a prime candidate for paleodietary reconstruction.

As was the case in geology, archeologists were first interested in measuring radiogenic isotope ratios, with radiocarbon dating applied as early as 1949 (Arnold and Libby, 1949). The advent of the radiocarbon method resulted in a veritable revolution in archeology, frequently considered as one of its most decisive development of the 20th century. Twenty years later, some plants were recognized to exhibit higher $\delta^{13}\text{C}$ values than others and erroneously produce older dates (Hall, 1967), foreshadowing and initiating investigations on dietary and environmental reconstructions using carbon stable isotopes. The cause was revealed by identifying differential fractionation of carbon isotopes during CO_2 fixation by plant groups with different photosynthetic pathways: C_3 and C_4 , and CAM to a lesser extent (Smith and Epstein, 1971; O'Leary, 1988; Farquhar et al., 1989). Plants using the C_3 photosynthesis pathway (trees, most shrubs, and temperate grasses) are characterized by low $\delta^{13}\text{C}$ values, ranging from -37‰ to -20‰ (Smith and Epstein, 1971; O'Leary, 1988; Farquhar et al., 1989; Kohn, 2010), while the C_4 plants (mostly tropical grasses) have higher values around -16‰ to -10‰ (Smith and Epstein, 1971; O'Leary, 1988; Farquhar et al., 1989; Basu et al., 2015). Isotopic compositions of carbon and nitrogen in animal tissues were subsequently studied (DeNiro and Epstein, 1978; DeNiro and Epstein, 1981), and their association with diet and fractionation along the food chain was quickly established.

Carbon isotope compositions are passed along in food webs with only secondary fractionation (e.g., Lee-Thorp et al., 1989; Cerling and Harris, 1999; Passey et al., 2005), resulting in consumers' tissues to reflect the relative proportion of a food web's primary carbon sources, namely of C_3 - (bushes, shrubs, and grasses) or C_4 -plants (mostly tropical and subtropical grasses, sedges) in their diet. This distinction quickly proved valuable in paleodietary studies, where it provided a sensitive proxy to the introduction of maize (a C_4 grass) domestication (Vogel and Merwe, 1977; Van der Merwe and Vogel, 1978), the contributions of marine resources, typically more ^{13}C -enriched than terrestrial carbon sources, into populations' diet (Tauber, 1981; Chisholm et al., 1982; Hobson and Collier, 1984; Sealy et al., 1986) and insights into the diet of early hominids (e.g., Lee-Thorp et al., 1994; Sponheimer and Lee-Thorp, 1999a; Sponheimer et al., 2006b). Additionally, in tropical and subtropical regions, forest and woodland habitats, and animals living in these environments, are associated with C_3 plants that exhibit low $\delta^{13}\text{C}$ values, whereas drier and more open environments are characterized by C_4 plants (i.e., mostly grasses) with high $\delta^{13}\text{C}$ values (e.g., Cerling et al., 1997; Zazzo et al., 2000; Sponheimer et al., 2006a; Cerling et al., 2015; Bacon et al., 2018a, 2018b). Additional insights into densely forested C_3 ecosystems can also be gleaned through low values that result from a "canopy effect" (van der Merwe and

Medina, 1991): the lowest $\delta^{13}\text{C}$ values are found in flora and fauna living on the forest floor (Vogel, 1978; Ehleringer et al., 1986; Medina et al., 1986; Ehleringer et al., 1987; Sternberg et al., 1989; van der Merwe and Medina, 1989, 1991; Krigbaum, 2003; Krigbaum et al., 2013; Graham et al., 2014; Blumenthal et al., 2016; Roberts et al., 2017b) and can consequently be used as a tracer to infer the density of a forest cover and its associated habitat type. The $\delta^{13}\text{C}$ values of consumers accordingly reflect these isotopically distinct carbon sources and thus allow the reconstruction of paleoenvironments and vegetation cover.

Substantial variability exists between ecosystems in nitrogen isotopic composition, reflecting an intricate balance between biological nitrogen fixation, recycling within the biosphere and soils, and re-release of N^2 (e.g., Shearer and Kohl, 1986; Ambrose, 1991; Robinson, 2001; Amundson et al., 2003; Evans, 2007). More importantly, nitrogen isotopes found in bone or dentin collagen vary according to the diet, specifically with trophic level. Indeed, a stepwise shift of +2–6‰ in $\delta^{15}\text{N}$ has been widely documented between consumers and their diet in various food webs (e.g., DeNiro and Epstein, 1981; Schoeninger and DeNiro, 1984; Minagawa and Wada, 1986; Sealy et al., 1987; Bocherens and Drucker, 2003; Passey et al., 2005; Fox-Dobbs et al., 2007), and even for breastfeeding (e.g., Fogel et al., 1989; Schurr, 1998; Richards et al., 2002; Fuller et al., 2006).

However, ecosystems have multiple food sources that exhibit distinct nitrogen stable isotope composition despite sharing a single trophic level. Differences in $\delta^{15}\text{N}$ values of primary consumers are governed mainly by a balance between atmospheric fixation, denitrification, and ammonia volatilization within the soil (e.g., Shearer and Kohl, 1986; Ambrose, 1991; Evans, 2007). Collectively, the primary consumers' isotopic compositions define an isotopic baseline specific to different regions or times, which needs to be accounted for when assessing trophic position using nitrogen stable isotope (Post, 2002; Casey and Post, 2011; Woodcock et al., 2012). By analyzing sympatric animals as a frame of reference for each trophic level, baseline variability can thus be assessed, and the stepwise trophic shift allows the use of $\delta^{15}\text{N}$ as a tool for evaluating the degree of animal-matter in the diet of past populations (e.g., Schoeninger et al., 1983; Ambrose, 1986; Bocherens et al., 1991; Richards and Hedges, 1999; Richards et al., 2001; Müldner and Richards, 2005; Fischer et al., 2007; Richards and Trinkaus, 2009). This method notably played a pivotal role in determining *Homo neanderthalensis* as apex predator with a meat-rich diet (e.g., Bocherens et al., 1991,

1999, 2005; Drucker and Bocherens, 2004; Richards and Trinkaus, 2009; Jaouen et al., 2019a; Wißing et al., 2019).

Compared to other sources of information on past diets, these two isotope systems provide a quantitative approach to assess the overall dietary reliance for an individual, i.e., they average out the whole diet over specific periods (bone formation and remodeling of the lifespan of an animal or human (e.g., Enlow, 1962; Enlow and Bangm 1965), and tooth enamel secretion and mineralization over the formation time of teeth (e.g., Dean, 2006; Lacruz et al., 2008, 2017; Bromage et al., 2012)). However, analyses of collagen are limited by the preservation of organic material (i.e., proteins), which typically does not survive in skeletal remains beyond the Late Pleistocene (van Klinken, 1999). This time frame is shorter (~15 ka) in arid or wet tropical environments (Ambrose, 1991; Krigbaum, 2005; Loosdrecht et al., 2018).

Moreover, the source material for biosynthesis determines what portions of the diet are represented in the stable nitrogen isotope compositions of tissues (e.g., Schoeller, 1999; Schwarcz 2000; Harrison and Katzenberg 2003), whereby collagen is more indicative of the protein portion of the diet (e.g., Ambrose and Norr, 1993; Tieszen and Fagre, 1993). Consequently, reconstructions of overall dietary reliance made through stable nitrogen isotope analysis of collagen are hampered by meat almost consistently containing more protein than plants (Phillips and Koch, 2002). As a result, animal-based dietary signals in $\delta^{15}\text{N}$ values are prevailing in humans (e.g., Richards et al., 2001; Bocherens et al., 2005; Richards and Trinkaus, 2009; Naito et al., 2016; Jaouen et al., 2019a), since the relative importance of plants in the diet is generally being overprinted by meat consumption. Additionally, as absolute values do not define trophic positions but are relative to others from specimens of known trophic position, variation in $\delta^{15}\text{N}$ baselines must be appropriately accounted for by defining a context for which consumers' $\delta^{15}\text{N}$ values can be directly compared, otherwise erroneous assessment of consumer trophic positions are likely to arise (Post, 2002; Casey and Post, 2011; Woodcock et al., 2012). These caveats represent severe limitations to paleodietary investigations across ecosystems and climatic zones, and limit insights that can be gleaned into human evolution.

Recently, developments in mass spectrometry have allowed the measurement of different natural stable isotope ratios for elements such as calcium, magnesium, strontium, and zinc (e.g., Chu et al., 2006; Knudson et al., 2010; Costas-Rodríguez et al., 2014; Martin et al., 2014), and collectively referred to as “non-traditional stable isotopes” (Albarède and Beard, 2004; Anbar and Rouxel, 2007; Weiss et al., 2008). It

was not long until studies on biological materials was carried out, such as plants and human or animal tissues (Skulan et al., 1997; Skulan and DePaolo, 1999; Walczyk and von Blanckenburg, 2002; Ohno et al., 2004, 2005; Weiss et al., 2005; Guelke and von Blanckenburg, 2007; Viers et al., 2007; Black et al., 2008; Moynier et al., 2009, 2013; von Blanckenburg et al., 2009; Balter et al., 2010, 2013; Aucour et al., 2011; Weinstein et al., 2011; Jouvin et al., 2012; Hindshaw et al., 2013).

While these non-traditional stable isotopes provided the opportunity to assess new types of information such as human metabolism (Walczyk and von Blanckenburg, 2005; Albarède et al., 2011; Heghe et al., 2012; Jaouen et al., 2012; Jaouen and Balter, 2014) and diseases (Krayenbuehl et al., 2005; Morgan et al., 2012; Aramendía et al., 2013; Balter et al., 2015; Lerner et al., 2015), one of the greatest potentials of these non-traditional isotopes rests in paleodietary studies. Indeed, the relation in isotopic composition to trophic level has already been demonstrated for calcium (Skulan et al., 1997; Skulan and DePaolo, 1999; Chu et al., 2006; Reynard et al., 2010; Heuser et al., 2011; Tacaíl et al., 2017, 2020; Hassler et al., 2018; Martin et al., 2020), stable strontium (Knudson et al., 2010; Weber et al., 2020), magnesium (Martin et al., 2014, 2015), and zinc (Jaouen et al., 2013, 2016a, 2016b, 2018; Costas-Rodríguez et al., 2014).

Moreover, these non-traditional stable isotopes can be measured in the bioapatite of vertebrates, the mineral part of bones, dentin, and tooth enamel. In particular, tooth enamel offers the potential of preserving biogenic diet-related isotope composition over millions of years and perhaps even over geological timescales (e.g., Copeland et al., 2011; Balter et al., 2012, 2019; Dean et al., 2018; Hassler et al., 2018). Indeed, the porosity of tooth enamel is low, it has a low content of organic matter, and has larger and more compact crystallites relative to bones, making it a mineral tissue that is less susceptible to diagenetic trace element exchange (e.g., Kyle, 1986; Wang and Cerling, 1994; Kohn et al., 1999; Schoeninger et al., 2003; Kocsis et al., 2010; McCormack et al., 2015). Moreover, tooth enamel mineralizes sequentially and remains compositionally and structurally stable during life, thus capturing and preserving environmental and dietary changes that occurred during the enamel mineralization phases in an individual's life (Dean, 2006; Lacruz et al., 2008, 2017; Bromage et al., 2012). The combination of trophic level proxy and high preservation potential is precisely what makes non-traditional stable isotopes such promising paleodietary tracers. They could provide a new tool to assess diet and trophic interaction in past food webs where the traditionally-used nitrogen isotope composition of collagen from

bone and dentin are affected by diagenetic alteration and limited by the degree of protein preservation.

1.3 Zinc stable isotope analysis in (paleo)dietary studies

Among these non-traditional stable isotope systems, the isotopes of the trace element zinc (Zn) constitute a promising dietary indicator (Jaouen et al., 2013, 2016a, 2016b, 2018; Costas-Rodríguez et al., 2014), yet the study of this system is still in its infancy.

Zinc is the second most abundant micronutrient in the human body after iron (Lim et al., 2013; Maret, 2016), and it is an essential agent in many biological processes and necessary for most living organisms (Vallee and Falchuk, 1993; Berg and Shi, 1996; Maret, 2017). In fact, it is estimated to bind as many as 2800 different proteins in the human body (Andreini et al., 2006), covering a wide variety of diverse functions (Matthews et al., 2009; King, 2011; Hara et al., 2017).

Zinc has to be continuously supplied by dietary intake (Rink, 2000) to ensure and support healthy zinc homeostasis in intestinal absorption (Krebs, 2000) and compensate endogenous zinc losses (Maret, 2006; Gibson et al., 2016). While the amount of absorbed zinc depends on the zinc content of the diet (Brown et al., 2004), zinc absorption is conditional on its intestinal bioaccessibility and bioavailability from the diet, as some food components can influence the available zinc concentration. Phytate, naturally found in many plants, is one such component that has been shown to decrease intestinal zinc bioavailability severely (e.g., Turnlund et al., 1984; Ferguson et al., 1988). Consequently, plant-based diets generally contain less intestinally-available zinc than meat-based diets (Kristensen et al., 2006; Foster and Samman, 2015). Conversely, dietary proteins correlate with higher zinc uptake (Sandström et al., 1980; Wapnir, 2000), and even more so for animal proteins (Sandström et al., 1983). Moreover, adding animal protein to plant-based diets appears to improve zinc bioavailability considerably (Sandström et al., 1989), because protein seemingly counteracts the impairing effects of phytate (Davidsson et al., 1996). The zinc content in animal products is also generally high, whereby meat and offals from some commonly-consumed terrestrial animals contain between 1000 to 7000 $\mu\text{g}/100\text{g}$ of zinc (e.g., Onianwa et al., 2001; Scherz and Kirchhoff, 2006). In comparison, the zinc content in most commonly-consumed plants is less than 1000 $\mu\text{g}/100\text{g}$, except for cereals, seeds, and nuts, where zinc content ranges from 2560 to 3700 $\mu\text{g}/100\text{g}$ (e.g., Onianwa et al., 2001; Scherz and Kirchhoff, 2006). However, while cereals, seeds, and

nuts contain a similarly high amount of zinc than animal products, they almost systematically also contain a high level of phytate compared to tubers, fruits, leaves, and vegetables (e.g., Reddy, 2002), severely decreasing the intestinal zinc bioavailability. In addition to zinc content and zinc bioavailability, zinc absorption also seemingly depends on individuals' overall zinc content in their diet, as zinc-deficient humans and animals exhibit increased and more efficient zinc absorption from dietary intakes (Istfan et al., 1983; Wada et al., 1985; Taylor et al., 1991; Hunt et al., 2008; Yasuno et al., 2011).

While zinc is not a transition metal, its properties are more similar to them than post-transition metals. It displays an average relative atomic mass of 65.38 (Ponzevera et al., 2006) and possesses five naturally occurring stable isotopes: ^{64}Zn (48.63%), ^{66}Zn (27.90%), ^{67}Zn (4.10%), ^{68}Zn (18.75%) and ^{70}Zn (0.62%) (Rosman and Taylor, 1998). Isotopic abundances are presented in δ (delta) notation expressed as deviation per mil (‰) using the two most abundant isotopes relative to the JMC-Lyon standard solution, as follows: $\delta^{66}\text{Zn} = \left(\frac{^{66}\text{Zn}/^{64}\text{Zn}_{\text{sample}}}{^{66}\text{Zn}/^{64}\text{Zn}_{\text{standard}}} - 1 \right) \times 1000$.

In 2012, Van Heghe and colleagues (Heghe et al., 2012) began investigating in humans the causes of the variability of zinc isotopes in a pilot study. Since then, work on mammals from modern food webs, first in Africa (Jaouen et al., 2013, 2016a) and then in the Canadian Arctic (Jaouen et al., 2016b), have further elucidated the relationship between zinc isotopes and diet. The few studies that have utilized stable zinc isotopes indicate that the method shows exceptional promise for paleodietary analysis in fossils (Jaouen et al., 2013, 2016a, 2016b, 2018, 2020; Bourgon et al., 2020, 2021; McCormack et al., 2021). Zinc is incorporated as a trace element in the mineral fraction (i.e., bioapatite) of tooth enamel. Consequently, it is not reliant on the preservation of organic material (in contrast to classical organic matter-bound nitrogen isotopes), representing a major advantage in archeological applications. As already mentioned, tooth enamel is crucially resistant to soil alteration and contamination (Lee-Thorp and van der Merwe, 1991; Michel et al., 1996; Kohn et al., 1999; Trueman and Tuross, 2002; Dauphin and Williams, 2004), and therefore can retain unaltered elemental signatures for millions of years. The potential for recovering dietary information beyond the reach of other conventional collagen-bound dietary tracers in ancient vertebrate fossils and environments adverse to organic matter preservation is thus consequential.

As currently understood, the primary source of zinc in a given terrestrial food web derives from plants. Two main parameters are then suggested to explain the zinc

isotope composition of plants: the initial zinc isotope ratios of the source-intake (Viers et al., 2007; Fekiacova et al., 2015) and the biological fractionation that occurs by and within the plant itself (Weiss et al., 2005; Viers et al., 2007, 2015; Moynier et al., 2009; Aucour et al., 2011, 2015; Tang et al., 2012, 2016; Deng et al., 2014; Caldelas and Weiss, 2017; van der Ent et al., 2021). For plants specifically, the initial source-intake is derived from the soil, whose isotopic composition is in turn controlled by the nature of the underlying bedrock, as well as chemical weathering in soils (e.g., Viers et al. 2007, 2015; Opfergelt et al. 2017; van der Ent et al., 2021). While igneous rocks exhibit a narrow range of $\delta^{66}\text{Zn}$ values ($+0.3 \pm 0.14 \text{ ‰}$ (2σ)) (Moynier et al., 2009, 2017), $\delta^{66}\text{Zn}$ values recorded in sedimentary rocks are more heterogeneous and variable, exhibiting higher values that can go as high as 1.4 ‰ in marine carbonates (Luck et al., 1999; Maréchal et al., 2000; Pichat et al., 2003; Cloquet et al., 2008; Moynier et al., 2017). Higher values in carbonate rock have been suggested to be the result of biological processes, whereby marine algae's uptake favors the lighter zinc isotopes and consequently induces a relative enrichment of $\delta^{66}\text{Zn}$ in the surface seawater zinc pool (Maréchal et al., 2000), leading to a similar enrichment in that of shell carbonate formed in isotopic equilibrium with ambient seawater (Pichat et al., 2003).

Following zinc intake in the rhizosphere, an initial fractionation through preferential absorption occurs in plants between the roots and the soil (Weiss et al., 2005; Aucour et al., 2011, 2015; Tang et al., 2016), leading to a general enrichment in heavy isotopes in the roots relative to the litter (**Figure 1**; Weiss et al., 2005; Viers et al., 2007; Moynier et al., 2009; Aucour et al., 2011, 2015; Tang et al., 2016; van der Ent et al., 2021). A correlation also possibly exists between $\delta^{66}\text{Zn}$ and the length of plants, both within a single plant and between species (**Figure 1**). Indeed, root-to-shoot zinc translocation leads to active uptake of heavy zinc isotopes out of the xylem, seemingly occurring during transport, and consequently favors the mobility of light zinc isotopes to the most aerial parts of the plants (**Figure 1**; Viers et al., 2007; Moynier et al., 2009). This active uptake during transport leads to lower $\delta^{66}\text{Zn}$ values observed for the most aerial parts of the plants (Weiss et al., 2005; Viers et al., 2007; Moynier et al., 2009; Tang et al., 2012, 2016; Deng et al., 2014; Caldelas and Weiss, 2017; van der Ent et al., 2021), and generally higher $\delta^{66}\text{Zn}$ values in low growing plants compared to high growing plants, respectively such as herbaceous species and trees (Weiss et al., 2005; Viers et al., 2007; Moynier et al., 2009).

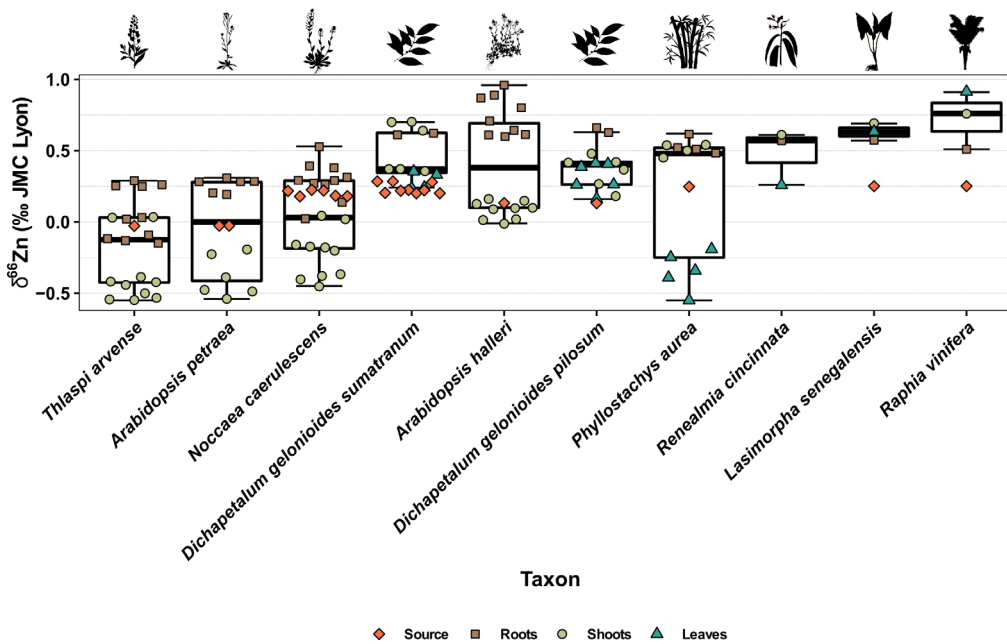


Figure 1. Box and whisker plots presenting the range of $\delta^{66}\text{Zn}$ values (‰, relative to the JMC-Lyon zinc isotope standard) in some plants (Viers et al., 2007; Moynier et al., 2009; Aucour et al., 2011; Tang et al., 2016; van der Ent et al., 2021), highlighting the general enrichment in heavy isotopes in the roots (brown square) relative to the source (orange diamond) and the general trend of lower $\delta^{66}\text{Zn}$ values in shoots (light green circle; here including stem and/or shoots data) and leaves (turquoise triangle) relative to the roots. The isotopic composition of the known or likely source (e.i., litter, soil, or nutrient solution in experimental settings) of zinc uptake from the plant does not contribute to the boxes and whiskers, which represent the 25th–75th percentiles, with the median represented by a bold horizontal line, for each plant.

Similar underlying principles then governs the zinc isotope composition in the tissues of subsequent trophic chains' consumers (i.e., animals): isotopic fractionations occurring within the consumer during intestinal absorption and the initial zinc isotope ratios of the food ingested (Turnlund et al., 1984; Cousins, 1985; Lönnerdal, 2000; Balter et al., 2010; Jaouen et al., 2013, 2017; Moynier et al., 2013). Naturally, the zinc isotope composition in animal tissues depends on the initial source intake, which varies according to what is consumed. Indeed, different species, organs, and tissues of plants and animals alike are likely to induce different $\delta^{66}\text{Zn}$ values in the consumer (**Figure 1 and 2; Supplementary Information (SI) Appendix, Table S1**; Balter et al., 2010, 2013; Moynier et al., 2013; Jaouen et al., 2013, 2016a; Costas-Rodríguez et al., 2014; Mahan et al., 2018). Additionally, while the physiological mechanisms (i.e., element cycling in the body) which drive zinc isotope fractionation are not yet well understood, biological activities fractionate zinc isotopes in the body among organs and account for variability in body tissues $\delta^{66}\text{Zn}$ values (**Figure 2; SI Appendix, Table S1**; Balter et al., 2010, 2013; Moynier et al., 2013; Mahan et al., 2018). Specifically, zinc isotopes can be used as ecological proxies precisely because the coordination of zinc with different ligands induces high isotopic fractionation within organisms. Indeed, heavy zinc isotopes tend to form stronger bonds that often involve oxygen in hydroxides, phosphates, carbonates, and nitrogen in histidine, whereas bonds involving sulfides

are enriched in lighter zinc (Balter et al., 2013). For example, mammal bones are typically enriched in heavy zinc because of the binding to phosphates, whereas the liver is conversely enriched in light zinc isotopes due to its bond to sulfur (Balter et al., 2010, 2013; Moynier et al., 2013; Mahan et al., 2018). As a result, muscles and most organs are typically ^{66}Zn depleted relative to the animal's diet (**Figure 2**; *SI Appendix, Table S1*; Balter et al., 2010, 2013; Moynier et al., 2013; Mahan et al., 2018) and thus inducing successively lower $\delta^{66}\text{Zn}$ value with increasing trophic level.

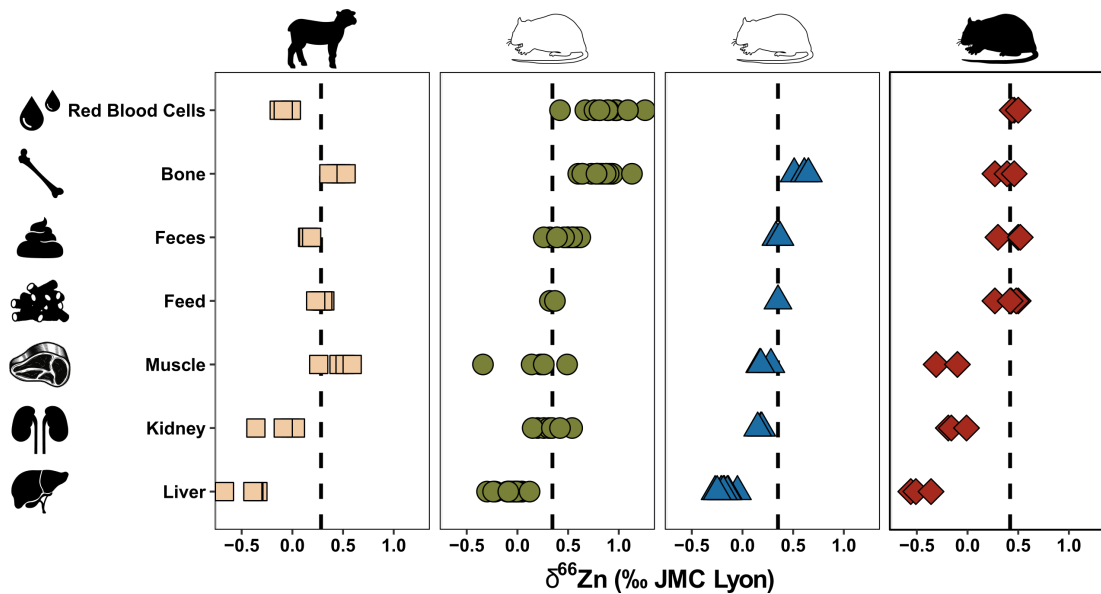


Figure 2. The zinc isotope compositions (‰, relative to the JMC-Lyon zinc isotope standard) of red blood cells, bones, feces, muscle, kidney, liver, and respective feeds of animals, as reported from controlled-feeding experiments, highlights the generally low $\delta^{66}\text{Zn}$ values in soft tissues and higher values in bones compared to the diet. The beige squares correspond to data from sheep of Balter et al. (2010), the green circles from mice of Moynier et al. (2013), blue triangles from mice of Balter et al. (2013), and red diamonds from rats of a preliminary dataset (*SI Appendix, Table S1*). The dashed lines correspond to the mean $\delta^{66}\text{Zn}$ values of the diet provided to the animals in each study.

Generally, plant-matter has relatively elevated $\delta^{66}\text{Zn}$ values (Costas-Rodríguez et al., 2014; Jaouen et al., 2016a), whereas muscles and other soft tissues exhibit low values (*SI Appendix, Table S1*; Balter et al., 2010, 2013; Jaouen et al., 2013, 2016a; Moynier et al., 2013; Costas-Rodríguez et al., 2014; Mahan et al., 2018). This difference leads to discrimination in $\delta^{66}\text{Zn}$ values between trophic levels within a given food web where higher trophic level consumers exhibit lower $\delta^{66}\text{Zn}$ values in their body tissues than primary consumers (Jaouen et al., 2013, 2016a, 2016b, 2018; Costas-Rodríguez et al., 2014). The underlying mechanism responsible for trophic level discrimination through zinc stable isotopes is thus different from that of the classical nitrogen stable isotopes, whereby $\delta^{15}\text{N}$ values instead allow trophic level assessment through a 'global' preferential uptake of ^{15}N relative to their diet (e.g., Ambrose and DeNiro, 1986; Ambrose, 1991; Kelly, 2000).

However, the implementation of zinc isotopic composition as trophic proxies is still in its infancy, with various ecological and physiological mechanisms that are poorly understood or not yet investigated. For example, it has not been directly tested if the underlying bedrock affects a whole food web's baseline $\delta^{66}\text{Zn}$ values. While its influence is indeed suspected (Jaouen et al., 2016a, 2016b), systematic assessment of local geology will be crucial to address this question as other factors could likely inhibit or offset this influence, such as preferential adsorption in plants (Weiss et al., 2005; Arnold Tim et al., 2009). Variability in $\delta^{66}\text{Zn}$ values for a given food web will also require further investigation. Different dietary habits, such as omnivorous, frugivorous, insectivorous, browsers, grazers, still have not been systematically assessed, and more rigorous trophic relations between different animals from a whole food web are needed. Above all else, the prospect of a high preservation potential of pristine diet-related zinc isotope ratios in fossils specimens is one of the primary interests for this method, but its application has yet to be attempted.

1.4 Hominin biogeography and tropical forest reliance in Southeast Asia during the Pleistocene

Through the course of this thesis, a focus was given to Late Pleistocene vertebrate fossil assemblages from cave settings in Laos in the Indochinese Peninsula of Southeast Asia, as it served various purposes. For the first time, zinc stable isotope analysis could be conducted on fossils to assess post-mortem taphonomic alteration and the preservation of pristine diet-related $\delta^{66}\text{Zn}$ values in tooth enamel, moreover under tropical conditions that are adverse for collagen preservation. The overall dietary reliance information can also reinforce a growing body of evidence for early human foragers' exploitation and occupation of tropical rainforest environments. Meanwhile, these results would pave the way to explore adaptations and dietary reliance of different fossil hominins, offering insights into palaeoanthropological and archeological research, whereby the hominin specimen record of Asia is the fastest-changing in this field of research.

Currently, the earliest hominin movements in East and Southeast Asia are attributed to *Homo erectus* populations (Swisher et al., 1994; Larick et al., 2001), which was widely dispersed by 700 ka (Brumm et al., 2016; Ingicco et al., 2018). Two insular dwarf hominins were later found in Southeast Asia: *Homo floresiensis* at 100 to 60 ka (Sutikna et al., 2016) and *Homo luzonensis* at 66.7 ± 1 ka (Détroit et al., 2019). More recently, genomic evidence from modern populations in New Guinea provided insights

into the arrival of another early hominin, the Denisovan, in insular Southeast Asia by about 363 ka (Jacobs et al., 2019). Anatomically modern humans first expanded into Southeast Asia by at least 70 ka (Demeter et al., 2017; Westaway et al., 2017; Shackelford et al., 2018) and encountered Denisovan lineages (Jacobs et al., 2019) and possibly other hominins. The Far East then witnessed a major turnover of hominins during the Late Pleistocene, with the extinction and replacement of all hominin groups following the arrival of *Homo sapiens* (Sutikna et al., 2016). However, much remains to be understood about population relationships and variability across the Pleistocene from East and Southeast Asia (Dennell and Roebroeks, 2005; Rabett, 2012; Dennell, 2016).

It was suggested that a shift in the transition between the Middle Pleistocene and the Late Pleistocene from open habitats (such as mixed savannah and woodland environments) into tropical lowland evergreen rainforests brought about the extinction of most hominins in East and Southeast Asia (Louys and Roberts, 2020). By contrast, the ability of *Homo sapiens* to adapt in such environments became increasingly evident as it expanded its niche in Southeast Asia to make use of resource-rich rainforest habitats (Barton, 2005; Barker et al., 2007; Summerhayes et al., 2010; Roberts et al., 2017a; Wedage et al., 2019; Langley et al., 2020).

However, the adaptation to rainforests by our species represents a somewhat new paradigm in itself, as *Homo sapiens* had long been seen as primarily adapted to open environments and especially savannahs (Fleagle et al., 2010; Norton and Braun, 2011). Moreover, it was also argued early on that human forager habitation of tropical forest environments was virtually impossible, owing to supposed dietary constraints imposed by spaced resources, seasonal availability, and scarcity of energy-rich wild foods (Hutterer, 1983; Hart and Hart, 1986; Headland, 1987; Bailey et al., 1989). Paleoanthropologists and archeologists then adopted these views, which led to tropical forests being seen as ‘barriers’ to human dispersal and occupation (e.g., Gamble, 1993; Bird et al., 2005; Boivin et al., 2013; Wurster and Bird, 2016) or simply avoided and under-studied. Since then, this paradigm slowly waned, whereby various studies highlighted that foraging lifestyles in tropical forests are possible, whether currently or in the past (Bahuchet et al., 1991; Brosius, 1991; Balée, 1999; Roberts and Petraglia, 2015). Importantly, archeological research firmly established that humans exploited tropical forest resources well into the Late Pleistocene (Barton, 2005; Barker et al., 2007; Summerhayes et al., 2010; Roberts et al., 2017a; Wedage et al., 2019; Langley et al., 2020). However, little is still known about the overall contribution of wild

tropical forest resources to the diet of fossil human foragers, whether relative to other habitats, other subsistence strategies, or relative to resource types (i.e., animal-matter or plant-matter).

Among others, the lack of archeological material and the poor preservation of organic matter in tropical latitudes limits the insights that can be gleaned into human dietary reliance on rainforest (Tappen, 1994), despite evidence of our species being present in these habitats since at least 70 ka (Demeter et al., 2017; Westaway et al., 2017; Shackelford et al., 2018). Indeed, the vertebrate assemblages from Southeast Asia are usually found in karst breccias and are governed by complicated and various sedimentary processes emanating from highly variable, climate-driven, and water-dependent environments (Duringer et al., 2012; Bacon et al., 2015, 2018b). Most notably, fossil assemblages undergo long transportation processes through subterranean cave networks with often multiple reworking episodes (Duringer et al., 2012; Bacon et al., 2015, 2018b). Conversely, while sedimentary sequences from caves and rock shelters that yield archeological material (e.g., lithic technology, hearth features, plant macro-remains, cut marks on bones) can offer insights into past human behaviors (Barker et al., 2007; Summerhayes et al., 2010; Perera et al., 2011), such depositional contexts are few in Southeast Asia. Furthermore, organic archeological material (particularly faunal and plant remains) from pre-Holocene contexts is found very seldomly. When available, stable isotope analysis of bones and teeth can provide insights into the diets of past humans from tropical rainforest environments, and such approaches were able to highlight a reliance on forest resources for Late Pleistocene forager populations from Sri Lanka (Roberts et al., 2015, 2017a). However, whether animal or plant resources were consumed cannot be determined from stable carbon isotopes due to the small trophic fractionation. Moreover, stable carbon and nitrogen isotope analysis of bone or dentin collagen is mostly unfeasible in tropical environments because collagen is generally absent due to poor protein preservation (van Klinken, 1999; Krigbaum, 2005; Clarkson et al., 2009). The classical dietary proxy $\delta^{15}\text{N}$, used to assess the degree of animal protein consumption and trophic level, is thus not suitable for these settings. As such, evaluating the overall dietary reliance of past human forager populations from tropical rainforests has proven complicated.

1.5 This study

This thesis explores the use of zinc stable isotope analyses of fossil teeth to generate direct evidence of overall dietary reliance, specifically for trophic level assessment. The work presented herein is structured as a series of interconnected projects prepared

for publication in international peer-reviewed scientific journals. The thesis focuses mainly on zinc isotope ($\delta^{66}\text{Zn}$) as dietary proxy applied to tooth enamel of a variety of species, but also uses a range of other isotopic methods such as carbon ($\delta^{13}\text{C}$), oxygen ($\delta^{18}\text{O}$), strontium ($^{87}\text{Sr}/^{86}\text{Sr}$), and nitrogen ($\delta^{15}\text{N}$) isotope analysis. In addition, various statistical modelings were conducted to further the interpretative framework and help identify controlling factors of variability in $\delta^{66}\text{Zn}$ values.

The first publication of this thesis (*Chapter 2*) demonstrates and outlines the preservation potential of pristine diet-related zinc isotopic composition in tooth enamel and its first application on fossil teeth, namely from a Late Pleistocene mammal assemblage from Laos, to assess the feeding ecology of these species. The second publication (*Chapter 3*) explores zinc contamination concerns from handling samples with standard disposable laboratory gloves during enamel sampling and chemical sample preparation. In parallel, the study explores variability in $\delta^{66}\text{Zn}$ values based on the developmental stage of the human teeth sampled. The third publication (*Chapter 4*) demonstrate the application of zinc stable isotope analysis to assess the overall dietary reliance and subsistence strategies of a Late Pleistocene human from Tam Pà Ling in Laos' rainforests. Moreover, this study illustrates how $\delta^{66}\text{Zn}$ analysis on teeth can be used for contexts where archeological material evidence is absent and other forms of trophic level assessment are impossible.

1.5.1 Aims and objectives

Chapter 2 – Publication 1

While stable nitrogen isotope analyses of collagen from bone and dentin have commonly been used for dietary reconstructions and trophic level assessment, protein preservation limits the use of this method. This publication explores zinc isotope ratios in tooth enamel as an alternative dietary and trophic level proxy by analyzing fossil mammals from the Late Pleistocene (38.4 to 13.5 ka) assemblage of the Tam Hay Marklot cave in northeastern Laos.

As observed in modern-day samples, this publication seeks to discern discrimination in zinc isotopes in mammals between different dietary behaviours (i.e., carnivorous, omnivorous and herbivorous diets), thus demonstrating that zinc isotopes can also be used in paleodietary studies of fossil hominins or other mammalian species. Notably, a key aim is to prove the preservation of pristine diet-related zinc isotope ratios, even under tropical conditions adverse to collagen preservation.

This article is published in *Proceedings of the National Academy of Sciences of the United States of America*: **Bourgon, N.**, Jaouen, K., Bacon, A.-M., Jochum, K.P., Dufour, E., Düringer, P., Ponche, J.-L., Joannes-Boyau, R., Boesch, Q., Antoine, P.-O., Hulot, M., Weis, U., Schulz-Kornas, E., Trost, M., Fiorillo, D., Demeter, F., Patole-Edoumba, E., Shackelford, L.L., Dunn, T.E., Zachwieja, A., Duangthongchit, S., Sayavonkhamdy, T., Sichanthongtip, P., Sihanam, D., Souksavatdy, V., Hublin, J.-J., Tütken, T., 2020. Zinc isotopes in Late Pleistocene fossil teeth from a Southeast Asian cave setting preserve paleodietary information. *Proc. Natl. Acad. Sci. U.S.A.* 117, 4675–4681.

doi.org/10.1073/pnas.1911744117

Chapter 3 – Publication 2

While zinc isotope ratios of tooth enamel are a promising tracer for paleodietary reconstruction, much work is still necessary to establish this method fully. Notably, contamination remains a possible issue and could consequently bias results. Indeed, the zinc content of sample solutions of tooth enamel can be as low as 400 ng and could thus be affected by exogenous zinc contributions during sampling and/or chemical preparation.

Following recent work, this publication aims to assess how different types of typical laboratory gloves specifically affect zinc isotope measurements of tooth enamel. Using different types of teeth coming from an early Holocene foragers population of Lapa do Santo (Brazil), a series of tests were conducted to evaluate the potential of zinc contamination from gloves handling during sample preparation and assess various sources of variability in zinc isotopic composition, including dietary transitions during childhood.

This article is published in *PLoS ONE*: Jaouen, K., Trost, M., **Bourgon, N.**, Colleter, R., Cabec, A.L., Tütken, T., Oliveira, R.E., Pons, M.L., Méjean, P., Steinbrenner, S., Chmeleff, J., Strauss, A., 2020. Zinc isotope variations in archeological human teeth (Lapa do Santo, Brazil) reveal dietary transitions in childhood and no contamination from gloves. *PLoS ONE* 15, e0232379.

doi.org/10.1371/journal.pone.0232379

Chapter 4 – Publication 3

Although evidence suggests our species' presence in Southeast Asia by at least 70 ka, the frequent lack of archeological material evidence (e.g., lithic technology, hearth features, plant macro-remains, cut marks on bones, etc.) and poor preservation of

organic matter in tropical latitudes limits our knowledge of human occupation and subsistence strategies on tropical rainforests.

In this publication, a multi-isotope study was conducted to determine the diet and ecological adaptations of the TPL1 *H. sapiens* individual from Tam Pà Ling (Laos), the oldest modern human individual (63–46 ka) found in South East Asia. By using zinc stable isotopes analyses, this study aims to investigate for the first time the reliance on plant or animal resources from Late Pleistocene rainforest human foragers and their adaptability in utilizing rainforests and not only open environments. Additionally, this publication serves as a case study illustrating the benefits of using the zinc isotopic approach for paleodietary reconstruction, especially when nitrogen stable isotope analysis of bone or dentin collagen is unsuccessful.

This article is published in *Journal of Human Evolution*: **Bourgon, N.**, Jaouen, K., Bacon, A.-M., Dufour, E., McCormack, J., Tran, N.-H., Trost, M., Fiorillo, D., Dunn, T.E., Zanolli, C., Zachwieja, A., Durringer, P., Ponche, J.-L., Boesch, Q., Antoine, P.-O., Westaway, K.E., Joannes-Boyau, R., Suzzoni, E., Frangeul, S., Crozier, F., Aubaile, F., Patole-Edoumba, E., Luangkhoth, T., Souksavatdy, V., Boualaphane, S., Sayavonkhamdy, T., Sichanthongtip, P., Sihanam, D., Demeter, F., Shackelford, L.L., Hublin, J.-J., Tütken, T., 2021. Trophic ecology of a Late Pleistocene early modern human from tropical Southeast Asia inferred from zinc isotopes. *J. Hum. Evol.* 161, 103075.

doi.org/10.1016/j.jhevol.2021.103075

Chapter 2

Preservation of diet-related zinc isotope ratios in fossil tooth enamel

Zinc isotopes in Late Pleistocene fossil teeth from a Southeast Asian cave setting preserve paleodietary information

Nicolas Bourgon, Klervia Jaouen, Anne-Marie Bacon, Klaus Peter Jochum, Elise Dufour, Philippe Durringer, Jean-Luc Ponche, Renaud Joannes-Boyau, Quentin Boesch, Pierre-Olivier Antoine, Manon Hullot, Ulrike Weis, Ellen Schulz-Kornas, Manuel Trost, Denis Fiorillo, Fabrice Demeter, Elise Patole-Edoumba, Laura L. Shackelford, Tyler E. Dunn, Alexandra Zachwieja, Somoh Duangthongchit, Thongsa Sayavonkhamdy, Phonephanh Sichanthongtip, Daovee Sihanam, Viengkeo Souksavatdy, Jean-Jacques Hublin, and Thomas Tütken

Contribution: Designing the research, performing research, analyzing the data, writing the article, and reviewing the article.

This manuscript is published in a similar version in *Proceedings of the National Academy of Sciences of the United States of America* vol 117, no. 9 (2020), p. 4675-4681. doi.org/10.1073/pnas.1911744117

Acknowledgements

We thank K. Schilling and B. Brumme (Department of Human Evolution, Max Planck Institute for Evolutionary Anthropology, Leipzig) as well as O. Tombret (UMR 7209 AASPE) for technical support; S. Steinbrenner (Department of Human Evolution, Max Planck Institute for Evolutionary Anthropology, Leipzig) who performed the carbon and nitrogen analysis; R. Mundry (Department of Primatology, Max Planck Institute for Evolutionary Anthropology, Leipzig) for his valuable help and insight with the LMM; R. Barr, C. Zickert, L. Därr, A. Salzer, and L. Schymanski (Multimedia Department, Max Planck Institute for Evolutionary Anthropology, Leipzig) for their help with pictures and figure presentation; Christine Lefèvre, Joséphine Lesur, and Aurélie Verguin of the UMR 7209 (AASPE), Muséum National d'Histoire Naturelle, in Paris, for the agreement and access to the mammal collection; and M. Sponheimer and P. Telouk for their helpful discussions. We would like to acknowledge the support and thank the Max Planck Society and the Deutsche Forschungsgemeinschaft ("PALÄODIET" Project 378496604) for funding this study. T.T. and K.J. received funding by the European Research Council under the European Union's Horizon 2020 research and innovation program Grant Agreements 681450 and 803676, respectively. Funding for the excavation of the Tam Hay Marklot cave in 2015 was provided by the University of Strasbourg (Unistra/EOST UMR 7516) and the Unité Propre de Recherche (UPR) 2147 of CNRS Dynamique de l'évolution humaine, France, and the University of Illinois at Urbana–Champaign. Finally, we would like also to thank V.S. and S. Luangaphay of the Department of National Heritage, Ministry of Information and Culture in Vientiane, Laos, for their authorization to study the Tam Hay Marklot fauna.

Abstract

Stable carbon and nitrogen isotope ratios of collagen from bone and dentin have frequently been used for dietary reconstruction, but this method is limited by protein preservation. Isotopes of the trace element zinc in bioapatite constitute a promising proxy to infer dietary information from extant and extinct vertebrates. The $^{66}\text{Zn}/^{64}\text{Zn}$ ratio (expressed as $\delta^{66}\text{Zn}$ value) shows an enrichment of the light isotope in mammals along each trophic step. However, preservation of diet-related $\delta^{66}\text{Zn}$ values in fossil teeth has not been assessed yet. Here, we analyzed the enamel of fossil teeth from the Late Pleistocene (38.4–13.5 ka) mammalian assemblage of the Tam Hay Marklot (THM) cave in northeastern Laos to reconstruct the food web and assess the preservation of original $\delta^{66}\text{Zn}$ values. Distinct enamel $\delta^{66}\text{Zn}$ values of the fossil taxa ($\delta^{66}\text{Zn}_{\text{carnivore}} < \delta^{66}\text{Zn}_{\text{omnivore}} < \delta^{66}\text{Zn}_{\text{herbivore}}$) according to their expected feeding habits were observed, with a trophic carnivore-herbivore spacing of +0.60 ‰ and omnivores having intermediate values. Zinc and trace element concentration profiles similar to those of modern teeth also indicate the minimal impact of diagenesis on the enamel. While further work is needed to explore preservation for settings with different taphonomic conditions, the diet-related $\delta^{66}\text{Zn}$ values in fossil enamel from THM cave suggest an excellent long-term preservation potential, even under tropical conditions that are well known to be adverse for collagen preservation. Zinc isotopes could thus provide a new tool to assess the diet of fossil hominins and associated fauna, as well as trophic relationships in past food webs.

Significance

Dietary habits, especially meat consumption, represent a key aspect in the behavior and evolution of fossil hominin species. Here, we explore zinc isotope ratios in tooth enamel of fossil mammals. We show discrimination between different trophic levels and demonstrate that zinc isotopes could prove useful in paleodietary studies of fossil hominin, or other mammalian species, to assess their consumption of animal versus plant resources. We also demonstrate the high preservation potential of pristine diet-related zinc isotope ratios, even under tropical conditions with poor collagen preservation, such as the studied depositional context in Southeast Asia. However, assessing the preservation of original $\delta^{66}\text{Zn}$ values is required for each fossil site as diagenesis may vary across and even within taphonomic settings.

2.1 Introduction

Stable isotope analyses in archeology and paleontology have been frequently used to explore the diet of past human populations. Nitrogen stable isotope ($\delta^{15}\text{N}$) analysis of bone or dentin collagen is an established method for the trophic level assessment (DeNiro and Epstein, 1981; Schoeninger and DeNiro, 1984). However, these analyses are confronted with the limitations that arise from the degree of protein preservation (van Klinken, 1999). Trophic level assessment of ancient mammals and hominins older than ~ 100 kyr are, due to the lack of collagen preservation, currently out of reach. This timeframe is even shorter (~ 15 kyr) in arid and wet tropical settings that nonetheless often represent key regions in human evolution, such as Africa (Ambrose, 1991; Loosdrecht et al., 2018) and Asia (Krigbaum, 2005; Clarkson et al., 2009). However, beyond the classical collagen-bound nitrogen isotopes, trophic level reconstructions from enamel with different isotope systems have become feasible (Chu et al., 2006; Knudson et al., 2010; Costas-Rodríguez et al., 2014, p.; Martin et al., 2014) and were recently applied to fossil and archeological specimens (Knudson et al., 2010; Martin et al., 2015, 2018; Jaouen et al., 2018; Balter et al., 2019). Using multi-collector inductively coupled plasma mass spectrometry (MC-ICP-MS) allows for the measurement of “nontraditional” stable isotopes from various elements (calcium, magnesium, zinc, and strontium). Among these, zinc isotope ratios ($^{66}\text{Zn}/^{64}\text{Zn}$, expressed as $\delta^{66}\text{Zn}$ value) constitute a promising dietary indicator (Jaouen et al., 2013, 2016a, 2016b, 2018; Costas-Rodríguez et al., 2014). Indeed, zinc is incorporated as a trace element in the enamel bioapatite and, thus, has a better long-term preservation potential compared to collagen-bound nitrogen, showing promise for dietary reconstructions in archeology and paleontology (Dean et al., 2018). It was not until 2012 that Van Heghe et al. began investigating the causes of the variability of $\delta^{66}\text{Zn}$ values in a pilot study. Since then, work on mammals from modern food webs, first in Africa (Jaouen et al., 2013, 2016a) and then in the Canadian Arctic (Jaouen et al., 2016b), have established the relationship between $\delta^{66}\text{Zn}$ of bioapatite and diet.

As currently understood, two factors influence the variability of $\delta^{66}\text{Zn}$ values in a food web: the initial zinc isotope composition from the source of intake and biological zinc isotope fractionation occurring within the organism itself. In plants, the initial bioavailable zinc isotope composition is derived from the soil, which is in turn controlled by the nature of the underlying bedrock. Igneous rocks exhibit relatively similar $\delta^{66}\text{Zn}$ values ($+0.3 \pm 0.14$ ‰ [2σ]) (Cloquet et al., 2008; Moynier et al., 2017). Sedimentary rocks show much more variable $\delta^{66}\text{Zn}$ values (Maréchal et al., 2000;

Cloquet et al., 2008; Moynier et al., 2017), with the highest values found in marine carbonates (+0.3 to +1.4 ‰) (Luck et al., 1999; Pichat et al., 2003). An initial biological fractionation in plants then occurs between the roots and the soil, which favors the absorption of heavy zinc isotopes relative to the litter layer in which they grow (Weiss et al., 2005; Viers et al., 2007; Moynier et al., 2009; Aucour et al., 2011). Active uptake of heavy zinc isotopes then enhances the intra-plant mobility of light zinc isotopes to the most aerial parts of the plants (Weiss et al., 2005; Viers et al., 2007; Moynier et al., 2009), leading to a general trend of progressively lower $\delta^{66}\text{Zn}$ values from root to leaves, i.e., within different parts of a single plant, but also leading to variable $\delta^{66}\text{Zn}$ values between different plant species (Weiss et al., 2005; Viers et al., 2007; Moynier et al., 2009). In animals, the body tissues' $\delta^{66}\text{Zn}$ values also depend on the zinc isotopic composition of the foods consumed. Different plants and parts of plants consumed will thus induce varying $\delta^{66}\text{Zn}$ values in herbivores. Similarly, the $\delta^{66}\text{Zn}$ values of body tissues in carnivores depend on the prey and parts of the prey consumed, with muscles usually exhibiting low $\delta^{66}\text{Zn}$ values compared to the average zinc isotopic composition of the body (Balter et al., 2010; Jaouen et al., 2013, 2016a; Costas-Rodríguez et al., 2014). Since plants usually have the most elevated $\delta^{66}\text{Zn}$ values (Costas-Rodríguez et al., 2014; Jaouen et al., 2016a) and muscles low values (Balter et al., 2010; Jaouen et al., 2013, 2016a; Costas-Rodríguez et al., 2014), the resulting $\delta^{66}\text{Zn}$ values of a trophic chain follow an opposite trend as to the classic trophic level proxy $\delta^{15}\text{N}$ collagen values, that increase about 3–4 ‰ per trophic level (Schoeninger and DeNiro, 1984). The higher the trophic level of an animal is, the lower the $\delta^{66}\text{Zn}$ values of its body tissues are (Balter et al., 2010; Jaouen et al., 2013, 2016a, 2016b, 2018; Costas-Rodríguez et al., 2014).

However, while enamel has been shown to be less prone to alteration than bone and dentin (Lee-Thorp and van der Merwe, 1991; Michel et al., 1996; Kohn et al., 1999; Budd et al., 2000; Trueman and Tuross, 2002; Dauphin and Williams, 2004), it is nevertheless not immune from diagenetic processes (Grandjean and Albarède, 1989; Michel et al., 1996; Kohn et al., 1999; Sponheimer and Lee-Thorp, 1999b, 2006; Trueman and Tuross, 2002; Schoeninger et al., 2003). One key predicament to investigating paleoecology through the analysis of trace elements (such as zinc) is thus the absence of diagenetic alteration. Additionally, generalized diagenetic effects on zinc from enamel still remain mostly uncertain, as they seem to vary considerably from site to site (Bocherens et al., 1994; Sponheimer and Lee-Thorp, 2006; Hinz and Kohn, 2010). Therefore, careful investigations of potential postmortem alteration on trace elements in fossil teeth are crucial for each taphonomic setting to separate genuine

ecological information from diagenetic alteration such as trace element incorporation, leaching, or replacement (Sponheimer and Lee-Thorp, 2006; Hinz and Kohn, 2010; Reynard and Balter, 2014).

Tam Hay Marklot (THM) cave (filling of the cave, and its associated fauna, dated to 38.4–13.5 ka by U-Th analysis on teeth, *SI Appendix, Supplementary information 1.1.3, Tables S9–S14, and Figures S43–S46*), in the northeastern part of Laos, Hua Pan Province, is situated in a subtropical latitudinal setting where preservation of organic material (i.e., collagen) is generally poor (Pestle and Colvard, 2012). This cave offers ideal conditions to rigorously assess the preservation potential of diet-related zinc isotopic composition in fossils when compared to organic matter-bound dietary proxies such as nitrogen isotopes. Indeed, the complex and diverse sedimentary processes encountered in mainland Southeast Asia often lead to atypical preservation of the vertebrate assemblages, almost always originating from karst breccias (Düringer et al., 2012; Bacon et al., 2015, 2018b). Subject to a highly variable climate- and water-dependent environment, these karst systems produce fossil assemblages that are often characteristic of long transportation processes through subterranean cave networks, often with multiple reworking episodes (Düringer et al., 2012; Bacon et al., 2015, 2018b). Furthermore, the surroundings of THM cave offer, at present-day and presumably also in the past, two types of photosynthetic pathways used by local plants, C₃ and C₄, thus allowing an additional and already well-established dietary tracer ($\delta^{13}\text{C}$) of the same specimens to be compared with the $\delta^{66}\text{Zn}$ results. A detailed description of the regional geology and sedimentary deposits is presented in *SI Appendix, Supplementary information 1.1.1*.

Here, a multi-isotope investigation was carried out on tooth enamel ($\delta^{66}\text{Zn}$, $^{87}\text{Sr}/^{86}\text{Sr}$, $\delta^{13}\text{C}$, $\delta^{18}\text{O}$) and dentin collagen ($\delta^{15}\text{N}$), if still preserved, from the Late Pleistocene (38.4–13.5 ka) fossiliferous assemblage newly recovered in the THM cave in 2015. The preservation of diet-related zinc isotopic composition in fossil enamel was systematically investigated to assess the potential application of zinc isotope analysis for dietary reconstruction in deep time. In order to cover a broad range of distinct trophic levels and dietary habits, tooth enamel from 72 specimens belonging to 22 mammalian taxa was analyzed (*SI Appendix, Table S2*). A variety of small-, medium- and large-sized species were selected, covering a wide range of feeding categories including carnivores, omnivores, and herbivores (where a species' specific trophic ecology was assigned based on analogous modern-day fauna's dietary behaviors; *SI Appendix, Table S2*).

Enamel from each specimen was sampled for $\delta^{66}\text{Zn}$, $^{87}\text{Sr}/^{86}\text{Sr}$, $\delta^{13}\text{C}$, and $\delta^{18}\text{O}$ isotope analyses (>5 mg per sample for zinc analysis; see *SI Appendix, Supplementary information 1.3.1*). Because kinetic and equilibrium biological fractionations of $^{87}\text{Sr}/^{86}\text{Sr}$ are negligible (Bentley, 2006; Price et al., 2012; Wright, 2012; Flockhart et al., 2015) and overwritten during normalization for instrumental mass bias (Bentley, 2006), radiogenic $^{87}\text{Sr}/^{86}\text{Sr}$ ratios in animal bones and teeth reflect those of local bioavailable strontium sources (Graustein, 1989; Bentley, 2006; Knudson et al., 2010; Lewis et al., 2017). Differences in $^{87}\text{Sr}/^{86}\text{Sr}$ would thus imply provenance from a distinct locality with a different geological bedrock type. The granitic bedrock found at THM locality is likely to exhibit higher $^{87}\text{Sr}/^{86}\text{Sr}$ associated with concomitant lower $\delta^{66}\text{Zn}$ values, while the limestone bedrock would show the opposite trend. This could thus explain some of the variability observed in enamel $\delta^{66}\text{Zn}$ values among the fossil teeth. The carbon isotopic composition ($\delta^{13}\text{C}$) of foods is incorporated into the tissues (i.e., bone and enamel) of the animals that eat them (DeNiro and Epstein, 1978; Lee-Thorp et al., 1989). In terrestrial animals, the carbon of food webs is derived from plants that undergo either C_3 or C_4 photosynthesis (Smith and Epstein, 1971), providing a complementary dietary tracer to $\delta^{66}\text{Zn}$ values. While an array of complex variables is likely to induce variations in the oxygen isotopic composition ($\delta^{18}\text{O}$) of tooth enamel in homeothermic vertebrates (Longinelli, 1984; Luz et al., 1984; Pederzani and Britton, 2019), the present study seeks to explore possible relation between $\delta^{18}\text{O}$ values and zinc isotopic composition, mostly relative to diet and physiology. A subsample of 23 specimens was also analyzed for dentin collagen $\delta^{13}\text{C}$ and $\delta^{15}\text{N}$ values in order to assess the preservation of organic material. When collagen preservation was sufficient (*SI Appendix, Supplementary information 1.3.5*), the $\delta^{15}\text{N}$ values ($n = 4$) were compared with $\delta^{66}\text{Zn}$ of the same specimen since the collagen-bound $\delta^{15}\text{N}$ values reflect the amount of animal protein in the diet and can thus be used to assess trophic level (Schoeninger and DeNiro, 1984). The impact of postmortem taphonomic alteration processes was assessed in situ with spatially resolved element concentration profiles on six fossil mammalian teeth as well as three modern ones for comparison, with distinct feeding behaviors (carnivorous, omnivorous, and herbivorous), digestive physiologies (foregut, hindgut, and carnivore) and phylogenetic histories (Artiodactyla, Perissodactyla, Carnivora, Rodentia, and Primates). Finally, in order to enhance the interpretative framework of zinc isotopic composition, we explored the relation between individual factors (diet, $^{87}\text{Sr}/^{86}\text{Sr}$, $\delta^{13}\text{C}_{\text{apatite}}$, $\delta^{18}\text{O}_{\text{apatite}}$, zinc concentration, and body mass) with $\delta^{66}\text{Zn}$ values, by fitting a linear mixed model (LMMs; Baayen, 2008) with a Gaussian error structure

and identity link (McCullagh and Nelder, 1989). A detailed description of the variation of the different stable isotope systems and the methods used in this study are presented in *SI Appendix, Supplementary information 1.2 and 1.3*.

2.2 Results

Measured $\delta^{66}\text{Zn}$, $^{87}\text{Sr}/^{86}\text{Sr}$, $\delta^{13}\text{C}$, $\delta^{18}\text{O}$, and $\delta^{15}\text{N}$ values for all specimens and reference materials are summarized in *SI Appendix, Supplementary information 1.4, Tables S4–S6, and Figures S8–S10*.

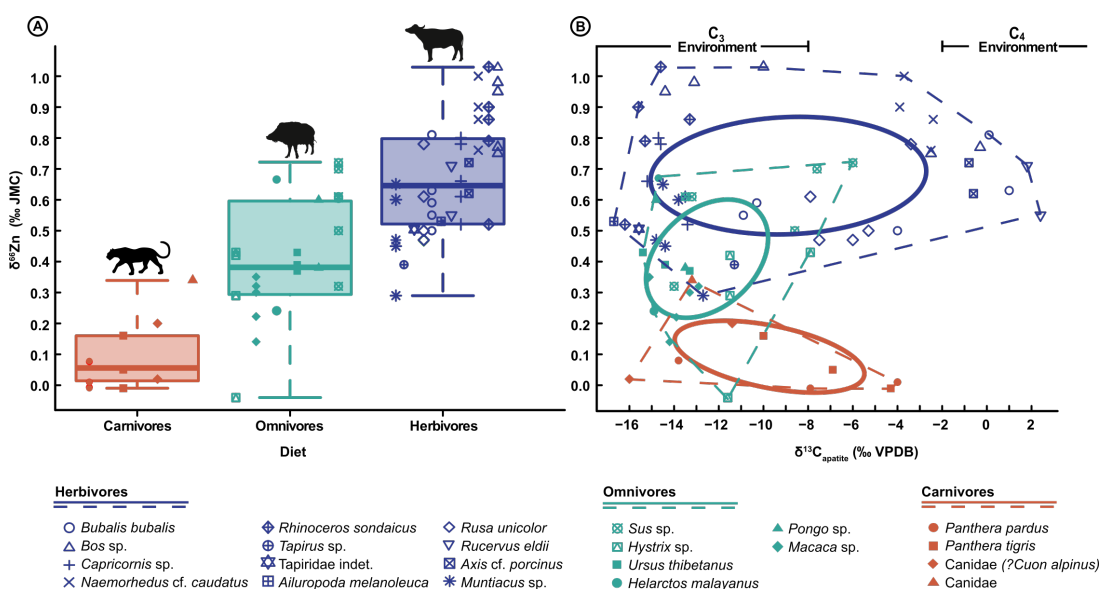


Figure 3. (A) Range of $\delta^{66}\text{Zn}$ values (relative to the JMC-Lyon zinc isotope standard; Maréchal et al., 1999) in tooth enamel for carnivores (red), omnivores (turquoise), and herbivores (blue) of the THM cave assemblage. The boxes from the box and whisker plots represent the 25th–75th percentiles, with the median as a bold horizontal line. (B) Distribution of enamel $\delta^{66}\text{Zn}$ versus $\delta^{13}\text{C}_{\text{apatite}}$ values of the THM cave assemblage (*SI Appendix, Table S4*), where “C₃ environment” and “C₄ environment” are defined by $\delta^{13}\text{C}_{\text{apatite}} < -8$ ‰ and > -2 ‰, respectively. Dashed lines represent the full range of variation, and full lines represent 40% predictive ellipses (using R statistical software and package “SIBER”; Jackson et al., 2011; R Core Team, 2018).

The total range of tooth enamel $\delta^{66}\text{Zn}$ values from THM cave is 1.07 ‰, ranging from -0.04 ‰ to $+1.03$ ‰ (**Figure 3**). Herbivores exhibit the highest $\delta^{66}\text{Zn}$ values ($\delta^{66}\text{Zn} = +0.68 \pm 0.38$ ‰ [2σ], $n = 41$), carnivores the lowest ($\delta^{66}\text{Zn} = 0.09 \pm 0.24$ ‰ [2σ], $n = 9$) and the $\delta^{66}\text{Zn}$ values of omnivores fall in between ($\delta^{66}\text{Zn} = +0.41 \pm 0.38$ ‰ [2σ], $n = 22$) (**Figure 1**; *SI Appendix, Table S4*). Omnivorous taxa, on average, show the highest variability in the intra-taxon ranges of their $\delta^{66}\text{Zn}$ values (average $\delta^{66}\text{Zn}$ range = 0.30 ± 0.34 ‰ [2σ]), compared to herbivores (average $\delta^{66}\text{Zn}$ range = 0.28 ± 0.24 ‰ [2σ]) and carnivores (average $\delta^{66}\text{Zn}$ range = 0.15 ± 0.10 ‰ [2σ]).

Sixty-nine of 72 specimens were analyzed for $^{87}\text{Sr}/^{86}\text{Sr}$. Enamel $^{87}\text{Sr}/^{86}\text{Sr}$ display a broad range, from 0.7097 to 0.7243 ($\Delta = 0.0146$); however, the majority of specimens clusters between 0.7135 and 0.7173 (52%, $n = 36$; *SI Appendix, Table S4*).

Enamel $\delta^{13}\text{C}$ values range from -16.70 ‰ to 2.40 ‰ ($n = 72$), covering the full spectrum of values typical for pure subcanopy to open woodland C_3 and C_4 plant feeders (**Figure 1B**; *SI Appendix, Table S4*). Fossil enamel from THM cave indicates that a predominant C_3 environment existed in the cave surroundings but with a definite C_4 grass component (Smith and Epstein, 1971). The enamel $\delta^{18}\text{O}$ values range from -5.85 ‰ to 0.2 ‰.

Collagen preservation of the teeth was poor, as only 4 (*Muntiacus* sp., *Bos* sp., *Sus* sp., and *Rhinoceros sondaicus*) of the 23 dentin samples yielded any collagen, and even these fell below the 1% limit ($\sim 0.46 \pm 0.48\%$ [2σ]; modern bones = $\sim 22\%$; van Klinken, 1999). Nonetheless, collagen extracts have C:N ratios characteristic of well-preserved collagen (3.26 ± 0.08 [2σ]) (van Klinken, 1999) (*SI Appendix, Table S5 and Figure S9*). The $\delta^{15}\text{N}_{\text{collagen}}$ values associated with these specimens range from $+3.15$ ‰ to $+10.56$ ‰ and the $\delta^{13}\text{C}_{\text{collagen}}$ values from -24.0 ‰ to -9.1 ‰. The higher $\delta^{15}\text{N}_{\text{collagen}}$ values are in agreement with associated lower $\delta^{66}\text{Zn}$ values, for taxa assigned an omnivorous diet (*Sus* sp. and *Muntiacus* sp.), and conversely the lower $\delta^{15}\text{N}_{\text{collagen}}$ values with higher $\delta^{66}\text{Zn}$ values, representative of an herbivorous diet (*Bos* sp. and *Rhinoceros sondaicus*). The $\delta^{13}\text{C}_{\text{collagen}}$ and $\delta^{13}\text{C}_{\text{apatite}}$ values are also consistent for each specimen (*SI Appendix, Tables S4 and S5*).

Zinc concentration distribution was investigated in 15 cross-sections from 6 fossil mammal teeth and compared to that of 10 cross-sections from 3 modern specimens to assess the impact of postmortem taphonomic processes on the enamel. Additionally, Fe, Mn, Al, Mg, and rare earth elements (REE, calculated as the sum of all measured REE concentrations), which are sensitive to diagenetic alteration, provided complementary tracers to discern the degree of diagenetic alteration of the enamel. Concentrations and distribution profiles of these elements were similar to those of modern teeth and were observed almost systematically across modern and fossil enamel samples, suggesting a lack of any significant diagenetic alteration (uptake or leaching) of trace elements in the latter. Similarly, an absence of a relationship between $\delta^{66}\text{Zn}$ values and average enamel concentration in various other trace elements, with potentially different susceptibilities for alteration (Reynard and Balter, 2014), can be observed (*SI Appendix, Figures S35–S39*). In contrast, the dentin and pulp cavity of the fossil teeth had higher concentrations of these elements, indicating diagenetic alteration (**Figure 2**). On 15 fossil tooth cross-sections, a total of 23 enamel segments were analyzed. Of these, only one enamel cross-section segment showed zinc concentration distribution that did not follow the characteristic pattern observed for

modern enamel ($n = 10$) of higher concentration in the outermost layer that decreases toward a constant level inward (*SI Appendix, Figure S30*) (Lee et al., 1999; Kohn et al., 2013; Tacail et al., 2017; Dean et al., 2018). While the distribution of this one segment may indicate some postmortem alteration, none of the other three enamel cross-section segments analyzed from that same specimen (*Panthera pardus*, 34505) displayed an atypical pattern. The absence of any significant postmortem zinc uptake is nonetheless further corroborated by the absence of a mixing line between zinc concentration and $\delta^{66}\text{Zn}$ values (*SI Appendix, Figure S32*). Altogether, good preservation of the enamel seems to prevail in the fossil specimens, suggesting no alteration of original zinc contents and, hence, preservation of pristine biogenic $\delta^{66}\text{Zn}$ values. Complete sets of spatial element concentration profiles are provided in *SI Appendix, Figures S12–S29*.

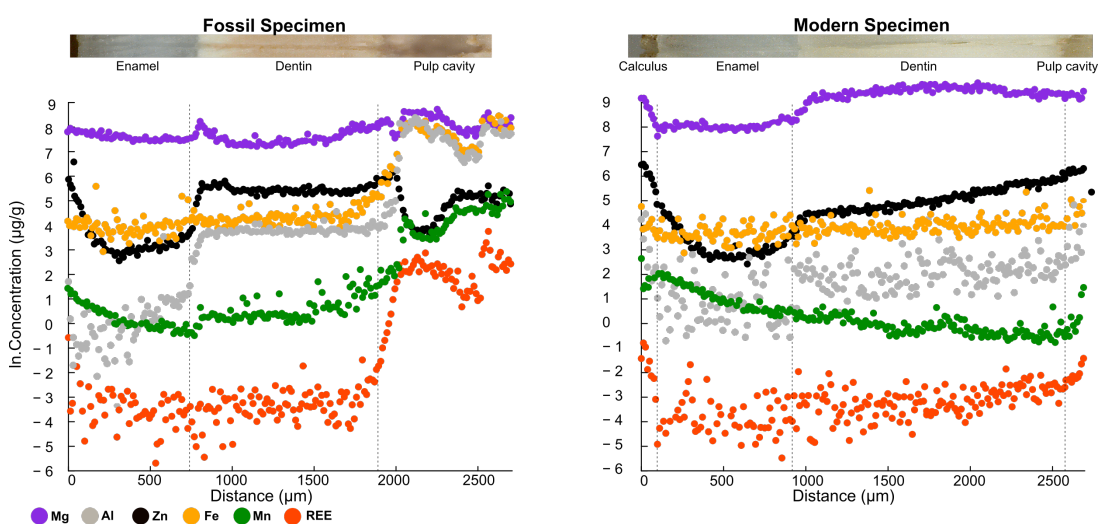


Figure 4. Natural log-transformed spatial element concentration profiles (ln.Concentration, as $\mu\text{g/g}$) of Zn, Fe, Mn, Al, Mg, and REE in caprine teeth for a fossil (*Capricornis* sp., left) and a modern (*H. jemtahicus*, right) specimen. The Fe, Mn, Al, and REE (calculated as the sum of all measured REE concentrations) were selected as tracers for diagenetic alteration because of their relative abundance in soil-matter, as well as their tendency to be enriched postmortem in fossil bioapatite. Thus, they most likely trace postmortem taphonomic alterations and element uptake from soil pore water. Note that in both photomicrographs the tracks of laser ablation line scans are visible.

Overall, the full-null LMM comparison was clearly significant (likelihood ratio test: $\chi^2 = 21.29$, $\text{df} = 2$, $P < 0.001$) and allowed to assess which of the tested predictors were associated with variations in $\delta^{66}\text{Zn}$ values. The $\delta^{13}\text{C}$ and $\delta^{18}\text{O}$ values, as well as the zinc concentration of each sample, appeared to have no significant relation with the variability of the $\delta^{66}\text{Zn}$ values response ($\delta^{13}\text{C}_{\text{apatite}}$ values likelihood ratio test: $\chi^2 = 0.230$, $\text{df} = 1$, $P = 0.632$; $\delta^{18}\text{O}_{\text{apatite}}$ values likelihood ratio test: $\chi^2 = 0.135$, $\text{df} = 1$, $P = 0.713$). Diet had a significant relation with $\delta^{66}\text{Zn}$ values whereby omnivores and herbivores had clearly elevated values as compared to carnivores (LMM diet $P < 0.05$; *SI Appendix, Table S7*). Finally, $^{87}\text{Sr}/^{86}\text{Sr}$ and body mass both displayed a significant relation with the variability of the $\delta^{66}\text{Zn}$ values ($^{87}\text{Sr}/^{86}\text{Sr}$ likelihood ratio test: $\chi^2 =$

12.101, $df = 1$, $P = 0.001$; body mass likelihood ratio test: $X^2 = 9.892$, $df = 1$, $P = 0.002$). While (G)LMMs do not allow to get an estimated effect size for individual predictors, the effect size for the entirety of the fixed effects (“marginal R^2 ”) is 0.63, and the one for the entirety of the fixed and random effects (“conditional R^2 ”) is 0.85 (Nakagawa et al., 2017).

2.3 Discussion

2.3.1 Preservation of diet-related zinc isotope compositions in fossils teeth

The ordering of fossil taxa from THM cave according to their enamel $\delta^{66}\text{Zn}$ values ($\delta^{66}\text{Zn}_{\text{carnivores}} < \delta^{66}\text{Zn}_{\text{omnivores}} < \delta^{66}\text{Zn}_{\text{herbivores}}$) reflects trophic level differences that are in good agreement with their expected dietary habits (**Figure 3**), as well as $\delta^{66}\text{Zn}$ values observed for modern mammals from similar feeding categories (Jaouen et al., 2013, 2016a, 2016b, 2018). This strongly suggests that the enamel of the 38.4–13.5 thousand-year-old fossil teeth from THM cave retained their original, diet-related zinc isotopic composition expected for each feeding category and, hence, was not altered by taphonomic processes. This is further supported by spatial distribution profiles of zinc across the fossil enamel with higher concentrations in the outermost enamel layer decreasing toward a constant level inward, which is a characteristic pattern for modern teeth (**Figure 4; SI Appendix, Figures S18–S20 and S27–S30**) (Lee et al., 1999; Kohn et al., 2013; Tacail et al., 2017; Dean et al., 2018). The higher concentration in zinc in the first few tenths of microns of the outermost enamel layer is believed to be a biochemical signal that could be associated with the termination of the enamel maturation (Tacail et al., 2017). While this pattern is systematically observed for all teeth (i.e., both fossil and modern ones), thus supporting the preservation of pristine biogenic zinc concentrations (and thus $\delta^{66}\text{Zn}$ signatures), it also poses a challenge for distinguishing between original biogenic signature and postmortem diagenetic uptake. However, this layer of higher zinc concentration is systematically only $<200\ \mu\text{m}$ thick (**Figure 3; SI Appendix, Figures S12–S29**) (Lee et al., 1999; Kohn et al., 2013; Tacail et al., 2017; Dean et al., 2018) and, thus, lends further support to the preservation of a biogenic pattern. Furthermore, this outer zinc-rich layer is routinely removed mechanically during the enamel cleaning process for stable isotope analysis.

Due to the tropical setting of THM cave, collagen preservation is limited, as reflected by low collagen extraction success rate (i.e., $n = 4$) and low collagen yield (<1%). Nevertheless, the few $\delta^{15}\text{N}_{\text{collagen}}$ values that were obtained follow the expected trend in $\delta^{66}\text{Zn}$ values, where relatively high $\delta^{15}\text{N}_{\text{collagen}}$ values are associated with relatively low $\delta^{66}\text{Zn}$ values (Jaouen et al., 2016b) (*SI Appendix, Figure S31*). Finally, the low in vivo-like Mn, Fe, Al, Mg, and bulk REE contents, typical for the enamel of modern mammal teeth (**Figure 4**), demonstrate the lack of any significant diagenetic uptake of trace elements from the soil environment rich in these elements. Although postmortem taphonomic processes can vary significantly from one location to another due to site formations processes, age, environmental conditions, and soil composition (Wang and Cerling, 1994; Kohn et al., 1999; Hedges, 2002), multiple lines of evidence presented in this study support the effective preservation of diet-related zinc isotopic composition in the enamel of the investigated fossil teeth despite the adverse tropical setting of THM cave. This is encouraging for future applications of zinc isotopes in the enamel of fossil teeth for dietary reconstructions.

2.3.2 Variation in zinc isotopic compositions in tooth enamel.

The overall mean value and range of $\delta^{66}\text{Zn}$ values for each diet category, as well as the intra-specific $\delta^{66}\text{Zn}$ variability of each taxon (*SI Appendix, Supplementary information 1.4.1*), are in agreement with their dietary habits and display nearly no overlap between carnivores and herbivores. Additionally, the LMM further confirmed that $\delta^{66}\text{Zn}$ values differ between each of the three dietary categories. Carnivores exhibit the lowest $\delta^{66}\text{Zn}$ values, in agreement with a strictly carnivorous diet and the smallest range of variation. In contrast, herbivores have significantly higher $\delta^{66}\text{Zn}$ values than carnivores and many omnivores (**Figure 3**). Herbivores also have a broad range of $\delta^{66}\text{Zn}$ values being consistent with the consumption of a variety of different plants, plant parts, and their specific digestive strategies (foregut and hindgut fermentation). Omnivores display mostly intermediate $\delta^{66}\text{Zn}$ values but occasionally exhibit values characteristic of carnivorous taxa or strictly herbivorous taxa (**Figure 3**). Thus, omnivores exhibit the largest range of $\delta^{66}\text{Zn}$ values covering all three dietary categories, most likely resulting from a varying proportion of meat (but also of plant- and animal-matter from vertebrates and invertebrates) in their diet. While not enough data are yet available to draw any definitive conclusions, it is likely that the lower end of their $\delta^{66}\text{Zn}$ range reflect diets that are mostly composed of animal-matter, whereas the upper range would be predominantly, if not entirely, comprised of plants. A single

herbivore specimen (*Muntiacus* sp.) falls within the range of carnivores. However, this taxon is known at times to exhibit omnivorous dietary habits, feeding on bird's eggs and small animals (Kurt, 1990; Jackson, 2002). Furthermore, its associated high $\delta^{15}\text{N}$ value attests to a diet that is, at the very least, not strictly limited to plant-matter. Finally, both its $\delta^{66}\text{Zn}$ and $\delta^{15}\text{N}$ values are similar to that of a *Sus* sp., further supporting an omnivorous diet for this *Muntiacus* specimen.

Overall, the range of $\delta^{66}\text{Zn}$ values for THM is smaller (1.07 ‰) than seen in a modern terrestrial food web of the Koobi Fora region of Turkana Basin in Kenya (1.24 ‰) (Jaouen et al., 2016a), and the absolute $\delta^{66}\text{Zn}$ values of the whole food web are also lower. This is likely the result of different faunal assemblages and environments between the two localities: THM cave was situated in a mostly forested setting, whereas Koobi Fora is mainly an open grassland landscape. Because trees are likely to exhibit lower $\delta^{66}\text{Zn}$ values in their leaves compared to low growing herbaceous vegetation (Viers et al., 2007; Weiss et al., 2008; Moynier et al., 2009), this could explain why herbivores, and consequently carnivores, have lower enamel $\delta^{66}\text{Zn}$ values at THM cave. The zinc isotopic composition of the local geology, seen as having a significant relation with $\delta^{66}\text{Zn}$ values of THM cave, could also in part explain differences observed between these sites. The trophic spacing observed between mammalian carnivore-herbivore is also larger at THM (+0.60 ‰) than at Koobi Fora (+0.40 ‰). This is likely the result of the faunal assemblage from Koobi Fora, as it contains fewer species and specimens ($n = 10$ and $n = 26$, respectively), carnivores that do not prey on most or any of the herbivores listed, and hyenas' higher $\delta^{66}\text{Zn}$ values probably caused by bone consumption (Jaouen et al., 2016a). As opposed to the Koobi Fora region, no clear distinction in $\delta^{66}\text{Zn}$ values can be drawn between grazers and browsers at THM. However, two groups can be discerned in the $\delta^{66}\text{Zn}$ values of browsers (established by $\delta^{13}\text{C}_{\text{apatite}} < -8$ ‰ characteristic for C_3 plant feeders), one with low ($+0.52 \pm 0.20$ ‰ [2σ], $n = 14$) and the other with high ($+0.90 \pm 0.20$ ‰ [2σ], $n = 9$) $\delta^{66}\text{Zn}$ values (**Figure 3**). In the upper range of the sampled browsers' $\delta^{66}\text{Zn}$ values (**Figure 3**), a mixture of both foregut and hindgut fermenters, as well as large and intermediate body-sized taxa, are present. Consequently, we conclude that digestive physiology and body mass can be ruled out as factors explaining this variability. Maternal effects linked to breastfeeding or in utero tooth formation were also ruled out as causes to intra-group $\delta^{66}\text{Zn}$ values variability, as the formation and emergence sequence of the sampled teeth (i.e., only teeth of adult individuals formed postweaning; *SI Appendix, Table S2*) goes against such interpretation. Therefore, the most likely explanation would be diet, most probably linked to the vertical layering of

the vegetation in a given habitat. Because of progressively lower $\delta^{66}\text{Zn}$ values observed within plants from root to leaves, browsing in lower vegetation layers on herbaceous understory plants should lead to higher grazer-like $\delta^{66}\text{Zn}$ values while browsing in upper vegetation layers like the canopy should lead to lower $\delta^{66}\text{Zn}$ values. This might be the reason for similar $\delta^{66}\text{Zn}$ values between some browsers (e.g., *Rhinoceros sondaicus* and *Bos* sp.) and grazers (e.g., *Rucervus eldii* and *Axis cf. porcinus*, with $\delta^{13}\text{C}_{\text{apatite}} > -2$ ‰ characteristic for C_4 plant feeders) (**Figure 3**).

Finally, the estimates obtained for $^{87}\text{Sr}/^{86}\text{Sr}$ and body mass from the LMM were in agreement with their respective expectation toward $\delta^{66}\text{Zn}$ values in a food web (**SI Appendix, Table S7**). Based on the strontium and zinc isotope composition of crustal rocks (Luck et al., 1999; Maréchal et al., 2000; Pichat et al., 2003; Cloquet et al., 2008; Moynier et al., 2017; Bataille et al., 2018), an increase in $^{87}\text{Sr}/^{86}\text{Sr}$ ratios associated with a decrease in $\delta^{66}\text{Zn}$ values was expected (**SI Appendix, Table S7**): Granitic bedrock usually exhibits higher $^{87}\text{Sr}/^{86}\text{Sr}$ associated with concomitant lower $\delta^{66}\text{Zn}$ values while limestone bedrock shows the opposite trend, both present at THM locality. Likewise, a positive relationship between $\delta^{13}\text{C}$ and body mass due to ^{13}C enrichment with increasing body mass was reported elsewhere (Tejada-Lara et al., 2018) and seems to also apply for $\delta^{66}\text{Zn}$ values (**SI Appendix, Table S7**). Conversely, no significant relation could be drawn between $\delta^{13}\text{C}$ and $\delta^{18}\text{O}$ values and $\delta^{66}\text{Zn}$ values relative to diet and physiology. The LMM thus allowed us to successfully identify which of the tested predictors showed a significant relation with $\delta^{66}\text{Zn}$ values, otherwise not always identified as such (**SI Appendix, Figure S10**). However, their respective impact on $\delta^{66}\text{Zn}$ values cannot be estimated, although it seems likely that its effect is limited since dietary habits are preserved. Further work (e.g., controlled-feeding experiments) will be necessary to ascertain and quantify the impact of these factors on $\delta^{66}\text{Zn}$ values in a broader and more general context, especially compared to diet.

2.4 Conclusion

In this study, the first zinc isotope dataset of fossil tooth enamel, from a Late Pleistocene Southeast Asian faunal assemblage (~38.4–13.5 ka) from the THM cave in northeastern Laos, Hua Pan Province, is presented. We show multiple lines of evidence that support the lack of significant postmortem diagenetic trace element uptake from the soil environment into the enamel of fossil teeth. Enamel profiles along

tooth cross sections do not display any identifiable postmortem alteration of biogenic zinc concentration gradients or diet-related $\delta^{66}\text{Zn}$ by postmortem processes. The classic trophic-level proxy $\delta^{15}\text{N}_{\text{collagen}}$ (only obtained for four samples) displayed an expected inverse trophic relation with $\delta^{66}\text{Zn}$ of the same teeth, further supporting the preservation of original $\delta^{66}\text{Zn}$ values. The Late Pleistocene mammal teeth from THM thus retained pristine, diet-related $\delta^{66}\text{Zn}$ values in their tooth enamel that are in good agreement with the expected dietary habits of the concerned taxa. For this fossil food web, a trophic level spacing of -0.60‰ between herbivores and carnivores was found, while omnivores had intermediate $\delta^{66}\text{Zn}$ values being 0.30‰ lower or higher to herbivores and carnivores, respectively. Thus, carnivores have the lowest, omnivores intermediate, and herbivores the highest $\delta^{66}\text{Zn}$ values. Contrary to what was previously observed in an African grassland environment regarding the distinction of browsers and grazers (Jaouen et al., 2016a), no obvious relation was found between $\delta^{13}\text{C}$ and $\delta^{66}\text{Zn}$ values. However, both the local geology and the body mass showed a significant relation with consumer's $\delta^{66}\text{Zn}$ values, as expected. Further studies from other sites and from controlled-feeding experiments will be necessary to ascertain the factors at play and their impact on the variability of $\delta^{66}\text{Zn}$ values in consumer (hard) tissues. While a systematic, site-specific assessment of the extent of diagenetic alterations of biogenic compositions in fossils is required, the results obtained from THM cave show promise for a high preservation potential of $\delta^{66}\text{Zn}$ values in fossil enamel. Applying $\delta^{66}\text{Zn}$ as dietary tracer could thus open new research avenues in paleontology and archeology, providing us with a powerful and much-needed isotopic trophic tracer for prehistoric and geological time periods ($>100\text{ kyr}$) or settings that lack collagen preservation, given pristine $\delta^{66}\text{Zn}$ values are preserved.

2.5 Methods

Sample Collection. The material used in this study consists of a selection of diverse taxa from the THM assemblage, covering a large range of distinct dietary habits. Within each taxon, the same teeth on the dental row (e.g., left p2), or different teeth but with various wear stages (e.g., left and right p2), were selected to ensure they belonged to different individuals. A total of 72 teeth, belonging to 22 distinct species and/or genera, were selected for the present isotopic analysis. One to six specimens per species were used (*SI Appendix, Table S2*).

Stable Isotope Analysis. Zinc and strontium isotopic ratios from teeth enamel were measured on a Thermo Scientific Neptune MC-ICP-MS, and carbon and nitrogen isotopic ratios from teeth dentin were conducted using a Thermo Finnigan Flash EA coupled to a Delta V isotope ratio mass spectrometer, at the Max Planck Institute for Evolutionary Anthropology in Leipzig, and following the protocols in *SI Appendix, Supplementary information 1.3.2, 1.3.3, and 1.3.5*. Stable carbon and oxygen isotopic compositions of every sample were analyzed using a Thermo Delta V Advantage isotopic mass spectrometer coupled to a Thermo Kiel IV Carbonate Device chemical preparer, at the “Service de Spectrométrie de Masse Isotopique du Muséum” in Paris, using the protocol described in *SI Appendix, Supplementary information 1.3.4*.

Spatial Element Concentration Profiles Analytical Technique. Spatial element concentration profiles were conducted on six fossil teeth (*Capricornis* sp., *Ursus thibetanus*, *P. pardus*, *Sus* sp. *Bubalus bubalis*, and *Macaca* sp.) and three modern teeth (*Bison bison*, *Hemitragus jemtanicus*, and *Pteronura brasiliensis*) of various feeding behaviors (carnivorous, omnivorous, and herbivorous), digestive physiologies (foregut, hindgut, and carnivore) and mammalian order (Artiodactyla, Perissodactyla, Carnivora, Rodentia, and Primates). The measurement routines were performed with a Thermo Scientific Element 2 single collector sector-field ICP-MS coupled with a New Wave UP213 Nd:YAG laser ablation system, at the Max Planck Institute for Chemistry (Mainz), as described in *SI Appendix, Supplementary information 1.3.6*.

Statistical Analysis. All statistical analyses were performed using the statistical program R (version 3.6.1) (R Core Team, 2018). To test our hypotheses of predictors associated with variability in $\delta^{66}\text{Zn}$ values, we fitted a LMM (Baayen, 2008) with a Gaussian error structure and identity link (McCullagh and Nelder, 1989) using the R-package “lme4” (version 1.1–17) (Bates et al., 2015). The full method is reported in *SI Appendix, Supplementary information 1.3.7*.

A complete description of the material and methods used in this study is presented in *SI Appendix, Supplementary information 1.3*. All data discussed in the paper is available to readers in *SI Appendix*.

Chapter 3

Assessment of contamination and dietary transitions on zinc isotope variations

Zinc isotope variations in archeological human teeth (Lapa do Santo, Brazil) reveal dietary transitions in childhood and no contamination from gloves

Klervia Jaouen, Manuel Trost, Nicolas Bourgon, Rozenn Colleter, Adeline Le Cabec, Thomas Tütken, Rodrigo Elias Oliveira, Marie Laure Pons, Pauline Méjean, Sven Steinbrenner, Jérôme Chmeleff, André Strauss

Contribution: Designing the research, performing research (measurements performed in Leipzig), analyzing the data (Linear mixed-model), writing the article (Linear mixed-model), and reviewing the article.

This manuscript is published in a similar version in *PLoS ONE*, 15(5): e0232379. doi.org/10.1371/journal.pone.0232379.

Acknowledgements

Max Planck Society funded the cost of isotope analyses, and FAPESP (04/01321-6, 08/51747-0, 17/16451-2), and CNPQ (435980/2018-1) supported investigation at Lapa do Santo to AS. Salary support was provided to NB and MT by the DFG (“PALÄODIET” project (378496604), to MLP by the MSCA (753059, SPECADIS), and to KJ and PM by the ERC ARCHEIS (Grant number: 803676).

Abstract

Zinc isotope ratios of dental enamel are a promising tracer for dietary reconstruction in archeology, but its use is still in its infancy. A recent study demonstrated a high risk of zinc contamination from nitrile and latex gloves used during chemical sample preparation. Here we assess the potential impact of the use of such gloves during enamel sampling on the zinc isotope composition of teeth from a population of early Holocene hunter-gatherers from Lapa do Santo, Lagoa Santa, Minas Gerais, Brazil. We first examined the amount of zinc and its isotopic composition released from the gloves used in this study by soaking them in weak nitric acid and water. We compared zinc isotope ratios obtained from teeth that were sampled wearing nitrile, latex, or no gloves. Finally, we performed a linear mixed model (LMM) to investigate post hoc the relationship between the gloves used for sampling and the zinc isotope variability in dental enamel. We found that the gloves used in this study released a similar amount of zinc compared to previous work, but only in acidic solution. Zinc isotope ratios of teeth and the LMM identified no sign of significant zinc coming from the gloves when teeth were handled for enamel sampling. We hypothesize that zinc in gloves is mostly released by contact with acids. We found that the main source of zinc isotope variability in the Lapa do Santo population was related to the developmental stage of the tooth tissues sampled. We report identical results for two individuals coming from a different archeological context. Tooth enamel formed in utero and/or during the two first years of life showed higher zinc isotope ratios than enamel formed after weaning. More work is required to systematically investigate if zinc isotopes can be used as a breastfeeding tracer.

3.1 Introduction

Geochemists performing ion-exchange column chromatography for zinc isotopes ($^{66}\text{Zn}/^{64}\text{Zn}$ expressed as $\delta^{66}\text{Zn}$ value) are well aware of contamination issues. The first work published on zinc stable isotope abundances by Maréchal et al. (1999) reports procedural zinc blanks of 50 ng. The zinc concentration used for isotopic analyses is typically 300 ng ml⁻¹. The origin of zinc contamination has been observed in different clean laboratories and investigated in detail in 2017 by Garçon et al. (2017). The main source of contamination comes from gloves, especially those made of nitrile, neoprene, and latex. Reagents (acids, resins, Milli-Q water) and laboratory facilities may also involve other potential sources of zinc contamination. It has been noted that other contaminants may directly be related to body hygiene or care products used by the experimenter, such as some types of shampoo, sunscreen, toothpaste, or make-up (LeBlanc et al., 1999; Lu et al., 2015; Fatima et al., 2016; Kaličanin and Velimirović, 2016). The elevated content of zinc in blanks can become a substantial problem when working with non-primate mammal teeth, which generally contain low amounts of zinc (Bourgon et al., 2020). Sample solutions of tooth enamel can contain zinc contents as low as 400 ng. Consequently, zinc isotope ratio analyses may become biased by substantial zinc contributions from glove contamination. Unfortunately, while the blanks assessed during ion-exchange column chromatography can detect contamination in the clean lab, these blanks cannot account for any zinc contamination occurring during tooth handling, enamel sampling, or during dilutions performed prior to zinc isotope analyses. As much as possible, the sampling procedure should not involve any direct contact between the sampled enamel and the gloves, as the experimenter should hold the tooth by the root, if formed and/or preserved, and use tweezers to collect the chunks of enamel. However, this contact may happen, especially when the experimenter is not aware of the risk of contamination or for teeth without any formed or preserved roots.

This study aims to assess how the use of gloves affects zinc isotope measurements of dental enamel and to propose safe sample-handling practices. To do so, we performed a series of tests to assess the potential of zinc contamination from several types of gloves used during the preparation of enamel samples later used in zinc isotope analyses (TEST 1). We specifically tested types of gloves, which were not mentioned in Garçon et al. (2017) and which are routinely used at the Max Planck Institute for Evolutionary Anthropology, where most of the preparatory and analytical work on dental enamel has been performed. We also considered the contamination coming from

the fingertips of the gloves—in comparison to the whole gloves—since they come into direct contact with the teeth if the experimenter used any gloves during sampling. In a second step (TEST 2), we analyzed teeth to assess if substantial variation could be attributed to potential contamination during sampling from the experimenter wearing the different types of gloves used in TEST 1 (nitrile, latex, vinyl, and no gloves). To perform TEST 2, we used different types of teeth (deciduous and permanent, premolars and molars) coming from a pre-colonial population from Brazil, the early Holocene foragers of Lapa do Santo, whose mobility and diet have been previously studied (Hermenegildo, 2009; Strauss et al., 2015, 2016). In a third test (TEST 3), we indirectly explored post hoc the contamination through nitrile and latex gloves used during the sampling of the Lapa do Santo teeth. We chose to use a linear mixed model (LMM) similar to the one used by Bourgon et al. (2020) to explore the source of zinc isotopic variability in dental enamel. We included in the model the amount of zinc loaded in acid onto the ion chromatographic column (abbreviated as “ALC”, which stands for Amount Loaded onto the Columns) as a predictor. This amount is different from the zinc concentration in the teeth (used as a predictor in the previous model, Bourgon et al., 2020) since the zinc ALC depends on the amount of dental enamel sampled, which can vary depending on the preservation, as well as the area of the tooth sampled. If the zinc ALC is small, the final $\delta^{66}\text{Zn}$ value is more likely to be impacted by the $\delta^{66}\text{Zn}$ of the gloves. The use of the LMM allows us to predict if other factors can explain the zinc isotope variability observed in the teeth, such as the tooth formation time or the strontium isotope composition—an indicator of the geographical origin of the humans from Lapa do Santo.

With these three tests, we confirm the high risk of zinc contamination coming from nitrile and latex gloves when working in the clean lab but also reveal the absence of detectable contamination when gloves are used during enamel sampling. We show that zinc isotope variations observed in the teeth of Lapa do Santo are due to dietary transitions: from the placental diet to breastfeeding as well as before and after weaning. To confirm this result, we undertook an additional experiment (for details, see *SI Appendix, Supplementary Information 2*). We systematically analyzed the teeth of an adult and of a child coming from a different archeological context, the early modern period Jacobins convent of Rennes, France. We then confirmed the trend observed in the Lapa do Santo population, which opens perspectives for the use of zinc isotopes as a potential tracer of the weaning age. Finally, the post hoc test performed using the LMM does not detect any contamination—the zinc ALC is indeed not a predictor for the variance of the zinc isotope ratios—whereas the LMM confirms the crown

formation time of the tooth (i.e., prenatally until ~2 years of age vs. after full weaning) as a main driver of zinc isotope variation in teeth.

3.2 Material and methods

3.2.1 Background information on cultural and dietary behavior of humans from Lapa do Santo

The teeth come from the Lapa do Santo archeological collection, a site from the Lagoa Santa region in east-central Brazil. The permit IPHAN 01514.002697/2011-97 allows the use of the selected teeth for isotope studies. Lagoa Santa has been well known to the academic community since the works of the Danish naturalist Peter Lund in the first half of the 19th century. Since then, hundreds of archeological sites have been located in this region, recording ~12,500 years of non-continuous human occupation in caves and open-air sites (Strauss, 2017). For the Early- and Middle-Holocene occupations, lithic technology, zooarcheology, osteological markers, and multi-isotopic analyses indicate groups of foragers with low mobility and a subsistence strategy focused on gathering plant foods and hunting small and mid-sized animals but no megafauna. A high frequency of caries indicative of elevated consumption of carbohydrates is observed among women but not men (Da-Gloria and Larsen, 2014). Lithics include small flakes and cores of quartz (Bueno and Isnardis, 2017) that were often used to process non-cooked starch plants (Ortega, 2019). Artifacts such as projectile points and axe blades occurred only marginally. Rock art abounds, including the oldest securely dated evidence of rock art in South America (10.5 cal ky BP). Representations include animals, filiform anthropomorphs, geometric motifs, manioc's tubers, and semi-lunar axes. Similar styles are found over a large area of Brazil (Neves et al., 2012).

Of particular importance are the numerous well-preserved Early Holocene (10.6–9.4 cal ky BP; 95.4% interval) skeletons recovered from the region, in general, and from Lapa do Santo, in particular. The skeletal population from Lapa do Santo is comprised of ~50 individuals of both sexes and all ages. At Lapa do Santo, funerary rituals include primary burials, reduction of the body, followed by secondary burial, and pits filled with disarticulated and fragmented bones of a single individual (Strauss et al., 2016).

Sample name	Type	Supplier	Model	Color	Size	Packaging	Ref. no.
N	Nitrile	Carl Roth	Rotiprotect® nitrile evo	Blue	M	Cardboard box	CPX7.1
LT	Latex textured	Carl Roth	Rotiprotect® -latex gloves Type 1 powder-free	White	M	Cardboard box	C269.1
LC	Latex coated	Carl Roth	Rotiprotect® -latex gloves Type 2 powder-free	White	M	Cardboard box	L.950.1
V	Vinyl	Carl Roth	Rotiprotect® -vinyl	Translucid	M	Cardboard box	6178.1

Table 1. List of the gloves tested in this study and associated characteristics. One glove per box was used.

Ancient DNA extracted from skeletons from Lapa do Santo indicates they are entirely nested within past and present Native American genetic diversity (Posth et al., 2018). Because of the tropical environment, very few individuals yield enough collagen to provide dietary information, but based on the few collagen $\delta^{13}\text{C}$ and $\delta^{15}\text{N}$ data and zooarcheology, it seems that the population relied on terrestrial resources with a small contribution of meat in their daily meals (Strauss et al., 2016). However, fish bones have also been found on the site (Villagran et al., 2017), revealing a broad dietary spectrum.

3.2.2 TEST 1: Experiments on gloves

Leaching experiments

Following the work by Garçon et al. (2017), we selected gloves that are commonly used in our laboratories (**Table 1**) and that had not been tested yet as sources of zinc contamination. The experiments were conducted in the Pico Trace clean lab at the Department of Human Evolution, Max Planck Institute for Evolutionary Anthropology in Leipzig, Germany. The acids used in the experiments were ultrapure, certified to contain less than 100 ppt of zinc. The resin was rinsed ten times with HNO_3 0.5 N, and the column steps included additional cleaning steps. All the lab consumables used for sample preparation and analyses were soaked 48 h in HCl 2 N. We used four different setups (**Figure 5**) to test the contamination issues. In order to avoid the sampling of their inner coating, the gloves were first tied with a knot (TESTS 1A and 1B). This, of course, does not apply to TESTS 1C and 1D, where the fingertips of the gloves were soaked. For TEST 1A, the complete gloves were soaked for 40 h in 100 ml of a solution of HNO_3 0.5 N in glass beakers (400 ml) first autoclaved and cleaned with Milli-Q water. The beakers were covered with parafilm and placed under a fume hood with laminar flow and extraction for the time of the experiment to avoid any external contamination. Duplicates were run in 200 ml of solution in 800 ml glass beakers. Then 10 ml of solution was sampled, placed in a Teflon beaker, and dried overnight. The residue was then digested in 1.5 N HBr and purified using the protocol described in Jaouen et al. (2016a) adapted from Moynier et al. (2006). Zinc isotope ratios and concentration were then directly measured on the Neptune MC-ICP-MS at the Max Planck Institute for Evolutionary Anthropology. For TEST 1B, a double-distilled water solution was used instead of the HNO_3 0.5 N. For TEST 1C, the fingertips (a circle of about 1 cm of diameter) of the gloves were cut using ceramic scissors and placed in beakers containing HNO_3 0.5 N for 15 min. For TEST 1D, the setup is that

of the TEST 1C but with a solution sampled after 40 h instead of 15 min. Ten ml of solution were first sampled, and a second sampling was performed 40 h later. The samples were then dried down on a hot plate, purified, and analyzed following the protocol described for TEST 1A. To test the reproducibility of the results, TEST 1A was repeated for the nitrile gloves, 1B for the latex gloves (coated), and 1C for the nitrile and latex gloves (textured). For those duplicate analyses, the samples were prepared in the laboratories of Leipzig but analyzed with a Neptune Plus at the Géosciences Environnement Toulouse department from the Observatoire Midi Pyrénées, France.

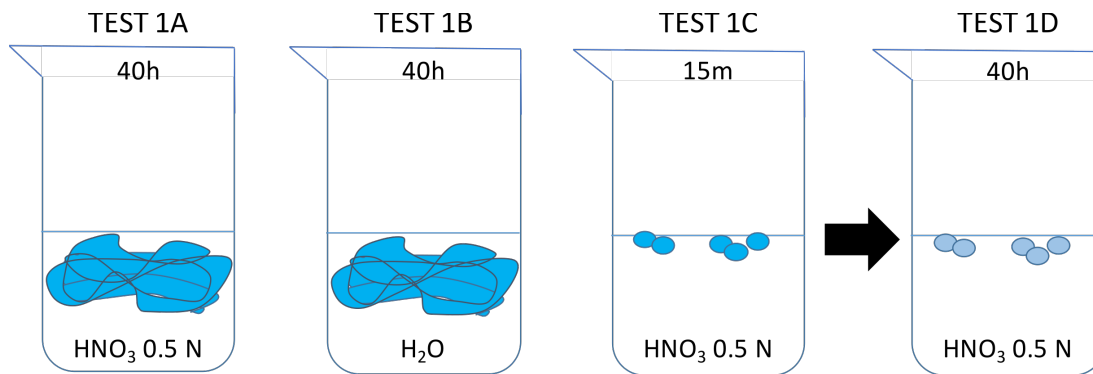


Figure 5. Schematic setup of the different leaching tests of gloves in acidic and aqueous solution. See text for more details.

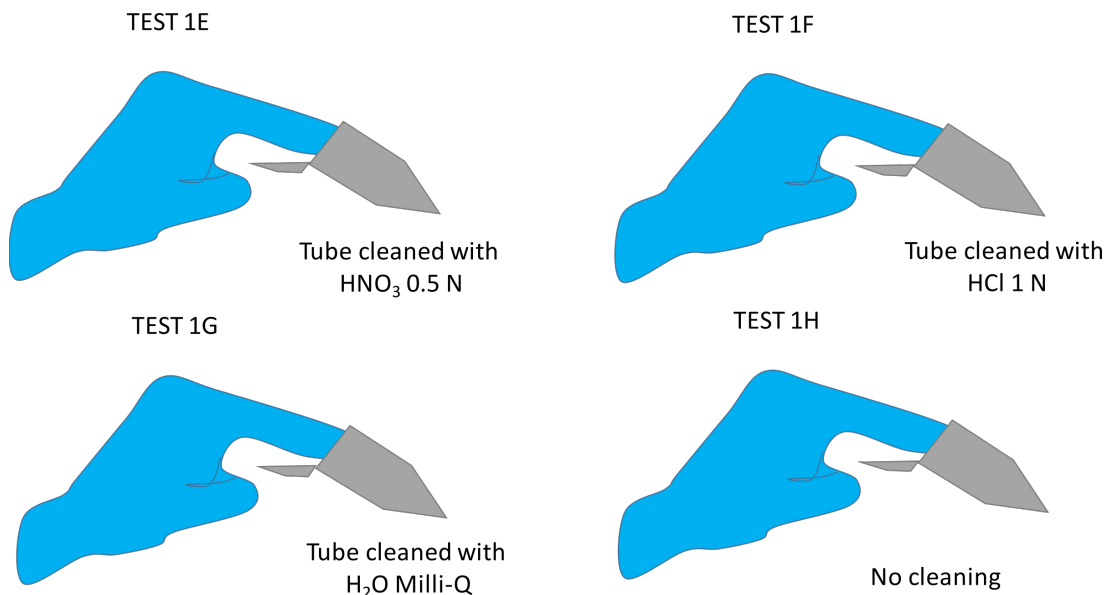


Figure 6. Schematic setup of the different dry contact tests with gloves and tubes cleaned in acidic and aqueous solutions. See text for more details.

Dry contact with tubes

Following the example of Garçon et al. (2017) again, we proceeded to a second glove contamination test in the context of dry contact with tubes. For this experiment, 5 ml-

Eppendorf tubes were cleaned with HNO₃ 0.5 N (TEST 1E), HCl 1 N—commonly used for labware cleaning—(TEST 1F), Milli-Q water (TEST 1G) or not cleaned at all (TEST 1H, **Figure 6**). The tubes cleaned with acids (TESTS E and F) were then soaked into water for one night, and all the tubes were dried under a fume hood. The experimenter then used the gloves listed in **Table 1**, introduced a finger for one second against the tube walls with a slight spin move, removed the finger, and then added 1 ml of Milli-Q water. The tube was then shaken so that the liquid came in contact with the whole surface of the tube walls, the solution was transferred to a clean Savillex, and the concentration was finally measured using the protocol described by Jaouen et al. (2016b).

3.2.3 TEST 2: Experiment sample contamination using different types of gloves

Twenty-six archeological human teeth (*SI Appendix, Table S18*) from 18 individuals of Lapa do Santo (Brazil) were sampled following our regular sampling technique using nitrile gloves (TEST 2A, $n = 26$), latex gloves (TEST 2B, $n = 26$) and no gloves at all (TEST 2C, $n = 6$). For this sampling technique, the enamel surface is first cleaned mechanically using a diamond-tipped burr before the chunk sampling (about 2 to 3 mm large and long). A microsaw is then used to sample a chunk of the tooth crown, from which the last traces of dentin are removed using a cleaned diamond-tipped burr so as to only keep the enamel. All the teeth were sampled for TEST 2A and TEST 2B, but unfortunately, only six teeth had enough material for further sampling for TEST 2C. The teeth were cleaned in Milli-Q water in glass beakers and put in an ultrasound bath for 15 min in order to remove the potential contaminants from the surface between each different test. In the case of TEST 2C, enamel powder was sampled rather than a chunk of tooth tissues to prevent the experimenters from injuring themselves while manipulating the microsaw on such a small object. Prior to zinc isotope analyses, the zinc from the gloves and the teeth was extracted and purified using the protocol described by Jaouen et al. (2016a) adapted from Moynier et al. (2006). The isotope analyses were all conducted using a Neptune MC-ICP-MS at the Department of Human Evolution, Max Planck Institute for Evolutionary Anthropology in Leipzig, Germany. It is worth noting that for the teeth prepared with nitrile gloves, isotope compositions were analyzed at the LGPTE of the Ecole Normale Supérieure of Lyon, France, with a Nu-500 MC-ICP-MS, and duplicates were run using the Neptune Plus at the Géosciences Environnement Toulouse department from the Observatoire Midi

Pyénées, France. For each batch, the in-house standard AZE and the reference material SRM 1400 were run for inter-lab and inter-batch comparison (*SI Appendix, Table S16*).

3.2.4 TEST 3: Post hoc assessment of contamination during sample preparation using linear mixed model

The linear mixed model (LMM) was performed using the statistical program R (version 3.6.1) (R Core Team, 2018). In order to test the hypothetic predictors associated with zinc isotope variability, the model was fitted (Baayen, 2008) with a Gaussian error structure and identity link (McCullagh and Nelder, 1989) using the R-package “lme4” (version 1.1–17) (Bates et al., 2015). The tested predictors were: the type of gloves (only nitrile and latex, samples obtained without gloves were excluded ($n = 6$) to ensure the model stability), $^{87}\text{Sr}/^{86}\text{Sr}$ isotope ratios-as a proxy for the geology-, the amount of zinc loaded on the column (ALC), the formation time of the tooth (group A: teeth formed before weaning, group B: teeth formed after weaning). All quantitative predictors were inspected for whether they were symmetrically distributed. They were also z-transformed to ease the model convergence (to a mean of zero and a standard deviation of one). In order to keep Type I error rate at the nominal level of 0.05, a random slope of ALC was included (Schielzeth and Forstmeier, 2009; Barr et al., 2013). We checked if residuals were normally distributed and homogeneous using a QQ plot (residuals plotted against fitted values) (Field, 2005). The model was tested on 52 teeth, coming from 18 individuals, and handled with two types of gloves.

3.3 Results

All zinc isotope results and concentrations obtained in this study are available in *SI Appendix, Tables S16-S19*. The column zinc blanks for all the tests were found to range from 2 to 5 ng. The standards (in-house AZE and NIST SRM 1400) gave results consistent with the values previously published, but we noticed that the AZE samples prepared with nitrile gloves for the clean lab step gave lower results than the ones prepared with latex gloves (*SI Appendix, Table S17*; Jaouen et al., 2016a, 2016b, 2018). All samples but one showed mass-dependent fractionation for $\delta^{66}\text{Zn}$, $\delta^{67}\text{Zn}$, and $\delta^{68}\text{Zn}$. The SRM 1400 standard gave consistent results in the three different

laboratories where it has been measured with three different MC-ICPMS (Neptune, Department of Human Evolution/ MPI-EVA, Leipzig; Nu 500 LGTPE/ ENS Lyon, Lyon; Neptune Plus, GET/OMP, Toulouse).

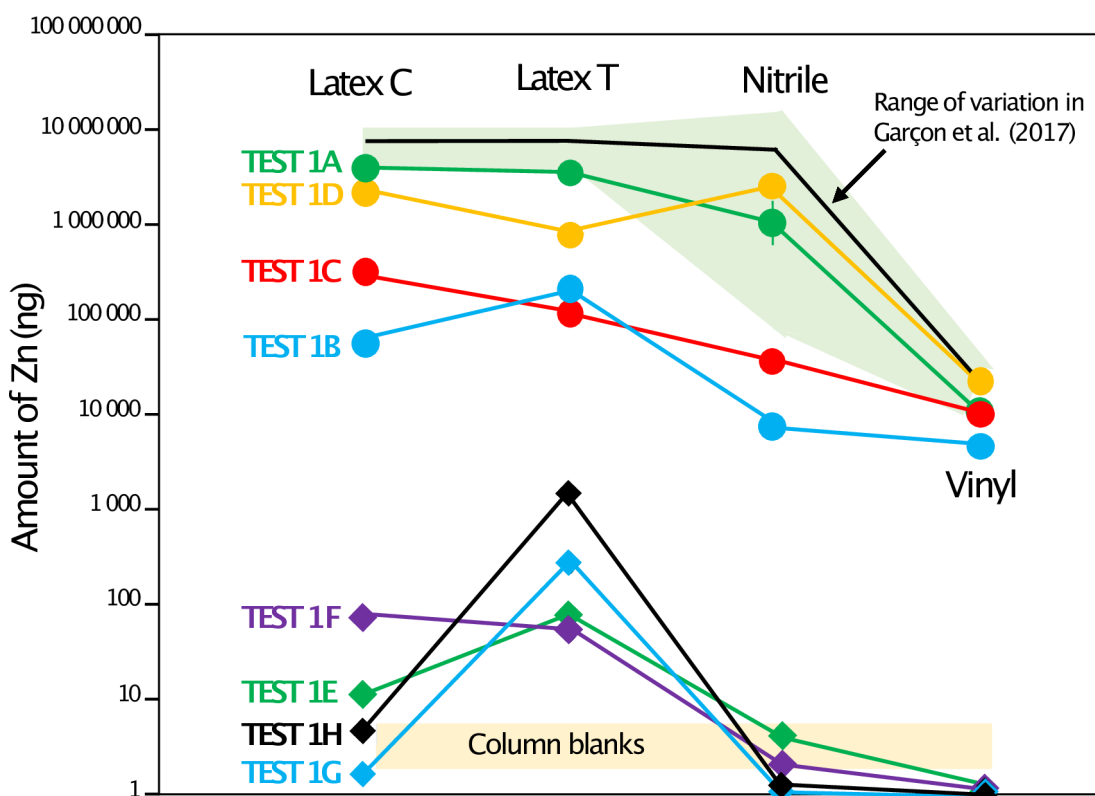


Figure 7. Amount of zinc obtained for each test and each type of gloves following the protocol described in **Figure 5** and the corresponding text. “Latex C” corresponds to the coated latex gloves and “Latex T” to the textured latex gloves.

3.3.1 TEST 1: Experiments on gloves

The amount of zinc released by the gloves following the tests by Garçon et al. (2017) corresponds to the range reported by these authors (Nitrile and latex gloves release several grams, vinyl gloves about 50 mg, TEST 1A, **Figure 7**). Compared to the column blanks associated with TEST 1 (2–3 ng), those amounts are enormous. The duplicates, ran in a different solution volume, released similar amounts of zinc (**SI Appendix, Table S17**). Because of the high matrix content of the samples, a column purification was performed prior to zinc isotope analyses of the glove test samples.

The isotope ratios for the nitrile gloves were found to be the lowest values reported for any type of gloves (**Figure 8**). The isotope results were exactly the same for 3 of the 4 duplicates, the last one being shifted by 0.2 ‰ (**Figure 8; SI Appendix, Table S17**). The tests on the fingertips (TEST 1C and 1D) reveal that 14% and 50% of the zinc accumulated over 40 h is released respectively from the latex (coated or textured) and

vinyl gloves in the first 15 min, while only 1% of the total amount of zinc recovered in 40 h from the nitrile gloves is released during this period.

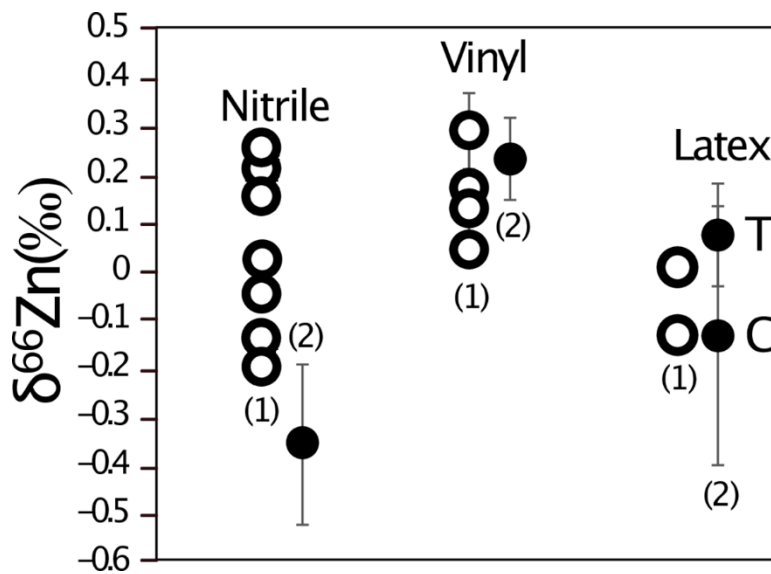


Figure 8. Zinc isotope composition of the gloves from (1) Garçon et al. (2017) (open circles) and (2) this study (filled circles). For this study, the symbols represent the average value for the four tests and the whiskers correspond to the standard deviation. T stands for textured, C for coated.

The amount of zinc released by the fingertips (TEST 1D) of the nitrile and latex gloves was comparable to the amount released by the whole gloves (TEST 1A, **Figure 5**). The latex gloves released the same amount in TEST 1A, while the fingertip tests (TESTS 1C and 1D) showed slightly higher amounts for the gloves with inner coating. This can be explained by a higher zinc content of this coating in comparison to the textured gloves since the coating was only exposed to the solution in TESTS 1C and 1D. TEST 1B shows that a small portion of zinc is released by the gloves when they are soaked into water (more than two orders of magnitude lower for the latex gloves).

As mentioned above, the column blanks are 2 to 3 ng. The blanks coming from the solutions in the glass beakers without gloves that were sampled (10 ml), evaporated, and purified on the columns like the actual samples (**Figure 5**) were also 3 ng, with the exception of two of them (100 ng). We assume that the contamination comes from the glass beakers, even though they were rinsed with Milli-Q water. The beakers were stored outside of the clean lab, used by experimenters working with nitrile gloves, and were possibly cleaned at different instances using an autoclave. The $\delta^{66}\text{Zn}$ values of the different tests show substantial variation, but there is no correlation between concentration and isotope ratios. There is also no systematic difference between the ratios measured in the TESTS 1D and 1C, which argues for the absence of kinetic zinc isotope fractionation. However, we noticed that the $\delta^{66}\text{Zn}$ values observed in TEST 1B are systematically lower than in the other tests (**Figure 9**).

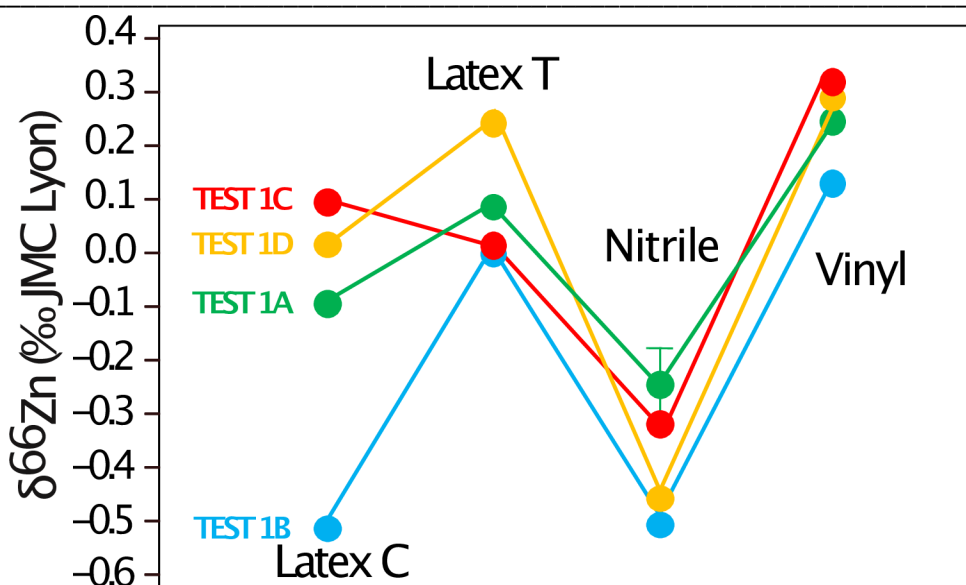


Figure 9. Zinc isotope ratios measured for the four types of gloves tested in this study. C stands for coated, T for textured. The description of the tests is provided in the text and **Figure 5**.

TESTS 1E, 1F, 1H, and 1G show similar amounts of zinc released from the gloves than those of TEST B from Garçon et al. (2017), except for the latex textured gloves that we tested, which release substantially more zinc during a one-second dry contact. Surprisingly, those gloves also released more zinc when the tubes were not cleaned with acids, in contrast to all the other gloves, which had the highest content in the tubes formerly cleaned with HNO₃ and HCl.

3.3.2 TEST 2: Experiment sample contamination using different types of gloves

For the 26 Lapa do Santo teeth sampled, 62% gave identical results in TESTS 2A and 2B. For the remaining 10 teeth, four showed higher zinc isotope ratio values when sampled using latex gloves, and six of them had higher values when sampled with nitrile gloves (**Figure 10**). TEST 2C only consists of six teeth sampled without using gloves. Among them, three showed values identical to those sampled with nitrile and latex gloves (**Figures 10 and 11**), and two had slightly lower values (0.1 to 0.2 ‰) than those sampled with latex and nitrile gloves, which were identical. The last sampled tooth showed a higher result in TEST 2B than in TEST 2A, whereas the value in TEST 2C was similar to that in TEST 2B.

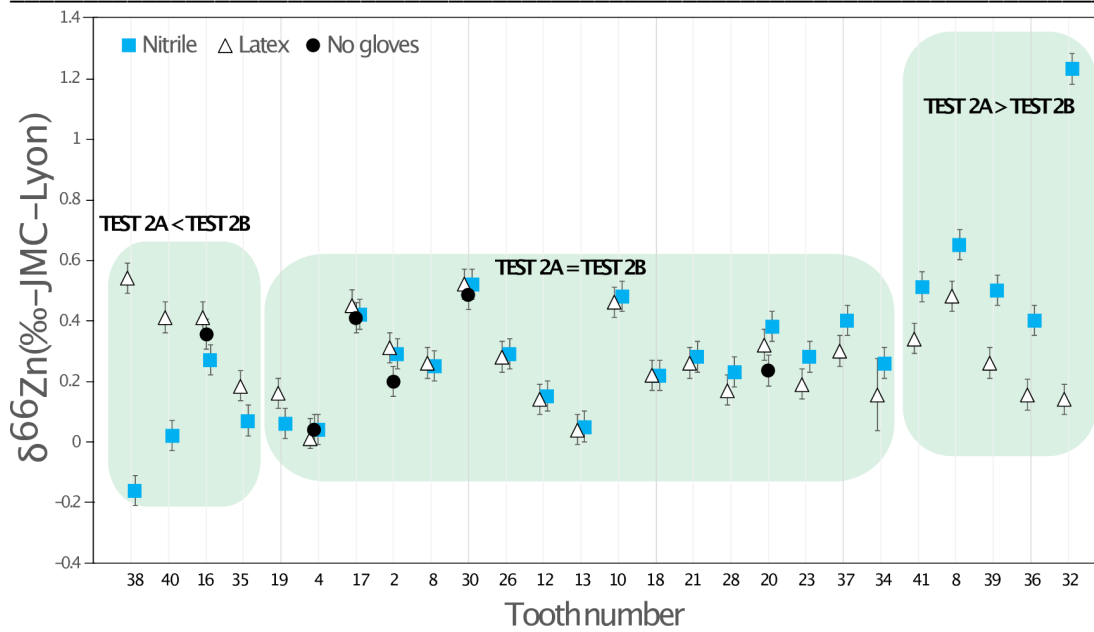


Figure 10. Zinc isotope ratios for each Lapa do Santo tooth sampled either with nitrile gloves (TEST 2A), latex gloves (TEST 2B), or without gloves (TEST 2C). The numbers on the x-axis correspond to the tooth specimen ID (see *SI Appendix, Table S18*), to note that several teeth may belong to the same individual. Typical analytical error for zinc isotope ratios is 0.05 ‰ to 0.08 ‰ (2σ), and the standard deviation of the different standards (AZE and SRM 1400) run on the columns ranges from 0.08 to 0.1 ‰ (2σ).

We observe no correlation between zinc concentrations and isotope ratios (**Figure 12**). This was also observed for the additional teeth from the Jacobins convent (Rennes, France), which are described in *SI Appendix, Supplementary Information 2.3*. There are two outliers, one with a very positive $\delta^{66}\text{Zn}$ value and another one with a low $\delta^{66}\text{Zn}$, which was sampled with nitrile gloves. The latter one is also the only sample showing mass-independent fractionation (see arrows on **Figure 12**), which is generally caused by isobaric interferences. This can happen when too much matrix is present in the solution knowing that the gloves release many other elements than just zinc (2017). The two outliers also have drastically different $\delta^{66}\text{Zn}$ values and zinc concentrations compared to the two samples extracted from the same teeth and prepared with nitrile and latex gloves (**Figure 13**).

In Lapa do Santo, no differences in $\delta^{66}\text{Zn}$ were observed between individuals identified as men or women (Kruskal-Wallis $\chi^2 = 0.3229$, $df = 1$, p -value = 0.57). The carbon, nitrogen, and strontium isotope data also did not reveal differences between sexes (Strauss et al., 2015, 2016). Interestingly, the type of tooth is strongly associated to specific $\delta^{66}\text{Zn}$ values

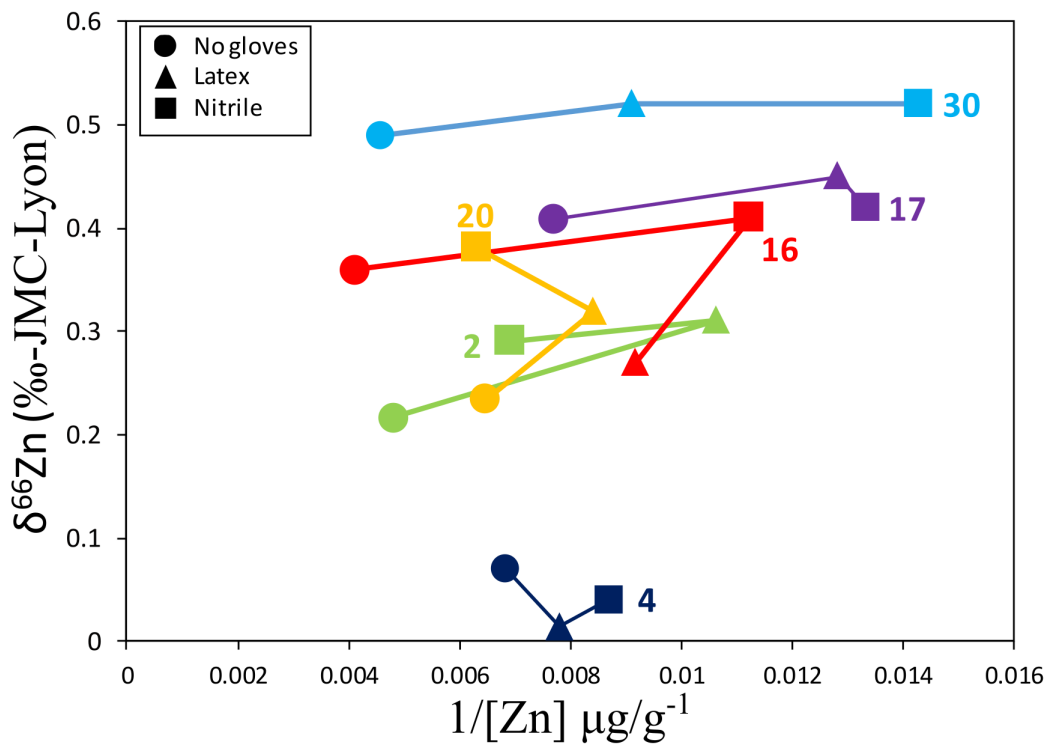


Figure 11. Relationship between zinc concentrations ($\mu\text{g/g}$) and isotope values for the six teeth on which all three TESTS 2 A, B, and C have been performed. The numbers 2 to 30 corresponds to the identification number of the teeth, which are also given in *SI Appendix, Table S18*.

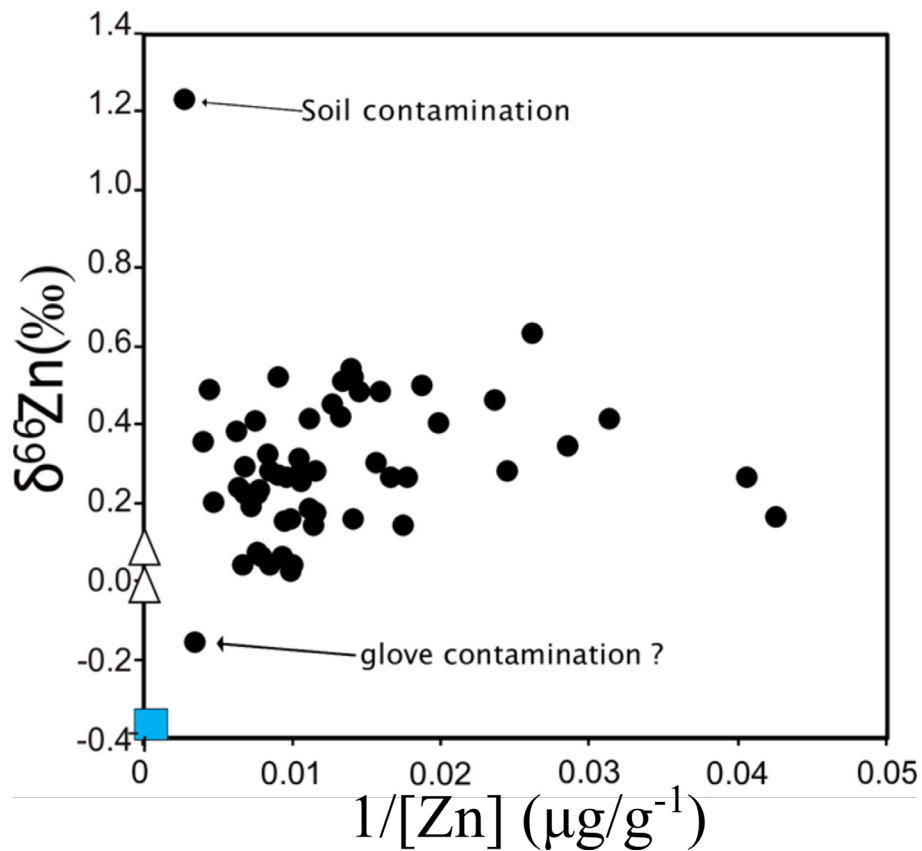


Figure 12. Relationship between zinc concentrations ($\mu\text{g/g}$) and $\delta^{66}\text{Zn}$ values for the Lapa do Santo teeth (black circles). All samples are plotted together, independently from the sampling method used. The blue square represents the nitrile gloves, and the empty triangles are the latex gloves.

(Kruskal-Wallis $\chi^2 = 28.32$, $df = 6$, $p\text{-value} = 0.000082$, all measurements taken together; $n = 77$ and Kruskal-Wallis $\chi^2 = 14.98$, $df = 6$, $p\text{-value} = 0.02$, average value per tooth, $n = 26$). This trend is even more significant (Kruskal-Wallis $\chi^2 = 27.35$, $df = 3$, $p\text{-value} = 0.0000050$, all measurements together, $n = 77$) when the teeth are grouped by formation periods, which are themselves related to dietary transitions in childhood (deciduous molars: placental and exclusive breastfeeding; permanent first molars (M1): breastfeeding, with and without solid food; permanent first premolars (P3): weaning and post-weaning diet; second premolars, permanent second and third molars (P4, M2, M3): post-weaning diet).

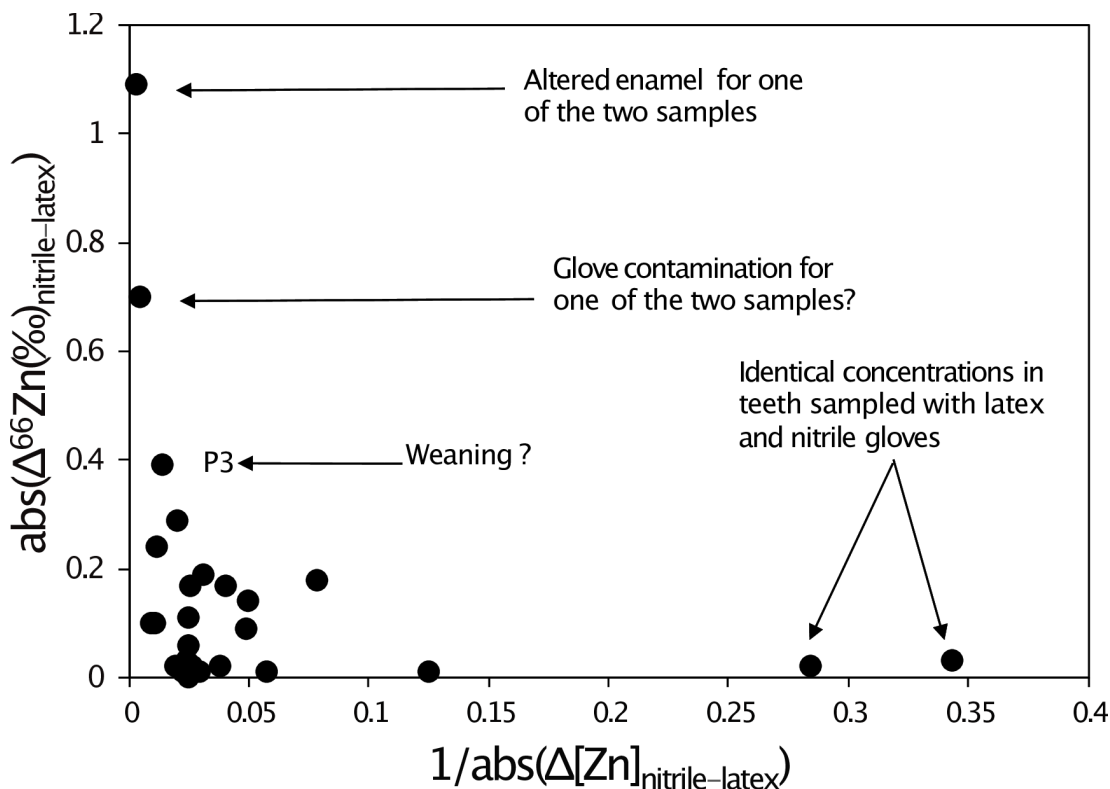


Figure 13. Correlation between the difference of concentration and the difference of $\delta^{66}\text{Zn}$ values of tooth samples from Lapa do Santo prepared with nitrile or latex gloves. P3 = first premolar. The typical analytical error for zinc isotope ratios ranges from 0.05 to 0.08 ‰ (2σ), and the standard deviation of the different standards (AZE and SRM 1400) run on the columns are 0.08 to 0.1 ‰ (2σ).

3.3.3 TEST 3: Post hoc assessment of contamination during sample preparation using linear mixed model

The full-null linear mixed model comparison was significant (likelihood ratio test: $\chi^2 = 10.62$, $df = 8$, $p\text{-value} = 4.95 \cdot 10^{-3}$) and allowed to assess which of the tested predictors were associated with variations in $\delta^{66}\text{Zn}$ values. The tooth formation time (i.e., in utero and before weaning vs. post-weaning) and the strontium isotope ratios showed a significant relation with $\delta^{66}\text{Zn}$ values (likelihood ratio test $p\text{-values}$ equal to

0.002 and 0.039, respectively). The ALC and the type of gloves used for sampling appeared to have no significant relation with the variability of the $\delta^{66}\text{Zn}$ values (likelihood ratio test p-values equal to 0.158 and 0.482, respectively).

3.4 Discussion

3.4.1 Zinc contamination during sample preparation in the clean lab

Our study confirms the strong risk of zinc contamination from nitrile and latex gloves, especially when working with acids. Vinyl gloves release a smaller amount of zinc (two orders of magnitude) during acid exposure than the two other types of gloves (nitrile and latex). Nitrile gloves release zinc that is depleted in heavy isotopes compared to the other brands of nitrile gloves studied by Garçon et al. (2017) (**Figure 8**). The four types of gloves release similar amounts of zinc in comparison to the study of Garçon et al. (2017) (**Figure 7**). This suggests that the conclusions of the two other experiments (TEST 2 and TEST 3) conducted on different types of gloves of the Rotiprotect brand can be of interest to users of other brands.

We recommend that when working with acids and wearing gloves made of latex, nitrile, or neoprene, the experimenters should wear a second pair of gloves on top made of vinyl to lower the risk of zinc contamination. Some laboratories also adopt the strategy to wash the gloves with water prior to zinc purification in the laboratory. However, our tests show that a limited amount of zinc is released in water.

As mentioned by Garçon et al. (2017), the best strategy is to avoid any contact between the gloves and the cleaning solutions for the beakers, the pipette tips, or any labware that comes in contact with the samples. This strategy has proved to be efficient in our clean lab, where the blanks are usually around 2 ng and never exceed 10 ng, since we have become aware of the contamination risk by gloves. We also noticed a small change of the $\delta^{66}\text{Zn}$ value of our inhouse zinc isotope standard and an improvement of the standard deviation around this value (*SI Appendix, Table S16*). This could be related to the reduction of potentially glove-derived zinc contamination (now measured around 1.59 ‰ instead of 1.51 ‰, see Bourgon et al. (2020) and Jaouen et al. (2016a)). We estimated that contamination of 50 ng in the clean lab and 10 ng during the sample dilution prior to zinc isotope analyses would trigger a shift of about -0.1 ‰ for this in-house standard. We observed consistent values between the two above-mentioned publications for the SRM 1400 ($\delta^{66}\text{Zn} = 1$ ‰; *SI Appendix, Table*

S16), but this standard contains more zinc (181 $\mu\text{g/g}$) than the in-house AZE (about 140 $\mu\text{g/g}$).

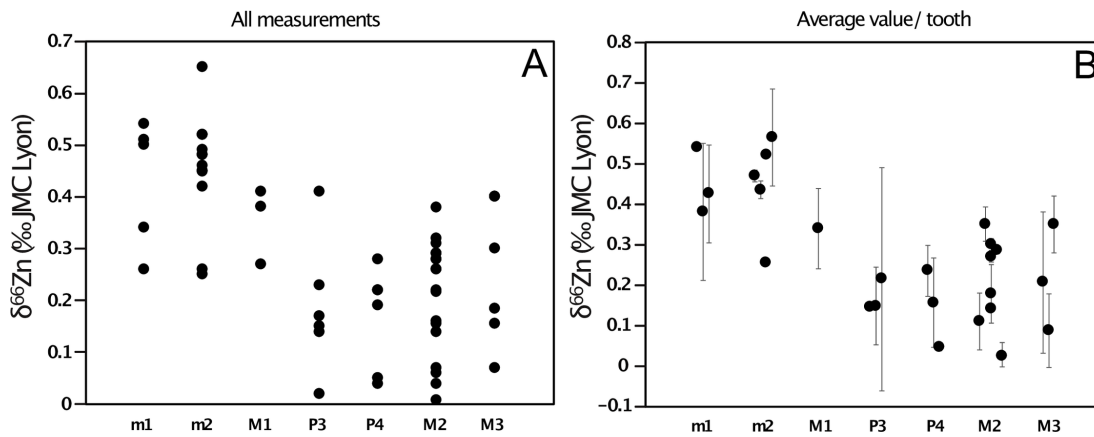


Figure 14. Zinc isotope values in teeth of the Lapa do Santo population. Tooth types are ordered from the earliest to the latest crown initiation and formation times: from in utero (deciduous molars) to puberty (permanent third molar). A) All single measurements pooled together (sample preparation with gloves nitrile or latex- or without), B) average $\delta^{66}\text{Zn}$ value per dental specimen. The error bars represent the variation within a tooth (1σ).

3.4.2 Zinc contamination during the enamel sampling procedure

Most of the teeth sampled with two different types of gloves showed identical $\delta^{66}\text{Zn}$ values in the analyzed enamel samples, whereas nitrile and latex gloves used for these experiments had very different $\delta^{66}\text{Zn}$ values. The multiple samples taken from a single tooth do not represent a homogenized powder but were rather taken from different parts of the tooth crown, thus corresponding to different times of enamel formation and thus potentially reflecting differences in diet-related $\delta^{66}\text{Zn}$ values. For the tooth samples showing different $\delta^{66}\text{Zn}$ values, no systematic trend towards more positive or negative values could be observed using one or another type of gloves or no gloves at all (**Figure 10**). The LMM results confirm the lack of influence of the glove type used for sampling on the zinc isotopic variability. This could result from the release of zinc mostly occurring in an acidic environment (see results from the TESTS 1 A to H). It appears that the teeth showing the maximum variation in $\delta^{66}\text{Zn}$ values form their enamel during major periods of dietary transition in human life history, which are birth and weaning (**Figure 14B**). The LMM also demonstrated that the $\delta^{66}\text{Zn}$ values are linked to the formation time of the tooth. Diet is usually known to be the main source of zinc isotope variations in human teeth (Jaouen et al., 2016a, 2016b, 2018). Strontium isotope ratios are related to the bioavailable strontium from the local bedrock substrate and therefore reflect the geographical origin of the studied individuals. In Lapa do Santo, these strontium isotope ratios were also found to correlate with $\delta^{66}\text{Zn}$ values, which was already highlighted for well-preserved fossil

mammal teeth by Bourgon et al. (2020) using a similar LMM. This means that, although zinc is mainly influenced by diet, the geology of the area where the food products come from can also influence, to a certain degree, the zinc isotope ratios recorded in teeth. This is expected since marine limestones, and some siliceous sediments show much higher $\delta^{66}\text{Zn}$ than other types of rocks (Moynier et al., 2017). Although both studies revealed the relationship between strontium and zinc isotope ratios, a potential bias in the Lapa do Santo teeth relates to the fact that the previously published strontium isotope ratios (Strauss et al., 2016) were obtained from teeth that may differ from those used in the present study. When multiple samples coming from different teeth or within a tooth of the same individuals were analyzed for zinc, a unique strontium isotope ratio was associated. Even if a potential bias exists for the relationship between strontium and zinc isotope data, the variation observed between the two or three sampling tests (**Figure 11**) is therefore biogenic and not due to contamination, with one possible exception (**Figure 10**). Contamination-related zinc isotopic shifts are often accompanied by a change of zinc concentration (**Figure 12**).

In summary, the teeth showing the largest isotopic variations may involve 1) soil contamination ($\delta^{66}\text{Zn} = 1.23 \text{ ‰}$, **Figures 10, 12 and 13**); 2) an analytical problem or glove contamination resulting in samples showing mass-independent fractionation ($\delta^{66}\text{Zn} = -0.16 \text{ ‰}$, **Figures 12 and 13**); 3) enamel forming during dietary transition periods. For this latter category, the maximal variation did not exceed 0.4 ‰ , which may reflect a dietary shift by one trophic level (Jaouen et al., 2016b, 2018; Bourgon et al., 2020).

3.4.3 Life history and dietary effects on human enamel $\delta^{66}\text{Zn}$ values

The zinc isotope composition of archeological teeth, when not impacted by glove contamination during sampling, is strongly related to the developmental times at which enamel starts forming. Little is known about zinc metabolism and absorption mechanisms during lifetime dietary transitions. Zinc absorption is not solely related to zinc intake (Dolphin and Goodman, 2009). Phytates contained in plants— especially in cereals—constitute inhibitors to zinc absorption. However, infants whose mothers feed on a cereal-based diet show higher Zn/Ca ratios in their prenatal enamel (i.e., formed in utero) than other infants (Dolphin and Goodman, 2009). This can be explained by the fact that during pregnancy, women having the lowest daily zinc intake also have the highest rate of zinc absorption (Fung et al., 1997). This regulation stops

during lactation. In another study, Donangelo et al. (2005) not only confirmed that the types of diet with a high amount of phytates were correlated with higher zinc absorption rates during pregnancy, but they also observed the effect during lactation. Zinc absorption among pregnant women remains generally higher than in non-pregnant and non-lactating women (Hambidge et al., 2006; Donangelo and King, 2012). Interestingly, however, Zn/Ca measured in modern populations from Mexico have been shown to be higher and more variable in enamel formed postnatally than prenatally (Dolphin et al., 2005; Garçon et al., 2017). Infants that are breastfed show a zinc absorption of around 41% (Sandström et al., 1983), while it does not exceed 30% in pregnant women (Fung et al., 1997), which might explain this observed difference. Zinc concentration has also been shown not to be a reliable trophic level indicator (Dolphin and Goodman, 2009) as opposed to zinc isotope ratios (Jaouen et al., 2016a, 2016b; Bourgon et al., 2020). Prior to the present study, no work has addressed the question of zinc isotope fractionation in enamel formed in utero and during breastfeeding.

For the Lapa do Santo site, we had access to seven tooth types. Two of them—deciduous first and second molars (m1 and m2, respectively)—had crowns partially formed in utero and during the first months of life (**Figure 14**; AlQahtani et al., 2010). The permanent first molars (M1) form their crown during the first three years of life, and therefore likely record the isotope signature associated not only with breastfeeding but also with the introduction of solid food in the infant's diet. The crown of the first premolar (P3) initiates around 1.5 years of age when most hunter-gatherer infants still breastfeed (Feitosa et al., 2010; Horta et al., 2013; Veile and Kramer, 2015; Stuart-Macadam and Dettwyler, 2017), although solid food has already largely been introduced in their diet. Zinc absorption in infants feeding on mother milk is also much higher (around 40%) than that of individuals with an omnivorous diet (around 24%, Sandström et al., 1983; Wessells and Brown, 2012) because zinc absorption is inhibited by phytates contained in plants, notably in high amounts in cereals (Lönnerdal, 2000). Therefore, the isotope signature of zinc might be strongly influenced by the signature of human milk even after the introduction of solid food. The second premolar (P4) crown starts forming two years after birth (AlQahtani et al., 2010) therefore recording a diet exclusively or mainly based on solid food. The second and third permanent molars (M2 and M3) are formed after weaning. When teeth are ranked depending on their time of initiation and formation, a trend in enamel $\delta^{66}\text{Zn}$ values can be seen, with the highest values in teeth initiating their enamel formation in utero and the lowest values in teeth formed after the weaning age (**Figure 14**).

In order to test the robustness of this ontogenetic trend, we decided to systematically analyze each tooth type from archeological remains of a child (estimated age at death: 5–9 years, see *SI Appendix, Supplementary Information 2.1*) and an adult. As it was not possible on the Lapa do Santo material, this was undertaken on two specimens belonging to a medieval population recovered at the Jacobin convent in Rennes, France. The diet of these individuals has already been extensively documented (Jaouen et al., 2018; Colleter et al., 2019). The procedure of this test is fully described in *SI Appendix, Supplementary Information 2.2*. Every tooth type analyzed from the two Les Jacobins individuals yielded a pattern very similar to that observed at the scale of the Lapa do Santo population (**Figure 15**). This test especially confirms that the teeth starting to form their crown around birth have the highest enamel zinc isotope ratios, while the post-weaning teeth show the lowest values. As expected, the M1 has intermediate isotope signatures, as its crown formation time ranges from in utero until ~3 years of age. The teeth sampled in Rennes allow to clearly confirm the trend observed (**Figures 15 and 16**).

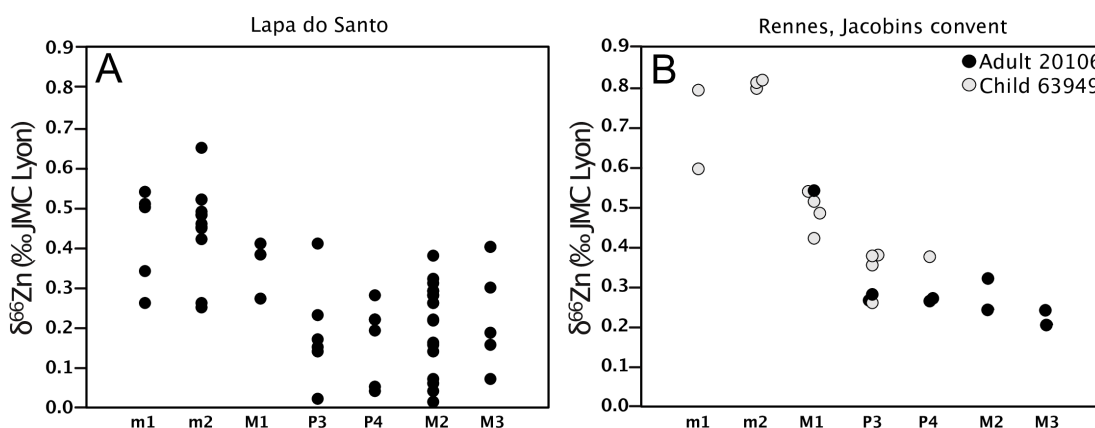


Figure 15. Zinc isotope values from the enamel of different tooth types at (A) Lapa do Santo (Brazil) and (B) Jacobins convent (Rennes, France). Note the trend of decreasing $\delta^{66}\text{Zn}$ values in enamel with increasing crown formation age for humans from both archeological sites.

For the Jacobin convent, we carefully documented the location of the sampling on the teeth, which allowed estimating the age of enamel formation for each sample (**Figure 15**; *SI Appendix, Table S19*, and **Figure S48**).

Many of the teeth presented in this study have formed their enamel during dietary transitions: milk teeth often record in utero and breastfeeding signatures. In some cases, they can even record a third dietary transition: the introduction of solid food. The M1 enamel also records successively: exclusive breastfeeding, breastfeeding in combination with solid food consumption, and to a lesser extent towards the end of the crown formation, post-weaning signatures.

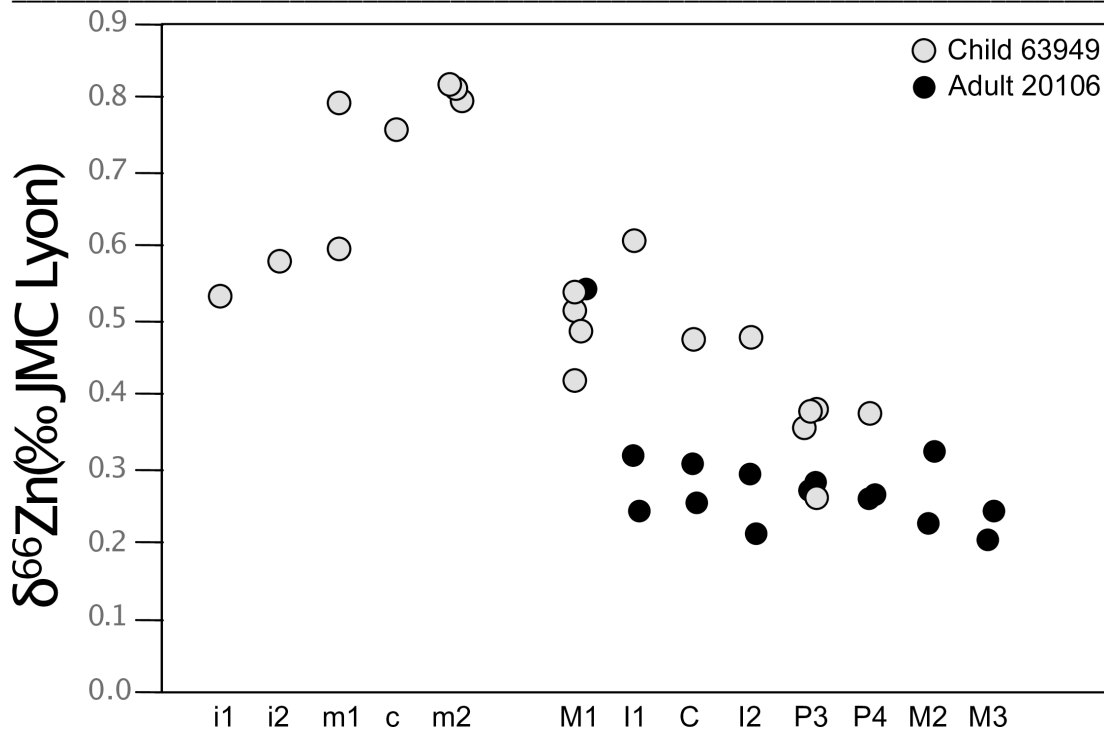


Figure 16. Zinc isotope compositions of all the tooth types sampled for two individuals of the Jacobins convent. The teeth are ranked from the earliest forming enamel to the latest forming crowns.

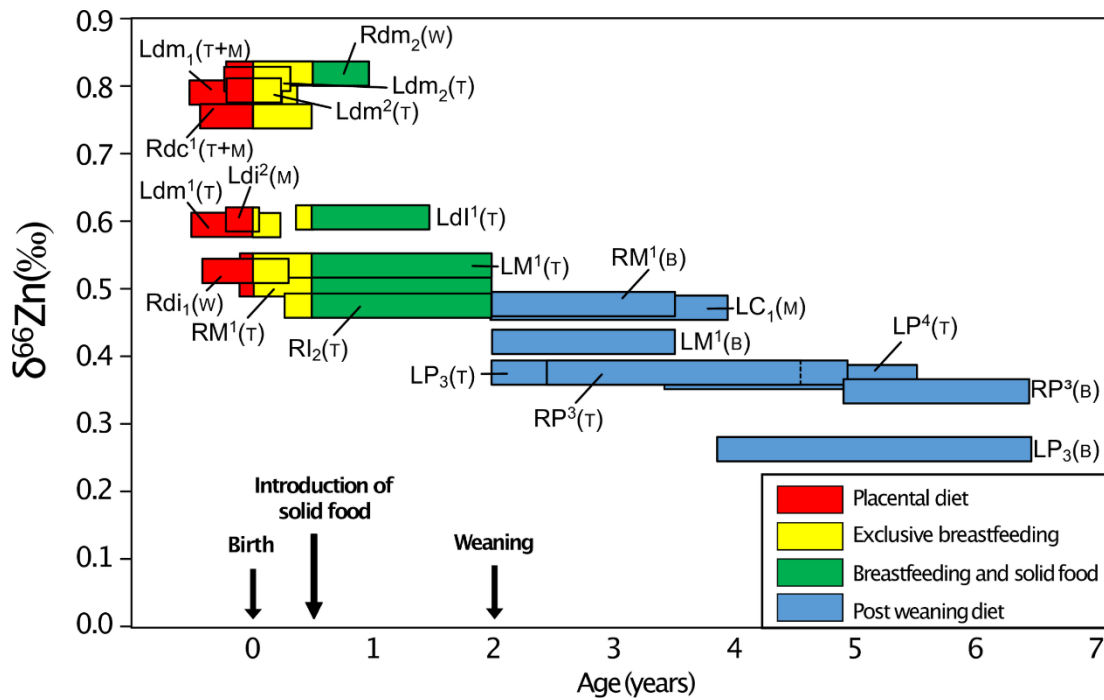


Figure 17. Zinc isotope ratios in the different teeth of Child 63949, recovered from the Jacobin convent (Rennes, France), with the corresponding formation ages of the areas of enamel sampled (*SI Appendix, Table S19*) (AlQahtani et al., 2010). Different parts of the tooth crowns were sampled: top (T); middle (M); bottom (B); whole height (W). The age at introduction of solid food and weaning is here fully hypothetical (i.e., there is no archeological record for this specimen) but is based on nitrogen isotope data measured in the tooth roots as well as historical data on the population (*SI Appendix, Supplementary Information 2.1 and 2.3*). Because the actual weaning age could be slightly younger or older, it is provided only for illustrative purposes.

Therefore, it remains difficult to identify with certainty which $\delta^{66}\text{Zn}$ values can be associated with dental enamel formed in utero, during the exclusive breastfeeding period, or when solid food is present in the diet. From the trend seen in **Figure 16**, we can suggest the two scenarios (**Figure 18**), described below, in order to explain what

causes zinc isotope variations between tooth types. Scenario 1 (S1): The lowest $\delta^{66}\text{Zn}$ values observed in the deciduous m1 could correspond to in utero life, while the highest values observed in all studied deciduous m1 and m2 would result from exclusive breastfeeding. Indeed, all m2 show higher $\delta^{66}\text{Zn}$ values than m1, after which they shortly started forming. The permanent M1, formed during the first three years after birth, would record a mixed signature of breastfeeding and solid food consumption. The P3, P4, M2, and M3 then record post-weaning $\delta^{66}\text{Zn}$ values. Scenario 2 (S2): The dental enamel formed in utero records the highest ratios, while post-weaning formed enamel shows the lowest. The mother milk would then have intermediate zinc isotope ratios between blood (placental diet) and bulk diet (solid food). In both scenarios, the variation of $\delta^{66}\text{Zn}$ values over time could also be due to a differential fractionation related to the maturation of the intestinal tract.

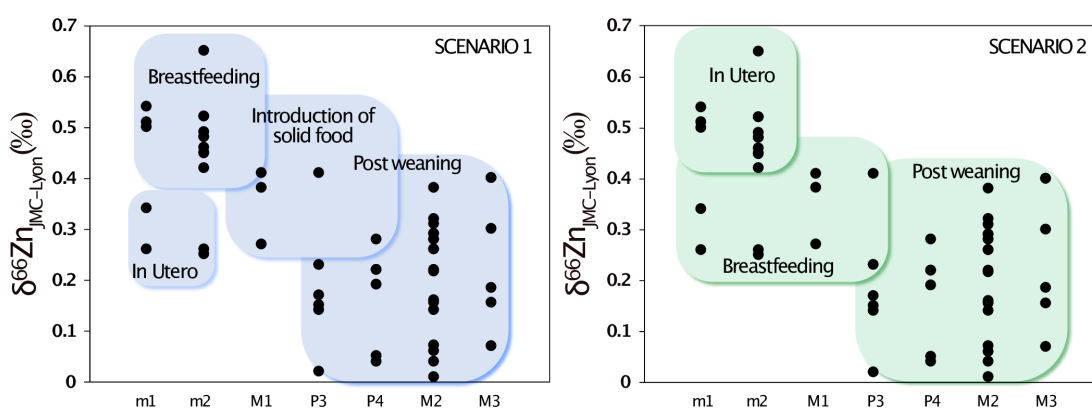


Figure 18. Possible scenarios for the evolution of enamel $\delta^{66}\text{Zn}$ values in teeth during childhood.

For the juvenile individual 63949 (Jacobin convent), the two deciduous m1 were sampled at the cusp tip of the crown to note that the sample of lower m1 includes some enamel from the middle part of the crown (*SI Appendix, Table S19*). This could explain the isotope difference observed between the two teeth, provided that the upper m1 sample exhibits a lower $\delta^{66}\text{Zn}$ and contains more enamel formed in utero (**Figures 15-17**). Moreover, the deciduous central incisors, which mainly form their enamel in utero, show the lowest zinc isotope ratio among all deciduous teeth. This would lend support to Scenario 1. The differences observed between the child and the adult at the Jacobin convent may first be related to the fact that the top of the crown (cuspal enamel) was often sampled for the child, while enamel was more frequently sampled in the middle of the crown (lateral enamel) for the adult. This means that the child's samples contain material from earlier stages of enamel formation, while the adult's samples reflect enamel from a time period when the individual was still breastfed. It may also be that the adult individual 20106 was weaned before the child 63949, a

likely scenario considering their different socio-economical group (*SI Appendix, Supplementary Information 2.1*).

Does Scenario 1 fit with what could be expected from the isotope composition of the food products and animal tissues? In animals, a pilot study showed that dairy products tend to have higher $\delta^{66}\text{Zn}$ values than meat products (Costas-Rodríguez et al., 2014). However, those $\delta^{66}\text{Zn}$ values are even higher in plant products. One could consider that a diet in which plants are the main source of proteins, as hypothesized for the Lapa do Santo population (Strauss et al., 2016), should be associated with higher $\delta^{66}\text{Zn}$ values (Wessells and Brown, 2012; Jaouen et al., 2018). Nevertheless, most of the zinc in the diet comes from animal products (Jaouen et al., 2017), and the adult diet of the individuals from Lapa do Santo did contain meat, as attested by the abundant presence of burnt bones of small and middle-sized animals in the site (Strauss et al., 2016). Moreover, it is not entirely clear what was the dietary source of animal protein in the Lapa do Santo population. On the one hand, carbon and nitrogen isotopic data indicate a low position in the trophic chain. On the other hand, there were abundant middle- and small-sized burnt bones of mammals like rodents, deer, peccary, and armadillo at the site, along with bone remains of reptiles and marsupials as well as the abundant shell remains from terrestrial snails (Strauss et al., 2016). The $\delta^{66}\text{Zn}$ values of non-mammalian tetrapods are still unknown (Strauss et al., 2016). In addition, the $\delta^{66}\text{Zn}$ values of the fauna of Lapa do Santo have not been analyzed yet, so the comparison with other existing $\delta^{66}\text{Zn}$ values on humans from other locations cannot be made. Possible site-specific effects (Jaouen et al., 2017; Bourgon et al., 2020) could indeed induce variation in local zinc isotope compositions of the food webs. Therefore, it is possible that the post-weaning diet of the Lapa do Santo population is associated with lower $\delta^{66}\text{Zn}$ values than the breastfeeding one. In Scenarios 1 and 2, we thus hypothesized that mother milk is enriched in heavy zinc isotopes compared to the main sources of zinc in Lapa do Santo individuals' diets.

Considering the question of the differences between the enamel parts formed in utero or during the child's infancy, Scenario 2 (S2) suggests that in utero $\delta^{66}\text{Zn}$ values might be 0.3 ‰ above that of the permanent teeth, which would correspond, somehow, to one trophic level below the post-weaning diet (Jaouen et al., 2016a, 2016b; Bourgon et al., 2020). This could be explained by the placental diet based on the nutrients coming from the mother's blood, in a way similar to what happens with calcium isotopes (Tacail et al., 2017). Indeed, $\delta^{66}\text{Zn}$ in human blood is enriched by 0.4 ‰ compared to human or animal muscles (Albarède et al., 2011; Jaouen et al., 2019b),

which corresponds to the above-mentioned difference between P4, M2, and M3 and the parts of m1 and m2 enamel assumed to be formed in utero (S2). However, based on the Jacobin convent isotope data, Scenario 1 would be the most likely. A progressive maturation of the intestinal tract may be associated with a differential fractionation of zinc over time, in a similar way to what happens for strontium and calcium (Lough et al., 1963), which are not discriminated by children's intestinal tracts. More work is needed to better understand the zinc isotopic differences between human milk and food products, as well as the associated fauna of the Lapa do Santo individuals to better constrain diet-related factors controlling intra-population and intra-individual variability of tooth enamel $\delta^{66}\text{Zn}$ values. However, the similarity of the patterns observed in two very contrasting contexts (the Paleoamericans and hunter-gatherers of the tropical and prehistorical site of Lapa do Santo, Brazil, and the medieval urban Bretons of the temperate site of the Jacobin convent, Rennes, France) is striking.

3.5 Conclusion

The release of zinc from different types of gloves into acidic solution confirms previous results and highlights the potential of zinc contamination during chemical sample treatment. Vinyl gloves showed the lowest contamination potential when quantifying zinc isotopic ratios, although they still release some zinc and are the less protective type of gloves for the experimenter against chemicals. A recommendation when working in the clean lab would be to wear two types of gloves, a pair of vinyl gloves (minimum contamination) superimposed on a pair of nitrile gloves (best protection for the user). Cleaning the gloves prior to utilization is not efficient because of the low amount of zinc released in water and the safety risks that would be associated with an acid step. However, we did not detect any zinc contamination during enamel sampling, although the enamel making the outer surface of the tooth crown may have accidentally been in contact with the nitrile or latex gloves. Thus, zinc is mostly released from gloves in the context of an acidic environment and not by mechanical contact with the tooth. Still, we would recommend not to wear any plastic gloves during tooth sampling, and if protection is needed, we recommend wearing textile gloves instead. The enamel $\delta^{66}\text{Zn}$ values of the Lapa do Santo humans display a trend where teeth formed during the earlier stages of life have the highest values, while teeth forming during later childhood show the lowest values. Enamel samples of deciduous teeth have the highest $\delta^{66}\text{Zn}$ values, which could be best explained by

elevated $\delta^{66}\text{Zn}$ values of maternal blood and milk, enriched in heavier zinc isotopes compared to the adult diet of the Lapa do Santo humans, as reflected in the lower $\delta^{66}\text{Zn}$ values of their permanent molars. Teeth mineralized during the first two years of life have intermediate enamel $\delta^{66}\text{Zn}$ values, probably due to the mixed signature of the consumption of solid food and mother milk. Future work on the faunal $\delta^{66}\text{Zn}$ values of this site will help to better interpret the diet of the different individuals of this population. More work is needed to explain the zinc isotope variations during childhood in this study to further explore if zinc can be a promising proxy to trace age at weaning—similarly to calcium isotopes. Moreover, this work confirms the interest to use zinc isotopes in dental enamel for dietary reconstructions of archeological mammals (fauna and humans) in tropical settings (Bourgon et al., 2020) since bone and tooth collagen preservation in Lapa do Santo was poor, while enamel $\delta^{66}\text{Zn}$ values seem pristine and a promising dietary tracer.

Chapter 4

Trophic ecology of a Late Pleistocene early modern human from tropical Southeast Asia

Trophic ecology of a Late Pleistocene early modern human from tropical Southeast Asia inferred from zinc isotopes

Nicolas Bourgon, Klervia Jaouen, Anne-Marie Bacon, Elise Dufour, Jeremy McCormack, N.-Han Tran, Manuel Trost, Denis Fiorillo, Tyler E. Dunn, Clément Zanolli, Alexandra Zachwieja, Philippe Durringer, Jean-Luc Ponche, Quentin Boesch, Pierre-Olivier Antoine, Kira E. Westaway, Renaud Joannes-Boyau, Eric Suzzoni, Sébastien Frangeul, Françoise Crozier, Françoise Aubaile, Elise Patole-Edoumba, Thonglith Luangkhoth, Viengkeo Souksavatdy, Souliphane Boualaphane, Thongsa Sayavonkhamdy, Phonephanh Sichanthongtip, Daovee Sihanam, Fabrice Demeter, Laura L. Shackelford, Jean-Jacques Hublin, Thomas Tütken

Contribution: Designing the research, performing research, analyzing the data, writing the article, and reviewing the article.

This manuscript is published in a similar version in *Journal of Human Evolution* vol 161 (2021), 103075. doi.org/10.1016/j.jhevol.2021.103075

Acknowledgements

The authors would like to thank O. Tombret (UMR 7209 AASPE) for technical support. Additional thanks go to Franziska Honigschnabel (Multimedia Department, Max Planck Institute for Evolutionary Anthropology, Leipzig) and Jonathan Schultz (Human Evolution Department, Max Planck Institute for Evolutionary Anthropology, Leipzig) for their help with picture and figure presentation. Finally, the authors would also like to thank V. Souksavatdy and S. Luangaphay of the Department of National Heritage, Ministry of Information and Culture in Vientiane, Laos, for their authorization to study the Nam Lot and Tam Pà Ling fossil collections. The authors would like to acknowledge the support and thank the Max Planck Society, the Deutsche Forschungsgemeinschaft ('PALÄODIET' project: 378496604) and Biologie, Anthropologie, Biométrie, Epigénétique, Lignées (BABEL; FRE 2029 CNRS) for funding this study. T. Tütken and K. Jaouen received funding from the European Research Council under the European Union's Horizon 2020 research and innovation program (grant agreement no. 681450 and no. 803676, respectively).

Abstract

Tam Pà Ling, a cave site in northeastern Laos, has yielded the earliest skeletal evidence of *Homo sapiens* in mainland Southeast Asia. The reliance of Pleistocene humans in rainforest settings on plant or animal resources is still largely unstudied, mainly due to poor collagen preservation in fossils from tropical environments precluding stable nitrogen isotope analysis, the classical trophic level proxy. However, isotopic ratios of zinc in bioapatite constitute a promising proxy to infer trophic and dietary information from fossil vertebrates, even under adverse tropical taphonomic conditions. Here, we analyzed the zinc isotope composition ($^{66}\text{Zn}/^{64}\text{Zn}$ expressed as $\delta^{66}\text{Zn}$ value) in the enamel of two teeth of the Late Pleistocene (63–46 ka) *H. sapiens* individual (TPL1) from Tam Pà Ling, as well as 76 mammal teeth from the same site and the nearby Nam Lot cave. The human individual exhibits relatively low enamel $\delta^{66}\text{Zn}$ values (+0.24 ‰) consistent with an omnivorous diet, suggesting a dietary reliance on both plant- and animal-matter. These findings offer direct evidence of the broad utilization of resources from tropical rainforests by one of the earliest known anatomically modern humans in Southeast Asia.

4.1 Introduction

Southeast Asia is a key region for understanding patterns of human dispersal into Asia and Australasia (Bae et al., 2017; Perry and Verdu, 2017; Rabett, 2018; Louys and Roberts, 2020). While traditional assumptions have often viewed tropical rainforest habitats as an obstacle to prehistoric human dispersal and occupation (Hutterer, 1983; Bailey et al., 1989; Bailey and Headland, 1991; Wurster and Bird, 2016), increasing evidence and novel analytic approaches have demonstrated human occupation and adaptation to rainforest habitats in Southeast Asia (Barton, 2005; Barker et al., 2007; Summerhayes et al., 2010; Roberts et al., 2015; Demeter et al., 2017; Westaway et al., 2017; Wedage et al., 2019; Langley et al., 2020). Indeed, it was suggested that adaptive plasticity allowed our species to remain in Southeast Asia through ever-increasing climatic instability in the Late Pleistocene and became the last surviving hominin, as opposed to *Homo erectus* and *Homo floresiensis*, for example (Roberts and Amano, 2019; Louys and Roberts, 2020).

The site of Tam Pà Ling (TPL), at Pà Hang Mountain in the Annamite mountain range of northeastern Laos (Huà Pan Province), has shown increasing significance in anthropological and archeological studies in Southeast Asia (Bae et al., 2017; Martín-Torres et al., 2017; McColl et al., 2018), with the oldest known and richest fossil record of our species in this region (Demeter et al., 2012, 2015; Shackelford et al., 2018). Alongside faunal remains, skeletal remains from at least five human individuals have been recovered to date from a chronologically well-constrained Late Pleistocene stratigraphic context (Demeter et al., 2012, 2015, 2017; Shackelford et al., 2018), providing direct evidence of long-term human occupation of the region. Located at the top of the Pà Hang Mountain, TPL cave has one main chamber, excavated at the east end of a gallery, at the base of the entrance's steep 65-m slope. The site's stratigraphy suggests a formation by periodic slope wash deposition coming from the cave's entrance (Demeter et al., 2012, 2015; Shackelford et al., 2018), with no evidence of human occupation on the surface. While the source of TPL fossils remains unknown, current evidence suggests that they originated at or near the cave's entrance before slope wash transport and burial. Various dating methods yielded an age range for the human fossil-bearing deposit at TPL of 63–46 ka (Demeter et al., 2012) for the TPL1 individual (a cranium with frontal, occipital, maxillae, and dentition showing derived modern human morphology), providing the earliest skeletal evidence of anatomically modern humans in mainland Southeast Asia.

Despite evidence of rainforest occupation by our species from at least 70 ka (Demeter et al., 2017; Westaway et al., 2017; Shackelford et al., 2018), poor organic matter preservation in tropical latitudes generally hinders our understanding of human dietary reliance on these habitats and their resources (Tappen, 1994). Occasionally, insights can be obtained when archeological material is preserved in cave and rock shelter sedimentary sequences (Barker et al., 2007; Summerhayes et al., 2010; Perera et al., 2011). However, such depositional contexts are rare in Southeast Asia, and archeological material (in particular faunal and plant remains) is seldom found in pre-Holocene contexts. As such, evaluating the overall dietary importance of tropical forest resources based on archeological material alone has proven to be difficult.

Stable isotope analysis of bones and teeth can provide direct evidence of dietary resources consumed in this tropical rainforest environment. Such methods have successfully highlighted reliance on forest resources for Late Pleistocene tropical rainforest forager populations from Sri Lanka (Roberts et al., 2015, 2017a). However, no information on the exact nature of these resources—whether animal or plant—can be obtained from stable carbon isotopes. In addition, nitrogen stable isotope ($\delta^{15}\text{N}$) analysis of bone or dentin collagen—an established method for investigating trophic relations (DeNiro and Epstein, 1981)—is mostly unsuccessful in tropical environments due to generally poor protein preservation (van Klinken, 1999; Krigbaum, 2005; Clarkson et al., 2009).

Recently, trophic level assessment from enamel using different ‘non-traditional’ stable isotope systems (calcium, magnesium, zinc, and strontium) has become possible through the use of multicollector inductively coupled plasma mass spectrometry (Chu et al., 2006; Knudson et al., 2010; Costas-Rodríguez et al., 2014; Martin et al., 2014), using amounts of material similar to or lower than traditional carbon and oxygen stable isotope analysis. These methods have been successfully applied to fossil and archeological specimens (Knudson et al., 2010; Martin et al., 2015, 2018; Jaouen et al., 2016a; Balter et al., 2019), bypassing the taphonomic limitations of collagen-bound nitrogen isotopes. In particular, the stable isotope ratios of the trace element zinc (including the $^{66}\text{Zn}/^{64}\text{Zn}$, expressed as $\delta^{66}\text{Zn}$ value) constitute a promising dietary indicator among these non-traditional isotope systems (Jaouen et al., 2013, 2016a, 2016b, 2018; Bourgon et al., 2020; McCormack et al., 2021).

Incorporated as a trace element in enamel bioapatite, zinc has better long-term preservation potential than collagen-bound nitrogen (Dean et al., 2018). Indeed, tooth

enamel is more resistant to diagenetic alteration (Kohn et al., 1999; Trueman and Tuross, 2002; Dauphin and Williams, 2004), and systematic variations in $\delta^{66}\text{Zn}$ values show promise for dietary reconstructions in archeology and paleontology, as recently demonstrated (Bourgon et al., 2020). Two key factors are currently known to control the variability of $\delta^{66}\text{Zn}$ values in animals. First, the $\delta^{66}\text{Zn}$ values of consumer body tissues depend on the zinc isotopic composition of the source intake, i.e., mainly the food ingested (Jaouen et al., 2013; Costas-Rodríguez et al., 2014). Second, biological zinc isotope fractionation occurring within an organism results in variation in $\delta^{66}\text{Zn}$ values between different plant parts or body tissues (Balter et al., 2013; Moynier et al., 2013). As such, a consumer's $\delta^{66}\text{Zn}$ value will ultimately be impacted by what plant or animal species were fed upon, as well as which parts of said food source. Other physiological factors such as metabolism and body size could also result in $\delta^{66}\text{Zn}$ variability, although such mechanisms are currently poorly understood or investigated. Given that plant material typically has higher $\delta^{66}\text{Zn}$ values relative to animal-matter (including insects; Evans et al., 2016), the resulting $\delta^{66}\text{Zn}$ values of a terrestrial trophic chain follow an opposite trend to the classic trophic level proxy $\delta^{15}\text{N}_{\text{collagen}}$ values (Schoeninger and DeNiro, 1984). Therefore, higher trophic levels are associated with lower tissue $\delta^{66}\text{Zn}$ values (Jaouen et al., 2013, 2016a, 2016b, 2018; Costas-Rodríguez et al., 2014).

Here, we apply a multi-isotope approach ($\delta^{66}\text{Zn}$, $^{87}\text{Sr}/^{86}\text{Sr}$, $\delta^{13}\text{C}_{\text{apatite}}$, $\delta^{18}\text{O}_{\text{apatite}}$) to the TPL1 individual from TPL to determine the diet and ecological adaptations of the oldest modern human individual found in Southeast Asia (Demeter et al., 2012). Specifically, the association at TPL of a rich human fossil record and fauna with taxa of known ecological preferences for tropical forests allows us to apply methodologies such as stable zinc isotope measurements. This association is crucially important in sites such as TPL where detailed archeological material evidence is absent (e.g., lithic technology, hearth features, plant macroremains, cut marks on bones), making isotopic approaches the only way to gain insight into past dietary reliance. We compared the variability in enamel $\delta^{66}\text{Zn}$ values to $^{87}\text{Sr}/^{86}\text{Sr}$ measurements from the same specimens to account for any potential $\delta^{66}\text{Zn}$ variability introduced by feeding on different bedrock (Graustein, 1989; Bentley, 2006; Bourgon et al., 2020). In addition, we used stable carbon isotope measurements ($\delta^{13}\text{C}_{\text{apatite}}$) as a complementary dietary tracer (Cerling and Harris, 1999; Cerling et al., 2015). The $\delta^{13}\text{C}$ values of bioapatite reflect the relative proportion in a consumer's diet of ingested carbon derived from the food web's primary sources, namely plants using either C_3 (trees, bushes, shrubs, and

grasses) or C_4 (grasses, sedges) photosynthetic pathways (Smith and Epstein, 1971; O'Leary, 1988; Farquhar et al., 1989). In tropical and subtropical regions, forest and woodland habitats are associated with C_3 plants that exhibit low $\delta^{13}C$ values, whereas drier and open environments are characterized by C_4 plants with high $\delta^{13}C$ values (Zazzo et al., 2000; Sponheimer et al., 2006a; Kohn, 2010; Cerling et al., 2015; Bacon et al., 2018a, 2018b). In addition, the lowest $\delta^{13}C$ values reflect densely forested conditions resulting from a 'canopy effect' (van der Merwe and Medina, 1991) and can thus be used to further differentiate between open and forested C_3 environments (i.e., the degree of tree cover). Using $\delta^{13}C_{\text{apatite}}$ values and diet enamel spacing (see *SI Appendix, Supplementary information 3.1*), we estimated the average $\delta^{13}C$ value of the diet ($\delta^{13}C_{\text{diet}}$) from each animal specimen. Stable oxygen isotope analysis ($\delta^{18}O_{\text{apatite}}$) was used to offer possible insights into physiology, water source, and diet (Pederzani and Britton, 2019). A description of the different stable isotope systems in a tropical context used in this study can be found in *SI Appendix, Supplementary information 3.1*.

4.2 Material and methods

The two *Homo sapiens* tooth samples analyzed in this study come from the lateral enamel of a first and second permanent upper left molar (M^1 and M^2) of the same TPL1 individual, dated to 63–46 ka (Demeter et al., 2012). Faunal remains from TPL are scarce and excavated from a chronologically long deposit (70–1.1 ka; Shackelford et al., 2018), rendering trophic relations among the taxa equivocal. To address this uncertainty, the Late Pleistocene fossiliferous assemblage from Nam Lot cave (NL; 86 to 72 ka; Bacon et al., 2015, 2018), a nearby cave site in the Pà Hang Mountain (≈ 150 m distance to TPL; *SI Appendix, Figure S52*), was also analyzed to assess consistency between trophic positions of similar fauna from the two different sites and to provide a more comprehensive ecological baseline for TPL1. In total, the dental enamel of 76 mammal specimens belonging to 18 taxa was analyzed (*SI Appendix, Table S20*), whereby 24 specimens come from TPL (70–1.1 ka) and 52 from NL (86–72 ka). The spotted hyena (*Crocuta crocuta*) was considered separately from other carnivorous taxa (herein assigned the 'bone-eating carnivore' dietary category), as it has been found to exhibit different $\delta^{66}Zn$ values from other sympatric carnivores (Jaouen et al., 2016a). Collagen extraction was attempted in the context of this study on a subselection of specimens from NL but was not successful (collagen yield $< 0.05\%$; *SI Appendix, Table S21*). Previously published enamel isotope data

($\delta^{66}\text{Zn}$, $^{87}\text{Sr}/^{86}\text{Sr}$, $\delta^{13}\text{C}_{\text{apatite}}$, and $\delta^{18}\text{O}_{\text{apatite}}$; $n = 72$) from the Late Pleistocene fauna of Tam Hay Marklot (THM; 38.4 to 13.5 ka), northeastern Laos (Huà Pan Province; Bourgon et al., 2020), were also used for comparison throughout this study to further enlarge the faunal dataset.

The tooth enamel samples used for zinc and strontium isotopic analysis were prepared following the protocols described in *SI Appendix, Supplementary information 3.2* and measured using Thermo Scientific Neptune multicollector inductively coupled plasma mass spectrometry at the Max Planck Institute for Evolutionary Anthropology in Leipzig. The stable carbon and oxygen isotope compositions of samples analyzed in this study were measured with a Thermo Delta V Advantage isotopic mass spectrometer coupled to a Thermo Kiel IV Carbonate Device chemical preparer, at the Service de Spectrométrie de Masse Isotopique du Muséum in Paris, using the protocol described in *SI Appendix, Supplementary information 3.2*.

Statistical analyses were performed in R v. 4.0.2 (R Core Team, 2018), using an alpha level for significance of 0.05. To explore sources of variability of $\delta^{66}\text{Zn}$ values in dental enamel, we fitted a linear mixed model (LMM; Baayen, 2008; similar to Bourgon et al., 2020) with a Gaussian error structure and identity link (McCullagh and Nelder, 1989) using the R package ‘lme4’ version 1.1–17 (Bates et al., 2015; *SI Appendix, Supplementary information 3.2*). Predictors included in the model were dietary category (carnivore, bone-eating carnivore, omnivore, and herbivore), site (THM, NL, and TPL), $^{87}\text{Sr}/^{86}\text{Sr}$, $\delta^{13}\text{C}_{\text{apatite}}$, $\delta^{18}\text{O}_{\text{apatite}}$, zinc concentration, and body mass. One-way analysis of variance (ANOVA) was also performed to determine statistical differences in $\delta^{66}\text{Zn}$ values between dietary categories. Where differences were found to be significant, Tukey's post-hoc pair-wise comparisons were carried out to determine which dietary categories were significantly different from each other. Isotopic niches were estimated using stable isotope Bayesian ellipses (Jackson et al., 2011), where the shape and size of the ellipses are defined by the covariance matrix of $\delta^{13}\text{C}$ and $\delta^{66}\text{Zn}$ values, while the position is defined by the means of both variables. All data discussed in the paper are provided in *SI Appendix, Tables S20–S27*.

4.3 Results

All measured $\delta^{66}\text{Zn}$, $^{87}\text{Sr}/^{86}\text{Sr}$, $\delta^{13}\text{C}$ (apatite and diet), and $\delta^{18}\text{O}_{\text{apatite}}$ values from TPL and NL can be found in *SI Appendix, Tables S22 and S23* and all values from reference

materials in *SI Appendix, Table S26*. Most values for $\delta^{13}\text{C}_{\text{apatite}}$ and $\delta^{18}\text{O}_{\text{apatite}}$ values from NL specimens ($n = 47$) are from previously published work (Bacon et al., 2018a).

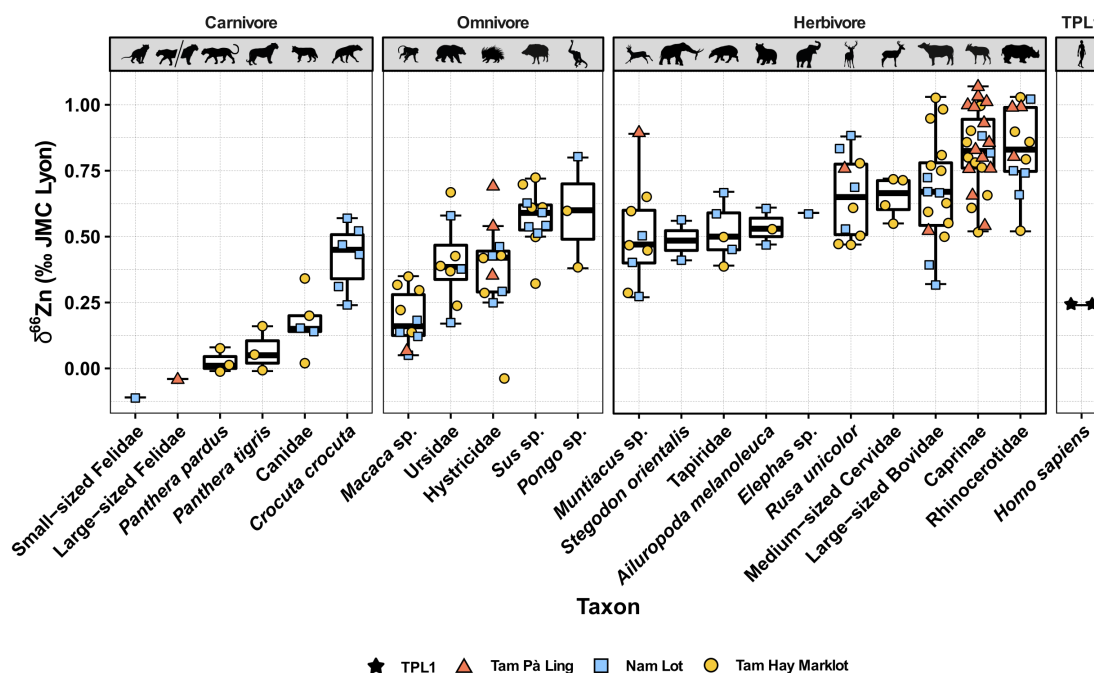


Figure 19. Box and whisker plots of the range of $\delta^{66}\text{Zn}$ values (relative to the JMC-Lyon zinc isotope standard) in tooth enamel for each taxon and the TPL1 *H. sapiens* individual (63–46 ka; black star). Each of the other colors and symbols represents specimens from different sites: Tam Pà Ling (70–1.1 ka; orange triangles), Nam Lot (86–72 ka; blue squares), and previously published data from Tam Hay Marklot (Bourgon et al., 2020; 38.4–13.5 ka; yellow circles). Note the inclusion of the bone-eating carnivore *C. crocuta* with other carnivores. The boxes represent the 25th–75th percentiles, with the median represented by a bold horizontal line. The average analytical repeatability of samples was 0.01 ‰.

The $\delta^{66}\text{Zn}$ values obtained from tooth enamel from TPL and NL caves range from -0.11 to $+1.07$ ‰ (Figure 19–21). The absence of a mixing line between zinc concentration and $\delta^{66}\text{Zn}$ values (Kendall's correlation test for TPL and NL, respectively: $\tau_b = 0.13$, $p = 0.34$, and $\tau_b = 0.15$, $p = 0.13$; *SI Appendix, Figure S53*) suggests no significant postmortem zinc uptake. Carnivores exhibit the lowest $\delta^{66}\text{Zn}$ values ($\delta^{66}\text{Zn} = +0.04 \pm 0.13$ ‰ 1σ , $n = 4$), herbivores the highest ($\delta^{66}\text{Zn} = +0.72 \pm 0.21$ ‰ 1σ , $n = 45$), while $\delta^{66}\text{Zn}$ values from omnivores are intermediate ($\delta^{66}\text{Zn} = +0.40 \pm 0.22$ ‰ 1σ , $n = 21$; *Figure 20; SI Appendix, Table S22*). Hyenas display higher values than those of other sympatric carnivores ($\delta^{66}\text{Zn} = +0.42 \pm 0.13$ ‰ 1σ , $n = 6$). Most notably, the TPL1 *H. sapiens* individual exhibits an identical $\delta^{66}\text{Zn}$ value of $+0.24$ ‰ for both M^1 and M^2 , corresponding to an intermediate value between carnivorous and herbivorous taxa (Figure 19).

Seventy-eight specimens were analyzed for $^{87}\text{Sr}/^{86}\text{Sr}$, displaying a broad range of values from 0.7103 to 0.7319, with TPL1 exhibiting a value of 0.7200. Most faunal specimens exhibit ratios between 0.7127 and 0.7179 (51%, $n = 40$; *SI Appendix, Table S22*). These ratios are similar to what was observed for THM (0.7135–0.7173; 52%, $n = 36$; Bourgon et al., 2020) and consistent with the complex local geology

composed of Late Carboniferous (Moscovian) to Permian limestone, Silurian sandstone, and Paleozoic granite (Bacon et al., 2011; Düringer et al., 2012).

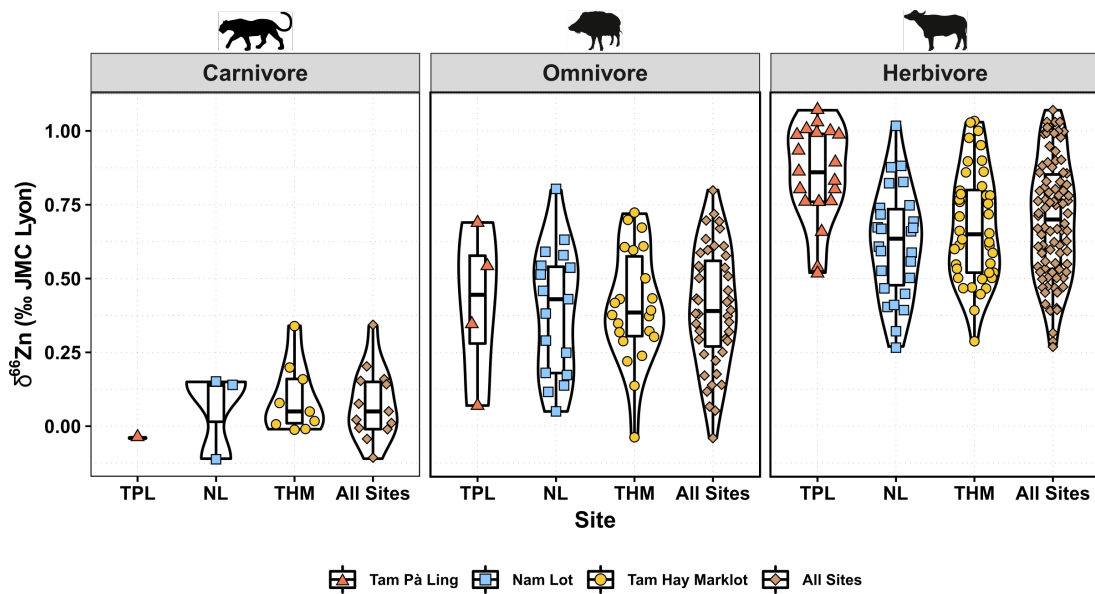


Figure 20. Violin plots presenting the range of $\delta^{66}\text{Zn}$ values (relative to the JMC-Lyon zinc isotope standard) of tooth enamel from each site for carnivores (excluding the bone-eating carnivore *C. crocuta*), omnivores, and herbivores. Each of the colors and symbols represents specimens coming from different sites: Tam Pà Ling (70–1.1 ka; orange triangles), Nam Lot (86–72 ka; blue squares), previously published data from Tam Hay Marklot (Bourgon et al., 2020; 38.4–13.5 ka; yellow circles), and all sites combined (brown diamonds). The outline of the plots illustrates kernel probability density, where the width represents the proportion of the data found therein. The boxes from the box and whisker plots inside the violin plots represent the 25th–75th percentiles, with the median represented by a bold horizontal line.

Stable carbon and oxygen isotope analyses were conducted on 32 specimens, the remaining having been previously analyzed and published (Bacon et al., 2018a). The enamel $\delta^{13}\text{C}_{\text{diet}}$ values of the fauna, ranging from -30.2 to -14.1 ‰ ($n = 32$), are typical of a wide range of feeding behaviors from pure subcanopy to open woodland C_3 plant feeders and C_4 plant feeders (i.e., grazers; Cerling and Harris, 1999; Cerling et al., 2004, 2015; Tejada et al., 2020; **Figure 21**; **SI Appendix, Table S23**), while the $\delta^{18}\text{O}_{\text{apatite}}$ values range from -9.4 to -0.6 ‰. TPL1 *H. sapiens* individual exhibits $\delta^{13}\text{C}_{\text{diet}}$ and $\delta^{18}\text{O}_{\text{apatite}}$ values of -26.4 ‰ and -6.4 ‰, respectively. While a C_4 grass component is present in the area surrounding the sites (as exemplified by $\delta^{13}\text{C}_{\text{apatite}}$ values for some herbivorous specimens at NL and TPL that are typical of C_4 feeders; Cerling and Harris, 1999; Cerling et al., 2015), the prevalence of low $\delta^{13}\text{C}_{\text{apatite}}$ values seen from the fossil mammal assemblage suggests a predominant C_3 environment (average $\delta^{13}\text{C}_{\text{apatite}} = -25.0 \pm 3.7$ ‰ 1σ , $n = 52$ and -24.9 ± 4.3 ‰ 1σ , $n = 28$, respectively, for NL and TPL).

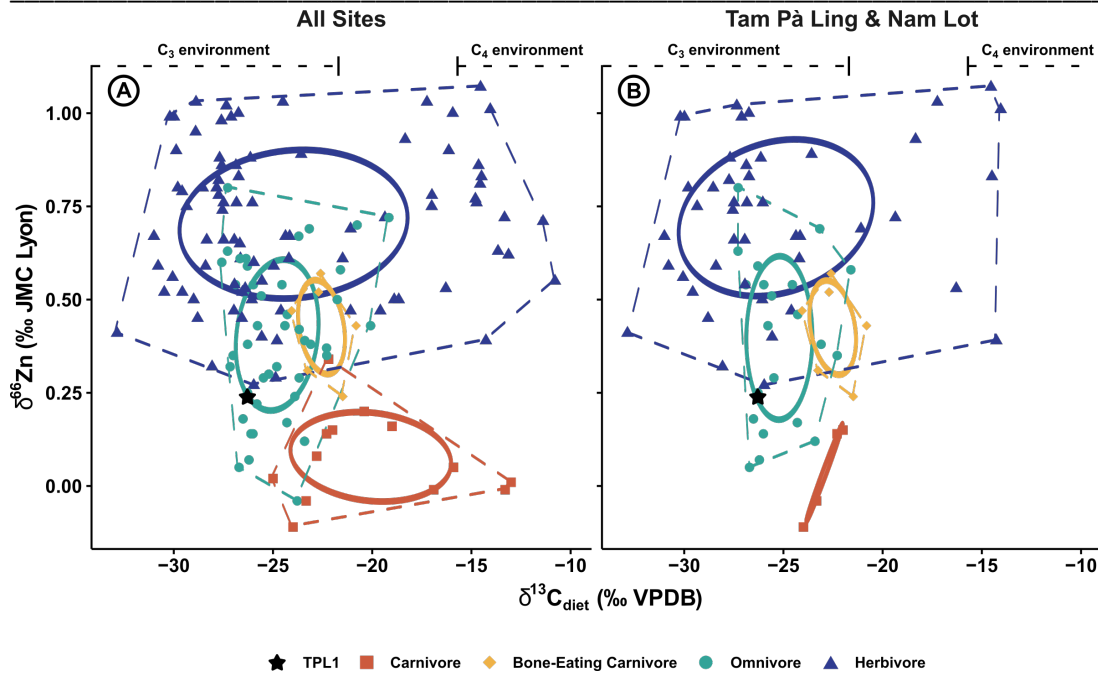


Figure 21. Distribution of enamel $\delta^{66}Zn$ versus $\delta^{13}C_{\text{diet}}$ values for TPL1 individual (black star), carnivores (red square), bone-eating carnivore *C. crocuta* (yellow diamond), omnivores (turquoise circle), herbivores (blue triangle) for A) all three Late Pleistocene sites of Tam Pà Ling (70–1.1 ka), Nam Lot (86–72 ka) and previously published data from Tam Hay Marklot (Bourgon et al., 2020; 38.4–13.5 ka) and B) only Tam Pà Ling and Nam Lot (this study and Bacon et al., 2018a). 'C₃ environment' and 'C₄ environment' are respectively defined by $\delta^{13}C_{\text{diet}} < -21.7$ ‰ and > -15.7 ‰. Dashed lines for convex hulls represent the full range of variation and full lines for ellipses represent 40% predictive ellipses. VPDB = Vienna Pee Dee Belemnite.

The full-null LMM comparison was significant (likelihood ratio test: $X^2 = 30.72$, $df = 3$, $p < 0.001$), allowing us to securely assess which tested predictors were associated with $\delta^{66}Zn$ variability. The $\delta^{13}C_{\text{apatite}}$ and $\delta^{18}O_{\text{apatite}}$ values, site and zinc concentration show no significant relationship ($p > 0.05$) to the variability of $\delta^{66}Zn$ (**SI Appendix, Table S24**). Contrary to what was seen in the THM fauna (Bourgon et al., 2020), body mass was not significantly associated with $\delta^{66}Zn$ variability (likelihood ratio test: $X^2 = 2.96$, $df = 1$, $p = 0.35$; **SI Appendix, Table S24**). Finally, significant relationships were observed between $\delta^{66}Zn$ variability and $^{87}Sr/^{86}Sr$ (likelihood ratio test: $X^2 = 19.40$, $df = 1$, $p < 0.001$; **SI Appendix, Table S19**), as well as with dietary categories whereby omnivores, bone-eating carnivores and herbivores all have higher values than carnivores (likelihood ratio test: $X^2 = 35.84$, $df = 3$, $p < 0.001$; **SI Appendix, Table S24**). ANOVA ($F(3,144) = 52.75$, $p < 0.001$) revealed that only the $\delta^{66}Zn$ values of omnivores and bone-eating carnivores are not significantly different ($p = 0.99$), whereas all other dietary categories are statistically distinct (**SI Appendix, Table S25**).

4.4 Discussion

4.4.1 Variability in tooth enamel $\delta^{66}\text{Zn}$ and trophic level

As at THM, the preservation of enamel-bound diet-related $\delta^{66}\text{Zn}$ signals is also demonstrated at NL and TPL (*SI Appendix, Figure S53*). No collagen could be successfully extracted from the dentin of the tooth samples (*SI Appendix, Table S21*), reinforcing the usefulness of zinc isotope analysis to assess trophic levels in a tropical context where generally poor preservation of organics makes the application of traditional collagen-bound stable nitrogen isotope analysis unfeasible. The LMM conducted on the THM, NL, and TPL datasets revealed that the faunal enamel $\delta^{66}\text{Zn}$ values associated with each trophic level were in agreement between sites (*SI Appendix, Table S24*), thus ensuring valid trophic relation comparisons. Just as for THM, the range of $\delta^{66}\text{Zn}$ values for TPL and NL are, however, slightly smaller (1.11 ‰ and 1.13 ‰, respectively) than those from the Koobi Fora region of Turkana Basin in Kenya (1.24 ‰; Jaouen et al., 2016a), and the absolute $\delta^{66}\text{Zn}$ values of the whole food web are also lower (~0.50 ‰). While more work is necessary to ascertain regional variability in $\delta^{66}\text{Zn}$ values—especially in other settings or parts of the world—these results are promising for paleodietary reconstruction as they suggest a certain degree of homogeneity in zinc isotopic compositions among taxa, at least on a regional scale.

ANOVA results demonstrate that $\delta^{66}\text{Zn}$ values are significantly different between all dietary categories except omnivores and bone-eating carnivores, whereby carnivores display the lowest mean $\delta^{66}\text{Zn}$ value and herbivores the highest, while omnivores and bone-eating carnivores fall in between (**Figure 20**). Indeed, the $\delta^{66}\text{Zn}$ values of hyenas are significantly higher than those of other sympatric carnivores, as also observed for the Koobi Fora region in Kenya (Jaouen et al., 2016a). Bone tissue generally exhibits higher $\delta^{66}\text{Zn}$ values than muscle tissues (Balter et al., 2013; Moynier et al., 2013), thus likely resulting in higher $\delta^{66}\text{Zn}$ values in taxa that regularly consume bones such as the spotted hyena (van Valkenburgh et al., 1990; van Valkenburgh, 1996).

Omnivores display a large range of $\delta^{66}\text{Zn}$ values, with the lower end of values likely representing a predominantly carnivorous and the upper range a primarily herbivorous diet. This distinction is supported by values from fossil orangutans (*Pongo* sp.) and wild boars (*Sus* sp.), whose modern diets are predominantly composed respectively of fruits (Fox et al., 2004; Wich et al., 2006; Kanamori et al., 2010; Hardus et al., 2012) and plant-matter (Barrios-Garcia and Ballari, 2012; Ballari

and Barrios-García, 2014). Indeed, while both orangutans and wild boars exhibit variability in their $\delta^{66}\text{Zn}$ values as expected from taxa that display omnivorous behaviors at times (Wich et al., 2006; Barrios-García and Ballari, 2012; Hardus et al., 2012; Ballari and Barrios-García, 2014), they still fall well within the range of values characteristic for herbivores (due to insufficient data to accurately determine a frugivorous range of $\delta^{66}\text{Zn}$ values, orangutans are herein considered as herbivores in terms of their $\delta^{66}\text{Zn}$ values as fruits are plant-matter). Moreover, the predictive Bayesian ellipse of omnivores does not overlap with that of carnivores and only minimally with that of herbivores, further supporting isotopically distinct $\delta^{66}\text{Zn}$ values for an omnivorous diet (**Figure 21**). Conversely, the convex hulls (comprising 100% of the data) show substantial overlap between omnivores and both herbivores and carnivores, suggesting that the lower end of $\delta^{66}\text{Zn}$ values in omnivores represent a predominantly carnivorous diet, while the upper range values represent a largely herbivorous diet. The $\delta^{66}\text{Zn}$ variability of herbivorous taxa across all sites is considerable ($\Delta^{66}\text{Zn}_{\text{max-min}} = 0.8 \text{ ‰}$; average $\delta^{66}\text{Zn} = +0.70 \pm 0.20 \text{ ‰ } 1\sigma, n = 86$), although identifying dietary trends associated with distinct $\delta^{66}\text{Zn}$ values is challenging. Moreover, no apparent differences in $\delta^{66}\text{Zn}$ can be seen between animals associated with C_3 and C_4 diets (i.e., browsers and grazers) according to the LMM, as was the case in the nearby site of THM (Bourgon et al., 2020; see *SI Appendix, Supplementary information 3.3* for further discussion). Thus, while $\delta^{66}\text{Zn}$ variability observed in herbivores shows potential to investigate dietary preferences of sympatric taxa, further work is needed to characterize and distinguish herbivorous dietary behaviors.

Finally, the estimates obtained from the LMM for $^{87}\text{Sr}/^{86}\text{Sr}$ (*SI Appendix, Table S24*) are in agreement with what was already highlighted for THM cave, whereby lower $\delta^{66}\text{Zn}$ values are associated with higher trophic levels and higher $^{87}\text{Sr}/^{86}\text{Sr}$ values. While $\delta^{66}\text{Zn}$ values recorded in tooth enamel are determined mainly by diet, local geology seems to also induce some variability in $\delta^{66}\text{Zn}$ values, albeit likely to a limited degree considering the good agreement between the different dietary categories across all three sites. Conversely, the LMM found no significant relation associated with average body mass on $\delta^{66}\text{Zn}$ variability. It is possible that larger mammals were coincidentally associated with higher $\delta^{66}\text{Zn}$ values in THM (Bourgon et al., 2020). In contrast, the current LMM—using a larger sample size with a more diverse faunal assemblage—likely better explained a relationship of $\delta^{66}\text{Zn}$ variability (here the lack thereof) to body mass. As was the case for THM (Bourgon et al., 2020), no clear differences in $\delta^{66}\text{Zn}$ can be seen between animals associated with C_3 and C_4 diets

according to the LMM (see *SI Appendix, Supplementary information 3.3 and Figure S54–S57* for further discussion on herbivores' $\delta^{66}\text{Zn}$ variability). Similarly, no relationship was drawn between variability in $\delta^{66}\text{Zn}$ values and zinc concentration, as demonstrated by the absence of a mixing line between variables (*SI Appendix, Figure S53*). This absence of a relationship further argues for the preservation of enamel-bound diet-related $\delta^{66}\text{Zn}$ signals, as opposed to higher zinc concentrations seen in diagenetically altered dental tissues compared to modern ones (Bourgon et al., 2020).

4.4.2 Stable zinc isotope measurements of the TPL1 *H. sapiens* individual

Owing to generally poor collagen preservation in fossils from tropical contexts, direct trophic assessment of pre-Holocene humans living in rainforests has been impossible using the traditional collagen-bound stable nitrogen isotope measurements (Krigbaum, 2005). Using zinc isotope measurements, a direct trophic assessment was successfully obtained for the TPL1 individual, allowing a better understanding of Late Pleistocene rainforest human dietary reliance. Additionally, this approach offers a unique opportunity to directly assess the diet of this individual in the absence of associated archeological evidence at TPL.

The $\delta^{66}\text{Zn}$ values obtained for the M¹ and M² of the TPL1 individual are identical ($\delta^{66}\text{Zn} = +0.24\text{‰}$) and argue for a post-weaning dietary signal when considering the typical development time of the M2 (Hillson, 1996; AlQahtani et al., 2010). When compared to $\delta^{66}\text{Zn}$ values from the fossil faunal assemblages, the zinc isotope composition of the TPL1 individual falls within the range of omnivorous taxa ($\delta^{66}\text{Zn}$ between -0.04 and 0.80‰ ; **Figure 19**) and, more importantly, within omnivores' isotopically distinct Bayesian ellipse (**Figure 21**). This strongly suggests that the diet of this individual contained both animal and plant material. Alternatively, a strictly carnivorous diet with the inclusion of bone marrow could induce similar omnivore-like values, as observed for the bone-eating carnivore spotted hyena. However, no evidence of bone marrow extraction was observed in Late Pleistocene Southeast Asia archeological records, although younger archeological records from terminal Late Pleistocene and Holocene Hoabinian period sites suggest the utilization of this resource (Forestier et al., 2015; Zeitoun et al., 2019). The $\delta^{66}\text{Zn}$ values of TPL1 also fall outside the range of bone-eating carnivores (**Figure 21**) and could further suggest

an omnivorous diet. However, a smaller proportion of bone marrow to the diet of TPL1 compared with that of the spotted hyenas could perhaps produce intermediate values to the carnivores' and bone-eating carnivores' dietary categories. Further work using other isotopic approaches such as stable calcium isotopes (Martin et al., 2018, 2020) could help to further address this question and more fully distinguish a bone-eating carnivore diet from an omnivorous one.

The position at the lower end of $\delta^{66}\text{Zn}$ values for omnivorous taxa suggests that a higher proportion of animal-matter was included in its diet compared with most other sympatric omnivorous mammalian species. This is supported by the higher $\delta^{66}\text{Zn}$ values seen in orangutans and wild boars, which provide a frame of reference for values reflecting mostly frugivorous (i.e., herbivorous in the larger sense) and herbivorous diets with some varying degrees of animal-matter consumption (Wich et al., 2006; Barrios-Garcia and Ballari, 2012; Hardus et al., 2012; Ballari and Barrios-García, 2014). Conversely, the relatively low $\delta^{66}\text{Zn}$ values of macaques (*Macaca* sp.) support the higher consumption of animal-matter as a likely driving factor to lower values in omnivores. This includes but is not limited to insects, as current data suggest depleted ^{66}Zn isotopic compositions (Evans et al., 2016) similar to what is observed for other animal-matter such as meat. Indeed, while macaque species show considerable flexibility in their dietary habits (Heesen et al., 2013; Kato et al., 2014; Huang et al., 2015; Sengupta and Radhakrishna, 2016; Ruslin et al., 2019; Khatiwada et al., 2020), fruits and leaves are often a staple component of their diet. However, the $\delta^{66}\text{Zn}$ values for macaques are likely not solely controlled by fruit consumption, as values similar to the predominantly frugivorous orangutans would be expected (>60% fruits; Fox et al., 2004; Wich et al., 2006; Hardus et al., 2012). As such, a comparatively higher proportion of animal-matter in their diet (primarily insects in this case, which exhibit low $\delta^{66}\text{Zn}$ values (Evans et al., 2016) similar to other animal-matter) is a reasonable inference for the position of macaques and other omnivorous taxa at the lower end on the omnivore spectrum of $\delta^{66}\text{Zn}$ values. Notwithstanding the evidence for animal-matter, the incorporation of plant-matter into the diet of TPL1 is still supported, as almost all carnivore specimens (92%, $n = 12$) exhibit lower $\delta^{66}\text{Zn}$ values, typically associated with a higher trophic level (Jaouen et al., 2016a, 2016b).

Furthermore, the $\delta^{66}\text{Zn}$ values from TPL1 are similar to those of the M² from the early Holocene tropical hunter-gatherer population of Lapa do Santo from Brazil ($\delta^{66}\text{Zn} = +0.26 \pm 0.14 \text{‰ } 1\sigma$, $n = 13$; Jaouen et al., 2020), whose diet was described as

a mixture of plants and small-to-mid-sized animals (Strauss et al., 2016, Strauss, 2017). However, this comparison with the TPL1 individual remains tentative, as trophic levels based on $\delta^{66}\text{Zn}$ could not be assigned to Lapa do Santo's individuals because no sympatric fauna from the site was analyzed. Nevertheless, $\delta^{15}\text{N}$ values also obtained from the Lapa do Santo individuals (Strauss, 2017) lend support to an omnivorous diet and thus further validate the interpretation of $\delta^{66}\text{Zn}$ values for TPL1 as indicative of a mixture of animal and plant material. Additional $\delta^{66}\text{Zn}$ data from human populations are available (Jaouen et al., 2017, 2018), but comparisons between TPL1 *H. sapiens* individuals and these human populations are ill-advised because they concern French individuals of the 13th to 20th century from various locations for which cultural, social, religious, and economic factors contributed to dietary choices (Quellier, 2013). While the absolute range of $\delta^{66}\text{Zn}$ values of previous studies (Jaouen et al., 2017, 2018) is similar to what is seen for the Laotian Late Pleistocene sites presented in the current study, data presented from Koobi Fora (where a defined food web was studied; Jaouen et al., 2016a) further highlight that baselines vary from one setting to another, just as they do for $\delta^{15}\text{N}$ values. Failure to properly account for baseline variation would lead to incorrect assessment of consumer trophic positions (Post, 2002; Woodcock et al., 2012).

The omnivorous diet determined for TPL1 strongly contrasts with most trophic level assessments obtained from nitrogen isotope data of humans in other regions of the world for that period, where a meat-rich diet is almost consistently observed (Richards et al., 2003; Bocherens et al., 2005; Richards and Trinkaus, 2009; Naito et al., 2016; Jaouen et al., 2019a). Even when data attest to plant consumption, their overall dietary contribution remains unknown (Henry et al., 2014; Power et al., 2018) or relatively low (Naito et al., 2016), while the $\delta^{15}\text{N}$ values remain high and within the range of other carnivores. Moreover, $\delta^{15}\text{N}$ values are biased from the relative importance of plants in the diet being overprinted by meat consumption, owing to the fact that plants usually contain much less protein than meat (Phillips and Koch, 2002). This bias consequently hampers accurate reconstruction of overall dietary reliance made through nitrogen stable isotope analysis by favoring animal-based diets, which is observed in most cases for other regions of the world for that period.

Even when considering only Southeast Asian sites from Late Pleistocene, the omnivorous diet assigned for TPL1 offers some much-needed insights into our species' overall dietary reliance and behaviors for this region of the world for that period. Indeed, current data are scarce and rely mostly on archeological material evidence

(Barker et al., 2007; Wedage et al., 2019; Langley et al., 2020) and, to a lesser extent, on carbon stable isotope measurements (Roberts et al., 2017a). Even when archaeological material such as organic remains (i.e., animal bones or plant remains) and stone tools are found, they mostly prove inadequate for reconstructing overall dietary reliance, as they offer indirect evidence of past human diets and may be unrepresentative of daily subsistence practices. In contrast, enamel $\delta^{66}\text{Zn}$ analysis provides new insights into human diets (i.e., degree of herbivory vs. faunivory) during the period of tooth crown formation. While differences between sites could also suggest different adaptations of humans to tropical forest environments, methods such as zinc stable isotope analysis offer additional insights and nuances by providing direct evidence of overall dietary reliance. The omnivorous diet determined for TPL1 could also be in line with behaviors associated with specialized adaptations to tropical rainforest environments seen from archeological records from other Southeast Asian sites, perhaps even such as exploitation and possible processing of plants (Barton, 2005; Barker et al., 2007; Summerhayes et al., 2010; Wedage et al., 2019) and diverse specialized hunting strategies (Barton et al., 2009; Bacon et al., 2015; Roberts et al., 2017a; Wedage et al., 2019; Langley et al., 2020).

Alongside trophic level assessment using $\delta^{66}\text{Zn}$ measurements, the stable carbon isotope analysis of the M¹ of TPL1 provides additional dietary information (**Figure 21**). The $\delta^{13}\text{C}_{\text{diet}}$ value of TPL1 is relatively low ($\delta^{13}\text{C}_{\text{diet}} = -26.4\text{‰}$) and falls well within the range of food obtained from a forested C₃ environment (Cerling and Harris, 1999; Cerling et al., 2015). This range of values is also in line with a humid climate and forested environments highlighted for northeast Laos before the onset of the Last Glacial Maximum (Milano et al., 2018). Within the studied Late Pleistocene food web of tropical forest, this value is most similar to that of taxa such as *Macaca* sp., *Sus* sp., and *Muntiacus* sp. The $\delta^{13}\text{C}_{\text{diet}}$ value of TPL1 is also similar to that of human specimens from terminal Pleistocene and Holocene deposits at Fa Hien-Lena and Balangoda Kuragala (~12–3 ka cal BP) and slightly lower than that from Late Pleistocene Batadomba-Lena fauna (dated to 36–12 ka; Roberts et al., 2015, 2017a). While studies from other Late Pleistocene Southeast Asian sites suggested that semi-open rainforest and rainforest edges were preferred by humans (Roberts et al., 2015, 2017a), the $\delta^{13}\text{C}_{\text{diet}}$ value from the TPL1 individual clearly highlights a strict reliance on dietary resources from forest environments. This value is also very close to the threshold ($\delta^{13}\text{C}_{\text{diet}} = -27.2\text{‰}$) established for a diet entirely consisting of resources from closed-canopy forests (Roberts et al., 2017a, 2018; Tejada et al.,

2020), further contrasting with an initial assessment that tropical forests could not support human foraging in the absence of agriculture (Bailey and Headland, 1991).

4.5 Conclusions

Collectively, $\delta^{66}\text{Zn}$ values from TPL1 and comparison with fauna strongly suggest that the diet of this *H. sapiens* individual contained both plant and animal material, while the $\delta^{13}\text{C}$ value indicates that the resources consumed came strictly from forested environments. This omnivorous diet contrasts with most trophic level assessments obtained from nitrogen isotope data of humans in other regions of the world for that period, where a meat-rich diet is almost consistently supported. The current results are also the oldest direct evidence of overall dietary reliance and subsistence strategies for Late Pleistocene humans in rainforests. These results clearly reinforce a growing body of evidence for early human foragers' exploitation of a broad resource base and long-term occupation of tropical rainforest environments. Moreover, this study demonstrates the potential of $\delta^{66}\text{Zn}$ analysis on teeth where archeological material evidence is absent, and other forms of trophic level assessment are not possible. Finally, distinctions observed between other sympatric primates suggest that $\delta^{66}\text{Zn}$ analysis proves especially valuable for studying the diet and ecology of fossil primates but, most importantly, to explore adaptations and dietary reliance of different fossil hominins.

Chapter 5

Synthesis and outlook

The studies carried out and presented in this thesis have important implications for trophic interactions in (paleo)dietary investigations, especially when reconstructing human diets. The following chapter summarizes the main findings of this thesis and examines their relevance to paleodietary reconstructions. The chapter then outlines persisting challenges and areas of development.

The first part of this thesis (*Chapter 2*) presents the first stable zinc isotope analyses conducted on tooth enamel of fossil specimens, namely from the Late Pleistocene Southeast Asian faunal assemblage (~38.4 to 13.5 ka) of Tam Hay Marklot cave in northeastern Laos, Hua Pan Province. Specifically, a crucial step to applying stable zinc isotope analysis for paleodietary studies was to establish that unaltered diet-related isotopic signals could be retained over long periods of time.

In this publication, various lines of evidence were consequently presented to demonstrate the absence of notable post-mortem diagenetic trace elements uptake into the enamel of fossil teeth. Spatial distribution profiles of zinc and diagenetically sensitive elements (e.g., iron, manganese, magnesium, uranium and rare earth elements) were investigated in cross-sections from fossil mammal teeth and compared to modern specimens to evaluate post-mortem taphonomic processes' impact on the enamel chemical composition. Zinc's and these elements' concentrations and distribution profiles were similar between fossil and modern enamel samples, suggesting that trace elements' diagenetic alteration was absent or negligible. In contrast, the dentin and pulp cavity of the fossil teeth displayed overall higher concentrations for all the investigated elements, most likely resulting from diagenetic alteration (which may also lead to zinc addition and/or exchange). Furthermore, no relationship between $\delta^{66}\text{Zn}$ values and average enamel concentration in the diagenetically sensitive elements can be discerned. Similarly, significant

modifications of the original enamel mineral elemental composition are equally refuted by the absence of a mixing line between $\delta^{66}\text{Zn}$ values and zinc concentration, supporting the absence of any significant postmortem zinc uptake from the embedding sediment.

Furthermore, the overall mean enamel value and range of $\delta^{66}\text{Zn}$ values for each diet category correspond to different dietary habits of the fossil mammals ($\delta^{66}\text{Zn}_{\text{carnivores}} < \delta^{66}\text{Zn}_{\text{omnivores}} < \delta^{66}\text{Zn}_{\text{herbivores}}$). This systematic stepwise trophic ordering further indicates that the enamel of the fossil teeth from Tam Hay Marklot cave retained their original zinc isotope composition. Beyond a clear distinction between carnivorous and herbivorous diet, an intermediate omnivorous range of $\delta^{66}\text{Zn}$ values could also be discerned. This differentiation is especially promising for paleodietary studies as no other geochemical proxy has so far parsimoniously identified and characterized a distinct omnivorous feeding habit. Fossil hominins could likely exhibit such dietary behaviors, thus making stable zinc isotope analysis a particularly appealing method in archeological research.

Finally, we investigated *post hoc* relationships between individual predictors (diet, $^{87}\text{Sr}/^{86}\text{Sr}$, $\delta^{13}\text{C}_{\text{apatite}}$, $\delta^{18}\text{O}_{\text{apatite}}$, zinc concentration and body mass) with $\delta^{66}\text{Zn}$ values, by fitting a linear mixed model (LMM). Contrary to expectations, no apparent relationship was observed between $\delta^{13}\text{C}$ and $\delta^{66}\text{Zn}$ values, whereby C_4 feeders would be expected to display higher $\delta^{66}\text{Zn}$ values due to a $\delta^{66}\text{Zn}$ -to-height gradient (Weiss et al., 2005; Viers et al., 2007; Moynier et al., 2009; Tang et al., 2012, 2016; Deng et al., 2014; Caldelas and Weiss, 2017; van der Ent et al., 2021) observed in plants and the generally lesser height of C_4 plants (i.e., primarily grasses) compared to many C_3 plants (which notably include trees, bushes, and shrubs). However, both local geology (expressed through $^{87}\text{Sr}/^{86}\text{Sr}$) and body mass revealed a significant relationship with $\delta^{66}\text{Zn}$ variability. Such exercise aimed to enhance the interpretative framework of variability in $\delta^{66}\text{Zn}$ values, allowing for a more comprehensive understating of the zinc isotope system and and potentially controlling factors of bioapatite $\delta^{66}\text{Zn}$ values, leading to more tailored studies in the future by identifying avenues of research.

The next section of this thesis (**Chapter 3**) examines specifically how laboratory gloves (all of which containing a variable amount of zinc) can affect zinc isotope composition and indicate that standard sample-handling practices are not leading to any measurable zinc contamination. This work follows up on findings from Garçon et al. (2017) where zinc contamination was investigated in detail for various clean laboratories and highlighted laboratory gloves as a serious contamination source. This risk of

contamination represents a major concern for stable zinc isotope measurements of tooth enamel since the zinc content of sample solutions can be as low as 400 ng and could thus easily be altered by exogenous zinc contributions. The $\delta^{66}\text{Zn}$ values for the in-house bovine liver reference material (AZE), routinely prepared alongside fossil enamel samples during each batch zinc separation on ion chromatographic columns, systematically yielded higher values in Bourgon et al. (2020) than previous studies (*SI Appendix, Table S16*; Jaouen et al., 2012, 2016a, 2016b, 2018). Among potential causes, zinc contamination was a reasonable culprit.

Various lines of evidence were thus explored by performing different experiments to investigate zinc contamination. In a first experiment, a series of tests were thus conducted to assess the potential of zinc contamination, whereby the types of gloves (i.e., the material of the gloves) used during chemical preparation were first investigated. This test highlighted that vinyl gloves showed the lowest contamination potential when working in cleanrooms during zinc separation.

In a second experiment, teeth were analyzed to assess if substantial variation in $\delta^{66}\text{Zn}$ could be attributed to contamination from manipulating samples during the sampling process. Different types of teeth (deciduous and permanent, premolars and molars) coming from an early Holocene forager population of Lapa do Santo Brazil (Strauss et al., 2016; Strauss, 2017) were sampled numerous times, each time with the experimenter using different types of gloves (nitrile, latex, vinyl and no gloves). In conjunction with the first experiment, this test concluded that zinc appears to be primarily released in an acidic environment and not through direct contact with the tooth.

Finally, the potential contamination from manipulating samples during the sampling process was explored *post hoc*. To this end, a linear mixed model was used to explore the source of zinc isotope variability in dental enamel, similar to the one developed in *Chapter 2*, using the different $\delta^{66}\text{Zn}$ values obtained from the same teeth using different types of gloves in their handling (from the aforementioned second experiment). The model could determine that the gloves used during the sampling process were not significantly associated with variability in zinc isotope composition, further arguing that glove contamination was negligible or absent. Additionally, the linear mixed model once again identified a significant relationship between zinc and strontium isotope composition (the latter was used as an indicator of the bedrock geology reflecting the geographical origin of the samples).

More importantly, the linear mixed model identified tooth formation stages as significantly associated with variability in $\delta^{66}\text{Zn}$ values. The deciduous teeth recorded the highest $\delta^{66}\text{Zn}$ values in the Lapa do Santo humans' enamel, followed by intermediate values for teeth mineralized during the first two years of life and the lowest values towards later stages of life (i.e., puberty and early adulthood). The association of tooth formation stages and $\delta^{66}\text{Zn}$ values has far-reaching implications for the interpretative framework of variability in $\delta^{66}\text{Zn}$ values of human and other mammal teeth and thus archeological applications, strongly suggesting that dietary transitions could be studied with this method: from placental diet to breastfeeding to before and after weaning. Because of the implication of such results, additional experiments were undertaken to confirm this trend. Accordingly, the teeth of an adult and a child from a different archeological context, the early modern period (16th to 18th centuries) Jacobins convent of Rennes (France), were thus analyzed. The results confirmed the Lapa do Santo's forager population's trend and consequently introduced new perspectives for using zinc isotopes as a tracer for assessing weaning practices.

Finally, **Chapter 4** employs the interpretative framework established from the two previous publications to explore the overall dietary reliance of a Late Pleistocene *Homo sapiens* from Tam Pà Ling, in the Annamite mountain range of north-eastern Laos (Huà Pan Province). More specifically, this study explores how stable zinc isotope analysis can be used to assess the type of resources consumed and how such data may inform us about human's adaptative plasticity. Indeed, it was suggested that the adaptive plasticity of *Homo sapiens* precisely provided our species with the capability to adapt and ultimately persist in Southeast Asia. Conversely, the ever-increasing climatic instability of the Late Pleistocene and the expansion of lowland tropical rainforests would have brought the extinction of other hominins, like *Homo erectus* and *Homo floresiensis*, for example (Roberts and Amano, 2019; Louys and Roberts, 2020). Moreover, despite evidence of rainforest occupation by our species from at least 70 ka (Demeter et al., 2017; Westaway et al., 2017; Shackelford et al., 2018), the poor preservation of organic matter in tropical latitudes (Tappen, 1994) and the rarity of occupation layers in Southeast Asia greatly hinders our understanding of humans' adaptation to these habitats and their resources.

Two *H. sapiens* tooth samples were analyzed in this study, coming from a first and second permanent upper left molar (M1 and M2) of the same TPL1 individual, dated to 63–46 ka (Demeter et al., 2012), the earliest skeletal evidence of anatomically-modern humans in mainland Southeast Asia. Specifically, the M2 of TPL1 was

analyzed to establish a potential dietary breastfeeding $\delta^{66}\text{Zn}$ value (or the lack thereof) recorded in the M1, as evidenced in the Lapa Do Santo and Jacobins' populations. Indeed, the enamel sample from the M1 would represent a formation period spanning from 1.5 to 2.5–3.5 years of age (Hillson, 1996; AlQahtani et al., 2010), whereas that from the M2 would cover from 5 to ~7–8 years of age (Hillson, 1996; AlQahtani et al., 2010). Tooth enamel of mammal specimens from the Tam Pà Ling (70–1.1 ka) and Nam Lot (86–72 ka) assemblages was also analyzed, and the isotope data from Tam Hay Marklot (38.4 to 13.5 ka) was also used for comparison and to enlarge the faunal dataset further.

Analyzing the TPL1 individual and the faunal assemblages is crucially relevant in sites such as Tam Pà Ling, where archeological evidence is lacking (e.g., lithic technology, hearth features, plant macro-remains, cut marks on bones), as isotopic approaches constitute the only means to assess past dietary reliance and ecological adaptations of fossil humans. A multi-isotope approach ($\delta^{66}\text{Zn}$, $^{87}\text{Sr}/^{86}\text{Sr}$, $\delta^{13}\text{C}_{\text{apatite}}$, $\delta^{18}\text{O}_{\text{apatite}}$) was thus employed to investigate the diet of the TPL1 individual, one of the oldest modern human individual found in South East Asia. This extensive sample size and isotopic proxies investigated in this study provided a comprehensive ecological baseline and presented exemplary practices for such an application study, especially in conjunction with a linear mixed model.

Like at Tam Hay Marklot, isotopically distinct $\delta^{66}\text{Zn}$ values for omnivorous diets could also be determined for Tam Pà Ling and Nam Lot fossil assemblages. Likewise, Nam Lot spotted hyenas' results confirmed earlier observations (Jaouen et al., 2016a) that bone consumption would induce higher $\delta^{66}\text{Zn}$ values in its consumer than in other sympatric carnivores. The systematic identification of these isotopically distinct dietary behaviors has tremendous implications for zinc stable isotopes as a (paleo)dietary tracer, as it seemingly indicates underlying ecological and dietary principles. It also highlights the potential for zinc stable isotopes to discern specific dietary behaviors beyond mere assessments of trophic levels.

Contrary to the previous chapter, the $\delta^{66}\text{Zn}$ values obtained from the M1 and M2 of the TPL1 individual were identical, arguing for a post-weaning dietary signal given the development timing of human's teeth (Hillson, 1996; AlQahtani et al., 2010). Indeed, it suggests a very consistent diet throughout the early years of the individual (spanning 1.5 to 8 years of age, based on typical formation time of humans' M1 and M2, and the enamel sample taken from TPL1), for which a gradual in the diet over this period during weaning is usually observed for archeological and non-industrialized

human populations (Sellen, 2001; Richards et al., 2003; Clayton et al., 2006; Guatelli-Steinberg et al., 2014; Tessone et al., 2015; Tsutaya et al., 2016; Konner, 2017). When considering the typical development time of an M2, the $\delta^{66}\text{Zn}$ values obtained for the TPL1 individual argue for a post-breastfeeding isotope composition and a substantial contribution of adult food resources to its diet.

Perhaps more importantly, the comparison with the $\delta^{66}\text{Zn}$ values from sympatric fauna strongly suggests that TPL1 included a substantial amount of both plant and animal material in its diet. This omnivorous diet strongly differs from meat-rich diets that were almost consistently observed in other fossil humans for that period (mostly from the classically-used nitrogen stable isotope proxy). These results also provide some much-needed insights into our species' overall dietary reliance for Southeast Asian sites from the Late Pleistocene. Indeed, current data are scarce and rely primarily on archeological material evidence (i.e., Barker et al., 2007; Wedage et al., 2019; Langley et al., 2020). Consequently, the implications proposed from such studies could very well be unrepresentative of the daily subsistence practices. While caution equally warrants using a single individual to investigate *Homo sapiens*' behaviors in Southeast Asia from the Late Pleistocene, the $\delta^{66}\text{Zn}$ values from TPL1 nonetheless provide direct and unequivocal insights into the diet of this specific individual.

Alongside the zinc isotope composition, a $\delta^{13}\text{C}$ value was obtained for the TPL1 individual and indicated that the resources consumed in the diet of the early modern human came strictly from forested environments. Moreover, the $\delta^{13}\text{C}$ value from the TPL1 individual is very close to values of diets relying entirely on resources from closed-canopy forests (Roberts et al., 2017a, 2018; Tejada et al., 2020). These results confirm that *Homo sapiens* could adapt to and thrive in rainforest environments, even without the need for open environments nearby. Indeed, other studies suggested semi-open rainforest and rain forest edges were still preferred by humans in other Late Pleistocene Southeast Asia sites (Roberts et al., 2015, 2017a). However, this study securely attests to early human foragers' exploitation of tropical rainforest environments by presenting the oldest direct evidence of overall dietary reliance and subsistence strategies for Late Pleistocene humans in rainforests.

While archeological material evidence is lacking at Tam Pà Ling, the implications of an omnivorous diet from a strictly forested environment for the TPL1 individual would suggest specialized adaptations to tropical rainforest environments, perhaps similar to those observed from archeological records from other Southeast Asian sites. Specifically, it could be reasonable to assume practices such as exploitation and

possible processing of plants (Barton, 2005; Barker et al., 2007; Summerhayes et al., 2010; Wedage et al., 2019), as well as specialized hunting strategies (Barton et al., 2009; Bacon et al., 2015; Roberts et al., 2017a; Wedage et al., 2019; Langley et al., 2020). Naturally, variations could also arise between sites due to different adaptations from human groups to tropical forest environments. Further studies in Southeast Asia of different archeological sites, ages, and even species could elucidate and help bring the subsistence strategies observed for the TPL1 individual into a broader context.

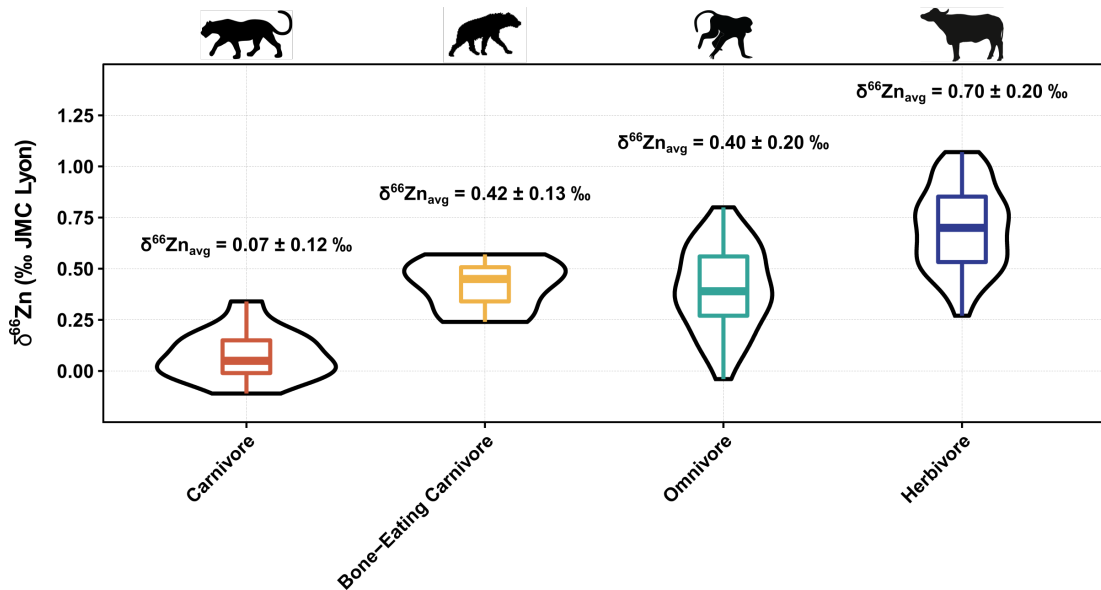


Figure 22. Violin plots presenting the range of $\delta^{66}\text{Zn}$ values (‰, relative to the JMC-Lyon zinc isotope standard) of tooth enamel in mammals, highlighting the low $\delta^{66}\text{Zn}$ values in carnivores (red), intermediate in bone-eating carnivores (yellow; here comprised only of *C. crocuta*) and omnivores (turquoise), and high in herbivores (blue). The data aggregates specimens of three Late Pleistocene sites of Laos ($n = 148$, of which 13 are carnivores, 6 are bone-eating carnivores, 43 are omnivores, and 86 are herbivores): Tam Pà Ling (70–1.1 ka), Nam Lot (86–72 ka), and Tam Hay Marklot (38.4–13.5 ka). The outline of the plots illustrates kernel probability density, where the width represents the proportion of the data found therein. The boxes from the box and whisker plots represent the 25th–75th percentiles, with the median represented by a bold horizontal line.

Among other things, the work presented in this thesis also outlines the potential of zinc stable isotopes as a tool for trophic and dietary assessments compared to other geochemical proxies. Indeed, the presence of isotopically distinct $\delta^{66}\text{Zn}$ values for omnivorous diets (**Figure 22**) suggests zinc isotope composition to be influenced to a much lesser extent by animal-matter consumption than the classically-used nitrogen stable isotope values (e.g., Ambrose, 2002; Sponheimer et al., 2003; Leichliter et al., 2021), all the while successfully discriminating carnivorous to herbivorous diets. While the novel and ground-breaking application of the oxidation-denitrification method allows the measurement of nitrogen stable isotopes in tooth enamel (Leichliter et al., 2021) and would likely enable the use of this proxy over geological timescale, the current limitations relative to the overestimated importance of animal-matter in the diet are likely to persist. Similarly, calcium stable isotopes require a marginal amount

of calcium-rich food items, such as bones and dairy products, to produce isotopic distinctions between individuals (for example, as low as only 0.6 to 1.5% of bone in the food; Heuser et al., 2011). Moreover, it can only determine the inclusion of such calcium-rich food items in the diet, nor seemingly quantify it, rather than directly trace trophic levels or diets. Meanwhile, other geochemical proxies, such as stable magnesium isotopes (e.g., Martin et al., 2014, 2015) and ratios of Sr/Ca and Ba/Ca (e.g., Burton et al., 1999; Balter et al., 2002), generally exhibit a low degree of discrimination between trophic levels. The studies presented in this dissertation thus demonstrate the potential of stable zinc isotopes analyses as (paleo)dietary proxy while also highlighting its various use and benefits. However, it also illustrates and exposes its current limitations, weaknesses, and future research directions.

Beyond confirming that stable zinc isotope analyses can be applied to fossil food webs, the preservation potential of diet-related zinc stable isotope values on a geological timescale still needs to be assessed, especially considering the timeframe currently covered by other dietary proxies such as calcium isotopes (e.g., Heuser et al., 2011; Hassler et al., 2018; Balter et al., 2019). Application studies on fossil assemblages beyond the Quaternary, both marine and terrestrial, will thus be crucial to firmly establish stable zinc isotopes as a paleodietary proxy. Such studies would require extensive investigation of post-mortem diagenetic alteration using various methods but also preferably analyze well-contextualized assemblages or taxa with closely-related modern counterparts.

Various sources of variability in $\delta^{66}\text{Zn}$ values for a given food web were investigated throughout this thesis, partly through statistical modelling. While diet consistently appears to be the primary source of variability in $\delta^{66}\text{Zn}$ values for the publications presented in this work, other suspected factors were determined. Indeed, all studies identified that the local geology (observed from $^{87}\text{Sr}/^{86}\text{Sr}$ values analyzed on the same teeth) induces variability in $\delta^{66}\text{Zn}$ values, albeit to a limited extent given the agreement in each study between different dietary categories or tooth formation in the case of Lapa Do Santo's population. However, the relationship between $^{87}\text{Sr}/^{86}\text{Sr}$ and $\delta^{66}\text{Zn}$ values is limited to some taxa and could thus hint that it is not the result of the bedrock's $\delta^{66}\text{Zn}$ values upon the food web. Instead, it could merely signify that some resources growing upon or located on a specific geologic substrate were consumed and not others. Some degree of soil consumption in the diet often seen in many mammals (Beyer et al., 1994; Abrahams, 2013) could also partly explain this relationship $\delta^{66}\text{Zn}$ values. Indeed, many of the taxa studied from the Southeast Asian assemblages are

known to exhibit varying degrees of geophagy or involuntary ingestion of soil (e.g., porcupine, tapir, rhinoceros, sambar, and large- and small-size bovids; Abrahams, 2013). Further work examining $\delta^{66}\text{Zn}$ values in various plants growing on different geological substrates will be necessary to formally ascertain whether the local geology induces variability in $\delta^{66}\text{Zn}$ values.

Similarly, a recently-published study observed remarkably low geographical $\delta^{66}\text{Zn}$ variability in *Pusa hispida* and *Ursus maritimus* bones from North-American Arctic (McCormack et al., 2021), thus already arguing for geographically homogenous values in marine contexts. While the results from Tam Hay Marklot, Tam Pà Ling, Nam Lot, and preliminary data from Late Pleistocene sites of Vietnam (Coc Muoi (148–117 ka) and Duoi U'Oi (70–60 ka); **SI Appendix, Table S28**) also argue for homogeneous values across the region and seemingly over 130 kyr, the $\delta^{66}\text{Zn}$ values from the studied Koobi Fora's food web are undoubtedly different (**Figure 23**).

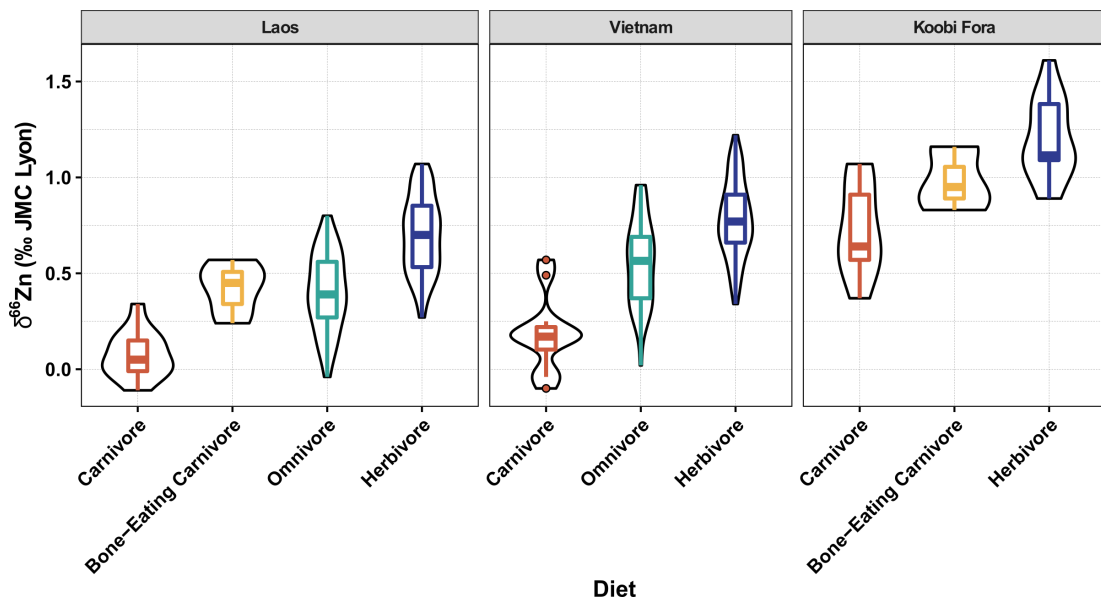


Figure 23. Violin plots presenting the range of $\delta^{66}\text{Zn}$ values (‰ and relative to the JMC-Lyon zinc isotope standard) of tooth enamel between broad localities for carnivores (red), bone-eating carnivores (yellow; here comprised only of *C. crocuta*), omnivores (turquoise), and herbivores (blue). The data aggregates specimens of different sites into three broad groups: Laos, Vietnam, and Koobi Fora. The Laos group ($n = 148$, of which 13 are carnivores from 5 different taxa, 6 are *C. crocuta* bone-eating carnivores, 43 are omnivores from 5 different taxa, and 86 are herbivores from 10 different taxa) includes data from Late Pleistocene sites of Tam Pà Ling (70–1.1 ka), Nam Lot (86–72 ka), and Tam Hay Marklot (38.4–13.5 ka). The Vietnam group ($n = 141$, of which 12 are carnivores from 4 different taxa, 52 are omnivores from 5 different taxa, and 77 are herbivores from 10 different taxa) includes preliminary data from Late Pleistocene sites of Coc Muoi (148–117 ka) and Duoi U'Oi (70–60 ka) (see **SI Appendix, Table S28**). The Koobi Fora group ($n = 26$, of which 9 are carnivores from 3 different taxa, 3 *C. crocuta* bone-eating carnivores, and 14 are herbivores from 6 different taxa) includes data of modern-day fauna from Koobi Fora (Jaouen et al., 2016a). The outline of the plots illustrates kernel probability density, where the width represents the proportion of the data found therein. The boxes from the box and whisker plots represent the 25th–75th percentiles, with the median represented by a bold horizontal line.

These results clearly attest to $\delta^{66}\text{Zn}$ baseline variabilities between different settings, at least in terrestrial contexts. Among other things, soil organic matter, soil acidification, litter recycling, and dissolved organic carbon appear to play a role in soil's $\delta^{66}\text{Zn}$ value

(Weiss et al., 2007; Viers et al., 2015; Opfergelt et al., 2017; van der Ent et al., 2021), and thus likely on its whole food web but it remains to be tested empirically. However, beyond observing higher or lower $\delta^{66}\text{Zn}$ values associated with each trophic level, the effects of $\delta^{66}\text{Zn}$ baselines upon a whole food web remain poorly understood, and the causes behind baseline variabilities even more so. Extensive studies will need to be conducted to firmly attest to these factors' impacts on $\delta^{66}\text{Zn}$ baselines and variability of a given terrestrial food web.

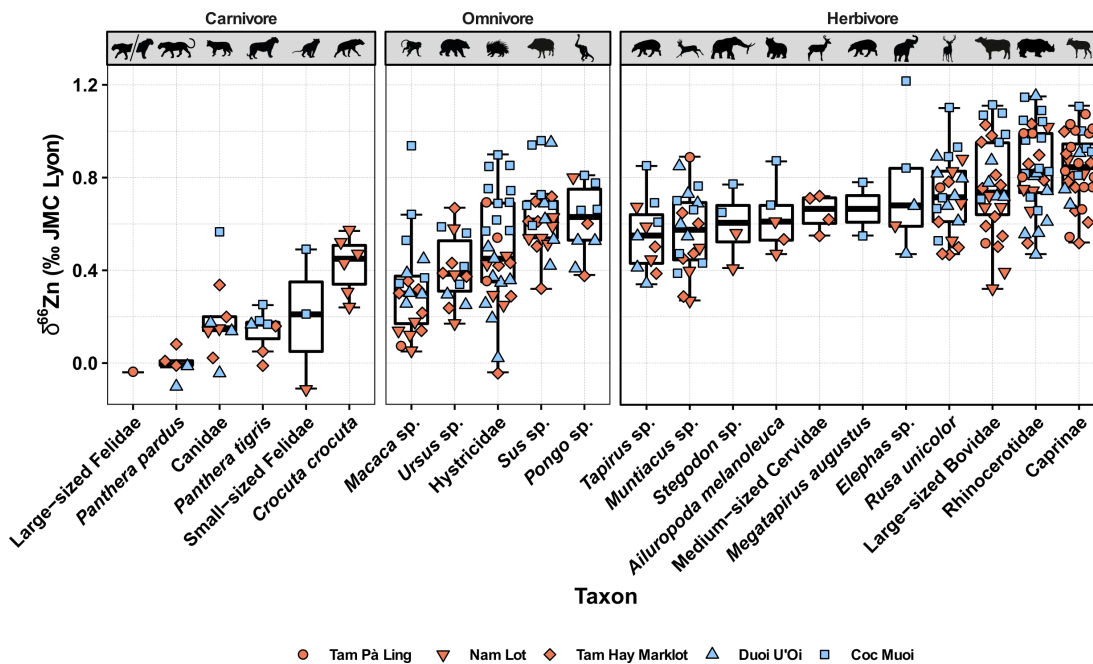


Figure 24. Box and whisker plots of the range of $\delta^{66}\text{Zn}$ values (relative to the JMC-Lyon zinc isotope standard) in tooth enamel for each taxon from Late Pleistocene sites from Laos and the preliminary data from Vietnam (see *SI Appendix, Table S28*). Each color corresponds to the two broad regional groups: Laos (orange) and Vietnam (light blue). Each of the symbols represents specimens from different sites: Tam Pà Ling (70–1.1 ka; circle), Nam Lot (86–72 ka; upside-down triangle), Tam Hay Marklot (38.4–13.5 ka; diamond), Duoi U'Oi (70–60 ka; triangle) and Coc Muoi (148–117 ka; square). Note the inclusion of the bone-eating carnivore *C. crocuta* with other carnivores. The boxes represent the 25th–75th percentiles, with the median represented by a bold horizontal line.

Beyond attesting to a seemingly homogenous regional baseline, the preliminary data from the Late Pleistocene sites of Vietnam (Coc Muoi (148–117 ka) and Duoi U'Oi (70–60 ka)) also highlights the variability in $\delta^{66}\text{Zn}$ values between sites for the same species (**Figure 24**). Differences can be discerned within carnivore and herbivore taxa but are especially pronounced within the omnivore taxa, consistent with their opportunistic feeding behaviors. This observed variability is encouraging for using zinc stable isotope composition as a dietary proxy because it highlights its potential to trace changes in the diet through time. To some extent, and perhaps more importantly, it also rules out species-specific causes and/or metabolism as major factors behind $\delta^{66}\text{Zn}$ values associated with a taxon or a dietary behavior. Indeed, between all Late Pleistocene sites of Laos and Vietnam, some omnivorous taxa (*Macaca* sp., *Ursus* sp., and Hystricidae) exhibit $\delta^{66}\text{Zn}$ values (respectively 0.05 to 0.94 ‰, 0.17 to 0.59 ‰,

and -0.04 to 0.90 ‰) that cover the typical ranges associated with carnivore, omnivore, and herbivore taxa (**Figure 24**).

Nonetheless, biological activity fractionates zinc isotopes in the body among organs of plants and animals, resulting in variability in body tissue $\delta^{66}\text{Zn}$ values (e.g., Weiss et al., 2005; Viers et al., 2007, 2015; Moynier et al., 2009, 2013; Balter et al., 2010, 2013; Aucour et al., 2011). In turn, this increased source of differential fractionation would suggest an increased variability in $\delta^{66}\text{Zn}$ values is expected in food webs. Indeed, the $\delta^{66}\text{Zn}$ values seem more variable in plants than what is observed for $\delta^{15}\text{N}$ values based on the results obtained thus far for herbivorous species. While this variability might prove challenging for establishing strictly defined cut-off values for different dietary behaviors or environments, it could instead prove invaluable in distinguishing the feeding ecology of extant animals. Moreover, it could provide the means to describe environments beyond the traditional C_3 - C_4 dichotomy or, better yet, identify and define further ecological partitioning within this traditional division. However, there is too little available data on plants' $\delta^{66}\text{Zn}$ values, but an already seemingly high variability between plants' organs (Weiss et al., 2005; Viers et al., 2007, 2015; Moynier et al., 2009; Aucour et al., 2011, 2015; Tang et al., 2012, 2016; Deng et al., 2014; van der Ent et al., 2021), to address this question adequately. Indeed, extensive work and considerable data collection from various ecosystems and controlled-growing environments will be necessary to establish a framework in plants' $\delta^{66}\text{Zn}$ variability and to define broad trends in their distribution, whether ecological (e.g., lowlight canopy forest, open savannah environment, temperate forests, cold steppes, and so forth) or related to plant-resources (e.g., fruits, leaves, grasses, and so forth).

Just as is the case with nitrogen stable isotopes, zinc stable isotope values would presumably favor dietary signals indicative of animal-matter consumption because of an increased zinc uptake and an improved zinc bioavailability when proteins, especially animal proteins, are included in the diet (Sandström et al., 1980, 1983, 1989; Wapnir, 2000). However, the data presented in this thesis undoubtedly demonstrate the capability of zinc stable isotope values to identify the presence of isotopically distinct $\delta^{66}\text{Zn}$ values for an omnivorous diet, seemingly indicating its lesser degree of predispositions toward animal-matter consumption compared to other geochemical dietary proxies. Indeed, it has been documented that protein content as low as 19% of the whole diet could nonetheless induce a carnivorous signal in consumers with nitrogen stable isotope values (e.g., Ambrose, 2002; Sponheimer et al., 2003;

Leichliter et al., 2021). Conversely, preliminary data from a controlled-feeding experiment study currently reflects no such discrimination in zinc stable isotope values (*SI Appendix, Table S1*). Instead, they seemingly appear wholly dependent on the zinc isotopic composition of the ingested food rather than its nature (i.e., meat-based or plant-based), unlike for collagen's $\delta^{13}\text{C}$ and $\delta^{15}\text{N}$ values that are rather indicative of the protein portion of the diet (e.g., Ambrose and Norr, 1993; Tieszen and Fagre, 1993). Indeed, these preliminary results also suggest no difference in diet-tissue fractionation relative to the nature of the food consumed (*SI Appendix, Table S1*). While the physiological mechanisms (i.e., element cycling and fractionation in the body) which drive variability in the zinc isotope system are not yet wholly nor well understood and variability in food resources, as stated above, not fully grasped, the mere outlook of confidently identifying omnivorous diets cannot be overstated enough for paleodietary reconstructions. More work is necessary to firmly establish and define the isotopically distinct $\delta^{66}\text{Zn}$ values for omnivorous diets, but its presence nonetheless holds exceptional promise in identifying and refining (paleo)dietary reconstructions for species that could exhibit omnivorous behaviors, especially for Hominids and primates. However, while statistical analyses unquestionably identify it as being isotopically distinct from the $\delta^{66}\text{Zn}$ values of carnivorous and herbivorous diets, the question remains as to whether it truly represents an omnivorous diet or not.

Indeed, omnivorous diets are currently defined based on $\delta^{66}\text{Zn}$ values of taxa that display omnivorous behaviors at times. As such, the $\delta^{66}\text{Zn}$ values are not empirically associated with omnivorous diets *per se* but rather with omnivorous taxa. These species display a large range of $\delta^{66}\text{Zn}$ values, whereby the majority display $\delta^{66}\text{Zn}$ values intermediate to those of carnivorous and herbivorous taxa. Consequently, the lower-end values likely represent a predominantly carnivorous and the upper range a primarily herbivorous diet, thus fully representing and consistent with the opportunistic feeding behaviors of omnivorous taxa. However, further work will be necessary to confirm this assumption through controlled-feeding experiments or multi-isotope analyses using other dietary proxies.

Among others, the combined investigation of stable zinc and nitrogen isotopes is a promising avenue. Indeed, the extensive knowledge available relative to stable nitrogen isotope variability and fractionation makes it an ideal candidate to pair with stable zinc isotope analyses. Moreover, stable nitrogen isotope values are usually much more sensitive to animal-based resources in the diet because meat almost consistently contains more protein, also often more readily bioavailable, than in plants (e.g., Kies,

1981; Sealy et al., 1987; Phillips and Koch, 2002). While it makes distinguishing an omnivorous diet difficult using this isotopic system alone, it could prove to be the ideal tool in assessing the validity of stable zinc isotopes' omnivorous values. Specifically, the novel application of the oxidation-denitrification method that allows the measurement of nitrogen stable isotopes in tooth enamel (Leichliter et al., 2021) could make it possible to directly compare $\delta^{66}\text{Zn}$ with classical $\delta^{15}\text{N}$ values from a single tooth enamel sample rather than using bone collagen. By using a diverse faunal assemblage covering an extensive range of distinct dietary habits, these combined methods could consequently investigate $\delta^{66}\text{Zn}$ variability in different omnivorous taxa or species whose diet is still highly debated. Going forward, developments in these areas can substantially improve the robusticity of stable zinc isotope analysis as a precise empirical tool for (paleo)dietary reconstructions and especially so for hominids.

Conclusion

The role of dietary behaviors in human evolution is one of the key questions in archeology and palaeoanthropology. However, archeological sites are rare, and most of the artifacts present when the site was formed have usually disappeared through time. Even when archeological material evidence is present (e.g., stone tools and animal bones), it cannot be unequivocally associated with daily subsistence practices of hominids and could thus offer a biased and unrepresentative view of past diets. While the use of bone collagen for stable nitrogen and carbon isotope analyses can circumvent these problems and provide overall dietary reliance information, such analyses are confronted with issues of their own that arise from the preservation of organic matter. This limitation consequently hinders their use for older periods and settings with adverse preservation conditions. However, this difficulty can now be overcome by conducting stable zinc isotope analyses, a novel dietary and trophic level proxy.

This thesis advances the interpretative framework of stable zinc isotope analysis of tooth enamel and promotes exemplary practices in (paleo)dietary reconstruction. Investigations of stable zinc isotope analyses of fossil teeth were thus conducted to generate direct evidence of overall dietary reliance, specifically for trophic level assessment.

The first publication of this thesis (*Chapter 2*) confirmed the preservation potential of pristine diet-related zinc isotopic composition in fossil specimens and established stable zinc isotope analyses as a noteworthy addition to paleodietary investigations' toolset. Variability in $\delta^{66}\text{Zn}$ values was also explored, and outlined factors of interest to be further investigated.

The second publication (*Chapter 3*) explored contamination concerns during enamel sampling and chemical sample preparation, identified as negligible, and proposed safe-handling procedures to perform reliable stable zinc isotope measurements. Additionally, variability in $\delta^{66}\text{Zn}$ values relative to the developmental stage of the teeth

sampled was revealed, consequently showing great promises to investigate past breastfeeding and weaning practices through stable zinc isotope analyses.

The third and final publication (**Chapter 4**) assesses the overall dietary reliance of a Late Pleistocene human hunter-gatherer from Tam Pà Ling in Laos' rainforests and illustrates how $\delta^{66}\text{Zn}$ analysis on teeth can be used where archeological material evidence is absent or other forms of trophic level assessment are impossible. The result obtained strongly suggest that the diet of this *H. sapiens* individual contained both plant and animal material, contrasting with a meat-rich diet almost systematically determined using collagen stable nitrogen isotope analyses from humans in other regions of the world for the Late Pleistocene.

A broader and more comprehensive application of stable zinc isotope analyses has significant potential for clarifying aspects of hominid behaviors and subsistence strategies in archeology, such as the timing of the introduction of animal-matter to the diet, the relationship between environment and dietary choices, breastfeeding and weaning practices, food selection or food processing. Future methodological developments, such as empirically determined diet-enamel spacing or extensive $\delta^{66}\text{Zn}$ dataset of plant resources and animal tissue, remain to be explored to increase further the precision and reliability of (paleo)dietary reconstruction using stable zinc isotope analyses in modern and past ecosystems.

Supplementary information appendix

Supplementary information 1

Supplementary information to Bourgon et al. (2020), Zinc isotopes in Late Pleistocene fossil teeth from a Southeast Asian cave setting preserve paleodietary information. *Proc. Natl. Acad. Sci. U.S.A.* 117, 4675–4681, doi.org/10.1073/pnas.1911744117.

Supplementary information 1.1: Context

1.1.1 Geology

Location and geological context

The studied area is located in the northeastern part of Laos, about 290 km NNE from Vientiane, in the Hua Pan province (**Figure S1**). The site can be reached by the road n°1C from Luang Prabang to the small city of Muang Hiam (also called Vieng Thong) (**Figure S2**), and from there, towards the north approximately 60 km to Xoneuna city (also called Muang Xon) (**Figure S3**). The cave is located 6 km SE from the center of the city.

The basement of the region consists of Palaeozoic granite and diorite (Saurin, 1961). These rocks are covered with a widespread light metamorphic sedimentary formation characterized by grey to yellow poorly cemented arkosic sandstones interbedded with pelites and attributed to the Silurian, or perhaps partly to the Devonian (Saurin, 1961). This latter formation is strongly deformed and folded. This detrital sedimentary formation is capped by a thick limestone unit still poorly dated and attributed by Saurin (Saurin, 1961) to an interval between the Late Carboniferous (Moscovian) and the Permian, some outcrops displaying many tabulate corals (mostly tetracorals). Furthermore, crinoidal remains, as well as calcified sponges (stromatoporoids)

developed in laminated calcite with some vertical pillars, are frequent. The karstic formation belongs to the northern Annamitic Chain oriented broadly NNW-SSE. Locally, the thick limestone unit forms a variety of tower karsts that emerge here and there from the forest. This unit consists of a pluri-decametric massive sparitic dark-grey carbonate without marl intercalation. Grey to black cherts occur in some places often reworked inside the cave. The mountain contains a widespread karstic network in which bone-rich breccias and sandy clays can be found.

The Tam Hay Marklot cave is located at the foot of a karstic hill totally covered by forest (**Figure S4a**). The entrance of the cave is constituted by a large and open chamber of about 10 m long and 8 m wide (**Figure S4b-c**), but the entrance of the well-developed gallery (very narrow, less than 0.60 m in diameter) (**Figure S4d-e**) is at the end of this chamber. The first passageway leads to the first chamber of about 15 m long, and the second passageway to the main gallery, which can be followed entirely to the end of the cavity. The 235 m long cave consists of a succession of wide to narrow galleries ranging from one to ten meters wide (**Figure S5**). The height of the main gallery is, on average, around three meters.

Some 150 m from the entrance, the gallery is partly flooded on about sixty meters. After, this part of the gallery narrows, gradually ending in a dead-end. The soil of the gallery from the entrance to about two-thirds of the cavity is entirely covered by a soft and partly wet light brown sediment formed by sandy to gravelly clays. The greatest part of the vertebrate remains was found in this soft sediment forming the soil of the cave until at least the drowned part of the gallery. After this part, the cave ground is made up of solid flowstone. The soft sediment has a thickness of at least one meter. The lower part is more gravelly. Since the vertebrate remains were mainly located in the first 40 cm, no further explorations were conducted deeper for the moment, but further investigations will be conducted in 2020.

Description and analysis of the sedimentary deposits

The karstic filling, homogeneous along the cave, is summarized in **Figure S6** through three sections. The roof and walls of the cave are formed by a compact grey-colored limestone. Four different deposits were recognized in the cave: soft sandy to gravelly clays on the soil; well-cemented conglomerate mixed with breccias plastered on the wall from the base up to two-thirds of the height of the gallery; speleothems cemented on both roof and walls included on the conglomerate; and a 1 to 4 cm dark brown mud

covering the soil and partly the walls from place to place. Details of the facies are given in **Figure S7**:

- The soft sandy to gravelly clays cover almost the entire soil of the cave. The sedimentary facies greatly vary from place to place inside the cave but generally display pure silty to sandy sticky clays in the first upper 30-60 cm, whereas the lower part up to a depth of one meter is made mainly of small to coarse-grained mixed gravels and clays. Furthermore, the lower part of the deposit is generally cross-bedded with numerous erosion surfaces. Most of the teeth come from the upper clayey sediment. Although the vertebrate remains can be found everywhere in the gallery, from the entry to the drowned part of the gallery, their richness in this soft sediment varies from place to place. In some places close to the wall of the gallery, the soft sediment can be poorly to hardly cemented by calcite (**Figure S7**). This calcitic cementation is a secondary diagenetic phenomenon due to the water circulation along the wall.
- The conglomerate and breccias plastered on the wall contain a large range of pebbles and cobbles up to 20 cm in size, cemented by small gravels and coarse-grained sandstones (**Figure S7a**). The maturity of the clasts is highly variable. Full-rounded pebbles and cobbles are mixed with very angular clasts generally in contact with each other. The greater quantity of clasts consists of full-rounded fine-grained yellow-colored sandstones sometimes rich in micas similar to the weakly metamorphic Devonian sandstones described above. The second type of clasts is constituted by angular square-shaped black cherts. The great hardness of these cryptocrystalline silica occurrences compared to the hardness of the sandstones can't explain the important difference in the maturity of the clasts. It is obvious that these two types of rocks of different maturity don't have the same sedimentary history. Cherts probably originated from the substratum of the cave (limestone formation) and have been transported over only short distances, whereas the composition of the sandstone suggests a long transport. In fact, similar black chert concretions can be found easily in situ in the limestone formation; thus, their local provenience is indisputable. Concerning the sandstone pebbles, they are similar to those observed in the river two hundred meters below the Tam Hay Marklot cave in the valley.
- The speleothems (in green on **Figure S7d**) cover the roof and walls (limestone substratum) in the entire gallery. In many places, speleothems

obviously cover the conglomerate plastered on the walls but are also covered by the soft clayey sediments, which are the last deposited sediments.

- The thinnest deposit is a centimetric scale brown-soft mud that covers all of the other deposits up to one-meter height from the floor of the gallery. This suggests episodic flooding of the cave during the rainy season, also explaining the cross-bedded sands and gravels in some places, on the soft sediment of the floor.

Cave filling history

The study of the cavity reveals a complicated depositional history, which consists of at least four types of deposits, roughly superimposed upon each other (**Figure S7**). The oldest deposit is the conglomerate/breccias covered by all of the other sediments (speleothems on the roof and walls, sandy to gravelly clays on the soil, and soft mud, successively).

The perfect imbrication of the flat pebbles (red arrow on **Figure S7a-b**) suggests a water flow orientated from inside to outside, which raises several questions. First, there is today no gallery or pipe being able to bring such conglomerate inside the cave. Secondly, there is today no likely origin on the top of the tower karst sandstone formation that could have provided all of this gravel/pebble material. Similar gravels and pebbles (mainly the sandstones) can be found in the current river crossing the town two hundred meters below, which also strongly suggests that this intra-karstic conglomerate could be very old. With an incision of 0.2 m per thousand years on average (Düringer et al., 2012), this deposit situated at least 200 m above the current alluvial plain could be potentially 2 million years old.

The presence of relicts of conglomerates plastered very high on the walls shows that the gallery was filled by sediment to the roof and then was almost entirely emptied before the sandy clay unit was deposited on the cave floor. That means that a major phase of karstic erosion separates the two described sedimentary units and that there is an extended range of time between the conglomerate and the clayey sediment (red line on **Figure S7d**). The numerous erosion surfaces inside the clayey deposits of the soil, as well as the vertical and lateral alternation of mud, sands, and small gravels, suggest that the deposit has been sedimented in several phases. Furthermore, the occurrence of a thin layer of sticky mud plastered on the wall, as well as marks of the level of the water at different heights inside the main gallery, are evidence that the

cave is still episodically flooded today most likely during the rainy seasons. This can also explain why the concentration of fossil remains is not uniform in the cave but occurs in placer-like loci. Furthermore, some marks of the level of the water in the cave (upper limit of the soft mud) correspond exactly to the height of the second passageway, which probably plays the role of a water outfall. The origin of vertebrate remains is, for the moment, unknown (primary deposit or reworking of old fossiliferous deposits).

In relation to the speleothems, we observed that their location is highly variable from place to place in the cave but that, in most cases, they occur between the conglomerate and the sandy clays deposits. In this case, their deposition obviously took place after the phase of emptying the major part of the conglomerate/breccias and before the deposit of the clayey sediment. The thin mud layer that covers all of the other facies is the result of episodic flooding of the cave and represents the last known deposit.

1.1.2 Faunal description

The full faunal analysis from the Tam Hay Marklot fauna are presented here and in **Table S8**.

Artiodactyla

Within bovids, 115 teeth show the basic pattern of Caprinae, with smooth enamel, styles and stylids more prominent than main cusps, and no ectostylid. Dental dimensions allow the clear distinction of two taxa, one of large size close to the modern *Capricornis* species (*C. sumatraensis* or *C. milneedwardsi*), and a second one of small size close to the modern *Naemorhedus* species (*N. goral* or *N. caudatus*, the dimensions of *C. crispus* being intermediar (Suraprasit et al., 2016)). We assign the Tam Hay Marklot specimens to *Capricornis* sp. and *Naemorhedus* cf. *caudatus* (P3 and P4 of square shape, metastyle well developed on M3). Dimensions of the large Caprinae from Tam Hay Marklot (*Capricornis* sp.) are comparable to those of late Middle to Late Pleistocene specimens (Tougaard, 1998; Bacon et al., 2008, 2011; Filoux et al., 2015; Suraprasit et al., 2016; Bacon et al., 2018b, 2018c).

In relation to the large-sized bovids, it seems that at least two taxa occurred at Tam Hay Marklot. The main differences are observable on lower premolars and m3. On the first set of premolars, the main cuspids (hypoconid, entoconid, protoconid, and

metaconid) appear well-developed buccolingually; the p2s are small mesiodistally and massive; on the lingual side, we observe the presence of deep valleys between cuspids, and the enamel is often thick, all are features encountered in *Bos* species. Some m1/m2 exhibit rounded and voluminous metaconid and entoconid, and m3s a salient entostylid, which forms a deep notch with the hypoconulid. These features are close to the morphology observed in the modern *Bos frontalis* (being aware that *Bos* species may be easily confused on size and morphology). On another set of teeth, premolars are flatter and more elongated (with a range of variation showing no overlap with that of *Bos*), with shallow valleys and grooves between cuspids and a thinner enamel, as in *Bubalus bubalis* (synonym to *B. arnee*). We assign cautiously the teeth to *Bos* sp. (close to *Bos* cf. *frontalis*) ($N = 37$) and *Bubalus bubalis* ($N = 40$), whereas 27 teeth remain difficult to identify.

The 287 suid specimens (277 permanent and 10 deciduous teeth) of Tam Hay Marklot show the typical morphological pattern of *Sus* (molar bunodont with bulky cusps and cuspids and numerous accessory tubercles, showing a star-like shape when worn). However, the teeth display differences that suggest the presence of two distinct species. This is particularly observable on third molars (m3 and M3) and upper premolars (P4), whereas we were not able to detect clear differences on the other cheek teeth (except one m2 much elongated). The great majority of M3s display a high degree of variation with well-developed anterior cingulum with bulky folds, well-developed median accessory cusps, and main cusps sometimes duplicated. The morphology of the posterior portion of the crowns is complex, with a pentacone associated with numerous tubercles on the labial side. Likewise, for m3s, with a large pentaconid surrounded by numerous tubercles. On P4s, the cingulum is anteriorly and posteriorly developed and ended at the base of their crowns by two small cusps. We also observe the presence of a posterior sagittal couplet. This morphology is characteristic of *Sus scrofa*. A small number of teeth (m3 and M3) shows a different pattern: on M3, the anterior cingulum is thinner with a crenulated enamel, the median cusp behind the first row (hyperpreconule) is few developed, whereas the median cusp behind the second row is absent (pentapreconule); on m3s, the accessory median cusp behind the talonid is particularly small, a feature observed in *Sus barbatus* (Badoux, 1959). On P4s, the cingulum is not marked, and the couplet is absent. Two taxa can be recorded at Tam Hay Marklot: *Sus scrofa*, which includes most likely a great number of teeth, and *Sus* cf. *barbatus* only recognized on a small number of teeth ($N = 17$). We didn't observe significant size differences between *S. scrofa* and *S. barbatus* at Tam Hay Marklot. Moreover, both species exhibit range variations comparable to

those of modern species, rather than to those of the late Middle Pleistocene specimens (Khok Sung and Thum Wiman Nakin (Tougaard, 1998; Suraprasit et al., 2016) for *S. barbatus*, and Coc Muoi (Bacon et al., 2018c) for *S. scrofa*).

Numerous teeth exhibit the morphological pattern and dimensions of the large deer, *Rusa unicolor* ($N = 390$): the presence of an anterior fold on m1/m2, well-developed on m3; ectostylid always present on m1/m2; the presence of a small anterior and, more rarely, posterior ectostylid on m3s; p4 molarized (Heintz, 1970); salient cusps and styles on upper premolars; large paracone and metacone on upper molars. The Tam Hay Marklot species overlap in morphology and dimensions with the modern and late Middle to Late Pleistocene species.

The identification of middle-sized and small-sized cervids is more difficult due to the large overlap in dimensions and morphology (Tougaard, 1998). Within these cervids, some teeth are slightly larger with these characteristics: parastylid few developed on p2; a small anterior first valley on p3/p4; an entoconid as developed as the metaconid and entostylid; the entoconid and entostylid fused at the mid-height of the crown on p4; cones and conids of molars with a rounded shape; on m3s, large and rounded hypoconulid; parastyle more developed than the other styles on upper molars. All of these features are present in *Rucervus eldii* ($N = 27$). Dimensions of the Tam Hay Marklot m3s, p3s/p4s, fall within the ranges of variation of the modern species (Suraprasit et al., 2016). We also recognized a different taxon on the basis of a slightly smaller size and features close to the *Axis porcinus* pattern ($N = 22$): parastylid well-developed forming a V-shaped valley with the paraconid; metaconid bilobed on p4s; entoconid and entostylid fused; V-shaped cones and conids on molars; on m3s, large and elongated hypoconulid. Specimens from the late Middle Pleistocene Thum Wiman Nakin site allocated to this species appear much greater (Tougaard, 1998).

Muntiacinae species also occur, which can be distinguished by the smallest dimensions of their teeth and the following features: few developed protoconid and parastylid oriented more anteriorly on lower premolars; few salient cones and conids on molars; upper molars with cone-shaped crowns; small styles on upper premolars and molars. However, the specimens remain difficult to identify at the species level (*Muntiacus* sp.) ($N = 105$). They are close in dimensions to the *Muntiacus* species of the Late Pleistocene Duoi U'Oi site (Bacon et al., 2018c) and to the modern *M. muntiacus grandicornis* measured by the authors at the Raffles Museum in Singapore.

Perissodactyla

The rhinocerotid sample consists of 32 dental elements, which unambiguously document at least two extant species, namely the Javan rhinoceros, *Rhinoceros sondaicus* ($N = 10$), and the Sumatran rhinoceros, *Dicerorhinus sumatrensis* ($N = 9$), whereas 13 tooth fragments could not be identified at the genus or species levels and were accordingly referred to as Rhinocerotina indet.

Rhinoceros sondaicus is notably documented by a right D2 with a medifossette and a sharp parastyle sagittally oriented. A fragmentary P2 has an oblique cingular spur at the entrance of the lingual valley. A fragment of one M1 displays a thick hypocone, lacking a lingual groove. The fragmentary M3 has a thick paracone rib, vanishing well before the neck. The d4 fragment has a quadrangular occlusal outline. One p4 has a very thick labial enamel, an oblique cingular spur at the ectolophid groove, the latter being pointing mesiodorsally in lateral view. All of these features are characteristic of *R. sondaicus*, based on comparison with the dental material from individuals either recent (MNHN-AC) or fossil (Punung locality, Java: Museum Naturalis of Leiden; Coc Muoi, Vietnam: Institute of Archeology, Ha Noi).

Dicerorhinus sumatrensis is recognized thanks to the presence of a mesiolingual groove on the sagittally pinched hypocone of one fragmentary D4 and on permanent teeth (broken M2). A fragment of one M3, also with a sagittally pinched hypocone, shows a slightly convex ectometaloph in occlusal view, with a distolingual cingulum restricted to a small spur, further determining a shallow groove lingual to it. The complete d2 falls within the size range of *D. sumatrensis*. It is narrower than d2s referred to as *R. sondaicus*, with a shallow anterolabial groove and a posterior valley closed. Several fragmentary d3s and d4s have unconstricted metaconid and entoconid, and a distal border of the metalophid straight and oblique, which allows to assign them to *D. sumatrensis*. The labial fragment of m1 has a vertical ectolophid groove reaching the neck. Together with small dimensions (especially regarding the width), all of these features are considered as diagnostic based on comparison with dental material from individuals either recent (MNHN-AC; Cambridge Museum) or fossil (Sibrambang and Lida Ajer Caves, Sumatra; Museum Naturalis of Leiden).

Two teeth of tapir are also recorded at Tam Hay Marklot: one lower left canine (Tapiridae indet.) and one fragment of a jugal tooth (*Tapirus* sp.).

Carnivora

In relation to the Felidae, we recognized a small-sized felid on one m1 (a very simple morphology with two sharp blades) and five small canines ($N = 6$). Within the sample of specimens belonging to large felids, several fragmentary large teeth (four P4, two p4, and one m1) and one complete upper I3 suggest the presence of *Panthera tigris* ($N = 7$). Four other complete premolars (one P3, two P4, and one p4) exhibit the morphology and size of *Panthera pardus* ($N = 4$), with dimensions falling in the range size of modern Asian *P. pardus* (taken by the authors at the Museum Naturalis in Leiden). The two P4 display well-developed cusps, one mesial in the line of blades and a second one oriented lingually. Six fragmentary canines are assigned to large Carnivora.

Four complete, one fragmentary, and two heavily worn upper M1 belong to a small-sized melinae, a badger, most likely *Arctonyx* on the basis of morphology and size (hypocone elongated distally, lingual cusps well-developed). The dimensions of M1s (length: 14-16.2 mm; width: 10.2-11.1 mm) are particularly small, close to those of modern species of *Arctonyx*: *A. dictator* (measurements taken by the authors at the National History Museum, London, and *A. collaris collaris* (Colbert and Hooijer, 1953), rather to that of Pleistocene specimens (de Vos and Long, 1993).

Four complete permanent teeth belong to a large-sized Canidae. However, this sample shows great variation in teeth dimensions, with one large P4 falling within that of *Cuon javanicus antiquus* (Colbert and Hooijer, 1953), one P3 and one m1 are small like in individuals from modern Asian populations, *C. a. adustus* (Myanmar), *C. a. sumatrensis* (Malaysia), *C. a. javanicus* (East Java) (measured by the authors at the National History Museum, London), whereas one very small M1 appears outside of the range of variation of modern and fossil populations.

Three ursids are present at Tam Hay Marklot: *Ursus thibetanus* has been identified based on 17 permanent teeth. The most striking characteristics are: the presence of a lingual cusp on P4; outline of the M1 crown elongated with a weak cingulum; a large paracone, and an elongated talonid on M2. Dimensions of the teeth are particularly great, in comparison with the other available but small modern and fossil samples (Colbert and Hooijer, 1953; de Vos and Long, 1993; Bacon et al., 2008, 2011, 2018b, 2018c). *Helarctos malayanus* is represented by seven permanent teeth. The occlusal outline of the M2s is squarer with a less developed talonid. One M2 is particularly massive (Badoux, 1959). One lower m2 is assigned to *Ailuropoda melanoleuca*. The

tooth is smaller than those measured in a recent population (Colbert and Hooijer, 1953).

Primates

Twenty-two permanent teeth conform to the morphology of the genus *Macaca* among Cercopithecidae. On the basis of the dimensions of upper molars, it seems that at least two species were present at Tam Hay Marklot. The large molars have the size of Late Pleistocene specimens (Duoi U'Oi, Tam Hang, and Lang Trang (de Vos and Long, 1993; Bacon et al., 2008, 2011), close to the modern *M. nemestrina* or *M. mulatta* (data taken by the authors at the National History Museum, London; and *M. nemestrina*, *M. mulatta* or *M. arctoides* (Takai et al., 2014)), whereas a set of small teeth appear close to *M. fascicularis* (data taken by the authors at the National History Museum, London). Other species are difficult to identify due to the large size overlap between taxa. Three *Pongo* teeth, two molars and one canine, are recorded, but these limited data preclude an assignment either to *Pongo pygmaeus* or to the Late Pleistocene *P. devosi* identified in China and Vietnam (Harrison et al., 2014).

Rodentia

Only teeth of large-sized rodents belonging to Hystricidae are recorded at Tam Hay Marklot ($N = 151$): 134 have the dimensions of the *Hystrix* species, whereas 17 smaller could be assigned to the genus *Atherurus*, most likely *A. macrourus*, the only species recorded in the Pleistocene of Southeast Asia. The length variations of upper (M1-M3) and lower (m1-m3) molars largely exceed those of modern *Hystrix* (*Acanthion*) *brachyura* s. l., and even those of the taller modern species *Hystrix* (*Hystrix*) *indica* (van Weers, 2005). While falling in size closer to *H. indica*, we allocate the Tam Hay Marklot teeth cautiously to *Hystrix* sp.

1.1.3 Direct dating of Tam Hay Marklot teeth

Material and methods

Samples

Four mammalian tooth samples of the Tam Hay Marklot assemblage discovered in 2015 and selected from the five samples exported in 2018 for direct dating (SCUMK-

01, SCUMK-02, SCUMK-03A, SCUMK-03B, and SCUMK-R1) were prepped for U-series dating and analyzed at Southern Cross University and the University of Wollongong (**Table S9**).

U-series dating protocol and parameters

Teeth were cut to expose the different dental tissues using a low-speed saw with a rotating diamond blade of 300 μm thickness. Each section was then analyzed by quadrupole LA-ICP-MS for uranium distribution and with a Neptune Plus LA-MC-ICP-MS for uranium-series measurements with the following setting: jet sample Ni 83506 and x skimmer Ni 76250 cones. The instrument was tuned with the NIST610 at 60% laser energy (2.49 J/cm^2), frequency 5 Hz, spot size 65 μm , scan speed of 5 $\mu\text{m}/\text{sec}$, He: 900 ml/min, N_2 : 10 ml/min with an obtained value of $^{238}\text{U}=1.28$ V, $^{232}\text{Th}=1.05$ V. Each sample was pre-ablated at 40% laser energy (3.3 J/cm^2), frequency 5 Hz, spot size 150 μm , and scan speed of 200 $\mu\text{m}/\text{sec}$, before conducting measurements of 310 μm rasters long at 80% laser energy (6.27 J/cm^2), frequency 20 Hz, spot size 150 μm , and scan speed of 5 $\mu\text{m}/\text{sec}$. For each sample, between 9 and 10 rasters were drawn on the samples perpendicular to the growth axis of the tooth (from the enamel tip to the pulp cavity). Each raster was analyzed twice consecutively, and then data were averaged to obtain one minimum U-series age. Therefore, for each sample, we have calculated several minimum U-series ages (depending on the number of rasters and the data quality). Ages were not calculated when U concentration was below 1 $\mu\text{g}/\text{g}$ or when U/Th ratio was below 500. When values permitted, using the raster's sequence along the growth axis, a modeled U-series age was calculated using a Diffusion-Adsorption-Decay (DAD) model (Grün et al., 2014). Baseline and drifts were corrected using a NIST 612 glass disc, while two coral reference materials (the MIS 7 Faviid and MIS5 Porites corals from the Southern Cook Islands (Woodroffe et al., 1991)) were used to correct $^{234}\text{U}/^{238}\text{U}$ and $^{230}\text{Th}/^{238}\text{U}$ ratios and assess the accuracy of measurements. Each coral reference material was analyzed by solution MC-ICPMS and used for reference. To account for potential matrix effects, a bovid tooth fragment from South Africa with known isotope concentrations was used to verify measurements. To account for tailing effects, measurements were carried out at half-masses of 229.5 and 230.5 for ^{230}Th and 233.5 and 234.5 for ^{234}U (Eggins et al., 2003).

Results

The U-series dating results for SCUMK-01, SCUMK-02, SCUMK-03, and SCUMK-R1 are presented in **Tables S10-S13**, and range between 37.4 ka +/- 0.9, and 13.1 ka +/- 0.5.

- 1) The ages for SCUMK-R1 ranges between 37.0 ka +/- 1.5 and 25.0 ka +/- 0.9 with a mean age estimated at 31.2 ka +/- 1.3.
- 2) The ages for SCUMK-01 ranges between 26.4.0 ka +/- 0.8 and 29.8 ka +/- 1.0 with a mean age estimated at 27.6 ka +/- 1.0.
- 3) The ages for SCUMK-02 ranges between 37.0 ka +/- 1.3 and 39.1 ka +/- 1.4 with a mean age estimated at 37.4 ka +/- 0.9.
- 4) The ages for SCUMK-03A ranges between 12.0 ka +/- 0.5 and 13.4 ka +/- 0.9 with a mean age estimated at 13.1 ka +/- 0.5.

The $^{234}\text{U}/^{238}\text{U}$ ratio was consistent between the samples, except for sample SCUMK-01 which had slightly lower values. Despite the important difference in minimum age between SCUMK-03A (13 ka) and SCUMK-02 (37 ka), it does not appear to be a different diffusion environment, and therefore the age discrepancy could only be an artifact of a later diffusion of U for SCUMK-03. Yet, because the distribution of U around the dental tissue in SCUMK-03A is rather uniform, it appears likely that the tooth represents a later deposition event than SCUMK-02.

In order to advance the dating accuracy, we have modeled each tooth using the DAD model (**Table S14 and Figures S42-45**), which takes into consideration the diffusion rate, the distance, and size of each dental tissue, and the diffusion pathway (Grün et al., 2014).

The difference between the mean U-series age and the model DAD age is within error the same and therefore indistinguishable (**Table S14**). The results show that the samples can be considered as closed-system and that the minimum ages obtained with the U-series are close to the 'true' age of the sample obtained by the DAD model. In other words, the results indicate that the teeth recovered from Tam Hay Marklot site have different ages.

1.1.4 General chronology and ecology of Tam Hay Marklot cave fauna

The mammalian faunal assemblage with the occurrence of modern taxa and the absence of archaic taxa (*Stegodon*, *Megatapirus*, or extinct rhinocerotid species), the dimensions of teeth close to those of the post-Middle Pleistocene taxa (species

experienced overall trends of dental size decrease throughout the Pleistocene), and the dating, which show an age range of 38.4–13.5 ka, document a mammalian assemblage during a time period which encompasses the later section of the glacial stage MIS 3 through all MIS 2, including the Last Glacial Maximum (26.5–19 ka). Isotopic results suggest a mixed environment from closed low-light tropical rainforest to open savannah. The dating of a tooth of orangutan (*Pongo* sp.) at 38.4 ka shows that during the periglacial MIS 3 period, at this latitude, the great ape still occupied closed, low-light tropical forests. In this mixed environment, the diet of the tiger (*Panthera tigris*) relied on prey species preferentially from open woodlands where they could find large-sized cervids and bovids, whereas the diet of canids much more relied on forest-dwelling species. The diet of the other large predator, the leopard (*P. pardus*) relied on prey species from both ecosystems.

Supplementary information 1.2: Stable isotope analyses

Stable isotope analysis is now a widely used method in archeological and paleontological fields, yielding new insights into the past of animals and humans alike (DeNiro and Epstein, 1978; McConnaughey and McRoy, 1979; DeNiro and Epstein, 1981; Schoeninger and DeNiro, 1984; Kelly, 2000; Richards et al., 2001). Although a large array of materials and tissues can be subjected to such analyses, dental enamel is of particular interest as it is metabolically inert after formation and is not very sensitive to post-mortem diagenesis and alteration (Lee-Thorp et al., 1989; Wang and Cerling, 1994; Kohn et al., 1999; Lee-Thorp, 2008). It thus consists of an important material for palaeodietary and paleoenvironmental research (Lee-Thorp et al., 1989; Cerling and Harris, 1999; Sponheimer and Lee-Thorp, 1999a; Kohn and Cerling, 2002). However, enamel bioapatite (a biological carbonate-bearing hydroxylapatite) records the isotopic composition of the “whole” diet consumed and this only over the growth and mineralization period of the teeth in animals (or hominins), thus representing a narrow subadult period (Hillson, 1996; Nanci, 2018).

1.2.1 Variation of zinc stable isotope values in tooth enamel

Zinc is an element of Group 2B of the periodic table, the last column of the *d* block. While it is not a transition metal *per se*, it is sometimes included with them as its properties are more similar to these than to the post-transition metals. Zinc possesses

five naturally occurring stable isotopes, ^{64}Zn (48.63%), ^{66}Zn (27.90%), ^{67}Zn (4.10%), ^{68}Zn (18.75%) (Rosman and Taylor, 1998), with an average relative atomic mass of 65.37777 (Ponzevera et al., 2006).

Zinc is a trace element, but it is an important agent in many biological processes and is vital for most living organisms. Indeed, it has reactive stability in a cellular environment governed by oxidation-reduction processes because of its single oxidation state (2+). Its ligands are multiples (Vallee and Falchuk, 1993), and it is involved in all six enzyme classes and most of the regulatory proteins (Berg and Shi, 1996), as well as being involved in many biochemical functions (Vallee and Falchuk, 1993).

In terrestrial contexts, the primary source of zinc in a given food web ultimately comes from the plants. Subsequently, two main parameters have been presented to explain the zinc isotope composition of plants: the initial zinc isotope ratios of the soil (Viers et al., 2007; Fekiacova et al., 2015) and the biological fractionation that occurs between the plant and the soil as well as within the plant itself during nutrient transport (Weiss et al., 2005; Viers et al., 2007, 2015; Moynier et al., 2009; Aucour et al., 2011).

The initial $^{66}\text{Zn}/^{64}\text{Zn}$ ratio (expressed as $\delta^{66}\text{Zn}$ value) of the soil is in turn controlled by the nature of the underlying bedrock. While igneous rocks exhibit a narrow and homogenous range of $\delta^{66}\text{Zn}$ values ($+0.3 \pm 0.14 \text{ ‰}$ (2σ)) (Moynier et al., 2009, 2017), sedimentary rocks exhibit a broader range of $\delta^{66}\text{Zn}$ values (Maréchal et al., 2000; Cloquet et al., 2008; Moynier et al., 2017) with the highest values observed for marine carbonates (up to $+1.4 \text{ ‰}$) (Luck et al., 1999; Pichat et al., 2003). In the case of Tam Hay Marklot cave, three major rock units are present at the local scale in the cave surrounding (see “*Supplementary information 1.1: Context - 1.1.1 Geology*”): an exposed magmatic bedrock composed of granite, widespread arkosic sandstone, and finally a sedimentary cover consisting of marine limestone. While $\delta^{66}\text{Zn}$ stable isotope analyses have not been conducted on any of these bedrocks, the limestone cover is likely to exhibit higher values than the other two. It is then reasonable to assume that local geology may impact local isotope ratios of the food web, thus possibly explaining some of the variability observed in enamel $\delta^{66}\text{Zn}$ values among the fossil teeth.

Within plants themselves, an initial fractionation occurs between the roots and the soil during zinc uptake in the rhizosphere (Weiss et al., 2005; Aucour et al., 2011). As a result, roots and shoots are generally enriched in heavy isotopes relative to the litter layer in which they grow (Weiss et al., 2005; Viers et al., 2007; Moynier et al., 2009;

Aucour et al., 2011). Additionally, low $\delta^{66}\text{Zn}$ values are systematically observed in the most aerial parts of the plants (Weiss et al., 2005; Viers et al., 2007; Moynier et al., 2009). It is believed that once the zinc is in the xylem, active uptake of heavy isotopes by cells out of the xylem occurs during its transport, thus favoring the mobility of light isotopes to the most aerial parts of the plants (Viers et al., 2007; Moynier et al., 2009). As such, a correlation seems to exist between $\delta^{66}\text{Zn}$ in leaves and the length of the plants, both within a single plant and between species. Generally speaking, low growing plants such as herbaceous species are thus expected to have higher $\delta^{66}\text{Zn}$ values compared to high growing plants like trees (Weiss et al., 2005; Viers et al., 2007; Moynier et al., 2009).

Similar to plants, the isotopic composition of zinc in trophic chains' consumers (i.e., animal tissues) is governed by two factors: the initial zinc isotope ratios of the food products (plants in the case of herbivores and animals in the case of carnivores) and the isotopic fractionation occurring during intestinal absorption (Turnlund et al., 1984; Cousins, 1985; Lönnnerdal, 2000; Balter et al., 2010; Jaouen et al., 2013, 2017; Moynier et al., 2013).

As was the case for plants, in $\delta^{66}\text{Zn}$ values is prompted by the initial zinc isotopic composition of the foods consumed. For plant consumption, different species and parts, as well as differences in growth height, are all likely to induce different $\delta^{66}\text{Zn}$ values in the consumer. Similarly, the $\delta^{66}\text{Zn}$ values of body tissues resulting from meat consumption will depend on which parts and organ were consumed, with muscles usually being ^{66}Zn depleted relative to the average isotopic composition of the body (Balter et al., 2010; Jaouen et al., 2013; Costas-Rodríguez et al., 2014; Jaouen et al., 2016a). It was suggested that biological activity fractionates zinc isotopes in the body among organs, thus explaining variability in body tissues (Balter et al., 2010; Moynier et al., 2013). Additionally, plant products usually have the most elevated $\delta^{66}\text{Zn}$ values (Costas-Rodríguez et al., 2014; Jaouen et al., 2016a), whereas muscles exhibit low values (Balter et al., 2010; Jaouen et al., 2013; Costas-Rodríguez et al., 2014; Jaouen et al., 2016a). Contrary to the classic trophic level proxy $\delta^{15}\text{N}_{\text{collagen}}$ values then, the higher the trophic level of an animal is, the lower are the zinc isotope ratios of its body tissues (Jaouen et al., 2013, 2016a, 2016b, 2018; Costas-Rodríguez et al., 2014).

1.2.2 Variation of strontium stable isotope values in tooth enamel

The geographical distribution of strontium isotopes is mostly determined by the evolution of ^{87}Sr in a geologic system. Contrary to the other strontium isotopes, ^{87}Sr is radiogenic as a result of the radioactive decay of ^{87}Rb . The relative content and ratio of ^{87}Sr to ^{86}Sr is thus a function of both the age of the rock and the original rubidium (Rb) amount of a given bedrock. This leads to a general trend of higher $^{87}\text{Sr}/^{86}\text{Sr}$ ratios in older rocks and lower values in younger rocks.

Strontium isotopes are widely used as geochemical signatures to “source” individuals (whether animals or humans) to a geologic area. This is because the $^{87}\text{Sr}/^{86}\text{Sr}$ ratio recorded in enamel is directly related to that of the diet and ultimately to that of the soils and water available to the plants at the very base of the food web. The underlying concept is that the strontium isotopic signature is mostly preserved and carried from the eroding geologic bedrock to the soil (Dasch, 1969) and then enters as bioavailable strontium into the plants (Hurst and Davis, 1981). This signature is then preserved in its consumers, no matter the trophic level (i.e., from plants to herbivores and from herbivores to carnivores) (Steadman et al., 1958). While there are additional non-geologic sources of variations in this $^{87}\text{Sr}/^{86}\text{Sr}$ ratio, an isotopic signature from specimens can then be associated with a biologically-available signature from a given location or region. This correlation between $^{87}\text{Sr}/^{86}\text{Sr}$ ratios within a food web with underlying geology signature was originally demonstrated in ecological studies (Gosz et al., 1983; Åberg, 1995; Koch, 1998) and quickly applied to archeological context (Ericson, 1985; Balasse, 2002; Bentley, 2006).

1.2.3 Variation of carbon and oxygen stable isotope values in tooth enamel

The carbon isotopic composition of bioapatite reflects that of diet, whereas the oxygen reflects mainly that of ingested water (DeNiro and Epstein, 1978; Sullivan and Krueger, 1981; Longinelli, 1984; Luz et al., 1984; Lee-Thorp et al., 1989; Cerling and Harris, 1999; Sponheimer and Lee-Thorp, 1999b; Passey et al., 2005).

Reliance on food resources can be assessed through the existence of “isotopically” distinct resources in the environment. In tropical contexts, there exists an isotopic distinction in $\delta^{13}\text{C}$ values between plants using C_3 and C_4 photosynthetic pathways (Smith and Epstein, 1971; O’Leary, 1988; Farquhar et al., 1989). The $\delta^{13}\text{C}$ values observed in studied faunal or hominin material thus convey the relative proportion of C_4 grassland and C_3 forest/woodland as carbon sources in their diet and, indirectly, to

their associated environments (Zazzo et al., 2000; M. Sponheimer et al., 2006a, 2006b; Codron et al., 2012; Bacon et al., 2018a, 2018b). C₃ plants predominate over the terrestrial vegetation biomass and are composed of trees, bushes, shrubs, and grasses (Smith and Epstein, 1971; O'Leary, 1988; Farquhar et al., 1989; Still et al., 2003). For the geographic area in this study, a $\delta^{13}\text{C}$ range of -37 ‰ to -23 ‰ is considered for C₃ plants, as higher values (>-23 ‰) are restricted to particular context and species (Smith and Epstein, 1971; O'Leary, 1988; Kohn, 2010). C₄ plants occur primarily in tropical and subtropical grassland and savanna regions, as well as in temperate grassland regions in North and South America and Africa (Still et al., 2003). They are mainly composed of grasses and sedges and present higher $\delta^{13}\text{C}$ values of -17 ‰ to -10 ‰ (Smith and Epstein, 1971; O'Leary, 1988).

It is noteworthy to mention that the terms C₃ and C₄ refer only to plants' photosynthetic pathways. Technically, they are therefore strictly appropriate to describe the diet of herbivores. However, these terms will be used for all taxa in the present study to refer to the exploitation of resources provided from an environment dominated by either C₃ or C₄ plants rather than the consumption of the plants themselves. Finally, the emission of burning fuel over the past 150 years has decreased the $\delta^{13}\text{C}$ of atmospheric CO₂, consequently influencing the $\delta^{13}\text{C}$ of all living organisms. As the $\delta^{13}\text{C}$ values of plants are based on modern samples, they must be corrected (~ 1.5 ‰) (Friedli et al., 1986) when comparing with organisms that predate the atmospheric CO₂ shift due to fossil fuel burning. Therefore, the upper $\delta^{13}\text{C}$ limit for C₃ used for the present study is shifted from -23 ‰ to -21.5 ‰, and the lower limit for C₄ plants from -17 ‰ to -15.5 ‰.

The diet's isotopic composition is then metabolized and incorporated into the tissues of animals (Lee-Thorp et al., 1989). Trophic fractionation occurs when the food's carbon is metabolized and incorporated into the tissues of animals (bone collagen, enamel carbonate, hair, etc.), but is not homogenous and varies across animals (DeNiro and Epstein, 1978; Lee-Thorp et al., 1989; Cerling and Harris, 1999; Passey et al., 2005). No $\delta^{13}\text{C}$ diet-enamel spacing was thus applied to tooth enamel $\delta^{13}\text{C}_{\text{apatite}}$ values in this paper because empirically determined diet-enamel ^{13}C enrichment factors (or closely related ones) are not determined for too many of the investigated fossil species. Thus, only $\delta^{13}\text{C}_{\text{apatite}}$ values are compared, which avoids the necessity of assumptions (however well-founded and logical) otherwise needed in order to assign diet-enamel $\delta^{13}\text{C}$ spacing to species with no such available data. However, this still enables the distinction between C₃ and C₄ plant-feeders.

The oxygen isotopic composition ($\delta^{18}\text{O}$) of tooth enamel in homeothermic animals is regulated by that of body water, which consists of a complex combination of the effect of climate, diet, and physiology (Longinelli, 1984; Luz et al., 1984; Ayliffe and Chivas, 1990; Bryant et al., 1994; Kohn, 1996; Kohn et al., 1996; Pederzani and Britton, 2018). Enamel oxygen isotope composition is nevertheless primarily controlled by the composition of drinking water and chemically-bound water in the diet, i.e., free water found in plants (Longinelli, 1984; Luz et al., 1984; Bryant and Froelich, 1995; Kohn et al., 1996; Fricke et al., 1998; Fricke et al., 1998). The isotopic composition of both of these is, in turn, mostly dependent on latitude and climate and temperature, moisture content, amount of precipitation, and isotopic composition of precipitation (Dansgaard, 1964; Longinelli, 1984; Kohn and Cerling, 2002). In tropical and subtropical regions, it has been shown that the $\delta^{18}\text{O}$ values of vegetation mostly reflect either evaporative potential or the source-effect of rainfall (Buchmann et al., 1997; Buchmann and Ehleringer, 1998; McCarroll and Loader, 2006).

Carbon and oxygen isotope compositions offer another insight into paleoenvironmental conditions in densely forested C_3 ecosystems through low values resulting from a “Canopy Effect” (van der Merwe and Medina, 1991). The lowest $\delta^{18}\text{O}$ and $\delta^{13}\text{C}$ values are found in flora and fauna living on the forest floor (Vogel, 1978; Ehleringer et al., 1986; Medina et al., 1986; Ehleringer et al., 1987; Sternberg et al., 1989; van der Merwe and Medina, 1989, 1991; Krigbaum, 2003; Krigbaum et al., 2013; Graham et al., 2014; Blumenthal et al., 2016; Roberts et al., 2017b) and can consequently be used as a tracer to infer the density of a forest cover. Additionally, $\delta^{18}\text{O}$ and $\delta^{13}\text{C}$ values from densely forested areas and ones that are more open will discriminate from one another with higher values associated with open settings (Roberts et al., 2015, 2017a, 2017b; Blumenthal et al., 2016).

1.2.4 Variation of nitrogen stable isotope values in collagen

Collagen-bound nitrogen isotope composition ($\delta^{15}\text{N}$) is usually 3 to 5 ‰ higher than dietary protein (Schoeninger and DeNiro, 1984; Hedges and Reynard, 2007; Katzenberg and Waters-Rist, 2018). This diet-consumer spacing can thus be used to assess the trophic level of an organism within a given food web and particularly to identify the consumption of animal protein in the diet. Herbivores from terrestrial food web thus usually show $\delta^{15}\text{N}$ values 3 to 5 ‰ higher than the plants (i.e., 3 to 7 ‰), whereas carnivores will exhibit values, again, of 3 to 5 ‰ higher than their prey (i.e.,

6 to 12 ‰). Omnivore's $\delta^{15}\text{N}$ values will usually fall between both ranges, according to the proportion of plant and animal proteins in their diet. However, the $\delta^{15}\text{N}$ values of plants are not homogeneous (Ambrose, 1991; Martinelli et al., 1999; Aranibar et al., 2008), which can lead to differences in absolute $\delta^{15}\text{N}$ values from one food web to another. Nevertheless, by comparing specimens from a wide range of diets (herbivores, omnivores, and carnivores) for a given food web, it is possible to assign trophic level positions to specimens. The same trophic level effect can also be observed in aquatic ecosystems, but because many more steps usually take place in the food chain in aquatic ecosystems, $\delta^{15}\text{N}$ values of top-level consumers tend to be much higher (Richards and Hedges, 1999).

Supplementary information 1.3: Methods

1.3.1 Sample collection

The material used in this study consists of a selection of diverse taxa from the Tam Hay Marklot cave assemblage, covering a large range of distinct dietary habits. Each of the species' specific trophic ecology was assigned based on analogous modern-day fauna's dietary behaviors (Nowak, 1999; Macdonald, 2009; Johnsingh and Manjrekar, 2013, 2015). A total of 72 teeth belonging to 22 taxa were selected for the present isotopic analysis. One to six specimens per species were used (**Table S2**). Within each taxon, the same types of teeth (ex: left p3) were selected to ensure they belonged to different individuals. However, the same "right" and "left" teeth were sometimes selected but were considered to belong to distinct individuals based on different dental wear stages. In addition to their original submitter number, each specimen was assigned a SEVA code associated with samples prepared at the Department of Human Evolution of the Max Planck Institute for Evolutionary Anthropology (Leipzig, Germany). Enamel was mechanically cleaned using a handheld drill equipped with a diamond-tipped burr to remove both adhering external material and a superficial layer of enamel. Subsequently, three different samples for each specimen was taken along the full height of the crown, using either a diamond-tip cutting wheel or diamond-tipped burr: 4.8 to 23.5 mg (average $10.5 \text{ mg} \pm 7.3 \text{ mg}$ (2σ)) for zinc isotope analysis (a minimum of 5 mg is recommended for the analysis), 9.4 to 25.8 mg for strontium isotope analysis and 4.1 to 13.7 mg for carbon and oxygen isotope analysis. The varying amount of material collected was due to differences in relative thickness of the enamel, the height of the crown and the overall aspect of the teeth.

1.3.2 Zinc analytical technique

Enamel samples were digested in 1 ml of HCl 1.0 N, then evaporated and dissolved again in HBr 1.5 N. Zinc was then purified in two steps the modified ion exchange method adapted from Moynier et al. (2006), first described in Jaouen et al. (2016a). Zinc was purified in pre-conditioned microcolumns on 1 ml AG-1x8 resin (200-400 dry mesh size, 106-180 μm wet bead size) using 2 ml of HBr 1.5 N for matrix residue elution and 5 ml of HNO₃ 0.5 N for zinc elution. Samples were then dried and re-dissolved in 1 ml HNO₃ 0.5 N. Every preparation batch of 13 samples included at least one reference material (in-house reference material AZE bone powder and/or the NIST SRM 1400 bone ash) and a blank in order to assess the quality of the column chromatography purification. These replicate measurements allow to correct values of the enamel samples run at the same time, while also controlling the precision of the mass spectrometer (2σ (AZE) = 0.08 ‰; 2σ (NIST SRM 1400) = 0.06 ‰). Zinc isotopic ratios were measured using the protocol of Toutain et al. (2008) and Cu doping, on a Thermo Neptune Multi-collector ICP-MS at the Max Planck Institute for Evolutionary Anthropology (Leipzig, Germany). The dentin and sediment samples were measured on a Thermo Neptune Plus Multi-collector ICP-MS at the “Observatoire Midi Pyrénées” (Toulouse, France). The in-house standard zinc AA-MPI was used for standard bracketing. Isotopic ratios were expressed relative to the international standard JMC-Lyon. Isotopic abundances are presented in δ (delta) notation expressed as deviation per mil (‰), as follows: $\delta^{66}\text{Zn} = \left(\frac{{}^{66}\text{Zn}}{{}^{64}\text{Zn}}_{\text{sample}} / \frac{{}^{66}\text{Zn}}{{}^{64}\text{Zn}}_{\text{standard}} - 1 \right) \times 1000$. Repeated analyses ($n = 89$) of almost every specimen were also performed to determine the homogeneity of the enamel samples. The overall average analytical repeatability for these fossil samples was ± 0.04 ‰ (2σ) (**Table S4**). Following a protocol adapted from the one used for strontium by Copeland et al. (2008) (Copeland et al., 2008) and first used in Jaouen et al. (2016b), regression equation based on the ⁶⁴Zn signal intensity (V) of three solutions with known concentrations (150, 300 and 600 ppb) were used to estimate the zinc concentrations of samples. The accuracy of these obtained zinc concentration was evaluated through the known concentration of international reference material NIST SRM 1400 (bone ash) and deemed accurate (expected zinc concentration = 181 ± 6 $\mu\text{g/g}$ (2σ); measured zinc concentration 190 ± 19.4 $\mu\text{g/g}$ (2σ)).

1.3.3 Strontium analytical technique

Sample preparation used a modified method of Copeland et al. (2008) (Copeland et al., 2008), as presented in Britton et al. (2009) (Britton et al., 2009). Enamel samples were digested in 2 ml of HNO₃ 14.3 N, then evaporated and dissolved in 1 ml HNO₃ 3.0 N. Samples are then loaded into 1 ml of pre-conditioned microcolumns containing Sr-specTM resin (50-100 μm particle size). Matrix residues were eluted with 1.2 ml HNO₃ 3 N and strontium was eluted from the resin with 1.5 ml ultrapure deionized water (18.2 MΩ), dried and then re-dissolved in 2 ml HNO₃ 0.5 N. Every preparation batch of 10 samples included at least one reference material (NIST SRM 1486 bone meal) and a blank in order to assess the quality of the column chromatography purification. Analyses of ⁸⁷Sr/⁸⁶Sr ratios were measured using a Thermo Scientific Neptune Multi-collector ICP-MS at the Max Planck Institute for Evolutionary Anthropology.

All ⁸⁷Sr/⁸⁶Sr measurements were corrected for interferences from rubidium (Rb) and normalized for instrumental mass bias to ⁸⁸Sr/⁸⁶Sr = 8.375209 (exponential law). External normalization of data was achieved with analysis of the international strontium isotope reference material NIST SRM 987 during each analytical session (⁸⁷Sr/⁸⁶Sr value = 0.7102957 ± 0.000021 (2σ) (n = 58)). All ⁸⁷Sr/⁸⁶Sr values reported here were adjusted so SRM987 = 0.710240 (Johnson and Fridrich, 1990), with a correction offset of + 0.000056 (n = 58). Strontium concentrations of the enamel samples were determined through regression equation based on the ⁸⁸Sr signal intensity (V) of three solutions with known concentrations (100, 400, and 700 ppb), using the method described in Copeland et al. (2008) (Copeland et al., 2008).

1.3.4 Carbonate carbon and oxygen analytical technique

Each sample was soaked in a 1 ml of 0.1 M acetic acid (CH₃COOH) solution for four hours at room temperature, rinsed three times in distilled water, and then dried overnight at 65 °C. Stable carbon and oxygen isotopic compositions of every sample were analyzed using a Thermo Scientific Delta V Advantage isotopic mass spectrometer coupled to a Thermo Scientific Kiel IV Carbonate Device chemical preparer, at the "Service de Spectrométrie de Masse Isotopique du Muséum (SSMIM)" in Paris. Isotopic abundances are presented in δ (delta) notation expressed as deviation per mil (‰), as follows: $\delta^{13}\text{C} = \left(\frac{^{13}\text{C}/^{12}\text{C}_{\text{sample}}}{^{13}\text{C}/^{12}\text{C}_{\text{standard}}} - 1 \right) \times 1000$ and $\delta^{18}\text{O} = \left(\frac{^{18}\text{O}/^{16}\text{O}_{\text{sample}}}{^{18}\text{O}/^{16}\text{O}_{\text{standard}}} - 1 \right) \times 1000$. Analyses of an internal laboratory reference

material (Marble LM) normalized to the International Atomic Energy Agency reference material (NBS-19) (**Table S6**) were performed alongside fossil samples during every mass spectrometer run. These replicate measurements allow to correct values of the carbonate enamel samples run at the same time, while also controlling the precision of the mass spectrometer (2σ ($\delta^{13}\text{C}$) = 0.06 ‰; 2σ ($\delta^{18}\text{O}$) = 0.12 ‰).

1.3.5 Collagen carbon and nitrogen analytical technique

A selection of specimens ($n = 23$) from various taxon ($n = 16$) was also taken to assess the preservation of organic material. Because most teeth from the assemblage show various degrees of porcupine gnawing of their roots, only 23 out of the 72 specimens had sufficient dentin material for such analysis. The root of the teeth was cleaned with a sandblaster using Korox® 50 (50 μm) 99.6% aluminum oxide sand. Samples were obtained by using a handheld drill equipped with a diamond-tip cutting wheel, where 198.2 to 677.5 mg of material was taken from the root area. Sample preparation for collagen extraction followed the protocol first described in Talamo and Richard (2011) (Talamo and Richards, 2011). Samples were demineralized with HCl 0.5 N while refrigerated for several days (until no effervescence was observed), then rinsed with deionized water. NaOH 0.1 N was then added for 30 minutes to remove humic acids, followed by an HCl 0.5 N step for 15 minutes, with deionized water rinses after both steps. Following Longin's protocol (1971) (Longin, 1971), samples are gelatinized at pH 3 in a heater block at 75 °C for 20 h, and then filtered (Eeze-Filter™, Elkay Laboratory Products (UK) Ltd.), to remove small particles (<80 μm), and ultrafiltered (Sartorius "Vivaspin Turbo" 30 KDa ultrafilters). Finally, samples were lyophilized for 48 h (~ -28 °C). The preservation of the collagen was assessed for the samples with a sufficient yield by evaluating C:N (between 2.9 and 3.6) ratios, %C, %N, collagen yield (ideally not less than 1% of weight), and $\delta^{13}\text{C}$ and $\delta^{15}\text{N}$ values (Ambrose, 1990; van Klinken, 1999). Stable isotope analysis was conducted using a Thermo Finnigan Flash EA coupled to a Delta V isotope ratio mass spectrometer. The $\delta^{13}\text{C}$ values are measured relative to the V-PDB standard, and $\delta^{15}\text{N}$ values are measured relative to the AIR standard.

1.3.6 Spatial element concentration profiles analytical technique

Spatial element concentration profiles were conducted on six fossils specimens (Tam Hay Marklot cave, Laos) and three modern ones (Center of Natural History of

Hamburg, originally zoo animals from Hagenbeck Tierpark in Hamburg). Each tooth was sectioned longitudinally along the buccolingual axis using an Isomet low-speed saw (Bühler, Lake Bluff, US). In order to obtain a plane surface, the resulting surface of each tooth was then polished using an Ecomet 4000 variable speed grinder-polisher (Bühler, Lake Bluff, US) with CarbiMet grit 360 [P600] (Bühler, Lake Bluff, US) paper. The measurement routines were performed with a Thermo Element2 single collector sector-field ICP-MS coupled with a New Wave UP213 Nd:YAG laser ablation system at the Max Planck Institute for Chemistry, Mainz. Spot analysis with a laser beam size of 80 μm and a pulse repetition rate of 10 Hz was performed in a line scan analysis at a speed of 10 $\mu\text{m}/\text{s}$ after a pre-ablation with 80 $\mu\text{m}/\text{s}$. Fluence (energy density) during the experiments was 13 J cm^{-2} .

Concentration of the following 36 selected isotopes were measured in the same run: Na^{23} , Mg^{25} , Al^{27} , Si^{29} , P^{31} , K^{39} , Ca^{43} , Mn^{55} , Fe^{57} , Cu^{63} , Zn^{66} , Zn^{67} , Zn^{68} , Rb^{85} , Sr^{86} , Sr^{88} , Cs^{133} , Ba^{137} , Ba^{138} , La^{139} , Ce^{140} , Pr^{141} , Nd^{143} , Sm^{147} , Eu^{151} , Gd^{157} , Tb^{159} , Dy^{161} , Ho^{165} , Er^{167} , Tm^{169} , Yb^{173} , Lu^{175} , Pb^{208} , Th^{232} and U^{238} . The synthetic glass NIST SRM 612 ($n = 6$) was used to calibrate element concentrations (Jochum et al., 2011). Each monitored isotope was normalized to ^{43}Ca as the internal standard. During each LA-ICP-MS sequence, the accuracy and precision of the analysis were assessed by measuring ca. 160 μm long line scans on a pressed powder pellet of NIST SRM 1400.

1.3.7 Statistical analysis

To test our hypotheses, analyses were performed using the statistical program R (version 3.6.1) (R Core Team, 2018). Our response variable was $\delta^{66}\text{Zn}$ values, and the tested predictors, associated with each $\delta^{66}\text{Zn}$ value were diet (carnivore, omnivore, and herbivore), taxon, $\delta^{13}\text{C}$ values, $\delta^{18}\text{O}$ values, $^{87}\text{Sr}/^{86}\text{Sr}$ isotope ratios, zinc concentration, and the average body mass for that specific species. We fitted a linear mixed model (LMMs) (Baayen, 2008) with a Gaussian error structure and identity link (McCullagh and Nelder, 1989) using the R-package “lme4” (version 1.1-17) (Bates et al., 2015).

All quantitative predictors were inspected for whether they were roughly symmetrically distributed and were, when they showed to have a skewed distribution (body mass and zinc concentration), log-transformed. In order to ease model convergence and achieve comparability of estimates, all quantitative predictors were subsequently z-transformed (to a mean of zero and a standard deviation of one). We included all predictors as fixed effects with the exception of taxon, which we included

as a random intercepts effect. Furthermore, to keep Type I error rate at the nominal level of 0.05, we included random slopes of $\delta^{13}\text{C}$, $\delta^{18}\text{O}$, $^{87}\text{Sr}/^{86}\text{Sr}$, and zinc concentration within taxon but no parameters for the correlations among random slopes and intercepts (Schielzeth and Forstmeier, 2009; Barr et al., 2013). Collinearity among predictors was assessed using the function *vif* of the R-package “car” (Fox and Weisberg, 2011) applied to a standard linear model, excluding the random effect, was low (maximum of squared n^{th} root of Generalized Variance Inflation Factors, with n being twice the degrees of freedom of the respective predictor: 1.56).

To assess model stability, we compared model estimates obtained from the full dataset with those obtained when excluding levels of the random effect (taxa) and as well as specimens, one at a time. This revealed model stability to be good. We checked whether the assumptions of normally distributed and homogeneous residuals were fulfilled by visual inspection of a QQ-plot (Field, 2005) of the residuals and residuals plotted against fitted values, which revealed no obvious violations of these assumptions. In order to test the significance of the key test predictors, $^{87}\text{Sr}/^{86}\text{Sr}$ and body mass, we compared the full model with a null model lacking these two terms to avoid multiple testing (Forstmeier and Schielzeth, 2011). For this we used a likelihood ratio test, approximated using a *chi*-square distribution (Dobson, 2002). We also tested the significance of individual fixed effect predictors using likelihood ratio tests comparing the full model and with models dropping predictors one at a time. We determined confidence intervals of model estimates by means of a parametric bootstrap (function *bootMer* of the package “lme4”) utilizing 1,000 bootstraps. The sample size for the model was 69 specimens from 22 taxa since three specimens could not be sampled for $^{87}\text{Sr}/^{86}\text{Sr}$ analysis.

Supplementary information 1.4: Results

1.4.1 Zinc stable isotope values ($\delta^{66}\text{Zn}$) in fossil tooth enamel from Tam Hay Marklot Cave

The zinc isotopic compositions of the 72 studied tooth enamel specimens from the Tam Hay Marklot fauna are presented here and in **Table S4**.

When every taxon and every diet category are considered, $\delta^{66}\text{Zn}$ values range from -0.04 ‰ (*Hystrix* sp.) to 1.03 ‰ (*Bos* sp.), with an average of 0.52 ‰ (± 0.54 ‰ (2σ)). Herbivores ($n = 41$; $\text{mean}\delta^{66}\text{Zn} = 0.68$ ‰ ± 0.38 ‰ (2σ)) exhibit $\delta^{66}\text{Zn}$ values ranging from 0.29 ‰ (*Muntiacus* sp.) to 1.03 ‰ (*Bos* sp.), carnivores ($n = 9$; $\text{mean}\delta^{66}\text{Zn} = 0.09$

± 0.24 ‰ (2σ) from -0.01 ‰ (*Panthera tigris*) to 0.34 ‰ (Canidae) and omnivores ($n = 22$; mean $\delta^{66}\text{Zn} = 0.41 \pm 0.54$ ‰ (2σ)) from -0.04 ‰ (*Hystrix* sp.) to 0.72 ‰ (*Sus* sp.).

Rhinoceros sondaicus ($n = 5$) exhibit the largest range of variation in $\delta^{66}\text{Zn}$ values (0.51 ‰) and *Ursus thibetanus* ($n = 3$) the smallest (0.05 ‰), with an average range throughout all different taxa of 0.27 ‰. When the mean intra-specific $\delta^{66}\text{Zn}$ ranges of variation of each taxon are taken together, omnivores exhibit the largest one (0.30 ‰), followed by herbivores (0.28 ‰) and then finally carnivores (0.15 ‰). It is also noteworthy to mention that the range of variation in $\delta^{66}\text{Zn}$ values of herbivores taxa is increased by that of *Rhinoceros sondaicus*, itself influenced by a single outlier. If this outlier were to be ignored, the range of variation observed in herbivores taxa $\delta^{66}\text{Zn}$ would decrease to 0.25 ‰.

The overall range of $\delta^{66}\text{Zn}$ values for each broad diet category, as well as their taxon intra-specific variations, is in agreement with dietary habits. Indeed, omnivorous taxa (which diets can consist of various proportions of meat, eggs, insects, grubs, fruits, roots, tubers, leaves, stems, bark, etc.) exhibit the largest range and variability of $\delta^{66}\text{Zn}$ values. They display $\delta^{66}\text{Zn}$ values ranging from those associated with carnivorous taxa to those of strict herbivorous, with the bulk, however, consisting of intermediate values between carnivores and herbivores. This, in turn, most likely results from a varying proportion of meat in the diet. Herbivorous taxa range of $\delta^{66}\text{Zn}$ values, albeit smaller than that of omnivores, is also coherent with expectations. Values are generally higher, and the relatively large range in $\delta^{66}\text{Zn}$ values is consistent with intake from different plants and plant parts (i.e., fruits, roots, tubers, leaves, stems, bark, etc.). Finally, carnivore taxa exhibit the lowest $\delta^{66}\text{Zn}$ values and the smallest range of variation, both being in agreement with a diet limited to meat consumption.

Additionally, sediment ($n = 5$) and dentin samples ($n = 13$, from 7 specimens) and were analyzed for $\delta^{66}\text{Zn}$ values (**Table S15**) in order to assess the trend of post-mortem diagenesis alteration. The $\delta^{66}\text{Zn}_{\text{dentin}}$ values range from 0.39 to 1.05 ‰ (**Table S15 and Figures S40-42**). The offset observed between $\delta^{66}\text{Zn}_{\text{dentin}}$ and $\delta^{66}\text{Zn}_{\text{enamel}}$ is $+0.22 \pm 0.26$ ‰ (2σ) (**Figure S40**), which is in agreement with $\delta^{66}\text{Zn}$ values obtained from modern fauna at Kobi Fora ($\Delta\delta^{66}\text{Zn}_{\text{bone-enamel}} \approx +0.2$ ‰) (Jaouen et al., 2016a). Additionally, the trophic levels difference can still be observed, with carnivores having the lowest $\delta^{66}\text{Zn}$ values. The $\delta^{66}\text{Zn}_{\text{sediment}}$ values range from 0.12 ‰ to 0.69 ‰ (**Table S15**). The clay sample exhibits the lowest $\delta^{66}\text{Zn}$ value, as can be expected from a usually silicate-rich mineral, and the highest $\delta^{66}\text{Zn}$ value is found in the cemented

fossil-bearing layer. When $\delta^{66}\text{Zn}$ values from both sediments and dentin samples are compared with their respective zinc concentration (**Figure S42**), no obvious trend could be observed. Thus, no clear post-mortem diagenesis alteration in dentin $\delta^{66}\text{Zn}$ values and zinc concentration can be observed.

1.4.2 Strontium radiogenic isotope ratios ($^{87}\text{Sr}/^{86}\text{Sr}$) in fossil tooth enamel from Tam Hay Marklot Cave

The radiogenic strontium isotope ratios ($^{87}\text{Sr}/^{86}\text{Sr}$) of 69 specimens from the Tam Hay Marklot fauna are presented here and in **Table S4 and Figures S10-11**. Only 69 specimens out of 72 were analyzed, as not enough material was available from three specimens.

The $^{87}\text{Sr}/^{86}\text{Sr}$ ratios range from 0.7097 (*Hystrix* sp.) to 0.7243 (*Helarctos malayanus*), with an average of 0.7154 ± 0.0062 (2σ). The majority of the specimens falls within a range of $^{87}\text{Sr}/^{86}\text{Sr}$ ratios from 0.7135 (1st Qu.) to 0.7173 (3rd Qu.). *Axis* cf. *porcinus* ($n = 2$) exhibit the smallest intra-specific variation in $^{87}\text{Sr}/^{86}\text{Sr}$ isotope (0.0001) and *Helarctos malayanus* ($n = 2$) display the largest (0.0122 ± 0.0172 (2σ)), while the average variation observed for each taxon is of 0.0044 ± 0.006 (2σ).

No bioavailable strontium isotope ratios are available for the studied region, and no local plants were analyzed in the current study. Description of the bedrocks geology is nonetheless available (Saurin, 1961) and reported in “**Supplementary information 1.1: Context - 1.1.1 Geology**”. Three major units are identified in the surrounding area of the Tam Hay Marklot cave: Palaeozoic granite basement, a widespread Silurian light metamorphic sedimentary formation composed primarily of arkosic sandstone, and finally, a thick limestone unit attributed to an interval between the Late Carboniferous (Moscovian) and the Permian (Saurin, 1961). Considering the local geology of Tam Hay Marklot cave’s region, it could be expected that the granite exhibits a higher $^{87}\text{Sr}/^{86}\text{Sr}$ value than the other two the sedimentary substratum. Accordingly, the granite would also be expected to display lower $\delta^{66}\text{Zn}$ values than both sedimentary rock formations (Luck et al., 1999; Maréchal et al., 2000; Pichat et al., 2003; Cloquet et al., 2008; Moynier et al., 2017). The preservation of pristine radiogenic strontium isotope ratios was investigated through a mixing line between strontium concentration and $^{87}\text{Sr}/^{86}\text{Sr}$ ratios (**Figure S11**). The absence of any significant post-mortem strontium uptake was corroborated by the absence of relation between the two variables, as well

as by the strontium concentrations also fall within the range of modern specimens (Figure S11).

1.4.3 Carbon ($\delta^{13}\text{C}$) and oxygen ($\delta^{18}\text{O}$) stable isotope values in fossil tooth enamel from Tam Hay Marklot Cave

The carbon and oxygen isotopic compositions of the 72 studied specimens from the Tam Hay Marklot cave fauna are presented here and in Table S4 and Figure S8.

Among the 22 taxa present in the sample, the $\delta^{13}\text{C}_{\text{apatite}}$ values range from -16.7 ‰ (*Ailuropoda melanoleuca*) to +2.4 ‰ (*Rucervus eldii*), with a mean $\delta^{13}\text{C}$ value of -10.11 ‰ (± 10.64 ‰ (2σ)). Herbivores ($n = 41$) present values -16.2 ‰ (*Rhinoceros sondaicus*) to +2.4 ‰ (*Rucervus eldii*), carnivores ($n = 9$) between -16.0 ‰ (Canidae (?*Cuon alpinus*)) and -4.0 ‰ (*Panthera pardus*) and omnivores ($n = 22$) between -15.4 ‰ (*Ursus thibetanus*) and -6.0 ‰ (*Sus* sp.). The majority of the specimens (65%, $n = 47$) display $\delta^{13}\text{C}_{\text{apatite}}$ values that reflect a C_3 diet ($\delta^{13}\text{C}_{\text{apatite}} < -8$ ‰), with a moderate amount (25%, $n = 18$) showing a mixed C_3/C_4 diet (-8 ‰ $> \delta^{13}\text{C}_{\text{apatite}} > -2$ ‰), and only few (10%, $n = 7$) being associated with a strict C_4 diet ($\delta^{13}\text{C}_{\text{apatite}} > -2$ ‰). Large bovids (*Bos* sp., *Bubalus bubalis*) and *Panthera pardus* exhibit the largest variations in $\delta^{13}\text{C}$ values (respectively $\Delta^{13}\text{C}$ 14.1 ‰, 11.9 ‰, and 9.8 ‰) and *Helarctos malayanus*, *Axis* cf. *porcinus* and *Rucervus eldii* exhibits the smallest ones (respectively $\Delta^{13}\text{C}$ 0.2 ‰, 0.2 ‰, and 0.6 ‰). The average overall variation is 4.3 ‰ and the median 2.6 ‰.

The $\delta^{13}\text{C}_{\text{apatite}}$ values of -14.0 ‰ or lower result from a strong canopy effect, thus representative of a mesic closed low-light tropical rainforest (Cerling et al., 1997, 2004, 2015; Cerling and Harris, 1999; Levin et al., 2008; Roberts et al., 2015, 2017a; Bacon et al., 2018a), with a relatively high proportion (30%, $n = 22$) of specimens from Tam Hay Marklot cave being associated with these values. All three dietary categories (carnivores, omnivores, and herbivores) are represented for a total of 12 different taxa. *Rhinoceros sondaicus* ($n = 5$), in particular, is well represented in this ecoregion, with only a single specimen falling out of the aforementioned range of $\delta^{13}\text{C}_{\text{apatite}}$ values. Higher $\delta^{13}\text{C}_{\text{apatite}}$ values, between -14 ‰ and -8 ‰, consist of diets reflecting a reliance on mostly C_3 environment resources. It encompasses a similar proportion of specimens (35%, $n = 25$) to those associated with a strong canopy effect and presents the highest diversity in species (14/22 taxa). However, these C_3 associated $\delta^{13}\text{C}_{\text{apatite}}$ values can reflect either a mixed dietary reliance from closed forests and open woodlands (Sponheimer et al., 2006a, 2006b; Levin et al., 2008; Roberts et al., 2015, 2017a) or a

reliance on strictly mesic forest environment (Erdelen, 1988; Roberts et al., 2015, 2017a; Bacon et al., 2018a). In the case of Tam Hay Marklot cave, the latter case seems the most coherent. Indeed, taxa associated with $\delta^{13}\text{C}_{\text{apatite}}$ values between -14.0 ‰ and -8.0 ‰, most notably but not restricted to *Pongo* sp. (orangutan), support the presence of forest habitat, albeit probably not as dense as that of a closed low-light tropical rainforest. A natural break in the $\delta^{13}\text{C}_{\text{apatite}}$ values can also be observed around -10.0 ‰. Finally, the highest end of $\delta^{13}\text{C}_{\text{apatite}}$ values encompass values reflecting mixed C₃-C₄ resources reliance (from -8.0 ‰ to -2.0 ‰) and strict C₄ plant-feeder (i.e., grazer) values (> -2.0 ‰). A fairly significant number of specimens (35%, $n = 25$) and taxa from Tam Hay Marklot (10/22) once again present such values. Such values cover a wide array of ecoregions going from mixed forests to C₃ xeric woodland to C₃-C₄ “savannah” environment. While it can be difficult to define a clear limit between these various different ecoregions, they nonetheless all consist of open settings of varying degrees.

The oxygen isotopic compositions of Tam Hay Marklot fauna vary from -10.0 ‰ (*Sus* sp.) to 0.2 ‰ (*Naemorhedus* cf. *caudatus*), with an average $\delta^{18}\text{O}_{\text{apatite}}$ values -5.7 ‰ (± 3.54 ‰ (2σ)). Herbivores display values of -7.6 ‰ (*Capricornis* sp.) to -4.2 ‰ (*Bos* sp.), carnivores from -7.3 ‰ (*Panthera pardus* and Canidae (?*Cuon alpinus*)) to -3.2 ‰ (Canidae (?*Cuon alpinus*)) and omnivores from -10.0 ‰ (*Sus* sp.) to -4.1 ‰ (*Pongo* sp.). The average variation seen within taxa is 2.6 ‰ and the median 2.8 ‰. Contrary to expectations, the taxa that exhibit the largest variation in their $\delta^{18}\text{O}_{\text{apatite}}$ values were not systematically those that showed large variation in their $\delta^{13}\text{C}$ values as well.

1.4.4 Carbon ($\delta^{13}\text{C}$) and nitrogen ($\delta^{15}\text{N}$) stable isotope values in fossil teeth root dentin from Tam Hay Marklot Cave

A sub-sample of 23 specimens from 16 different taxa was processed for collagen extraction to assess the preservation of organic material. The preservation of the collagen was assessed for the samples with a sufficient yield by evaluating C:N (between 2.9 and 3.6) ratios, %C, %N, collagen yield (not less than 1% of weight), and $\delta^{13}\text{C}$ and $\delta^{15}\text{N}$ values (Ambrose, 1990; van Klinken, 1999). The collagen-bound stable carbon and nitrogen isotopic composition of the four specimens that yielded collagen are presented here and in **Table S5 and Figure S9**.

Individuals with the highest to the lowest $\delta^{15}\text{N}_{\text{collagen}}$ are: *Muntiacus* sp. (10.56 ‰), *Sus* sp. (8.07 ‰), *Rhinoceros sondaicus* (6.63 ‰), and *Bos* sp. (3.15 ‰). The associated $\delta^{13}\text{C}_{\text{collagen}}$ values are -21.0 ‰, -21.7 ‰, -24.0 ‰ and -9.1 ‰, respectively.

The low $\delta^{15}\text{N}_{\text{collagen}}$ value of *Bos* sp. can be explained by the fact that the food resources consumed by this specimen come from a C_4 environment, and thus more open and dry than that associated with the other three specimens (Aranibar et al., 2008). Its trophic level is nevertheless consistent with a herbivorous diet (Schoeninger and DeNiro, 1984; Kelly, 2000; Hedges and Reynard, 2007; Katzenberg and Waters-Rist, 2018). The $\delta^{15}\text{N}_{\text{collagen}}$ value of the *Sus* sp. specimen, when compared to herbivorous *Rhinoceros sondaicus* specimen, is consistent with that of an omnivorous diet, as it is higher (+1.49 ‰) but not by a full trophic level (Schoeninger and DeNiro, 1984; Hedges and Reynard, 2007; Katzenberg and Waters-Rist, 2018). *Muntiacus* sp. exhibits the highest $\delta^{15}\text{N}_{\text{collagen}}$, which is almost a trophic level higher (+2.49 ‰) than that of *Sus* sp. and a full trophic level higher than that of *Rhinoceros sondaicus* (+3.93 ‰). This is surprising given that even an omnivorous diet is debated for the muntjac. While some studies suggest that they exhibit omnivore habits (Kurt, 1990; Jackson, 2002), others show that it is not the case (Jackson and Chapman, 1977; Ilyas and Khan, 2003; Johnsingh and Manjrekar, 2015). At the very least, a full trophic level above herbivores, and slightly higher than that of *Sus* sp., is unexpected. The $\delta^{13}\text{C}_{\text{collagen}}$ values are consistent with those ranging from mammals feeding in a C_4 open environment to a closed low-light tropical rainforest. They also mirror the $\delta^{13}\text{C}_{\text{apatite}}$ values obtained for the same specimens. A fairly constant $\delta^{13}\text{C}_{\text{apatite-collagen}}$ spacing (from 7.8 to 8.8 ‰; 8.2 ± 1.0 ‰ (2σ)) can also be observed and is slightly larger than expected spacings, especially for omnivores (Krueger and Sullivan, 1984; Lee-Thorp et al., 1989; Passey et al., 2005).

1.4.5 Spatial element concentration profiles

Spatial element concentration profiles analysis was carried on (*Capricornis* sp., *Ursus thibetanus*, *Panthera pardus*, *Sus* sp., and *Macaca* sp.) and three modern teeth (*Bison bison*, *Hemitragus jemlahicus*, and *Pteronura brasiliensis*) of various feeding behaviors (carnivorous, omnivorous, and herbivorous). From the 36 selected isotopes measured, sets of spatial element concentration profiles are provided in **Figures S12-S29** for the following elements: zinc (Zn), iron (Fe), manganese (Mn), aluminum (Al), magnesium (Mg), strontium (Sr), REE (rare earth elements, calculated as the sum of

all measured REE concentrations), lead (Pb) and uranium (U). Elements such as iron, manganese, and aluminium and were used as diagenetic tracers because their ionic radius is close to that of zinc, making them more likely to share similar behaviors and consequently to be altered in similar ways (Jaouen et al., 2018). In addition, rare earth elements, lead, and uranium were used to assess the presence of diagenesis in a broader sense. Indeed, because their ionic radius differs widely from that of zinc, they behave in a very different way and are not a reliable specific diagenesis tracer for elements such as zinc (Reynard and Balter, 2014).

Similar concentrations and undisturbed distribution profiles of these elements were observed almost systematically across modern and fossil enamel samples, while in contrast the dentin and pulp cavity in fossil teeth displayed an increase or decrease of these elements, indicating diagenetic alteration. A total of 23 enamel cross-section segments were analyzed over the 15 analyses conducted on the six fossil specimens. Only one, from the *Panthera pardus* specimen, showed zinc concentration distribution that deviates from the pattern found in modern teeth. However, this was only observed for one of the cross-section segments analyzed on this specimen.

Supplementary information 2

Supplementary information to Jaouen et al. (2020), Zinc isotope variations in archeological human teeth (Lapa do Santo, Brazil) reveal dietary transitions in childhood and no contamination from gloves. PLoS ONE 15, e0232379. doi.org/10.1371/journal.pone.0232379

Supplementary information 2.1: Archeological context

The samples come from the site of the convent of the Jacobins, Rennes, France. The diet of many individuals from this convent has been investigated in two previous studies (Jaouen et al., 2018; Colleter et al., 2019). They revealed a diet rich in animal proteins during the 16th to 18th centuries for the well-off individuals (Group A) as well as the intermediate socio-economical group (Group B). The two individuals analyzed for this study are a 5 to 9-year-old child belonging to Group A (Grave 291, US 63949, buried in one of the chapels of the convent church), and an adult belonging to Group B (Grave 300, US 20106) buried in the west yard, out of the convent walls (Le Cloirec, 2016). The adult died between 20 and 49 years of age (AlQahtani et al., 2010) and was quite tall compared to the rest of the Jacobin population (178.6 cm).

Supplementary information 2.2: Methods

Prior to destructive sampling, the teeth were scanned on a Diondo d3 micro-CT scanner in the Department of Human Evolution at the Max Planck Institute for Evolutionary Anthropology in Leipzig. The following parameters were used for μ CT-scanning the lower left M1: voltage of 130 kV, a current of 80 μ A, frame average of 2, 2430 projections, a resolution of 9.1366 μ m (isometric voxels), X-Ray beam filtered by 0.5 mm of Brass; the scan took 1h4min. The data were routinely reconstructed as described in Le Cabec et al. (2013). Virtual 2D sections and 3D models were generated in VGSTUDIO MAX 3.2.0.

The teeth were sampled following the protocol described in the main text using vinyl gloves. The sampling areas were carefully chosen (reported in **Table S19**) to be able to estimate the associated age of enamel formation (**Figure S48**). The collagen was extracted following the protocol of Talamo and Richards (2011) without the ultrafiltration step in order to obtain enough material on the milk teeth. All the teeth

were analyzed at the GET/OMP lab using a Neptune Plus MC-ICP-MS for zinc isotopes and with EA-IRMS for C/N isotopes.

Supplementary information 2.3: Results and discussion

Isotope data for the samples and standards can be found in **Tables S16 and S19**, as well as **Chapter 3, Figures 13 and 14**. The collagen extraction was successful for all the samples tested, and the C/N ratio corresponds to the modern range (van Klinken, 1999). For zinc isotopes, the differences between the adult and the child for the I1, I2, C, P3, and P4 can be partially explained by the fact that the sampled areas were at the tip of the crown for the child (cuspal enamel), and the middle for the adult (lateral enamel). However, we have two samples horizontally (parallelly to the enamel dentin junction) taken for all the adult teeth except the M1, and they gave consistent results. Therefore, the child samples reveal earlier stages of formation when the individual was still breastfed. Based on Figure 12, we can assume the child was weaned at 2 years of age. It also matches the results obtained on nitrogen isotopes (**Figure S49**). According to nitrogen isotopes, the diet of the child significantly changed after weaning, including much more animal proteins around 5 years of age. The fact that the incisors and canines of the adult are not different from the premolars and molars suggests an earlier age at weaning, probably around 1 year of age. It is known that urban populations were using wet nurses in the countryside, who had to care for more than one child, and were weaning the children with porridge (Stuart-Macadam and Dettwyler, 2017). The richer families used to hire and host directly in their home a private wet nurse, which triggered less hygienic and milk deficiency issues and therefore involved later weaning ages. However, the shift of nitrogen isotopes observed for the child after weaning age (**Figure S49**) could suggest that the child first grew up at the wet nurse's residence and was weaned on a plant-based diet. The child then moved to his or her biological family, where animal resources were more available. However, it could also suggest metabolic stress since the roots were still forming when the individual died: nitrogen isotope ratios can increase in association to nutritional stress (Hobson et al., 1993; Mekota et al., 2006). Many intense and regular stress events were observed in the dentin of the M1 (see μ CT data, **Figure S50**). This is consistent and would lend support to explain the elevated $\delta^{15}\text{N}$ values obtained from the M1 dentin.

The previous works by Dolphin and collaborators (Dolphin et al., 2005; Dolphin and Goodman, 2009) suggested that postnatal enamel should exhibit higher zinc

concentrations than prenatal one, which we did not observe (**Figure S51**). In general, no correlation was observed between zinc isotope ratios and concentrations. It is probably explained by the fact that superficial enamel has a very high zinc content (Tacail et al., 2007) and that depending on the depth of the sampling, it might impact the zinc concentration of a sample whatever formation time it would correspond to.

Supplementary information 3

Supplementary information to Bourgon et al. (2021), Trophic ecology of a Late Pleistocene early modern human from tropical Southeast Asia inferred from zinc isotopes. J. Hum. Evol. 161, 103075, doi.org/10.1016/j.jhevol.2021.103075.

Supplementary information 3.1: Stable isotope analyses

3.1.1 Variation of zinc stable isotope values in tooth enamel

In a terrestrial context, the primary source of zinc in a given food web originates from its primary producers—plants. Two main parameters have been shown to account for the zinc isotope composition of plants: initial zinc isotope ratios of the source uptake, i.e., soil (Viers et al., 2007; Fekiacova et al., 2015), and biological fractionation (Weiss et al., 2005; Viers et al., 2007, 2015; Moynier et al., 2009; Aucour et al., 2011). For plants specifically, the initial source uptake is derived from the soil, the isotopic composition of which is in turn controlled by the nature of the underlying bedrock. The $\delta^{66}\text{Zn}$ value of the soil itself is determined by the nature of the underlying bedrock, where igneous rocks exhibit a narrow range of $\delta^{66}\text{Zn}$ values ($+0.3 \pm 0.14\text{‰}$, 2σ ; Moynier et al., 2009, 2017) and sedimentary rocks exhibit a broader range (Maréchal et al., 2000; Cloquet et al., 2008; Moynier et al., 2017) with the highest values observed for marine carbonates (up to $+1.4\text{‰}$; Luck et al., 1999; Pichat et al., 2003). Within plants themselves, biological fractionation first occurs between the roots and the soil, specifically through zinc uptake in the rhizosphere. Roots, but also shoots, thus generally display higher $\delta^{66}\text{Zn}$ values relative to the litter layer in which they grow (Weiss et al., 2005; Viers et al., 2007; Moynier et al., 2009; Aucour et al., 2011). Additional fractionation within plants also seems to occur through an active uptake of zinc heavy isotopes by cells out of the xylem during its transport. This consequently favors the mobility of light isotopes to the most aerial parts of the plants, which in turn exhibit low $\delta^{66}\text{Zn}$ values (Weiss et al., 2005; Viers et al., 2007; Moynier et al., 2009). As a result, a correlation is often observed between the $\delta^{66}\text{Zn}$ in leaves and the height of the plants, both within a single plant and between plant species. Accordingly, low-growing plants such as herbaceous species are expected to display higher $\delta^{66}\text{Zn}$ values compared to high-growing plants like trees (Weiss et al., 2005; Viers et al., 2007; Moynier et al., 2009). Subsequently, the isotopic composition of zinc in a consumer's body tissues is governed by the same two factors, namely, zinc isotopic composition of the source uptake (i.e., the food ingested, whether plant or animal; Jaouen et al.,

2013; Costas-Rodríguez et al., 2014) and the isotopic fractionation occurring within an organism (Turnlund et al., 1984; Cousins, 1985; Lönnerdal, 2000; Balter et al., 2010; Jaouen et al., 2013, 2017; Moynier et al., 2013). It has been suggested that biological activity fractionates zinc isotopes in the body, thus explaining variability in body tissues (Balter et al., 2010; Moynier et al., 2013). As such, a consumer's $\delta^{66}\text{Zn}$ values will reflect which plant or animal species was fed upon as well as which parts or tissues of said food source. This also applies to breastfeeding milk, which was recently demonstrated to induce an isotopically distinct composition to that of an adult diet (Jaouen et al., 2020).

3.1.2 Variation of strontium isotope values in tooth enamel

The $^{87}\text{Sr}/^{86}\text{Sr}$ of the underlying soil/rock substrate mainly controls the geographical distribution of strontium isotopes. Contrary to other strontium isotopes, ^{87}Sr is radiogenic, resulting from the radioactive decay of ^{87}Rb . As such, the relative content and ratio of ^{87}Sr to ^{86}Sr of a given bedrock is a function of the age of the rock but also of its original rubidium (Rb) amount. A general trend of higher $^{87}\text{Sr}/^{86}\text{Sr}$ in older rocks and of lower values in younger rocks is thus typical.

Strontium isotopes are the principal geochemical proxy used to trace migration and to determine the provenance of individuals (whether animals or humans) from a geologic area, originally demonstrated in ecological studies (Gosz et al., 1983; Åberg, 1995; Koch, 1998) and then frequently applied to archeological contexts (Ericson, 1985; Balasse, 2002; Bentley, 2006). This is because the geogenic $^{87}\text{Sr}/^{86}\text{Sr}$ is mostly transferred from the eroding geologic bedrock to the soil (Dasch, 1969) and then enters as bioavailable strontium into the plants (Hurst and Davis, 1981). This $^{87}\text{Sr}/^{86}\text{Sr}$ is then preserved within a food web, regardless of the trophic level (Steadman et al., 1958; Blum et al., 2000). Indeed, kinetic and equilibrium biological fractionations of $^{87}\text{Sr}/^{86}\text{Sr}$ are negligible (Bentley, 2006; Price et al., 2012; Wright, 2012; Flockhart et al., 2015) and normalization to an $^{86}\text{Sr}/^{88}\text{Sr}$ value of 0.1194 to correct for instrumental mass bias (Bentley, 2006) subsequently removes all fractionation arising from natural processes and measurement. As such, radiogenic $^{87}\text{Sr}/^{86}\text{Sr}$ ratios in animal bones and teeth are passed along trophic levels and reflect those of local bioavailable strontium sources (Graustein, 1989; Bentley, 2006; Knudson et al., 2010; Lewis et al., 2017). The $^{87}\text{Sr}/^{86}\text{Sr}$ from specimens can thus be associated with a biologically available signature from a given location or region.

3.1.3 Variation of carbon and oxygen stable isotope values in tooth enamel

The carbon isotopic composition ($\delta^{13}\text{C}$) of bioapatite can be used to assess the reliance on food resources through the existence of ‘isotopically’ distinct resources in the environment. In a tropical setting, the $\delta^{13}\text{C}$ values distinguish plants undergoing C_3 and C_4 photosynthetic pathways (Smith and Epstein, 1971; O’Leary, 1988; Farquhar et al., 1989). The $\delta^{13}\text{C}$ values observed in studied faunal or hominin material reflect that of the carbon sources, and consequently convey the relative proportion of C_3 forest/woodland and C_4 grassland in their diet, and indirectly to their associated environments (Zazzo et al., 2000; Sponheimer et al., 2006a; Codron et al., 2012; Bacon et al., 2018a, 2018b). C_3 plants encompass trees, bushes, shrubs, and C_3 grasses (Smith and Epstein, 1971; O’Leary, 1988; Farquhar et al., 1989; Still et al., 2003). For the geographic area in this study, the $\delta^{13}\text{C}$ values of C_3 plants are considered to fall in the range of -37 to -23 ‰, as higher values (>-23 ‰) are limited to species from particularly dry environments (Smith and Epstein, 1971; O’Leary, 1988; Kohn, 2010). Low $\delta^{13}\text{C}$ values (<-27.2 ‰ (Cerling et al., 2004; Levin et al., 2008; Tejada et al., 2020)) offer additional insight into paleoenvironmental conditions, as they result from a ‘canopy effect’ (van der Merwe and Medina, 1991) found in densely forested C_3 ecosystems. C_4 plants mainly consist of grasses and sedges that primarily occur in tropical and subtropical grassland and savannah regions (Still et al., 2003). They display higher $\delta^{13}\text{C}$ values of -17 to -10 ‰ (Smith and Epstein, 1971; O’Leary, 1988), thus allowing for a clear C_4 to C_3 distinction in environments where both photosynthetic pathways are found. However, the burning of fossil fuels over the past 150 years has decreased the $\delta^{13}\text{C}$ of atmospheric CO_2 and consequently influenced the $\delta^{13}\text{C}$ of all living organisms. As the $\delta^{13}\text{C}$ values of plants used in paleontological and archeological research are based on modern samples, a correction must be applied (~ 1.3 ‰; Friedli et al., 1986) when studying organisms that predate this atmospheric CO_2 shift. Therefore, the upper $\delta^{13}\text{C}$ limit for C_3 used for the present study is shifted from -23 to -21.7 ‰, and the lower limit for C_4 plants from -17 to -15.7 ‰. The upper limit for a closed-canopy C_3 environment is -27.2 ‰, following recent work by Tejada et al. (2020), and already accounts for the correction of the modern-day atmospheric CO_2 shift. Finally, the tissues of animals subsequently metabolized and incorporated the isotopic composition of the diet (Lee-Thorp et al., 1989). However, trophic fractionation occurring between consumer and diet varies between body tissues and across animals (DeNiro and Epstein, 1978; Lee-Thorp et al., 1989; Cerling and Harris, 1999; Passey et al., 2005). Indeed, some comparable modern data are available (Lee-Thorp and Van der Merwe, 1987; Cerling and Harris, 1999, 1999; Balasse, 2002;

Bocherens, 2002; Cerling et al., 2004; Passey et al., 2005; Bocherens et al., 2011; Codron et al., 2012) and more recently, Tejada-Lara et al., 2018 established a relationship where body mass can be used to predict ^{13}C isotope enrichment in mammals. In the current paper, species-specific enrichment factors were used for each taxon, following the equations proposed by Tejada-Lara et al. (2018) in most cases.

As explained in Tejada-Lara et al. (2018), the equations use log-transformed (\ln) body mass. The obtained diet-bioapatite (ε^*) also needs to be inverted (e^x) in order to obtain the ‰ isotope enrichment value. This results in the following equations:

$$\text{General: } \varepsilon^*_{\text{diet-bioapatite}} = e^{2.4 + 0.034 (\ln \text{BM})}$$

$$\text{Foregut fermenter: } \varepsilon^*_{\text{diet-bioapatite}} = e^{2.34 + 0.05 (\ln \text{BM})}$$

$$\text{Hindgut fermenter: } \varepsilon^*_{\text{diet-bioapatite}} = e^{2.42 + 0.032 (\ln \text{BM})}$$

The enrichment factor of the giant panda (*Ailuropoda melanoleuca*) was not calculated, as Tejada-Lara et al. (2018) clearly demonstrated that the giant panda's calculated enrichment factor was incorrect. Instead, a $\varepsilon^*_{\text{diet-bioapatite}}$ $\delta^{13}\text{C}$ enrichment of +9.7 ‰ from Han et al. (2016) was used for the giant panda (*Ailuropoda melanoleuca*). Similarly, species-specific enrichment factors of specimens from the carnivore guild were not calculated, but rather we used the theoretical +9 ‰ diet-enamel spacing (Lee-Thorp et al., 1989). Species for which this diet-enamel spacing was used include: Canidae, large-sized Felidae, *Panthera pardus*, *Panthera tigris*, small-sized Felidae, *Crocuta crocuta*, and Ursidae. We report both $\delta^{13}\text{C}_{\text{apatite}}$ and $\delta^{13}\text{C}_{\text{diet}}$ values in the present study.

The oxygen isotopic composition ($\delta^{18}\text{O}_{\text{apatite}}$) of bioapatite reflects mainly that of ingested water (DeNiro and Epstein, 1978; Sullivan and Krueger, 1981; Longinelli, 1984; Luz et al., 1984; Lee-Thorp et al., 1989; Cerling and Harris, 1999; Sponheimer and Lee-Thorp, 1999b; Passey et al., 2005). In homoeothermic animals, this composition is regulated by that of body water, which results from a complex combination of diet, physiology, and various effects of climate (Longinelli, 1984; Luz et al., 1984; Ayliffe and Chivas, 1990; Bryant et al., 1994; Kohn, 1996; Kohn et al., 1996; Pederzani and Britton, 2019). Nevertheless, the oxygen isotopic composition from drinking water and chemically-bound water in the diet (i.e., free water found in plants) remain the primary source of variation in $\delta^{18}\text{O}_{\text{apatite}}$ of enamel (Longinelli, 1984; Luz et al., 1984; Bryant and Froelich, 1995; Kohn et al., 1996; Fricke et al., 1998a, b). The $\delta^{18}\text{O}$ of this water is primarily controlled by latitude, climate, temperature, moisture content, amount, and isotopic composition of precipitation

(Dansgaard, 1964; Longinelli, 1984; Kohn and Cerling, 2002). For tropical and subtropical regions specifically, the $\delta^{18}\text{O}$ values of vegetation mostly reflect either evaporative potential, amount- or source-effect of rainfall (Buchmann et al., 1997; Buchmann and Ehleringer, 1998; McCarroll and Loader, 2006). While $\delta^{13}\text{C}_{\text{apatite}}$ values were converted to $\delta^{13}\text{C}_{\text{diet}}$, the $\delta^{18}\text{O}_{\text{apatite}}$ values were not similarly converted to drinking water $\delta^{18}\text{O}$ values, as empirically-determined water-enamel ^{18}O fractionation are not known for many of the investigated fossil taxa (or closely related ones).

Supplementary information 3.2: Material and methods

3.2.1 Sample collection

The faunal material comprises a selection from the TPL and NL assemblages (70–1.1 ka, Shackelford et al., 2018; **Table S20**; and 86–72 ka, Bacon et al., 2015, respectively), covering a large range of distinct dietary habits. Only one sample from TPL is very young ($<1.1 \pm 0.2$ ka), whereas all others are at least 14 ± 2 ka or older (Shackelford et al., 2018; **Table S27**). A wide range of taxa covering distinct trophic levels and dietary habits was selected—including carnivores, omnivores, and herbivores—with each taxon assigned to a feeding category based on modern-day observations of its dietary behaviors (**Table S20**). One to 15 specimens per species were analyzed (**Table S20**). Only 32 specimens were analyzed for carbon and oxygen isotopes (**Table S23**), as the majority had already been measured and published in Bacon et al., 2018a. Species-specific trophic ecology (carnivore, omnivore, and herbivore) was assigned based on modern-day analogous fauna's dietary behaviors (Nowak, 1999; Macdonald, 2009; Johnsingh and Manjrekar, 2013, 2015). Previously published data ($\delta^{66}\text{Zn}$, $^{87}\text{Sr}/^{86}\text{Sr}$, $\delta^{13}\text{C}_{\text{apatite}}$ and $\delta^{18}\text{O}_{\text{apatite}}$; $n = 72$) were also included from the site of Tam Hay Marklot (THM) cave (Bourgon et al., 2020), north-eastern Laos (Huà Pan Province). Some species and genera were grouped together into 21 taxonomic units of upper rank (i.e., *Capricornis* sp. and *Naemorhedus* sp. grouped into Caprinae; see 'Taxon' and 'Taxonomic Unit' in **Table S20**) and referred herein as 'taxon' in this study, 18 of which are present in TPL and NL datasets.

3.2.2 Enamel sampling for isotope analysis

Enamel was first cleaned mechanically using a handheld dental drill equipped with a diamond-tip burr. Using either a diamond-tip cutting wheel or a diamond-tip burr, up

to three different samples—powder or fragment—were then taken along the full height of the crown for each specimen. Overall, 4.2 to 20.2 mg (average 10.4 mg \pm 3.8 mg, 1 σ) were used for zinc isotope analysis (a least 5 mg is usually recommended), 4.8 to 22.4 mg (average 13.6 mg \pm 4.8 mg, 1 σ) for strontium isotope analysis and 4.1 to 10.6 mg (average 5.8 mg \pm 1.7 mg, 1 σ) for carbon and oxygen isotope analysis. Larger amounts of material were used when chips of enamel had broken off, or alternatively in some high-crowned teeth in order to have a homogenized sample of the full height of the tooth. As samples were taken along the full height of the crown, samples for each specimen correspond to a time span of a few months to a few years depending on the species and tooth selected (and the extent of tooth wear; Passey and Cerling, 2002; Teaford et al., 2007; Berkovitz and Shellis, 2018). The isotopic values are thus also timed-average and represent a long-term averaged value over that period (Fricke et al., 1998a; Sharp and Cerling, 1998; Balasse, 2002).

The sample from the left M¹ from TPL1 consisted of a lingual fragment of enamel that had already chipped off, which made up the entire lateral height of the crown. To avoid extensive surface modification and to reduce the risk of breakage, the left M² TPL1 specimen was only sampled for zinc isotopic ratio measurement with light abrasion all over the lateral surface of its crown. For TPL1 specifically, the enamel samples from the M¹ would represent a period spanning from 1.5 years of age to 2.5–3.5 years of age (Hillson, 1996; AlQahtani et al., 2010), whereas that from the M² would cover from 5 to ~7–8 years of age (Hillson, 1996; AlQahtani et al., 2010). The M² was analyzed to control for a potential dietary breastfeeding $\delta^{66}\text{Zn}$ value recorded in the M¹, as has recently been documented (Jaouen et al., 2020). When sampling an enamel fragment rather than powder, the complete enamel pieces were crushed, powdered, and homogenized using an agate mortar and pestle, and then powder aliquots were divided accordingly for each isotopic analytical technique.

3.2.3 Zinc isotope analytical technique

Enamel samples from 78 specimens were digested in 1 ml of HCl 1.0 N, evaporated, and then re-dissolved in 1 ml HBr 1.5 N. Using a modified ion exchange method adapted from Moynier et al. (2009) and first described in Jaouen et al. (2016a), zinc was purified in two steps using pre-conditioned microcolumns on 1 ml AG-1x8 resin (200–400 dry mesh size, 106–180 μm wet bead size). Two ml of HBr 1.5 N was used for matrix residue elution, followed by 5 ml of HNO₃ 0.5 N for zinc elution. Finally,

samples were dried and re-dissolved in 1 ml HNO₃ 0.5 N before measurements. At least one reference material (in-house reference material AZE bone powder and/or the NIST SRM 1400 bone ash) and a blank were included and prepared alongside every batch of archeological samples (usually 13 at a time). Zinc isotopic ratios measurements were performed on a Thermo Scientific Neptune Multi-collector ICP-MS at the Max Planck Institute for Evolutionary Anthropology (Leipzig, Germany), using the Cu-doping protocol of Toutain et al. (2008). Zinc isotope ratios are expressed relative to the JMC-Lyon isotope standard, and isotopic abundances are presented in δ (delta) notation expressed as deviation per mil (‰), as follows: $\delta^{66}\text{Zn} = \left(\frac{{}^{66}\text{Zn}/{}^{64}\text{Zn}_{\text{sample}}}{{}^{66}\text{Zn}/{}^{64}\text{Zn}_{\text{standard}}} - 1 \right) \times 1000$. The in-house standard zinc AA-MPI was used for standard bracketing. Repeated analyses ($n = 126$) of every specimen were also performed to determine the homogeneity of the enamel samples. The overall average analytical repeatability for these fossil samples was 0.01 ‰, 1 σ ; **Table S22**) and those of the in-house reference material AZE bone powder and the NIST SRM 1400 bone ash are 0.00 ‰ (1 σ ; $n = 5$) and ± 0.01 ‰, 1 σ ; $n = 8$), respectively (**Table S26**). Estimates for zinc concentrations of samples were obtained with a regression equation based on the ⁶⁴Zn signal intensity (V) of three solutions with known concentrations (150, 300, and 600 $\mu\text{g/g}$), following a protocol adapted from the one used for strontium by Copeland et al., 2008 and first used for zinc in Jaouen et al. (2016b).

3.2.4 Strontium isotope analytical technique

Following a modified method of Copeland et al. (2008), first presented in Britton et al. (2009), 78 enamel samples were digested in 2 ml of HNO₃ 14.3 N, evaporated, and then dissolved in 1 ml HNO₃ 3.0 N. Samples were then loaded on 1 ml of Sr-spec™ resin (50–100 μm particle size) in pre-conditioned microcolumns. Matrix residues were eluted with 1.2 ml HNO₃ 3.0 N, while strontium was eluted with 1.5 ml ultrapure deionized water (18.2 M Ω). Samples were then dried and re-dissolved in 2 ml HNO₃ 0.5 N for measurements. Each preparation batch of archeological samples also includes at least one reference material (NIST SRM 1486 bone meal) and a blank. Analysis of ⁸⁷Sr/⁸⁶Sr was performed with a Thermo Scientific Neptune Multi-collector ICP-MS at the Max Planck Institute for Evolutionary Anthropology. Interferences from rubidium (Rb) were corrected from every ⁸⁷Sr/⁸⁶Sr measurement and normalized for instrumental mass bias to ⁸⁸Sr/⁸⁶Sr = 8.375209 (exponential law). Analysis of the international strontium isotope reference material NIST SRM 987 was performed during each analytical session for external normalization of data (⁸⁷Sr/⁸⁶Sr value =

0.7102852 ± 0.000011 , 1σ ; $n = 59$). All $^{87}\text{Sr}/^{86}\text{Sr}$ values reported were adjusted so $\text{SRM 987} = 0.710240$ (Johnson and Fridrich, 1990) with a correction offset of $+0.000045$ ($n = 59$). Following the method described in Copeland et al. (2008), a regression equation based on the ^{88}Sr signal intensity (V) of three solutions with known concentrations (100, 400, and 700 $\mu\text{g/g}$) was used to estimate the strontium concentration for each specimen.

3.2.5 Carbonate carbon and oxygen isotope analytical technique

Powdered enamel samples of 32 teeth were soaked in 1 ml of (CH_3COOH) 0.1 N for four hours at room temperature, rinsed in distilled water, and dried overnight at 65°C . Stable carbon and oxygen isotopic ratios measurement from the carbonate phase of enamel were performed at the Service de Spectrométrie de Masse Isotopique du Muséum in Paris, using a Thermo Scientific Delta V Advantage isotopic mass spectrometer coupled to a Thermo Scientific Kiel IV Carbonate Device chemical preparer. Isotopic abundances are presented in δ (delta) notation expressed relative to the Vienna Pee Dee Belemnite isotope standard as deviation per mil (‰), where: $\delta^{13}\text{C} = (^{13}\text{C}/^{12}\text{C}_{\text{sample}}/^{13}\text{C}/^{12}\text{C}_{\text{standard}} - 1) \times 1000$ and $\delta^{18}\text{O} = (^{18}\text{O}/^{16}\text{O}_{\text{sample}}/^{18}\text{O}/^{16}\text{O}_{\text{standard}} - 1) \times 1000$. An internal laboratory standard (Marble LM), normalized to the International Atomic Energy Agency reference material (NBS 19; **Table S26**) was analyzed alongside fossil enamel samples during every mass spectrometer run and used for one-point calibration, allowing correction for the structurally bound carbonate of the enamel samples while also controlling for the precision of the mass spectrometer (1σ [$\delta^{13}\text{C}$] = 0.03 ‰; 1σ [$\delta^{18}\text{O}$] = 0.09 ‰; **Table S26**). Two faunal specimens from Tam Pà Ling (SEVA number 35424 and 35958) were analyzed for carbon and oxygen isotopic compositions but not for zinc or strontium.

3.2.6 Statistical analysis

The sample size for the linear mixed model (LLM) was 145 specimens from 21 (generalized) taxa using datasets of TPL (this study), Nam Lot cave (NL; this study and Bacon et al., 2018a), and THM (Bourgon et al., 2020).

The investigated response variable was $\delta^{66}\text{Zn}$ values, and the tested predictors were: diet (carnivore, omnivore, and herbivore), site (THM, NL and TPL) taxon, $\delta^{13}\text{C}_{\text{apatite}}$ values, $\delta^{18}\text{O}_{\text{apatite}}$ values, $^{87}\text{Sr}/^{86}\text{Sr}$, zinc concentration, and average body mass for each

species (estimated from modern-day analogous species (Nowak, 1999; Macdonald, 2009; Johnsingh and Manjrekar, 2013, 2015). All quantitative predictors underwent visual inspection to check that they were roughly symmetrically distributed. Those showing a skewed distribution (body mass and zinc concentration) were then log-transformed. Additionally, all quantitative predictors were z-transformed (to a mean of zero and a standard deviation of one) to ease model convergence and achieve comparability of estimates. Every predictor was used as fixed effects with the exception of taxon, which was included as a random intercept effect. Furthermore, collinearity among predictors was assessed by calculating variation inflation factors (Fox and Weisberg, 2011) to a standard linear model in which the random effect was excluded. The model stability was subsequently assessed by comparing the model estimates obtained from the full dataset to those excluding levels of the random effect (taxon) as well as specimens, one at a time. Assumptions of normally distributed and homogeneous residuals were examined by visual inspection.

To test the significance of the key predictors (site, $^{87}\text{Sr}/^{86}\text{Sr}$ and body mass), the full model was compared with a null model lacking these terms (Forstmeier and Schielzeth, 2011) by using a likelihood ratio test, approximated using a chi-square distribution (Dobson, 2002). Similarly, the significance of individual fixed effect predictors was also tested by using likelihood ratio tests between the full model and models that exclude predictors one at a time and then adjusted using Holm-Bonferroni correction for multi-testing (Holm, 1979). Confidence intervals of the model's estimate were obtained with parametric bootstrap (Bates et al., 2015), utilizing 1000 bootstraps. Finally, while no effect size estimate for individual predictors can be obtained for (Generalized)LMMs, the effect size for all combined fixed effects was calculated ('marginal r^2 ' = 0.57), as well as the one also incorporating random effects ('conditional r^2 ' = 0.72; Nakagawa et al., 2017).

Descriptive statistics (e.g., sample size, mean, median, quartiles, standard deviations), as well as the LMM results, revealed that the overall $\delta^{66}\text{Zn}$ distribution for herbivores at TPL deviated from THM and NL. To further investigate the $\delta^{66}\text{Zn}$ distribution from TPL fauna and evaluate the potential mechanisms underlying the difference from the other sites, we ran two simulations.

The goal of the first simulation (**Figure S56**) was to evaluate where the observed $\delta^{66}\text{Zn}$ distribution for each taxon and dietary group in TPL is located in comparison to the theoretical distribution for each taxon and dietary group. To do this, $\delta^{66}\text{Zn}$ distribution was separately simulated for herbivores, omnivores, and carnivores (excluding the

bone-eating carnivore *C. crocuta*) from a multivariate normal distribution. Each dietary group comprised of various simulated taxa (herbivores = 10, omnivores = 5 and carnivores = 4). A total of 1000 observations for each taxon was simulated. The empirical mean and standard deviation of the observed $\delta^{66}\text{Zn}$ distribution for each taxon aggregated over every site was used for the simulations. The $\delta^{66}\text{Zn}$ values for taxa in the same dietary group were assumed to be slightly correlated 0.2, as species in the same dietary category correlate a little with each other in their $\delta^{66}\text{Zn}$ values since they potentially eat overlapping food resources.

To further investigate whether the observed difference in mean $\delta^{66}\text{Zn}$ values for herbivores from TPL could be due to sampling variability, we ran a second simulation (**Figure S57**) to evaluate whether incomplete data could exhibit $\delta^{66}\text{Zn}$ distributions similar to the one observed from TPL. Zinc stable isotopes distribution was separately simulated for herbivores, omnivores, and carnivores from a multivariate normal distribution. The simulation structure was identical to the previous simulation. After complete simulated data were obtained for $\delta^{66}\text{Zn}$ values for each dietary group (**Figure S56**), two kinds of missingness were introduced to the simulated data: missingness on the taxa and missingness on the dietary group. In TPL, the sample for each taxon ranged from 1 to 15; missingness was thus introduced on the taxa so that 1 to 15 remained for each taxon. Subsequently, missingness was introduced at the dietary level equivalent to the missingness in the observed $\delta^{66}\text{Zn}$ values per dietary group. Ten data sets were simulated according to this setup to compare them to the TPL dataset.

Finally, the proportion of overlap between overlapping areas of kernel density estimations was calculated (Pastore, 2018) for $\delta^{66}\text{Zn}$ values from each dietary category (**Figure S58**).

Supplementary information 3.3: Variation of zinc stable isotope values in fossil tooth enamel from Tam Pà Ling and Nam Lot

Each diet category from TPL and NL displays an overall mean $\delta^{66}\text{Zn}$ value and range that is well in agreement with the expected dietary habits. However, the overall mean for herbivores is higher for TPL compared to those of NL and THM (**Chapter 4, Figure 18**), although the overall mean $\delta^{66}\text{Zn}$ values of carnivores and omnivores from TPL are similar to the other two sites, and each taxon shows similar $\delta^{66}\text{Zn}$ values between sites. This is likely the result of the smaller ($n = 19$) and less diverse herbivore

faunal assemblage from TPL. Indeed, many herbivorous taxa associated with lower values (i.e., Tapiridae, *Ailuropoda melanoleuca* and *Muntiacus* sp.) are absent or very few in number in TPL, and comparatively more Caprinae, associated with higher $\delta^{66}\text{Zn}$ values, are present (**Figure S54**). Multivariate-normal simulations were able to replicate these findings and further support that the faunal assemblage composition—and not different values per se—explains the higher mean $\delta^{66}\text{Zn}$ value of herbivores at TPL (*SI Appendix, Supplementary information 3.2.6; Figures S56 and S57*).

Herbivores from NL and TPL display a broad range of $\delta^{66}\text{Zn}$ values (+0.27 to +1.07 ‰) similar to those of THM. A difference in diet linked to a broad grazer-browser distinction could also be suggested, as it was observed for the Koobi Fora region (Jaouen et al., 2016a). However, no clear distinction in $\delta^{66}\text{Zn}$ values could be drawn between taxa with $\delta^{13}\text{C}_{\text{apatite}}$ values from C_3 and C_4 feeders at TPL and NL, nor could THM (Bourgon et al., 2020). Because of the $\delta^{66}\text{Zn}$ -to-height correlation observed in plants, it is possible that lower consumption of plant-matter from vegetation layers on C_3 understory plants leads to equally high grazer-like $\delta^{66}\text{Zn}$ values, regardless of the photosynthetic pathways. This could thus explain the absence of correlation between $\delta^{66}\text{Zn}$ values and $\delta^{13}\text{C}_{\text{apatite}}$ values from C_3 - C_4 feeders. Presumable grazer-browser dietary ecology could be tentatively assigned to each herbivorous taxon using analogous modern-day fauna's dietary behaviors. However, the fauna from Southeast Asia is particularly stable and homogenous throughout a vast period and geographic range (from Thailand to Borneo, and often even including India), covering vastly different environments. In fact, synecological analyses have long struggled with this consistency in faunal assemblages (Medway, 1977; de Vos and Long, unpub. rep., 1993; van den Bergh et al., 2001). Assigning typical habitat or dietary behaviors—such as grazer or browser—was shown to be mostly ineffective for many animal species found in Southeast Asia and wholly dependent on the exact locality (and time period studied; Bacon et al., 2018a, 2018b; Suraprasit et al., 2018, 2020; Ma et al., 2019; Bourgon et al., 2020). As such, no 'grazer' or 'browser' feeding ecology was assigned to herbivorous taxa for the present study. Comparisons in $\delta^{66}\text{Zn}$ variability between herbivorous taxa are thus strictly based on $\delta^{13}\text{C}_{\text{apatite}}$ values, distinguishing C_3 from C_4 feeders, i.e., reflecting the diet actually ingested by the analyzed individuals.

Currently, the most likely explanation for this variability is the consumption of a variety of different plants species and plant parts, perhaps also linked to the vertical layering of the vegetation and its postulated $\delta^{66}\text{Zn}$ -to-height gradient. Indeed, while

lower values could be associated with consumption of high-growing plants or more aerial parts due to active uptake of heavy zinc isotopes out of the xylem during transport (Weiss et al., 2005; Viers et al., 2007; Moynier et al., 2009), no clear distinction can be established between the various dietary habits of the herbivorous taxa. Additionally, as the same range of $\delta^{66}\text{Zn}$ values can be observed for both foregut and hindgut fermenters, digestive physiology was ruled out as a factor explaining this variability. Maternal effects linked to breastfeeding or tooth formation in utero were also ruled out as causes for intra-group $\delta^{66}\text{Zn}$ variability, as no clear trend can be observed relative to the formation and emergence sequence of the sampled teeth. The estimate obtained from the LMM for $^{87}\text{Sr}/^{86}\text{Sr}$ (**Table S24**) provides insights into $\delta^{66}\text{Zn}$ variability of herbivores and for that of other dietary categories. However, the relationship between $^{87}\text{Sr}/^{86}\text{Sr}$ and $\delta^{66}\text{Zn}$ values is limited to some taxa (**Figure S55**), potentially hinting that this relationship is not the result of the bedrock's $\delta^{66}\text{Zn}$ values upon the food web. Rather, it could simply be that some food items—growing upon or located on a certain geologic substrate—and not others were consumed. Perhaps some degree of soil consumption in the diet—often seen in many animals (Beyer et al., 1994; Abrahams, 2013)—also has to be accounted for as partly explaining their $\delta^{66}\text{Zn}$ values. In fact, many of the taxa found at TPL, NL, and THM are known to exhibit some degree of geophagy or involuntary ingestion of soil (e.g., porcupine, tapir, rhinoceros, sambar, and large- and small-size bovids; Abrahams, 2013) and indeed show a clearer relationship between $^{87}\text{Sr}/^{86}\text{Sr}$ and $\delta^{66}\text{Zn}$ values.

Supplementary information tables

SEVA	Specimen no.	Diet	Diet type	Material	$\delta^{66}\text{Zn}$	$\delta^{67}\text{Zn}$	$\delta^{68}\text{Zn}$	[Zn] (ug/g)
35108	1ERB6B2	Bone	Pellet	Bone	0.32	0.57	0.69	73
35111	1ERB6B2	Bone	Pellet	Liver	-1.03	-1.60	-1.99	38
35114	1ERB6B2	Bone	Pellet	Kidney	-0.73	-1.09	-1.37	60
35117	1ERB6B2	Bone	Pellet	Muscle	-0.88	-1.27	-1.66	23
35120	1ERB6B2	Bone	Pellet	Feces	0.09	0.12	0.23	157
35131	1ERB6B2	Bone	Pellet	Hair	0.31	0.58	0.73	85
35135	1ERB6B2	Bone	Pellet	RBC	-0.08	-0.15	-0.11	8
35136	1ERB6B2	Bone	Pellet	Plasma	-0.16	0.41	-0.14	2
35129	N/A	Bone	Pellet	Feed	0.00	0.09	0.15	88
35107	1ARA5B1	Animal	Pellet	Bone	0.22	0.37	0.48	81
35226	1ARA5B1	Animal	Pellet	Feces	-0.12	-0.16	-0.22	265
35230	1ARA5B1	Animal	Pellet	Hair	0.10	0.17	0.18	161
35234	1ARA5B1	Animal	Pellet	Kidney	-0.91	-1.33	-1.54	86
35238	1ARA5B1	Animal	Pellet	Liver	-1.15	-1.64	-2.19	90
35242	1ARA5B1	Animal	Pellet	Muscle	-0.94	-1.29	-1.77	30
35254	1ARA5B1	Animal	Pellet	Plasma	-0.26	-0.21	-0.40	1
35258	1ARA5B1	Animal	Pellet	RBC	-0.18	-0.24	-0.32	6
35337	1ARA5B1	Animal	Pellet	RBC	-0.20	-0.13	-0.36	0
35127	N/A	Animal	Pellet	Feed	-0.09	-0.10	-0.12	67
36026	1BRA1B1	Breeder	Pellet	Bone	0.46	0.74	0.96	139
36033	1BRA1B1	Breeder	Pellet	Feces	0.52	0.93	1.14	121
36736	1BRA1B1	Breeder	Pellet	Kidney	-0.01	0.06	0.15	63
36743	1BRA1B1	Breeder	Pellet	Liver	-0.36	-0.46	-0.57	64
36749	1BRA1B1	Breeder	Pellet	Muscle	-0.10	-0.01	0.15	31
36025	1BRC1B1	Breeder	Pellet	Bone	0.39	0.64	0.83	135
36032	1BRC1B1	Breeder	Pellet	Feces	0.30	0.52	0.65	208
36735	1BRC1B1	Breeder	Pellet	Kidney	-0.16	-0.13	-0.14	68
36742	1BRC1B1	Breeder	Pellet	Liver	-0.51	-0.70	-0.82	73
35223	1BRC4B1	Breeder	Pellet	Bone	0.27	0.47	0.52	140
35227	1BRC4B1	Breeder	Pellet	Feces	0.50	0.77	0.97	151
35231	1BRC4B1	Breeder	Pellet	Hair	0.08	0.12	0.20	208
35235	1BRC4B1	Breeder	Pellet	Kidney	-0.19	-0.20	-0.28	97
35239	1BRC4B1	Breeder	Pellet	Liver	-0.56	-0.78	-1.08	87
35243	1BRC4B1	Breeder	Pellet	Muscle	-0.31	-0.42	-0.54	64
35255	1BRC4B1	Breeder	Pellet	Plasma	0.36	0.96	0.93	1
35257	1BRC4B1	Breeder	Pellet	RBC	0.46	0.69	0.92	4
35336	1BRC4B1	Breeder	Pellet	RBC	0.44	0.80	0.88	0
35340	1BRC4B1	Breeder	Pellet	RBC	0.50	0.74	1.02	5
35126	N/A	Breeder	Pellet	Feed	0.27	0.44	0.53	37
35248	N/A	Breeder	Pellet	Feed	0.43	0.65	0.90	70
36037	N/A	Breeder	Pellet	Feed	0.50	0.81	1.11	79

36038	N/A	Breeder	Pellet	Feed	0.48	0.78	1.14	67
36039	N/A	Breeder	Pellet	Feed	0.42	0.84	0.99	70
35109	2AA6B1	Chicks	Natural	Bone	0.33	0.54	0.71	115
35112	2AA6B1	Chicks	Natural	Liver	-0.72	-1.10	-1.37	121
35115	2AA6B1	Chicks	Natural	Kidney	-0.51	-0.72	-0.97	55
35118	2AA6B1	Chicks	Natural	Muscle	-0.45	-0.58	-0.86	21
35121	2AA6B1	Chicks	Natural	Feces	0.34	0.42	0.73	312
35122	2AA6B1	Chicks	Natural	Hair	0.19	0.13	0.42	78
35138	2AA6B1	Chicks	Natural	WB	0.23	0.25	0.47	6
35139	2AA6B1	Chicks	Natural	RBC	0.23	0.29	0.49	9
35140	2AA6B1	Chicks	Natural	Plasma	0.27	0.73	0.63	5
35141	2AA6B1	Chicks	Natural	Bone	0.28	0.46	0.58	92
35142	2AA6B1	Chicks	Natural	Liver	-0.71	-1.09	-1.38	54
35143	2AA6B1	Chicks	Natural	Kidney	-0.53	-0.82	-1.03	75
35125	N/A	Chicks	Natural	Feed	0.31	0.58	0.73	32
35106	1ARA4B2	Insect	Pellet	Bone	0.26	0.30	0.55	101
35225	1ARA4B2	Insect	Pellet	Feces	-0.50	-0.77	-0.96	229
35229	1ARA4B2	Insect	Pellet	Hair	-0.02	0.01	-0.03	163
35233	1ARA4B2	Insect	Pellet	Kidney	-0.91	-1.34	-1.63	100
35237	1ARA4B2	Insect	Pellet	Liver	-1.21	-1.75	-2.30	92
35241	1ARA4B2	Insect	Pellet	Muscle	-0.77	-1.10	-1.48	33
35253	1ARA4B2	Insect	Pellet	Plasma	-0.28	-0.05	-0.32	1
35259	1ARA4B2	Insect	Pellet	RBC	-0.13	-0.18	-0.25	3
35338	1ARA4B2	Insect	Pellet	RBC	-0.15	-0.07	-0.22	0
35128	N/A	Insect	Pellet	Feed	-0.04	-0.07	-0.01	69
35105	1ARB1B1	Plant	Pellet	Bone	0.23	0.52	0.48	125
35110	1ARB1B1	Plant	Pellet	Liver	-1.30	-1.88	-2.53	53
35113	1ARB1B1	Plant	Pellet	Kidney	-0.92	-1.31	-1.74	36
35116	1ARB1B1	Plant	Pellet	Muscle	-1.04	-1.60	-1.97	21
35119	1ARB1B1	Plant	Pellet	Feces	-0.27	-0.36	-0.47	143
35132	1ARB1B1	Plant	Pellet	RBC	-0.29	-0.51	-0.56	
35133	1ARB1B1	Plant	Pellet	Plasma	-0.36	-0.19	-0.59	
35249	1ARB1B1	Plant	Pellet	Hair	-0.01	0.02	0.01	185
36027	1ARB1B2	Plant	Pellet	Bone	0.23	0.47	0.53	153
36034	1ARB1B2	Plant	Pellet	Feces	-0.31	-0.39	-0.51	201
36044	1ARB1B2	Plant	Pellet	Hair	0.13	0.34	0.36	181
36737	1ARB1B2	Plant	Pellet	Kidney	-0.85	-1.11	-1.45	82
36744	1ARB1B2	Plant	Pellet	Liver	-1.18	-1.70	-2.21	89
36750	1ARB1B2	Plant	Pellet	Muscle	-0.89	-1.20	-1.55	31
36028	1ARB1G1	Plant	Pellet	Bone	0.28	0.47	0.61	155
36035	1ARB1G1	Plant	Pellet	Feces	-0.21	-0.22	-0.33	193
36045	1ARB1G1	Plant	Pellet	Hair	0.10	0.32	0.37	188
36738	1ARB1G1	Plant	Pellet	Kidney	-0.92	-1.28	-1.53	64
36745	1ARB1G1	Plant	Pellet	Liver	-1.28	-1.81	-2.39	85
36751	1ARB1G1	Plant	Pellet	Muscle	-1.01	-1.44	-1.76	25

36029	1ARB1G2	Plant	Pellet	Bone	0.30	0.44	0.65	158
36036	1ARB1G2	Plant	Pellet	Feces	-0.32	-0.40	-0.54	234
36046	1ARB1G2	Plant	Pellet	Hair	0.08	0.27	0.32	187
36739	1ARB1G2	Plant	Pellet	Kidney	-0.91	-1.33	-1.62	76
36746	1ARB1G2	Plant	Pellet	Liver	-1.24	-1.75	-2.33	84
36752	1ARB1G2	Plant	Pellet	Muscle	-0.89	-1.20	-1.56	33
36030	1ARB1R1	Plant	Pellet	Bone	0.25	0.43	0.56	158
36042	1ARB1R1	Plant	Pellet	Feces	-0.34	-0.47	-0.57	197
36047	1ARB1R1	Plant	Pellet	Hair	0.13	0.35	0.39	183
36740	1ARB1R1	Plant	Pellet	Kidney	-0.85	-1.20	-1.55	80
36747	1ARB1R1	Plant	Pellet	Liver	-1.29	-1.82	-2.44	92
36753	1ARB1R1	Plant	Pellet	Muscle	-0.95	-1.32	-1.65	27
36031	1ARB1R2	Plant	Pellet	Bone	0.20	0.34	0.47	159
36043	1ARB1R2	Plant	Pellet	Feces	-0.26	-0.28	-0.42	280
36048	1ARB1R2	Plant	Pellet	Hair	0.17	0.42	0.50	157
36741	1ARB1R2	Plant	Pellet	Kidney	-0.89	-1.27	-1.46	59
36748	1ARB1R2	Plant	Pellet	Liver	-1.26	-1.80	-2.37	85
36754	1ARB1R2	Plant	Pellet	Muscle	-0.80	-1.08	-1.36	31
35124	N/A	Plant	Pellet	Feed	-0.25	-0.35	-0.45	48
36040	N/A	Plant	Pellet	Feed	-0.32	-0.41	-0.53	106
36041	N/A	Plant	Pellet	Feed	-0.33	-0.42	-0.53	101
35224	2AA1G1	Vegetable	Natural	Bone	0.37	0.58	0.72	139
35228	2AA1G1	Vegetable	Natural	Feces	0.25	0.45	0.55	129
35232	2AA1G1	Vegetable	Natural	Hair	0.23	0.32	0.46	191
35236	2AA1G1	Vegetable	Natural	Kidney	-0.26	-0.36	-0.47	91
35240	2AA1G1	Vegetable	Natural	Liver	-0.62	-0.90	-1.20	91
35244	2AA1G1	Vegetable	Natural	Muscle	-0.43	-0.49	-0.68	38
35250	2AA1G1	Vegetable	Natural	Hair	0.18	0.27	0.37	164
35256	2AA1G1	Vegetable	Natural	Plasma	0.33	0.76	0.71	1
35260	2AA1G1	Vegetable	Natural	RBC	0.36	0.56	0.71	7
35339	2AA1G1	Vegetable	Natural	RBC	0.33	0.70	0.69	0
35341	2AA1G1	Vegetable	Natural	RBC	0.36	0.54	0.73	6
35245	N/A	Vegetable	Natural	Feed	0.45	0.84	0.92	24

Table S1. Preliminary $\delta^{66}\text{Zn}$ results (in ‰) of rats from a controlled-feeding experiment. Animals were fed a custom-made diets, either pelleted (plant-, insect-, meat-based or meat-based & bone) or natural (day-old-chicks and vegetable mix). The diet "Bone" consist in an animal-based pelleted diet with an addition of 14% of bone-like supplement. Various material (tissues, organs, body fluids and feeds) were analyzed for their zinc stable isotope compositions to investigate biological fractionation and specific diet-tissue spacings. Abbreviation: SEVA = Stable isotope-Evolutionary Anthropology (the numbering system used in the Human Evolution department of the Max Planck Institute for Evolution Anthropology, Leipzig, for every sample analyzed for isotope analysis), RBC = Red blood cell, WB = Whole blood.

Taxon	SEVA	#ref	Diet^(1,2,3,4)	Element
<i>Capricornis</i> sp.	34489	MI-20	Herbivore	m3 inf. right
<i>Capricornis</i> sp.	34490	MI-21	Herbivore	m3 inf. right
<i>Capricornis</i> sp.	34491	MI-22	Herbivore	m3 inf. right
<i>Capricornis</i> sp.	34492	MI-23	Herbivore	m3 inf. right
<i>Capricornis</i> sp.	34493	MI-24	Herbivore	m3 inf. right
<i>Naemorhedus</i> cf. <i>caudatus</i>	34494	MI-25	Herbivore	m3 inf. left
<i>Naemorhedus</i> cf. <i>caudatus</i>	34495	MI-26	Herbivore	m3 inf. left
<i>Naemorhedus</i> cf. <i>caudatus</i>	34496	MI-27	Herbivore	m3 inf. left
<i>Naemorhedus</i> cf. <i>caudatus</i>	34497	MI-28	Herbivore	m3 inf. left
<i>Helarctos malayanus</i>	34498	MI-103	Omnivore	M2 sup. left
<i>Helarctos malayanus</i>	34499	MI-121	Omnivore	M2 sup. left
<i>Ursus thibetanus</i>	34500	MI-117	Omnivore	M2 sup. right
<i>Ursus thibetanus</i>	34501	MI-119	Omnivore	M2 sup. left
<i>Ursus thibetanus</i>	34502	MI-122	Omnivore	M2 sup. left
<i>Panthera pardus</i>	34503	MI-134	Carnivore	P3 sup. right
<i>Panthera pardus</i>	34504	MI-135	Carnivore	p4 inf. left
<i>Panthera pardus</i>	34505	MI-136	Carnivore	P4 sup. left
<i>Rusa unicolor</i>	34506	MI-166	Herbivore	m3 inf. left
<i>Rusa unicolor</i>	34507	MI-180	Herbivore	m3 inf. left
<i>Rusa unicolor</i>	34508	MI-185	Herbivore	m3 inf. left
<i>Rusa unicolor</i>	34509	MI-187	Herbivore	m3 inf. left
<i>Rusa unicolor</i>	34510	MI-191	Herbivore	m3 inf. left
<i>Rucervus eldii</i>	34511	MI-512	Herbivore	m3 inf. left
<i>Rucervus eldii</i>	34512	MI-595	Herbivore	m3 inf. left
<i>Axis</i> cf. <i>porcinus</i>	34513	MI-556	Herbivore	m3 inf. left
<i>Axis</i> cf. <i>porcinus</i>	34514	MI-557	Herbivore	m3 inf. left
<i>Muntiacus</i> sp.	34515	MI-627	Herbivore	m3 inf. right
<i>Muntiacus</i> sp.	34516	MI-628	Herbivore	m3 inf. right
<i>Muntiacus</i> sp.	34517	MI-629	Herbivore	m3 inf. right
<i>Muntiacus</i> sp.	34518	MI-630	Herbivore	m3 inf. right
<i>Muntiacus</i> sp.	34519	MI-631	Herbivore	m3 inf. right
<i>Bubalus bubalis</i>	34520	MI-650	Herbivore	p2 (p3?) inf. right
<i>Bubalus bubalis</i>	34521	MI-651	Herbivore	p2 (p3?) inf. right
<i>Bubalus bubalis</i>	34522	MI-652	Herbivore	p2 (p3?) inf. left
<i>Bubalus bubalis</i>	34523	MI-653	Herbivore	p2 (p3?) inf. left
<i>Bubalus bubalis</i>	34524	MI-654	Herbivore	p2 (p3?) inf. left
<i>Bos</i> sp.	34525	MI-655	Herbivore	p2 inf. right
<i>Bos</i> sp.	34526	MI-656	Herbivore	p2 inf. right
<i>Bos</i> sp.	34527	MI-657	Herbivore	p2 inf. right
<i>Bos</i> sp.	34528	MI-658	Herbivore	p2 inf. left
<i>Bos</i> sp.	34529	MI-659	Herbivore	p2 inf. left
<i>Panthera tigris</i>	34530	MI-130	Carnivore	frag. p4 inf. right
<i>Panthera tigris</i>	34531	MI-693	Carnivore	frag. P4 sup. left
<i>Panthera tigris</i>	34532	MI-694	Carnivore	frag. P4 sup. left
<i>Sus</i> sp.	34533	MI-662	Omnivore	p4 inf. left
<i>Sus</i> sp.	34534	MI-663	Omnivore	p4 inf. left

<i>Sus</i> sp.	34535	MI-664	Omnivore	p4 inf. left
<i>Sus</i> sp.	34536	MI-665	Omnivore	p4 inf. left
<i>Sus</i> sp.	34537	MI-666	Omnivore	p4 inf. left
<i>Sus</i> sp.	34538	MI-667	Omnivore	p4 inf. left
Canidae (? <i>Cuon alpinus</i>)	34539	MI-131	Carnivore	m1 inf. right
Canidae (? <i>Cuon alpinus</i>)	34540	MI-681	Carnivore	P3 sup. right
Canidae	34543	MI-682	Carnivore	M1 sup. left
<i>Pongo</i> sp.	34541	MI-683	Omnivore	Canine
<i>Pongo</i> sp.	34542	MI-685	Omnivore	M sup. left
<i>Ailuropoda melanoleuca</i>	34544	MI-684	Herbivore	m2 inf. right
Tapiridae indet.	34545	MI-691	Herbivore	canine inf. left
<i>Tapirus</i> sp.	34546	MI-692	Herbivore	frag. dent jugale
<i>Macaca</i> sp.	34547	MI-695	Omnivore	m1/m2 inf. left
<i>Macaca</i> sp.	34548	MI-696	Omnivore	m1/m2 inf. left
<i>Macaca</i> sp.	34549	MI-697	Omnivore	pm inf. right
<i>Macaca</i> sp.	34550	MI-698	Omnivore	m1/m2 inf. left
<i>Macaca</i> sp.	34551	MI-699	Omnivore	pm inf. right
<i>Hystrix</i> sp.	34552	MI-700	Omnivore	incisor
<i>Hystrix</i> sp.	34553	MI-701	Omnivore	incisor
<i>Hystrix</i> sp.	34554	MI-702	Omnivore	incisor
<i>Hystrix</i> sp.	34555	MI-703	Omnivore	incisor
<i>Rhinoceros sondaicus</i>	34556	MI-686	Herbivore	m3 inf. left
<i>Rhinoceros sondaicus</i>	34557	MI-687	Herbivore	m3 inf. left
<i>Rhinoceros sondaicus</i>	34558	MI-688	Herbivore	m2 inf. left
<i>Rhinoceros sondaicus</i>	34559	MI-689	Herbivore	d3 inf. left
<i>Rhinoceros sondaicus</i>	34560	MI-690	Herbivore	d3 inf. right

Table S2. Full list of fossil tooth specimens from Tam Hay Marklot cave (Laos) analyzed in this study, with corresponding SEVA number, original number, broad dietary category and anatomical element. The dietary category assigned to each taxon was taken from Nowak (1999)⁽¹⁾, Macdonalds (2009)⁽²⁾ and Johnsingh and Manjrekar (2013, 2015)⁽³⁻⁴⁾. Abbreviation: SEVA = Stable isotope-Evolutionary Anthropology (the numbering system used in the Human Evolution department of the Max Planck Institute for Evolution Anthropology, Leipzig, for every sample analyzed for isotope analysis).

Sample	Sample matrix	SEVA	$\delta^{66}\text{Zn}$
Sandy to gravelly silty clays (fossil-bearing layer)	Sediment	35342	0.60
Calclitic cementation (fossil-bearing layer)	Sediment	35343	0.69
Clay from conglomerate	Sediment	35344	0.12
Conglomerate/breccias	Sediment	35345	0.53
Sediment attached to the enamel surface of sample 34556 (<i>Rhinoceros sondaicus</i>)	Sediment	34556-D_9	0.55
<i>Rhinoceros sondaicus</i>	Dentin	34556-D_1	0.65
<i>Rhinoceros sondaicus</i>	Dentin	34556-D_2	0.77
<i>Rhinoceros sondaicus</i>	Dentin	34556-D_3	0.82
<i>Rhinoceros sondaicus</i>	Dentin	34556-D_4	0.73
<i>Rhinoceros sondaicus</i>	Dentin	34556-D_7	0.71
<i>Rhinoceros sondaicus</i>	Dentin	34556-D_10	0.65
<i>Rhinoceros sondaicus</i>	Dentin	34556-D_mean	0.72
<i>Capricornis</i> sp.	Dentin	34489-D	0.81
<i>Capricornis</i> sp.	Dentin	34490-D	1.05
<i>Capricornis</i> sp.	Dentin	34492-D	0.99
<i>Helarctos malayanus</i>	Dentin	34498-D	0.73
<i>Panthera pardus</i>	Dentin	34505-D	0.39
<i>Bubalus bubalus</i>	Dentin	34524-D	0.85

Table S3. Sediment and dentin $\delta^{66}\text{Zn}$ isotope values (‰) from Tam Hay Marklot cave (Laos) used to assess the impact of diagenesis on $\delta^{66}\text{Zn}$ values. Abbreviation: SEVA = Stable isotope-Evolutionary Anthropology (the numbering system used in the Human Evolution department of the Max Planck Institute for Evolution Anthropology, Leipzig, for every sample analyzed for isotope analysis).

Taxon	SEVA	Diet	$\delta^{13}\text{C}$ (‰)	$\delta^{18}\text{O}$ (‰)	$^{87}\text{Sr}/^{86}\text{Sr}$	$\delta^{66}\text{Zn}$ (‰)	$\delta^{66}\text{Zn}$ 2σ (‰)
<i>Capricornis</i> sp.	34489	Herbivore	-13.4	-2.2	0.7136	0.52	0.02
<i>Capricornis</i> sp.	34490	Herbivore	-14.7	-5.2	0.7098	0.81	0.03
<i>Capricornis</i> sp.	34491	Herbivore	-15.2	-5.2	0.7112	0.67	0.05
<i>Capricornis</i> sp.	34492	Herbivore	-13.5	-7	0.7148	0.61	0.02
<i>Capricornis</i> sp.	34493	Herbivore	-14.6	-7.6	0.7148	0.78	0.04
<i>Naemorhedus</i> cf. <i>caudatus</i>	34494	Herbivore	-2.4	+0.2	0.7103	0.86	0.00
<i>Naemorhedus</i> cf. <i>caudatus</i>	34495	Herbivore	-3.9	-2.5	0.7109	0.90	0.01
<i>Naemorhedus</i> cf. <i>caudatus</i>	34496	Herbivore	-3.7	-1.8	0.7105	0.99	0.07
<i>Naemorhedus</i> cf. <i>caudatus</i>	34497	Herbivore	-2.5	-1.6	0.7123	0.76	0.01
<i>Helarctos</i> <i>malayanus</i>	34498	Omnivore	-14.7	-3.9	0.7121	0.67	0.01
<i>Helarctos</i> <i>malayanus</i>	34499	Omnivore	-14.9	-5.5	0.7243	0.24	0.04
<i>Ursus</i> <i>thibetanus</i>	34500	Omnivore	-15.4	-7.4	0.7166	0.43	0.03
<i>Ursus</i> <i>thibetanus</i>	34501	Omnivore	-13.3	-6.6	0.7188	0.37	0.03
<i>Ursus</i> <i>thibetanus</i>	34502	Omnivore	-14.4	-6.3	0.7177	0.39	0.02
<i>Panthera</i> <i>pardus</i>	34503	Carnivore	-7.9	-7.3	0.7135	-0.01	0.05
<i>Panthera</i> <i>pardus</i>	34504	Carnivore	-4.0	-7.3	0.7113	0.01	0.02
<i>Panthera</i> <i>pardus</i>	34505	Carnivore	-13.8	-6.8		0.08	0.03
<i>Rusa unicolor</i>	34506	Herbivore	-7.5	-5.7	0.7159	0.47	0.06
<i>Rusa unicolor</i>	34507	Herbivore	-5.3	-4.4	0.7149	0.50	
<i>Rusa unicolor</i>	34508	Herbivore	-6	-4.9	0.7185	0.47	
<i>Rusa unicolor</i>	34509	Herbivore	-3.4	-4.9	0.7117	0.78	0.12
<i>Rusa unicolor</i>	34510	Herbivore	-7.9	-6.1	0.7147	0.61	
<i>Rucervus eldii</i>	34511	Herbivore	+2.4	-5.3	0.7144	0.55	0.01
<i>Rucervus eldii</i>	34512	Herbivore	+1.8	-3.1	0.7140	0.71	0.03
<i>Axis</i> cf. <i>porcinus</i>	34513	Herbivore	-0.8	-5.8	0.7117	0.72	0.08
<i>Axis</i> cf. <i>porcinus</i>	34514	Herbivore	-0.6	-5.3	0.7118	0.62	
<i>Muntiacus</i> sp.	34515	Herbivore	-13.8	-7.4	0.7160	0.60	0.07
<i>Muntiacus</i> sp.	34516	Herbivore	-14.8	-8.1	0.7174	0.47	0.01
<i>Muntiacus</i> sp.	34517	Herbivore	-12.7	-8.1	0.7195	0.29	0.20

<i>Muntiacus</i> sp.	34518	Herbivore	-14.4	-5	0.7163	0.46	0.04
<i>Muntiacus</i> sp.	34519	Herbivore	-14.5	-7.5	0.7158	0.64	0.02
<i>Bubalus bubalis</i>	34520	Herbivore	-10.3	-6.0	0.7151	0.59	
<i>Bubalus bubalis</i>	34521	Herbivore	-4.0	-6.6		0.50	0.10
<i>Bubalus bubalis</i>	34522	Herbivore	+1.0	-4.7		0.63	0.08
<i>Bubalus bubalis</i>	34523	Herbivore	-10.9	-6.3	0.7159	0.55	0.13
<i>Bubalus bubalis</i>	34524	Herbivore	+0.1	-5.9	0.7139	0.81	0.01
<i>Bos</i> sp.	34525	Herbivore	-2.5	-4.2	0.7160	0.75	
<i>Bos</i> sp.	34526	Herbivore	-14.4	-6.1	0.7165	0.95	
<i>Bos</i> sp.	34527	Herbivore	-0.3	-4.6	0.7173	0.77	
<i>Bos</i> sp.	34528	Herbivore	-10.0	-7.6	0.7156	1.03	0.01
<i>Bos</i> sp.	34529	Herbivore	-13.1	-5.9	0.7154	0.98	0.05
<i>Panthera tigris</i>	34530	Carnivore	-4.3	-3.2	0.7126	-0.01	0.09
<i>Panthera tigris</i>	34531	Carnivore	-6.9	-3.5	0.7147	0.05	0.06
<i>Panthera tigris</i>	34532	Carnivore	-10.0	-6.8	0.7170	0.16	0.07
<i>Sus</i> sp.	34533	Omnivore	-7.6	-7.5	0.7149	0.70	0.03
<i>Sus</i> sp.	34534	Omnivore	-8.6	-10	0.7210	0.50	0.04
<i>Sus</i> sp.	34535	Omnivore	-6.0	-5.9	0.7168	0.72	0.03
<i>Sus</i> sp.	34536	Omnivore	-13.5	-5.8	0.7181	0.61	0.05
<i>Sus</i> sp.	34537	Omnivore	-14.0	-7.6	0.7154	0.32	0.16
<i>Sus</i> sp.	34538	Omnivore	-13.2	-5.4	0.7202	0.61	0.06
Canidae (? <i>Cuon alpinus</i>)	34539	Carnivore	-16.0	-7.3	0.7205	0.02	0.08
Canidae (? <i>Cuon alpinus</i>)	34540	Carnivore	-11.4	-3.2		0.20	0.07
Canidae	34543	Carnivore	-13.2	-6		0.60	0.01
<i>Pongo</i> sp.	34541	Omnivore	-14.8	-4.1	0.7159	0.38	
<i>Pongo</i> sp.	34542	Omnivore	-13.5	-4.6	0.7103	0.34	0.02
<i>Ailuropoda melanoleuca</i>	34544	Herbivore	-16.7	-6.3	0.7121	0.53	0.01
Tapiridae indet.	34545	Herbivore	-15.5	-5.9	0.7211	0.50	0.04
<i>Tapirus</i> sp.	34546	Herbivore	-11.3	-7.9	0.7200	0.39	0.06
<i>Macaca</i> sp.	34547	Omnivore	-13.9	-5.3	0.7158	0.22	0.01
<i>Macaca</i> sp.	34548	Omnivore	-14.2	-5.3	0.7178	0.15	0.06
<i>Macaca</i> sp.	34549	Omnivore	-15.1	-5.6	0.7182	0.35	0.01
<i>Macaca</i> sp.	34550	Omnivore	-13.3	-4.7	0.7166	0.30	0.01
<i>Macaca</i> sp.	34551	Omnivore	-12.9	-4.6	0.7107	0.32	0.07
<i>Hystrix</i> sp.	34552	Omnivore	-11.5	-7.6	0.7134	0.42	0.01
<i>Hystrix</i> sp.	34553	Omnivore	-11.5	-5.5	0.7147	0.29	0.06
<i>Hystrix</i> sp.	34554	Omnivore	-7.9	-5.2	0.7097	0.43	0.03
<i>Hystrix</i> sp.	34555	Omnivore	-11.6	-8.5	0.7168	-0.04	0.07

<i>Rhinoceros sondaicus</i>	34556	Herbivore	-16.2	-6.5	0.7199	0.52	0.01
<i>Rhinoceros sondaicus</i>	34557	Herbivore	-13.3	-5.5	0.7173	0.86	
<i>Rhinoceros sondaicus</i>	34558	Herbivore	-15.6	-6.3	0.7156	0.90	
<i>Rhinoceros sondaicus</i>	34559	Herbivore	-15.3	-7.1	0.7186	0.79	0.11
<i>Rhinoceros sondaicus</i>	34560	Herbivore	-14.6	-7.5	0.7150	1.03	

Table S4. Enamel stable isotope results of $\delta^{13}\text{C}_{\text{apatite}}$, $\delta^{18}\text{O}_{\text{apatite}}$, $^{87}\text{Sr}/^{86}\text{Sr}$ and $\delta^{66}\text{Zn}$ from the 72 fossil tooth specimens from Tam Hay Marklot cave (Laos). Abbreviation: SEVA = Stable isotope-Evolutionary Anthropology (the numbering system used in the Human Evolution department of the Max Planck Institute for Evolution Anthropology, Leipzig, for every sample analyzed for isotope analysis).

SEVA	Taxon	% Coll	$\delta^{13}\text{C}_{\text{collagen}}$	$\delta^{15}\text{N}_{\text{collagen}}$	%C	%N	C:N ratio
34517	<i>Muntiacus</i> sp.	0.70	-21.03	+10.56	43.97	15.86	3.23
34527	<i>Bos</i> sp.	0.59	-9.15	+3.15	44.29	15.92	3.25
34537	<i>Sus</i> sp.	0.37	-21.68	+8.07	34.72	12.54	3.23
34556	<i>Rhinoceros sondaicus</i>	0.17	-24.04	+6.63	40.92	14.39	3.32

Table S5. Dentin $\delta^{13}\text{C}$ and $\delta^{15}\text{N}$ values (‰) from collagen extraction for the four of the 23 of the sub sample of 23 dentin samples, for which collagen extraction was attempted. Abbreviation: SEVA = Stable isotope-Evolutionary Anthropology (the numbering system used in the Human Evolution department of the Max Planck Institute for Evolution Anthropology, Leipzig, for every sample analyzed for isotope analysis).

Reference material	Element	Substance	Measured value	SD	n	Expected value	SD
Marbre-LM ⁽¹⁾ (theoretical value normalized to NBS-19)	C&O	Carbonate (in-house)	+2.17 ‰ (δ ¹³ C)	0.05	24	+2.13 ‰ (δ ¹³ C)	NA
			-2.00 ‰ (δ ¹⁸ O)	0.03		-1.83 ‰ (δ ¹⁸ O)	
EVA-0009 Methionine ⁽²⁾	C&N	Methionine (in-house)	-28.28 ‰ (δ ¹³ C)	0.09	7	-28.28 ‰ (δ ¹³ C)	NA
			-4.88 ‰ (δ ¹⁵ N)	0.26		-4.98 ‰ (δ ¹⁵ N)	
IAEA-N-1 (153–156)	N	Ammonium Sulfate	+0.43 ‰ (δ ¹⁵ N)	N/A	1	+0.40 ‰ (δ ¹⁵ N)	0.2
IAEA-CH-6 (153, 157)	C	Sucrose	-10.31 ‰ (δ ¹³ C)	N/A	1	-10.45 ‰ (δ ¹³ C)	0.033
IAEA-N-2 (153–156)	N	Ammonium Sulfate	+20.31 ‰ (δ ¹⁵ N)	N/A	1	+20.30 ‰ (δ ¹⁵ N)	0.2
IAEA-CH-7 (153, 157)	C	Polyethylene foil	-31.74 ‰ (δ ¹³ C)	N/A	1	-32.15 ‰ (δ ¹³ C)	0.05
NIST SRM 1577b ⁽²⁾	C&N	Bovine liver	-21.24 ‰ (δ ¹³ C)	0.04	2	-21.40 ‰ (δ ¹³ C)	NA
			+7.61 ‰ (δ ¹⁵ N)	0.04		7.60 ‰ (δ ¹⁵ N)	
NIST SRM 1486 ⁽³⁾	Sr	Bone meal	0.709306 (⁸⁷ Sr/ ⁸⁶ Sr)	0.000026	7	0.709299	0.000027
AZE ⁽³⁾	Zn	Dentin (in-house)	+1.59 ‰ (δ ⁶⁶ Zn)	0.04	11	+1.50 ‰ (δ ⁶⁶ Zn)	0.1
NIST SRM 1400 ⁽³⁾	Zn	Bone ash	+0.95 ‰ (δ ⁶⁶ Zn)	0.03	6	+1.0 ‰ (δ ⁶⁶ Zn)	0.04

Table S6. List of reference materials with their respective measured and expected values for different isotopes.

(1) Expected values obtained through in-house long-term measurements at the "Service de Spectrométrie de Masse Isotopique du Muséum (SSMIM)" in Paris.

(2) Expected values obtained through in-house long-term measurements at the Max Planck Institute for Evolutionary Anthropology, in Leipzig.

(3) Expected values taken from Jaouen et al. (2018).

	Est.	SE	LowerCI	UpperCI	X ²	Df	P	Min	Max
Intercept	0.074	0.078	-0.086	0.230			-	0.008	0.135
Diet ⁽¹⁾	NA	NA			23.289	2	0.000		
Diet _{Herbivore}	0.523	0.088	0.340	0.701				0.461	0.582
Diet _{Omnivore}	0.441	0.095	0.249	0.633				0.384	0.520
⁸⁷ Sr/ ⁸⁶ Sr ⁽²⁾	-0.097	0.023	-0.144	-0.050	12.101	1	0.001	-0.109	-0.079
$\delta^{13}\text{C}_{\text{apatite}}$ ⁽³⁾	-0.008	0.023	-0.058	0.041	0.230	1	0.632	-0.043	-0.005
$\delta^{18}\text{O}_{\text{apatite}}$ ⁽⁴⁾	0.006	0.027	-0.051	0.063	0.135	1	0.713	-0.005	0.030
Zinc concentration ⁽⁵⁾	-0.050	0.036	-0.133	0.031	2.163	1	0.141	-0.101	0.002
Body mass ⁽⁶⁾	0.116	0.035	0.047	0.187	9.892	1	0.002	0.095	0.143

Table S7. Results of the linear mixed model modelling $\delta^{66}\text{Zn}$ values as a function of several predictors (estimates and standard errors, confidence limits of the model, results of likelihood ratio tests, and the range of estimates obtained for the model when dropping levels of random effects one at a time).

(1) Dummy coded with carnivores being the reference category

(2) z-transformed to a mean of 0 and a standard deviation of 1; whereas the original mean and sd were 0.7154 and 0.0031 ⁸⁷Sr/⁸⁶Sr, respectively

(3) z-transformed to a mean of 0 and a standard deviation of 1; whereas the original mean and sd were -9.99‰ and 5.4‰ $\delta^{13}\text{C}_{\text{apatite}}$, respectively

(4) z-transformed to a mean of 0 and a standard deviation of 1; whereas the original mean and sd were -5.71‰ and 1.78‰ $\delta^{18}\text{O}_{\text{apatite}}$, respectively

(5) z-transformed to a mean of 0 and a standard deviation of 1; whereas the original mean and sd were 114.32 and 140.35 $\mu\text{g/g}$, respectively (before log-transformed)

(6) z-transformed to a mean of 0 and a standard deviation of 1; whereas the original mean and sd were 330.51 and 497.07 kg, respectively (before natural log-transformed)

Taxa	Permanent teeth	Deciduous teeth	Total
Artiodactyla			
<i>Rusa unicolor</i>	367	23	390
<i>Rucervus eldii</i>	17	10	27
<i>Axis cf. porcinus</i>	18	4	22
<i>Muntiacus</i> sp.	101	4	105
Middle-sized Cervidae	29	1	30
<i>Bos</i> sp. (<i>Bos</i> cf. <i>frontalis</i>)	37	-	37
<i>Bubalus bubalis</i>	40	-	40
Large-sized Bovidae (<i>Bos/Bubalus</i>)	27	7	34
<i>Capricornis</i> sp. (<i>Capricornis</i> cf. <i>sumatrensis</i>)	83	-	83
<i>Naemorhedus</i> cf. <i>caudatus</i>	32	-	32
<i>Sus</i> sp. (<i>S. scrofa/S. barbatus</i>)	264	10	274
<i>Sus</i> cf. <i>barbatus</i>	17	-	17
Proboscidea			
<i>Elephas</i> sp.	-	1	1
Perissodactyla			
<i>Rhinoceros sondaicus</i>	7	3	10
<i>Dicerorhinus sumatrensis</i>	4	5	9
Rhinocerotina indet.	≥7	≥4	13
Tapiridae indet.	1	-	1
<i>Tapirus</i> sp.	1	-	1
Carnivora			
Canidae (? <i>Cuon alpinus</i>)	4	-	4
<i>Panthera pardus</i>	4	-	4
<i>Panthera tigris</i>	7	-	7
Small-sized Felidae	6	-	6
Large Carnivora	6	-	6
<i>Ursus thibetanus</i>	17	-	17
<i>Helarctos malayanus</i>	7	-	7
Ursidae indet. (<i>U. thibetanus/H. malayanus</i>)	5	-	5
Small-sized melinae (<i>Arctonyx</i> sp.)	7	-	7
<i>Ailuropoda melanoleuca</i>	1	-	1
Primates			
<i>Macaca</i> sp.	22	-	22
<i>Pongo</i> sp.	3	-	3
Rodentia			
<i>Hystrix</i> sp.	134	-	134
<i>Atherurus</i> cf. <i>macrourus</i>	17	-	17
		-	
Total (NISP)	1292	72	1364

Table S8. Inventory of specimens (isolated teeth) of mammals recovered at the Tam Hay Marklot site. *N*: Total number of specimens.

Sample name	Field number	Taxon	Tooth type
SCUMK-01	1092	Large bovid (<i>Bos/Bubalus</i>)	M ₁ or M ₂
SCUMK-02	3	<i>Pongo</i> sp.	R-M ₁
SCUMK-03A	1003	<i>Bos</i> cf. <i>frontalis</i>	R-P ₃
SCUMK-03B	1005	<i>Bos</i> cf. <i>frontalis</i>	R-P ₃
SCUMK-R1	1058	<i>Dicerorhinus sumatrensis</i>	L-P ₃

Table S9. Sample description from fossil teeth of the Tam Hay Marklot assemblage prepared for U-series dating.

Sample	U	U/Th	²³⁰ Th/ ²³⁸ U	2 SE	²³⁴ U/ ²³⁸ U	2 SE	Age (ka)	2 SE
SCUMKR1_1	-0.02	0	-5.3000	5.3000	1.4600	0.5300		
SCUMKR1_2	-0.12	-1473	0.5270	0.0340	1.4710	0.0300		
SCUMKR1_3	-0.12	1192	0.4990	0.0410	1.4590	0.0100		
SCUMKR1_4	-0.12	315	0.4960	0.0570	1.4480	0.0120		
SCUMKR1_5	-0.11	463	0.4780	0.0560	1.5110	0.0270		
SCUMKR1_6	3.46	20353	0.3880	0.0140	1.4880	0.0110	37.0	1.5
SCUMKR1_7	3.68	26286	0.3582	0.0090	1.4770	0.0120	35.0	1.5
SCUMKR1_8	5.10	25500	0.3320	0.0140	1.4790	0.0120	32.0	1.6
SCUMKR1_9	6.21	51750	0.2653	0.0057	1.4651	0.0081	25.0	0.9
SCUMKR1_10	5.98	-31474	0.2866	0.0079	1.4660	0.0110	27.0	1.1
SCUMKR1 mean age							31.2	1.3

Table S10. U-series results for the Tam Hay Marklot rhinoceros tooth specimen SCUMKR1 (*Dicerorhinus sumatrensis*).

Sample	U	U/Th	$^{230}\text{Th}/^{238}\text{U}$	2 SE	$^{234}\text{U}/^{238}\text{U}$	2 SE	Age (ka)	2 SE
SCUMK01_1	-0.01	-1	-0.1000	2.0000	0.4400	0.7600		
SCUMK01_2	-0.07	-84	1.3000	1.2000	1.9000	0.7000		
SCUMK01_3	-0.07	-1470	0.5900	0.1600	1.4610	0.0920		
SCUMK01_4	0.61	-6100	0.1120	0.0560	1.4130	0.0510		
SCUMK01_5	9.73	57235	0.2738	0.0049	1.4014	0.0062	26.9	0.6
SCUMK01_6	12.13	8308	0.2914	0.0063	1.3987	0.0089	27.7	0.9
SCUMK01_7	10.47	7027	0.2840	0.0120	1.4000	0.0110	27.5	1.7
SCUMK01_8	10.74	3556	0.2732	0.0057	1.3981	0.0069	26.4	0.8
SCUMK01_9	7.90	600	0.3110	0.0100	1.3640	0.0150	29.8	1.0
SCUMK01 mean age							27.6	1.0

Table S11. U-series results for the Tam Hay Marklot bovid tooth specimen SCUMK01 (large bovid).

Sample	U	U/Th	$^{230}\text{Th}/^{238}\text{U}$	2 SE	$^{234}\text{U}/^{238}\text{U}$	2 SE	Age (ka)	2 SE
SCUMK02_1	-0.12	293	0.5400	0.0110	1.4518	0.0065		
SCUMK02_2	-0.12	-2306	0.5340	0.0350	1.4580	0.0120		
SCUMK02_3	6.70	-26800	0.3803	0.0081	1.4680	0.0077	37.2	1.1
SCUMK02_4	12.50	-113636	0.4160	0.0270	1.4729	0.0092	37.2	0.9
SCUMK02_5	16.01	53367	0.3889	0.0055	1.4730	0.0048	37.2	0.5
SCUMK02_6	16.47	1647000	0.3872	0.0042	1.4717	0.0051	37.3	0.6
SCUMK02_7	16.03	320600	0.3884	0.0050	1.4706	0.0061	37.0	1.3
SCUMK02_8	17.73	1773000	0.3870	0.0100	1.4714	0.0084	39.1	1.4
SCUMK02_9	17.28	7714	0.3906	0.0069	1.4730	0.0067	37.3	0.8
SCUMK02_10	17.10	13680	0.3929	0.0061	1.4718	0.0064	37.4	0.7
SCUMK02 mean age							37.4	0.9

Table S12. U-series results for the Tam Hay Marklot orangutan tooth specimen SCUMK02 (*Pongo* sp.).

Sample	U	U/Th	$^{230}\text{Th}/^{238}\text{U}$	2 SE	$^{234}\text{U}/^{238}\text{U}$	2 SE	Age (ka)	2 SE
SCUMK03_1	-0.03	-32	0.1700	0.2000	0.9300	0.3800		
SCUMK03_2	0.11	335	0.1360	0.0610	1.5000	0.1300		
SCUMK03_3	4.42	19217	0.1443	0.0049	1.4360	0.0130	13.1	0.5
SCUMK03_4	5.30	589	0.1392	0.0080	1.4240	0.0300	12.0	0.5
SCUMK03_5	5.10	9273	0.1482	0.0050	1.4430	0.0082	13.4	0.5
SCUMK03_6	5.16	5864	0.1475	0.0043	1.4358	0.0092	13.4	0.4
SCUMK03_7	4.70	1382	0.1477	0.0055	1.4465	0.0093	13.3	0.5
SCUMK03_8	4.20	592	0.1465	0.0049	1.4270	0.0110	13.4	0.5
SCUMK03_9	3.87	2037	0.1473	0.0091	1.4430	0.0140	13.4	0.9
SCUMK03A mean age							13.1	0.5

Table S13. U-series results for the Tam Hay Marklot bovid tooth specimen SCUMK03 (*Bos* sp. (*Bos* cf. *frontalis*)).

Sample	Mean Age U-series (ka)	Number of rasters	Age DAD (ka)	2 SE
SCUMK-R1	31.2ka \pm 1.3	5	31.4	+2.9/-2.7
SCUMK-01	27.6ka \pm 1.0	7	28.1	+1.2/-1.2
SCUMK-02	37.4ka \pm 0.9	8	38.4	+1.0/-1.2
SCUMK-03A	13.1ka \pm 0.5	7	13.5	+1.0/-1.0

Table S14. DAD model results for each fossil tooth sample from the Tam Hay Marklot assemblage prepared for U-series dating.

Sample	Sample matrix	SEVA	$\delta^{66}\text{Zn}$
Sandy to gravelly silty clays (fossil-bearing layer)	Sediment	35342	0.60
Calcitic cementation (fossil-bearing layer)	Sediment	35343	0.69
Clay from conglomerate	Sediment	35344	0.12
Conglomerate/breccias	Sediment	35345	0.53
Sediment attached to the enamel surface of sample 34556 (<i>Rhinoceros sondaicus</i>)	Sediment	34556-D_9	0.55
<i>Rhinoceros sondaicus</i>	Dentin	34556-D_1	0.65
<i>Rhinoceros sondaicus</i>	Dentin	34556-D_2	0.77
<i>Rhinoceros sondaicus</i>	Dentin	34556-D_3	0.82
<i>Rhinoceros sondaicus</i>	Dentin	34556-D_4	0.73
<i>Rhinoceros sondaicus</i>	Dentin	34556-D_7	0.71
<i>Rhinoceros sondaicus</i>	Dentin	34556-D_10	0.65
<i>Rhinoceros sondaicus</i>	Dentin	34556-D_mean	0.72
<i>Capricornis</i> sp.	Dentin	34489-D	0.81
<i>Capricornis</i> sp.	Dentin	34490-D	1.05
<i>Capricornis</i> sp.	Dentin	34492-D	0.99
<i>Helarctos malayanus</i>	Dentin	34498-D	0.73
<i>Panthera pardus</i>	Dentin	34505-D	0.39
<i>Bubalus bubalus</i>	Dentin	34524-D	0.85

Table S15. Sediment and dentin $\delta^{66}\text{Zn}$ isotope values (‰) from Tam Hay Marklot cave (Laos) used to assess the impact of diagenesis on $\delta^{66}\text{Zn}$ values. Abbreviation: SEVA = Stable isotope-Evolutionary Anthropology (numbering system used in the Human Evolution department of the Max Planck Institute for Evolution Anthropology, Leipzig, for every sample analyzed for isotope analysis).

Reference material	Source	$\delta^{66}\text{Zn}$ (‰)	SD	n	Gloves	Laboratory	ICPMS	Zn separation protocol
NIST SRM 1400	This study	1.00	0.01	2	Vinyl	Leipzig	Neptune	Moynier et al. (2006)
NIST SRM 1400	This study	1.07	NA	1	Nitrile	Lyon	Nu 500	Moynier et al. (2006)
NIST SRM 1400	This study	0.94	0.05	3	Vinyl	Toulouse	Neptune Plus	Moynier et al. (2006)
	Average	1.00	0.07					
NIST SRM 1400	Jaouen et al. (2018)	1.00	0.04		Nitrile	Lyon	Nu 500	Moynier et al. (2006)
NIST SRM 1400	Bourgon et al. (2020)	0.94	0.05	6	Vinyl	Leipzig	Neptune	Moynier et al. (2006)
	Average	0.97	0.04					
AZE	This study	1.53	0.05	3	Nitrile	Lyon	Nu 500	Moynier et al. (2006)
AZE	This study	1.61	0.03	2	Vinyl	Leipzig	Neptune	Moynier et al. (2006)
AZE	This study	1.62	NA	1	Vinyl	Toulouse	Neptune Plus	Moynier et al. (2006)
	Average	1.59	0.05					
AZE 7 ⁽¹⁾	This study	1.56	0.11	1	Nitrile	Lyon	Nu 500	Moynier et al. (2006)
AZE 7 ⁽¹⁾	This study	1.54	0.00	1	Nitrile	Leipzig	Neptune	Moynier et al. (2006)
AZE	Jaouen (2012)	1.50	0.04	10	Various	Lyon	Nu 500	Maréchal et al. (1999) Moynier et al. (2006)
AZE	Jaouen et al. (2016a)	1.47	0.11	8	Nitrile	Leipzig	Neptune	Moynier et al. (2006)
AZE	Jaouen (2016b)	1.51	0.12	2	Nitrile	Leipzig	Neptune	Maréchal et al. (1999) Moynier et al. (2006)
AZE	Jaouen et al. (2018)	1.51	0.14	5	Nitrile	Lyon	Nu 500	Moynier et al. (2006)
AZE	Bourgon et al. (2020)	1.59	0.05	11	Latex	Leipzig	Neptune	Moynier et al. (2006)
	Average	1.56	0.05					

Table S16. Measured and expected $\delta^{66}\text{Zn}$ values for NIST SRM 1400 and in-house AZE reference materials used in this study, and information about the type of gloves used during sample preparation and instrument (ICPMS) used for measurements.

⁽¹⁾ Reference material AZE #7 was measured in different laboratories for inter-lab comparison; standard deviations reported are thus not inter-samples.

Test	Gloves									
	Latex C		Latex T		Nitrile		Vinyl			
	$\delta^{66}\text{Zn}$ (‰)	Zn (ng)	$\delta^{66}\text{Zn}$ (‰)	Zn (ng)	$\delta^{66}\text{Zn}$ (‰)	Zn (ng)	$\delta^{66}\text{Zn}$ (‰)	Zn (ng)	$\delta^{66}\text{Zn}$ (‰)	Zn (ng)
TEST 1A	-0.11	3437443	0.07	2516074	-0.14	1229122	0.23	11401		
TEST 1B	-0.52	50178	-0.01	426144	-0.51	9563	0.11	5942		
TEST 1C	0.08	299260	0.00	108640	-0.33	40124	0.30	10528		
TEST 1D	0.00	2290117	0.22	843458	-0.46	2788904	0.27	27297		
TEST 1E		11.8		83.6		4.3		0.5		
TEST 1F		78.0		77.0		2.9		0.4		
TEST 1G		2.8		1671.9		0.7		0.4		
TEST 1H		4.7		311.6		1.1		0.8		

Table S17. The $\delta^{66}\text{Zn}$ values (‰) and zinc content (ng) for each of the glove tests and different type of gloves used in this study.

33944	m2	85	17	Burial 23, Subadult 1	Subadult	2 to 4	n/a	0.42	75	0.45 0.45	78	0.45 0.37 0.41	130
33945	m2	85	18	Burial 23, Subadult 2	Subadult	2 to 4	n/a	0.48	68	0.46 0.46	42		
33946	M2	27	19	Burial 23, Adult 1	Adult	n/a	n/a	0.06	123	0.16 0.16	23		
33947	M2	27	20	Burial 23, Adult 2	Adult	n/a	n/a	0.38	158	0.32 0.32	119	0.22 0.25 0.24	154
33948	M2	27	21	Burial 16	Young adult	18 to 21	Female	0.28	93	0.26 0.26	56		
33949	P4	45	23	Burial 34	Adult	24 to 49	Male	0.28	115	0.19 0.19	135		
33950	P4	25	26	Burial 05	Adult	24 to 49	Female	0.22	144	0.20 0.24 0.22	140		
33951	P3?	34?	28	Burial 21	Adult	24 to 40	Male	0.23	127	0.20 0.14 0.17	85		
33952	m2	75	30	Burial 27	Subadult	4 to 6	n/a	0.52	70	0.52 0.52	109	0.49 0.48 0.49	219
33953	M2	27	32	Burial 16	Young adult	18 to 21	Female	1.23	342	0.14 0.14	57		

33954	M2	27	34	Burial 11	Young adult	17 to 24	Female	0.26	102	0.07 0.24 0.16	70	
33955	M3	18	35	Burial 23, Adult #1	Adult	n/a	n/a	0.07	128	0.18 0.19 0.19	89	
33956	M3	18	36	Burial 15	Adult	26 to 64	Male	0.4	50	0.11 0.20 0.16	99	
33957	M3	28	37	Burial 23, Adult 2	Adult	n/a	n/a	NA	4	0.30 0.30	64	
33958	m1	64	38	Burial 23, Subadult 2	Subadult	2 to 4	n/a	-0.16	278	0.54 0.54	71	
33959	m1	64	39	PN-2253	Subadult	n/a	n/a	0.5	53	0.26 0.26	25	
33960	P3	44	40	Burial 10	Adult	> 24	Female	0.02	100	0.41 0.41	32	
33961	m1	64	41	Burial 23, Subadult 1	Subadult	2 to 4	n/a	0.51	74	0.34 0.34	35	

Table S18. Tooth enamel $\delta^{66}\text{Zn}$ values (‰) and zinc concentration ($\mu\text{g/g}$) from the Lapa do Santo (Minas Gerais, Brazil) hunter-gatherers, with anthropological data. Abbreviation: SEVA = Stable isotope-Evolutionary Anthropology (the numbering system used in the Human Evolution department of the Max Planck Institute for Evolution Anthropology, Leipzig, for every sample analyzed for isotope analysis).

(1) *Individual 2, PN-01.08.0637*

SEVA	Tooth	Ena. part sampled	Ena. init. (year)	Ena. compl. (year)	$\delta^{66}\text{Zn}$	$\delta^{67}\text{Zn}$	$\delta^{68}\text{Zn}$	[Zn] ($\mu\text{g/g}$)	Root init. (year)	Root compl. (year)	$\delta^{13}\text{C}$	$\delta^{15}\text{N}$	%C	%N	C/N
35197-1a	UR I1	Middle	0.9	2.5	0.24	0.39	0.51	105	5	10	-19.4	13.3	41.9	15.8	3.1
35197-1b	UR I1	Middle/Up	0.6	1.8	0.31	0.55	0.64	102							
35197-2a	LLI2	Middle	2	3.3	0.21	0.34	0.44	74	5.25	10.5	-19.4	13.4	43.5	16.6	3.1
35197-2b	LLI2	Middle/Up	1	2.5	0.29	0.42	0.58	149							
35197-3a	UL P4	Middle	5	6.3	0.26	0.41	0.5	81	7.5	14	-19.3	13.7	42.3	16.1	3.1
35197-3b	UL P4	Middle/Up	4.5	5.8	0.26	0.56	0.57	53							
35197-4a	UR C1	Middle	3	5	0.25	0.42	0.51	71	6.5	15	-19.0	13.1	43.0	16.3	3.1
35197-4b	UR C1	Middle/Up	1.5	4	0.3	0.52	0.62	91							
35197-5a	UP3	Middle	4	5.5	0.28	0.49	0.54	98	7	13	-19.1	13.6	42.7	16.1	3.1
35197-5b	UP3	Middle/Up	3.5	4.8	0.27	0.48	0.52	67							
35197-6a	UM3	Middle	11.8	13	0.24	0.43	0.52	141	14	23	-19.4	12.7	42.9	16.2	3.1
35197-6b	UM3	Middle/Up	10.5	12.3	0.2	0.28	0.41	88							
35197-7	UR M1	Middle	1.8	3	0.54	0.86	1.11	69	3	10	-19.3	13.5	43.2	16.1	3.1
35197-8a	UR M2	Middle	6.3	7	0.32	0.55	0.72	155	8.5	16	-19.7	13.6	44.6	16.6	3.1
35197-8b	UR M2	Middle/Up	5	6.5	0.22	0.41	0.45	105							
35198-2a	URM1	Top	-0.08	2	0.51	0.76	1.03	129	3	9	-19.6	13.0	40.9	15.7	3.1
35198-2b	URM1	Bottom	2	3.5	0.48	0.71	1	154	3	9	-19.6	13.0	40.9	15.7	3.1
35198-3a	ULM1	Top	-0.08	2	0.54	0.86	1.06	156	3	9	-19.7	12.9	41.2	15.7	3.1
35198-3b	ULM1	Bottom	2	3.5	0.42	0.79	0.84	58	3	9	-19.7	12.9	41.2	15.7	3.1
35198-5	ULdm1	Top	-0.5	0.25	0.59	0.87	1.17	105	0.5	2.5	-20.6	12.7	41.9	15.9	3.1
35198-6	ULP4	Top	3.5	5.5	0.37	0.61	0.78	46							
35198-7	ULC	Middle	2	4	0.47	0.78	0.94	131							

35198-12	LRI2	Top	0.3	3	0.48	0.75	0.94	130							
35198-13a	URP3	Top	2.5	5	0.38	0.72	0.84	104							
35198-13b	URP3	Bottom	5	6.5	0.35	0.62	0.72	79							
35198-14	ULI1	Top	0.38	1.5	0.61	0.99	1.2	145							
35198-15	ULdm2	Top	-0.21	0.25	0.79	1.28	1.6	92	1	3	-20.3	11.9	39.2	15.0	3.1
35198-17	ULdi2	Middle	-0.17	0.08	0.6	0.96	1.22	87							
35198-18	LRdi1	Whole height	-0.38	0.25	0.53	0.82	1.07	109	0.3	2	-20.4	13.2	40.8	15.6	3.1
35198-19	LLdm1	Top+Middle	-0.5	0.38	0.79	1.23	1.57	86	0.5	2	-20.4	12.6	42.2	16.1	3.1
35198-20	LRdc	Top+Middle	-0.42	0.5	0.75	1.02	1.47	159	0.8	3.25	-20.4	12.1	41.4	15.7	3.1
35198-21	LLdm2	Top	-0.21	0.33	0.81	1.21	1.65	85	1	3	-20.0	11.7	41.8	15.9	3.1
35198-22	LRdm2	Whole height	-0.2	1	0.82	1.2	1.61	89	1	3	-20.1	11.8	39.2	15.0	3.0
35198-23a	LLP3	top	2	4	0.38	0.55	0.72	117							

Table S19. Isotope data for the Couvent des Jacobins teeth (individual 63049 and 20106). The $\delta^{66}\text{Zn}$ values are obtained from the enamel, whereas the $\delta^{13}\text{C}$ and $\delta^{15}\text{N}$ from collagen extracted from the teeth's root. Delta values are expressed in ‰. The type of teeth sampled, the part sampled as well as the corresponding forming ages (init. and compl.: respectively the age of initiation and completion of the sampled enamel (ena.) and root) are also listed. Abbreviation: SEVA = Stable isotope-Evolutionary Anthropology (the numbering system used in the Human Evolution department of the Max Planck Institute for Evolution Anthropology, Leipzig, for every sample analyzed for isotope analysis).

SEVA	#Ref	Site	Taxon	Vernacular taxon name	Taxonomic unit	Diet	Tooth type
34438	NL-8	Nam Lot I	<i>Capricornis</i> sp.	Serow	Caprinae	Herbivore	rM ₃
34439	NL-9	Nam Lot I	<i>Capricornis</i> sp.	Serow	Caprinae	Herbivore	rM ₃
34441	NL-19	Nam Lot I	<i>Rusa unicolor</i>	Sambar deer	<i>Rusa unicolor</i>	Herbivore	IM ₁ /M ₂
34442	NL-29	Nam Lot I	<i>Rusa unicolor</i>	Sambar deer	<i>Rusa unicolor</i>	Herbivore	rP ₃
34443	NL-22	Nam Lot I	<i>Rusa unicolor</i>	Sambar deer	<i>Rusa unicolor</i>	Herbivore	IP ₃
34444	NL-24	Nam Lot I	<i>Rusa unicolor</i>	Sambar deer	<i>Rusa unicolor</i>	Herbivore	IM ₁ /M ₂
34445	NL-63-1	Nam Lot I	<i>Muntiacus</i> sp.	Muntjac	<i>Muntiacus</i> sp.	Herbivore	rM
34446	NL-65-1	Nam Lot I	<i>Muntiacus</i> sp.	Muntjac	<i>Muntiacus</i> sp.	Herbivore	rM
34447	NL-69	Nam Lot I	<i>Muntiacus</i> sp.	Muntjac	<i>Muntiacus</i> sp.	Herbivore	IM
34448	NL-116	Nam Lot I	Bovidae indet.	Large bovid	Large-sized Bovidae	Herbivore	IM ₃
34449	NL-117	Nam Lot I	Bovidae indet.	Large bovid	Large-sized Bovidae	Herbivore	M
34450	NL-125	Nam Lot I	Bovidae indet.	Large bovid	Large-sized Bovidae	Herbivore	M
34451	NL-161	Nam Lot I	Rhinocerotidae indet.	Rhinoceros	Rhinocerotidae	Herbivore	IP/M (fragment)
34452	NL-162	Nam Lot I	Rhinocerotidae indet.	Rhinoceros	Rhinocerotidae	Herbivore	milk tooth left (fragment)
34453	NL-254-1-1	Nam Lot I	Rhinocerotidae indet.	Rhinoceros	Rhinocerotidae	Herbivore	milk tooth left (fragment)
34454.1	NL-256-1	Nam Lot I	Rhinocerotidae indet.	Rhinoceros	Rhinocerotidae	Herbivore	milk tooth (fragment)
34455	NL-139	Nam Lot I	Bovidae (Bos sp.)	Large bovid	Large-sized Bovidae	Herbivore	rP ₄

34456	NL-143	Nam Lot I	Bovidae (Bos sp.)	Large bovid	Large-sized Bovidae	Herbivore	IP ₄
34457	NL-186	Nam Lot I	<i>Ailuropoda melanoleuca</i>	Giant panda	<i>Ailuropoda melanoleuca</i>	Herbivore	rM ₁
34458	NL-277	Nam Lot I	<i>Ailuropoda melanoleuca</i>	Giant panda	<i>Ailuropoda melanoleuca</i>	Herbivore	IM ²
34459	NL-162	Nam Lot I	<i>Sus sp.</i>	Wild boar	<i>Sus sp.</i>	Omnivore	rM ₁
34460	NL-208	Nam Lot I	<i>Sus sp.</i>	Wild boar	<i>Sus sp.</i>	Omnivore	rP ₄
34461	NL-216	Nam Lot I	<i>Sus sp.</i>	Wild boar	<i>Sus sp.</i>	Omnivore	rP ₄
34462	NL-218	Nam Lot I	<i>Sus sp.</i>	Wild boar	<i>Sus sp.</i>	Omnivore	rP ₄
34463	NL-SS-1	Nam Lot I	<i>Sus sp.</i>	Wild boar	<i>Sus sp.</i>	Omnivore	fragment
34465	NL-258	Nam Lot I	<i>Tapirus sp.</i>	Tapir	Tapiridae	Herbivore	IM
34466	NL-259	Nam Lot I	<i>Tapirus sp.</i>	Tapir	Tapiridae	Herbivore	II ₁
34467	NL-260	Nam Lot I	<i>Tapirus sp.</i>	Tapir	Tapiridae	Herbivore	II ¹
34468	NL-286	Nam Lot I	<i>Cuon alpinus</i>	Dhole	Canidae	Carnivore	P
34469	NL-368	Nam Lot I	<i>Cuon alpinus</i>	Dhole	Canidae	Carnivore	IP ₃
34470	NL-269	Nam Lot I	<i>Ursus thibetanus</i>	Asian black bear	Ursidae	Omnivore	rM ₃
34471	NL-271	Nam Lot I	<i>Ursus thibetanus</i>	Asian black bear	Ursidae	Omnivore	rM ₃
34472	NL-275	Nam Lot I	<i>Ursus thibetanus</i>	Asian black bear	Ursidae	Omnivore	IP ⁴
34474	NL-288	Nam Lot I	<i>Crocuta crocuta</i>	Spotted hyena	<i>Crocuta crocuta</i>	Bone-Eating Carnivore	IP ₃
34475	NL-295	Nam Lot I	<i>Crocuta crocuta</i>	Spotted hyena	<i>Crocuta crocuta</i>	Bone-Eating Carnivore	P
34476	NL-HS	Nam Lot I	<i>Pongo sp.</i>	Orang-utan	<i>Pongo sp.</i>	Omnivore	incisor
34478	NL-297	Nam Lot I	<i>Macaca sp.</i>	Macaque	<i>Macaca sp.</i>	Omnivore	incisor
34479	NL-314	Nam Lot I	<i>Macaca sp.</i>	Macaque	<i>Macaca sp.</i>	Omnivore	rM ₃

34480	NL-323	Nam Lot I	<i>Macaca sp.</i>	Macaque	<i>Macaca sp.</i>	Omnivore	rM ₃
34481	NL-357	Nam Lot I	<i>Macaca sp.</i>	Macaque	<i>Macaca sp.</i>	Omnivore	incisor
34482	NL-362	Nam Lot I	<i>Elephas sp.</i>	Elephant	<i>Elephas sp.</i>	Herbivore	milk tooth
34483	NL-365	Nam Lot I	<i>Stegodon orientalis</i>	Stegodon	<i>Stegodon orientalis</i>	Herbivore	milk tooth (fragment)
34484	NL-367	Nam Lot I	<i>Stegodon orientalis</i>	Stegodon	<i>Stegodon orientalis</i>	Herbivore	milk tooth (fragment)
34485	NL-369	Nam Lot I	<i>Hystrix sp.</i>	Porcupine	Hystriidae	Omnivore	P/M
34486	NL-385	Nam Lot I	<i>Hystrix sp.</i>	Porcupine	Hystriidae	Omnivore	incisor
34487	NL-392	Nam Lot I	<i>Hystrix sp.</i>	Porcupine	Hystriidae	Omnivore	P/M
34488	NL-397	Nam Lot I	<i>Hystrix sp.</i>	Porcupine	Hystriidae	Omnivore	P/M
35941	NLII-1	Nam Lot II	<i>Crocuta crocuta</i>	Spotted hyena	<i>Crocuta crocuta</i>	Bone-Eating Carnivore	rP ₂
35942	NLII-2	Nam Lot II	<i>Crocuta crocuta</i>	Spotted hyena	<i>Crocuta crocuta</i>	Bone-Eating Carnivore	rP ₃ (fragment)
35943	NLII-3	Nam Lot II	<i>Crocuta crocuta</i>	Spotted hyena	<i>Crocuta crocuta</i>	Bone-Eating Carnivore	IP ² (fragment)
35944	NLII-4	Nam Lot II	<i>Crocuta crocuta</i>	Spotted hyena	<i>Crocuta crocuta</i>	Bone-Eating Carnivore	IP ² (fragment)
35945	NLII-5	Nam Lot II	Small-sized Felidae	Small-sized Felidae	Small-sized Felidae	Carnivore	IP ³
35416	M33	Tam Pà Ling	<i>Capricornis sp.</i>	Serow	Caprinae	Herbivore	IM ₁ /M ₂
35417	M31	Tam Pà Ling	<i>Capricornis sp.</i>	Serow	Caprinae	Herbivore	IM
35418	M35	Tam Pà Ling	<i>Naemorhedus sp.</i>	Goral	Caprinae	Herbivore	rM ₁ /M ₂
35419	M31	Tam Pà Ling	<i>Naemorhedus sp.</i>	Goral	Caprinae	Herbivore	IM ₁ /M ₂
35420	K32	Tam Pà Ling	<i>Naemorhedus sp.</i>	Goral	Caprinae	Herbivore	rM ₁ /M ₂
35421	K32	Tam Pà Ling	<i>Naemorhedus sp.</i>	Goral	Caprinae	Herbivore	IM ³
35422	M35	Tam Pà Ling	Caprinae	Caprinae	Caprinae	Herbivore	ID ³

35423	L33	Tam Pà Ling	Caprinae	Caprinae	Caprinae	Caprinae	Herbivore	ID2
35424	M32	Tam Pà Ling	<i>Muntiacus</i> sp.	Muntjac	<i>Muntiacus</i> sp.	Herbivore	Herbivore	Canine
35425	K32	Tam Pà Ling	<i>Macaca</i> sp.	Macaque	<i>Macaca</i> sp.	Omnivore	Omnivore	IM
35426	L33	Tam Pà Ling	<i>Naemorhedus</i> sp.	Goral	Caprinae	Herbivore	Herbivore	ID ₃
35427	M31	Tam Pà Ling	<i>Rhinoceros</i> cf. <i>unicornis</i>	Indian rhinoceros	Rhinocerotidae	Herbivore	Herbivore	ID ₂
35428	M31	Tam Pà Ling	<i>Dicerorhinus sumatrensis</i>	Sumatran rhinoceros	Rhinocerotidae	Herbivore	Herbivore	ID ³
35429	K33	Tam Pà Ling	Caprinae	Caprinae	Caprinae	Herbivore	Herbivore	M ₁ /M ₂
35492	TPL1	Tam Pà Ling	<i>Homo sapiens</i>	Human	<i>Homo sapiens</i>	Herbivore	Herbivore	M ¹
35946	H33	Tam Pà Ling	<i>Capricornis sumatrensis</i>	Serow	Caprinae	Herbivore	Herbivore	IM ₃
35947	M32	Tam Pà Ling	Bovidae indet.	Large bovid	Large-sized Bovidae	Herbivore	Herbivore	rD ₃
35948	M32	Tam Pà Ling	Hystricidae (<i>Atherurus</i> sp.)	Porcupine	Hystricidae	Omnivore	Omnivore	incisor
35949	M29-30	Tam Pà Ling	Hystricidae (<i>Hystrix</i> sp.)	Porcupine	Hystricidae	Omnivore	Omnivore	incisor
35950	K33	Tam Pà Ling	Hystricidae	Porcupine	Hystricidae	Omnivore	Omnivore	incisor
35951	L32	Tam Pà Ling	<i>Rusa unicorn</i>	Sambar deer	<i>Rusa unicorn</i>	Herbivore	Herbivore	M ₃ (frag)
35952	K33	Tam Pà Ling	Caprinae	Caprinae	Caprinae	Herbivore	Herbivore	incisor (bottom) (left)
35954	L32	Tam Pà Ling	<i>Muntiacus</i> sp.	Muntjac	<i>Muntiacus</i> sp.	Herbivore	Herbivore	rD ³
35955	J31	Tam Pà Ling	Caprinae	Caprinae	Caprinae	Herbivore	Herbivore	rD ²
35956	M31	Tam Pà Ling	Large-sized Felidae	Large-sized Felidae	Large-sized Felidae	Carnivore	Carnivore	Milk canine
35957	O32	Tam Pà Ling	Large-sized Felidae	Large-sized Felidae	Large-sized Felidae	Carnivore	Carnivore	I ³

35958	K35	Tam Pà Ling	<i>Rhinoceros sondaicus</i>	Javan rhinoceros	Rhinocerotidae	Herbivore	IM ¹
36146	TPL1	Tam Pà Ling	<i>Homo sapiens</i>	Human	<i>Homo sapiens</i>		M ²

Table S20. Full list of Late Pleistocene fossil tooth specimens from Nam Lot and Tam Pà Ling cave (Laos) analyzed for $\delta^{66}\text{Zn}$ and $^{87}\text{Sr}/^{86}\text{Sr}$ in this study, with corresponding laboratory internal SEVA number, original sample number, broad dietary category and tooth type. Taxonomic units range from species to family levels. The dietary category assigned to each taxon was taken from Nowak (1999), Macdonald (2009) and Johnsingh and Manjrekar (2013, 2015). Abbreviations: SEVA = Stable isotope-Evolutionary Anthropology (the numbering system used in the Human Evolution department of the Max Planck Institute for Evolution Anthropology, Leipzig; for every sample analyzed for isotope analysis), r = right, l = left.

Table S16SEVA	Taxon	Sample mass (mg)	Collagen mass (mg)	% collagen
34441	<i>Rusa unicolor</i>	615.5	1.3	0.21
34442	<i>Rusa unicolor</i>	536	1.7	0.32
34448	Large-sized Bovidae	518.6	0.3	0.06
34450	Large-sized Bovidae	325.3	0.4	0.12
34451	Rhinocerotidae	456.9	1.3	0.28
34452	Rhinocerotidae	362.6	1.1	0.3
34457	<i>Ailuropoda melanoleuca</i>	519.6	1.4	0.27
34460	<i>Sus</i> sp.	485.7	0.7	0.15
34463	<i>Sus</i> sp.	454	0.3	0.07
34465	Tapiridae	418.4	1	0.23
34466	Tapiridae	295.4	1.3	0.44
34469	Canidae	502.8	1.2	0.24
34470	Ursidae	439.1	0.7	0.16
34474	<i>Crocuta crocuta</i>	405.3	0	0
34477	<i>Pongo</i> sp.	451.4	0	0
34483	<i>Stegodon orientalis</i>	457.6	1.3	0.28
34484	<i>Stegodon orientalis</i>	545.8	0.5	0.09

Table S21. Full list of the Late Pleistocene fossil tooth specimens sub sample from Nam Lot cave (Laos) for which dentin collagen extraction was attempted. Abbreviation: SEVA = Stable isotope-Evolutionary Anthropology (the numbering system used in the Human Evolution department of the Max Planck Institute for Evolution Anthropology, Leipzig, for every sample analyzed for isotope analysis).

SEVA	Site	Taxon	Diet	$\delta^{66}\text{Zn}$ (‰)	$\delta^{66}\text{Zn}$ 1 σ	Concentration Zn [$\mu\text{g/g}$]	$87\text{Sr}/86\text{Sr}$	Concentration Sr [$\mu\text{g/g}$]
34438	Nam Lot I	Caprinae	Herbivore	0.82	0.00	76	0.71125	141
34439	Nam Lot I	Caprinae	Herbivore	0.88	0.00	55	0.71069	56
34441	Nam Lot I	<i>Rusa unicorn</i>	Herbivore	0.68	0.02	25	0.71339	82
34442	Nam Lot I	<i>Rusa unicorn</i>	Herbivore	0.88	0.01	33	0.71278	95
34443	Nam Lot I	<i>Rusa unicorn</i>	Herbivore	0.83	0.01	102	0.71064	141
34444	Nam Lot I	<i>Rusa unicorn</i>	Herbivore	0.53	0.01	98	0.71309	107
34445	Nam Lot I	<i>Muntiacus</i> sp.	Herbivore	0.40	0.01	61	0.72733	84
34446	Nam Lot I	<i>Muntiacus</i> sp.	Herbivore	0.27	0.02	44	0.72689	116
34447	Nam Lot I	<i>Muntiacus</i> sp.	Herbivore	0.50	0.01	43	0.71253	138
34448	Nam Lot I	Large-sized Bovidae	Herbivore	0.67	0.01	73	0.72095	138
34449	Nam Lot I	Large-sized Bovidae	Herbivore	0.39	0.01	23	0.71577	82
34450	Nam Lot I	Large-sized Bovidae	Herbivore	0.32	0.01	24	0.71942	134
34451	Nam Lot I	Rhinocerotidae	Herbivore	0.72	0.11	15	0.71302	462
34452	Nam Lot I	Rhinocerotidae	Herbivore	1.01	0.08	11	0.71264	131
34453	Nam Lot I	Rhinocerotidae	Herbivore	0.66	0.00	64	0.71956	155
34454.1	Nam Lot I	Rhinocerotidae	Herbivore	0.75	0.00	78	0.71874	367
34455	Nam Lot I	Large-sized Bovidae	Herbivore	0.71	0.04	23	0.71844	171
34456	Nam Lot I	Large-sized Bovidae	Herbivore	0.67	0.01	50	0.71979	66
34457	Nam Lot I	<i>Ailuropoda melanoleuca</i>	Herbivore	0.61	0.01	28	0.71692	335
34458	Nam Lot I	<i>Ailuropoda melanoleuca</i>	Herbivore	0.47	0.05	16	0.71499	146
34459	Nam Lot I	<i>Sus</i> sp.	Omnivore	0.54	0.02	57	0.71673	193
34460	Nam Lot I	<i>Sus</i> sp.	Omnivore	0.51	0.03	96	0.71516	417
34461	Nam Lot I	<i>Sus</i> sp.	Omnivore	0.54	0.01	41	0.71655	360

34462	Nam Lot I	<i>Sus</i> sp.	Omnivore	0.63	0.00	91	0.72207	392
34463	Nam Lot I	<i>Sus</i> sp.	Omnivore	0.60	0.00	123	0.72249	124
34465	Nam Lot I	Tapiridae	Herbivore	0.66	0.02	27	0.71439	98
34466	Nam Lot I	Tapiridae	Herbivore	0.59	0.01	70	0.71618	81
34467	Nam Lot I	Tapiridae	Herbivore	0.45	0.04	14	0.71574	253
34468	Nam Lot I	Canidae	Carnivore	0.14	0.00	48	0.71734	169
34469	Nam Lot I	Canidae	Carnivore	0.15	0.02	82	0.71724	158
34470	Nam Lot I	Ursidae	Omnivore	0.17	0.00	26	0.73001	163
34471	Nam Lot I	Ursidae	Omnivore	0.38	0.01	37	0.71513	128
34472	Nam Lot I	Ursidae	Omnivore	0.58	0.03	153	0.71415	78
34474	Nam Lot I	<i>Crocota crocuta</i>	Bone-eating Carnivore	0.52	0.01	52	0.71562	85
34475	Nam Lot I	<i>Crocota crocuta</i>	Bone-eating Carnivore	0.56	0.02	64	0.71461	112
34476	Nam Lot I	<i>Pongo</i> sp.	Omnivore	0.81	0.02	263	0.71419	76
34478	Nam Lot I	<i>Macaca</i> sp.	Omnivore	0.14	0.02	131	0.72444	139
34479	Nam Lot I	<i>Macaca</i> sp.	Omnivore	0.13	0.03	163	0.72398	30
34480	Nam Lot I	<i>Macaca</i> sp.	Omnivore	0.06	0.02	126	0.72529	168
34481	Nam Lot I	<i>Macaca</i> sp.	Omnivore	0.18	0.03	121	0.71670	31
34482	Nam Lot I	<i>Elephas</i> sp.	Herbivore	0.56	0.02	173	0.71793	333
34483	Nam Lot I	<i>Stegodon orientalis</i>	Herbivore	0.41	0.00	107	0.71434	563
34484	Nam Lot I	<i>Stegodon orientalis</i>	Herbivore	0.57	0.02	62	0.71431	387
34485	Nam Lot I	Hystriidae	Omnivore	0.43	0.01	55	0.71576	63
34486	Nam Lot I	Hystriidae	Omnivore	0.46	0.04	66	0.72695	188
34487	Nam Lot I	Hystriidae	Omnivore	0.25	0.01	76	0.72297	284
34488	Nam Lot I	Hystriidae	Omnivore	0.29	0.02	61	0.73192	106
35416	Tam Pa Ling	Caprinae	Herbivore	0.77	0.00	120	0.71128	45
35417	Tam Pa Ling	Caprinae	Herbivore	1.00	0.00	128	0.71116	46

35418	Tam Pa Ling	Caprinae	Herbivore	1.04	0.02	45	0.71056	40
35419	Tam Pa Ling	Caprinae	Herbivore	0.80	0.00	46	0.71033	45
35420	Tam Pa Ling	Caprinae	Herbivore	1.08	0.01	48	0.71041	52
35421	Tam Pa Ling	Caprinae	Herbivore	0.54	0.02	96	0.71199	34
35422	Tam Pa Ling	Caprinae	Herbivore	0.52	0.00	30	0.71679	34
35423	Tam Pa Ling	Caprinae	Herbivore	0.95	0.01	39	0.71068	32
35424	Tam Pa Ling	<i>Muntiacus</i> sp.	Herbivore	0.94	0.01	102	0.71298	148
35425	Tam Pa Ling	<i>Macaca</i> sp.	Omnivore	0.08	0.01	167	0.71745	155
35426	Tam Pa Ling	Caprinae	Herbivore	0.78	0.02	53	0.71080	23
35427	Tam Pa Ling	Rhinocerotidae	Herbivore	0.99	0.02	15	0.71747	105
35428	Tam Pa Ling	Rhinocerotidae	Herbivore	0.80	0.01	19	0.71755	112
35429	Tam Pa Ling	Caprinae	Herbivore	0.86	0.00	92	0.71829	37
35492	Tam Pa Ling	<i>Homo sapiens</i>	Herbivore	0.24	0.01	95	0.72003	110
35941	Nam Lot II	<i>Crocuta crocuta</i>	Bone-eating Carnivore	0.31	0.02	150	0.71753	62
35942	Nam Lot II	<i>Crocuta crocuta</i>	Bone-eating Carnivore	0.23	0.01	88	0.71438	187
35943	Nam Lot II	<i>Crocuta crocuta</i>	Bone-eating Carnivore	0.47	0.01	137	0.71431	141
35944	Nam Lot II	<i>Crocuta crocuta</i>	Bone-eating Carnivore	0.42	0.01	346	0.71583	209
35945	Nam Lot II	Small-sized Felidae	Carnivore	-0.11	0.00	90	0.71765	90
35946	Tam Pa Ling	Caprinae	Herbivore	1.00	0.00	91	0.71121	52
35947	Tam Pa Ling	Large-sized Bovidae	Herbivore	0.66	0.01	20	0.71791	90
35948	Tam Pa Ling	Hystriidae	Omnivore	0.70	0.00	28	0.71186	65
35949	Tam Pa Ling	Hystriidae	Omnivore	0.34	0.01	27	0.71558	83
35950	Tam Pa Ling	Hystriidae	Omnivore	0.54	0.02	30	0.71093	67
35951	Tam Pa Ling	<i>Rusa unicorn</i>	Herbivore	0.76	0.02	103	0.71120	42
35952	Tam Pa Ling	Caprinae	Herbivore	0.83	0.01	77	0.71150	43
35954	Tam Pa Ling	<i>Muntiacus</i> sp.	Herbivore	0.89	0.00	21	0.71051	29

35955	Tam Pa Ling	Caprinae	Herbivore	1.02	0.00	57	0.71152	76
35956	Tam Pa Ling	Large-sized Felidae	Carnivore	0.88	0.01	159	0.71498	124
35957	Tam Pa Ling	Large-sized Felidae	Carnivore	-0.03	0.01	250	0.71469	157
35958	Tam Pa Ling	Rhinocerotidae	Herbivore	1.00	0.00	91	0.71453	101
36146	Tam Pa Ling	<i>Homo sapiens</i>		0.24	0.01	84		

Table S22. Enamel zinc and strontium stable isotope results ($^{87}\text{Sr}/^{86}\text{Sr}$ and $\delta^{66}\text{Zn}$) and concentration (Zn [$\mu\text{g/g}$] and Sr [$\mu\text{g/g}$]) from the Late Pleistocene fossil tooth specimens from Nam Lot and Tam Pà Ling caves (Laos). Abbreviation: SEVA = Stable isotope-Evolutionary Anthropology (the numbering system used in the Human Evolution department of the Max Planck Institute for Evolution Anthropology, Leipzig, for every sample analyzed for isotope analysis).

SEVA	Site	Taxon	Diet	Body mass (kg)	$\delta^{13}\text{C}_{\text{apatite}}$ (‰)	$\delta^{18}\text{O}_{\text{apatite}}$ (‰)	$\delta^{13}\text{C}$ Enrichment factor	$\delta^{13}\text{C}_{\text{diet}}$ (‰)
35941 ^(a)	Nam Lot II	<i>Crocota crocuta</i>	Bone-Eating Carnivore	70	-14.3	-6.6	9.0	-23.3
35942 ^(a)	Nam Lot II	<i>Crocota crocuta</i>	Bone-Eating Carnivore	70	-12.5	-6.8	9.0	-21.5
35943 ^(a)	Nam Lot II	<i>Crocota crocuta</i>	Bone-Eating Carnivore	70	-15.1	-6.2	9.0	-24.1
35944 ^(a)	Nam Lot II	<i>Crocota crocuta</i>	Bone-Eating Carnivore	70	-11.8	-7.2	9.0	-20.8
35945 ^(a)	Nam Lot II	Small-sized Felidae	Carnivore	18	-15.0	-6.6	9.0	-24.0
35416 ^(a)	Tam Pà Ling	<i>Capricornis</i> sp.	Herbivore	112	-12.9	-5.8	13.1	-26.0
35417 ^(a)	Tam Pà Ling	<i>Capricornis</i> sp.	Herbivore	112	-13.6	-6.2	13.1	-26.7
35418 ^(a)	Tam Pà Ling	<i>Naemorhedus</i> sp.	Herbivore	27	-5	-3.1	12.2	-17.2
35419 ^(a)	Tam Pà Ling	<i>Naemorhedus</i> sp.	Herbivore	27	-16.3	-2.1	12.2	-28.5
35420 ^(a)	Tam Pà Ling	<i>Naemorhedus</i> sp.	Herbivore	27	-2.3	-3.3	12.2	-14.5
35421 ^(a)	Tam Pà Ling	<i>Naemorhedus</i> sp.	Herbivore	27	-14.7	-5.8	12.2	-26.9
35422 ^(a)	Tam Pà Ling	Bovidae indet.	Herbivore	875	-15	-2.7	14.6	-29.6
35423 ^(a)	Tam Pà Ling	Caprinae	Herbivore	70	-5.5	-0.6	12.8	-18.3
35424 ^(a)	Tam Pà Ling	<i>Muntiacus</i> sp.	Herbivore	24	-9.6	-5.3	12.2	-21.8
35425 ^(a)	Tam Pà Ling	<i>Macaca</i> sp.	Omnivore	6	-14.3	-5	11.9	-26.2
35426 ^(a)	Tam Pà Ling	<i>Naemorhedus</i> sp.	Herbivore	27	-14.6	-3.3	12.2	-26.8
35427 ^(a)	Tam Pà Ling	<i>Rhinoceros</i> cf. <i>unicornis</i>	Herbivore	2250	-15.8	-9.1	14.4	-30.2
35428 ^(a)	Tam Pà Ling	<i>Dicerorhinus sumatrensis</i>	Herbivore	950	-15.8	-8.9	14.0	-29.8
35429 ^(a)	Tam Pà Ling	Caprinae	Herbivore	70	-14.0	-8.0	12.8	-26.9
35492 ^(a)	Tam Pà Ling	<i>Homo sapiens</i>	Herbivore	62	-13.7	-6.4	12.7	-26.4

35946 ^(a)	Tam Pà Ling	<i>Capricornis</i> sp.	Herbivore	112	-14.0	-6.5	13.1	-27.1
35947 ^(a)	Tam Pà Ling	Caprinae	Herbivore	70	-14.7	-6.3	12.8	-27.5
35948 ^(a)	Tam Pà Ling	Hystriidae	Omnivore	12	-11.0	-6.4	12.2	-23.2
35949 ^(a)	Tam Pà Ling	Hystriidae	Omnivore	12	-10.1	-9.4	12.2	-22.3
35950 ^(a)	Tam Pà Ling	Hystriidae	Omnivore	12	-12.4	-5.5	12.2	-24.6
35951 ^(a)	Tam Pà Ling	<i>Rusa unicorn</i>	Herbivore	220	-13.9	-6.4	13.6	-27.5
35952 ^(a)	Tam Pà Ling	Caprinae	Herbivore	70	-13.9	-4.2	12.8	-26.7
35954 ^(a)	Tam Pà Ling	<i>Muntiacus</i> sp.	Herbivore	24	-11.4	-6.6	12.2	-23.6
35955 ^(a)	Tam Pà Ling	Caprinae	Herbivore	70	-1.2	-6.5	12.8	-14.1
35956 ^(a)	Tam Pà Ling	<i>Panthera</i> sp.	Carnivore	212	-14.7	-6.2	9.0	-23.7
35957 ^(a)	Tam Pà Ling	<i>Panthera</i> sp.	Carnivore	212	-14.3	-6.5	9.0	-23.3
35958 ^(a)	Tam Pà Ling	<i>Rhinoceros sondaicus</i>	Herbivore	1750	-15.7	-3.6	14.3	-30.0
34438	Nam Lot	<i>Capricornis</i> sp.	Herbivore	112	-14.6	-4.1	13.1	-27.7
34439	Nam Lot	<i>Capricornis</i> sp.	Herbivore	112	-13.0	-3.3	13.1	-26.1
34441	Nam Lot	<i>Rusa unicorn</i>	Herbivore	220	-7.5	-5.8	13.6	-21.1
34442	Nam Lot	<i>Rusa unicorn</i>	Herbivore	220	-14.1	-6.7	13.6	-27.7
34443	Nam Lot	<i>Rusa unicorn</i>	Herbivore	220	-0.9	-5.5	13.6	-14.5
34444	Nam Lot	<i>Rusa unicorn</i>	Herbivore	220	-2.7	-6.1	13.6	-16.3
34445	Nam Lot	<i>Muntiacus</i> sp.	Herbivore	24	-13.4	-6.4	12.2	-25.6
34446	Nam Lot	<i>Muntiacus</i> sp.	Herbivore	24	-13.8	-7.3	12.2	-26.0
34447	Nam Lot	<i>Muntiacus</i> sp.	Herbivore	24	-13.9	-3.3	12.2	-26.1
34448	Nam Lot	Bovidae indet.	Herbivore	875	-9.8	-5.9	14.6	-24.4
34449	Nam Lot	Bovidae indet.	Herbivore	875	0.3	-4.9	14.6	-14.3
34450	Nam Lot	Bovidae indet.	Herbivore	875	-13.5	-4.7	14.6	-28.1

34451	Nam Lot	Rhinocerotidae indet.	Herbivore	1650	-13.3	-5.9	14.3	-27.6
34452	Nam Lot	Rhinocerotidae indet.	Herbivore	1650	-13.1	-2.5	14.3	-27.4
34453	Nam Lot	Rhinocerotidae indet.	Herbivore	1650	-12.7	-6.7	14.3	-27.0
34454	Nam Lot	Rhinocerotidae indet.	Herbivore	1650	-15.1	-6.6	14.3	-29.4
34455	Nam Lot	Bovidae indet.	Herbivore	875	-4.7	-6.5	14.6	-19.3
34456	Nam Lot	Bovidae indet.	Herbivore	875	-9.5	-4.4	14.6	-24.1
34457	Nam Lot	<i>Ailuropoda melanoleuca</i>	Herbivore	92	-14.5	-6.2	9.7	-24.2
34458	Nam Lot	<i>Ailuropoda melanoleuca</i>	Herbivore	92	-14.9	-4.2	9.7	-24.6
34459	Nam Lot	<i>Sus</i> sp.	Omnivore	137	-13.7	-5.7	13.2	-26.9
34460	Nam Lot	<i>Sus</i> sp.	Omnivore	137	-12.4	-6	13.2	-25.6
34461	Nam Lot	<i>Sus</i> sp.	Omnivore	137	-12.8	-5.3	13.2	-26.0
34462	Nam Lot	<i>Sus</i> sp.	Omnivore	137	-14.1	-6.8	13.2	-27.3
34463	Nam Lot	<i>Sus</i> sp.	Omnivore	137	-13.1	-6	13.2	-26.3
34465	Nam Lot	<i>Tapirus</i> sp.	Herbivore	300	-17.5	-6.4	13.5	-31.0
34466	Nam Lot	<i>Tapirus</i> sp.	Herbivore	300	-14.9	-6.8	13.5	-28.4
34467	Nam Lot	<i>Tapirus</i> sp.	Herbivore	300	-15.3	-5	13.5	-28.8
34468	Nam Lot	Canidae	Carnivore	15	-13.3	-6.4	9.0	-22.3
34469	Nam Lot	Canidae	Carnivore	15	-13.0	-3	9.0	-22.0
34470	Nam Lot	<i>Ursus thibetanus</i>	Omnivore	100	-15.3	-9	9.0	-24.3
34471	Nam Lot	<i>Ursus thibetanus</i>	Omnivore	100	-14.1	-8.3	9.0	-23.1
34472	Nam Lot	<i>Ursus thibetanus</i>	Omnivore	100	-12.6	-6.5	9.0	-21.6

34474	Nam Lot	<i>Crocota crocuta</i>	Bone-Eating Carnivore	70	-13.7	-6.4	9.0	-22.7
34475	Nam Lot	<i>Crocota crocuta</i>	Bone-Eating Carnivore	70	-13.6	-6.1	9.0	-22.6
34476	Nam Lot	<i>Pongo</i> sp.	Omnivore	55	-14.5	-3.3	12.8	-27.3
34478	Nam Lot	<i>Macaca</i> sp.	Omnivore	6	-14.1	-4.8	11.9	-26.0
34479	Nam Lot	<i>Macaca</i> sp.	Omnivore	6	-11.5	-3.7	11.9	-23.4
34480	Nam Lot	<i>Macaca</i> sp.	Omnivore	6	-14.8	-6.1	11.9	-26.7
34481	Nam Lot	<i>Macaca</i> sp.	Omnivore	6	-14.6	-3.6	11.9	-26.5
34482	Nam Lot	<i>Elephas</i> sp.	Herbivore	4250	-16.1	-6.2	14.7	-30.8
34483	Nam Lot	<i>Stegodon orientalis</i>	Herbivore	4000	-18.2	-4.3	14.7	-32.9
34484	Nam Lot	<i>Stegodon orientalis</i>	Herbivore	4000	-15.4	-6.5	14.7	-30.1
34485	Nam Lot	Hystriidae	Omnivore	12	-13.6	-6.5	12.2	-25.8
34486	Nam Lot	Hystriidae	Omnivore	12	-12.1	-5.7	12.2	-24.3
34487	Nam Lot	Hystriidae	Omnivore	12	-14.1	-5.2	12.2	-26.3
34488	Nam Lot	Hystriidae	Omnivore	12	-13.3	-5.7	12.2	-25.5
34489	Tam Hay Marklot	<i>Capricornis</i> sp.	Herbivore	112	-13.4	-2.2	13.1	-26.5
34490	Tam Hay Marklot	<i>Capricornis</i> sp.	Herbivore	112	-14.7	-5.2	13.1	-27.8
34491	Tam Hay Marklot	<i>Capricornis</i> sp.	Herbivore	122	-15.2	-5.2	13.1	-28.3
34492	Tam Hay Marklot	<i>Capricornis</i> sp.	Herbivore	112	-13.5	-7	13.1	-26.6
34493	Tam Hay Marklot	<i>Capricornis</i> sp.	Herbivore	112	-14.6	-7.6	13.1	-27.7
34494	Tam Hay Marklot	<i>Naemorhedus</i> sp.	Herbivore	27	-2.4	0.2	12.2	-14.6
34495	Tam Hay Marklot	<i>Naemorhedus</i> sp.	Herbivore	27	-3.9	-2.5	12.2	-16.1
34496	Tam Hay Marklot	<i>Naemorhedus</i> sp.	Herbivore	27	-3.7	-1.8	12.2	-15.9
34497	Tam Hay Marklot	<i>Naemorhedus</i> sp.	Herbivore	27	-2.5	-1.6	12.2	-14.7
34498	Tam Hay Marklot	<i>Helarctos malayanus</i>	Omnivore	50	-14.7	-3.9	9.0	-23.7
34499	Tam Hay Marklot	<i>Helarctos malayanus</i>	Omnivore	50	-14.9	-5.5	9.0	-23.9

34500	Tam Hay Marklot	<i>Ursus thibetanus</i>	Omnivore	100	-15.4	-7.4	9.0	-24.4
34501	Tam Hay Marklot	<i>Ursus thibetanus</i>	Omnivore	100	-13.3	-6.6	9.0	-22.3
34502	Tam Hay Marklot	<i>Ursus thibetanus</i>	Omnivore	100	-14.4	-6.3	9.0	-23.4
34503	Tam Hay Marklot	<i>Panthera pardus</i>	Carnivore	41	-7.9	-7.3	9.0	-16.9
34504	Tam Hay Marklot	<i>Panthera pardus</i>	Carnivore	41	-4.0	-7.3	9.0	-13.0
34505	Tam Hay Marklot	<i>Panthera pardus</i>	Carnivore	41	-13.8	-6.8	9.0	-22.8
34506	Tam Hay Marklot	<i>Rusa unicorn</i>	Herbivore	220	-7.5	-5.7	13.6	-21.1
34507	Tam Hay Marklot	<i>Rusa unicorn</i>	Herbivore	220	-5.3	-4.4	13.6	-18.9
34508	Tam Hay Marklot	<i>Rusa unicorn</i>	Herbivore	220	-6.0	-4.9	13.6	-19.6
34509	Tam Hay Marklot	<i>Rusa unicorn</i>	Herbivore	220	-3.4	-4.9	13.6	-17.0
34510	Tam Hay Marklot	<i>Rusa unicorn</i>	Herbivore	220	-7.9	-6.1	13.6	-21.5
34511	Tam Hay Marklot	<i>Rucervus eldii</i>	Herbivore	123	2.4	-5.3	13.2	-10.8
34512	Tam Hay Marklot	<i>Rucervus eldii</i>	Herbivore	123	1.8	-3.1	13.2	-11.4
34513	Tam Hay Marklot	<i>Axis cf. porcinus</i>	Herbivore	43	-0.8	-5.8	12.5	-13.3
34514	Tam Hay Marklot	<i>Axis cf. porcinus</i>	Herbivore	43	-0.6	-5.3	12.5	-13.1
34515	Tam Hay Marklot	<i>Muntiacus sp.</i>	Herbivore	24	-13.8	-7.4	12.2	-26.0
34516	Tam Hay Marklot	<i>Muntiacus sp.</i>	Herbivore	24	-14.8	-8.1	12.2	-27.0
34517	Tam Hay Marklot	<i>Muntiacus sp.</i>	Herbivore	24	-12.7	-8.1	12.2	-24.9
34518	Tam Hay Marklot	<i>Muntiacus sp.</i>	Herbivore	24	-14.4	-5	12.2	-26.6
34519	Tam Hay Marklot	<i>Muntiacus sp.</i>	Herbivore	24	-14.5	-7.5	12.2	-26.7
34520	Tam Hay Marklot	<i>Bubalus bubalis</i>	Herbivore	1000	-10.3	-6	14.7	-25.0
34521	Tam Hay Marklot	<i>Bubalus bubalis</i>	Herbivore	1000	-4.0	-6.6	14.7	-18.7
34522	Tam Hay Marklot	<i>Bubalus bubalis</i>	Herbivore	1000	1.0	-4.7	14.7	-13.7
34523	Tam Hay Marklot	<i>Bubalus bubalis</i>	Herbivore	1000	-10.9	-6.3	14.7	-25.6
34524	Tam Hay Marklot	<i>Bubalus bubalis</i>	Herbivore	1000	0.1	-5.9	14.7	-14.6
34525	Tam Hay Marklot	<i>Bos sp.</i>	Herbivore	800	-2.5	-4.2	14.5	-17.0

34526	Tam Hay Marklot	<i>Bos</i> sp.	Herbivore	800	-14.4	-6.1	14.5	-28.9
34527	Tam Hay Marklot	<i>Bos</i> sp.	Herbivore	800	-0.3	-4.6	14.5	-14.8
34528	Tam Hay Marklot	<i>Bos</i> sp.	Herbivore	800	-10.0	-7.6	14.5	-24.5
34529	Tam Hay Marklot	<i>Bos</i> sp.	Herbivore	800	-13.1	-5.9	14.5	-27.6
34530	Tam Hay Marklot	<i>Panthera tigris</i>	Carnivore	212	-4.3	-3.2	9.0	-13.3
34531	Tam Hay Marklot	<i>Panthera tigris</i>	Carnivore	212	-6.9	-3.5	9.0	-15.9
34532	Tam Hay Marklot	<i>Panthera tigris</i>	Carnivore	212	-10.0	-6.8	9.0	-19.0
34533	Tam Hay Marklot	<i>Sus</i> sp.	Omnivore	137	-7.6	-7.5	13.2	-20.8
34534	Tam Hay Marklot	<i>Sus</i> sp.	Omnivore	137	-8.6	-10	13.2	-21.8
34535	Tam Hay Marklot	<i>Sus</i> sp.	Omnivore	137	-6.0	-5.9	13.2	-19.2
34536	Tam Hay Marklot	<i>Sus</i> sp.	Omnivore	137	-13.5	-5.8	13.2	-26.7
34537	Tam Hay Marklot	<i>Sus</i> sp.	Omnivore	137	-14.0	-7.6	13.2	-27.2
34538	Tam Hay Marklot	<i>Sus</i> sp.	Omnivore	137	-13.2	-5.4	13.2	-26.4
34539	Tam Hay Marklot	Canidae	Carnivore	15	-16.0	-7.3	9.0	-25.0
34540	Tam Hay Marklot	Canidae	Carnivore	15	-11.4	-3.2	9.0	-20.4
34541	Tam Hay Marklot	<i>Pongo</i> sp.	Omnivore	55	-14.8	-4.1	12.8	-27.6
34542	Tam Hay Marklot	<i>Pongo</i> sp.	Omnivore	55	-13.5	-4.6	12.8	-26.3
34543	Tam Hay Marklot	Canidae	Carnivore	15	-13.2	-6	9.0	-22.2
34544	Tam Hay Marklot	<i>Ailuropoda melanoleuca</i>	Herbivore	92	-16.7	-6.3	9.7	-26.4
34545	Tam Hay Marklot	Tapiridae indet.	Herbivore	300	-15.5	-5.9	13.5	-29.0
34546	Tam Hay Marklot	<i>Tapirus</i> sp.	Herbivore	300	-11.3	-7.9	13.5	-24.8
34547	Tam Hay Marklot	<i>Macaca</i> sp.	Omnivore	6	-13.9	-5.3	11.9	-25.8
34548	Tam Hay Marklot	<i>Macaca</i> sp.	Omnivore	6	-14.2	-5.3	11.9	-26.1
34549	Tam Hay Marklot	<i>Macaca</i> sp.	Omnivore	6	-15.1	-5.6	11.9	-27.0
34550	Tam Hay Marklot	<i>Macaca</i> sp.	Omnivore	6	-13.3	-4.7	11.9	-25.2

34551	Tam Hay Marklot	<i>Macaca</i> sp.	Omnivore	6	-12.9	-4.6	11.9	-24.8
34552	Tam Hay Marklot	Hystriidae	Omnivore	12	-11.5	-7.6	12.2	-23.7
34553	Tam Hay Marklot	Hystriidae	Omnivore	12	-11.5	-5.5	12.2	-23.7
34554	Tam Hay Marklot	Hystriidae	Omnivore	12	-7.9	-5.2	12.2	-20.1
34555	Tam Hay Marklot	Hystriidae	Omnivore	12	-11.6	-8.5	12.2	-23.8
34556	Tam Hay Marklot	<i>Rhinoceros sondaicus</i>	Herbivore	1750	-16.2	-6.5	14.3	-30.5
34557	Tam Hay Marklot	<i>Rhinoceros sondaicus</i>	Herbivore	1750	-13.3	-5.5	14.3	-27.6
34558	Tam Hay Marklot	<i>Rhinoceros sondaicus</i>	Herbivore	1750	-15.6	-6.3	14.3	-29.9
34559	Tam Hay Marklot	<i>Rhinoceros sondaicus</i>	Herbivore	1750	-15.3	-7.1	14.3	-29.6
34560	Tam Hay Marklot	<i>Rhinoceros sondaicus</i>	Herbivore	1750	-14.6	-7.5	14.3	-28.9

Table S23. Enamel $\delta^{13}\text{C}_{\text{apatite}}$ and $\delta^{18}\text{O}_{\text{apatite}}$ stable isotope results, as well as body mass (kg), $\delta^{13}\text{C}$ (‰) enrichment factor and $\delta^{13}\text{C}_{\text{diet}}$ (‰) from the Late Pleistocene fossil tooth specimens from Tam Pà Ling, Nam Lot and Tam Hay Marklot caves (Laos). Average body mass for each species was estimated from modern day analogous species (Nowak, 1999; Macdonald, 2009; Johnsingh and Manjrekar, 2013, 2015). Most of Nam Lot $\delta^{13}\text{C}_{\text{apatite}}$ and $\delta^{18}\text{O}_{\text{apatite}}$ values used in this study had already been measured and published (Bacon et al., 2018a), as were the $\delta^{13}\text{C}_{\text{apatite}}$ and $\delta^{18}\text{O}_{\text{apatite}}$ values from Tam Hay Marklot (Bourgon et al., 2020). The M² from TPL-1 individual was not measured for $\delta^{13}\text{C}_{\text{apatite}}$ and $\delta^{18}\text{O}_{\text{apatite}}$ analysis due to lack of material. Abbreviation: SEVA = Stable isotope-Evolutionary Anthropology (the numbering system used in the Human Evolution department of the Max Planck Institute for Evolution Anthropology, Leipzig, for every sample analyzed for isotope analysis).

^a SEVA numbers indicating new original data from this study vs. data already published.

Variable	Estimate	SE	Lower CI	Upper CI	X ²	DF	p-value ^(a)	Min	Max
Intercept	0.023	0.068	-0.112	0.157				-0.031	0.056
Diet ^(b)					35.836	3	0.000		
diet ^{Herbivore}	0.572	0.079	0.417	0.720				0.519	0.625
diet ^{Omnivore}	0.449	0.082	0.293	0.616				0.402	0.518
diet ^{Bone-Eating Carnivore}	0.414	0.133	0.147	0.667				0.387	0.483
Site ^(c)					5.418	2	0.335		
Site ^{Nam Lot}	0.011	0.031	-0.048	0.073				-0.006	0.041
Site ^{Tam Pà Ling}	0.088	0.040	0.006	0.166				0.066	0.118
⁸⁷ Sr/ ⁸⁶ Sr ^(d)	-0.068	0.015	-0.096	-0.038	19.392	1	0.000	-0.090	-0.060
$\delta^{13}\text{C}_{\text{apatite}}$ ^(e)	0.022	0.016	-0.010	0.054	1.957	1	0.486	-0.002	0.037
$\delta^{18}\text{O}_{\text{apatite}}$ ^(f)	0.007	0.015	-0.022	0.038	0.322	1	0.570	-0.007	0.013
Zinc conc ^(g)	-0.014	0.015	-0.043	0.015	1.239	1	0.532	-0.023	-0.010
Body mass ^(h)	0.041	0.027	0.013	0.092	2.959	1	0.346	0.028	0.076

Table S24. Results of the linear mixed model modeling $\delta^{66}\text{Zn}$ values as a function of several predictors (diet: carnivore, bone-eating carnivore, omnivore and herbivore; $^{87}\text{Sr}/^{86}\text{Sr}$, $\delta^{13}\text{C}_{\text{apatite}}$, $\delta^{18}\text{O}_{\text{apatite}}$, locality, zinc concentration and body mass). The table shows the estimates and standard errors (SE), lower and upper confidence limits of the model (CI), results of likelihood ratio tests, and the range of estimates obtained for the model when dropping levels of random effects one at a time (Min, Max). A total of 145 specimens was used from all three Late Pleistocene Southeast Asian cave sites (Laos) of Nam Lot, Tam Pà Ling and published data from Tam Hay Marklot (Bourgon et al., 2020). Abbreviation: CI = confidence interval.

^(a)z- using the Holm-Bonferroni correction for multiple statistical tests (Holm, 1979).

^(b)Dummy coded with carnivores being the reference category.

^(c)Dummy coded with Tam Hay Marklot being the reference category.

^(d)z-transformed to a mean of 0 and a standard deviation of 1; whereas the original mean and sd were 0.71586 and 0.0041 $^{87}\text{Sr}/^{86}\text{Sr}$, respectively.

^(e)z-transformed to a mean of 0 and a standard deviation of 1; whereas the original mean and sd were -1.36 ‰ and 4.8 ‰ $\delta^{13}\text{C}_{\text{apatite}}$, respectively.

^(f)z-transformed to a mean of 0 and a standard deviation of 1; whereas the original mean and sd were -5.70 ‰ and 1.73 ‰ $\delta^{18}\text{O}_{\text{apatite}}$, respectively.

^(s)z-transformed to a mean of 0 and a standard deviation of 1; whereas the original mean and sd were 94.24 µg/g and 107.70 µg/g, respectively (before log-transformed).

^(b)z-transformed to a mean of 0 and a standard deviation of 1; whereas the original mean and sd were 372.60 kg and 701.89 kg, respectively (before natural log-transformed).

Reference material	Element	Substance	Measured value	SD	n	Expected value	SD	n
Marble-LM ^(a) (theoretical value normalized to NBS-19)	C & O	Carbonate (in-house)	+2.18 ‰ (δ ¹³ C) -2.03 ‰ (δ ¹⁸ O)	0.03 0.09	20	+2.13 ‰ (δ ¹³ C) -1.83 ‰ (δ ¹⁸ O)		
NIST SRM 1486	Sr	Bone meal	0.709298 (⁸⁷ Sr/ ⁸⁶ Sr)	0.000025	10	0.709299	0.000027	
AZE ^(b)	Zn	Dentin (in-house)	+1.60 ‰ (δ ⁶⁶ Zn)	0.00	5	+1.60 ‰ (δ ⁶⁶ Zn)	0.03	22
NIST SRM 1400 ^(b)	Zn	Bone ash	+0.96 ‰ (δ ⁶⁶ Zn)	0.01	8	+0.96 ‰ (δ ⁶⁶ Zn)	0.04	75

Table S25. List of reference materials with their respective measured and expected values for different isotopes.

^(a)Expected values obtained through in-house long-term measurements at the Service de Spectrométrie de Masse Isotopique du Muséum in Paris.

^(b)Expected values obtained through in-house long-term measurements at the Max Planck Institute for Evolutionary Anthropology, in Leipzig.

Dietary category 1	Dietary category 2	Mean difference	Lower CI	Upper CI	Adjusted <i>p</i> -value
Bone-eating Carnivore	Carnivore	0.35	0.10	0.60	<0.001
Omnivore	Carnivore	0.33	0.17	0.49	<0.001
Omnivore	Bone-eating carnivore	-0.02	-0.24	0.20	0.99
Herbivore	Carnivore	0.62	0.47	0.77	<0.001
Herbivore	Bone-eating carnivore	0.28	0.06	0.49	0.01
Herbivore	Omnivore	0.30	0.20	0.39	<0.001

Table S26. Results of Tukey post-hoc pair-wise comparisons for $\delta^{66}\text{Zn}$ values between dietary categories (bone-eating carnivore, omnivore, herbivore, and carnivore). A total of 145 specimens was used from all three Late Pleistocene Southeast Asian cave sites (Laos) of Nam Lot, Tam Pà Ling and published data from Tam Hay Marklot (Bourgon et al., 2020). Abbreviation: CI = confidence interval.

SEVA	Ref. #	Taxon	Depth recovered (m)	Age (and dating method)
35421	K32	<i>Naemorhedus</i> sp.	0.97	between $1.1 \pm 0.2\text{ka}$ and $2.8 \pm 0.2\text{ka}$ (cal. C14)
35951	L32	<i>Rusa unicolor</i>	1.42	between $14 \pm 2\text{ ka}$ and $23 \pm 2\text{ka}$ (OSL)
35957	O32	<i>Panthera</i> sp.	1.55	between $14 \pm 2\text{ ka}$ and $23 \pm 2\text{ka}$ (OSL)
35420	K32	<i>Naemorhedus</i> sp.	1.75	$23 \pm 2\text{ka}$ (OSL)
35954	L32	<i>Muntiacus</i> sp.	1.85	Between $23 \pm 2\text{ ka}$ and $33 \pm 3\text{ka}$ (OSL)
35948	M32	Hystriidae	1.88	Between $23 \pm 2\text{ ka}$ and $33 \pm 3\text{ka}$ (OSL)
35955	J31	Caprinae	1.80-1.90	Between $23 \pm 2\text{ ka}$ and $33 \pm 3\text{ ka}$ (OSL)
35419	M31	<i>Naemorhedus</i> sp.	2.05	$33 \pm 3\text{ka}$ (OSL)
35417	M31	<i>Capricornis</i> sp.	2.22	between $33 \pm 3\text{ ka}$ and $43 \pm 7\text{ ka}$ (OSL and IRSL respectively)
35425	K32	<i>Macaca</i> sp.	2.23	between $33 \pm 3\text{ ka}$ and $43 \pm 7\text{ ka}$ (OSL and IRSL respectively)
35946	H33	<i>Capricornis</i> sp.	2.32	between $33 \pm 3\text{ ka}$ and $43 \pm 7\text{ ka}$ (OSL and IRSL respectively)
35427	M31	<i>Rhinoceros</i> cf. <i>unicornis</i>	2.44	between $33 \pm 3\text{ ka}$ and $43 \pm 7\text{ ka}$ (OSL and IRSL respectively)

35416	M33	<i>Capricornis</i> sp.	2.50	between 43 ± 7 ka and 46 ± 6 ka (IRSL)
35428	M31	<i>Dicerorhinus sumatrensis</i>	2.51	between 43 ± 7 ka and 46 ± 6 ka (IRSL)
35952	K33	Caprinae	2.59	between 43 ± 7 ka and 46 ± 6 ka (IRSL)
35947	M32	<i>Capricornis</i> sp.	2.78	between 43 ± 7 ka and 46 ± 6 ka (IRSL)
35949	M29-30	Hystricidae	2.85	between 43 ± 7 ka and 46 ± 6 ka (IRSL)
35418	M35	<i>Naemorhedus</i> sp.	3.00	46 ± 6 ka (IRSL)
35950	K33	Hystricidae	3.07	46 ± 6 ka (IRSL)
35423	L33	Caprinae	3.29	between 46 ± 6 ka and 56 ± 6 ka (IRSL)
35426	L36	<i>Naemorhedus</i> sp.	3.50	between 46 ± 6 ka and 56 ± 6 ka (IRSL)
35422	M35	Bovidae indet.	3.80	between 46 ± 6 ka and 56 ± 6 ka (IRSL)
35429	K33	Caprinae	4.20	56 ± 6 ka (IRSL)
35958	K35	<i>Rhinoceros sondaicus</i>	6.60	>70 ± 8 ka (IRSL)

Table S27. List of samples from Tam Pà Ling with their associated depth at which they were recovered and their associated dating according to the latest chronology of the site (Shackelford et al., 2018). Abbreviation: SEVA = Stable isotope-Evolutionary Anthropology (numbering system used in the Human Evolution department of the Max Planck Institute for Evolution Anthropology, Leipzig, for every sample analyzed for isotope analysis), C14 = Radiocarbon dating (also referred to as carbon dating or carbon-14 dating), OSL = Optically-stimulated luminescence dating, IRSL = Infrared stimulated luminescence dating.

SEVA	Site	Taxon	Tooth	Diet	$\delta^{66}\text{Zn}$	$\delta^{67}\text{Zn}$	$\delta^{68}\text{Zn}$	[Zn] (ug/g)
34818	Duoi U'Oi	<i>Sus</i> sp.	p4 left	Omnivore	0.53	1.06	1.12	54
34819	Duoi U'Oi	<i>Sus</i> sp.	p4 left	Omnivore	0.62	1.21	1.32	38
34820	Duoi U'Oi	<i>Sus</i> sp.	p4 left	Omnivore	0.95	1.67	1.95	39
34821	Duoi U'Oi	<i>Sus</i> sp.	p4 left	Omnivore	0.69	1.30	1.44	36
34822	Duoi U'Oi	<i>Sus</i> sp.	p4 left	Omnivore	0.42	1.29	1.14	27
34823	Duoi U'Oi	<i>Rusa unicorn</i>	m3 left	Herbivore	0.61	1.53	1.49	31
34824	Duoi U'Oi	<i>Rusa unicorn</i>	m3 left	Herbivore	0.80	1.41	1.65	66
34825	Duoi U'Oi	<i>Rusa unicorn</i>	m3 left	Herbivore	0.82	1.42	1.67	141
34826	Duoi U'Oi	<i>Rusa unicorn</i>	m3 left	Herbivore	0.89	1.46	1.81	128
34827	Duoi U'Oi	<i>Rusa unicorn</i>	m3 left	Herbivore	0.68	1.39	1.53	37
34828	Duoi U'Oi	<i>Rusa unicorn</i>	m3 left	Herbivore	0.72	1.70	1.76	26
34829	Duoi U'Oi	<i>Muntiacus</i> sp.	m3 left	Herbivore	0.85	1.61	1.86	39
34830	Duoi U'Oi	<i>Muntiacus</i> sp.	m3 left	Herbivore	0.60	1.18	1.31	38
34831	Duoi U'Oi	<i>Muntiacus</i> sp.	m3 left	Herbivore	0.73	1.42	1.57	23
34832	Duoi U'Oi	<i>Muntiacus</i> sp.	m3 left	Herbivore	0.69	1.43	1.46	19
34833	Duoi U'Oi	<i>Muntiacus</i> sp.	m3 left	Herbivore	0.55	1.19	1.22	25
34834	Duoi U'Oi	Caprinae	m3 right	Herbivore	0.75	1.31	1.55	71
34835	Duoi U'Oi	Caprinae	m3 right	Herbivore	0.68	1.19	1.38	69
34836	Duoi U'Oi	Caprinae	m3 left	Herbivore	0.91	1.55	1.85	78
34837	Duoi U'Oi	Large-sized Bovidae	m	Herbivore	0.78	1.40	1.61	59
34838	Duoi U'Oi	Large-sized Bovidae	m	Herbivore	0.87	1.47	1.75	56
34839	Duoi U'Oi	Large-sized Bovidae	m	Herbivore	0.72	1.58	1.62	42
34840	Duoi U'Oi	Large-sized Bovidae	m	Herbivore	0.72	1.53	1.59	41

34841	Duoi U'Oi	Hystriidae	incisor	Omnivore	0.45	1.16	1.09	43
34842	Duoi U'Oi	Hystriidae	incisor	Omnivore	0.50	1.14	1.12	30
34843	Duoi U'Oi	Hystriidae	incisor	Omnivore	0.35	1.16	0.98	23
34844	Duoi U'Oi	Hystriidae	incisor	Omnivore	0.26	0.96	0.69	22
34845	Duoi U'Oi	Hystriidae	incisor	Omnivore	0.19	1.01	0.66	21
34846	Duoi U'Oi	Hystriidae	incisor	Omnivore	0.37	0.99	0.86	21
34847	Duoi U'Oi	Hystriidae	incisor	Omnivore	0.36	1.08	0.86	17
34848	Duoi U'Oi	Hystriidae	incisor	Omnivore	0.02	0.15	0.07	12
34849	Duoi U'Oi	Ursus sp.	I3 right	Omnivore	0.25	0.76	0.63	33
34850	Duoi U'Oi	Ursus sp.	I3 right	Omnivore	0.30	0.73	0.66	43
34851	Duoi U'Oi	Canidae	P4 left	Carnivore	0.17	0.74	0.48	22
34852	Duoi U'Oi	Canidae	P4 left	Carnivore	-0.04	0.17	-0.01	64
34853	Duoi U'Oi	Canidae	P4 left	Carnivore	0.14	0.62	0.40	26
34854	Duoi U'Oi	<i>Panthera pardus</i>	p4 left	Carnivore	-0.01	0.20	0.04	77
34855	Duoi U'Oi	<i>Panthera pardus</i>	p4 left	Carnivore	-0.10	0.19	-0.11	62
34856	Duoi U'Oi	<i>Panthera tigris</i>	m1 right	Carnivore	0.17	0.51	0.39	74
34857	Duoi U'Oi	<i>Macaca</i> sp.	incisor	Omnivore	0.26	0.61	0.57	122
34858	Duoi U'Oi	<i>Macaca</i> sp.	incisor	Omnivore	0.45	0.82	0.94	162
34859	Duoi U'Oi	<i>Macaca</i> sp.	incisor	Omnivore	0.30	0.68	0.64	96
34860	Duoi U'Oi	<i>Macaca</i> sp.	incisor	Omnivore	0.30	0.61	0.66	101
34861	Duoi U'Oi	<i>Macaca</i> sp.	incisor	Omnivore	0.39	0.82	0.80	105
34862	Duoi U'Oi	Rhinocerotidae	M2 right	Herbivore	0.74	1.46	1.61	8
34863	Duoi U'Oi	Rhinocerotidae	M3 right	Herbivore	0.56	0.80	1.15	15
34864	Duoi U'Oi	Rhinocerotidae	M3 right	Herbivore	0.81	1.61	1.71	32
34865	Duoi U'Oi	Rhinocerotidae	M3 right	Herbivore	1.15	2.01	2.37	59

34866	Duoi U'Oi	Rhinocerotidae	M3 right	Herbivore	0.82	1.43	1.72	90
34867	Duoi U'Oi	Rhinocerotidae	p2 right	Herbivore	0.47	0.94	1.04	72
34868	Duoi U'Oi	Rhinocerotidae	M3 right	Herbivore	0.56	1.20	1.23	33
34869	Duoi U'Oi	Rhinocerotidae	M2 right	Herbivore	0.61	1.19	1.33	39
34870	Duoi U'Oi	<i>Tapirus</i> sp.	M1/M2 left	Herbivore	0.41	1.23	1.07	21
34871	Duoi U'Oi	<i>Tapirus</i> sp.	P/M left	Herbivore	0.34	1.06	0.82	23
34872	Duoi U'Oi	<i>Tapirus</i> sp.	P/M left	Herbivore	0.55	0.74	1.11	10
34873	Duoi U'Oi	<i>Pongo</i> sp.	p3 right	Omnivore	0.41	0.69	0.87	275
34874	Duoi U'Oi	<i>Pongo</i> sp.	p3 right	Omnivore	0.53	0.96	1.12	245
34875	Duoi U'Oi	<i>Pongo</i> sp.	p3 right	Omnivore	0.53	0.89	1.08	306
34876	Duoi U'Oi	<i>Elephas</i> sp.	milk tooth	Herbivore	0.68	1.32	1.45	45
34878	Coc Muoi	<i>Muntiacus</i> sp.	m3 left	Herbivore	0.76	1.25	1.61	55
34879	Coc Muoi	<i>Muntiacus</i> sp.	m3 left	Herbivore	0.39	0.80	0.95	23
34880	Coc Muoi	<i>Muntiacus</i> sp.	P2/P3 left	Herbivore	0.47	0.85	1.04	59
34881	Coc Muoi	<i>Muntiacus</i> sp.	P3/P4 left	Herbivore	0.43	0.82	1.00	41
34882	Coc Muoi	<i>Muntiacus</i> sp.	P3/P4 left	Herbivore	0.66	1.12	1.38	69
34883	Coc Muoi	<i>Muntiacus</i> sp.	P2/P3 left	Herbivore	0.70	1.18	1.47	46
34884	Coc Muoi	<i>Sus</i> sp.	m3	Omnivore	0.94	1.56	1.92	116
34885	Coc Muoi	<i>Sus</i> sp.	m3 left	Omnivore	0.68	1.19	1.44	54
34886	Coc Muoi	<i>Sus</i> sp.	m3 left	Omnivore	0.73	1.31	1.55	42
34887	Coc Muoi	<i>Sus</i> sp.	m3 left	Omnivore	0.68	1.16	1.42	69
34888	Coc Muoi	<i>Sus</i> sp.	m3 left	Omnivore	0.96	1.55	1.98	65
34889	Coc Muoi	<i>Sus</i> sp.	m3 left	Omnivore	0.59	1.13	1.38	32
34890	Coc Muoi	<i>Ailuropoda melanoleuca</i>	M1 left	Herbivore	0.68	1.18	1.46	80
34891	Coc Muoi	<i>Ailuropoda melanoleuca</i>	M1 left	Herbivore	0.87	1.48	1.85	64

34893	Coc Muoi	<i>Ursus</i> sp.		M1 left	Omnivore	0.59	1.02	1.29	77
34894	Coc Muoi	<i>Ursus</i> sp.		m3 right	Omnivore	0.42	0.81	0.98	66
34896	Coc Muoi	<i>Ursus</i> sp.		M1 left	Omnivore	0.34	0.60	0.78	80
34897	Coc Muoi	<i>Ursus</i> sp.		M2 left	Omnivore	0.56	1.03	1.31	57
34898	Coc Muoi	<i>Pongo</i> sp.		I1 left	Omnivore	0.66	0.99	1.33	493
34899	Coc Muoi	<i>Pongo</i> sp.		M1 right	Omnivore	0.78	1.21	1.58	256
34900	Coc Muoi	<i>Pongo</i> sp.		M left	Omnivore	0.81	1.29	1.66	250
34901	Coc Muoi	<i>Pongo</i> sp.		m1 left	Omnivore	0.66	1.03	1.37	220
34902	Coc Muoi	<i>Macaca</i> sp.		Canine left	Omnivore	0.64	0.98	1.33	219
34903	Coc Muoi	<i>Macaca</i> sp.		canine	Omnivore	0.94	1.41	1.90	134
34904	Coc Muoi	<i>Macaca</i> sp.		m1/m2 left	Omnivore	0.53	0.81	1.07	145
34905	Coc Muoi	<i>Macaca</i> sp.		M3 left	Omnivore	0.37	0.58	0.78	150
34906	Coc Muoi	<i>Macaca</i> sp.		canine left	Omnivore	0.34	0.56	0.71	269
34907	Coc Muoi	<i>Panthera tigris</i>		P3 left	Carnivore	0.17	0.32	0.41	87
34908	Coc Muoi	<i>Panthera tigris</i>		P3 left	Carnivore	0.18	0.34	0.44	285
34909	Coc Muoi	<i>Panthera tigris</i>		m1 left	Carnivore	0.25	0.43	0.55	96
34910	Coc Muoi	Canidae		P4 right	Carnivore	0.57	0.93	1.18	70
34911	Coc Muoi	Small-sized Felidae		P4 right	Carnivore	0.49	0.87	1.05	99
34912	Coc Muoi	Small-sized Felidae		P4 right	Carnivore	0.21	0.41	0.47	116
34913	Coc Muoi	Hystricidae		incisor	Omnivore	0.57	0.92	1.19	64
34914	Coc Muoi	Hystricidae		incisor	Omnivore	0.85	1.32	1.73	60
34915	Coc Muoi	Hystricidae		incisor	Omnivore	0.69	1.07	1.43	26
34916	Coc Muoi	Hystricidae		incisor	Omnivore	0.74	1.18	1.54	29
34917	Coc Muoi	Hystricidae		incisor	Omnivore	0.57	0.94	1.21	50
34918	Coc Muoi	Hystricidae		incisor	Omnivore	0.62	0.96	1.29	42

34919	Coc Muoi	Hystricidae	incisor	Omnivore	0.85	1.29	1.73	40
34920	Coc Muoi	Hystricidae	incisor	Omnivore	0.69	1.09	1.41	80
34922	Coc Muoi	Hystricidae	incisor	Omnivore	0.75	1.17	1.54	71
34923	Coc Muoi	Hystricidae	incisor	Omnivore	0.90	1.42	1.84	93
34924	Coc Muoi	<i>Rusa unicorn</i>	m3 right	Herbivore	0.93	1.51	1.94	64
34925	Coc Muoi	<i>Rusa unicorn</i>	m3 left	Herbivore	1.10	1.71	2.23	65
34926	Coc Muoi	<i>Rusa unicorn</i>	m3 left	Herbivore	0.53	0.83	1.11	37
34927	Coc Muoi	<i>Rusa unicorn</i>	m3 left	Herbivore	0.89	1.42	1.80	35
34928	Coc Muoi	<i>Rusa unicorn</i>	m3 right	Herbivore	0.71	1.17	1.47	57
34929	Coc Muoi	<i>Rusa unicorn</i>	m3 right	Herbivore	0.67	1.10	1.39	42
34930	Coc Muoi	Caprinae	m1/m2 right	Herbivore	0.81	1.33	1.68	46
34931	Coc Muoi	Caprinae	m1/m2 left	Herbivore	0.93	1.46	1.87	64
34932	Coc Muoi	Caprinae	m1/m2 left	Herbivore	1.11	1.75	2.25	63
34933	Coc Muoi	Caprinae	m1/m2 right	Herbivore	1.00	1.57	2.04	66
34934	Coc Muoi	Caprinae	m1/m2 left	Herbivore	0.91	1.40	1.87	55
34935	Coc Muoi	Large-sized Bovidae	m3 right	Herbivore	0.95	1.54	1.93	80
34936	Coc Muoi	Large-sized Bovidae	m3 right	Herbivore	1.11	1.85	2.34	62
34937	Coc Muoi	Large-sized Bovidae	m3 right	Herbivore	1.07	1.68	2.18	65
34938	Coc Muoi	Large-sized Bovidae	m3 right	Herbivore	1.08	1.69	2.17	770
34939	Coc Muoi	Large-sized Bovidae	m3 right	Herbivore	0.99	1.52	2.01	52
34940	Coc Muoi	Large-sized Bovidae	m3 right	Herbivore	0.71	1.26	1.57	43
34941	Coc Muoi	Rhinocerotidae	p4	Herbivore	0.96	1.63	2.07	25
34942	Coc Muoi	Rhinocerotidae	p4	Herbivore	0.82	1.39	1.74	25
34943	Coc Muoi	Rhinocerotidae	p4	Herbivore	0.72	1.19	1.52	26
34944	Coc Muoi	Rhinocerotidae	p4	Herbivore	1.04	1.65	2.12	32

34945	Coc Muoi	Rhinocerotidae	p4	Herbivore	0.66	1.21	1.45	40
34946	Coc Muoi	Rhinocerotidae	p4	Herbivore	1.05	1.73	2.17	49
34947	Coc Muoi	Rhinocerotidae	p4	Herbivore	0.84	1.39	1.83	37
34948	Coc Muoi	Rhinocerotidae	p4	Herbivore	1.15	1.82	2.34	53
34949	Coc Muoi	Rhinocerotidae	M3	Herbivore	0.99	1.66	2.13	45
34950	Coc Muoi	Rhinocerotidae	M3	Herbivore	0.83	1.30	1.72	51
34951	Coc Muoi	Rhinocerotidae	m3	Herbivore	1.09	1.67	2.18	143
34952	Coc Muoi	Rhinocerotidae	m3	Herbivore	0.97	1.53	1.99	31
34953	Coc Muoi	<i>Megatapirus augustus</i>	m	Herbivore	0.55	0.89	1.16	67
34954	Coc Muoi	<i>Megatapirus augustus</i>	p3	Herbivore	0.78	1.25	1.60	76
34955	Coc Muoi	<i>Tapirus</i> sp.	p3	Herbivore	0.61	1.08	1.34	35
34956	Coc Muoi	<i>Tapirus</i> sp.	p4	Herbivore	0.69	1.11	1.40	68
34957	Coc Muoi	<i>Tapirus</i> sp.	p4	Herbivore	0.85	1.34	1.73	38
34958	Coc Muoi	<i>Stegodon</i> sp.	milk tooth	Herbivore	0.77	1.22	1.54	157
34959	Coc Muoi	<i>Stegodon</i> sp.	milk tooth	Herbivore	0.65	1.08	1.42	72
34960	Coc Muoi	<i>Elephas</i> sp.	m	Herbivore	0.84	1.31	1.67	767
34961	Coc Muoi	<i>Elephas</i> sp.	m1	Herbivore	1.22	2.04	2.53	102
35039	Duoi U'Oi	<i>Elephas</i> sp.	milk tooth	Herbivore	0.47	1.24	1.09	50

Table S28. Preliminary $\delta^{66}\text{Zn}$ results from the Late Pleistocene sites of Duoi U'Oi and Coc Muoi, Vietnam, respectively 70-60 ka and 148-117 ka. Abbreviation: SEVA = Stable isotope-Evolutionary Anthropology (the numbering system used in the Human Evolution department of the Max Planck Institute for Evolution Anthropology, Leipzig, for every sample analyzed for isotope analysis).

Supplementary information figures



Figure S1. Map of the Indochinese Peninsula with the location of the studied area in northeast Laos.

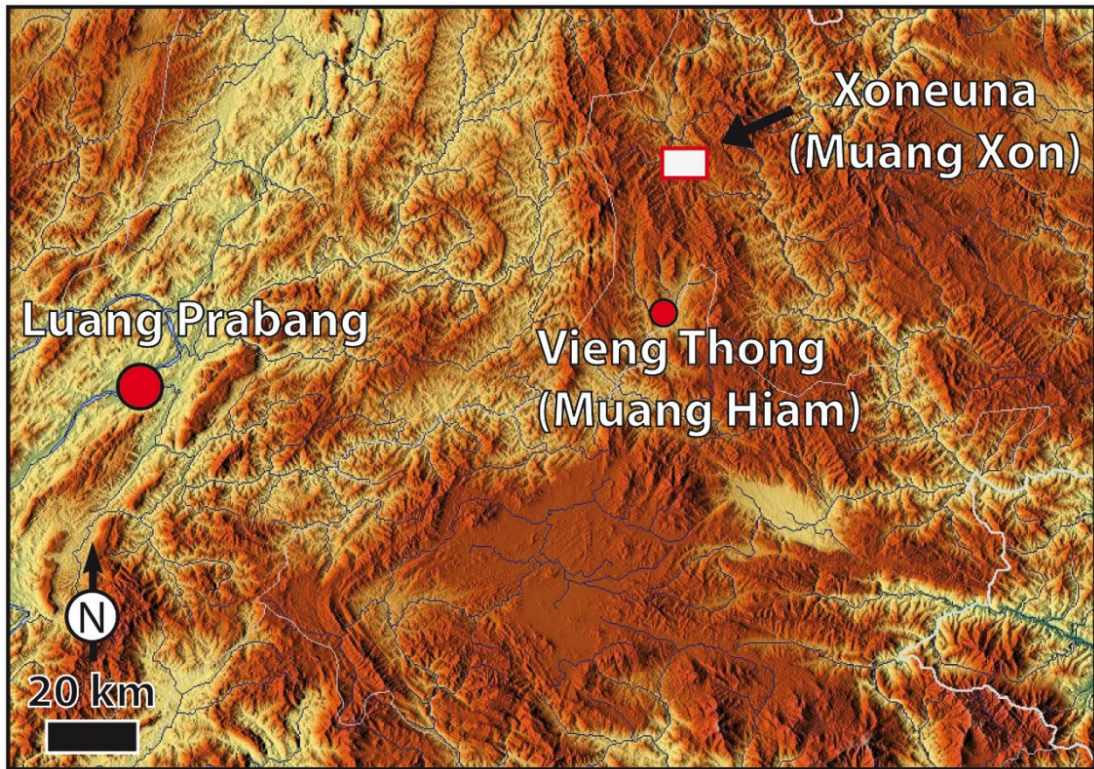


Figure S2. Map of Laos showing the studied area in the Hua Pan Province, 130 km NNE from Luang Prabang.



Figure S3. Satellite view of the studied area with the location of the cave 6 km SE from the city of Xoneuna (Muang Xon).

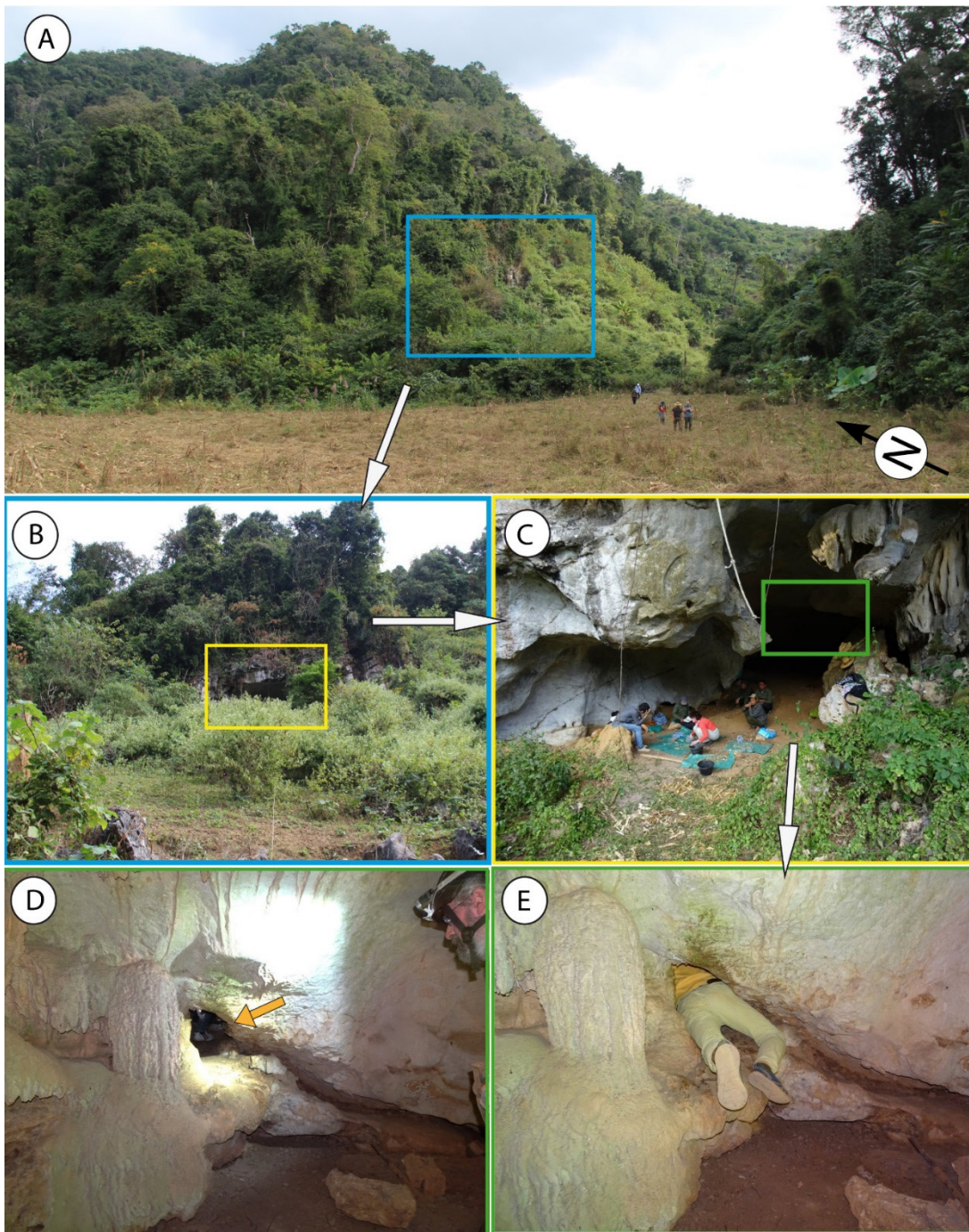


Figure S4. (A) Tam Hay Marklot cave at the foot of a tower karst covered by the forest, and (B, C) the first chamber at the entrance. (D, E) First passageway that leads to the gallery.

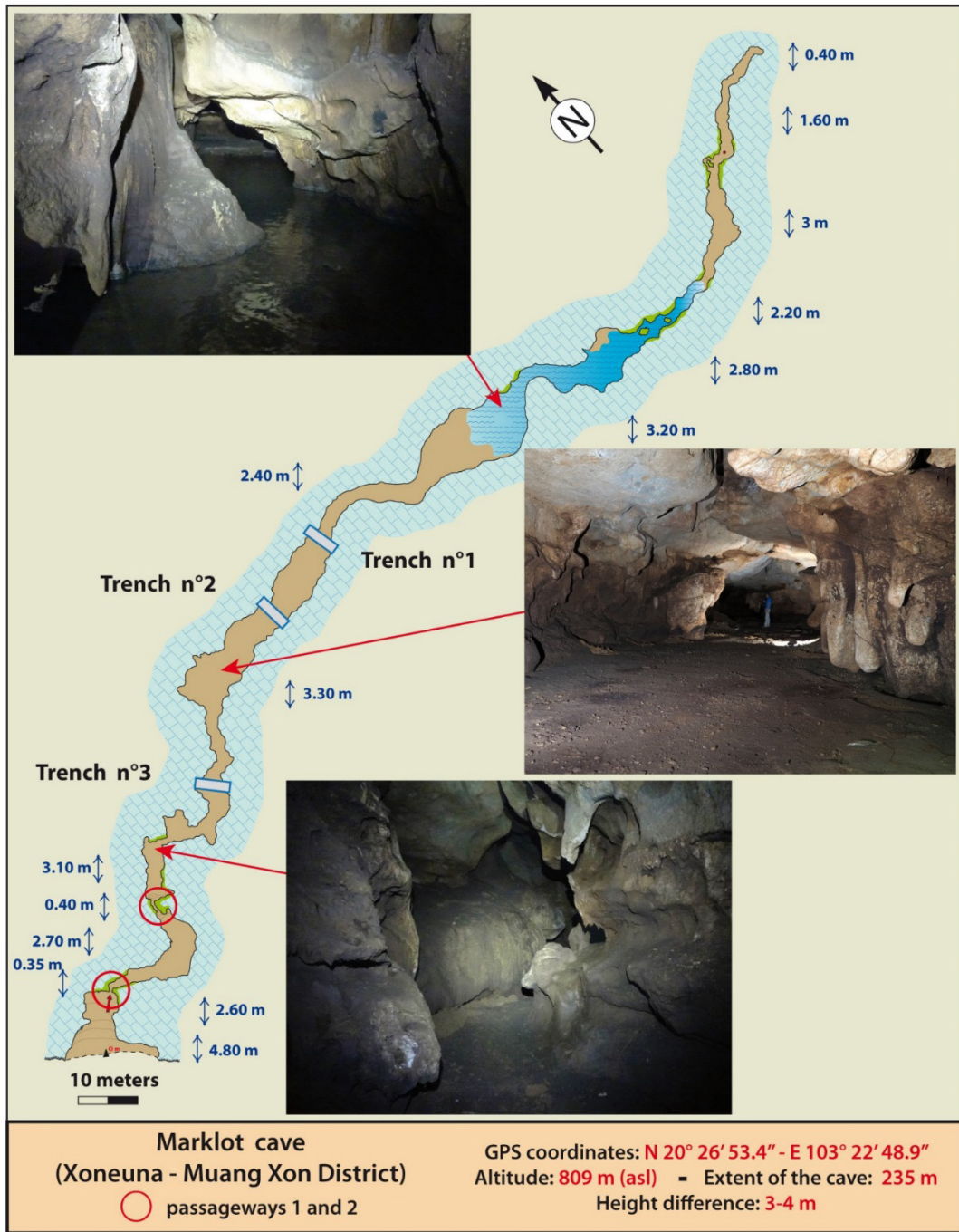


Figure S5. Map of the entire Tam Hay Marklot cave from the first chamber at the entrance to the dead-end after a 235 m extent, with three views of the gallery.

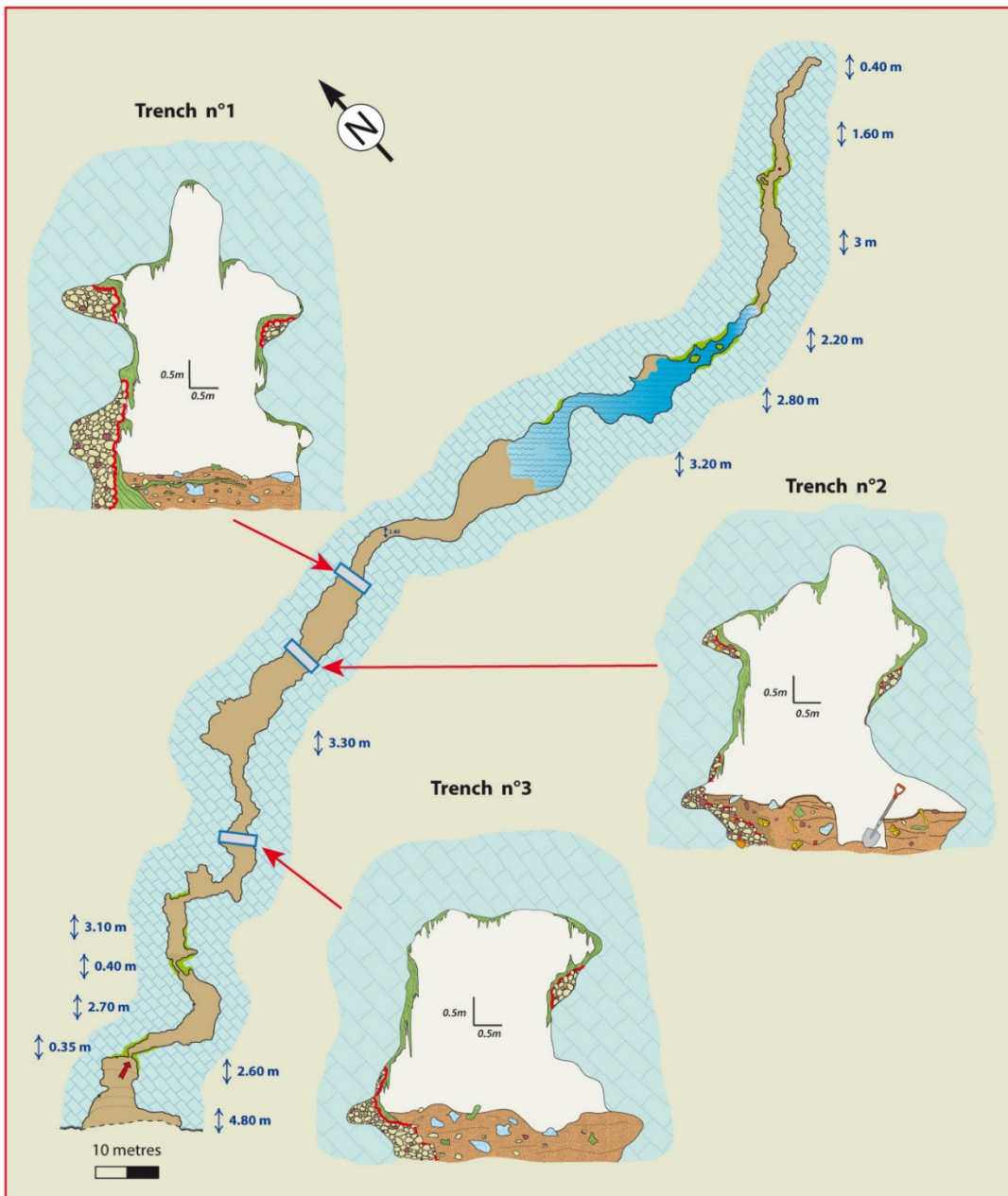


Figure S6. Map of the Tam Hay Marklot cave showing the three sections of the cave and their sedimentary fillings (see **Figure S7** for the legend of sedimentary sections).

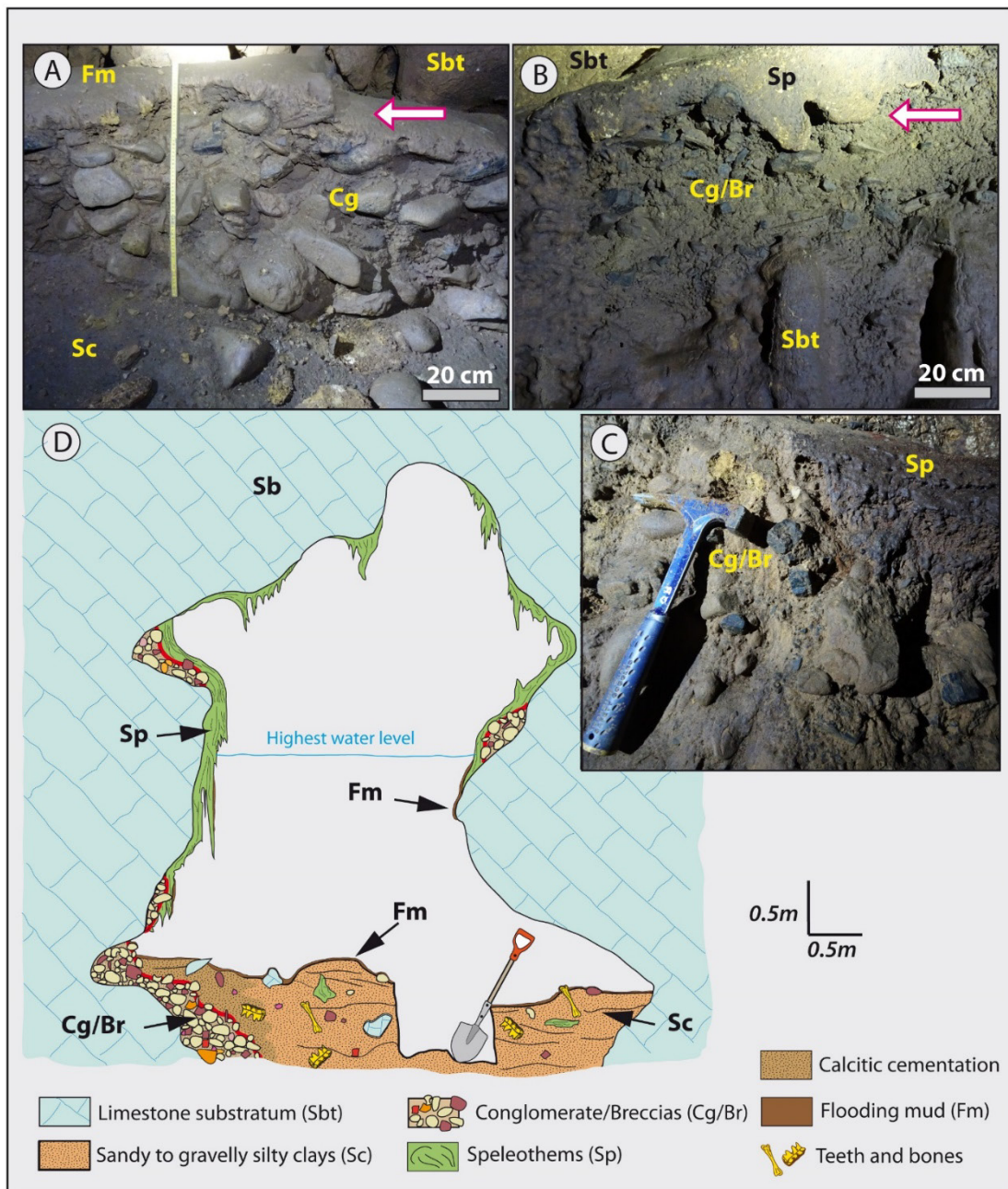


Figure S7. Detail of the section/trench 2 showing the main sedimentary facies of the cave. In A and B, the arrows give the direction of the paleocurrents from inside to outside of the cave.

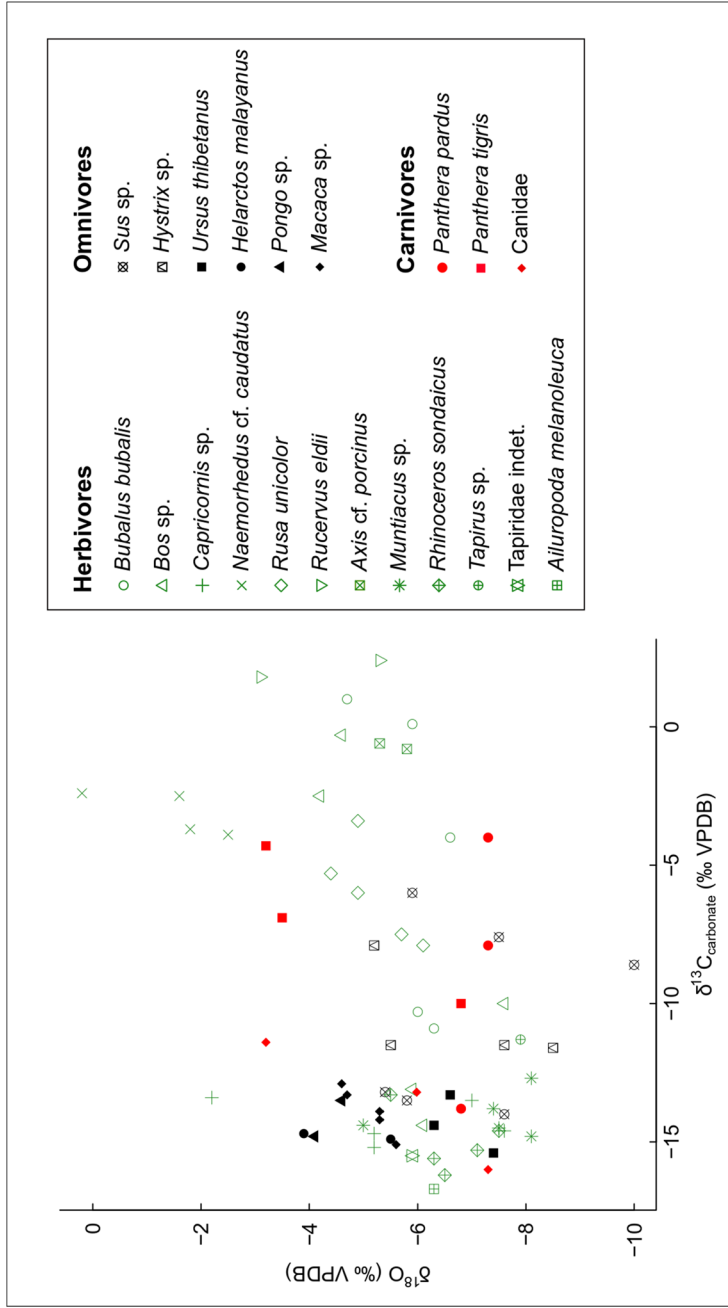


Figure S8. Distribution of carbon ($\delta^{13}\text{C}_{\text{apatitic}}$) and oxygen ($\delta^{18}\text{O}_{\text{apatitic}}$) stable isotope values in fossil tooth enamel from Tam Hay Marklot cave.

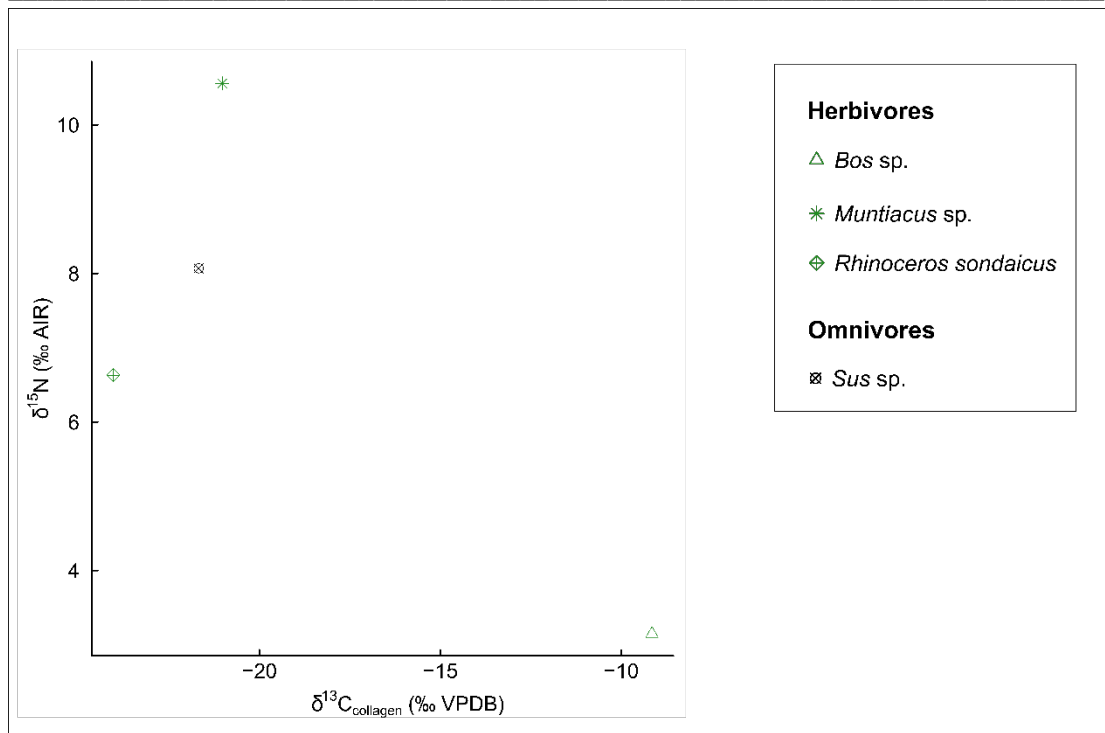


Figure S9. Distribution of carbon ($\delta^{13}\text{C}_{\text{collagen}}$) and nitrogen ($\delta^{15}\text{N}_{\text{collagen}}$) stable isotope values in root dentin of the few fossil teeth from Tam Hay Marklot cave with collagen preservation.

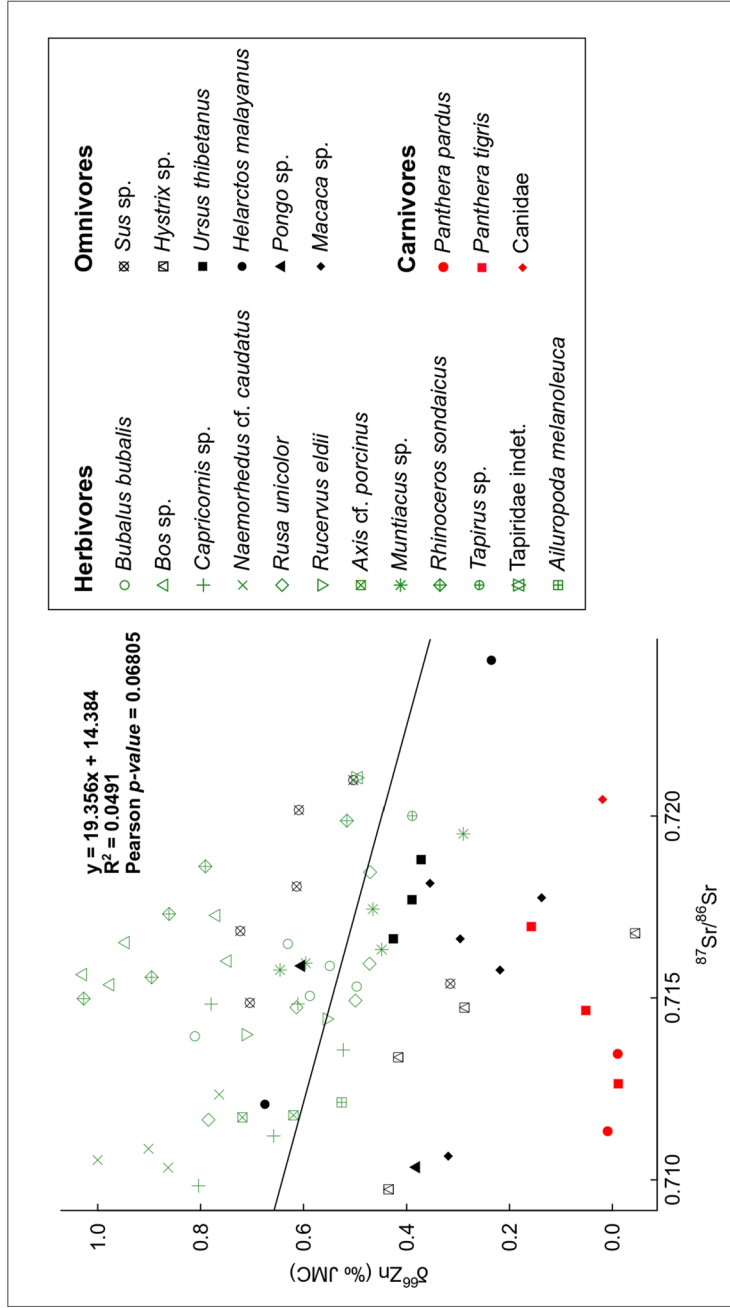


Figure S10. Relationship between radiogenic strontium isotope ratios ($^{87}\text{Sr}/^{86}\text{Sr}$) and zinc ($\delta^{66}\text{Zn}$) stable isotope values in enamel of fossil teeth from Tam Hay Marklot cave.

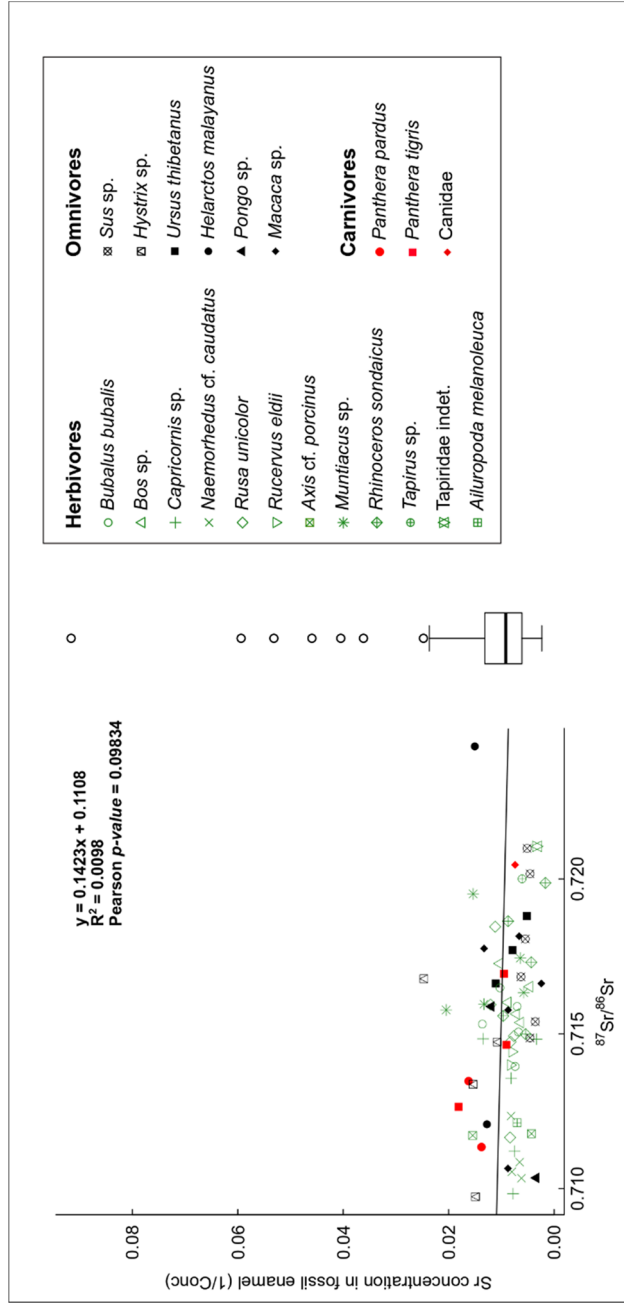


Figure S11. Relationship between the strontium concentration (1/Conc, as $\mu\text{g/g}$) and the radiogenic strontium isotope ratios ($^{87}\text{Sr}/^{86}\text{Sr}$) in enamel of fossil teeth from Tam Hay Marklot cave. The boxes from the box and whisker plot represent the 25th–75th percentiles, with the median as a bold horizontal line, of Sr concentration from modern enamel of mammal teeth found elsewhere (Copeland et al., 2008; Britton et al., 2009; Kohn et al., 2013).

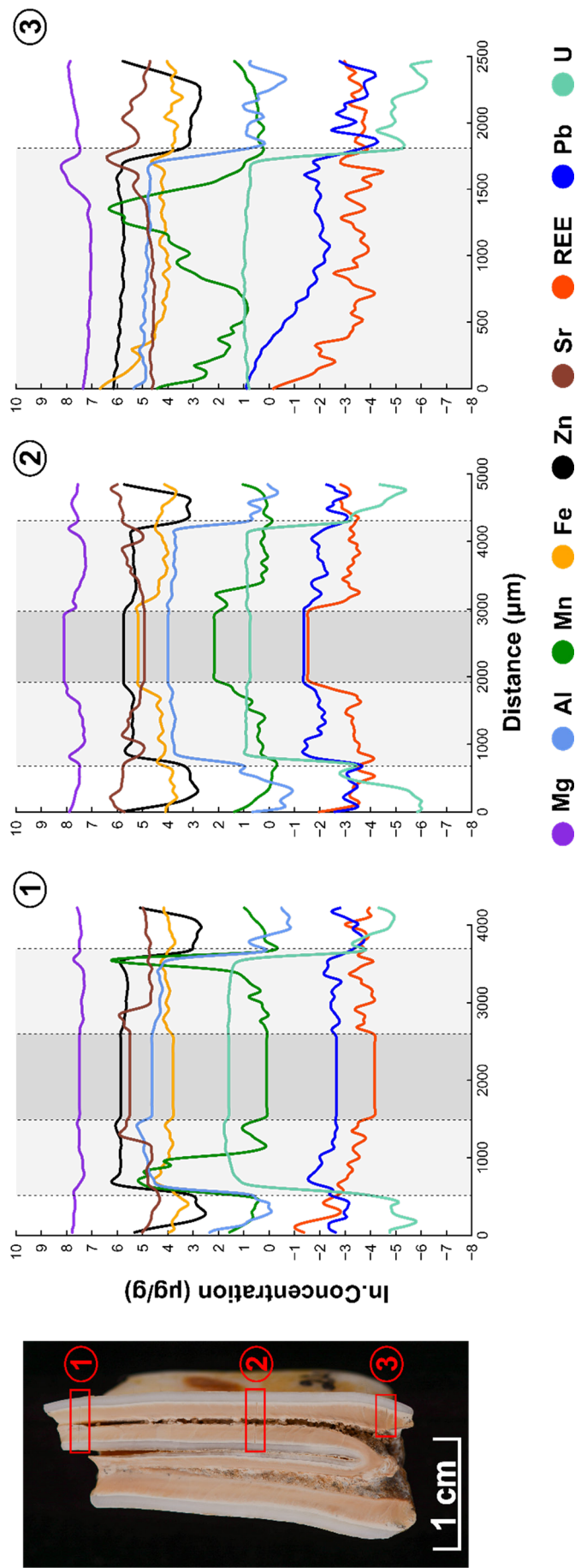


Figure S12. Spatial element concentration profiles for the element Zn, Fe, Mn, Al, Mg, Sr, Pb, U and rare earth elements (REE, calculated as the sum of all measured REE concentrations) of all LA-ICP-MS linescan analysis (1 to 3) of the Tam Hay Marklot cave fossil tooth (m3 right specimen 34493 (*Capricornis* sp.)). All concentration data ($\mu\text{g/g}$) were natural log transformed (\ln .Concentration). The different shaded areas, delimited by dotted lines, represent the different histological parts: white for enamel, light gray for dentin and medium gray for pulp cavity. The profiles follow a left-to-right direction as seen from the picture on the left.

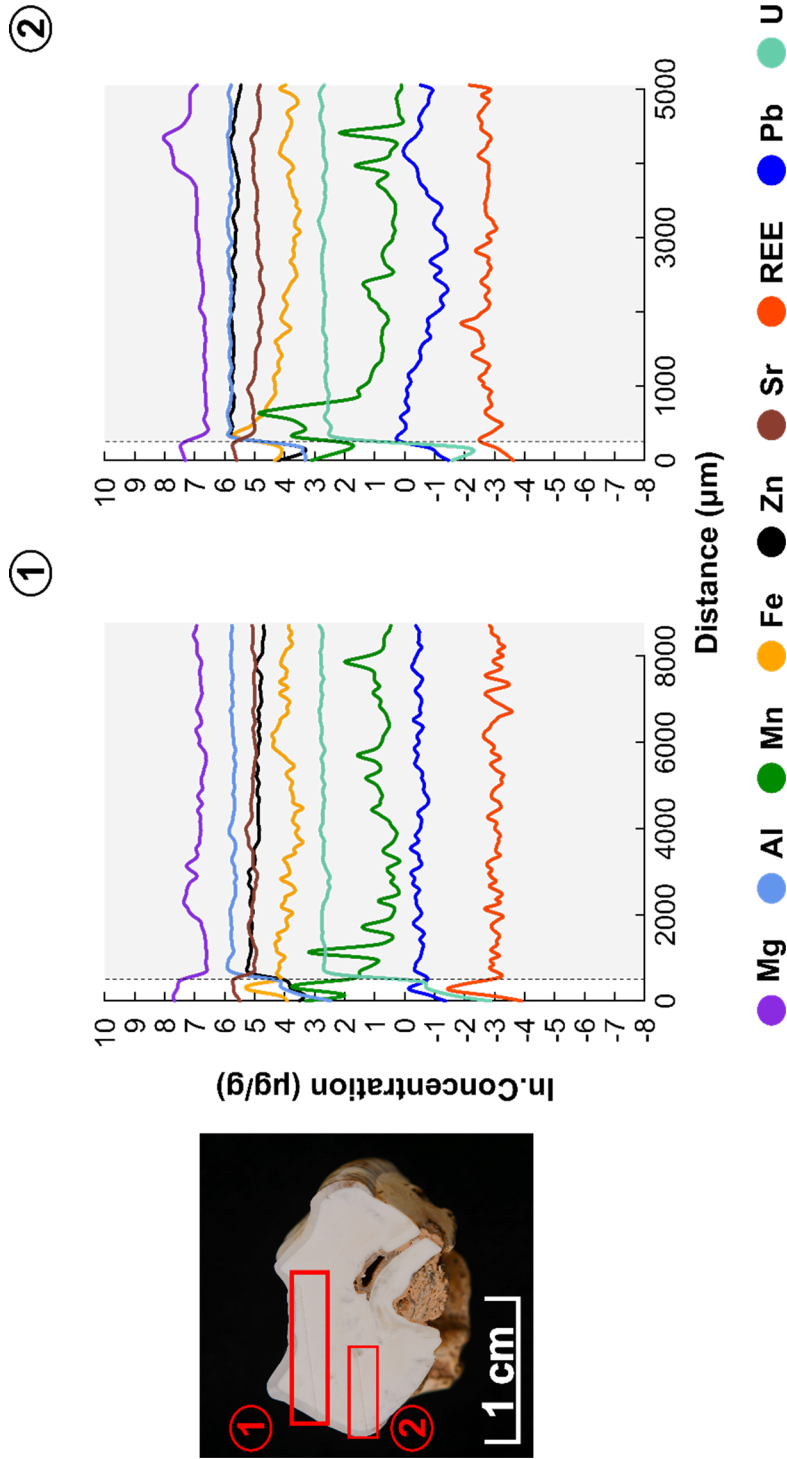


Figure S13. Spatial element concentration profiles for the element Zn, Fe, Mn, Al, Mg, Sr, Pb, U and rare earth elements (REE, calculated as the sum of all measured REE concentrations) of all LA-ICP-MS linescan analysis (1 and 2) of the Tam Hay Marklot cave fossil tooth (M2 left) specimen 34501 (*Ursus thibetanus*). All concentration data (µg/g) were natural log-transformed (ln.Concentration). The different shaded areas, delimited by dotted lines, represent the different histological parts: white for enamel, and light gray for dentin. The profiles follow a left-to-right direction as seen from the picture on the left.

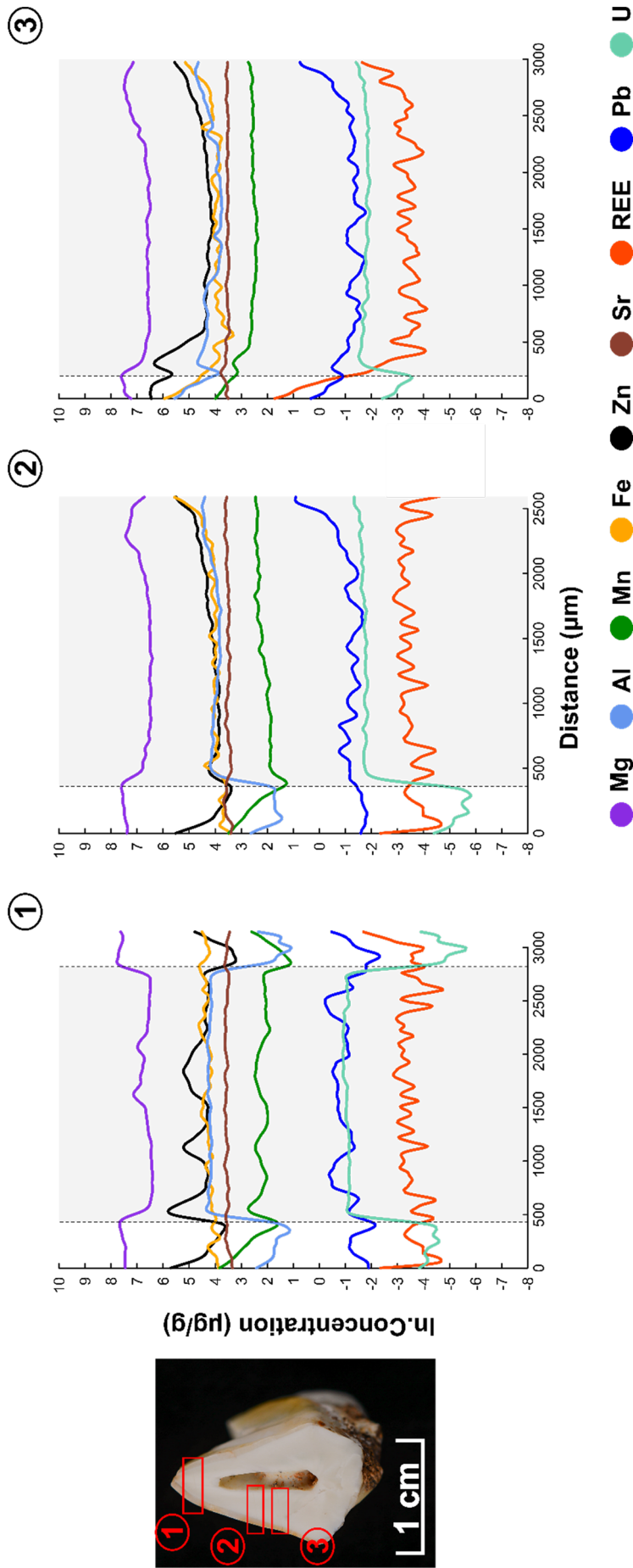


Figure S14. Spatial element concentration profiles for the element Zn, Fe, Mn, Al, Mg, Sr, Pb, U and rare earth elements (REE, calculated as the sum of all measured REE concentrations) of all LA-ICP-MS linescan analysis (1 to 3) of the Tam Hay Marklot cave fossil tooth (P4 left) specimen 34505 (*Panthera pardus*). All concentration data (µg/g) were natural log-transformed (ln. Concentration). The different shaded areas, delimited by dotted lines, represent the different histological parts: white for enamel, and light gray for dentin. The profiles follow a left-to-right direction as seen from the picture on the left

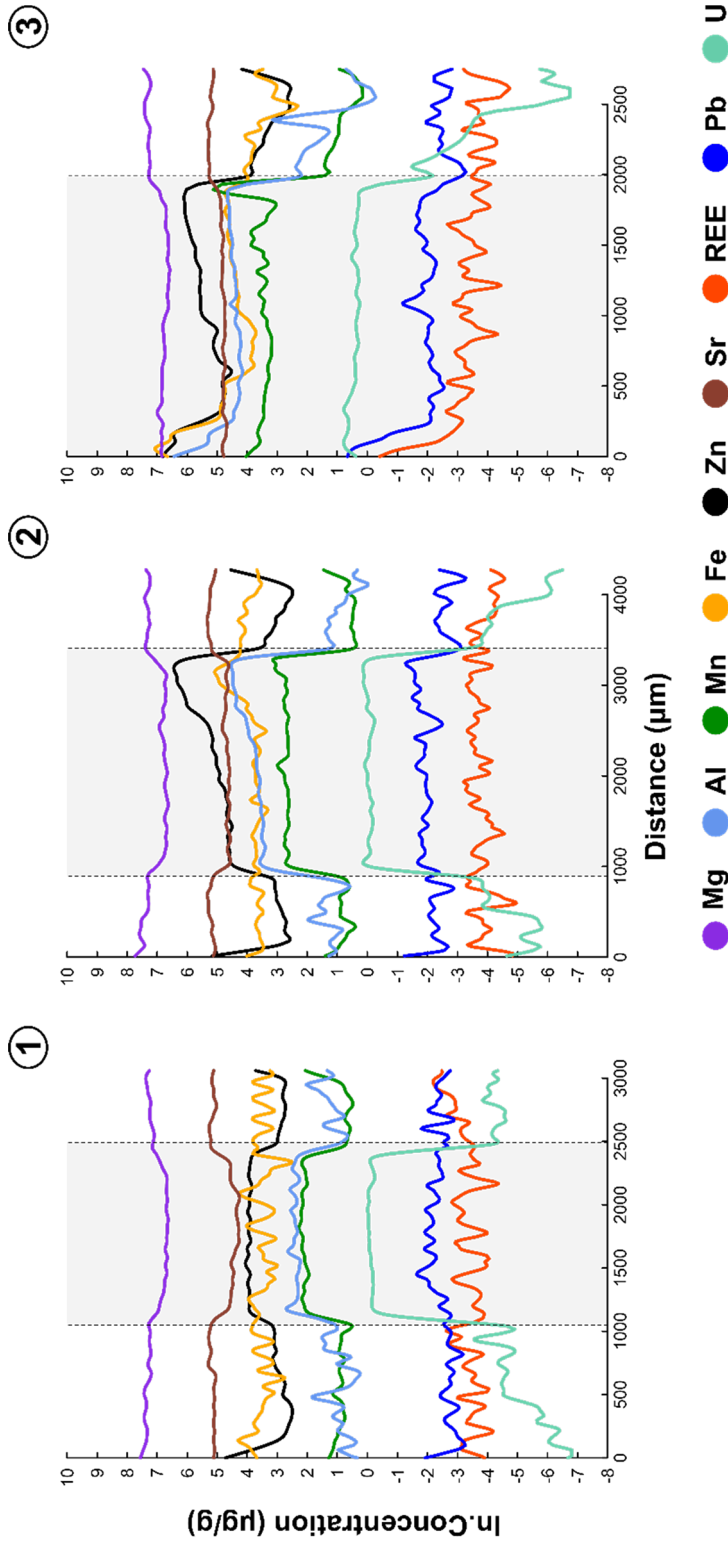


Figure S15. Spatial element concentration profiles for the element Zn, Fe, Mn, Al, Mg, Sr, Pb, U and rare earth elements (REE, calculated as the sum of all measured REE concentrations) of all LA-ICP-MS linescan analysis (1 to 3) of the Tam Hay Marklot cave fossil tooth (p2/p3 left) specimen 34524 (*Bubalus bubalis*). All concentration data ($\mu\text{g/g}$) were natural log.transformed (ln.Concentration). The different shaded areas, delimited by dotted lines, represent the different histological parts: white for enamel, and light gray for dentin. The profiles follow a left-to-right direction as seen from the picture on the left.

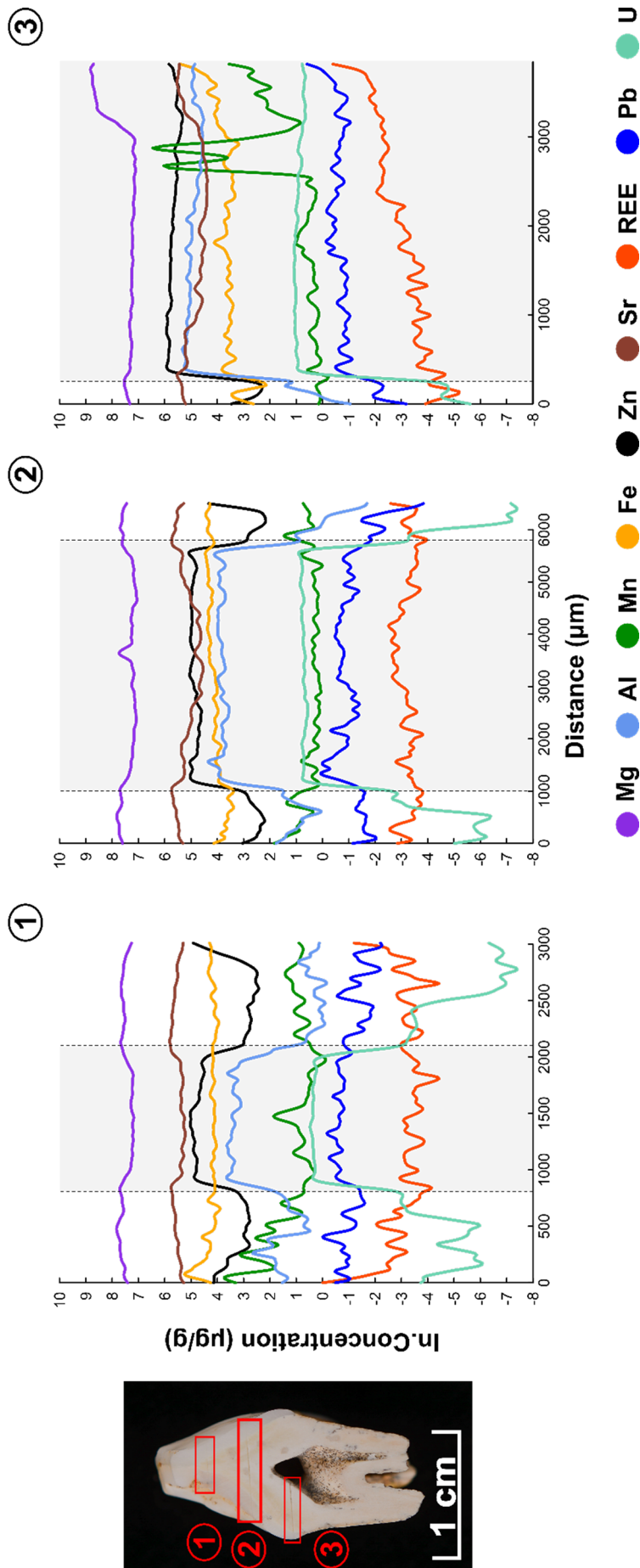


Figure S16. Spatial element concentration profiles for the element Zn, Fe, Mn, Sr, Pb, U and rare earth elements (REE, calculated as the sum of all measured REE concentrations) of all LA-ICP-MS linescan analysis (1 to 3) of the Tam Hay Marklot cave fossil tooth (p4 left) specimen 34538 (*Sus* sp.). All concentration data (µg/g) were natural log-transformed (ln. Concentration). The different shaded areas, delimited by dotted lines, represent the different histological parts: white for enamel, and light gray for dentin. The profiles follow a left-to-right direction as seen from the picture on the left.

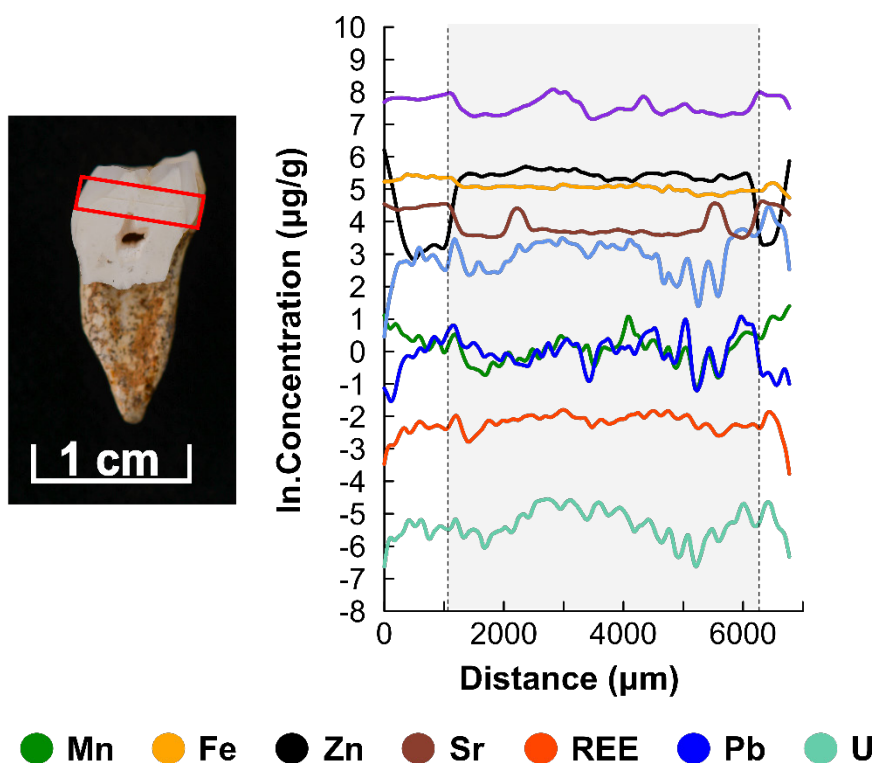


Figure S17. Spatial element concentration profiles for the element Zn, Fe, Mn, Al, Mg, Sr, Pb, U and rare earth elements (REE, calculated as the sum of all measured REE concentrations) of the single LA-ICP-MS linescan analysis of the Tam Hay Marklot cave fossil tooth (m1/m2 left) specimen 34548 (*Macaca* sp.). All concentration data ($\mu\text{g/g}$) were natural log.transformed (ln.Concentration). The different shaded areas, delimited by dotted lines, represent the different histological parts: white for enamel, and light gray for dentin. The profiles follow a left-to-right direction as seen from the picture on the left.

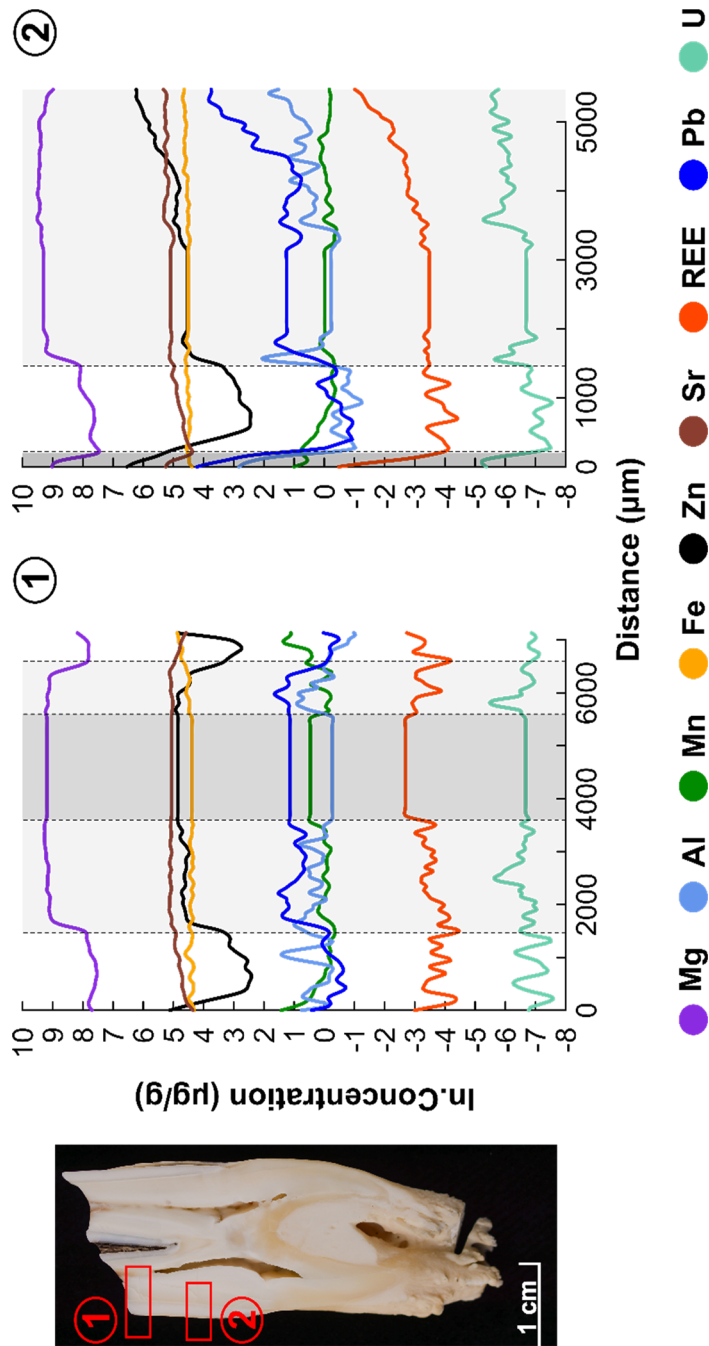


Figure S18. Spatial element concentration profiles for the element Zn, Fe, Mn, Al, Mg, Sr, Pb, U and rare earth elements (REE, calculated as the sum of all measured REE concentrations) of all LA-ICP-MS linescan analysis (1 and 2) of the Center of Natural History of Hamburg modern tooth (m3 right) specimen SEVA 34707 / ZMH-S-10461 (*Bison bison*). All concentration data ($\mu\text{g/g}$) were natural log-transformed (ln.Concentration). The different shaded areas, delimited by dotted lines, represent the different histological parts: white for enamel, light gray for dentin, medium gray for pulp cavity, and dark gray for calculus. The profiles follow a left-to-right direction as seen from the picture on the left.

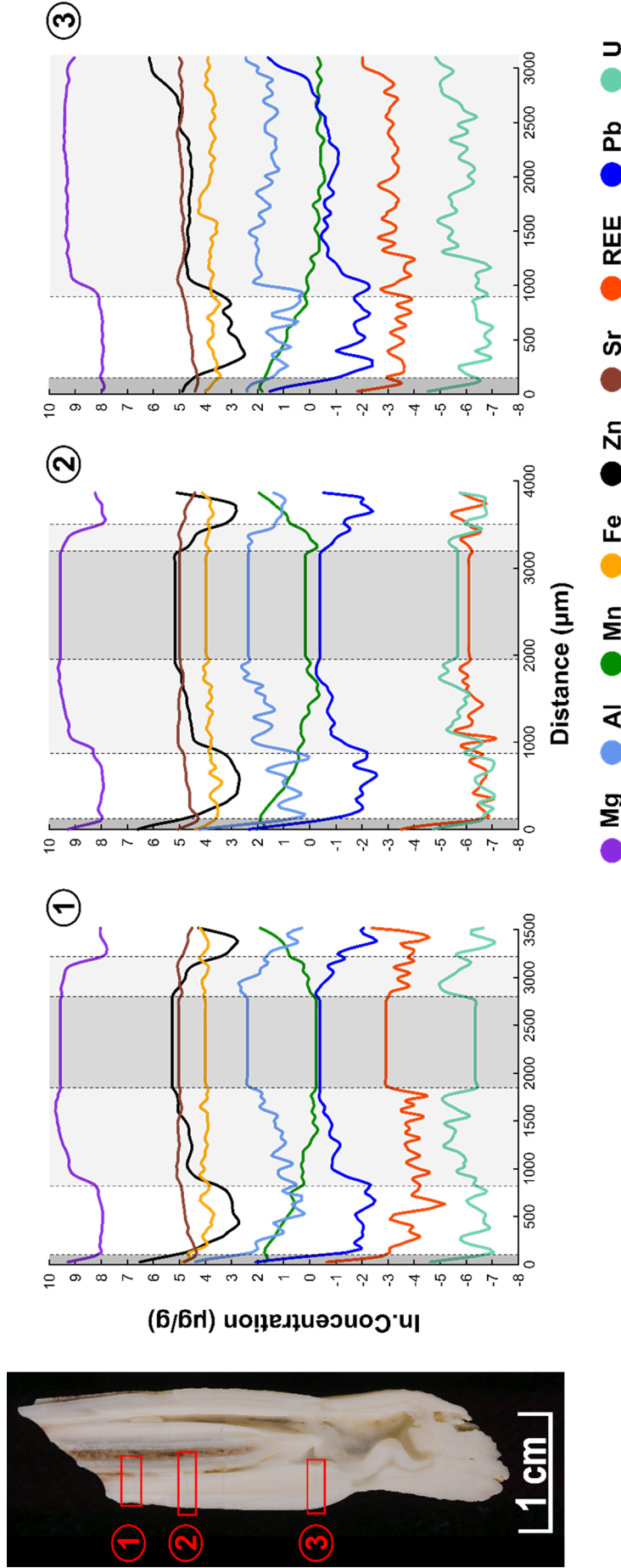


Figure S19. Spatial element concentration profiles for the element Zn, Fe, Mn, Al, Mg, Sr, Pb, U and rare earth elements (REE), calculated as the sum of all measured REE concentrations) of all LA-ICP-MS linescan analysis (1 to 3) of the Center of Natural History of Hamburg modern tooth (m3 left) specimen SEVA 34708 / ZMH-S-10963 (*Hemitragus jemtahicus*). All concentration data ($\mu\text{g/g}$) were natural log-transformed (ln.Concentration). The different shaded areas, delimited by dotted lines, represent the different histological parts: white for enamel, light gray for dentin, medium gray for pulp cavity, and dark gray for calculus. The profiles follow a left-to-right direction as seen from the picture on the left.

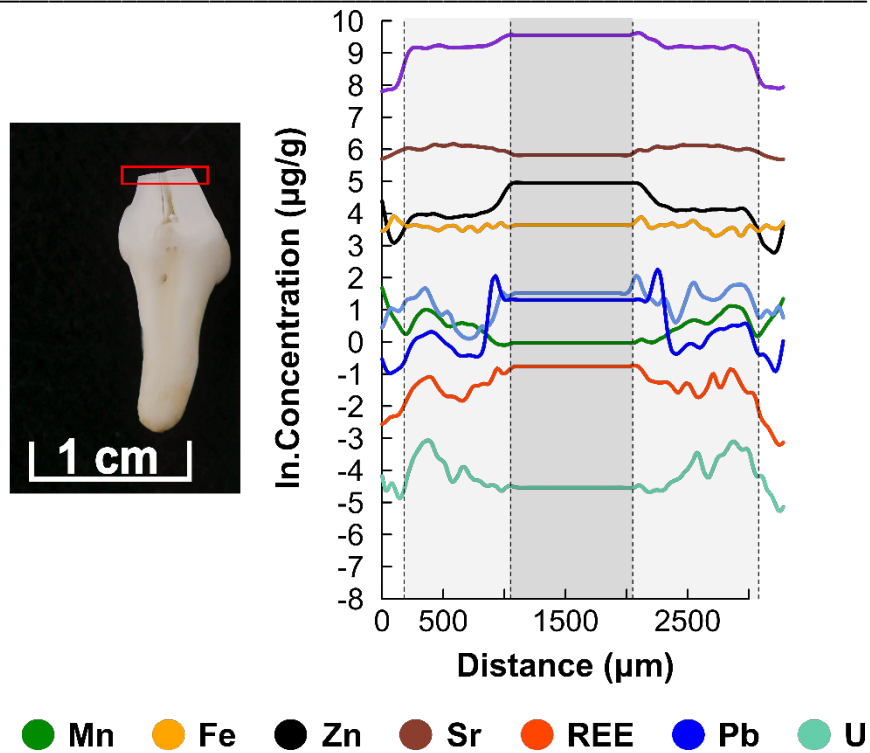


Figure S20. Spatial element concentration profiles for the element Zn, Fe, Mn, Al, Mg, Sr, Pb, U and rare earth elements (REE, calculated as the sum of all measured REE concentrations) of the single LA-ICP-MS linescan analysis of the Center of Natural History of Hamburg modern tooth (p3/p4) specimen SEVA 34709/ZMH-S-10612 (*Pteronura brasiliensis*). All concentration data ($\mu\text{g/g}$) were natural log.transformed (ln.Concentration). The different shaded areas, delimited by dotted lines, represent the different histological parts: white for enamel, light gray for dentin, and medium gray for pulp cavity. The profiles follow a left-to-right direction as seen from the picture on the left.

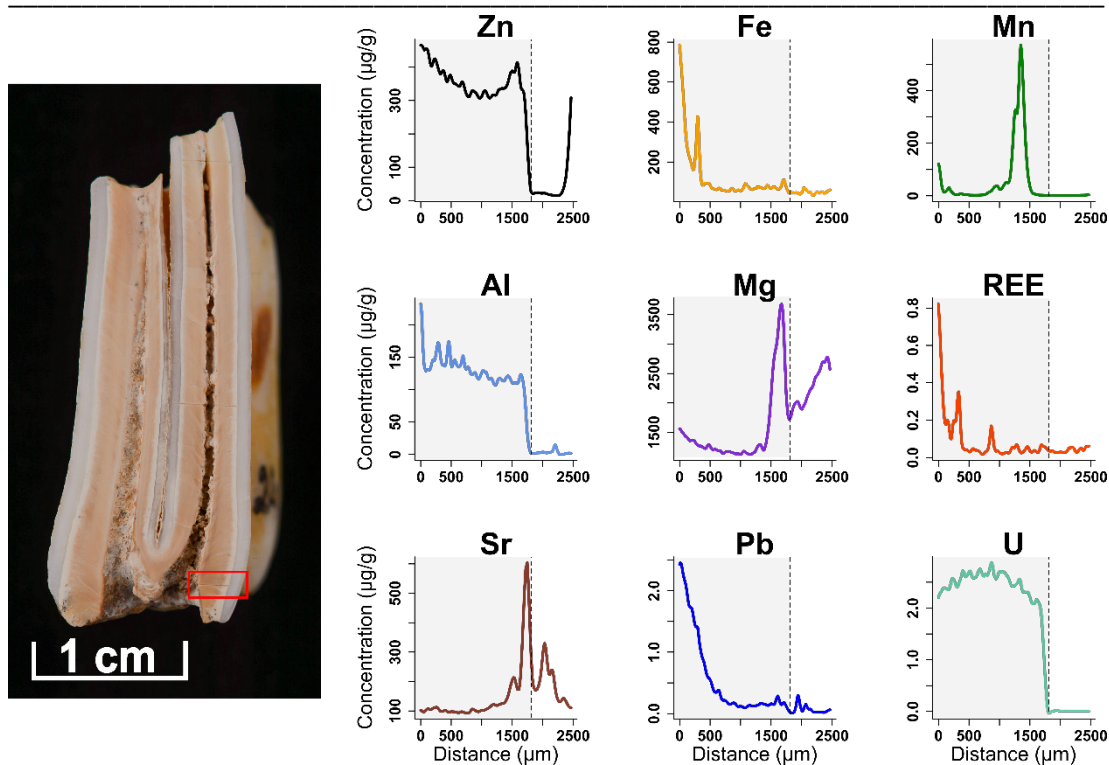


Figure S21. Typical concentrations ($\mu\text{g/g}$) observed through spatial element concentration profiles for the element Zn, Fe, Mn, Al, Mg, Sr, Pb, U and rare earth elements (REE, calculated as the sum of all measured REE concentrations) of the Tam Hay Marklot cave fossil tooth (m3 right) specimen 34493 (*Capricornis* sp.). The different shaded areas, delimited by dotted lines, represent the different histological parts: white for enamel, light gray for dentin, and medium gray for pulp cavity. The profiles follow a left-to-right direction as seen from the picture on the left.

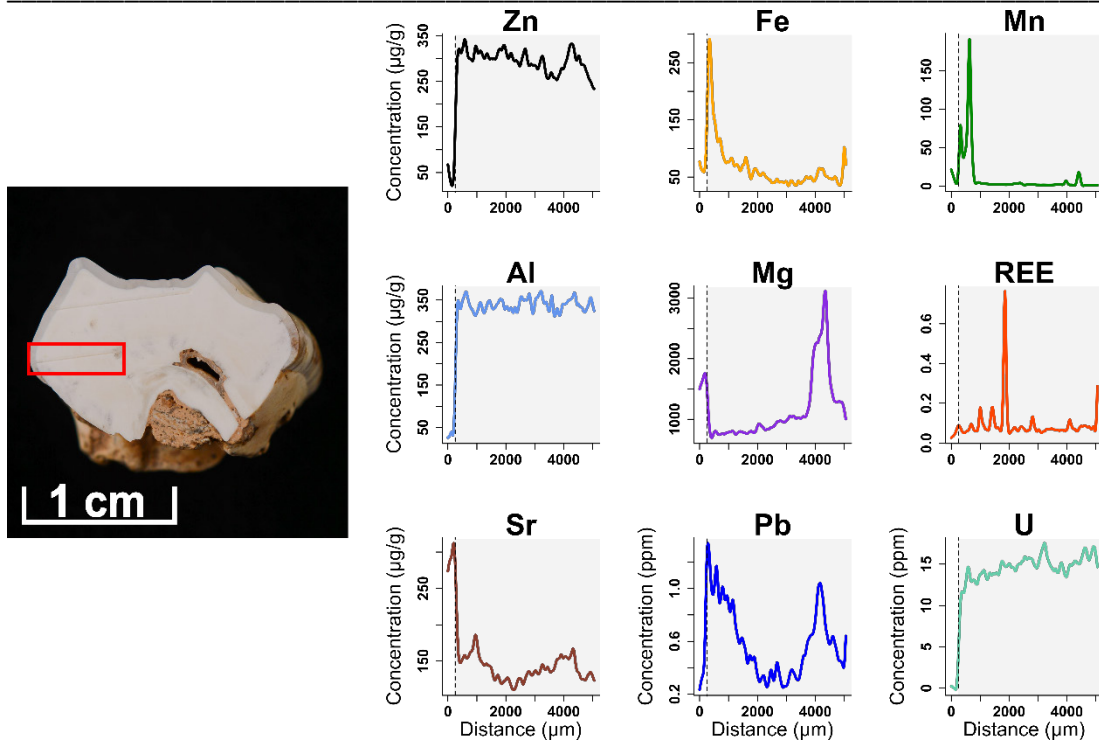


Figure S22. Typical concentrations ($\mu\text{g/g}$) observed through spatial element concentration profiles for the element Zn, Fe, Mn, Al, Mg, Sr, Pb, U and rare earth elements (REE, calculated as the sum of all measured REE concentrations) of the Tam Hay Marklot cave fossil tooth (M2 left) specimen 34501 (*Ursus thibetanus*). The different shaded areas, delimited by dotted lines, represent the different histological parts: white for enamel, and light gray for dentin. The profiles follow a left-to-right direction as seen from the picture on the left.

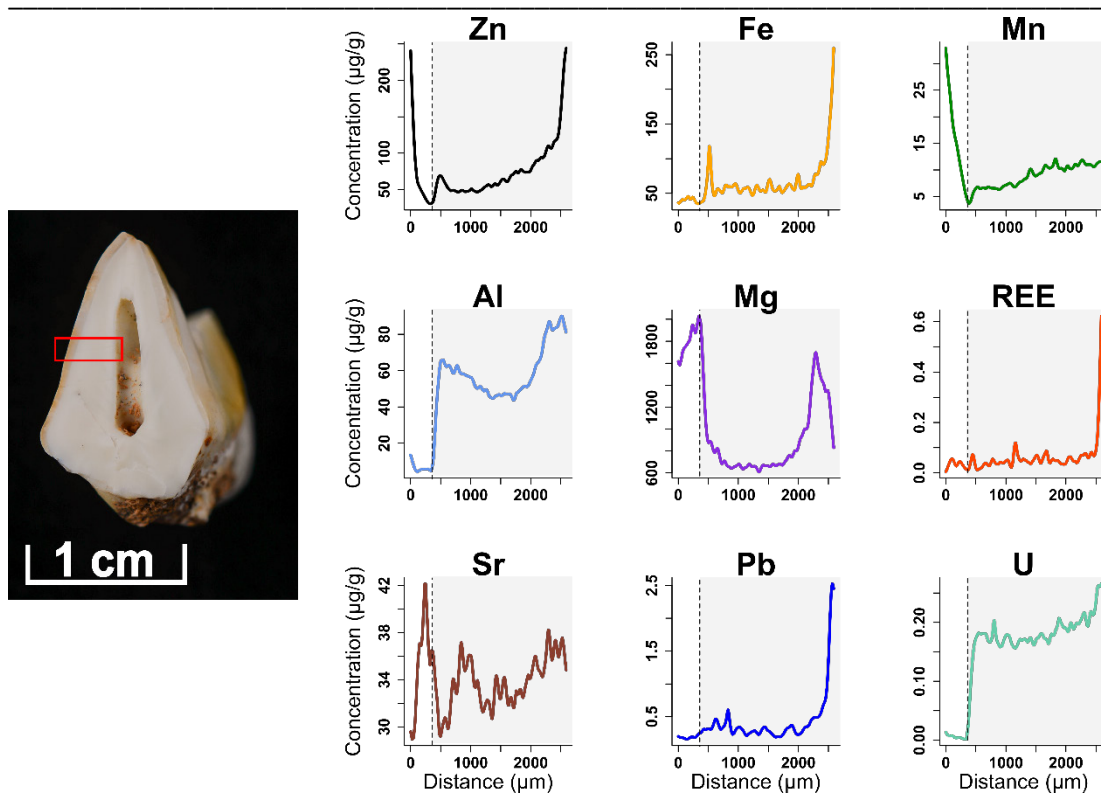


Figure S23. Typical concentrations ($\mu\text{g/g}$) observed through spatial element concentration profiles for the element Zn, Fe, Mn, Al, Mg, Sr, Pb, U and rare earth elements (REE, calculated as the sum of all measured REE concentrations) of the Tam Hay Marklot cave fossil tooth (P4 left) specimen 34505 (*Panthera pardus*). The different shaded areas, delimited by dotted lines, represent the different histological parts: white for enamel, and light gray for dentin. The profiles follow a left-to-right direction as seen from the picture on the left.

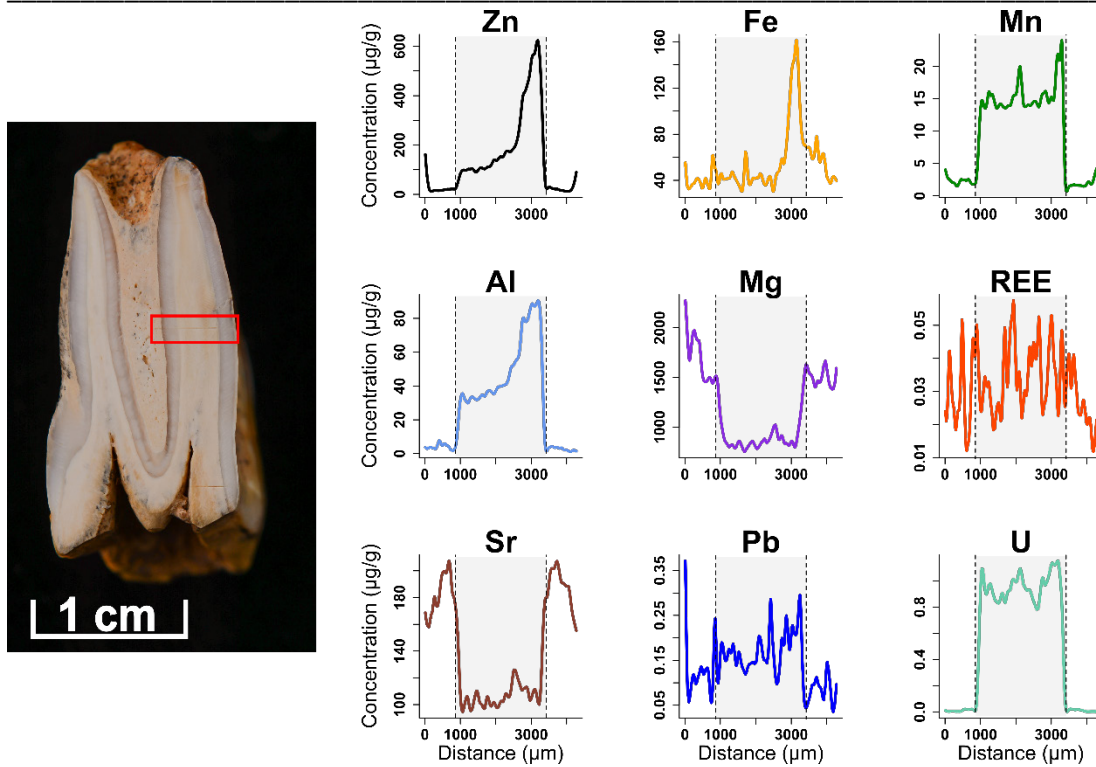


Figure S24. Typical concentrations ($\mu\text{g/g}$) observed through spatial element concentration profiles for the element Zn, Fe, Mn, Al, Mg, Sr, Pb, U and rare earth elements (REE, calculated as the sum of all measured REE concentrations) of the Tam Hay Marklot cave fossil tooth (p2/p3 left) specimen 34524 (*Bubalus bubalis*). The different shaded areas, delimited by dotted lines, represent the different histological parts: white for enamel, and light gray for dentin. The profiles follow a left-to-right direction as seen from the picture on the left.

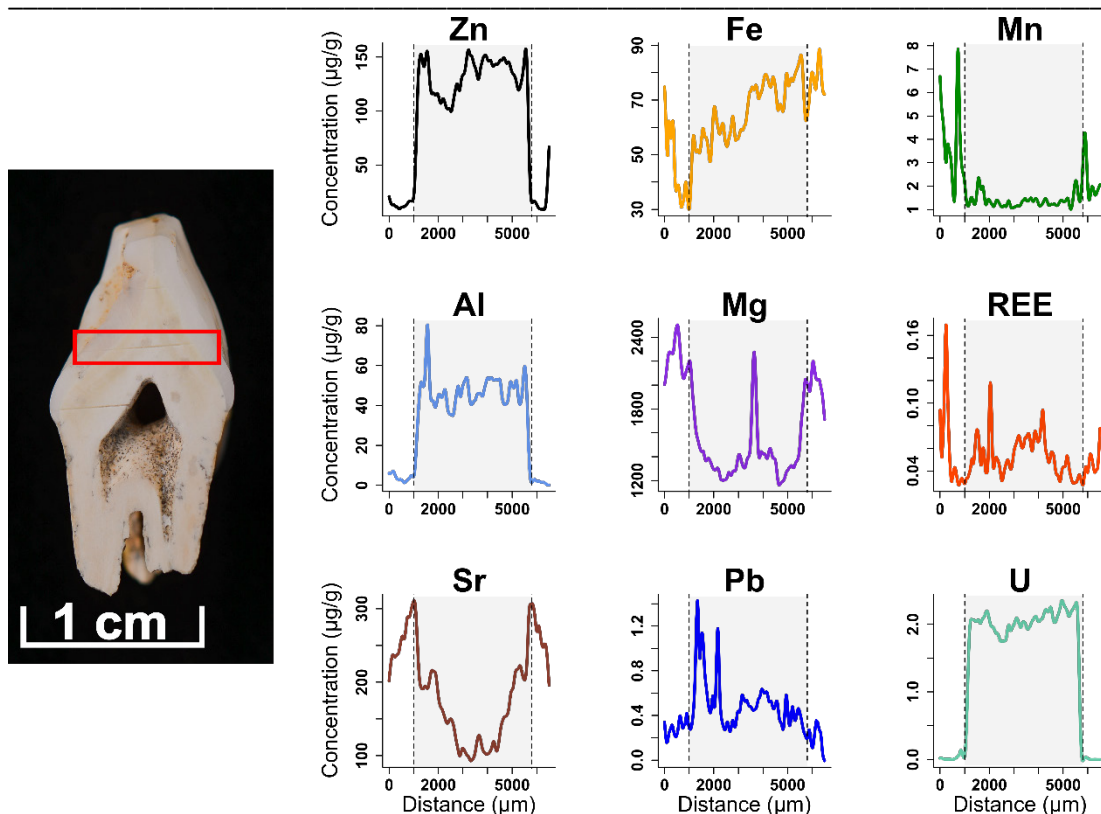


Figure S25. Typical concentrations ($\mu\text{g/g}$) observed through spatial element concentration profiles for the element Zn, Fe, Mn, Al, Mg, Sr, Pb, U and rare earth elements (REE, calculated as the sum of all measured REE concentrations) of the Tam Hay Marklot cave fossil tooth (p4 left) specimen 34538 (*Sus* sp.). The different shaded areas, delimited by dotted lines, represent the different histological parts: white for enamel, and light gray for dentin. The profiles follow a left-to-right direction as seen from the picture on the left.

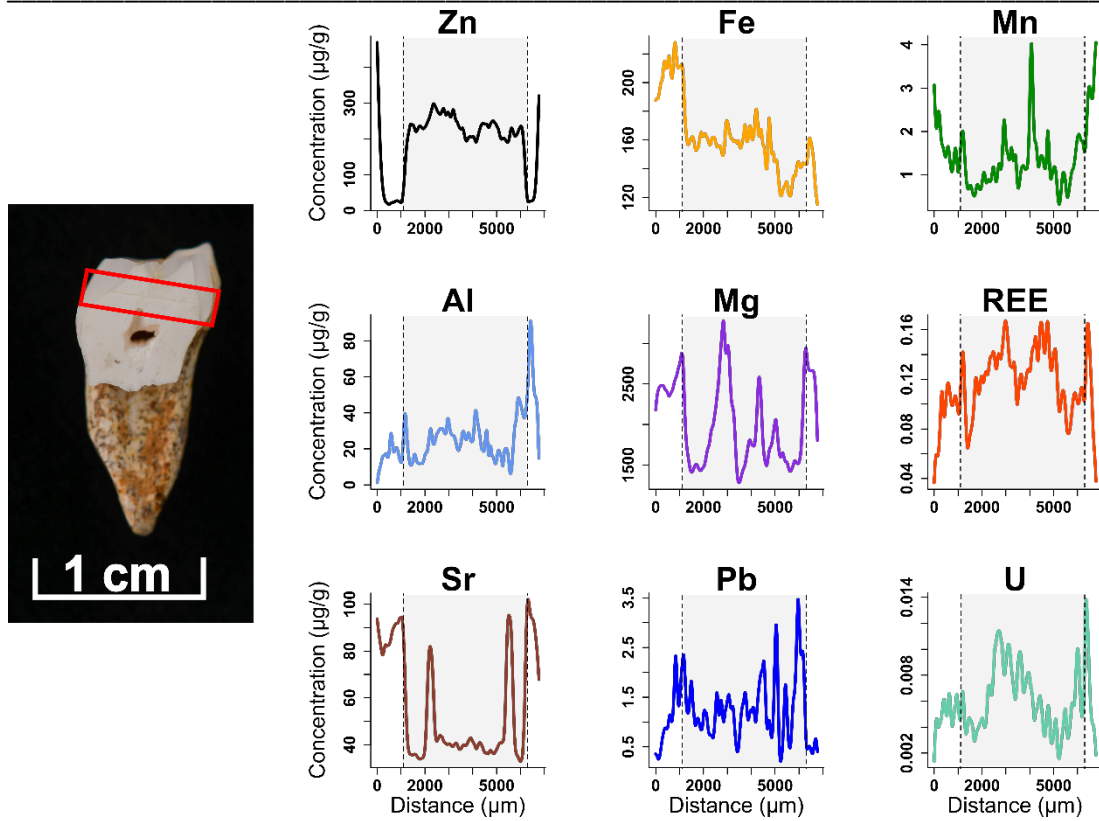


Figure S26. Typical concentrations ($\mu\text{g/g}$) observed through spatial element concentration profiles for the element Zn, Fe, Mn, Al, Mg, Sr, Pb, U and rare earth elements (REE, calculated as the sum of all measured REE concentrations) of the Tam Hay Marklot cave fossil tooth (m1/m2 left) specimen 34548 (*Macaca* sp.). The different shaded areas, delimited by dotted lines, represent the different histological parts: white for enamel, and light gray for dentin. The profiles follow a left-to-right direction as seen from the picture on the left.

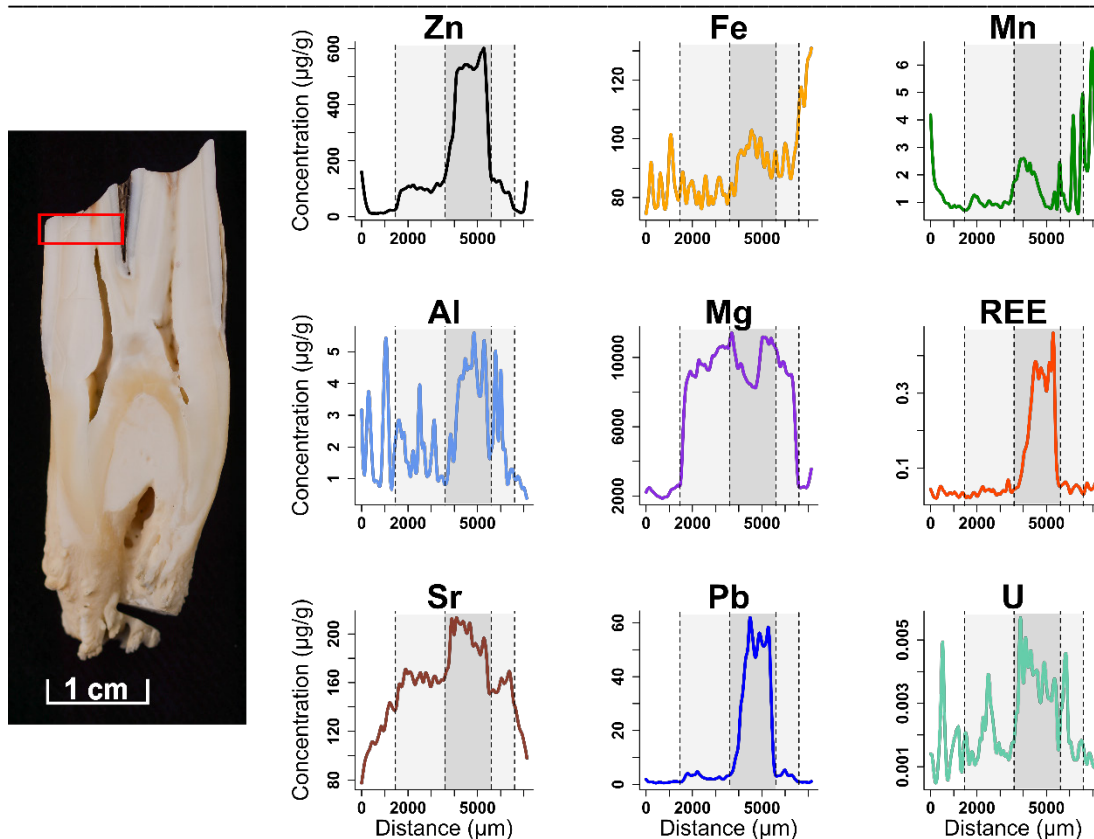


Figure S27. Typical concentrations ($\mu\text{g/g}$) observed through spatial element concentration profiles for the element Zn, Fe, Mn, Al, Mg, Sr, Pb, U and rare earth elements (REE, calculated as the sum of all measured REE concentrations) of the Center of Natural History of Hamburg modern tooth (m3 right) specimen SEVA 34707 / ZMH-S-10461 (*Bison bison*). The different shaded areas, delimited by dotted lines, represent the different histological parts: white for enamel, light gray for dentin, and medium gray for pulp cavity. The profiles follow a left-to-right direction as seen from the picture on the left.

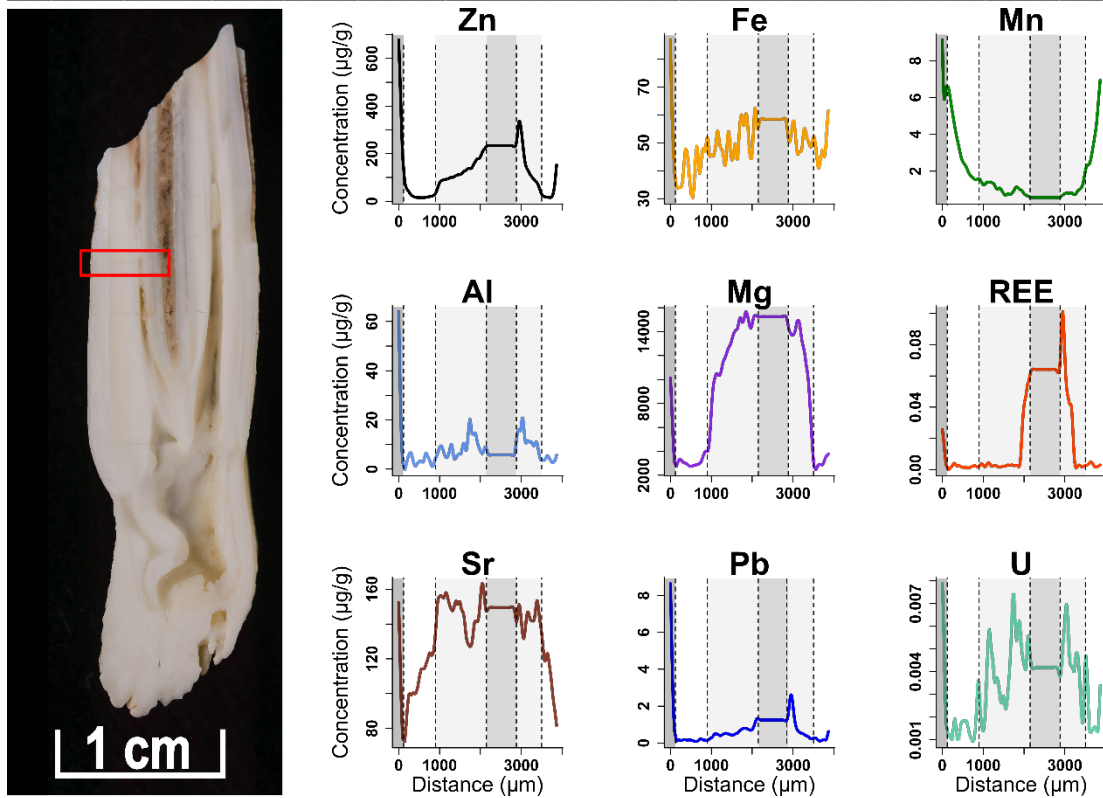


Figure S28. Typical concentrations ($\mu\text{g/g}$) observed through spatial element concentration profiles for the element Zn, Fe, Mn, Al, Mg, Sr, Pb, U and rare earth elements (REE, calculated as the sum of all measured REE concentrations) of the Center of Natural History of Hamburg modern tooth (m3 left) specimen SEVA 34708 / ZMH-S-10963 (*Hemitragus jemlahicus*). The different shaded areas, delimited by dotted lines, represent the different histological parts: white for enamel, light gray for dentin, medium gray for pulp cavity, and dark gray for calculus. The profiles follow a left-to-right direction as seen from the picture on the left.

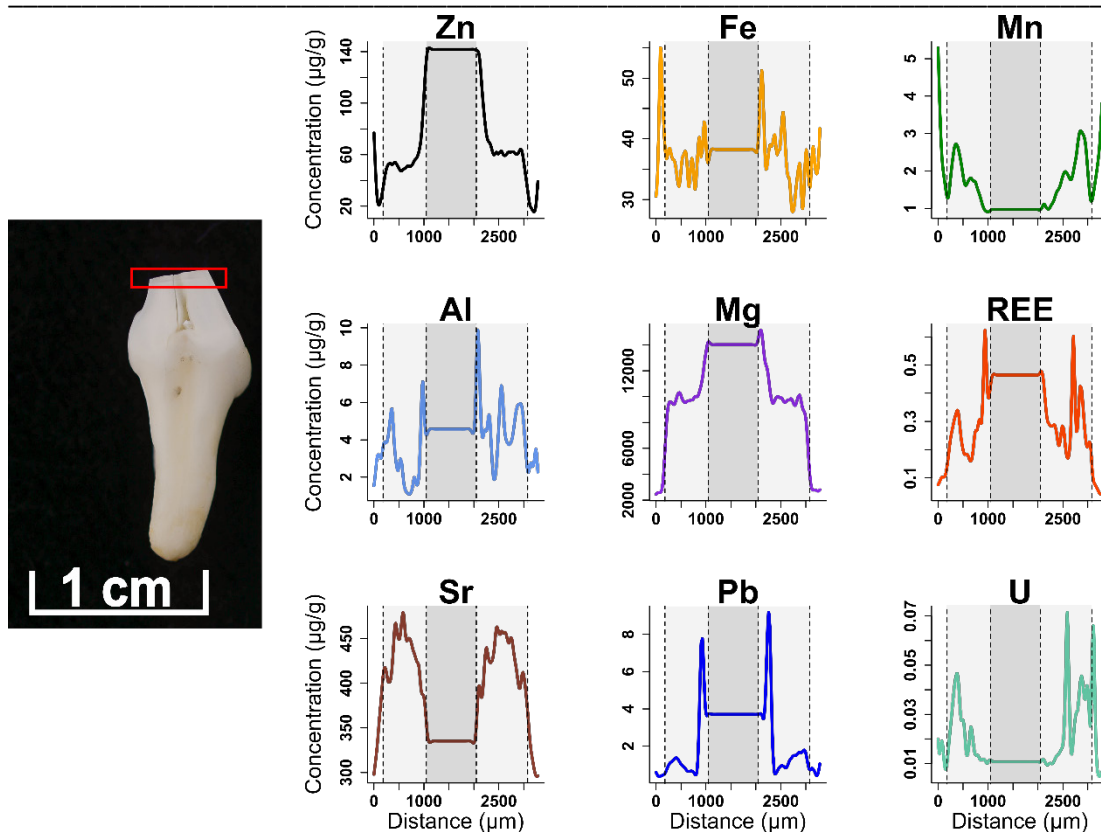


Figure S29. Typical concentrations ($\mu\text{g/g}$) observed through spatial element concentration profiles for the element Zn, Fe, Mn, Al, Mg, Sr, Pb, U and rare earth elements (REE, calculated as the sum of all measured REE concentrations) of the Center of Natural History of Hamburg modern tooth (p3/p4) specimen SEVA 34709/ZMH-S-10612 (*Pteronura brasiliensis*). The different shaded areas, delimited by dotted lines, represent the different histological parts: white for enamel, light gray for dentin, and medium gray for pulp cavity. The profiles follow a left-to-right direction as seen from the picture on the left.

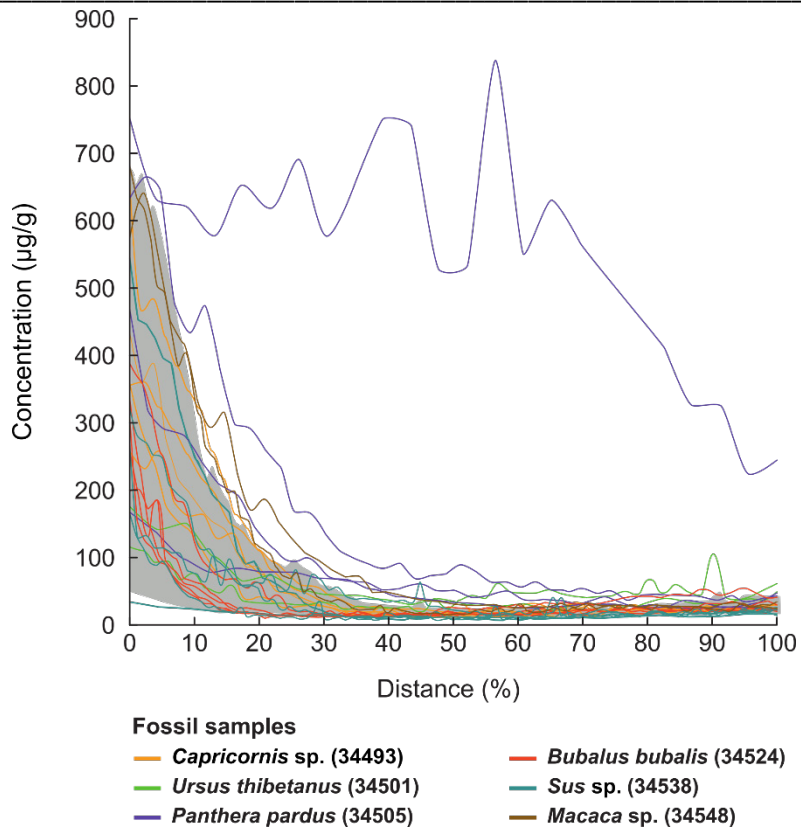


Figure S30. Zinc concentration ($\mu\text{g/g}$) distribution of every analyzed fossil enamel cross section segment, normalized to the relative enamel thickness (0% = outermost enamel layer, 100% = full thickness prior to analysis of enamel-dentin mixture). The gray area represents the concentration range observed in modern enamel cross section segments, colored lines those of the fossil enamel.

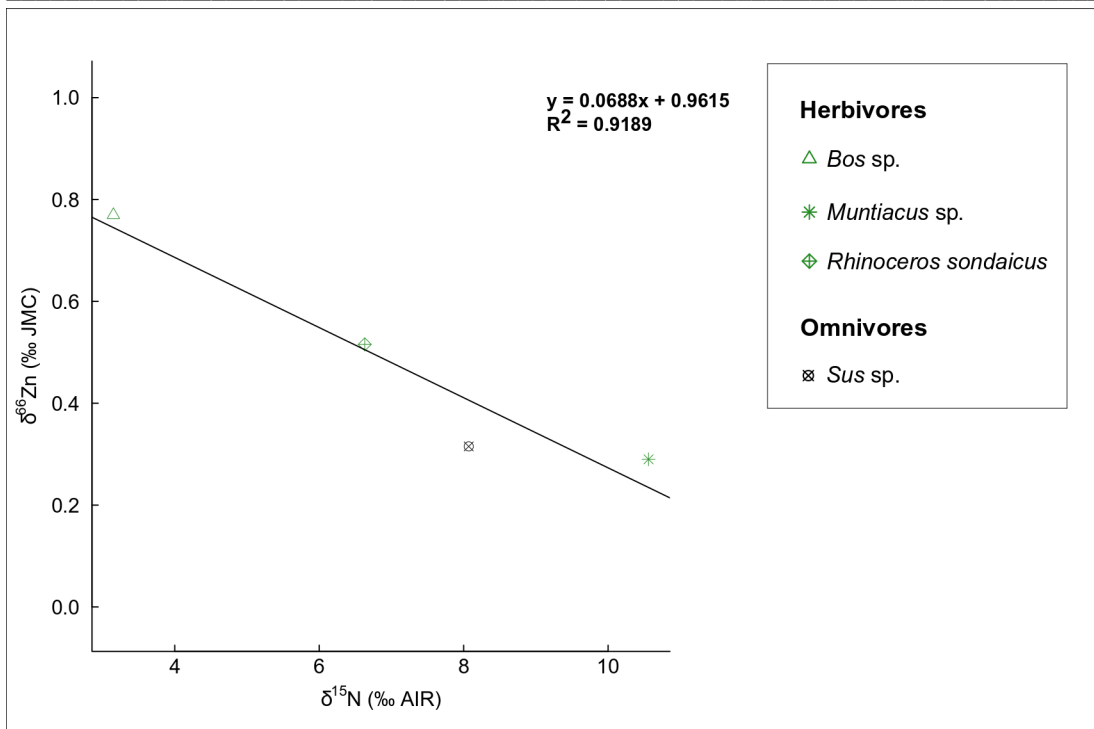


Figure S31. Relationship between $\delta^{15}\text{N}_{\text{collagen}}$ and $\delta^{66}\text{Zn}_{\text{enamel}}$ stable isotope values in fossil teeth from Tam Hay Marklot cave that yielded collagen from the dentin.

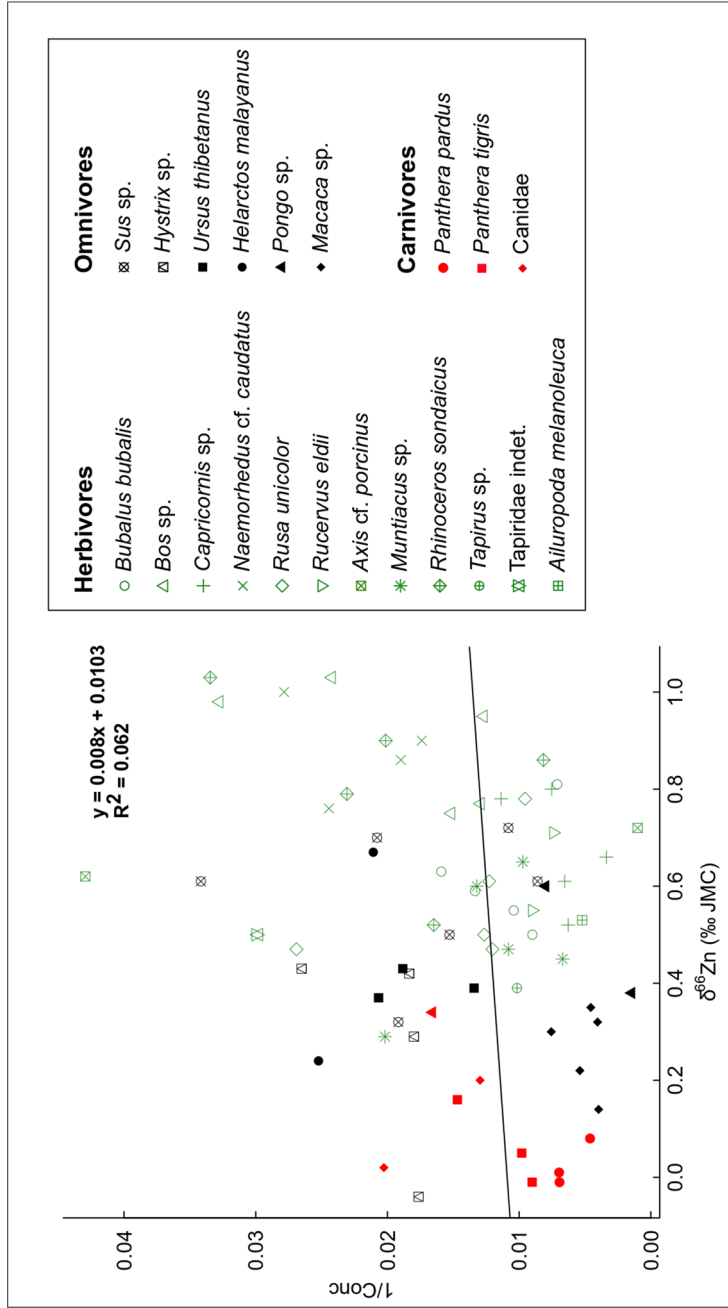


Figure S32. Relationship between the zinc concentration (1/Conc [$\mu\text{g/g}$]) and $\delta^{66}\text{Zn}$ stable isotope values in enamel of fossil teeth from Tam Hay Marklot cave.

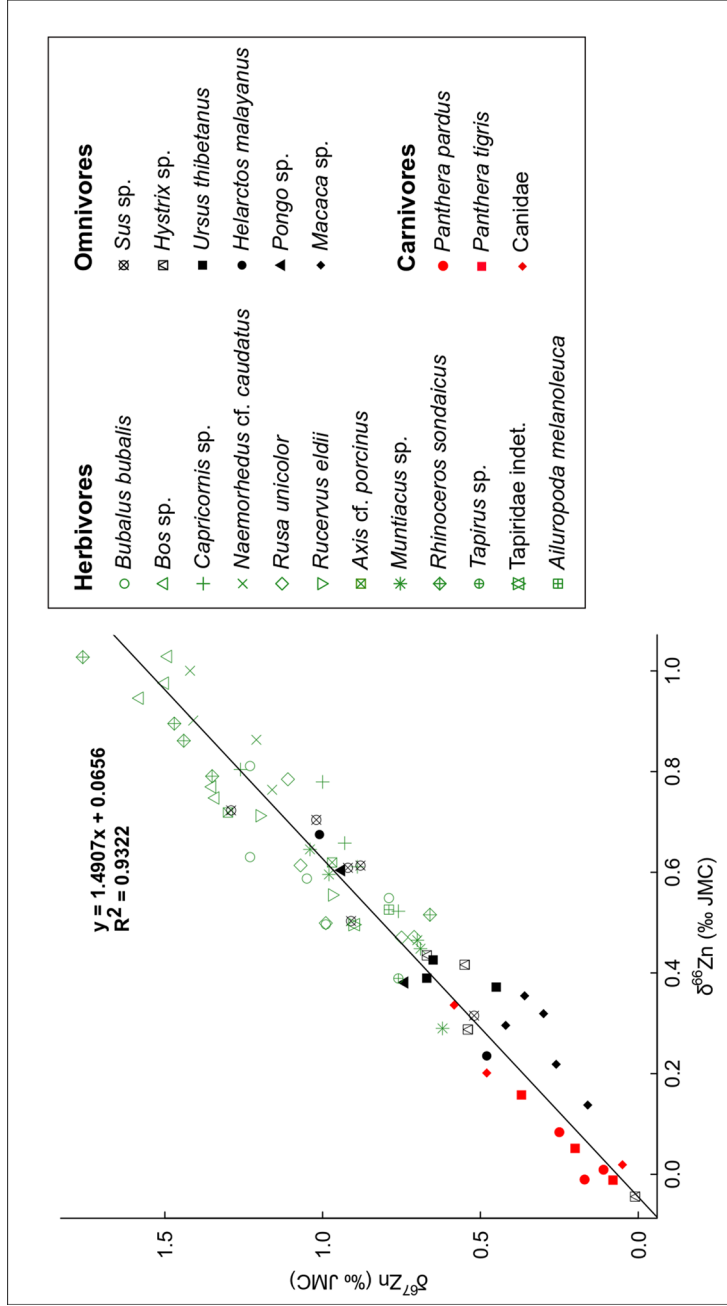


Figure S33. Relationship between $\delta^{67}\text{Zn}$ and $\delta^{66}\text{Zn}$ stable isotope values in enamel of fossil teeth from Tam Hay Marklot cave.

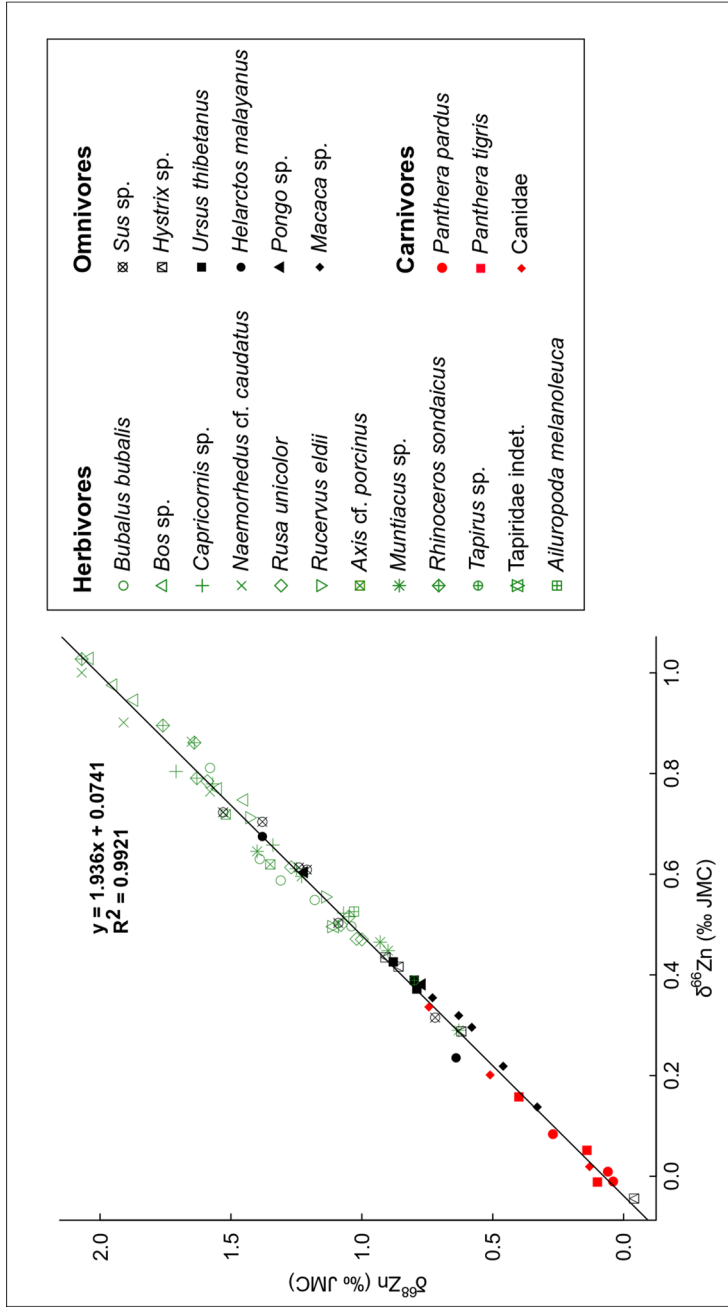


Figure S34. Relationship between $\delta^{68}\text{Zn}$ and $\delta^{66}\text{Zn}$ stable isotope values in enamel of fossil teeth from Tam Hay Marklot cave.

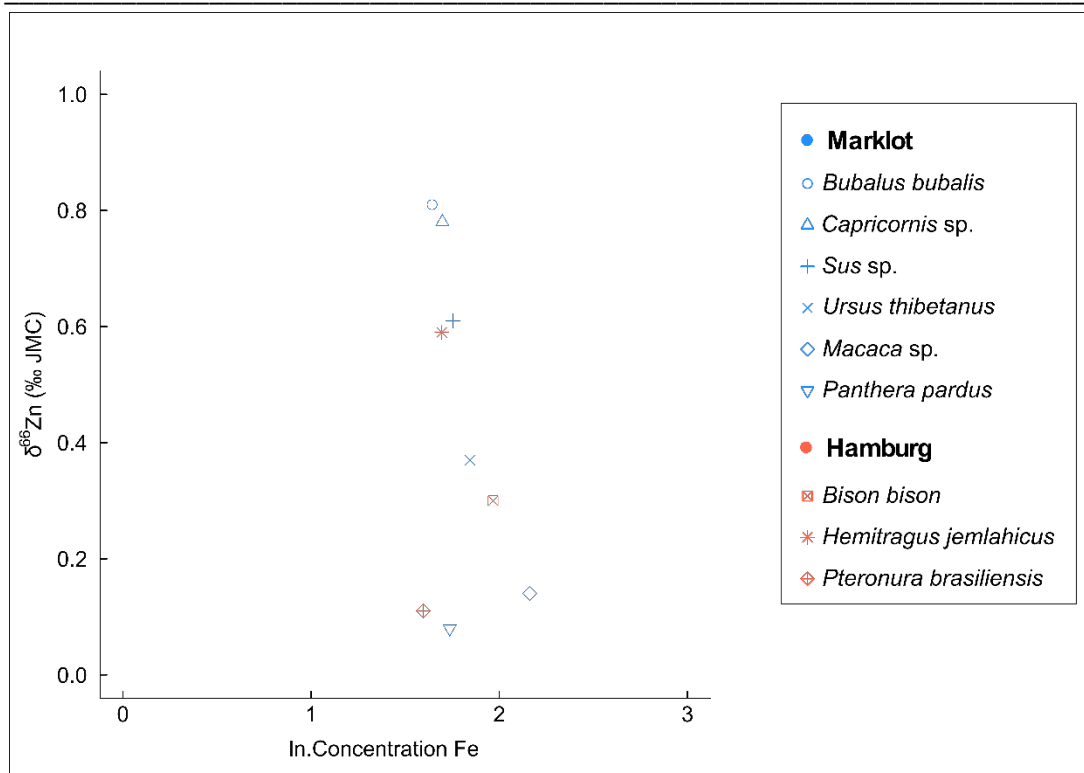


Figure S35. Distribution between ln.Concentration Fe ($\mu\text{g/g}$) and $\delta^{66}\text{Zn}$ stable isotope values in enamel of fossil (Marklot: Tam Hay Marklot) and modern (Hamburg: Center of Natural History of Hamburg, originally zoo animals from Hagenbeck Tierpark in Hamburg) teeth.

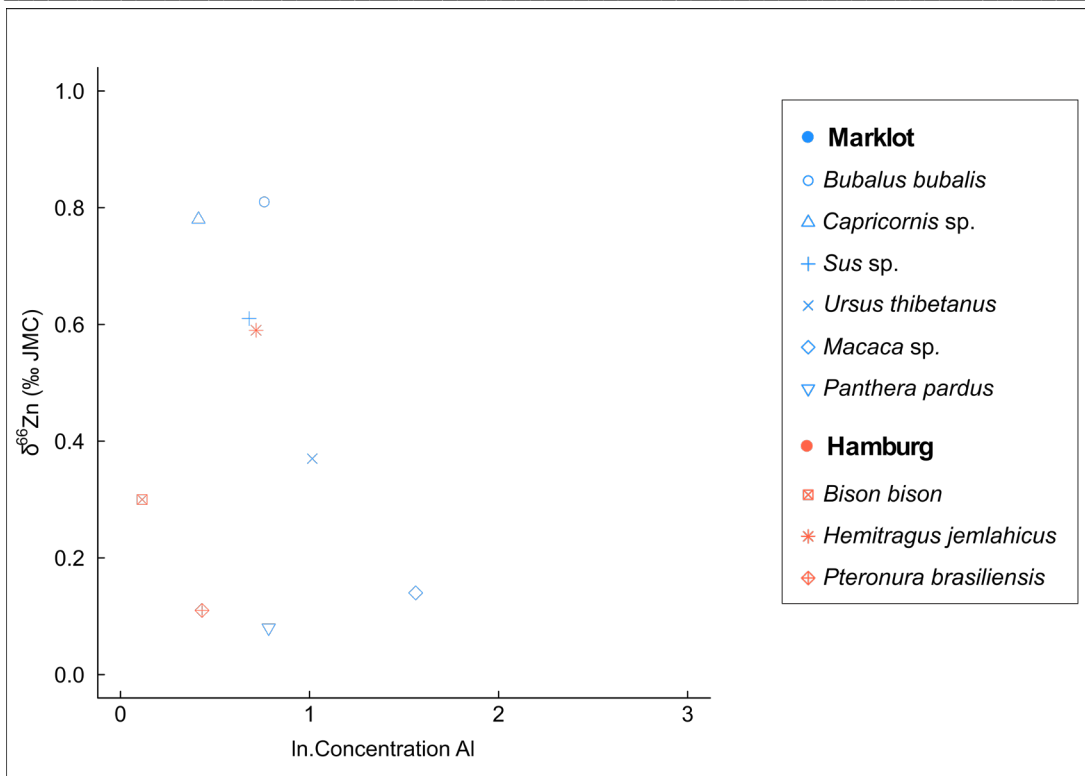


Figure S36. Distribution between ln.Concentration Al ($\mu\text{g/g}$) and $\delta^{66}\text{Zn}$ stable isotope values in enamel of fossil (Marklot: Tam Hay Marklot) and modern (Hamburg: Center of Natural History of Hamburg, originally zoo animals from Hagenbeck Tierpark in Hamburg) teeth.

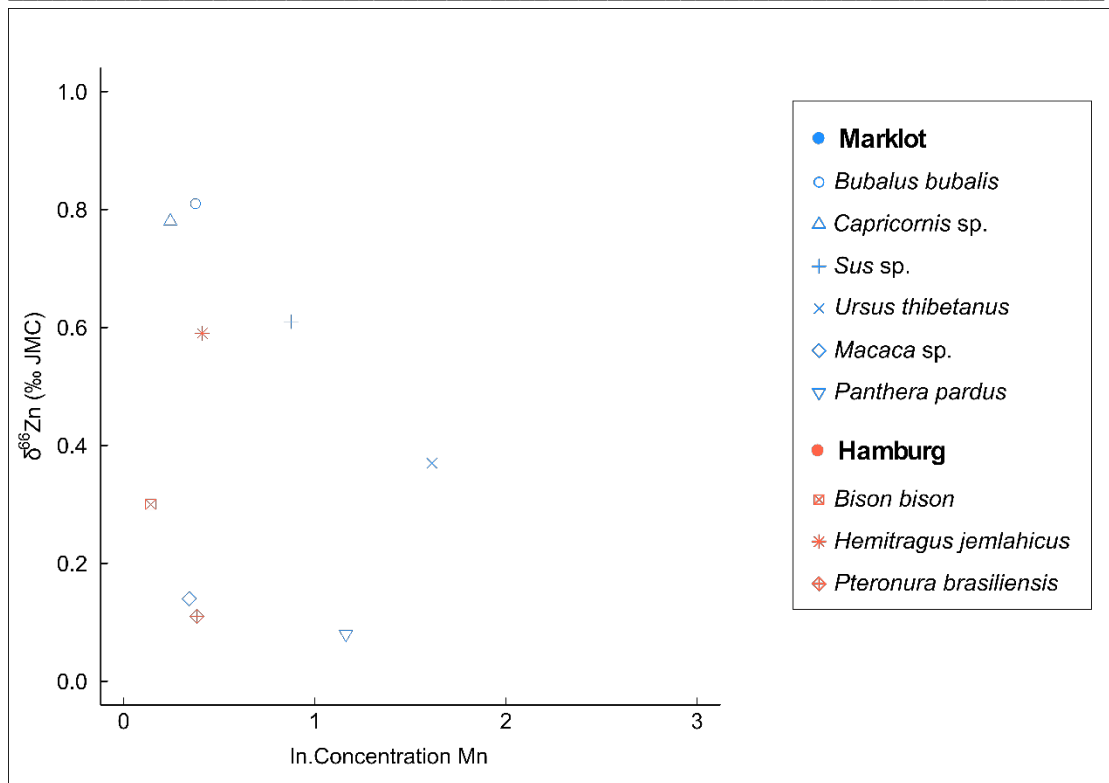


Figure S37. Distribution between ln.Concentration Mn ($\mu\text{g/g}$) and $\delta^{66}\text{Zn}$ stable isotope values in enamel of fossil (Marklot: Tam Hay Marklot) and modern (Hamburg: Center of Natural History of Hamburg, originally zoo animals from Hagenbeck Tierpark in Hamburg) teeth.

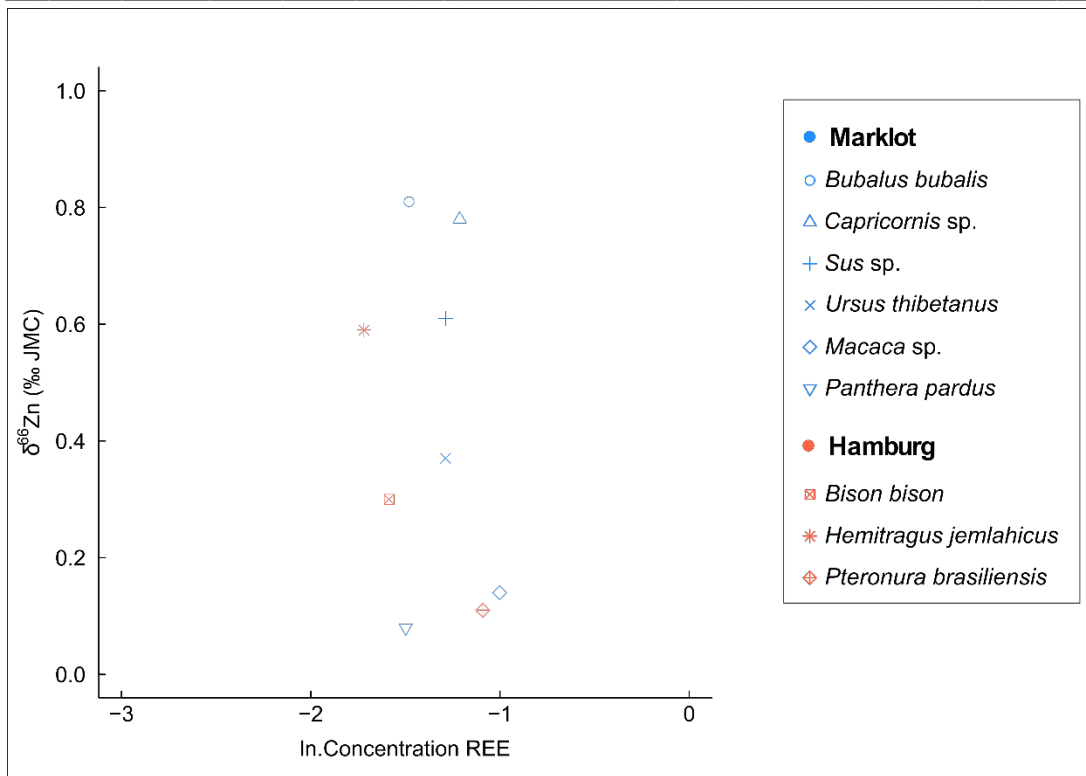


Figure S38. Distribution between ln.Concentration REE ($\mu\text{g/g}$; calculated as the sum of all measured REE concentrations) and $\delta^{66}\text{Zn}$ stable isotope values in enamel of fossil (Marklot: Tam Hay Marklot) and modern (Hamburg: Center of Natural History of Hamburg, originally zoo animals from Hagenbeck Tierpark in Hamburg) teeth.

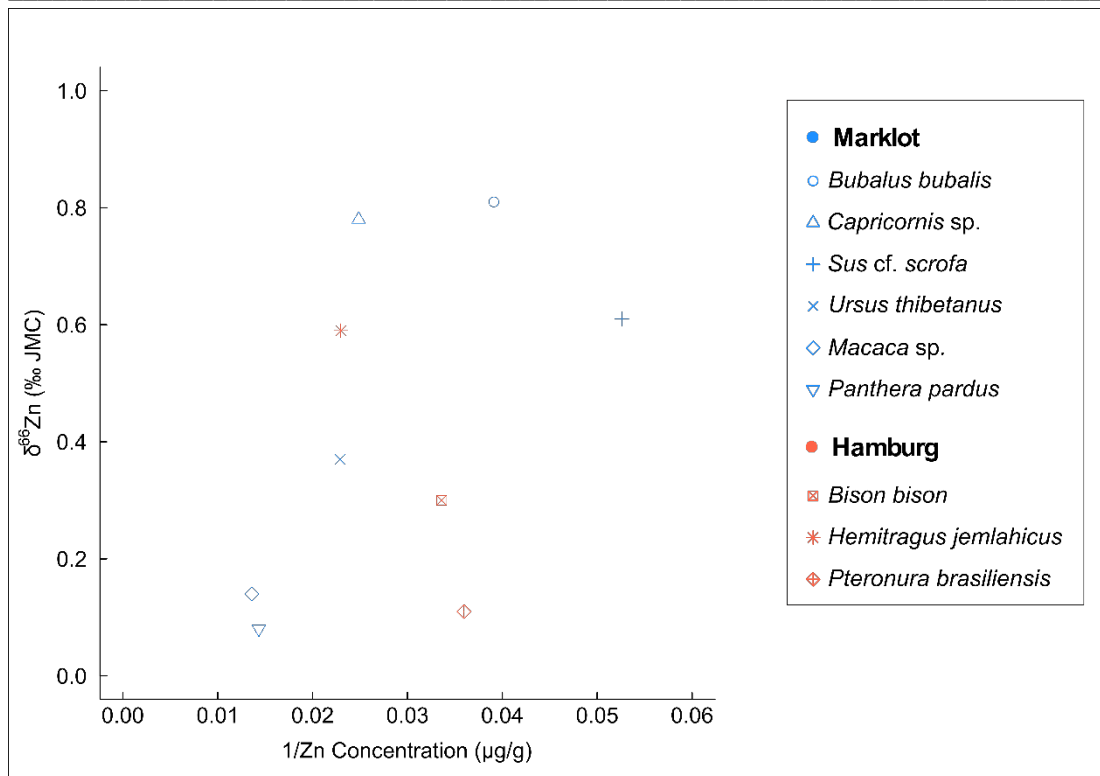


Figure S39. Distribution between the zinc concentration (1/Zn Concentration, µg/g) and $\delta^{66}\text{Zn}$ stable isotope values in enamel of fossil (Marklot: Tam Hay Marklot) and modern (Hamburg: Center of Natural History of Hamburg, originally zoo animals from Hagenbeck Tierpark in Hamburg) teeth.

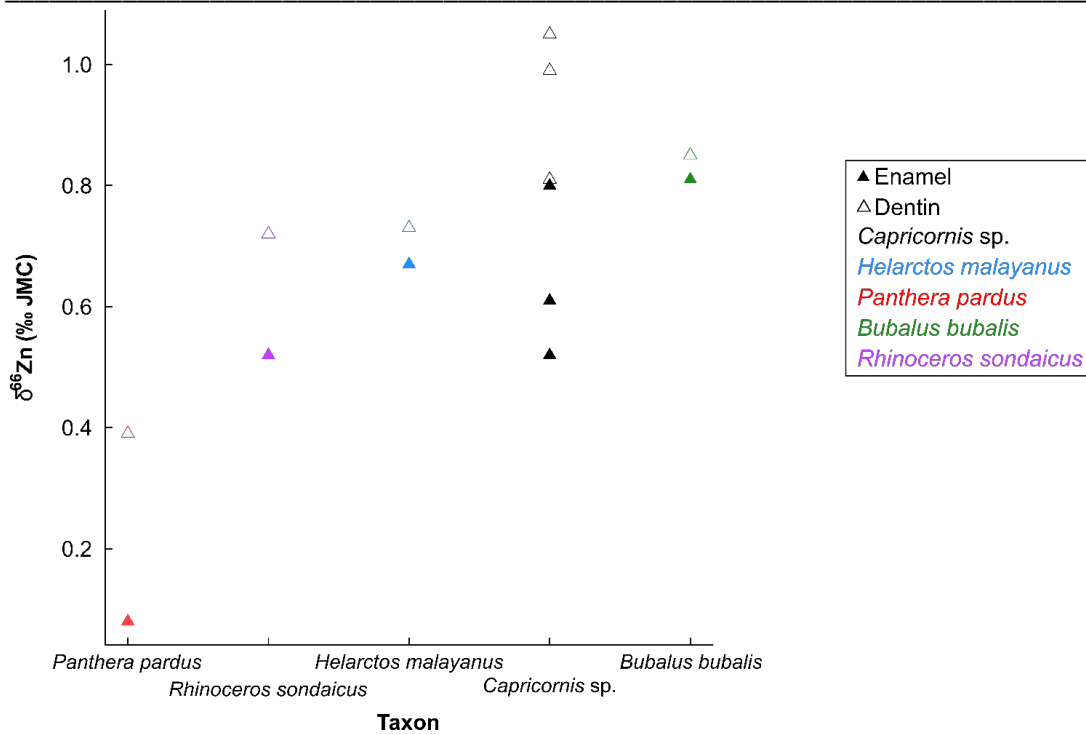


Figure S40. Distribution of $\delta^{66}\text{Zn}$ stable isotope values in dentin and enamel of fossil teeth from Tam Hay Marklot cave. Fossil teeth from various taxa: *Capricornis sp.* (34489, 34490 and 34492), *Helarctos malayanus* (34498), *Panthera pardus* (34505), *Bubalus bubalis* (34524) and *Rhinoceros sondaicus* (34556) were analyzed. Note that enamel has systematically lower $\delta^{66}\text{Zn}$ values compared to dentin of the same tooth.

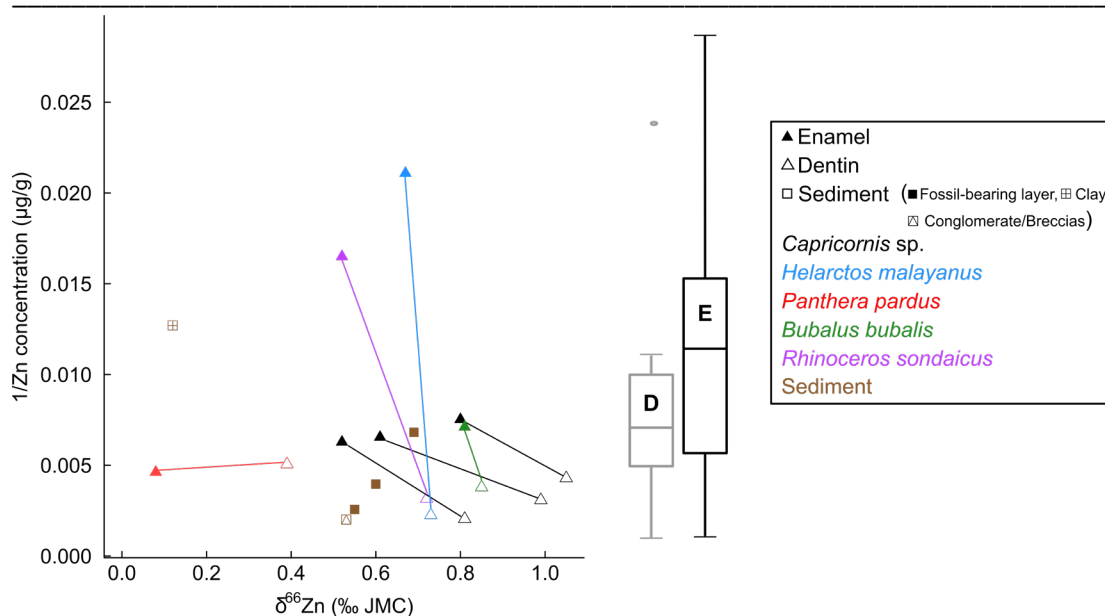


Figure S41. Distribution of zinc concentration ($1/\text{Zn}$ Concentration, $\mu\text{g/g}$) and $\delta^{66}\text{Zn}$ stable isotope values in dentin and enamel of fossil teeth, and sediment from Tam Hay Marklot cave. The line between samples indicate they are from the same specimen. Samples of fossil teeth include specimens from various taxa: *Capricornis* sp. (34489, 34490 and 34492), *Helarctos malayanus* (34498), *Panthera pardus* (34505), *Bubalus bubalis* (34524) and *Rhinoceros sondaicus* (34556). Sediment samples include fossiliferous layer (sandy to gravelly silty clay, with calcitic cementation), conglomerate/breccias from adjacent layer, and clay from the conglomerate). The boxes from the box and whisker plots represent the 25th–75th percentiles, with the median as a bold horizontal line, of zinc concentration from modern dentin (D) and enamel (E) found elsewhere (Lappalainen et al., 1981; Falla-Sotelo et al., 2005; Kohn et al., 2013; Teruel et al., 2015; Jaouen et al., 2016a).

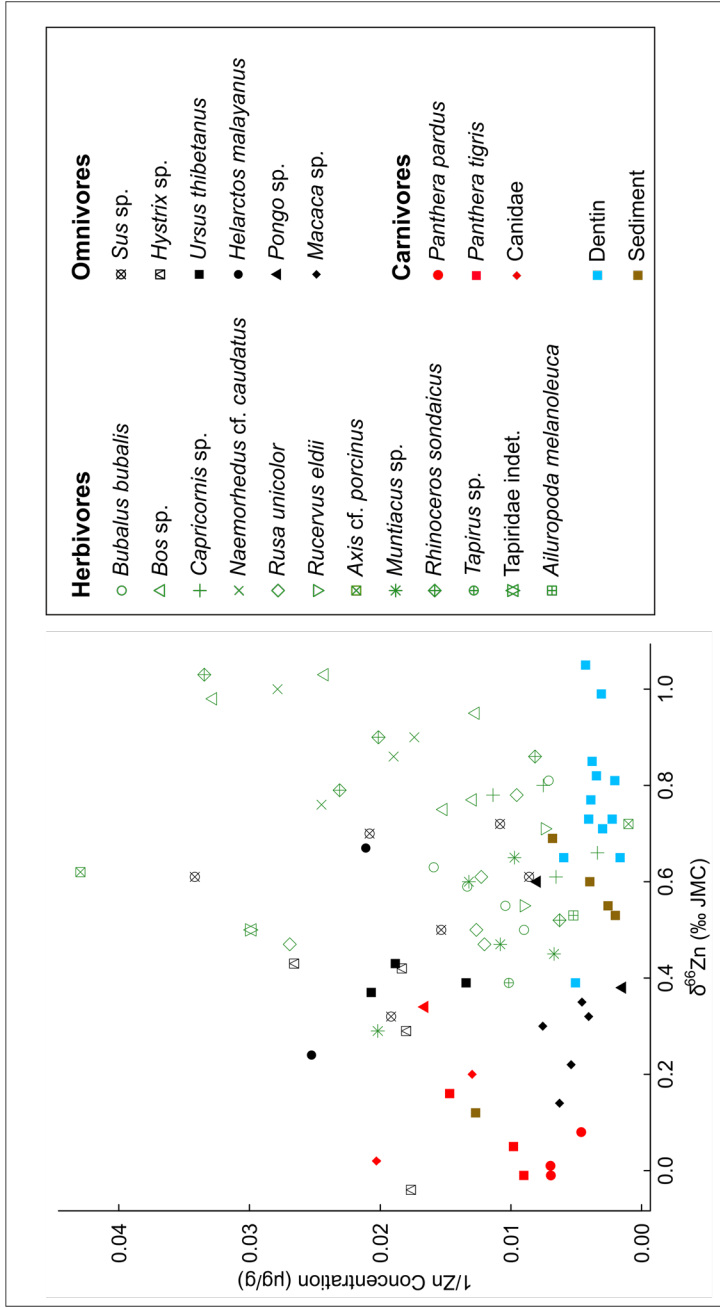


Figure S42. Distribution between the zinc concentration (1/Zn Concentration, µg/g) and $\delta^{66}\text{Zn}$ stable isotope values in enamel and dentin of fossil teeth and sediment from Tam Hay Marklot cave.

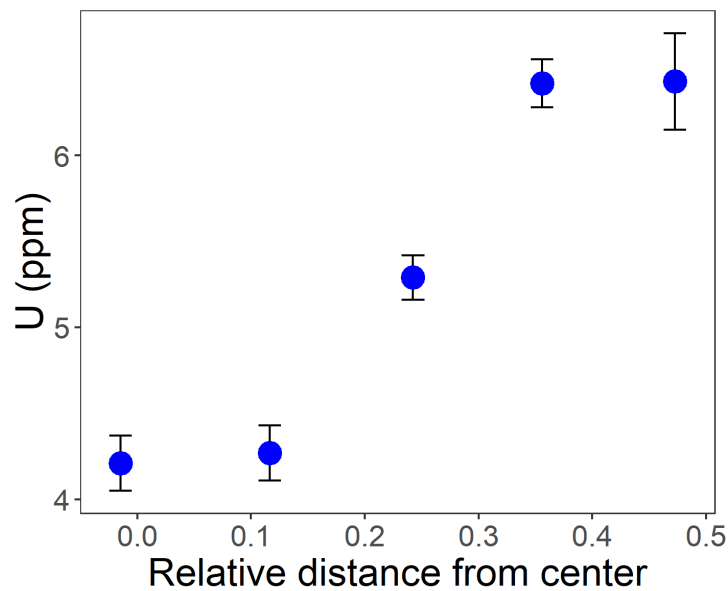


Figure S43. DAD model for the Tam Hay Marklot tooth specimen SCUMK-R1 (*Dicerorhinus sumatrensis*) that was prepared and analyzed for U/Th series dating. Relative distance is calculated from the EDJ to the extremity of the dental tissues between $[-1;1]$, being respectively the enamel tip in contact with the sediment and the pulp cavity.

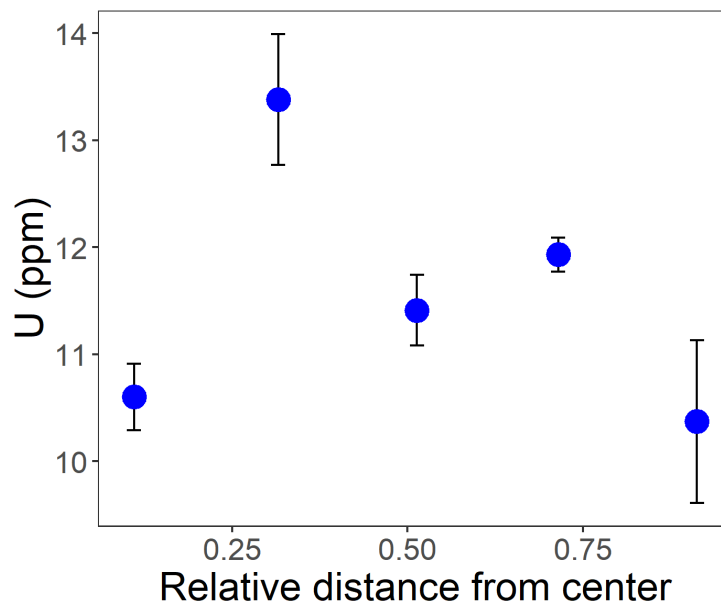


Figure S44. DAD model for the Tam Hay Marklot tooth specimen SCUMK-01 (large Bovid) that was prepared and analyzed for U/Th series dating. Relative distance is calculated from the EDJ to the extremity of the dental tissues between $[-1;1]$, being respectively the enamel tip in contact with the sediment and the pulp cavity.

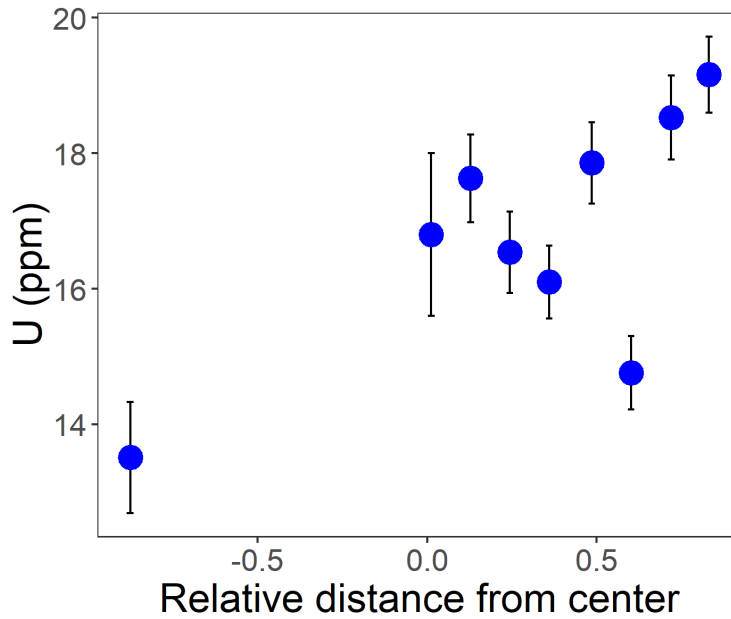


Figure S45. DAD model for the Tam Hay Marklot tooth specimen SCUMK-02 (*Pongo* sp.) that was prepared and analyzed for U/Th series dating. Relative distance is calculated from the EDJ to the extremity of the dental tissues between [-1;1], being respectively the enamel tip in contact with the sediment and the pulp cavity.

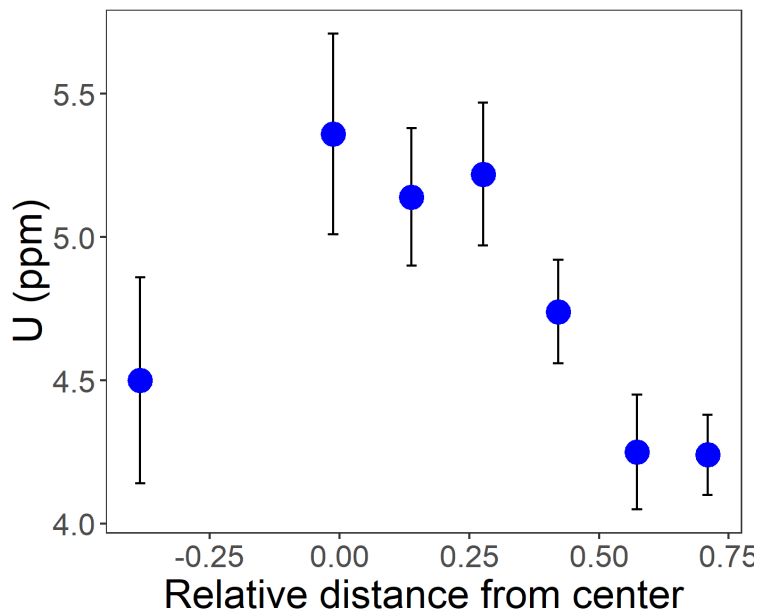


Figure S46. DAD model for the Tam Hay Marklot tooth specimen SCUMK-03A (*Bos* sp. (*Bos* cf. *frontalis*)) that was prepared and analyzed for U/Th series dating. Relative distance is calculated from the EDJ to the extremity of the dental tissues between [-1;1], being respectively the enamel tip in contact with the sediment and the pulp cavity.

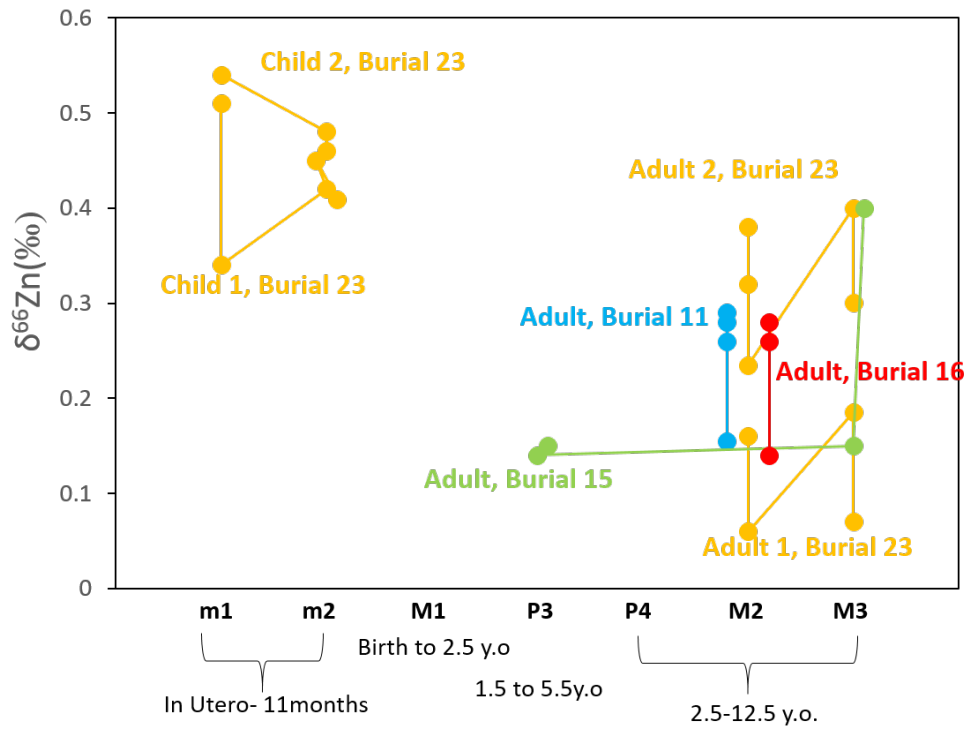


Figure S47. Zinc isotope composition in different teeth coming from the same Lapa do Santo individuals. Single enamel $\delta^{66}\text{Zn}$ measurements per tooth and of each individual are connected by a line. Burial 23 contains 4 individuals (yellow), while burials 11, 15 and 16 involve only one individual (blue, green and red respectively).

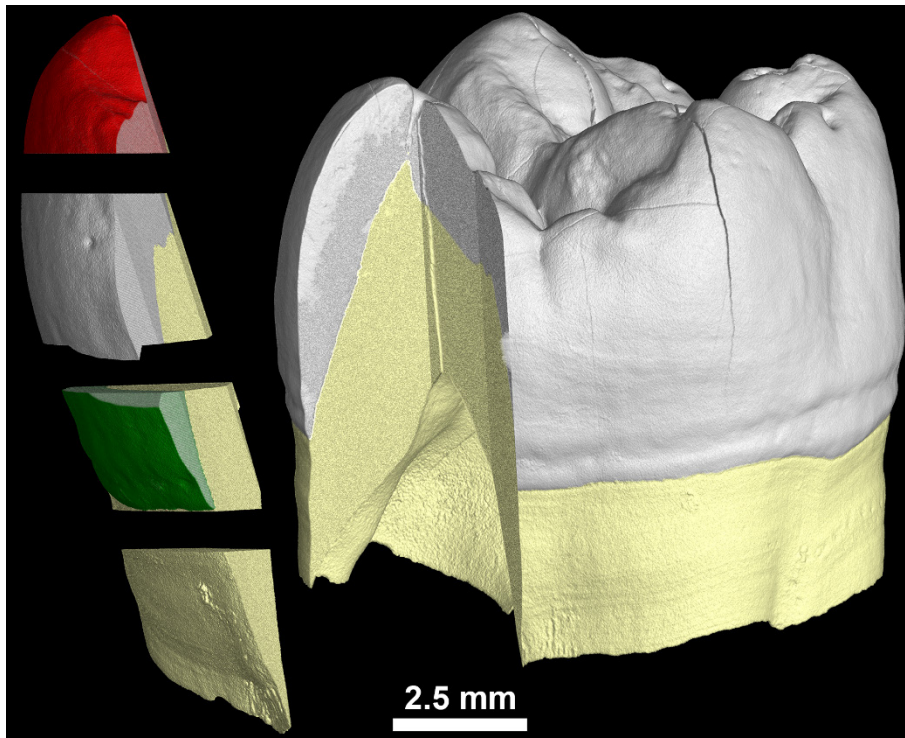


Figure S48. Three-dimensional model of the left permanent maxillary first molar (Specimen ID: SEVA 3598_3) of the Jacobins convent child showing the sampling strategy used for the zinc isotope analysis. A chunk of enamel and dentin is first detached from the crown using a pre-existing fracture (darker grey in the sectioned enamel). This piece of tooth is then cut in three sub-samples, from which the dentin will be removed to leave only the enamel to be used for the zinc analyses. The middle portion of the sample (natural colors) is preserved and was not used for analyses. The red subsample concerns the cuspal part of the crown and thus represents the earliest stages of enamel growth (until ~1.5 years), while the green subsample represents crown completion (~until 3 years of age).

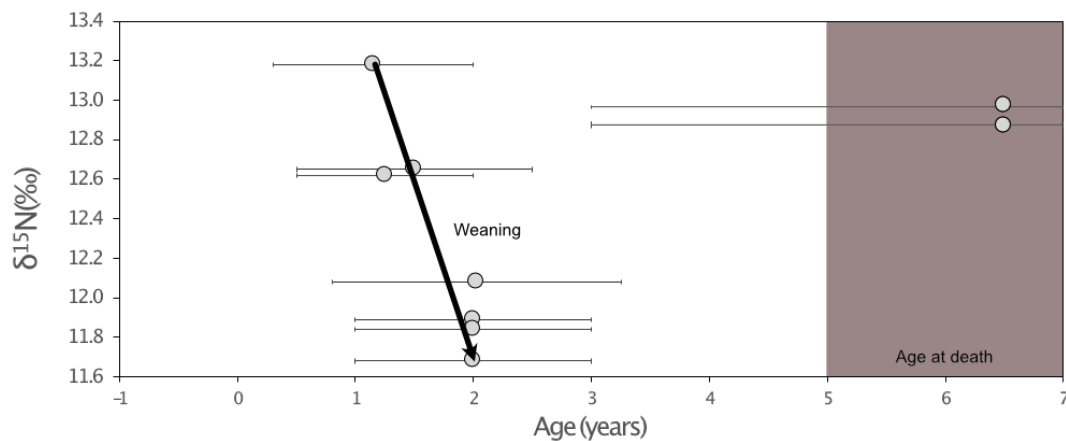


Figure S49. Nitrogen isotopes obtained on the tooth roots of the child 63949 (Jacobins convent, Rennes).

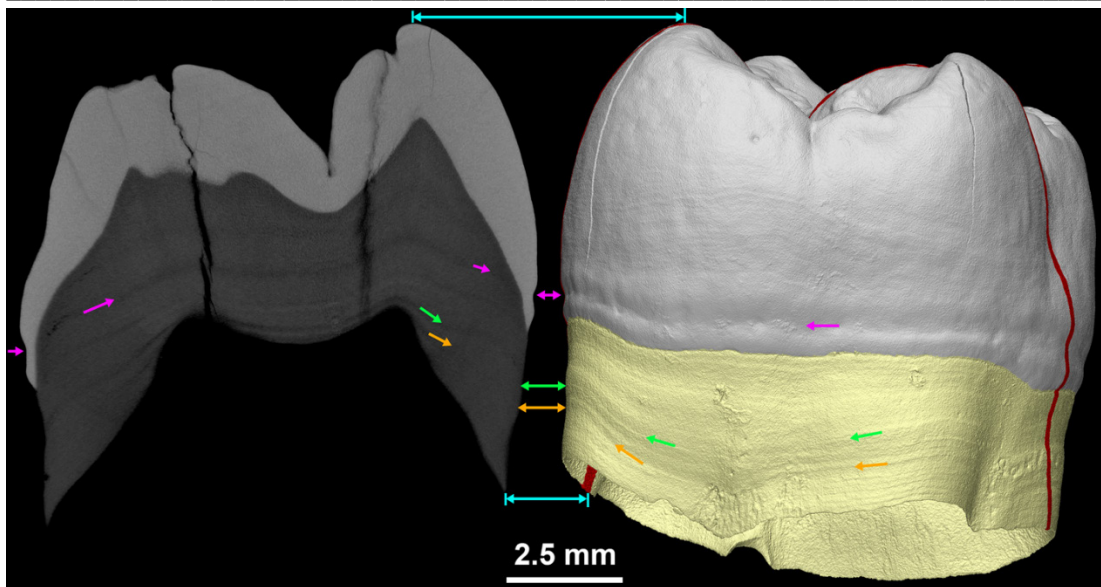


Figure S50. Matching of the stress events observed in the dentin on the 3D model of the lower left M1 of the child of the Jacobins convent and a 200 μm -thick virtual 2D section (taken where the red line is on the 3D model). The turquoise arrows show the perfect alignment of the virtual 2D section and the 3D model. A strong stress precedes crown completion (pink arrows in enamel and dentin) and produce a marked enamel hypoplasia on the enamel outer surface. From crown completion (~ 3 years) to death (~ 6 years), the child has undergone strong and chronic stress events (green and orange).

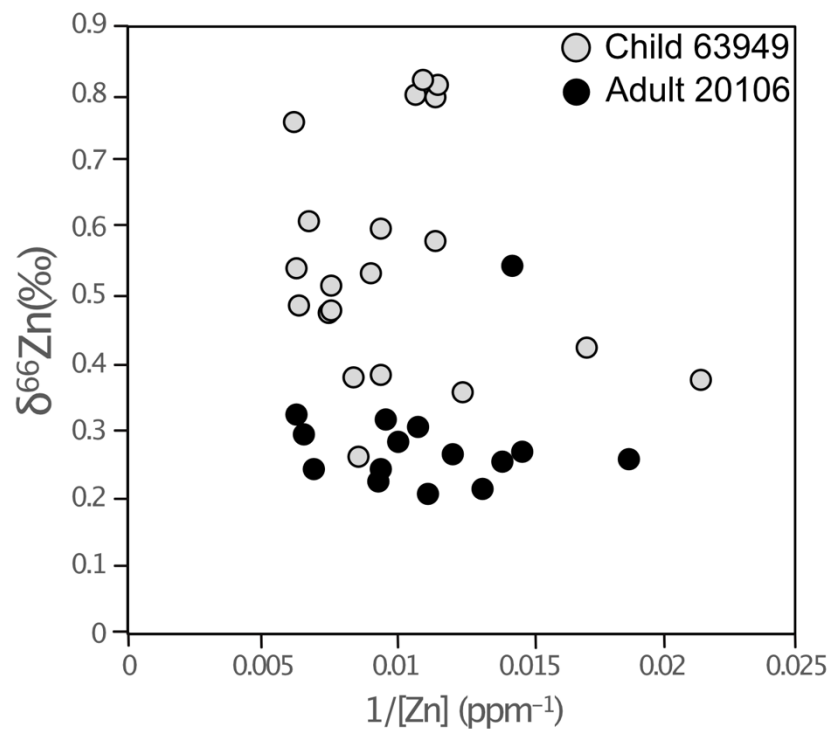


Figure S51. Relationship between zinc concentrations (ppm, as $\mu\text{g/g}$) and isotope ratios in the teeth of the child and the adult from the Jacobins convent.

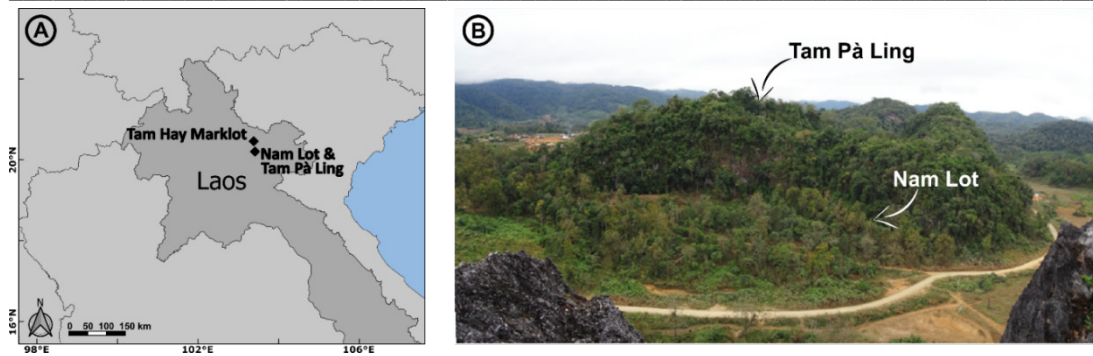


Figure S52. A) Map of Laos showing the geographical locations of the three fossiliferous Late Pleistocene karst cave sites of Tam Pà Ling, Nam Lot and Tam Hay Marklot (~50 km north of TPL and NL). B) Photograph of Pà Hang mountain (1170 m a.s.l), showing the close proximity (~150 m) of Tam Pà Ling and Nam Lot caves. Note that the *H. sapiens* TPL1 was found in the Tam Pà Ling cave.

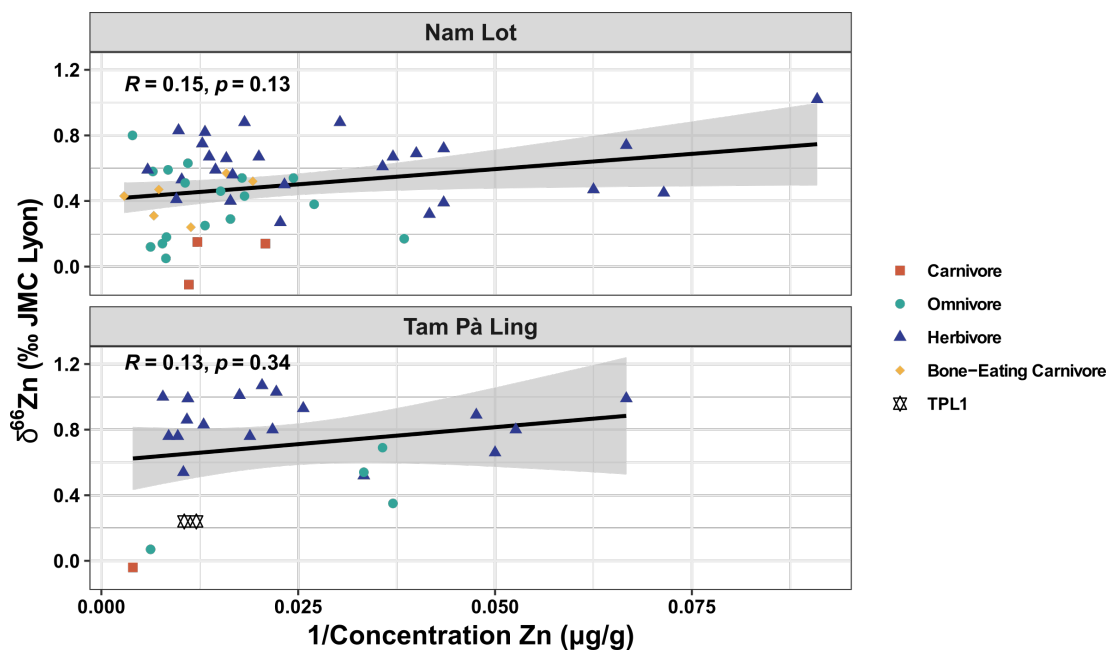


Figure S53. Non-significant relationship between the zinc concentration ($1/\text{Zn}$ concentration, $\mu\text{g/g}$) and $\delta^{66}\text{Zn}$ values in enamel of fossil teeth of carnivores (red squares), omnivores (turquoise circles), herbivores (blue triangles), bone-eating carnivore *C. crocuta* (yellow diamonds) and TPL1 individual (white six-pointed stars), from Nam Lot (top) and Tam Pà Ling (bottom) caves.

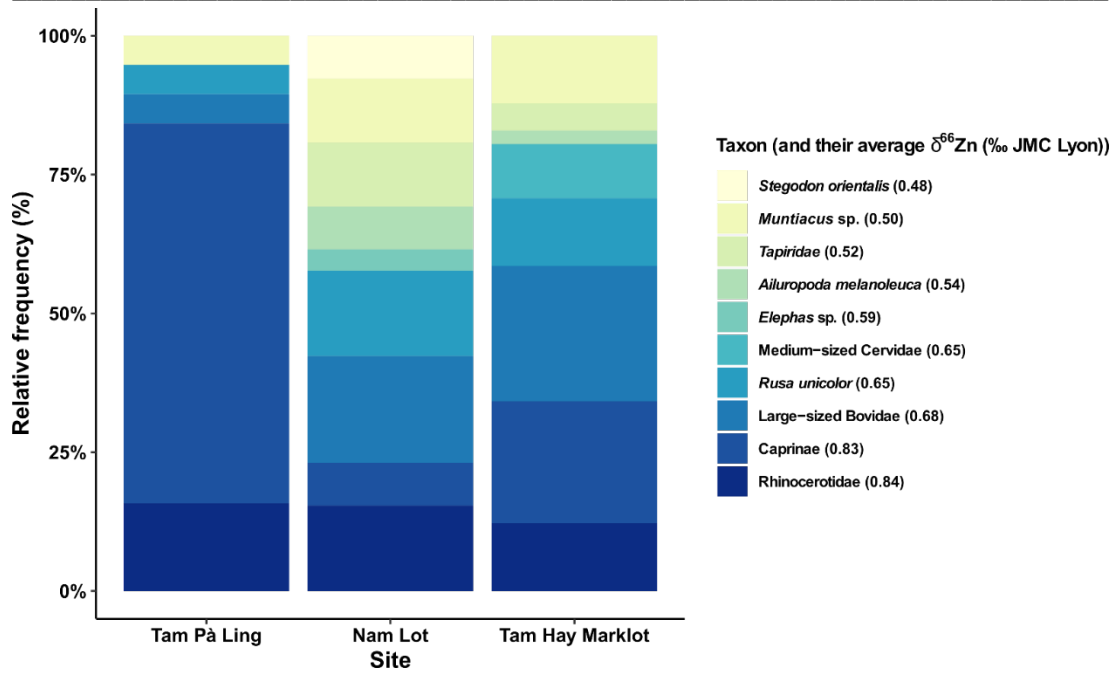


Figure S54. Relative frequency (%) of each herbivorous taxon from Tam Pà Ling (70–1.1 ka), Nam Lot (86–72 ka) and published data from Tam Hay Marklot (38.4–13.5 ka) (Bourgon et al., 2020), ordered by their overall across-sites average $\delta^{66}\text{Zn}$ values.

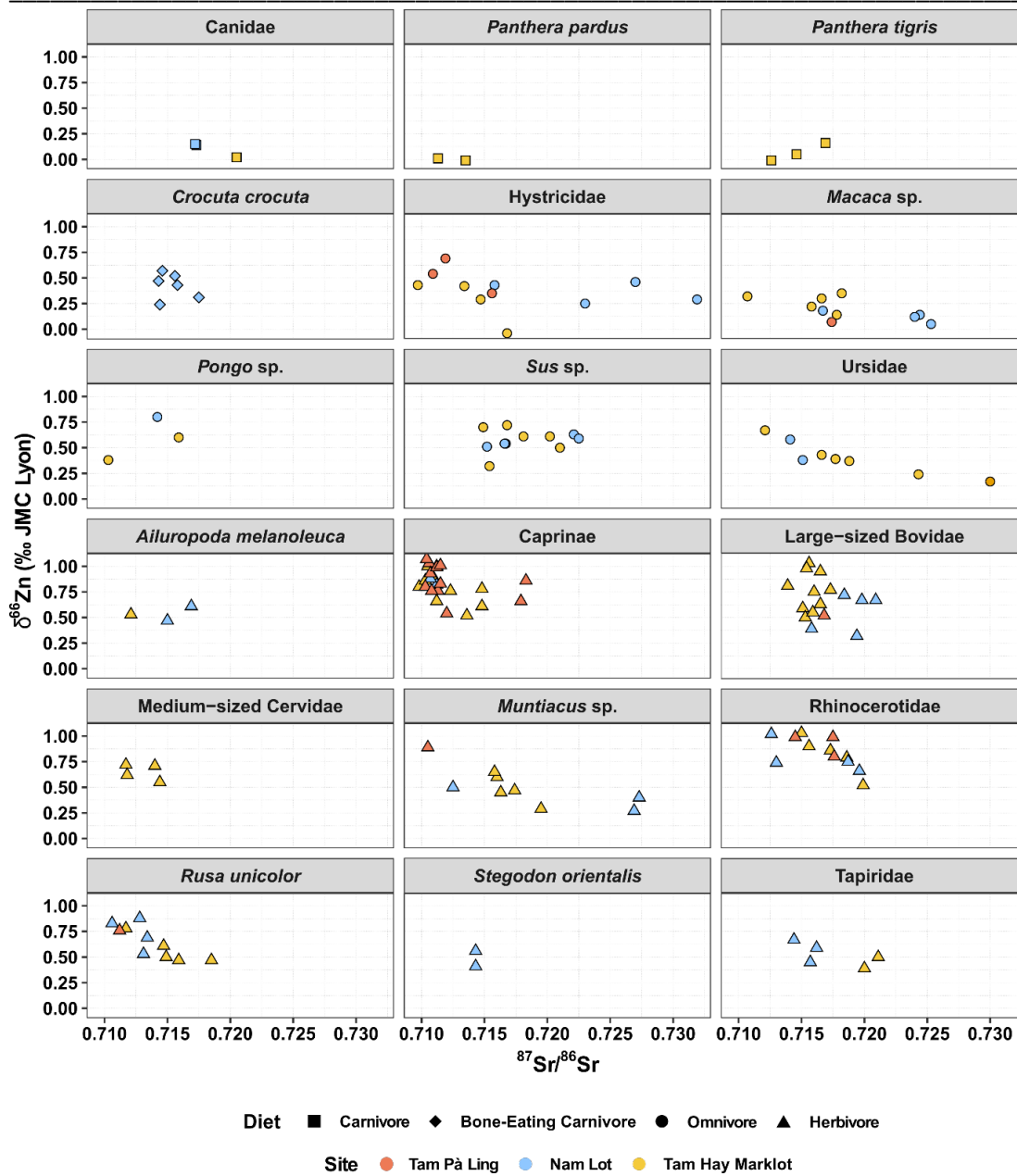


Figure S55. Distribution of radiogenic strontium isotope ratios ($^{87}\text{Sr}/^{86}\text{Sr}$) and zinc ($\delta^{66}\text{Zn}$) stable isotope values in enamel of fossil teeth of each taxon from the three Late Pleistocene cave sites (Laos) of Tam Pà Ling (orange), Nam Lot (blue) and published data from Tam Hay Marklot (Bourgon et al., 2020; yellow). Small-sized Felidae, large-sized Felidae, *Elephas* sp. and TPL1 were excluded here as they only have one $^{87}\text{Sr}/^{86}\text{Sr}$ observation each.

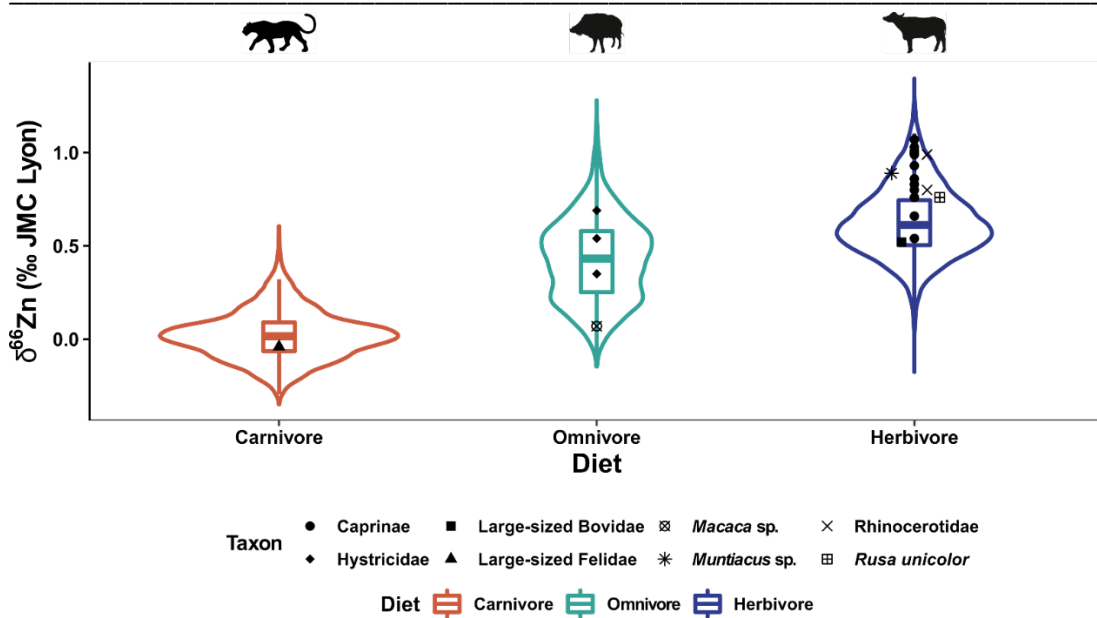


Figure S56. Violin plots of theoretical $\delta^{66}\text{Zn}$ values distribution for each dietary group and observed taxon and $\delta^{66}\text{Zn}$ values from TPL. Carnivore (red), omnivore (turquoise) and herbivore (blue). The plots illustrate the simulated theoretical $\delta^{66}\text{Zn}$ distribution for each dietary group. The observed $\delta^{66}\text{Zn}$ values for each taxon (point and shapes) from TPL are plotted on the violin plots to show where the TPL samples are located on the theoretical $\delta^{66}\text{Zn}$ distribution.

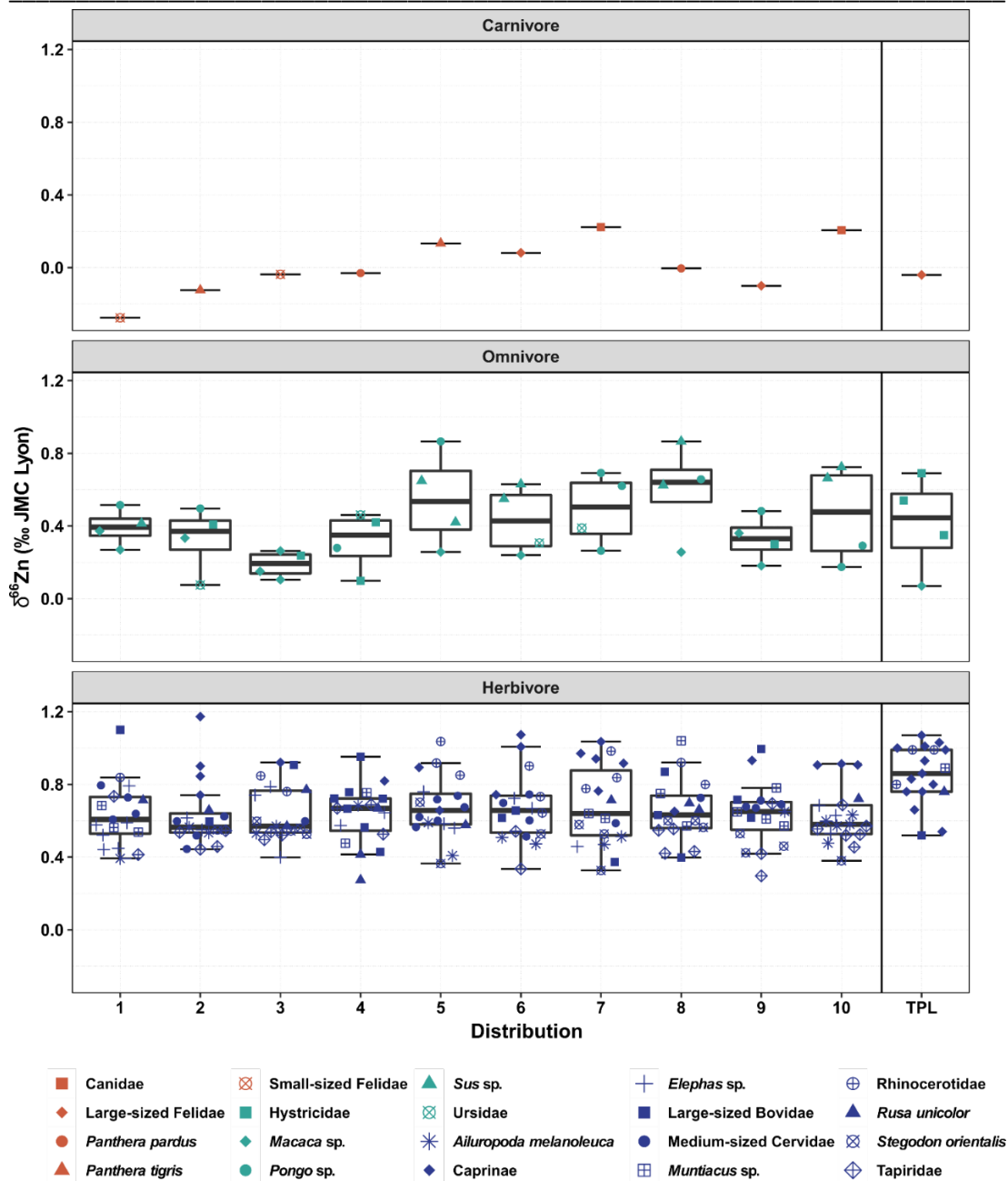


Figure S57. Box and whisker plots of distributions of simulated $\delta^{66}\text{Zn}$ datasets (simulation runs 1 to 10) with introduced missingness, compared to the distribution from the fossiliferous assemblage of Tam Pà Ling (TPL). The total number of specimen and the number of specimens per taxon mirror that of TPL, so that each simulation has 24 specimens and each taxon 1 to 15. The number of taxa per dietary category were randomly selected from the full dataset from Nam Lot, Tam Pà Ling and published data from Tam Hay Marklot (Bourgon et al., 2020). Carnivore (red), omnivore (turquoise) and herbivore (blue). The boxes represent the 25th–75th percentiles, with the median represented by a bold horizontal line.

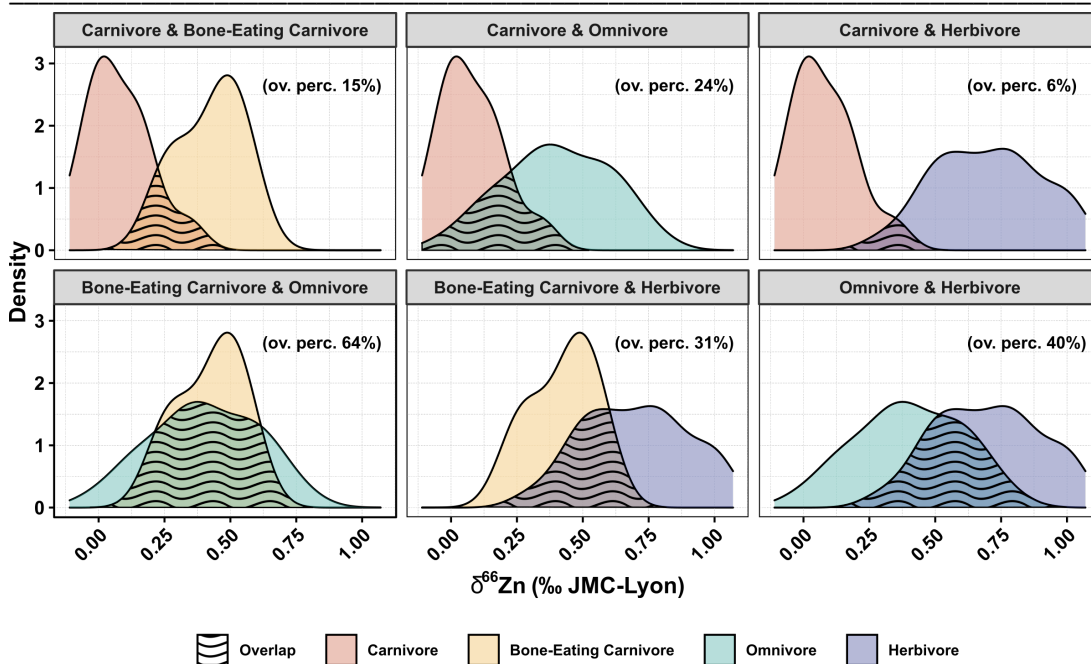


Figure S58. Proportion of overlap (as overlap percentage: ov. perc.) between overlapping area (represented by black wavy lines) of kernel density estimations for $\delta^{66}\text{Zn}$ values from each dietary category (carnivore = red, bone-eating carnivore *C. crocuta* = yellow, omnivores = turquoise, and herbivores = blue). ‘Overlapping’ can be defined as the area intersected by two (or more) probability density functions.

References

- Åberg, G., 1995. The use of natural strontium isotopes as tracers in environmental studies. *Water Air Soil Pollut.* 79, 309–322.
- Abrahams, P.W., 2013. Geophagy and the involuntary ingestion of soil. In: Selinus, O. (Ed.), *Essentials of medical geology: Revised edition*. Springer Netherlands, Dordrecht, pp. 433–454.
- Aiello, L.C., Wheeler, P., 1995. The expensive-tissue hypothesis: The brain and the digestive system in human and primate evolution. *Curr. Anthropol.* 36, 199–221.
- Albarède, F., Beard, B., 2004. Analytical methods for non-traditional isotopes. *Rev. Mineral. Geochem.* 55, 113–152.
- Albarède, F., Telouk, P., Lamboux, A., Jaouen, K., Balter, V., 2011. Isotopic evidence of unaccounted for Fe and Cu erythropoietic pathways. *Metallomics.* 3, 926–933.
- AlQahtani, S.J., Hector, M.P., Liversidge, H.M., 2010. Brief communication: The London atlas of human tooth development and eruption. *Am. J. Phys. Anthropol.* 142, 481–490.
- Ambrose, S.H., 1986. Stable carbon and nitrogen isotope analysis of human and animal diet in Africa. *J. Hum. Evol.* 15, 707–731.
- Ambrose, S.H., 1990. Preparation and characterization of bone and tooth collagen for isotopic analysis. *J. Archaeol. Sci.* 17, 431–451.
- Ambrose, S.H., 1991. Effects of diet, climate and physiology on nitrogen isotope abundances in terrestrial foodwebs. *J. Archaeol. Sci.* 18, 293–317.
- Ambrose, S.H., 2002. Controlled diet and climate experiments on nitrogen isotope ratios of rats. In: Ambrose, S.H., Katzenberg, M.A. (Eds.), *Biogeochemical*

- approaches to paleodietary analysis, *Advances in archaeological and museum science*. Springer, Boston, pp. 243–259.
- Ambrose, S.H., DeNiro, M.J., 1986. The isotopic ecology of East African mammals. *Oecologia*. 69, 395–406.
- Ambrose, S.H., Norr, L., 1993. Experimental evidence for the relationship of the carbon isotope ratios of whole diet and dietary protein to those of bone collagen and carbonate. In: Lambert, J.B., Grupe, G. (Eds.), *Prehistoric human bone: Archaeology at the molecular level*. Springer Berlin, Heidelberg, pp. 1–37.
- Amundson, R., Austin, A.T., Schuur, E. a. G., Yoo, K., Matzek, V., Kendall, C., Uebersax, A., Brenner, D., Baisden, W.T., 2003. Global patterns of the isotopic composition of soil and plant nitrogen. *Global Biogeochem. Cycles*. 17.
- Anbar, A.D., Rouxel, O., 2007. Metal stable isotopes in paleoceanography. *Annu. Rev. Earth Planet. Sci.* 35, 717–746.
- Andreini, C., Banci, L., Bertini, I., Rosato, A., 2006. Counting the zinc-proteins encoded in the human genome. *J. Proteome Res.* 5, 196–201.
- Aramendía, M., Rello, L., Resano, M., Vanhaecke, F., 2013. Isotopic analysis of Cu in serum samples for diagnosis of Wilson's disease: A pilot study. *J. Anal. At. Spectrom.* 28, 675–681.
- Aranibar, J.N., Anderson, I.C., Epstein, H.E., Feral, C.J.W., Swap, R.J., Ramontsho, J., Macko, S.A., 2008. Nitrogen isotope composition of soils, C₃ and C₄ plants along land use gradients in southern Africa. *J. Arid Environ.* 72, 326–337.
- Arnold Tim, Kirk Guy J. D., Wissuwa Matthias, Frei Michael, Zhao Fang-Jie, Mason Thomas F. D., Weiss Dominik J., 2009. Evidence for the mechanisms of zinc uptake by rice using isotope fractionation. *Plant Cell Environ.* 33, 370–381.
- Arnold, J.R., Libby, W.F., 1949. Age determinations by radiocarbon content: Checks with samples of known age. *Science*. 110, 678–680.
- Aucour, A.M., Pichat, S., Macnair, M.R., Oger, P., 2011. Fractionation of stable zinc isotopes in the zinc hyperaccumulator *Arabidopsis halleri* and nonaccumulator *Arabidopsis petraea*. *Environ. Sci. Technol.* 45, 9212–9217.
- Aucour, A.-M., Bedell, J.-P., Queyron, M., Magnin, V., Testemale, D., Sarret, G., 2015. Dynamics of Zn in an urban wetland soil–plant system: Coupling isotopic and EXAFS approaches. *Geochim. Cosmochim. Acta.* 160, 55–69.

- Ayliffe, L.K., Chivas, A.R., 1990. Oxygen isotope composition of the bone phosphate of Australian kangaroos: Potential as a palaeoenvironmental recorder. *Geochim. Cosmochim. Acta.* 54, 2603–2609.
- Baayen, R.H., 2008. *Analyzing linguistic data: A practical introduction to statistics using R*, 1st ed. Cambridge University Press, Cambridge.
- Bacon, A.-M., Demeter, F., Düringer, P., Helm, C., Bano, M., Vu The Long, Kim Thuy, N.T., Antoine, P.-O., Thi Mai, B., Huong, N.T.M., Dodo, Y., Chabaux, F., Rihs, S., 2008. The Late Pleistocene Duoi U’Oi cave in northern Vietnam: Palaeontology, sedimentology, taphonomy and palaeoenvironments. *Quat. Sci. Rev.* 27, 1627–1654.
- Bacon, A.-M., Düringer, P., Antoine, P.-O., Demeter, F., Shackelford, L., Sayavongkhamdy, T., Sichanthongtip, P., Khamdalavong, P., Nokhamaomphu, S., Sysuphanh, V., Patole-Edoumba, E., Chabaux, F., Pelt, E., 2011. The Middle Pleistocene mammalian fauna from Tam Hang karstic deposit, northern Laos: New data and evolutionary hypothesis. *Quat. Int.* 245, 315–332.
- Bacon, A.-M., Westaway, K., Antoine, P.-O., Düringer, P., Blin, A., Demeter, F., Ponche, J.-L., Zhao, J.-X., Barnes, L.M., Sayavonkhamdy, T., Thuy, N.T.K., Long, V.T., Patole-Edoumba, E., Shackelford, L., 2015. Late Pleistocene mammalian assemblages of Southeast Asia: New dating, mortality profiles and evolution of the predator–prey relationships in an environmental context. *Palaeogeogr. Palaeoclimatol. Palaeoecol.* 422, 101–127.
- Bacon, A.-M., Bourgon, N., Dufour, E., Zanolli, C., Düringer, P., Ponche, J.-L., Antoine, P.-O., Shackelford, L., Huong, N.T.M., Sayavonkhamdy, T., Patole-Edoumba, E., Demeter, F., 2018a. Nam Lot (MIS 5) and Duoi U’Oi (MIS 4) Southeast Asian sites revisited: Zooarchaeological and isotopic evidences. *Palaeogeogr. Palaeoclimatol. Palaeoecol.* 512, 132–144.
- Bacon, A.-M., Düringer, P., Westaway, K., Joannes-Boyau, R., Zhao, J., Bourgon, N., Dufour, E., Pheng, S., Tep, S., Ponche, J.-L., Barnes, L., Blin, A., Patole-Edoumba, E., Demeter, F., 2018b. Testing the savannah corridor hypothesis during MIS2: The Boh Dambang hyena site in southern Cambodia. *Quat. Int.* 464, 417–439.

- Bacon, A.-M., Antoine, P.-O., Huong, N.T.M., Westaway, K., Tuan, N.A., Durringer, P., Zhao, J., Ponche, J.-L., Dung, S.C., Nghia, T.H., Minh, T.T., Son, P.T., Boyon, M., Thuy, N.T.K., Blin, A., Demeter, F., 2018c. A rhinocerotid-dominated megafauna at the MIS6-5 transition: The late Middle Pleistocene Coc Muoi assemblage, Lang Son province, Vietnam. *Quat. Sci. Rev.* 186, 123–141.
- Badoux, D.M., 1959. Fossil mammals from two deposits at Punung (Java) (Doctoral dissertation). Utrecht University (Kemink en Zoon, N.V).
- Bae, C.J., Douka, K., Petraglia, M.D., 2017. On the origin of modern humans: Asian perspectives. *Science* 358.
- Bahuchet, S., McKey, D., de Garine, I., 1991. Wild yams revisited: Is independence from agriculture possible for rain forest hunter-gatherers? *Hum. Ecol.* 19, 213–243.
- Bailey, R.C., Head, G., Jenike, M., Owen, B., Rechtman, R., Zechenter, E., 1989. Hunting and gathering in tropical rain forest: Is it possible? *Am. Anthropol.* 91, 59–82.
- Bailey, R.C., Headland, T.N., 1991. The tropical rain forest: Is it a productive environment for human foragers? *Hum. Ecol.* 19, 261–285.
- Balasse, M., 2002. Reconstructing dietary and environmental history from enamel isotopic analysis: Time resolution of intra-tooth sequential sampling. *Int. J. Osteoarchaeol.* 12, 155–165.
- Balée, W.L., 1999. Footprints of the forest: Ka'apar ethnobotany - The historical ecology of plant utilization by an Amazonian people. Columbia University Press, New York.
- Ballari, S.A., Barrios-García, M.N., 2014. A review of wild boar *Sus scrofa* diet and factors affecting food selection in native and introduced ranges. *Mamm. Rev.* 44, 124–134.
- Balter, V., Bocherens, H., Person, A., Labourdette, N., Renard, M., Vandermeersch, B., 2002. Ecological and physiological variability of Sr/Ca and Ba/Ca in mammals of West European mid-Würmian food webs. *Palaeogeogr. Palaeoclimatol. Palaeoecol.* 186, 127–143.

- Balter, V., Zazzo, A., Moloney, A.P., Moynier, F., Schmidt, O., Monahan, F.J., Albarède, F., 2010. Bodily variability of zinc natural isotope abundances in sheep. *Rapid Commun. Mass Spectrom.* 24, 605–612.
- Balter, V., Braga, J., Télouk, P., Thackeray, J.F., 2012. Evidence for dietary change but not landscape use in South African early hominins. *Nature.* 489, 558–560.
- Balter, V., Lamboux, A., Zazzo, A., Télouk, P., Leverrier, Y., Marvel, J., P. Moloney, A., J. Monahan, F., Schmidt, O., Albarède, F., 2013. Contrasting Cu, Fe, and Zn isotopic patterns in organs and body fluids of mice and sheep, with emphasis on cellular fractionation. *Metallomics* 5, 1470–1482.
- Balter, V., Costa, A.N. da, Bondanese, V.P., Jaouen, K., Lamboux, A., Sangrajrang, S., Vincent, N., Fourel, F., Télouk, P., Gigou, M., Lécuyer, C., Srivatanakul, P., Bréchet, C., Albarède, F., Hainaut, P., 2015. Natural variations of copper and sulfur stable isotopes in blood of hepatocellular carcinoma patients. *Proc. Natl. Acad. Sci. U.S.A.* 112, 982–985.
- Balter, V., Martin, J.E., Tacail, T., Suan, G., Renaud, S., Girard, C., 2019. Calcium stable isotopes place Devonian conodonts as first level consumers. *Geochem. Perspect. Lett.* 10, 36–39.
- Barker, G., Barton, H., Bird, M., Daly, P., Datan, I., Dykes, A., Farr, L., Gilbertson, D., Harrison, B., Hunt, C., Higham, T., Kealhofer, L., Krigbaum, J., Lewis, H., McLaren, S., Paz, V., Pike, A., Piper, P., Pyatt, B., Rabett, R., Reynolds, T., Rose, J., Rushworth, G., Stephens, M., Stringer, C., Thompson, J., Turney, C., 2007. The ‘human revolution’ in lowland tropical Southeast Asia: The antiquity and behavior of anatomically modern humans at Niah Cave (Sarawak, Borneo). *J. Hum. Evol.* 52, 243–261.
- Barr, D.J., Levy, R., Scheepers, C., Tily, H.J., 2013. Random effects structure for confirmatory hypothesis testing: Keep it maximal. *J. Mem. Lang.* 68, 255–278.
- Barrios-Garcia, M.N., Ballari, S.A., 2012. Impact of wild boar (*Sus scrofa*) in its introduced and native range: A review. *Biol. Invasions* 14, 2283–2300.
- Barton, H., 2005. The case for rainforest foragers: The starch record at Niah Cave, Sarawak. *Asian Perspect.* 44, 56–72.

- Barton, H., Piper, P.J., Rabett, R., Reeds, I., 2009. Composite hunting technologies from the Terminal Pleistocene and Early Holocene, Niah Cave, Borneo. *J. Archaeol. Sci.* 36, 1708–1714.
- Basu, S., Agrawal, S., Sanyal, P., Mahato, P., Kumar, S., Sarkar, A., 2015. Carbon isotopic ratios of modern C₃–C₄ plants from the Gangetic Plain, India and its implications to paleovegetational reconstruction. *Palaeogeogr. Palaeoclimatol. Palaeoecol.* 440, 22–32.
- Bataille, C.P., Holstein, I.C.C. von, Laffoon, J.E., Willmes, M., Liu, X.-M., Davies, G.R., 2018. A bioavailable strontium isoscape for Western Europe: A machine learning approach. *PLoS ONE.* 13, e0197386.
- Bates, D., Mächler, M., Bolker, B., Walker, S., 2015. Fitting linear mixed-effects models using lme4. *J. Stat. Softw.* 67, 1–48.
- Bentley, R.A., 2006. Strontium isotopes from the earth to the archaeological skeleton: A review. *J. Archaeol. Method Theory.* 13, 135–187.
- Berg, J.M., Shi, Y., 1996. The galvanization of biology: A growing appreciation for the roles of zinc. *Science.* 271, 1081–1085.
- Beyer, W.N., Connor, E.E., Gerould, S., 1994. Estimates of soil ingestion by wildlife. *J. Wildl. Manage.* 58, 375–382.
- Bird, M.I., Taylor, D., Hunt, C., 2005. Palaeoenvironments of insular Southeast Asia during the Last Glacial Period: A savanna corridor in Sundaland? *Quat. Sci. Rev.* 24, 2228–2242.
- Black, J.R., Epstein, E., Rains, W.D., Yin, Q., Casey, W.H., 2008. Magnesium-isotope fractionation during plant growth. *Environ. Sci. Technol.* 42, 7831–7836.
- Blumenthal, S.A., Rothman, J.M., Chritz, K.L., Cerling, T.E., 2016. Stable isotopic variation in tropical forest plants for applications in primatology. *Am. J. Primatol.* 78, 1041–1054.
- Bocherens, H., Fizet, M., Mariotti, A., Lange-Badre, B., Vandermeersch, B., Borel, J.P., Bellon, G., 1991. Isotopic biogeochemistry (¹³C, ¹⁵N) of fossil vertebrate collagen: Application to the study of a past food web including Neandertal man. *J. Hum. Evol.* 20, 481–492.

- Bocherens, H., Brinkman, D.B., Dauphin, Y., Mariotti, A., 1994. Microstructural and geochemical investigations on Late Cretaceous archosaur teeth from Alberta, Canada. *Can. J. Earth Sci.* 31, 783–792.
- Bocherens, H., Billiou, D., Mariotti, A., Patou-Mathis, M., Otte, M., Bonjean, D., Toussaint, M., 1999. Palaeoenvironmental and palaeodietary implications of isotopic biogeochemistry of Last Interglacial Neanderthal and mammal bones in Scladina Cave (Belgium). *J. Archaeol. Sci.* 26, 599–607.
- Bocherens, H., Drucker, D., 2003. Trophic level isotopic enrichment of carbon and nitrogen in bone collagen: Case studies from recent and ancient terrestrial ecosystems. *Int. J. Osteoarchaeol.* 13, 46–53.
- Bocherens, H., Drucker, D.G., Billiou, D., Patou-Mathis, M., Vandermeersch, B., 2005. Isotopic evidence for diet and subsistence pattern of the Saint-Césaire I Neanderthal: Review and use of a multi-source mixing model. *J. Hum. Evol.* 49, 71–87.
- Bohlke, J.K., Gwinn, C.J., Coplen, T.B., 1993. New reference materials for nitrogen-isotope-ratio measurements. *Geostand. Newsl.* 17, 159–164.
- Boivin, N., Fuller, D.Q., Dennell, R., Allaby, R., Petraglia, M.D., 2013. Human dispersal across diverse environments of Asia during the Upper Pleistocene. *Quat. Int.* 300, 32–47.
- Bourgon, N., Jaouen, K., Bacon, A.-M., Jochum, K.P., Dufour, E., Düringer, P., Ponche, J.-L., Joannes-Boyau, R., Boesch, Q., Antoine, P.-O., Hullot, M., Weis, U., Schulz-Kornas, E., Trost, M., Fiorillo, D., Demeter, F., Patole-Edoumba, E., Shackelford, L.L., Dunn, T.E., Zachwieja, A., Duangthongchit, S., Sayavonkhamdy, T., Sichanthongtip, P., Sihanam, D., Souksavatdy, V., Hublin, J.-J., Tütken, T., 2020. Zinc isotopes in Late Pleistocene fossil teeth from a Southeast Asian cave setting preserve paleodietary information. *Proc. Natl. Acad. Sci. U.S.A.* 117, 4675–4681.
- Braun, D.R., Harris, J.W.K., Levin, N.E., McCoy, J.T., Herries, A.I.R., Bamford, M.K., Bishop, L.C., Richmond, B.G., Kibunjia, M., 2010. Early hominin diet included diverse terrestrial and aquatic animals 1.95 Ma in East Turkana, Kenya. *Proc. Natl. Acad. Sci. U.S.A.* 107, 10002–10007.
- Britton, K., Grimes, V., Dau, J., Richards, M.P., 2009. Reconstructing faunal migrations using intra-tooth sampling and strontium and oxygen isotope

- analyses: A case study of modern caribou (*Rangifer tarandus granti*). *J. Archaeol. Sci.* 36, 1163–1172.
- Bromage, T.G., Hogg, R.T., Lacruz, R.S., Hou, C., 2012. Primate enamel evinces long period biological timing and regulation of life history. *J. Theor. Biol.* 305, 131–144.
- Brosius, J.P., 1991. Foraging in tropical rain forests: The case of the penan of Sarawak, East Malaysia (Borneo). *Hum. Ecol.* 19, 123–150.
- Brown, K.H., Rivera, J.A., Bhutta, Z., Gibson, R.S., King, J.C., Lönnnerdal, B., Ruel, M.T., Sandtröm, B., Wasantwisut, E., Hotz, C., 2004. International Zinc Nutrition Consultative Group (IZiNCG) technical document #1: Assessment of the risk of zinc deficiency in populations and options for its control. *Food Nutr. Bull.* 25, S99-203.
- Brumm, A., van den Bergh, G.D., Storey, M., Kurniawan, I., Alloway, B.V., Setiawan, R., Setiyabudi, E., Grün, R., Moore, M.W., Yurnaldi, D., Puspaningrum, M.R., Wibowo, U.P., Insani, H., Sutisna, I., Westgate, J.A., Pearce, N.J.G., Duval, M., Meijer, H.J.M., Aziz, F., Sutikna, T., Kaars, S. van der, Flude, S., Morwood, M.J., 2016. Age and context of the oldest known hominin fossils from Flores. *Nature.* 534, 249–253.
- Bryant, J.D., Luz, B., Froelich, P.N., 1994. Oxygen isotopic composition of fossil horse tooth phosphate as a record of continental paleoclimate. *Palaeogeogr. Palaeoclimatol. Palaeoecol.* 107, 303–316.
- Bryant, J.D., Froelich, P.N., 1995. A model of oxygen isotope fractionation in body water of large mammals. *Geochim. Cosmochim. Acta.* 59, 4523–4537.
- Buchmann, N., Guehl, J.-M., Barigah, T.S., Ehleringer, J.R., 1997. Interseasonal comparison of CO₂ concentrations, isotopic composition, and carbon dynamics in an Amazonian rainforest (French Guiana). *Oecologia.* 110, 120–131.
- Buchmann, N., Ehleringer, J.R., 1998. CO₂ concentration profiles, and carbon and oxygen isotopes in C₃ and C₄ crop canopies. *Agric. For. Meteorol.* 89, 45–58.
- Budd, P., Montgomery, J., Barreiro, B., Thomas, R.G., 2000. Differential diagenesis of strontium in archaeological human dental tissues. *J. Appl. Geochem.* 15, 687–694.

- Bueno, L. de M.R., Isnardis, A., 2017. Lithic technology in Lagoa Santa in the Early Holocene. In: Da-Gloria, P., Neves, W.A., Hubbe, M. (Eds.), *Archaeological and paleontological research in Lagoa Santa: The quest for the First Americans*. Springer International Publishing, Cham, pp. 345–371.
- Burton, J.H., Price, T.D., Middleton, W.D., 1999. Correlation of bone Ba/Ca and Sr/Ca due to biological purification of calcium. *J. Archaeol. Sci.* 26, 609–616.
- Caldelas, C., Weiss, D.J., 2017. Zinc homeostasis and isotopic fractionation in plants: A review. *Plant Soil.* 411, 17–46.
- Casey, M.M., Post, D.M., 2011. The problem of isotopic baseline: Reconstructing the diet and trophic position of fossil animals. *Earth-Sci. Rev.* 106, 131–148.
- Cerling, T.E., Harris, J.M., Ambrose, S.H., Leakey, M.G., Solounias, N., 1997. Dietary and environmental reconstruction with stable isotope analyses of herbivore tooth enamel from the Miocene locality of Fort Ternan, Kenya. *J. Hum. Evol.* 33, 635–650.
- Cerling, T.E., Harris, J.M., 1999. Carbon isotope fractionation between diet and bioapatite in ungulate mammals and implications for ecological and paleoecological studies. *Oecologia.* 120, 347–363.
- Cerling, T.E., Hart, J.A., Hart, T.B., 2004. Stable isotope ecology in the Ituri Forest. *Oecologia.* 138, 5–12.
- Cerling, T.E., Andanje, S.A., Blumenthal, S.A., Brown, F.H., Chritz, K.L., Harris, J.M., Hart, J.A., Kirera, F.M., Kaleme, P., Leakey, L.N., Leakey, M.G., Levin, N.E., Manthi, F.K., Passey, B.H., Uno, K.T., 2015. Dietary changes of large herbivores in the Turkana Basin, Kenya from 4 to 1 Ma. *Proc. Natl. Acad. Sci. U.S.A.* 112, 11467–11472.
- Chisholm, B.S., Nelson, D.E., Schwarcz, H.P., 1982. Stable-carbon isotope ratios as a measure of marine *versus* terrestrial protein in ancient diets. *Science.* 216, 1131–1132.
- Dean, C. M., 2006. Tooth microstructure tracks the pace of human life-history evolution. *Proc. Royal Soc. B.* 273, 2799–2808.
- Chu, N.-C., Henderson, G.M., Belshaw, N.S., Hedges, R.E.M., 2006. Establishing the potential of Ca isotopes as proxy for consumption of dairy products. *J. Appl. Geochem.* 21, 1656–1667.

- Clarkson, C., Petraglia, M., Korisettar, R., Haslam, M., Boivin, N., Crowther, A., Ditchfield, P., Fuller, D., Miracle, P., Harris, C., Connell, K., James, H., Koshy, J., 2009. The oldest and longest enduring microlithic sequence in India: 35 000 years of modern human occupation and change at the Jwalapuram Locality 9 rockshelter. *Antiquity* 83, 326–348.
- Clayton, F., Sealy, J., Pfeiffer, S., 2006. Weaning age among foragers at Matjes River rock shelter, South Africa, from stable nitrogen and carbon isotope analyses. *Am. J. Phys. Anthropol.* 129, 311–317.
- Cloquet, C., Carignan, J., Lehmann, M.F., Vanhaecke, F., 2008. Variation in the isotopic composition of zinc in the natural environment and the use of zinc isotopes in biogeosciences: A review. *Anal. Bioanal. Chem.* 390, 451–463.
- Codron, D., Sponheimer, M., Codron, J., Newton, I., Lanham, J.L., Clauss, M., 2012. The confounding effects of source isotopic heterogeneity on consumer–diet and tissue–tissue stable isotope relationships. *Oecologia*. 169, 939–953.
- Colbert, E.H., Hooijer, D.A., 1953. Pleistocene mammals from the limestone fissures of Szechwan, China. *Bull. Am. Mus. Nat.* 7–134.
- Colleter, R., Clavel, B., Pietrzak, A., Duchesne, S., Schmitt, L., Richards, M.P., Telmon, N., Crubézy, É., Jaouen, K., 2019. Social status in late medieval and early modern Brittany: Insights from stable isotope analysis. *Archaeol. Anthropol. Sci.* 11, 823–837.
- Copeland, S.R., Sponheimer, M., Roux, P.J. le, Grimes, V., Lee-Thorp, J.A., Ruiters, D.J. de, Richards, M.P., 2008. Strontium isotope ratios ($^{87}\text{Sr}/^{86}\text{Sr}$) of tooth enamel: A comparison of solution and laser ablation multicollector inductively coupled plasma mass spectrometry methods. *Rapid Commun. Mass Spectrom.* 22, 3187–3194.
- Copeland, S.R., Sponheimer, M., de Ruiters, D.J., Lee-Thorp, J.A., Codron, D., le Roux, P.J., Grimes, V., Richards, M.P., 2011. Strontium isotope evidence for landscape use by early hominins. *Nature*. 474, 76–78.
- Coplen, T.B., Brand, W.A., Gehre, M., Gröning, M., Meijer, H.A.J., Toman, B., Verkouteren, R.M., 2006. New Guidelines for $\delta^{13}\text{C}$ Measurements. *Anal. Chem.* 78, 2439–2441.

- Costas-Rodríguez, M., Van Heghe, L., Vanhaecke, F., 2014. Evidence for a possible dietary effect on the isotopic composition of Zn in blood via isotopic analysis of food products by multi-collector ICP-mass spectrometry. *Metallomics*. 6, 139–146.
- Cousins, R.J., 1985. Absorption, transport, and hepatic metabolism of copper and zinc: Special reference to metallothionein and ceruloplasmin. *Physiol. Rev.* 65, 238–309.
- Da-Gloria, P., Larsen, C.S., 2014. Oral health of the Paleoamericans of Lagoa Santa, central Brazil. *Am. J. Phys. Anthropol.* 154, 11–26.
- Dansgaard, W., 1964. Stable isotopes in precipitation. *Tellus*. 16, 436–468.
- Dasch, E.J., 1969. Strontium isotopes in weathering profiles, deep-sea sediments, and sedimentary rocks. *Geochim. Cosmochim. Acta.* 33, 1521–1552.
- Dauphin, Y., Williams, C.T., 2004. Diagenetic trends of dental tissues. *C. R. Palevol.* 3, 583–590.
- Davidsson, L., Almgren, A., Sandström, B., Juillerat, M.E.-A., Hurrell, R.F., 1996. Zinc absorption in adult humans: The effect of protein sources added to liquid test meals. *Br. J. Nutr.* 75, 607–613.
- de Vos, J., Long, V.T., 1993. Systematic discussion of the Lang Trang fauna, Unpublished Report.
- Dean, C., Le Cabec, A., Spiers, K., Zhang, Y., Garrevoet, J., 2018. Incremental distribution of strontium and zinc in great ape and fossil hominin cementum using synchrotron X-ray fluorescence mapping. *J. R. Soc. Interface* 15, 20170626.
- Demeter, F., Shackelford, L., Westaway, K., Barnes, L., Durringer, P., Ponche, J.-L., Dumoncel, J., Sénégas, F., Sayavongkhamdy, T., Zhao, J.-X., Sichanthongtip, P., Patole-Edoumba, E., Dunn, T., Zachwieja, A., Coppens, Y., Willerslev, E., Bacon, A.-M., 2017. Early modern humans from Tam Pà Ling, Laos: Fossil review and perspectives. *Curr. Anthropol.* 58, S527–S538.
- Demeter, F., Shackelford, L., Westaway, K., Durringer, P., Bacon, A.-M., Ponche, J.-L., Wu, X., Sayavongkhamdy, T., Zhao, J.-X., Barnes, L., Boyon, M., Sichanthongtip, P., Sénégas, F., Karpoff, A.-M., Patole-Edoumba, E., Coppens, Y., Braga, J., 2015. Early modern humans and morphological

- variation in Southeast Asia: Fossil evidence from Tam Pa Ling, Laos. *PLoS ONE* 10, e0121193.
- Demeter, F., Shackelford, L.L., Bacon, A.-M., Durringer, P., Westaway, K., Sayavongkhamdy, T., Braga, J., Sichanthongtip, P., Khamdalavong, P., Ponche, J.-L., Wang, H., Lundstrom, C., Patole-Edoumba, E., Karpoff, A.-M., 2012. Anatomically modern human in Southeast Asia (Laos) by 46 ka. *Proc. Natl. Acad. Sci. U.S.A.* 109, 14375–14380.
- Deng, T.-H.-B., Cloquet, C., Tang, Y.-T., Sterckeman, T., Echevarria, G., Estrade, N., Morel, J.-L., Qiu, R.-L., 2014. Nickel and zinc isotope fractionation in hyperaccumulating and nonaccumulating plants. *Environ. Sci. Technol.* 48, 11926–11933.
- DeNiro, M.J., Epstein, S., 1978. Influence of diet on the distribution of carbon isotopes in animals. *Geochim. Cosmochim. Acta.* 42, 495–506.
- DeNiro, M.J., Epstein, S., 1981. Influence of diet on the distribution of nitrogen isotopes in animals. *Geochim. Cosmochim. Acta.* 45, 341–351.
- Dennell, R., 2016. Life without the Movius Line: The structure of the East and Southeast Asian Early Palaeolithic. *Quat. Int.* 400, 14–22.
- Dennell, R., Roebroeks, W., 2005. An Asian perspective on early human dispersal from Africa. *Nature.* 438, 1099–1104.
- Détroit, F., Mijares, A.S., Corny, J., Daver, G., Zanolli, C., Dizon, E., Robles, E., Grün, R., Piper, P.J., 2019. A new species of *Homo* from the Late Pleistocene of the Philippines. *Nature.* 568, 181–186.
- Dibble, H.L., Chase, P.G., McPherron, S.P., Tuffreau, A., 1997. Testing the reality of a “living floor” with archaeological data. *Am. Antiq.* 62, 629–651.
- Dobson, A.J., 2002. *An introduction to generalized linear models*, 2nd ed. Chapman and Hall/CRC, Boca Raton.
- Dolphin, A.E., Goodman, A.H., 2009. Maternal diets, nutritional status, and zinc in contemporary Mexican infants’ teeth: Implications for reconstructing paleodiets. *Am. J. Phys. Anthropol.* 140, 399–409.
- Dolphin, A.E., Goodman, A.H., Amarasiriwardena, D.D., 2005. Variation in elemental intensities among teeth and between pre- and postnatal regions of enamel. *Am. J. Phys. Anthropol.* 128, 878–888.

- Donangelo, C.M., King, J.C., 2012. Maternal zinc intakes and homeostatic adjustments during pregnancy and lactation. *Nutrients*. 4, 782–798.
- Donangelo, C.M., Vargas Zapata, C.L., Woodhouse, L.R., Shames, D.M., Mukherjea, R., King, J.C., 2005. Zinc absorption and kinetics during pregnancy and lactation in Brazilian women. *Am. J. Clin. Nutr.* 82, 118–124.
- Drucker, D., Bocherens, H., 2004. Carbon and nitrogen stable isotopes as tracers of change in diet breadth during Middle and Upper Palaeolithic in Europe. *Int. J. Osteoarchaeol.* 14, 162–177.
- Duringer, P., Bacon, A.-M., Sayavongkhamdy, T., Nguyen, T.K.T., 2012. Karst development, breccias history, and mammalian assemblages in Southeast Asia: A brief review. *C. R. Palevol* 11, 133–157.
- Eggins, S., Grün, R., Pike, A.W.G., Shelley, M., Taylor, L., 2003. ^{238}U , ^{232}Th profiling and U-series isotope analysis of fossil teeth by laser ablation-ICPMS. *Quat. Sci. Rev.* 22, 1373–1382.
- Ehleringer, J.R., Field, C.B., Lin, Z., Kuo, C., 1986. Leaf carbon isotope and mineral composition in subtropical plants along an irradiance cline. *Oecologia*. 70, 520–526.
- Ehleringer, J.R., Lin, Z.F., Field, C.B., Sun, G.C., Kuo, C.Y., 1987. Leaf carbon isotope ratios of plants from a subtropical monsoon forest. *Oecologia*. 72, 109–114.
- Enlow, D.H., 1962. A study of the post-natal growth and remodeling of bone. *Am. J. Anat.* 110, 79–101.
- Enlow, D.H., Bang, S., 1965. Growth and remodeling of the human maxilla. *Am. J. Orthod.* 51, 446–464.
- Erdelen, W., 1988. Forest ecosystems and nature conservation in Sri Lanka. *Biol. Conserv.* 43, 115–135.
- Ericson, J.E., 1985. Strontium isotope characterization in the study of prehistoric human ecology. *J. Hum. Evol.* 14, 503–514.
- Evans, R.D., 2007. Soil nitrogen isotope composition. In: Michener, R., Lajtha, K. (Eds.), *Stable isotopes in ecology and environmental science*. Blackwell Publishing, Chichester, pp. 83–98.

- Evans, R.D., Wang, W., Evans, H.E., Georg, R.B., 2016. Variation in Zn, C, and N isotope ratios in three stream insects. *FACETS* 1, 205–216.
- Falla-Sotelo, F.O., Rizzutto, M.A., Tabacniks, M.H., Added, N., Barbosa, M.D.L., Markarian, R.A., Quinelato, A., Mori, M., Youssef, M., 2005. Analysis and discussion of trace elements in teeth of different animal species. *Braz. J. Phys.* 35, 761–762.
- Farquhar, G.D., Ehleringer, J.R., Hubick, K.T., 1989. Carbon isotope discrimination and photosynthesis. *Annu. Rev. Plant Physiol. Plant Mol. Biol.* 40, 503–537.
- Fatima, T., Haji Abdul Rahim, Z.B., Lin, C.W., Qamar, Z., 2016. Zinc: A precious trace element for oral health care? *J. Pak. Med. Assoc.* 66, 1019–1023.
- Feitosa, S.F., Garrafa, V., Cornelli, G., Tardivo, C., Carvalho, S.J. de, 2010. Bioethics, culture and infanticide in Brazilian indigenous communities: The Zuruahá case. *Cad. Saúde Pública.* 26, 853–865.
- Fekiacova, Z., Cornu, S., Pichat, S., 2015. Tracing contamination sources in soils with Cu and Zn isotopic ratios. *Sci. Total Environ.* 517, 96–105.
- Ferguson, E.L., Gibson, R.S., Thompson, L.U., Ounpuu, S., Berry, M., 1988. Phytate, zinc, and calcium contents of 30 East African foods and their calculated phytate: Zn, Ca:phytate, and $[Ca][\text{phytate}]/[Zn]$ molar ratios. *J. Food Compos. Anal.* 1, 316–325.
- Field, A., 2005. Exploratory factor analysis. In: *Discovering statistics using SPSS*. Sage Publications, London, pp. 619–680.
- Filoux, A., Wattanapituksakul, A., Lespes, C., Thongcharoenchaikit, C., 2015. A Pleistocene mammal assemblage containing *Ailuropoda* and *Pongo* from Tham Prakai Phet cave, Chaiyaphum Province, Thailand. *Geobios.* 48, 341–349.
- Fischer, A., Olsen, J., Richards, M., Heinemeier, J., Sveinbjörnsdóttir, Á.E., Bennike, P., 2007. Coast–inland mobility and diet in the Danish Mesolithic and Neolithic: Evidence from stable isotope values of humans and dogs. *J. Archaeol. Sci.* 34, 2125–2150.
- Fleagle, J.G., Shea, J.J., Grine, F.E., Baden, A.L., Leakey, R.E., 2010. *Out of Africa I: The first hominin colonization of Eurasia, Vertebrate Paleobiology and Paleoanthropology*. Springer Science & Business Media, Dordrecht.

- Flockhart, D.T.T., Kyser, T.K., Chipley, D., Miller, N.G., Norris, D.R., 2015. Experimental evidence shows no fractionation of strontium isotopes ($^{87}\text{Sr}/^{86}\text{Sr}$) among soil, plants, and herbivores: Implications for tracking wildlife and forensic science. *Isotopes Environ. Health Stud.* 51, 372–381.
- Fogel, M., Tuross, N., DW, O., 1989. Nitrogen isotope tracers of human lactation in modern and archaeological populations. *Carnegie. Inst. Yr. Bk.* 88, 111–117.
- Forestier, H., Sophady, H., Puaud, S., Celiberti, V., Frère, S., Zeitoun, V., Mourer-Chauviré, C., Mourer, R., Than, H., Billault, L., 2015. The Hoabinhian from Laang Spean Cave in its stratigraphic, chronological, typo-technological and environmental context (Cambodia, Battambang province). *J. Archaeol. Sci. Rep.* 3, 194–206.
- Forstmeier, W., Schielzeth, H., 2011. Cryptic multiple hypotheses testing in linear models: Overestimated effect sizes and the winner's curse. *Behav. Ecol. Sociobiol.* 65, 47–55.
- Foster, M., Samman, S., 2015. Vegetarian diets across the lifecycle: Impact on zinc intake and status. *Adv. Food Nutr. Res.* 74, 93–131.
- Fox, E.A., Schaik, C.P. van, Sitompul, A., Wright, D.N., 2004. Intra- and interpopulational differences in orangutan (*Pongo pygmaeus*) activity and diet: Implications for the invention of tool use. *Am. J. Phys. Anthropol.* 125, 162–174.
- Fox, J., Weisberg, S., 2011. Multivariate linear models in R. In: *An R companion to applied regression*. Sage publications, Thousand Oaks, p. 31.
- Fox-Dobbs, K., Bump, J.K., Peterson, R.O., Fox, D.L., Koch, P.L., 2007. Carnivore-specific stable isotope variables and variation in the foraging ecology of modern and ancient wolf populations: Case studies from Isle Royale, Minnesota, and La Brea. *Can. J. Zool.* 85, 458–471.
- Fricke, Henry C, Clyde, W.C., O'Neil, J.R., 1998. Intra-tooth variations in $\delta^{18}\text{O}$ (PO_4) of mammalian tooth enamel as a record of seasonal variations in continental climate variables. *Geochim. Cosmochim. Acta.* 62, 1839–1850.
- Fricke, Henry C., Clyde, W.C., O'Neil, J.R., Gingerich, P.D., 1998. Evidence for rapid climate change in North America during the latest Paleocene thermal

- maximum: Oxygen isotope compositions of biogenic phosphate from the Bighorn Basin (Wyoming). *Earth Planet. Sci. Lett.* 160, 193–208.
- Friedli, H., Löttscher, H., Oeschger, H., Siegenthaler, U., Stauffer, B., 1986. Ice core record of the $^{13}\text{C}/^{12}\text{C}$ ratio of atmospheric CO_2 in the past two centuries. *Nature*. 324, 237.
- Fuller, B.T., Fuller, J.L., Harris, D.A., Hedges, R.E.M., 2006. Detection of breastfeeding and weaning in modern human infants with carbon and nitrogen stable isotope ratios. *Am. J. Phys. Anthropol.* 129, 279–293.
- Fung, E.B., Ritchie, L.D., Woodhouse, L.R., Roehl, R., King, J.C., 1997. Zinc absorption in women during pregnancy and lactation: A longitudinal study. *Am. J. Clin. Nutr.* 66, 80–88.
- Gamble, C., 1993. *Timewalkers: The prehistory of global colonization*. Penguin Books, London.
- Garçon, M., Sauzéat, L., Carlson, R.W., Shirey, S.B., Simon, M., Balter, V., Boyet, M., 2017. Nitrile, Latex, Neoprene and Vinyl Gloves: A primary source of contamination for trace element and Zn isotopic analyses in geological and biological samples. *Geostand. Geoanal. Res.* 41, 367–380.
- Garvey, R., 2018. Current and potential roles of archaeology in the development of cultural evolutionary theory. *Philos. Trans. R. Soc. Lond. B Biol. Sci.* 373, 20170057.
- Gibson, R.S., King, J.C., Lowe, N., 2016. A review of dietary zinc recommendations. *Food Nutr. Bull.* 37, 443–460.
- Gonfiantini, R., 1984. Advisory group meeting on stable isotope reference samples for geochemical and hydrochemical investigations, IAEA. International Atomic Energy Agency, Vienna, Austria.
- Gosz, J.R., Brookins, D.G., Moore, D.I., 1983. Using strontium isotope ratios to estimate inputs to ecosystems. *BioScience*. 33, 23–30.
- Graham, H.V., Patzkowsky, M.E., Wing, S.L., Parker, G.G., Fogel, M.L., Freeman, K.H., 2014. Isotopic characteristics of canopies in simulated leaf assemblages. *Geochim. Cosmochim. Acta.* 144, 82–95.

- Grandjean, P., Albarède, F., 1989. Ion probe measurement of rare earth elements in biogenic phosphates. *Geochim. Cosmochim. Acta.* 53, 3179–3183.
- Graustein, W.C., 1989. $^{87}\text{Sr}/^{86}\text{Sr}$ ratios measure the sources and flow of strontium in terrestrial ecosystems. In: Rundel, P.W., Ehleringer, J.R., Nagy, K.A. (Eds.), *Stable isotopes in ecological research*. Springer New York, New York, pp. 491–512.
- Grün, R., Eggins, S., Kinsley, L., Moseley, H., Sambridge, M., 2014. Laser ablation U-series analysis of fossil bones and teeth. *Palaeogeogr. Palaeoclimatol. Palaeoecol.* 416, 150–167.
- Guatelli-Steinberg, D., Stinespring-Harris, A., Reid, D.J., Larsen, C.S., Hutchinson, D.L., Smith, T., 2014. Chronology of linear enamel hypoplasia formation in the Krapina Neanderthals. *PaleoAnthropology.* 431, 445.
- Guelke, M., von Blanckenburg, F., 2007. Fractionation of Stable Iron Isotopes in Higher Plants. *Environ. Sci. Technol.* 41, 1896–1901.
- Hall, R.L., 1967. Those late corn dates: isotopic fractionation as a source of error in carbon-14 dates. *Mich. Arch.* 13, 171–180.
- Hambidge, K.M., Abebe, Y., Gibson, R.S., Westcott, J.E., Miller, L.V., Lei, S., Stoecker, B.J., Arbide, I., Teshome, A., Bailey, K.B., Krebs, N.F., 2006. Zinc absorption during late pregnancy in rural southern Ethiopia. *Am. J. Clin. Nutr.* 84, 1102–1106.
- Hara, T., Takeda, T., Takagishi, T., Fukue, K., Kambe, T., Fukada, T., 2017. Physiological roles of zinc transporters: Molecular and genetic importance in zinc homeostasis. *J. Physiol. Sci.* 67, 283–301.
- Hardus, M.E., Lameira, A.R., Zulfa, A., Atmoko, S.S.U., de Vries, H., Wich, S.A., 2012. Behavioral, ecological, and evolutionary aspects of meat-eating by Sumatran orangutans (*Pongo abelii*). *Int. J. Primatol.* 33, 287–304.
- Harrison, R.G., Katzenberg, M.A., 2003. Paleodiet studies using stable carbon isotopes from bone apatite and collagen: Examples from Southern Ontario and San Nicolas Island, California. *J. Anthropol. Archaeol.* 22, 227–244.
- Harrison, T., Jin, C., Zhang, Y., Wang, Y., Zhu, M., 2014. Fossil *Pongo* from the Early Pleistocene *Gigantopithecus* fauna of Chongzuo, Guangxi, southern China. *Quat. Int.* 354, 59–67.

- Hart, T.B., Hart, J.A., 1986. The ecological basis of hunter-gatherer subsistence in African Rain Forests: The Mbuti of Eastern Zaire. *Hum. Ecol.* 14, 29–55.
- Hassler, A., Martin, J.E., Amiot, R., Tacail, T., Godet, F.A., Allain, R., Balter, V., 2018. Calcium isotopes offer clues on resource partitioning among Cretaceous predatory dinosaurs. *Proc. R. Soc. B.* 285, 20180197.
- Headland, T.N., 1987. The wild yam question: How well could independent hunter-gatherers live in a tropical rain forest ecosystem? *Hum. Ecol.* 15, 463–491.
- Hedges, R.E.M., 2002. Bone diagenesis: An overview of processes. *Archaeometry.* 44, 319–328.
- Hedges, R.E.M., Reynard, L.M., 2007. Nitrogen isotopes and the trophic level of humans in archaeology. *J. Archaeol. Sci.* 34, 1240–1251.
- Heesen, M., Rogahn, S., Ostner, J., Schülke, O., 2013. Food abundance affects energy intake and reproduction in frugivorous female Assamese macaques. *Behav. Ecol. Sociobiol.* 67, 1053–1066.
- Heghe, L.V., Engström, E., Rodushkin, I., Cloquet, C., Vanhaecke, F., 2012. Isotopic analysis of the metabolically relevant transition metals Cu, Fe and Zn in human blood from vegetarians and omnivores using multi-collector ICP-mass spectrometry. *J. Anal. At. Spectrom.* 27, 1327–1334.
- Heintz, E., 1970. *Les Cervidés villafranchiens de France et d'Espagne*. Édition du Muséum, Paris.
- Henry, A.G., Brooks, A.S., Piperno, D.R., 2014. Plant foods and the dietary ecology of Neanderthals and early modern humans. *J. Hum. Evol.* 69, 44–54.
- Hermenegildo, T., 2009. *Reconstituição da dieta e dos padrões de subsistência das populações pré-históricas de caçadores-coletores do Brasil Central através da ecologia isotópica* (Master's Dissertation). Universidade de São Paulo, Piracicaba.
- Heuser, A., Tütken, T., Gussone, N., Galer, S.J.G., 2011. Calcium isotopes in fossil bones and teeth — Diagenetic versus biogenic origin. *Geochim. Cosmochim. Acta.* 75, 3419–3433.
- Hillson, S., 1996. *Dental Anthropology*. Cambridge University Press, Cambridge.

- Hindshaw, R.S., Reynolds, B.C., Wiederhold, J.G., Kiczka, M., Kretzschmar, R., Bourdon, B., 2013. Calcium isotope fractionation in alpine plants. *Biogeochemistry*. 112, 373–388.
- Hinz, E.A., Kohn, M.J., 2010. The effect of tissue structure and soil chemistry on trace element uptake in fossils. *Geochim. Cosmochim. Acta*. 74, 3213–3231.
- Hobson, K.A., Collier, S., 1984. Marine and terrestrial protein in Australian aboriginal diets. *Curr. Anthropol*. 25, 238–240.
- Hobson, K.A., Alisauskas, R.T., Clark, R.G., 1993. Stable-nitrogen isotope enrichment in avian tissues due to fasting and nutritional stress: Implications for isotopic analyses of diet. *Condor*. 95, 388–394.
- Holm, S., 1979. A simple sequentially rejective multiple test procedure. *Scand. J. Stat.* 6, 65–70.
- Horta, B.L., Santos, R.V., Welch, J.R., Cardoso, A.M., dos Santos, J.V., Assis, A.M.O., Lira, P.C., Coimbra Jr, C.E., 2013. Nutritional status of indigenous children: findings from the First National Survey of Indigenous People's Health and Nutrition in Brazil. *Int. J. Equity Health*. 12, 23.
- Huang, Z., Huang, C., Tang, C., Huang, L., Tang, H., Ma, G., Zhou, Q., 2015. Dietary adaptations of Assamese macaques (*Macaca assamensis*) in limestone forests in Southwest China. *Am. J. Primatol.* 77, 171–185.
- Hunt, J.R., Beiseigel, J.M., Johnson, L.K., 2008. Adaptation in human zinc absorption as influenced by dietary zinc and bioavailability. *Am. J. Clin. Nutr.* 87, 1336–1345.
- Hurst, R.W., Davis, T.E., 1981. Strontium isotopes as tracers of airborne fly ash from coal-fired power plants. *Geo*. 3, 363–367.
- Hutterer, K.L., 1983. The natural and cultural history of Southeast Asian Agriculture: Ecological and evolutionary considerations. *Anthropos*. 78, 169–212.
- Ilyas, O., Khan, J.A., 2003. Food habits of barking deer (*Muntiacus muntjak*) and goral (*Naemorhedus goral*) in Binsar Wildlife Sanctuary, India. *Mammalia*. 67, 521–532.
- Ingicco, T., van den Bergh, G.D., Jago-on, C., Bahain, J.-J., Chacón, M.G., Amano, N., Forestier, H., King, C., Manalo, K., Nomade, S., Pereira, A., Reyes, M.C.,

- Sémah, A.-M., Shao, Q., Voinchet, P., Falguères, C., Albers, P.C.H., Lising, M., Lyras, G., Yurnaldi, D., Rochette, P., Bautista, A., de Vos, J., 2018. Earliest known hominin activity in the Philippines by 709 thousand years ago. *Nature*. 557, 233–237.
- International Atomic Energy Agency, 1995. Reference and Intercomparison Materials for Stable Isotopes of Light Elements. International Atomic Energy Agency, Vienna.
- Istfan, N.W., Janghorbani, M., Young, V.R., 1983. Absorption of stable⁷⁰ Zn in healthy young men in relation to zinc intake. *Am. J. Clin. Nutr.* 38, 187–194.
- Jackson, A., 2002. *Muntiacus muntjak* (Indian muntjac). Animal Diversity Web. URL https://animaldiversity.org/accounts/Muntiacus_muntjak/ (accessed 12.13.18).
- Jackson, A.L., Inger, R., Parnell, A.C., Bearhop, S., 2011. Comparing isotopic niche widths among and within communities: SIBER – Stable Isotope Bayesian Ellipses in R. *J. Anim. Ecol.* 80, 595–602.
- Jackson, J.E., Chapman, D.I., 1977. A note on the food of Muntjac deer (*Muntiacus reevesi*). *J. Zool.* 183, 546–548.
- Jacobs, G.S., Hudjashov, G., Saag, L., Kusuma, P., Darusallam, C.C., Lawson, D.J., Mondal, M., Pagani, L., Ricaut, F.-X., Stoneking, M., Metspalu, M., Sudoyo, H., Lansing, J.S., Cox, M.P., 2019. Multiple deeply divergent Denisovan ancestries in Papuans. *Cell*. 177, 1010-1021.e32.
- Jaouen, K., 2012. Les isotopes des métaux de transition (Cu, Fe, Zn) au service de l'anthropologie (Doctoral dissertation). Ecole Normale Supérieure de Lyon, Lyon.
- Jaouen, K., Balter, V., 2014. Menopause effect on blood Fe and Cu isotope compositions. *Am. J. Phys. Anthropol.* 153, 280–285.
- Jaouen, K., Balter, V., Herrscher, E., Lamboux, A., Telouk, P., Albarède, F., 2012. Fe and Cu stable isotopes in archeological human bones and their relationship to sex. *Am. J. Phys. Anthropol.* 148, 334–340.
- Jaouen, K., Pons, M.-L., Balter, V., 2013. Iron, copper and zinc isotopic fractionation up mammal trophic chains. *Earth Planet. Sci. Lett.* 374, 164–172.

- Jaouen, K., Beasley, M., Schoeninger, M., Hublin, J.-J., Richards, M.P., 2016a. Zinc isotope ratios of bones and teeth as new dietary indicators: Results from a modern food web (Koobi Fora, Kenya). *Sci. Rep.* 6, 26281.
- Jaouen, K., Szpak, P., Richards, M.P., 2016b. Zinc isotope ratios as indicators of diet and trophic level in arctic marine mammals. *PLoS ONE*. 11, e0152299.
- Jaouen, K., Herrscher, E., Balter, V., 2017. Copper and zinc isotope ratios in human bone and enamel. *Am. J. Phys. Anthropol.* 162, 491–500.
- Jaouen, K., Colleter, R., Pietrzak, A., Pons, M.-L., Clavel, B., Telmon, N., Crubézy, É., Hublin, J.-J., Richards, M.P., 2018. Tracing intensive fish and meat consumption using Zn isotope ratios: Evidence from a historical Breton population (Rennes, France). *Sci. Rep.* 8, 5077.
- Jaouen, K., Richards, M.P., Cabec, A.L., Welker, F., Rendu, W., Hublin, J.-J., Soressi, M., Talamo, S., 2019a. Exceptionally high $\delta^{15}\text{N}$ values in collagen single amino acids confirm Neandertals as high-trophic level carnivores. *Proc. Natl. Acad. Sci. U.S.A.* 116, 4928–4933.
- Jaouen, K., Pouilloux, L., Balter, V., Pons, M.-L., Hublin, J.-J., Albarède, F., 2019b. Dynamic homeostasis modeling of Zn isotope ratios in the human body. *Metallomics*. 11, 1049–1059.
- Jaouen, K., Trost, M., Bourgon, N., Colleter, R., Le Cabec, A., Tütken, T., Oliveira, R.E., Pons, M.-L., Méjean, P., Steinbrenner, S., Chmeleff, J., Strauss, A., 2020. Zinc isotope variations in archeological human teeth (Lapa do Santo, Brazil) reveal dietary transitions in childhood and no contamination from gloves, *PLoS ONE*, 15 (2020), p. e0232379
- Jochum, K.P., Weis, U., Stoll, B., Kuzmin, D., Yang, Q., Raczek, I., Jacob, D.E., Stracke, A., Birbaum, K., Frick, D.A., Günther, D., Enzweiler, J., 2011. Determination of reference values for NIST SRM 610–617 glasses following ISO guidelines. *Geostand. Geoanal. Res.* 35, 397–429.
- Johnsingh, A., Manjrekar, N., 2013. *Mammals of South Asia Vol. 1*. Universities Press (India) Limited, Hyderabad.
- Johnsingh, A., Manjrekar, N., 2015. *Mammals of South Asia Vol. 2*. Universities Press (India) Limited, Hyderabad.

- Johnson, C.M., Fridrich, C.J., 1990. Non-monotonic chemical and O, Sr, Nd, and Pb isotope zonations and heterogeneity in the mafic- to silicic-composition magma chamber of the Grizzly Peak Tuff, Colorado. *Contrib. to Mineral. Petrol.* 105, 677–690.
- Jouvin, D., Weiss, D.J., Mason, T.F.M., Bravin, M.N., Louvat, P., Zhao, F., Ferec, F., Hinsinger, P., Benedetti, M.F., 2012. Stable isotopes of Cu and Zn in higher plants: Evidence for Cu reduction at the root surface and two conceptual models for isotopic fractionation processes. *Environ. Sci. Technol.* 46, 2652–2660.
- Kaličanin, B., Velimirović, D., 2016. A study of the possible harmful effects of cosmetic beauty products on human health. *Biol. Trace Elem. Res.* 170, 476–484.
- Kanamori, T., Kuze, N., Bernard, H., Malim, T.P., Kohshima, S., 2010. Feeding ecology of Bornean orangutans (*Pongo pygmaeus morio*) in Danum Valley, Sabah, Malaysia: A 3-year record including two mast fruitings. *Am. J. Primatol.* 72, 820–840.
- Kato, A., Tang, N., Borries, C., Papakyrikos, A.M., Hinde, K., Miller, E., Kunimatsu, Y., Hirasaki, E., Shimizu, D., Smith, T.M., 2014. Intra- and interspecific variation in macaque molar enamel thickness. *Am. J. Phys. Anthropol.* 155, 447–459.
- Katzenberg, M.A., Waters-Rist, A.L., 2018. Stable isotope analysis. In: Katzenberg, M.A., Grauer, Anne.L. (Eds.), *Biological anthropology of the human skeleton*. John Wiley & Sons, Ltd, Hoboken, pp. 467–504
- Kelly, J.F., 2000. Stable isotopes of carbon and nitrogen in the study of avian and mammalian trophic ecology. *Can. J. Zool.* 78, 1–27.
- Kendall, C., Grim, E., 1990. Combustion tube method for measurement of nitrogen isotope ratios using calcium oxide for total removal of carbon dioxide and water. *Anal. Chem.* 62, 526–529.
- Khatiwada, S., Paudel, P.K., Chalise, M.K., Ogawa, H., 2020. Comparative ecological and behavioral study of *Macaca assamensis* and *M. mulatta* in Shivapuri Nagarjun National Park, Nepal. *Primates* 61, 603–621.

- Kidwell, S.M., Behrensmeyer, A.K., 1993. Taphonomic approaches to time resolution in fossil assemblages: Introduction. *Short courses paleontol.* 6, 1–8.
- Kies, C., 1981. Bioavailability: A factor in protein quality. *J. Agric. Food Chem.* 29, 435–440.
- King, J.C., 2011. Zinc: An essential but elusive nutrient. *Am. J. Clin. Nutr.* 94, 679S–684S.
- Knudson, K.J., Williams, H.M., Buikstra, J.E., Tomczak, P.D., Gordon, G.W., Anbar, A.D., 2010. Introducing $\delta^{88/86}\text{Sr}$ analysis in archaeology: A demonstration of the utility of strontium isotope fractionation in paleodietary studies. *J. Archaeol. Sci.* 37, 2352–2364.
- Koch, P.L., 1998. Isotopic reconstruction of past continental environments. *Annu. Rev. Earth Planet. Sci.* 26, 573–613.
- Kocsis, L., Trueman, C.N., Palmer, M.R., 2010. Protracted diagenetic alteration of REE contents in fossil bioapatites: Direct evidence from Lu–Hf isotope systematics. *Geochim. Cosmochim. Acta.* 74, 6077–6092.
- Kohn, M.J., 1996. Predicting animal $\delta^{18}\text{O}$: Accounting for diet and physiological adaptation. *Geochim. Cosmochim. Acta.* 60, 4811–4829.
- Kohn, M.J., 2010. Carbon isotope compositions of terrestrial C_3 plants as indicators of (paleo)ecology and (paleo)climate. *Proc. Natl. Acad. Sci. U.S.A.* 107, 19691–19695.
- Kohn, M.J., Cerling, T.E., 2002. Stable isotope compositions of biological apatite. *Rev. Mineral. Geochem.* 48, 455–488.
- Kohn, M.J., Schoeninger, M.J., Valley, J.W., 1996. Herbivore tooth oxygen isotope compositions: Effects of diet and physiology. *Geochim. Cosmochim. Acta.* 60, 3889–3896.
- Kohn, M.J., Schoeninger, M.J., Barker, W.W., 1999. Altered states: Effects of diagenesis on fossil tooth chemistry. *Geochim. Cosmochim. Acta.* 63, 2737–2747.
- Kohn, M.J., Morris, J., Olin, P., 2013. Trace element concentrations in teeth – A modern Idaho baseline with implications for archeometry, forensics, and palaeontology. *J. Archaeol. Sci.* 40, 1689–1699.

- Konner, M., 2017. Hunter-gatherer infancy and childhood : The !Kung and others. In: Hewlett, B.S. (Ed.), *Hunter-gatherer childhoods: Evolutionary, developmental, and cultural perspectives*. Routledge, New York, NY, pp. 19–64.
- Krayenbuehl, P.-A., Walczyk, T., Schoenberg, R., von Blanckenburg, F., Schulthess, G., 2005. Hereditary hemochromatosis is reflected in the iron isotope composition of blood. *Blood*. 105, 3812–3816.
- Krebs, N.F., 2000. Overview of zinc absorption and excretion in the human gastrointestinal tract. *J. Nutr.* 130, 1374S-1377S.
- Krigbaum, J., 2003. Neolithic subsistence patterns in northern Borneo reconstructed with stable carbon isotopes of enamel. *J. Anthropol. Archaeol.* 22, 292–304.
- Krigbaum, J., 2005. Reconstructing human subsistence in the West Mouth (Niah Cave, Sarawak) burial series using stable isotopes of carbon. *Asian Perspect.* 44, 73–89.
- Krigbaum, J., Berger, M.H., Daegling, D.J., McGraw, W.S., 2013. Stable isotope canopy effects for sympatric monkeys at Taï Forest, Côte d’Ivoire. *Biol. Lett.* 9, 20130466.
- Kristensen, M.B., Hels, O., Morberg, C.M., Marving, J., Büge, S., Tetens, I., 2006. Total zinc absorption in young women, but not fractional zinc absorption, differs between vegetarian and meat-based diets with equal phytic acid content. *Br. J. Nutr.* 95, 963–967.
- Krueger, H.W., Sullivan, C.H., 1984. Models for carbon isotope fractionation between diet and bone. In: Turnlund, J.R., Johnson, P.E. (Eds.), *Stable Isotopes in Nutrition*, ACS Symposium Series. American Chemical Society, Washington, D.C, pp. 205–220.
- Kurt, F., 1990. Muntjac deer. In: *Grzimek’s encyclopedia of mammals*. McGraw-Hill Publishing Company, New York, pp. 137–139.
- Kyle, J.H., 1986. Effect of post-burial contamination on the concentrations of major and minor elements in human bones and teeth—The implications for palaeodietary research. *J. Archaeol. Sci.* 13, 403–416.
- Lacruz, R.S., Dean, M.C., Ramirez-Rozzi, F., Bromage, T.G., 2008. Megadontia, striae periodicity and patterns of enamel secretion in Plio-Pleistocene fossil hominins. *J. Anat.* 213, 148–158.

- Lacruz, R.S., Habelitz, S., Wright, J.T., Paine, M.L., 2017. Dental enamel formation and implications for oral health and disease. *Physiol. Rev.* 97, 939–993.
- Langley, M.C., Amano, N., Wedage, O., Deraniyagala, S., Pathmalal, M.M., Perera, N., Boivin, N., Petraglia, M.D., Roberts, P., 2020. Bows and arrows and complex symbolic displays 48,000 years ago in the South Asian tropics. *Sci. Adv.* 6, eaba3831.
- Lappalainen, R., Knuutila, M., Salminen, R., 1981. The concentrations of Zn and Mg in human enamel and dentine related to age and their concentrations in the soil. *Arch. Oral Biol.* 26, 1–6.
- Larick, R., Ciochon, R.L., Zaim, Y., Sudijono, Suminto, Rizal, Y., Aziz, F., Reagan, M., Heizler, M., 2001. Early Pleistocene $^{40}\text{Ar}/^{39}\text{Ar}$ ages for Bapang Formation hominins, Central Jawa, Indonesia. *Proc. Natl. Acad. Sci. U.S.A.* 98, 4866–4871.
- Larner, F., Woodley, L.N., Shousha, S., Moyes, A., Humphreys-Williams, E., Strekopytov, S., Halliday, A.N., Rehkämper, M., Coombes, R.C., 2015. Zinc isotopic compositions of breast cancer tissue. *Metallomics.* 7, 112–117.
- LeBlanc, A., Dumas, P., Lefebvre, L., 1999. Trace element content of commercial shampoos: Impact on trace element levels in hair. *Sci. Total Environ.* 229, 121–124.
- Le Cabec, A., Gunz, P., Kupczik, K., Braga, J., Hublin, J.-J., 2013. Anterior tooth root morphology and size in Neanderthals: Taxonomic and functional implications. *J. Hum. Evol.* 64, 169–193.
- Le Cloirec, G., 2016. Couvent des Jacobins : Du quartier antique à l'établissement dominicain. Rapport de fouille (Archeological excavation No. RAP03324). INRAP, Service régional de l'archéologie de Bretagne, Rennes (Ille-et-Vilaine).
- Lee, K.M., Appleton, J., Cooke, M., Keenan, F., Sawicka-Kapusta, K., 1999. Use of laser ablation inductively coupled plasma mass spectrometry to provide element versus time profiles in teeth. *Anal. Chim. Acta.* 395, 179–185.
- Lee-Thorp, J.A., 2008. On isotopes and old bones. *Archaeometry.* 50, 925–950.

- Lee-Thorp, J.A., Sealy, J.C., van der Merwe, N.J., 1989. Stable carbon isotope ratio differences between bone collagen and bone apatite, and their relationship to diet. *J. Archaeol. Sci.* 16, 585–599.
- Lee-Thorp, J.A., van der Merwe, N.J., 1991. Aspects of the chemistry of modern and fossil biological apatites. *J. Archaeol. Sci.* 18, 343–354.
- Lee-Thorp, J.A., van der Merwe, N.J., Brain, C.K., 1994. Diet of *Australopithecus robustus* at Swartkrans from stable carbon isotopic analysis. *J. Hum. Evol.* 27, 361–372.
- Leichliter, J.N., Lüdecke, T., Foreman, A.D., Duprey, N.N., Winkler, D.E., Kast, E.R., Vonhof, H., Sigman, D.M., Haug, G.H., Clauss, M., Tütken, T., Martínez-García, A., 2021. Nitrogen isotopes in tooth enamel record diet and trophic level enrichment: Results from a controlled feeding experiment. *Chem. Geol.* 563, 120047.
- Levin, N.E., Simpson, S.W., Quade, J., Cerling, T.E., Frost, S.R., 2008. Herbivore enamel carbon isotopic composition and the environmental context of *Ardipithecus* at Gona, Ethiopia. *Geol. Soc. Am. Spec. Pap.* 446, 215–234.
- Lewis, J., Pike, A.W.G., Coath, C.D., Evershed, R.P., 2017. Strontium concentration, radiogenic ($^{87}\text{Sr}/^{86}\text{Sr}$) and stable ($\delta^{88}\text{Sr}$) strontium isotope systematics in a controlled feeding study. *STAR.* 3, 53–65.
- Lim, K.H.C., Riddell, L.J., Nowson, C.A., Booth, A.O., Szymlek-Gay, E.A., 2013. Iron and zinc nutrition in the economically-developed world: A review. *Nutrients.* 5, 3184–3211.
- Longin, R., 1971. New method of collagen extraction for radiocarbon dating. *Nature.* 230, 241–242.
- Longinelli, A., 1984. Oxygen isotopes in mammal bone phosphate: A new tool for paleohydrological and paleoclimatological research? *Geochim. Cosmochim. Acta.* 48, 385–390.
- Lönnerdal, B., 2000. Dietary factors influencing zinc absorption. *J. Nutr.* 130, 1378S–1383S.
- Loosdrecht, M. van de, Bouzouggar, A., Humphrey, L., Posth, C., Barton, N., Aximu-Petri, A., Nickel, B., Nagel, S., Talbi, E.H., Hajraoui, M.A.E., Amzazi, S., Hublin, J.-J., Pääbo, S., Schiffels, S., Meyer, M., Haak, W., Jeong, C., Krause,

- J., 2018. Pleistocene North African genomes link Near Eastern and sub-Saharan African human populations. *Science*. 360, 548–552.
- Lough, S.A., Rivera, J., Comar, C.L., 1963. Retention of strontium, calcium, and phosphorus in human infants. *Proc. Soc. Exp. Biol. Med.* 112, 631–636.
- Louys, J., Roberts, P., 2020. Environmental drivers of megafauna and hominin extinction in Southeast Asia. *Nature*. 586, 402–406.
- Lu, P.-J., Huang, S.-C., Chen, Y.-P., Chiueh, L.-C., Shih, D.Y.-C., 2015. Analysis of titanium dioxide and zinc oxide nanoparticles in cosmetics. *J. Food Drug Anal.* 23, 587–594.
- Luck, J.-M., Ben Othman, D., Albarède, F., Télouk, P., 1999. Pb, Zn and Cu isotopic variations and trace elements in rain. In: Bauer, A., Velde, B.D. (Eds.), *Geochemistry of the Earth's surface*. CRC Press, Reykjavik, pp. 199–203.
- Luz, B., Kolodny, Y., Horowitz, M., 1984. Fractionation of oxygen isotopes between mammalian bone-phosphate and environmental drinking water. *Geochim. Cosmochim. Acta*. 48, 1689–1693.
- Macdonald, D.W., 2009. *The encyclopedia of mammals*, 2nd ed. Oxford University Press, Oxford.
- Mahan, B., Moynier, F., Jørgensen, A.L., Habekost, M., Siebert, J., 2018. Examining the homeostatic distribution of metals and Zn isotopes in Göttingen minipigs. *Metallomics*. 10, 1264–1281.
- Maréchal, C.N., Télouk, P., Albarède, F., 1999. Precise analysis of copper and zinc isotopic compositions by plasma-source mass spectrometry. *Chem. Geol.* 156, 251–273.
- Maréchal, C.N., Nicolas, E., Douchet, C., Albarède, F., 2000. Abundance of zinc isotopes as a marine biogeochemical tracer. *Geochem. Geophys. Geosyst.* 1.
- Maret, W., Sandstead, H.H., 2006. Zinc requirements and the risks and benefits of zinc supplementation. *J. Trace Elem. Med. Biol.* 20, 3–18.
- Maret, W., 2016. The metals in the biological periodic system of the elements: Concepts and conjectures. *Int. J. Mol. Sci.* 17, 66.
- Maret, W., 2017. Zinc in cellular regulation: The nature and significance of “zinc signals.” *Int. J. Mol. Sci.* 18, 2285.

- Martin, J.E., Vance, D., Balter, V., 2014. Natural variation of magnesium isotopes in mammal bones and teeth from two South African trophic chains. *Geochim. Cosmochim. Acta.* 130, 12–20.
- Martin, J.E., Vance, D., Balter, V., 2015. Magnesium stable isotope ecology using mammal tooth enamel. *Proc. Natl. Acad. Sci. U.S.A.* 112, 430–435.
- Martin, J.E., Tacail, T., Cerling, T.E., Balter, V., 2018. Calcium isotopes in enamel of modern and Plio-Pleistocene East African mammals. *Earth Planet. Sci. Lett.* 503, 227–235.
- Martin, J.E., Tacail, T., Braga, J., Cerling, T.E., Balter, V., 2020. Calcium isotopic ecology of Turkana Basin hominins. *Nat. Commun.* 11, 3587.
- Martinelli, L.A., Piccolo, M.C., Townsend, A.R., Vitousek, P.M., Cuevas, E., McDowell, W., Robertson, G.P., Santos, O.C., Treseder, K., 1999. Nitrogen stable isotopic composition of leaves and soil: Tropical versus temperate forests. *Biogeochemistry.* 46, 45–65.
- Martinón-Torres, M., Wu, X., Bermúdez de Castro, J.M., Xing, S., Liu, W., 2017. *Homo sapiens* in the Eastern Asian Late Pleistocene. *Curr. Anthropol.* 58, S434–S448.
- Matthews, J.M., Bhati, M., Lehtomaki, E., Mansfield, R.E., Cubeddu, L., Mackay, J.P., 2009. It takes two to tango: The structure and function of LIM, RING, PHD and MYND domains. *Curr. Pharm. Des.* 15, 3681–3696.
- McCarroll, D., Loader, N.J., 2006. Isotopes in tree rings. In: Leng, M.J. (Ed.), *Isotopes in palaeoenvironmental research*. Springer Netherlands, Dordrecht, pp. 67–116.
- McColl, H., Racimo, F., Vinner, L., Demeter, F., Gakuhari, T., Moreno-Mayar, J.V., Driem, G. van, Wilken, U.G., Seguin-Orlando, A., Castro, C. de la F., Wasef, S., Shoocongdej, R., Souksavatdy, V., Sayavongkhamdy, T., Saidin, M.M., Allentoft, M.E., Sato, T., Malaspinas, A.-S., Aghakhanian, F.A., Korneliussen, T., Prohaska, A., Margaryan, A., Damgaard, P. de B., Kaewsutthi, S., Lertrit, P., Nguyen, T.M.H., Hung, H., Tran, T.M., Truong, H.N., Nguyen, G.H., Shahidan, S., Wiradnyana, K., Matsumae, H., Shigehara, N., Yoneda, M., Ishida, H., Masuyama, T., Yamada, Y., Tajima, A., Shibata, H., Toyoda, A., Hanihara, T., Nakagome, S., Deviese, T., Bacon, A.-M., Durringer, P., Ponche, J.-L., Shackelford, L., Patole-Edoumba, E., Nguyen, A.T., Bellina-Pryce, B.,

- Galipaud, J.-C., Kinaston, R., Buckley, H., Pottier, C., Rasmussen, S., Higham, T., Foley, R.A., Lahr, M.M., Orlando, L., Sikora, M., Phipps, M.E., Oota, H., Higham, C., Lambert, D.M., Willerslev, E., 2018. The prehistoric peopling of Southeast Asia. *Science* 361, 88–92.
- McConnaughey, T., McRoy, C.P., 1979. Food-web structure and the fractionation of carbon isotopes in the Bering Sea. *Mar. Biol.* 53, 257–262.
- McCormack, J., Szpak, P., Bourgon, N., Richards, M., Hyland, C., Méjean, P., Hublin, J.-J., Jaouen, K., 2021. Zinc isotopes from archaeological bones provide reliable trophic level information for marine mammals. *Commun. Biol.* 4, 1–11.
- McCormack, J.M., Bahr, A., Gerdes, A., Tütken, T., Prinz-Grimm, P., 2015. Preservation of successive diagenetic stages in Middle Triassic bonebeds: Evidence from in situ trace element and strontium isotope analysis of vertebrate fossils. *Chem. Geol.* 410, 108–123.
- McCullagh, P., Nelder, J.A., 1989. *Generalized linear models*, 2nd edition. CRC Press, London.
- Medina, E., Montes, G., Cuevas, E., Rokzandic, Z., 1986. Profiles of CO₂ concentration and $\delta^{13}\text{C}$ values in tropical rain forests of the upper Rio Negro Basin, Venezuela. *J. Trop. Ecol.* 2, 207–217.
- Mekota, A.-M., Grupe, G., Ufer, S., Cuntz, U., 2006. Serial analysis of stable nitrogen and carbon isotopes in hair: Monitoring starvation and recovery phases of patients suffering from anorexia nervosa. *Rapid Commun. Mass Spectrom.* 20, 1604–1610.
- Michel, V., Ildefonse, Ph., Morin, G., 1996. Assessment of archaeological bone and dentine preservation from Lazaret Cave (Middle Pleistocene) in France. *Palaeogeogr. Palaeoclimatol. Palaeoecol.* 126, 109–119.
- Miksicek, C.H., 1987. Formation processes of the archaeobotanical record. In: Schiffer, M.B. (Ed.), *Advances in archaeological method and theory*. Academic Press, San Diego, pp. 211–247.
- Milano, S., Demeter, F., Hublin, J.-J., Düringer, P., Patole-Edoumba, E., Ponche, J.-L., Shackelford, L., Boesch, Q., Houg, N.T.M., Lan, L.T.P., Duangthongchit, S., Sayavonkhamdy, T., Sichanthongtip, P., Sihanam, D., Souksavatdy, V.,

- Westaway, K., Bacon, A.-M., 2018. Environmental conditions framing the first evidence of modern humans at Tam Pà Ling, Laos: A stable isotope record from terrestrial gastropod carbonates. *Palaeogeogr. Palaeoclimatol. Palaeoecol.* 511, 352-363.
- Minagawa, M., Wada, E., 1986. Nitrogen isotope ratios of red tide organisms in the East China Sea: A characterization of biological nitrogen fixation. *Mar. Chem.* 19, 245–259.
- Morgan, J.L.L., Skulan, J.L., Gordon, G.W., Romaniello, S.J., Smith, S.M., Anbar, A.D., 2012. Rapidly assessing changes in bone mineral balance using natural stable calcium isotopes. *Proc. Natl. Acad. Sci. U.S.A.* 109, 9989–9994.
- Moynier, F., Albarède, F., Herzog, G.F., 2006. Isotopic composition of zinc, copper, and iron in lunar samples. *Geochim. Cosmochim. Acta.* 70, 6103–6117.
- Moynier, F., Fujii, T., S. Shaw, A., Borgne, M.L., 2013. Heterogeneous distribution of natural zinc isotopes in mice. *Metallomics.* 5, 693–699.
- Moynier, F., Pichat, S., Pons, M.-L., Fike, D., Balter, V., Albarède, F., 2009. Isotopic fractionation and transport mechanisms of Zn in plants. *Chem. Geol.* 267, 125–130.
- Moynier, F., Vance, D., Fujii, T., Savage, P., 2017. The Isotope geochemistry of zinc and copper. *Rev. Mineral. Geochem.* 82, 543–600.
- Müldner, G., Richards, M.P., 2005. Fast or feast: Reconstructing diet in later medieval England by stable isotope analysis. *J. Archaeol. Sci.* 32, 39–48.
- Naito, Y.I., Chikaraishi, Y., Drucker, D.G., Ohkouchi, N., Semal, P., Wißing, C., Bocherens, H., 2016. Ecological niche of Neanderthals from Spy Cave revealed by nitrogen isotopes of individual amino acids in collagen. *J. Hum. Evol.* 93, 82–90.
- Nakagawa, S., Johnson, P.C.D., Schielzeth, H., 2017. The coefficient of determination R^2 and intra-class correlation coefficient from generalized linear mixed-effects models revisited and expanded. *J. R. Soc. Interface.* 14, 20170213.
- Nanci, A., 2018. Ten Cate's oral histology: Development, structure, and function, 9th edition. Elsevier Health Sciences, St-Louis.

- Neves, W.A., Araujo, A.G.M., Bernardo, D.V., Kipnis, R., Feathers, J.K., 2012. Rock art at the Pleistocene/Holocene boundary in eastern South America. *PLoS ONE*. 7, e32228.
- Norton, C.J., Braun, D.R. (Eds.), 2011. *Asian paleoanthropology: From Africa to China and beyond*. Springer Netherlands, Dordrecht.
- Nowak, R.M., 1999. *Walker's Mammals of the World*, 6th edition. Johns Hopkins University Press, Baltimore.
- O'Leary, M.H., 1988. Carbon isotopes in photosynthesis fractionation techniques may reveal new aspects of carbon dynamics in plants. *BioScience*. 38, 328–336.
- Ohno, T., Shinohara, A., Chiba, M., Hirata, T., 2005. Precise Zn isotopic ratio measurements of human red blood cell and hair samples by multiple collector-ICP-mass spectrometry. *Anal. Sci.* 21, 425–428.
- Ohno, T., Shinohara, A., Kohge, I., Chiba, M., Hirata, T., 2004. Isotopic analysis of Fe in human red blood cells by multiple collector-ICP-mass spectrometry. *Anal. Sci.* 20, 617–621.
- Onianwa, P.C., Adeyemo, A.O., Idowu, O.E., Ogabiela, E.E., 2001. Copper and zinc contents of Nigerian foods and estimates of the adult dietary intakes. *Food Chem.* 72, 89–95.
- Opfergelt, S., Cornéilis, J.T., Houben, D., Givron, C., Burton, K.W., Mattielli, N., 2017. The influence of weathering and soil organic matter on Zn isotopes in soils. *Chem. Geol.* 466, 140–148.
- Ortega, D.D., 2019. *Microvestígios botânicos em artefatos líticos do sítio Lapa do Santo (Lagoa Santa, Minas Gerais) (Master's Dissertation)*. Universidade de São Paulo, São Paulo.
- Passey, B.H., Robinson, T.F., Ayliffe, L.K., Cerling, T.E., Sponheimer, M., Dearing, M.D., Roeder, B.L., Ehleringer, J.R., 2005. Carbon isotope fractionation between diet, breath CO₂, and bioapatite in different mammals. *J. Archaeol. Sci.* 32, 1459–1470.
- Pederzani, S., Britton, K., 2019. Oxygen isotopes in bioarchaeology: Principles and applications, challenges and opportunities. *Earth Sci. Rev.* 188, 77–107.

- Perera, N., Kourampas, N., Simpson, I.A., Deraniyagala, S.U., Bulbeck, D., Kamminga, J., Perera, J., Fuller, D.Q., Szabó, K., Oliveira, N.V., 2011. People of the ancient rainforest: Late Pleistocene foragers at the Batadomba-lena rockshelter, Sri Lanka. *J. Hum. Evol.* 61, 254–269.
- Perry, G.H., Verdu, P., 2017. Genomic perspectives on the history and evolutionary ecology of tropical rainforest occupation by humans. *Quat. Int.* 448, 150–157.
- Pestle, W.J., Colvard, M., 2012. Bone collagen preservation in the tropics: A case study from ancient Puerto Rico. *J. Archaeol. Sci.* 39, 2079–2090.
- Phillips, D.L., Koch, P.L., 2002. Incorporating concentration dependence in stable isotope mixing models. *Oecologia*. 130, 114–125.
- Pichat, S., Douchet, C., Albarède, F., 2003. Zinc isotope variations in deep-sea carbonates from the eastern equatorial Pacific over the last 175 ka. *Earth Planet. Sci. Lett.* 210, 167–178.
- Ponzevera, E., Quétel, C.R., Berglund, M., Taylor, P.D.P., Evans, P., Loss, R.D., Fortunato, G., 2006. Mass discrimination during MC-ICPMS isotopic ratio measurements: Investigation by means of synthetic isotopic mixtures (IRMM-007 series) and application to the calibration of natural-like zinc materials (including IRMM-3702 and IRMM-651). *J. Am. Soc. Mass Spectrom.* 17, 1413–1427.
- Post, D.M., 2002. Using stable isotopes to estimate trophic position: Models, methods, and assumptions. *Ecology*. 83, 703–718.
- Posth, C., Nakatsuka, N., Lazaridis, I., Skoglund, P., Mallick, S., Lamnidis, T.C., Rohland, N., Nägele, K., Adamski, N., Bertolini, E., Broomandkhoshbacht, N., Cooper, A., Culleton, B.J., Ferraz, T., Ferry, M., Furtwängler, A., Haak, W., Harkins, K., Harper, T.K., Hünemeier, T., Lawson, A.M., Llamas, B., Michel, M., Nelson, E., Oppenheimer, J., Patterson, N., Schiffels, S., Sedig, J., Stewardson, K., Talamo, S., Wang, C.-C., Hublin, J.-J., Hubbe, M., Harvati, K., Nuevo Delaunay, A., Beier, J., Francken, M., Kaulicke, P., Reyes-Centeno, H., Rademaker, K., Trask, W.R., Robinson, M., Gutierrez, S.M., Prufer, K.M., Salazar-García, D.C., Chim, E.N., Müller Plumm Gomes, L., Alves, M.L., Liryo, A., Inglez, M., Oliveira, R.E., Bernardo, D.V., Barioni, A., Wesolowski, V., Scheifler, N.A., Rivera, M.A., Plens, C.R., Messineo, P.G., Figuti, L., Corach, D., Scabuzzo, C., Eggers, S., DeBlasis, P., Reindel, M., Méndez, C.,

- Politis, G., Tomasto-Cagigao, E., Kennett, D.J., Strauss, A., Fehren-Schmitz, L., Krause, J., Reich, D., 2018. Reconstructing the deep population history of Central and South America. *Cell*. 175, 1185-1197.e22.
- Power, R.C., Salazar-García, D.C., Rubini, M., Darlas, A., Harvati, K., Walker, M., Hublin, J.-J., Henry, A.G., 2018. Dental calculus indicates widespread plant use within the stable Neanderthal dietary niche. *J. Hum. Evol.* 119, 27–41.
- Price, T.D., Burton, J.H., Cucina, A., Zabala, P., Frei, R., Tykot, R.H., Tiesler, V., 2012. Isotopic studies of human skeletal remains from a sixteenth to seventeenth century AD churchyard in Campeche, Mexico: Diet, place of origin, and age. *Curr. Anthropol.* 53, 396–433.
- Quellier, F., 2013. *La table des Français: Une histoire culturelle (XVe - XIXe Siècle)*. Presses Universitaires de Rennes, Rennes.
- R Core Team, 2018. *R: A language and environment for statistical computing*. R Foundation for Statistical Computing, Vienna. 14.
- Rabett, R.J., 2012. *Human adaptation in the Asian Palaeolithic: Hominin dispersal and behaviour during the Late Quaternary*. Cambridge University Press, Cambridge.
- Rabett, R.J., 2018. The success of failed *Homo sapiens* dispersals out of Africa and into Asia. *Nat. Ecol. Evol.* 2, 212–219.
- Reddy, N.R., 2002. Occurrence, distribution, content, and dietary intake of phytate. In: Reddy, N.R., Sathé, S.K. (Eds.), *Food phytates*. CRC Press, Boca Raton, pp. 37–63.
- Reynard, B., Balter, V., 2014. Trace elements and their isotopes in bones and teeth: Diet, environments, diagenesis, and dating of archeological and paleontological samples. *Palaeogeogr. Palaeoclimatol. Palaeoecol.* 416, 4–16.
- Reynard, L.M., Henderson, G.M., Hedges, R.E.M., 2010. Calcium isotope ratios in animal and human bone. *Geochim. Cosmochim. Acta.* 74, 3735–3750.
- Richards, M.P., Hedges, R.E.M., 1999. Stable isotope evidence for similarities in the types of marine foods used by Late Mesolithic humans at sites along the Atlantic coast of Europe. *J. Archaeol. Sci.* 26, 717–722.

- Richards, M.P., Mays, S., Fuller, B.T., 2002. Stable carbon and nitrogen isotope values of bone and teeth reflect weaning age at the Medieval Wharram Percy site, Yorkshire, UK. *Am. J. Phys. Anthropol.* 119, 205–210.
- Richards, M.P., Pearson, J.A., Molleson, T.I., Russell, N., Martin, L., 2003. Stable isotope evidence of diet at Neolithic Çatalhöyük, Turkey. *J. Archaeol. Sci.* 30, 67–76.
- Richards, M.P., Pettitt, P.B., Stiner, M.C., Trinkaus, E., 2001. Stable isotope evidence for increasing dietary breadth in the European mid-Upper Paleolithic. *Proc. Natl. Acad. Sci. U.S.A.* 98, 6528–6532.
- Richards, M.P., Trinkaus, E., 2009. Isotopic evidence for the diets of European Neanderthals and early modern humans. *Proc. Natl. Acad. Sci. U.S.A.* 106, 16034–16039.
- Rink, L., 2000. Zinc and the immune system. *Proc. Nutr. Soc.* 59, 541–552.
- Roberts, P., Perera, N., Wedage, O., Deraniyagala, S., Perera, J., Eregama, S., Gledhill, A., Petraglia, M.D., Lee-Thorp, J.A., 2015. Direct evidence for human reliance on rainforest resources in late Pleistocene Sri Lanka. *Science*. 347, 1246–1249.
- Roberts, P., Perera, N., Wedage, O., Deraniyagala, S., Perera, J., Eregama, S., Petraglia, M.D., Lee-Thorp, J.A., 2017a. Fruits of the forest: Human stable isotope ecology and rainforest adaptations in Late Pleistocene and Holocene (~36 to 3 ka) Sri Lanka. *J. Hum. Evol.* 106, 102–118.
- Roberts, P., Blumenthal, S.A., Dittus, W., Wedage, O., Lee-Thorp, J.A., 2017b. Stable carbon, oxygen, and nitrogen, isotope analysis of plants from a South Asian tropical forest: Implications for primatology. *Am. J. Primatol.* 79, e22656.
- Roberts, P., Gillingwater, T.H., Lahr, M.M., Lee-Thorp, J., MacCallum, M., Petraglia, M., Wedage, O., Heenbanda, U., Wainnya-laeto, U., 2018. Historical tropical forest reliance amongst the Wanniyalaeto (Vedda) of Sri Lanka: An isotopic perspective. *Hum. Ecol.* 46, 435–444.
- Roberts, P., Petraglia, M., 2015. Pleistocene rainforests: barriers or attractive environments for early human foragers? *World Archaeol.* 47, 718–739.
- Roberts, P., Amano, N., 2019. Plastic pioneers: Hominin biogeography east of the Movius Line during the Pleistocene. *Archaeol. Res. Asia.* 17, 181–192.

- Robinson, D., 2001. $\delta^{15}\text{N}$ as an integrator of the nitrogen cycle. *Trends Ecol. Evol.* 16, 153–162.
- Rosman, K.J.R., Taylor, P.D.P., 1998. Isotopic compositions of the elements 1997 (Technical Report). *Pure Appl. Chem.* 70, 217–235.
- Ruslin, F., Matsuda, I., Md-Zain, B.M., 2019. The feeding ecology and dietary overlap in two sympatric primate species, the long-tailed macaque (*Macaca fascicularis*) and dusky langur (*Trachypithecus obscurus obscurus*), in Malaysia. *Primates* 60, 41–50.
- Sandström, B., Arvidsson, B., Cederblad, A., Björn-Rasmussen, E., 1980. Zinc absorption from composite meals: The significance of wheat extraction rate, zinc, calcium, and protein content in meals based on bread. *Am. J. Clin. Nutr.* 33, 739–745.
- Sandström, B., Cederblad, Å., Lönnerdal, B., 1983. Zinc absorption from human milk, cow's milk, and infant formulas. *Am. J. Dis. Child.* 137, 726–729.
- Sandström, B., Almgren, A., Kivistö, B., Cederblad, Å., 1989. Effect of protein level and protein source on zinc absorption in humans. *J. Nutr.* 119, 48–53.
- Saurin, E., 1961. Carte géologique du Laos, feuille Luang Prabang Est.
- Scherz, H., Kirchhoff, E., 2006. Trace elements in foods: Zinc contents of raw foods—A comparison of data originating from different geographical regions of the world. *J. Food Comp. Anal.* 19, 420–433.
- Schielzeth, H., Forstmeier, W., 2009. Conclusions beyond support: Overconfident estimates in mixed models. *Behav Ecol.* 20, 416–420.
- Schoeninger, M.J., DeNiro, M.J., 1984. Nitrogen and carbon isotopic composition of bone collagen from marine and terrestrial animals. *Geochim. Cosmochim. Acta.* 48, 625–639.
- Schoeninger, M.J., DeNiro, M.J., Tauber, H., 1983. Stable nitrogen isotope ratios of bone collagen reflect marine and terrestrial components of prehistoric human diet. *Science.* 220, 1381–1383.
- Schoeninger, M.J., Hallin, K., Reeser, H., Valley, J.W., Fournelle, J., 2003. Isotopic alteration of mammalian tooth enamel. *Int. J. Osteoarchaeol.* 13, 11–19.

- Schoeller, D.A., 1999. Isotope fractionation: Why aren't we what we eat? *J. Archaeol. Sci.* 26, 667–673.
- Schurr, M.R., 1998. Using stable nitrogen-isotopes to study weaning behavior in past populations. *World Archaeol.* 30, 327–342.
- Schwarcz, H.P., 2002. Some biochemical aspects of carbon isotopic paleodiet studies. In: Ambrose, S.H., Katzenberg, M.A. (Eds.), *Biogeochemical approaches to paleodietary analysis, advances in archaeological and museum science*. Springer US, Boston, pp. 189–209.
- Sealy, J.C., van der Merwe, N.J., Hobson, K.A., Horton, D.R., Lewis, R.B., Parkington, J., Robertshaw, P., Schwarcz, H.P., 1986. Isotope assessment and the seasonal-mobility hypothesis in the Southwestern Cape of South Africa. *Curr. Anthropol.* 27, 135–150.
- Sealy, J.C., van der Merwe, N.J., Thorp, J.A.L., Lanham, J.L., 1987. Nitrogen isotopic ecology in southern Africa: Implications for environmental and dietary tracing. *Geochim. Cosmochim. Acta.* 51, 2707–2717.
- Sellen, D.W., 2001. Comparison of infant feeding patterns reported for nonindustrial populations with current recommendations. *J. Nutr.* 131, 2707–2715.
- Sengupta, A., Radhakrishna, S., 2016. Influence of fruit availability on fruit consumption in a generalist primate, the rhesus macaque *Macaca mulatta*. *Int. J. Primatol.* 37, 703–717.
- Shackelford, L., Demeter, F., Westaway, K., Durringer, P., Ponche, J.-L., Sayavongkhamdy, T., Zhao, J.-X., Barnes, L., Boyon, M., Sichanthongtip, P., Sénégas, F., Patole-Edoumba, E., Coppens, Y., Dumoncel, J., Bacon, A.-M., 2018. Additional evidence for early modern human morphological diversity in Southeast Asia at Tam Pa Ling, Laos. *Quat. Int.* 466, 93–106.
- Shearer, G., Kohl, D.H., 1986. N₂-fixation in field settings: Estimations based on natural ¹⁵N abundance. *Aust. J. Plant Physiol.* 13, 699–756.
- Skulan, J., DePaolo, D.J., Owens, T.L., 1997. Biological control of calcium isotopic abundances in the global calcium cycle. *Geochim. Cosmochim. Acta.* 61, 2505–2510.

- Skulan, J., DePaolo, D.J., 1999. Calcium isotope fractionation between soft and mineralized tissues as a monitor of calcium use in vertebrates. *Proc. Natl. Acad. Sci. U.S.A.* 96, 13709–13713.
- Smith, B.N., Epstein, S., 1971. Two categories of $^{13}\text{C}/^{12}\text{C}$ ratios for higher plants. *Plant Physiol.* 47, 380–384.
- Sponheimer, M., Lee-Thorp, J.A., 1999a. Isotopic evidence for the diet of an early hominid, *Australopithecus africanus*. *Science*. 283, 368–370.
- Sponheimer, M., Lee-Thorp, J.A., 1999b. Oxygen isotopes in enamel carbonate and their ecological significance. *J. Archaeol. Sci.* 26, 723–728.
- Sponheimer, M., Robinson, T., Ayliffe, L., Roeder, B., Hammer, J., Passey, B., West, A., Cerling, T., Dearing, D., Ehleringer, J., 2003. Nitrogen isotopes in mammalian herbivores: Hair $\delta^{15}\text{N}$ values from a controlled feeding study. *Int. J. Osteoarchaeol.* 13, 80–87.
- Sponheimer, M., Lee-Thorp, J.A., 2006. Enamel diagenesis at South African Australopithecus sites: Implications for paleoecological reconstruction with trace elements. *Geochim. Cosmochim. Acta.* 70, 1644–1654.
- Sponheimer, M., Loudon, J.E., Codron, D., Howells, M.E., Pruett, J.D., Codron, J., de Ruiter, D.J., Lee-Thorp, J.A., 2006a. Do “savanna” chimpanzees consume C_4 resources? *J. Hum. Evol.* 51, 128–133.
- Sponheimer, M., Passey, B.H., Ruiters, D.J. de, Guatelli-Steinberg, D., Cerling, T.E., Lee-Thorp, J.A., 2006b. Isotopic evidence for dietary variability in the Early Hominin *Paranthropus robustus*. *Science*. 314, 980–982.
- Sponheimer, M., Alemseged, Z., Cerling, T.E., Grine, F.E., Kimbel, W.H., Leakey, M.G., Lee-Thorp, J.A., Manthi, F.K., Reed, K.E., Wood, B.A., Wynn, J.G., 2013. Isotopic evidence of early hominin diets. *Proc. Natl. Acad. Sci. U.S.A.* 110, 10513–10518.
- Steadman, L.T., Brudevold, F., Smith, F.A., 1958. Distribution of strontium in teeth from different geographic areas. *J. Am. Dent. Assoc.* 57, 340–344.
- Sternberg, L. da S.L., Mulkey, S.S., Wright, S.J., 1989. Oxygen isotope ratio stratification in a tropical moist forest. *Oecologia*. 81, 51–56.

- Still, C.J., Berry, J.A., Collatz, G.J., DeFries, R.S., 2003. Global distribution of C₃ and C₄ vegetation: Carbon cycle implications. *Global Biogeochem. Cycles*. 17, 1006.
- Strauss, A., 2017. Burial practices in the Lagoa Santa region. In: Da-Gloria, P., Neves, W.A., Hubbe, M. (Eds.), *Archaeological and paleontological research in Lagoa Santa: The quest for the First Americans*. Springer International Publishing, Cham, pp. 275–295.
- Strauss, A., Oliveira, R.E., Bernardo, D.V., Salazar-García, D.C., Talamo, S., Jaouen, K., Hubbe, M., Black, S., Wilkinson, C., Richards, M.P., Araujo, A.G.M., Kipnis, R., Neves, W.A., 2015. The oldest case of decapitation in the New World (Lapa do Santo, east-central Brazil). *PLoS ONE*. 10, e0137456.
- Strauss, A., Oliveira, R.E., Villagran, X.S., Bernardo, D.V., Salazar-García, D.C., Bissaro, M.C., Pugliese, F., Hermenegildo, T., Santos, R., Barioni, A., Oliveira, E.C. de, Sousa, J.C.M. de, Jaouen, K., Ernani, M., Hubbe, M., Inglez, M., Gratão, M., Rockwell, H., Machado, M., Souza, G. de, Chemale, F., Kawashita, K., O’Connell, T.C., Israde, I., Feathers, J., Campi, C., Richards, M., Wahl, J., Kipnis, R., Araujo, A., Neves, W., 2016. Early Holocene ritual complexity in South America: The archaeological record of Lapa do Santo (east-central Brazil). *Antiquity*. 90, 1454–1473.
- Stuart-Macadam, P., Dettwyler, K.A. (Eds.), 2017. *Breastfeeding: Biocultural perspectives*. Routledge, New York.
- Sullivan, C.H., Krueger, H.W., 1981. Carbon isotope analysis of separate chemical phases in modern and fossil bone. *Nature*. 292, 333–335.
- Summerhayes, G.R., Leavesley, M., Fairbairn, A., Mandui, H., Field, J., Ford, A., Fullagar, R., 2010. Human adaptation and plant use in highland New Guinea 49,000 to 44,000 years ago. *Science*. 330, 78–81.
- Suraprasit, K., Jaeger, J.-J., Chaimanee, Y., Chavasseau, O., Yamee, C., Tian, P., Panha, S., 2016. The Middle Pleistocene vertebrate fauna from Khok Sung (Nakhon Ratchasima, Thailand): Biochronological and paleobiogeographical implications. *Zookeys*. 1–157.
- Sutikna, T., Tocheri, M.W., Morwood, M.J., Saptomo, E.W., Jatmiko, Awe, R.D., Wasisto, S., Westaway, K.E., Aubert, M., Li, B., Zhao, J., Storey, M., Alloway, B.V., Morley, M.W., Meijer, H.J.M., van den Bergh, G.D., Grün, R., Dosseto,

- A., Brumm, A., Jungers, W.L., Roberts, R.G., 2016. Revised stratigraphy and chronology for *Homo floresiensis* at Liang Bua in Indonesia. *Nature*. 532, 366–369.
- Swisher, C.C., Curtis, G.H., Jacob, T., Getty, A.G., Suprijo, A., Widiasmoro, 1994. Age of the earliest known hominids in Java, Indonesia. *Science*. 263, 1118–1121.
- Tacail, T., Kovačiková, L., Brůžek, J., Balter, V., 2017. Spatial distribution of trace element Ca-normalized ratios in primary and permanent human tooth enamel. *Sci. Total Environ.* 603–604, 308–318.
- Tacail, T., Thivichon-Prince, B., Martin, J.E., Charles, C., Viriot, L., Balter, V., 2017. Assessing human weaning practices with calcium isotopes in tooth enamel. *Proc. Natl. Acad. Sci. U.S.A.* 114, 6268–6273.
- Tacail, T., Le Houedec, S., Skulan, J.L., 2020. New frontiers in calcium stable isotope geochemistry: Perspectives in present and past vertebrate biology. *Chem. Geol.* 537, 119471.
- Takai, M., Zhang, Y., Kono, R.T., Jin, C., 2014. Changes in the composition of the Pleistocene primate fauna in southern China. *Quat. Int.* 354, 75–85.
- Talamo, S., Richards, M., 2011. A comparison of bone pretreatment methods for AMS dating of samples >30,000 BP. *Radiocarbon*. 53, 443–449.
- Tang, Y.-T., Cloquet, C., Deng, T.-H.-B., Sterckeman, T., Echevarria, G., Yang, W.-J., Morel, J.-L., Qiu, R.-L., 2016. Zinc isotope fractionation in the hyperaccumulator *Noccaea caerulescens* and the nonaccumulating plant *Thlaspi arvense* at low and high Zn supply. *Environ. Sci. Technol.* 50, 8020–8027.
- Tang, Y.-T., Cloquet, C., Sterckeman, T., Echevarria, G., Carignan, J., Qiu, R.-L., Morel, J.-L., 2012. Fractionation of stable zinc isotopes in the field-grown zinc hyperaccumulator *Noccaea caerulescens* and the zinc-tolerant plant *Silene vulgaris*. *Environ. Sci. Technol.* 46, 9972–9979.
- Tappen, M., 1994. Bone weathering in the tropical rain forest. *J. Archaeol. Sci.* 21, 667–673.
- Tauber, H., 1981. ¹³C evidence for dietary habits of prehistoric man in Denmark. *Nature*. 292, 332–333.

- Taylor, C.M., Bacon, J.R., Aggett, P.J., Bremner, I., 1991. Homeostatic regulation of zinc absorption and endogenous losses in zinc-deprived men. *Am. J. Clin. Nutr.* 53, 755–763.
- Teaford, M.F., Ungar, P.S., 2000. Diet and the evolution of the earliest human ancestors. *Proc. Natl. Acad. Sci. U.S.A.* 97, 13506–13511.
- Tejada, J.V., Flynn, J.J., Antoine, P.-O., Pacheco, V., Salas-Gismondi, R., Cerling, T.E., 2020. Comparative isotope ecology of western Amazonian rainforest mammals. *Proc. Natl. Acad. Sci. U.S.A.* 117, 26263–26272.
- Tejada-Lara, J.V., MacFadden, B.J., Bermudez, L., Rojas, G., Salas-Gismondi, R., Flynn, J.J., 2018. Body mass predicts isotope enrichment in herbivorous mammals. *Proc. R. Soc. B.* 285, 20181020.
- Teruel, J. de D., Alcolea, A., Hernández, A., Ruiz, A.J.O., 2015. Comparison of chemical composition of enamel and dentine in human, bovine, porcine and ovine teeth. *Arch. Oral Biol.* 60, 768–775.
- Tessone, A., Guraieb, S.G., Goñi, R.A., Panarello, H.O., 2015. Isotopic evidence of weaning in hunter-gatherers from the late Holocene in Lake Salitroso, Patagonia, Argentina. *Am. J. Phys. Anthropol.* 158, 105–115.
- Tieszen, L.L., Fagre, T., 1993. Effect of diet quality and composition on the isotopic composition of respiratory CO₂, bone collagen, bioapatite, and soft tissues. In: Lambert, J.B., Grupe, G. (Eds.), *Prehistoric human bone: Archaeology at the molecular level*. Springer Berlin, Heidelberg, pp. 121–155.
- Tougaard, C., 1998. Les faunes de grands mammifères du Pléistocène moyen terminal de Thaïlande dans leur cadre phylogénétique, paléoécologique et biochronologique. (Doctoral dissertation). Université de Montpellier II.
- Trueman, C.N., Tuross, N., 2002. Trace elements in recent and fossil bone apatite. *Rev. Mineral. Geochem.* 48, 489–521.
- Tsutaya, T., Shimomi, A., Fujisawa, S., Katayama, K., Yoneda, M., 2016. Isotopic evidence of breastfeeding and weaning practices in a hunter-gatherer population during the Late/Final Jomon period in eastern Japan. *J. Archaeol. Sci.* 76, 70–78.

- Turnlund, J.R., King, J.C., Keyes, W.R., Gong, B., Michel, M.C., 1984. A stable isotope study of zinc absorption in young men: Effects of phytate and a-cellulose. *Am J Clin Nutr.* 40, 1071–1077.
- Vallee, B.L., Falchuk, K.H., 1993. The biochemical basis of zinc physiology. *Physiol. Rev.* 73, 79–118.
- van der Ent, A., Nkrumah, P.N., Aarts, M.G.M., Baker, A.J.M., Degryse, F., Wawryk, C., Kirby, J.K., 2021. Isotopic signatures reveal zinc cycling in the natural habitat of hyperaccumulator *Dichapetalum gelonioides* subspecies from Malaysian Borneo. *BMC Plant Biol.* 21, 437.
- van der Merwe, N.J., Medina, E., 1989. Photosynthesis and $^{13}\text{C}/^{12}\text{C}$ ratios in Amazonian rain forests. *Geochim. Cosmochim. Acta.* 53, 1091–1094.
- van der Merwe, N.J., Medina, E., 1991. The canopy effect, carbon isotope ratios and foodwebs in Amazonia. *J. Archaeol. Sci.* 18, 249–259.
- van der Merwe, N.J., Vogel, J.C., 1978. ^{13}C Content of human collagen as a measure of prehistoric diet in woodland North America. *Nature.* 276, 815–816.
- van Klinken, G.J., 1999. Bone collagen quality indicators for palaeodietary and radiocarbon measurements. *J. Archaeol. Sci.* 26, 687–695.
- van Valkenburgh, B., 1996. Feeding behavior in free-ranging, large African carnivores. *J. Mammal.* 77, 240–254.
- van Valkenburgh, B., Teaford, M.F., Walker, A., 1990. Molar microwear and diet in large carnivores: Inferences concerning diet in the sabretooth cat, *Smilodon fatalis*. *J. Zool.* 222, 319–340.
- van Weers, D.J., 2005. A taxonomic revision of the Pleistocene *Hystrix* (Hystricidae, Rodentia) from Eurasia with notes on the evolution of the family. *Contrib. Zool.* 74, 301–312.
- Veile, A., Kramer, K., 2015. Birth and breastfeeding dynamics in a modernizing indigenous community. *J. Hum. Lact.* 31, 145–155.
- Viers, J., Oliva, P., Nonell, A., Gélabert, A., Sonke, J.E., Freydier, R., Gainville, R., Dupré, B., 2007. Evidence of Zn isotopic fractionation in a soil–plant system of a pristine tropical watershed (Nsimi, Cameroon). *Chem. Geol.* 239, 124–137.

- Viers, J., Prokushkin, A.S., Pokrovsky, O.S., Kirilyanov, A.V., Zouiten, C., Chmeleff, J., Meheut, M., Chabaux, F., Oliva, P., Dupré, B., 2015. Zn isotope fractionation in a pristine larch forest on permafrost-dominated soils in Central Siberia. *Geochemical Trans.* 16, 3.
- Villagran, X.S., Strauss, A., Miller, C., Ligouis, B., Oliveira, R., 2017. Buried in ashes: Site formation processes at Lapa do Santo rockshelter, east-central Brazil. *J. Archaeol. Sci.* 77, 10–34.
- Vogel, J.C., 1978. Isotopic assessment of the dietary habits of ungulates. *S. Afr. J. Sci.* 74, 298–301.
- Vogel, J.C., Merwe, N.J.V.D., 1977. Isotopic evidence for early maize cultivation in New York State. *Am. Antiq.* 42, 238–242.
- von Blanckenburg, F., von Wirén, N., Guelke, M., Weiss, D.J., Bullen, T.D., 2009. Fractionation of metal stable isotopes by higher plants. *Elements.* 5, 375–380.
- Wada, L., Turnlund, J.R., King, J.C., 1985. Zinc utilization in young men fed adequate and low zinc intakes. *J. Nutr.* 115, 1345–1354.
- Walczyk, T., von Blanckenburg, F., 2002. Natural iron isotope variations in human blood. *Science.* 295, 2065–2066.
- Walczyk, T., von Blanckenburg, F., 2005. Deciphering the iron isotope message of the human body. *Int. J. Mass Spectrom.* 242, 117–134.
- Wang, Y., Cerling, T.E., 1994. A model of fossil tooth and bone diagenesis: Implications for paleodiet reconstruction from stable isotopes. *Palaeogeogr. Palaeoclimatol. Palaeoecol.* 107, 281–289.
- Wapnir, R.A., 2000. Zinc deficiency, malnutrition and the gastrointestinal tract. *J. Nutr.* 130, 1388S–1392S.
- Weber, M., Tacail, T., Lugli, F., Clauss, M., Weber, K., Leichliter, J., Winkler, D.E., Mertz-Kraus, R., Tütken, T., 2020. Strontium uptake and intra-population $^{87}\text{Sr}/^{86}\text{Sr}$ variability of bones and teeth—Controlled feeding experiments with rodents (*Rattus norvegicus*, *Cavia porcellus*). *Front. Ecol. Evol.* 8.
- Wedage, O., Amano, N., Langley, M.C., Douka, K., Blinkhorn, J., Crowther, A., Deraniyagala, S., Kourampas, N., Simpson, I., Perera, N., Picin, A., Boivin, N., Petraglia, M., Roberts, P., 2019. Specialized rainforest hunting by *Homo sapiens* ~45,000 years ago. *Nat. Commun.* 10, 1–8.

- Weinstein, C., Moynier, F., Wang, K., Paniello, R., Foriel, J., Catalano, J., Pichat, S., 2011. Isotopic fractionation of Cu in plants. *Chem. Geol.* 286, 266–271.
- Weiss, D.J., Mason, T.F.D., Zhao, F.J., Kirk, G.J.D., Coles, B.J., Horstwood, M.S.A., 2005. Isotopic discrimination of zinc in higher plants. *New Phytol.* 165, 703–710.
- Weiss, D.J., Rehkämper, M., Schoenberg, R., McLaughlin, M., Kirby, J., Campbell, P.G.C., Arnold, T., Chapman, J., Peel, K., Gioia, and S., 2008. Application of nontraditional stable-isotope systems to the study of sources and fate of metals in the environment. *Environ. Sci. Technol.* 42, 655–664.
- Wessells, K.R., Brown, K.H., 2012. Estimating the global prevalence of zinc deficiency: Results based on zinc availability in national food supplies and the prevalence of stunting. *PLoS ONE.* 7, e50568.
- Westaway, K.E., Louys, J., Awe, R.D., Morwood, M.J., Price, G.J., Zhao, J. -x, Aubert, M., Joannes-Boyau, R., Smith, T.M., Skinner, M.M., Compton, T., Bailey, R.M., van den Bergh, G.D., de Vos, J., Pike, A.W.G., Stringer, C., Saptomo, E.W., Rizal, Y., Zaim, J., Santoso, W.D., Trihascaryo, A., Kinsley, L., Sulistyanto, B., 2017. An early modern human presence in Sumatra 73,000–63,000 years ago. *Nature.* 548, 322–325.
- Wich, S.A., Utami-Atmoko, S.S., Mitra Setia, T., Djoyosudharmo, S., Geurts, M.L., 2006. Dietary and energetic responses of *Pongo abelii* to fruit availability fluctuations. *Int. J. Primatol.* 27, 1535–1550.
- Wißing, C., Rougier, H., Baumann, C., Comeyne, A., Crevecoeur, I., Drucker, D.G., Gaudzinski-Windheuser, S., Germonpré, M., Gómez-Olivencia, A., Krause, J., Matthies, T., Naito, Y.I., Posth, C., Semal, P., Street, M., Bocherens, H., 2019. Stable isotopes reveal patterns of diet and mobility in the last Neandertals and first modern humans in Europe. *Sci Rep.* 9, 4433.
- Woodcock, P., Edwards, D.P., Newton, R.J., Edwards, F.A., Khen, C.V., Bottrell, S.H., Hamer, K.C., 2012. Assessing trophic position from nitrogen isotope ratios: Effective calibration against spatially varying baselines. *Naturwissenschaften.* 99, 275–283.
- Woodroffe, C.D., Short, S.A., Stoddart, D.R., Spencer, T., Harmon, R.S., 1991. Stratigraphy and chronology of Late Pleistocene reefs in the southern Cook Islands, South Pacific. *Quat. Res.* 35, 246–263.

- Wright, P.J., 2010. Methodological issues in paleoethnobotany: A consideration of issues, methods, and cases. In: VanDerwarker, A.M., Peres, T.M. (Eds.), *Integrating zooarchaeology and paleoethnobotany: A consideration of issues, methods, and cases*. Springer, New York, pp. 37–64.
- Wright, L.E., 2012. Immigration to Tikal, Guatemala: Evidence from stable strontium and oxygen isotopes. *J. Anthropol. Archaeol.* 31, 334–352.
- Wurster, C.M., Bird, M.I., 2016. Barriers and bridges: Early human dispersals in equatorial SE Asia. *Geol. Soc. Lond. Spec. Publ.* 411, 235–250.
- Yasuno, T., Okamoto, H., Nagai, M., Kimura, S., Yamamoto, T., Nagano, K., Furubayashi, T., Yoshikawa, Y., Yasui, H., Katsumi, H., Sakane, T., Yamamoto, A., 2011. The disposition and intestinal absorption of zinc in rats. *Eur. J. Pharm. Sci.* 44, 410–415.
- Zazzo, A., Bocherens, H., Billiou, D., Mariotti, A., Brunet, M., Vignaud, P., Beauvilain, A., Mackaye, H.T., 2000. Herbivore paleodiet and paleoenvironmental changes in Chad during the Pliocene using stable isotope ratios of tooth enamel carbonate. *Paleobiology.* 26, 294–309.
- Zeitoun, V., Auetrakulvit, P., Zazzo, A., Pierret, A., Frère, S., Forestier, H., 2019. Discovery of an outstanding Hoabinhian site from the Late Pleistocene at Doi Pha Kan (Lampang province, northern Thailand). *Archaeol. Res. Asia.* 18, 1–16.